NUMERICAL INVESTIGATIONS OF AIRFLOW AND HEAT TRANSFER IN TRADITIONAL BALINESE BUILDINGS

A thesis submitted for the degree of Doctor of Philosophy

by

I Gusti Bagus Wijaya Kusuma

Department of Mechanical Engineering, Brunel University

September 1999

ABSTRACT

Traditional Balinese architecture is commonly related to culture and traditional reasoning. When subjected to several modern problems such as energy demand, pollution, and impact of urbanisation and tourism, traditional architecture becomes less attractive since the definitions behind traditional reasoning are not clear and can be interpreted in different ways. To understand this feature, the study of traditional Balinese architecture starts by using several key parameters such as wind engineering and heat transfer, as presented and used in several countries.

The flow patterns around a cubic building have been studied by many researchers. The velocity profile at the model position and the local surface roughness are specific to each building model and cannot be estimated from general tests of a standard building shape, therefore specific velocity profiles and conditions are used in this particular study.

The air flow around a cluster of traditional Balinese buildings is extremely complicated and difficult to determine by modelling an isolated building (via symmetric conditions) since the buildings are linked to each other. Full scale models of traditional buildings have been investigated by using *CFD* to predict the above aspects. Simulations using this method can be done more quickly and less expensively than with wind tunnel experiments, and are capable of delivering more detailed and comprehensive information about the flow structure.

Two-dimensional models of traditional Balinese building arrangements are simulated by using a commercial code *Fidap* based on the finite element method to assess the effects of type of roof, fence and surface roughness. Three-dimensional models are simulated by using a commercial code *CFX* based on the finite volume method to verify some traditional definitions.

A standard k-ε model is adopted because it needs less computational power and has achieved notable successes in calculating a wide variety of thin shear layer and recirculating flows without the need of adjustment of the model constants, but with the imposition of boundary conditions to reduce the over-prediction near windward edges. Adopting lower values of k and ε combined with multi-blocks is shown to reduce this over-estimation. For a cubic building, the results can be compared with several other turbulence models.

It appears that traditional Balinese architecture has a strong and significant correlation with several engineering fields, therefore traditional communities can develop by considering the *Tri Hita Karana* concept in order to improve thermal comfort and reduce cooling loads, with corresponding energy savings.

ACKNOWLEDGEMENTS

It gives me great pleasure to express my deepest gratitude to Professor L.C. Wrobel for his guidance, suggestions, help, information and encouragement throughout my studies.

I am grateful to Professor N. Ladommatos, the Head of the Mechanical Engineering Department, for the provision of supporting resources.

Particular thanks go to Professor T.V. Duggan, International Educational and Engineering Consultant, for his enthusiasm in supporting my PhD studies at Brunel University.

I would like to thank the Indonesian Government, Ministry of Education and Culture of the Republic of Indonesia for their financial support, Ir. Suherman, M. Eng., Director of the Engineering Education Development Project -ADB Loan No. 1432- for his support and suggestions throughout these studies, and all staff at the Central Project Implementation Unit, Jakarta, and at the Local Project Implementation Unit, Denpasar, for their help and assistance.

Very special thanks to my mother MK. Padmi, who always supported the fundamental nature of anything, during the course of my studies. Many thanks to my wife Laksmi, for her love, patience and encouragement. Special gratitude goes to my child, my inspiration. To my brothers and sister, for their support throughout this research.

Many thanks to the staff of the Mechanical Engineering Department, Brunel University; Callum Downie, Doug Clancy, Robert W Webb, and also special thanks to Sukin Natarajan and Francisco A Andrade who gave generously their time and effort throughout this work.

Finally, we give offerings to the gods of Bali, who play a prominent role in the success of our ventures.

I dedicate this research

to my father,

the late I Gusti Ngurah Soewandi,

for his ideas, motivation, suggestions and inspiration.

You are nowhere but everywhere.

CONTENTS

CHAPTER SIX THREE-DIMENSIONAL MODELLING OF TRADITIONAL BALINESE BUILDINGS

LIST OF FIGURES

CHAPTER FOUR

CHAPTER FIVE

LIST OF TABLES

NOTATION

κ, von Karman's constant ≈ 0.41

Re, ***Pe***, Reynolds and Peclet numbers, respectively

CFD, Computational Fluid Dynamics

k-ε, standard turbulence model

EVM, Eddy Viscosity turbulence model

ASM, Algebraic Stress turbulence model

LES, Large Eddy Simulation turbulence model

DSM, Differential Stress turbulence model

RNG- k-ε, re-normalisation group of standard turbulence model

CPU, Central Processor Unit

CFX, a commercial CFD code based on Finite Volume methods

Fidap, a commercial CFD code based on Finite Element methods

SIMPLE, Semi-Implicit Method for Pressure Linked Equations

SIMPLER, SIMPLE Revised

SIMPLEC, SIMPLE-Consistent

PISO, Pressure Implicit with Splitting of Operators

d_p, the distance between the first grid line and solid boundaries

r, the grid expanding factor for each region starting from the solid boundaries

P, k and ε, represent pressure, turbulent kinetic and energy dissipation, respectively

e and ***w***, represent the faces of a general node at *east* and *west* of the mid-point

E and ***P***, and ***W*** and ***P***, represent *East* and *Centre*, and *West* and *Centre*, respectively

f_W and f_P, the interpolation factor at points ***W*** and ***P***, respectively

Γ_w, Γ_P and Γ_E, diffusion coefficients at points ***W, P*** and ***E***, respectively

δx_{Ww} and δx_{wP}, distance between points

δx_{Pe} and δx_{eE}, distance between point and node

u, v and *w*, velocity components in *x*, *y* and *z* directions, respectively

h or ***H***, objects' or fences' or buildings' or tunnels' height

$\mathbf{U}_{inlet}$, inlet velocity

I, turbulence intensity, ranges between 1 and 7%

ρ, air density

n, the outward unit normal vector

u, velocity vector

d, the viscous stress tensor

μ, dynamic viscosity of air

u_t, tangential velocity

u_n, the outward normal velocity

∇_τ, the gradient operator in the tangent plane

$F_n = n.\ F$, normal force

$F_t = \tau.\ F$, tangential force

f_n and f_t, normal and tangential components of the traction forces, respectively

u', v', the fluctuating velocity components of fluid

P_w, the pressure at the wall

τ_w, the shear stress at solid walls, $\tau_w \equiv \mu \left.\frac{dU}{dy}\right|_{y=0}$

u_τ, friction velocity at a solid wall, $u_\tau = \sqrt{\tau_w / \rho}$

y^+, distance normal to a solid wall, $y^+ = \rho y u_\tau / \mu$

T_s, T_o and T_g, temperature on the object, at the inlet and on the ground, respectively

$\overline{u_y}, \overline{u_{10m}}$, mean speed of air at height y and 10 m, respectively

y_0, roughness length (0.010 m for a cut grass fetch)

T_0, inlet temperature = 301 K

$\sigma_k, \sigma_\varepsilon, C_1$ and C_2, constants of the model, with $\sigma_k = 1.0, \sigma_\varepsilon = 1.3, C_1 = 1.44$ and $C_2 = 1.92$

l, L, distance between two objects, length of objects, respectively

q'', heat flux on the surface

e/H, relative surface roughness

U_g, z_g, reference velocity of air and height, respectively

$\sigma_{T,l}$, $\sigma_{T,t}$, the laminar and turbulent Prandtl's number, respectively

CHAPTER ONE

INTRODUCTION

1.1 Traditional Balinese Architecture

Culture is a result of the interrelationship between humans and their environment. Traditional Balinese architecture as part of culture has its background on Hindu religion laws, customs and manners. It has always been followed by the people of Bali, and contains exalted values which are considered eternal [1].

The Balinese believe that three factors are crucial to a person's well-being, happiness and health:

The microcosm (*Bhuwana Alit*) which is made up of individual persons

The macrocosm (*Bhuwana Agung*) which comprises the universe

The supreme God (*Hyang Widhi Wasa*)

In their daily lives, the Balinese strive to keep the three factors in equilibrium, a concept called *Tri Hita Karana. Kaja* (towards the mountain, upwards) leads towards the sacred; *kelod* (towards the sea, downwards) leads to demons or evil; and the middle world, secular and without special forces, is where people live. Similarly, the village is located between the temple (upwards) and the haunted graveyard (downwards), and the house should be located between the house shrine and the refuse pit. *Natar* (centre) harmony and balance are unconsciously striven for in many aspects of thought, emotion and behaviour in daily living [2].

Traditional reasoning of zoning area follows the physics of microcosms (*Bhuwana Alit*) and macrocosms (*Bhuwana Agung*). The region is divided into three sub-areas called Poverty, Middle, and Primary areas (*Nista*, *Madya*, and *Utama*, respectively).

According to four palm leaf manuscripts (named *Lontar*) the *Asta Kosala*, *Asta Kosali*, *Asta Patali* and *Swakarman* [3, 4, 5 and 6], the housing area is divided into nine regions. In traditional Balinese architecture, people follow the upwards and downwards directions (*hulu* and *teben*, respectively). Upwards and downwards directions are defined following the movement of the sun or the mount - sea direction.

Sun-rises upwards and sun-sets downwards, or the mount is upwards and the sea is downwards. The *Sanga Mandala* concepts are shown in Fig.1.1.1, 1.1.2, 1.1.3 and 1.1.4 and the *Sanga Mandala* concept of Bali Island is shown in Fig.1.1.5.

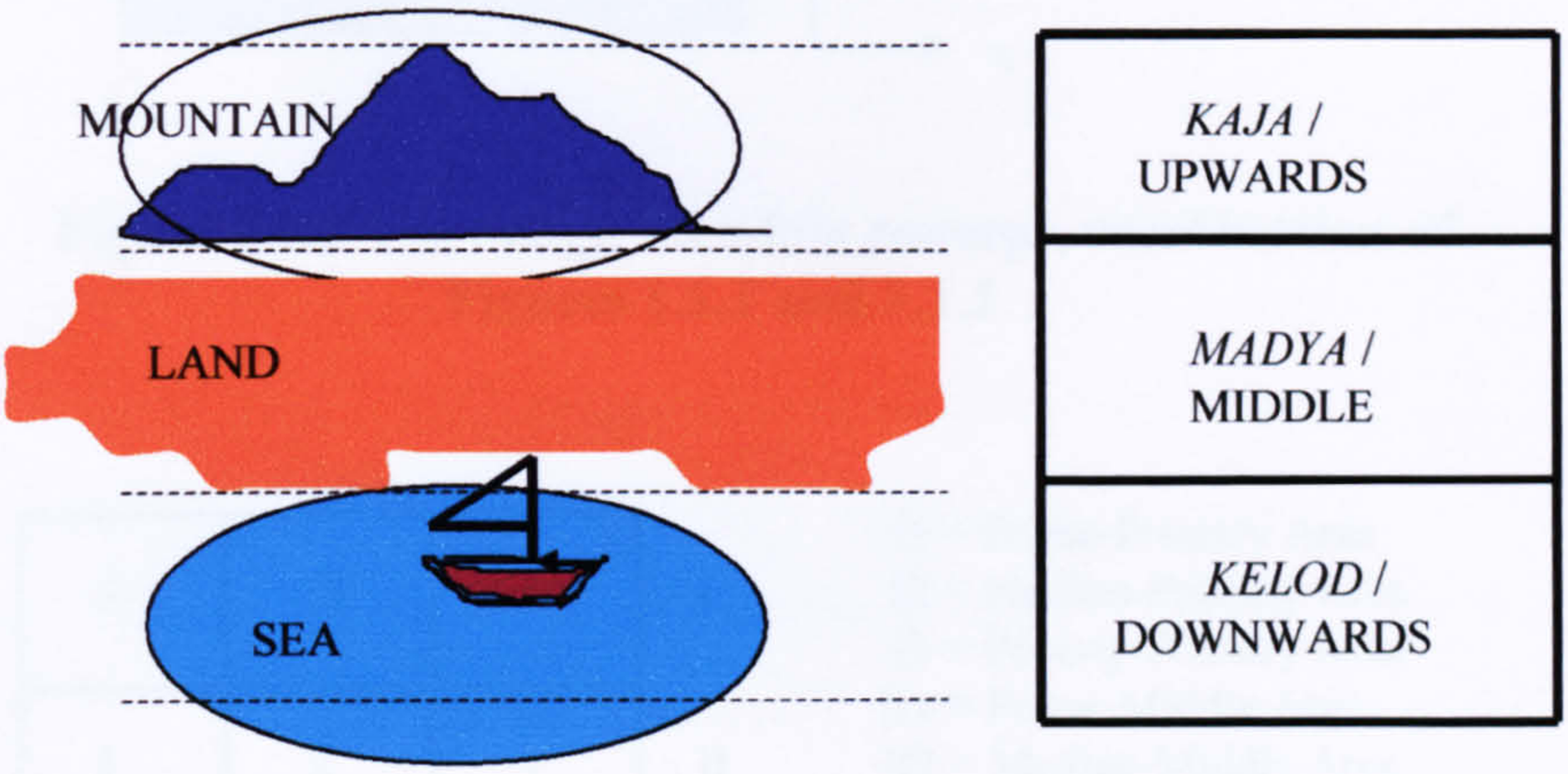

Figure 1.1.1 The *Sanga Mandala* concept following the mount-sea direction

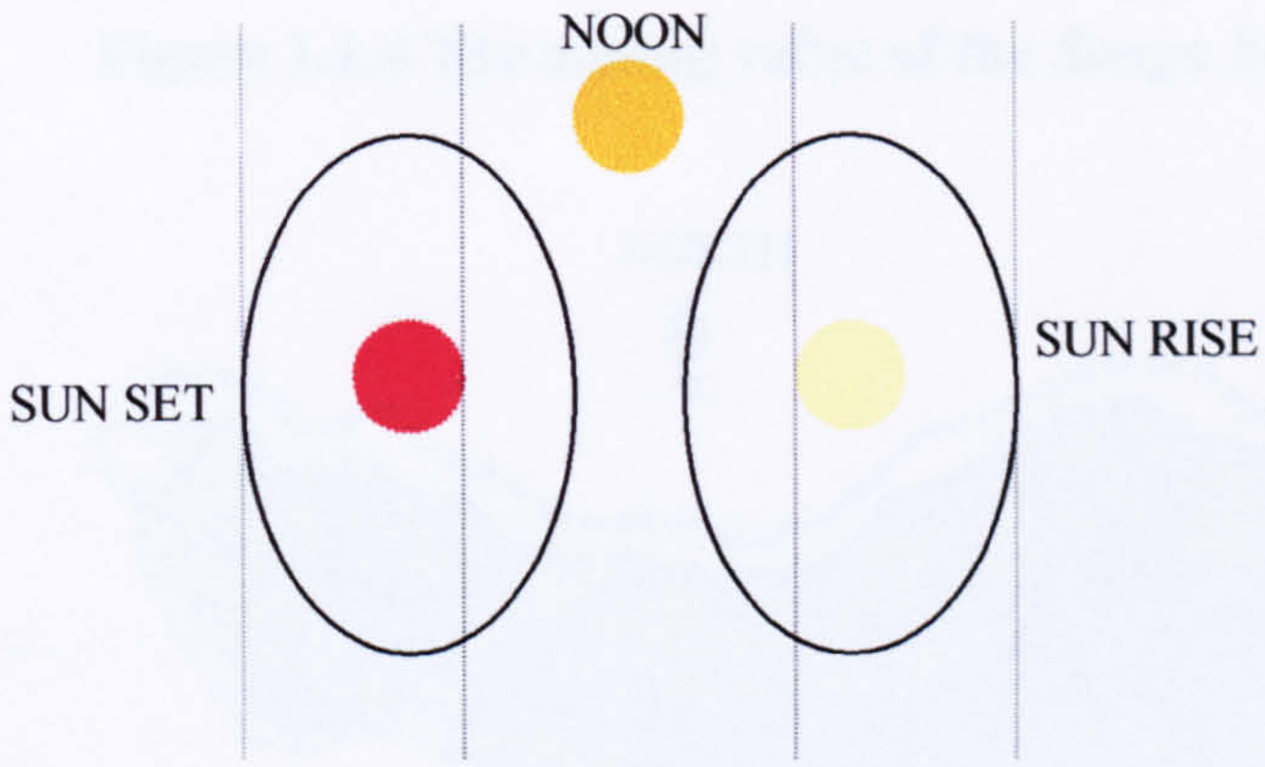

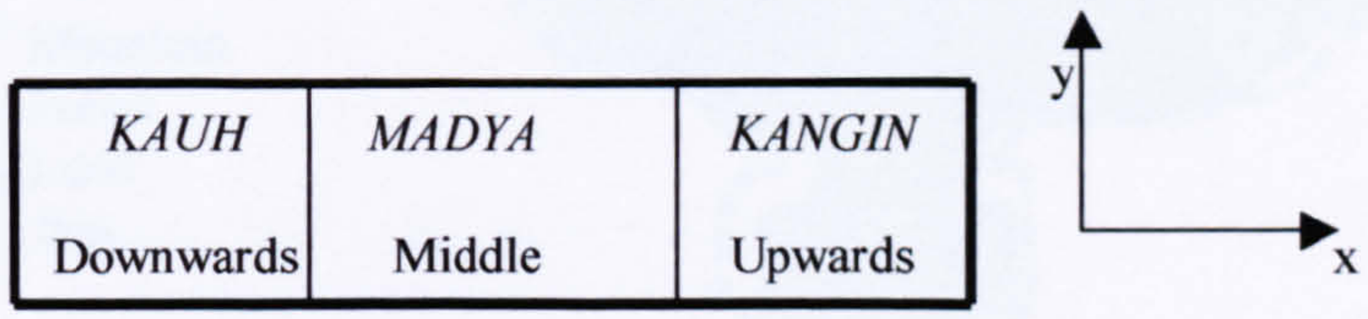

Figure 1.1.2 The *Sanga Mandala* concept following the sun-rise and sun-set directions

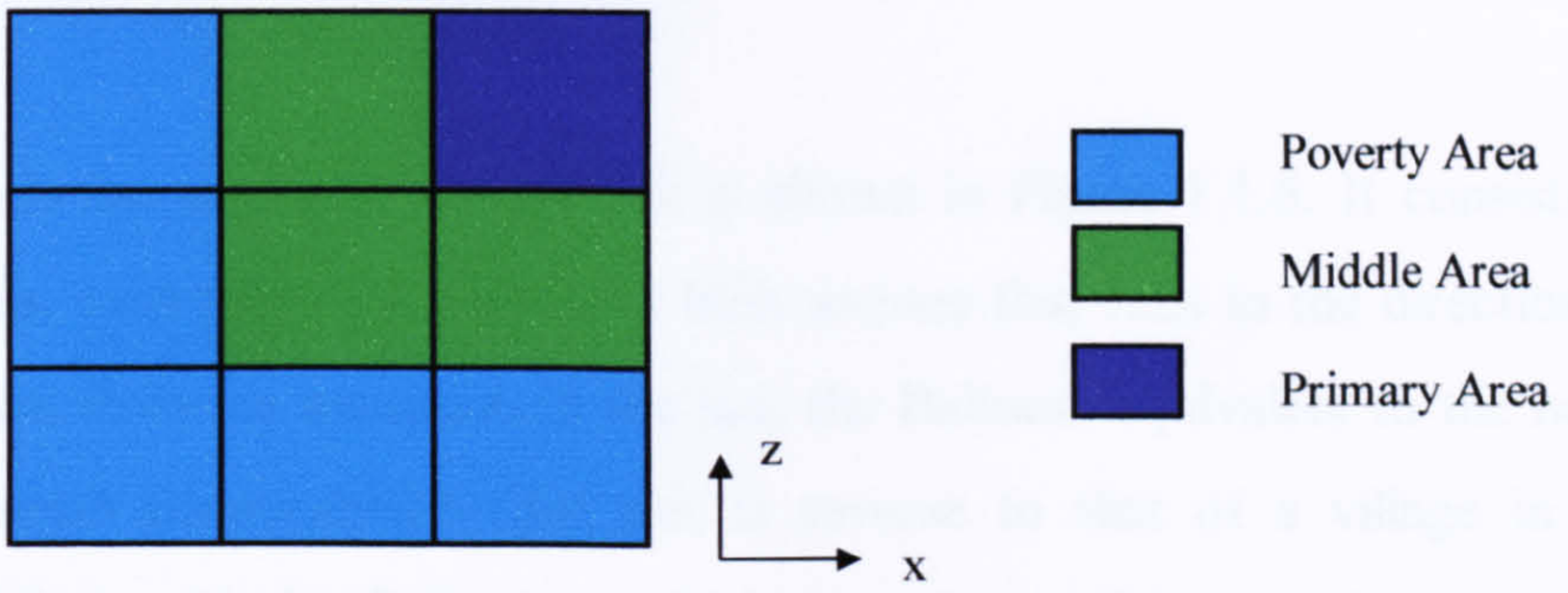

Figure 1.1.3 The *Sanga Mandala* concept, combination of Figures 1.1.1 and 1.1.2

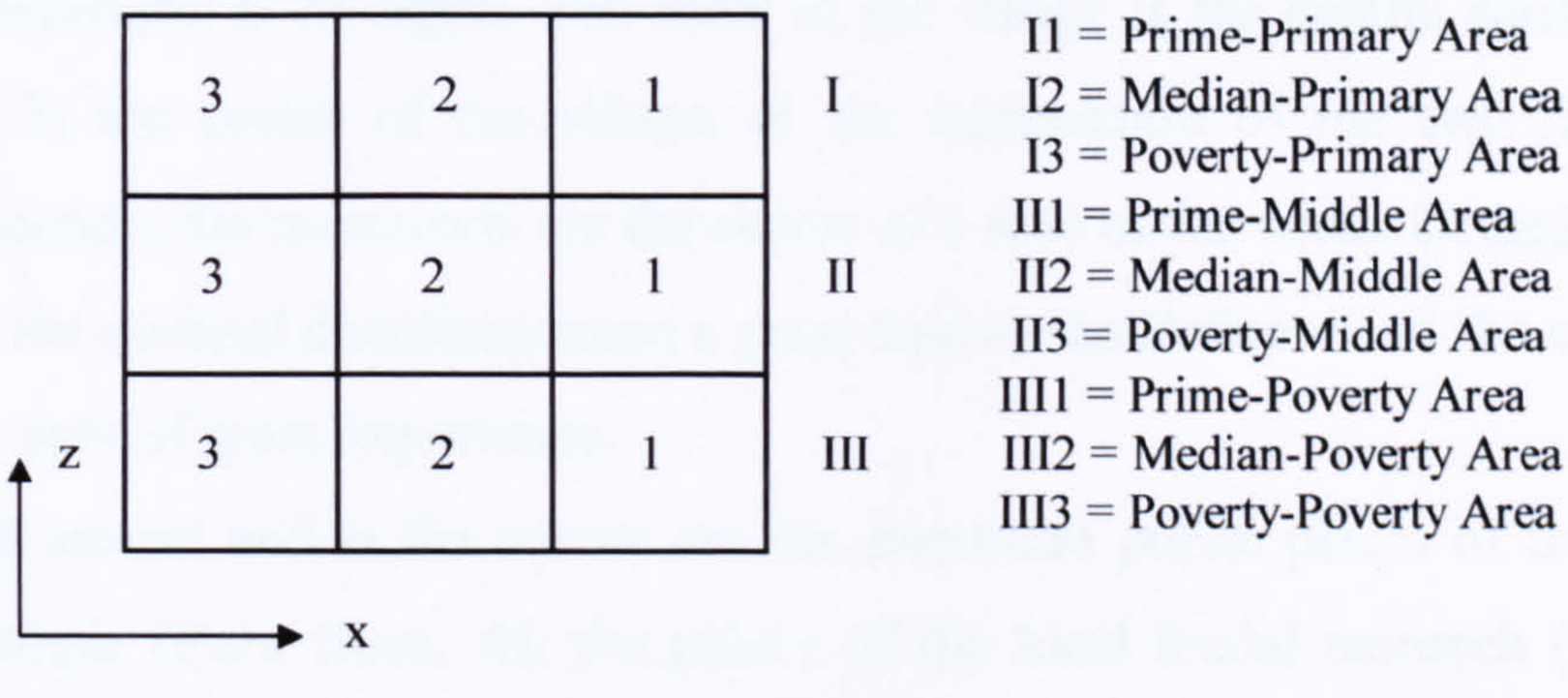

Figure 1.1.4 The zoning value of the *Sanga Mandala* concept

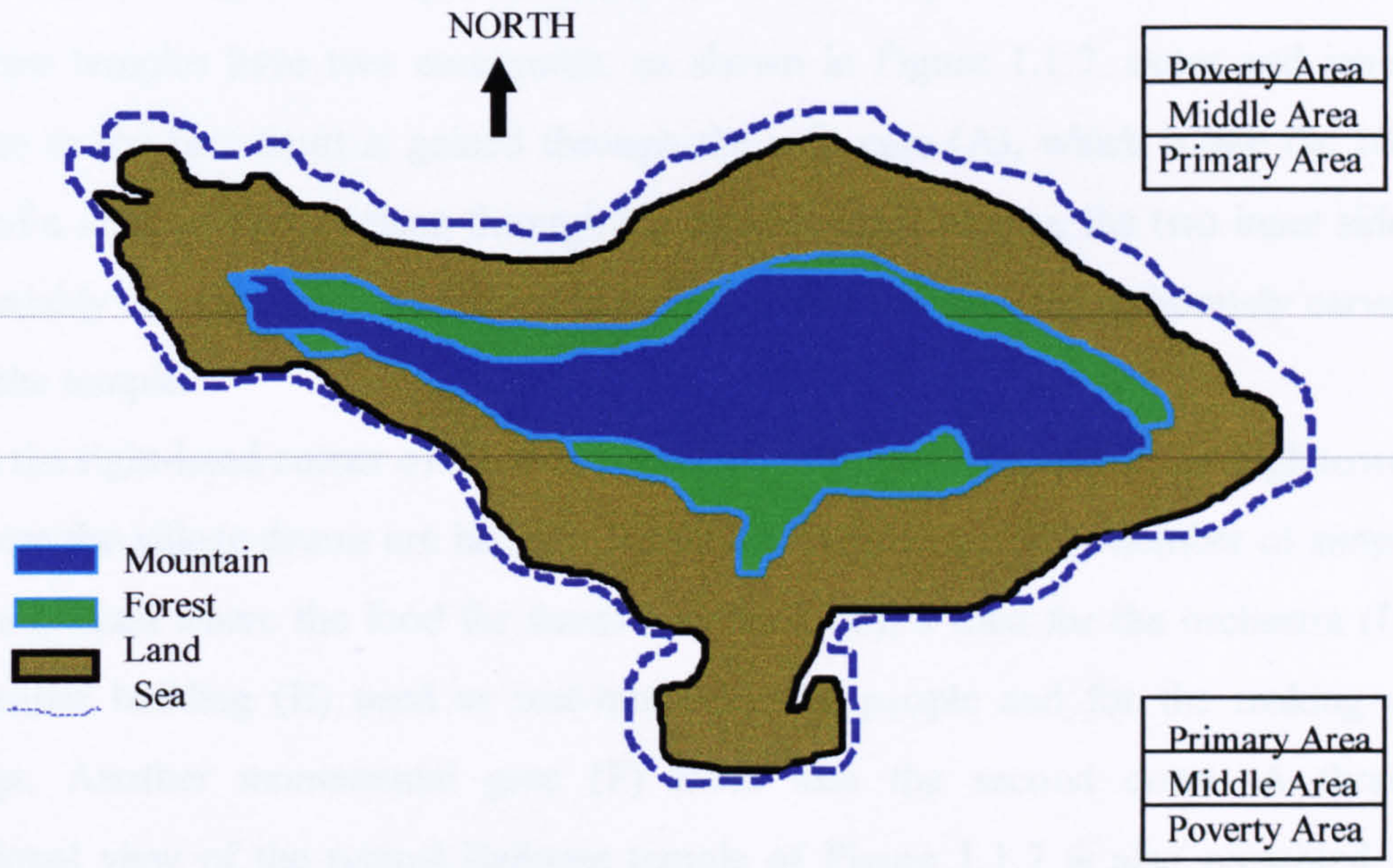

Figure 1.1.5 The *Sanga Mandala* concept of Bali island

1.1.1 Traditional Balinese Community

A simple village in the southern part of Bali is shown in Figure 1.1.6. It consists of family compounds, each side of a wide well built avenue that runs in the direction of the cardinal points; from the mountain to the sea, the Balinese equivalent to the north (upwards) and south (downwards). But this is reverse to that of a village in the northern part of Bali, with the Balinese equivalent to the south (upwards) and north (downwards). The Balinese make a clear differentiation between the dwelling-grounds and the unlived parts of the village, those for public use such as temples, assembly halls and market. The village is a unified organism in which every individual is a body and every institution is an organ. The heart of the village is the central square, invariably located in the centre of the village, at the intersection of the two main avenues. Consequently, the crossroads are the centre of a rose of the winds formed by the entire village, the cardinal directions mean a great deal to the Balinese and the crossroads are a magic spot of great importance.

All around and in the square are the important public places of the village: the town temple (*Pura Desa*, A), the palace of the local feudal monarch (*Puri*, B), the market (C), the assembly hall (*Wantilan*, D) the elaborate tower of drum alarm (*Kulkul* tower, E), a giant banyan, the sacred tree of the Hindus (*Waringin*, F) and, in the outskirts of the village, the temple of dead (*Pura Dalem*, G).

Most temples have two courtyards, as shown in Figure 1.1.7, outer and inner. Entrance to the first court is gained through the split gate (A), which is like the two halves of a solid tower cut clean through the middle. Furthermore, the two inner sides are invariably smooth, clean surfaces that shine by contrast with the elaborately carved rest of the temple.

In the right-hand corner of the first courtyard or outside the gate is the high tower (B) where the village drums are hanged. Inside the outer court are a number of simple sheds: a kitchen where the food for feasts is cooked (C), a shed for the orchestra (D) and another building (E) used as rest-house by the people and for the making of offerings. Another monumental gate (F) leads into the second court. A three-dimensional view of the typical Balinese temple of Figure 1.1.7 is also presented in Figure 1.1.8 which is taken from Covarrubias [7].

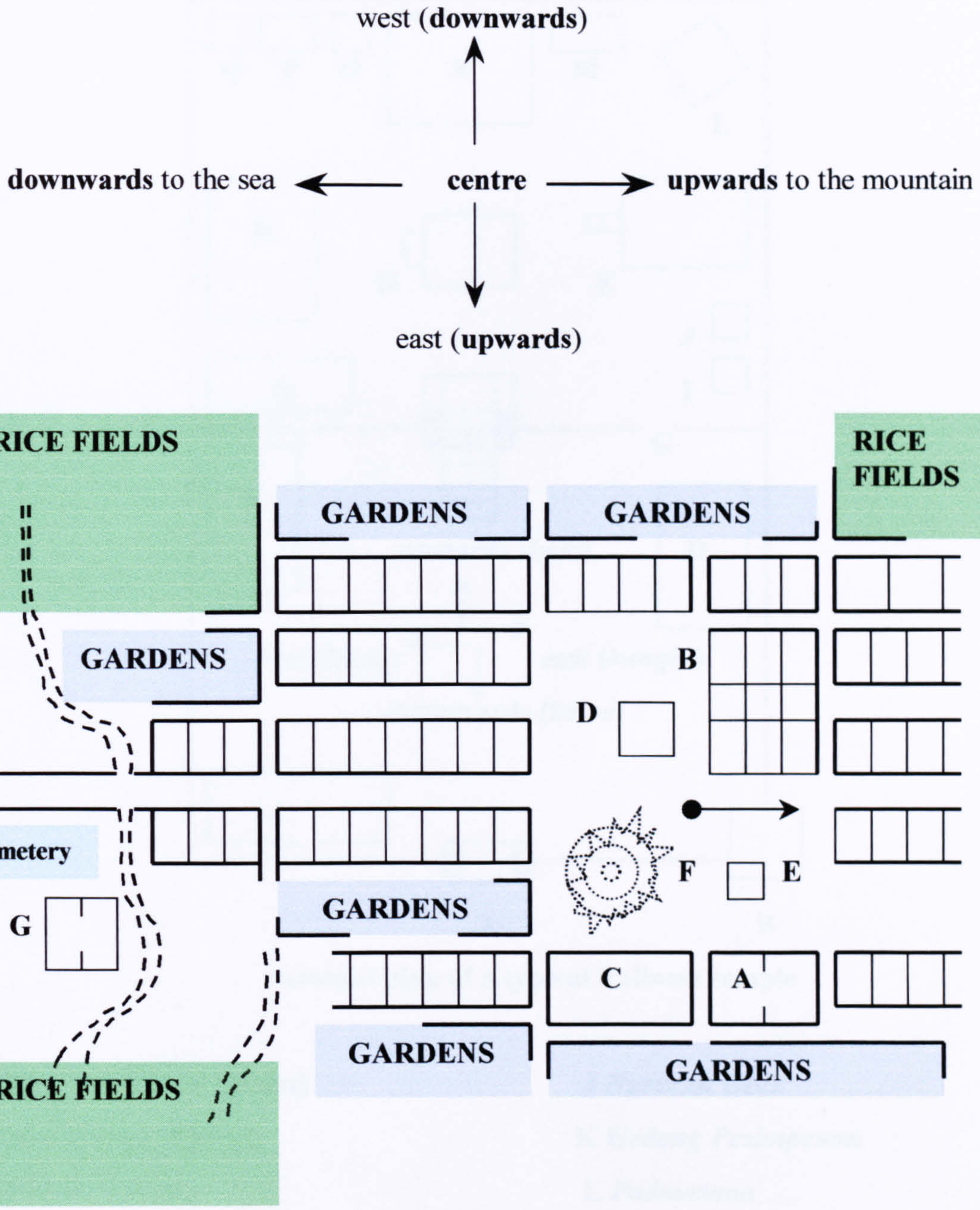

A TYPICAL VILLAGE

A	**TEMPLE TOWN (*PURA DESA*)**	**E**	**DRUM TOWER (*KULKUL*)**
B	**PALACE (*PURI*)**	**F**	**BANYAN TREE (*WARINGIN*)**
C	**MARKET**	**G**	**TEMPLE OF DEATH (*PURA DALEM*)**
D	**ASSEMBLY HALL(*WANTILAN*)**		

Figure 1.1.6 Village community

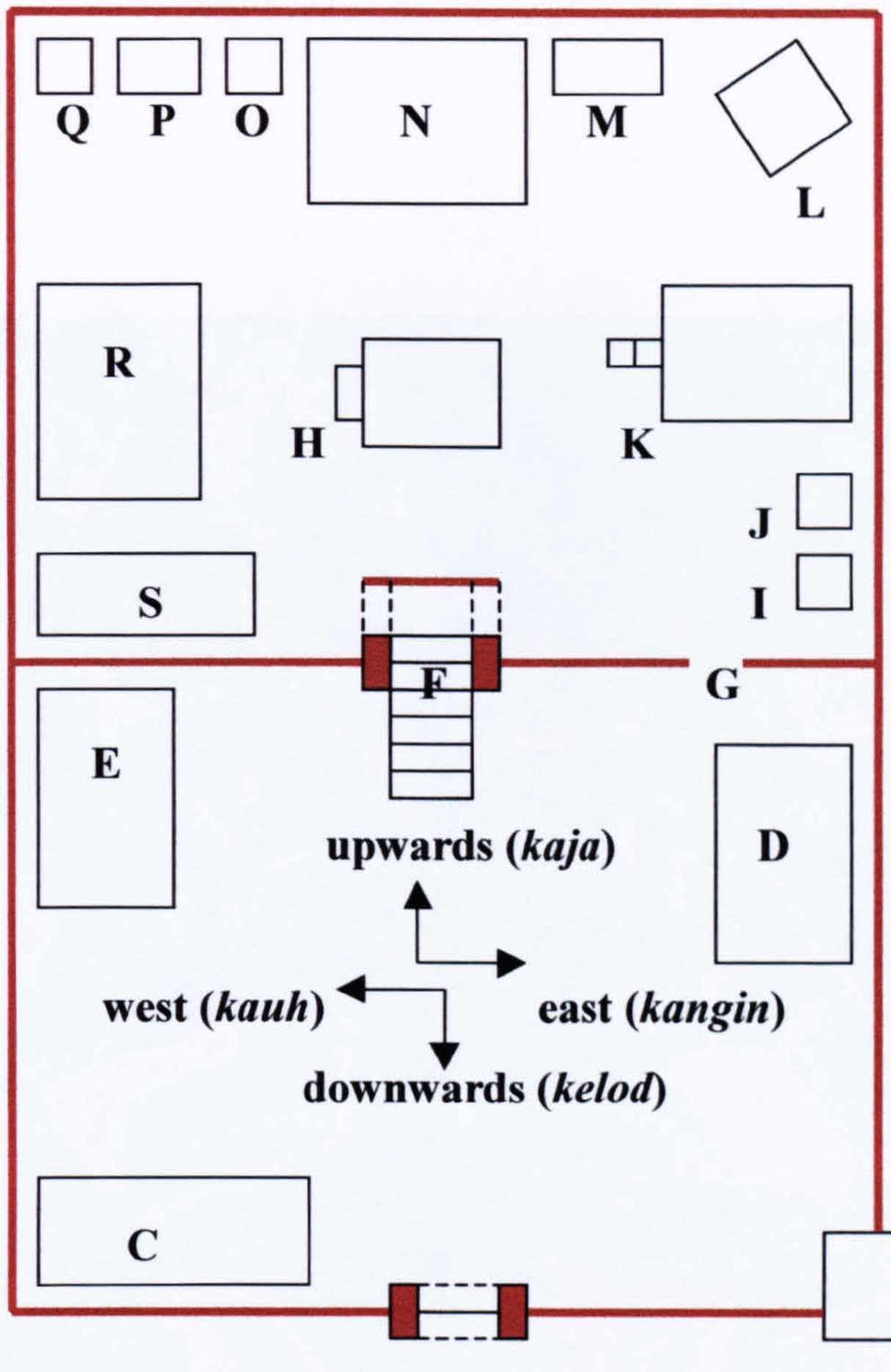

Ground plan of a typical Balinese temple

A Split Gate (*Candi Bentar*)

B Drum Tower (*Kulkul*)

C Kitchen (*Pawon*)

D Orchestral hall (*Balé Gong*)

E Hall for pilgrims (*Wantilan*)

F Ceremonial gate (*Paduraksa*)

G Side gate

H *Paruman*

I *Ngrurah Alit*

J *Ngrurah Gede*

K *Gedong Pesimpenan*

L *Padmasana*

M *Gunung Agung*

N *Meru*

O *Gunung Batur*

P *Maospait*

Q *Taksu*

R *Balé Piasan*

S *Balé*

Figure 1.1.7 Layout of Balinese temple

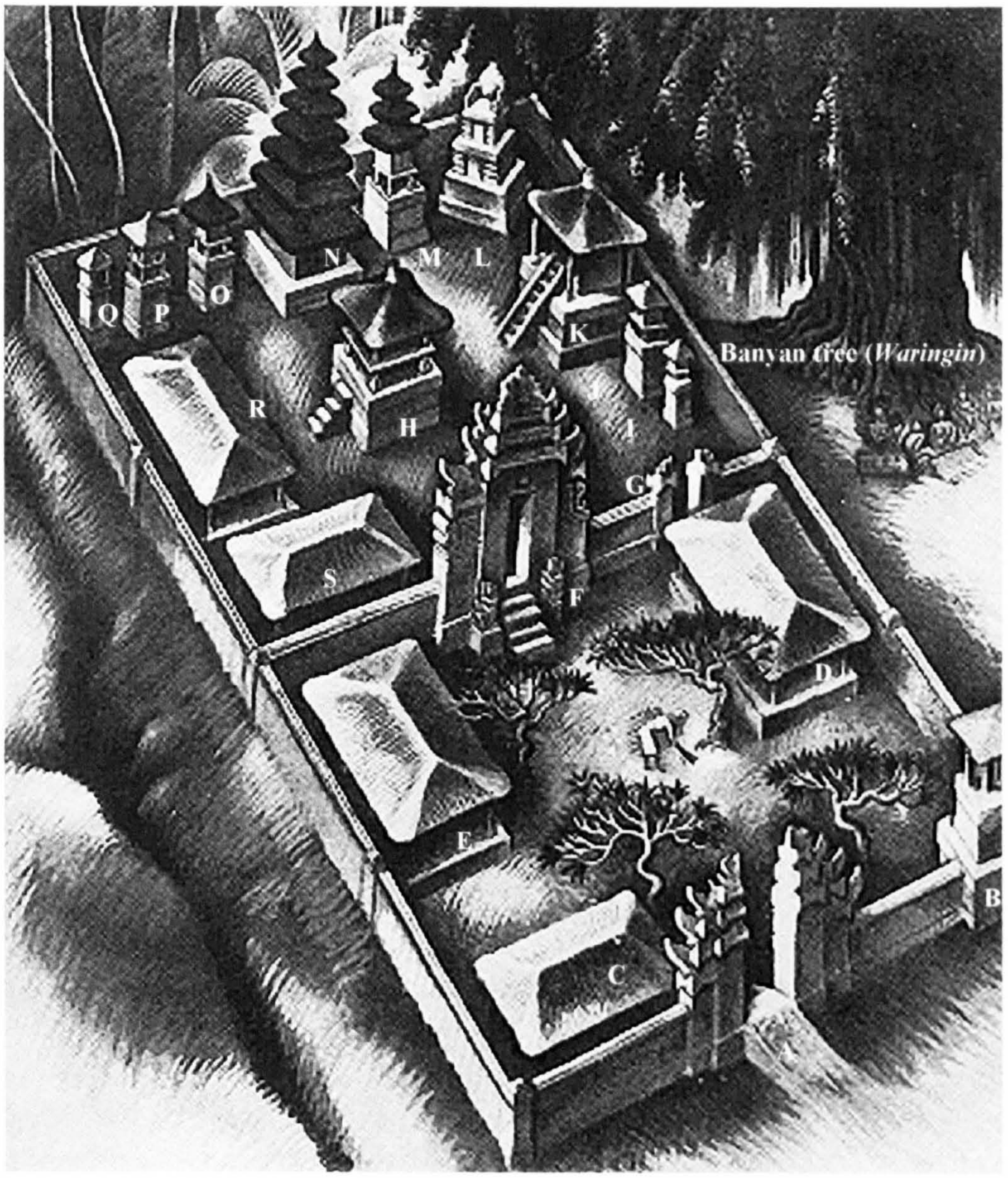

Figure 1.1.8 A typical Balinese temple

1.1.2 Buildings Location

a. Zoning of living

Zoning of traditional Balinese architecture is divided into nine regions following the wind-rose directions: East, south-east, South, south-west, West, north-west, North, north-east, and Centre. These nine regions, named *Sanga Mandala* (*Sanga* = nine , *Mandala* = region), were shown in Figure 1.1.4. Buildings are placed following this arrangement [8],

1. The Holy Place, shrines of the gods (*Merajan*),

   The place to pray, must lie in the upwards zone or primary zone

2. Bedroom (*Balé*),

   This is placed in the middle of the primary zone

3. Assembly Hall (*Balé Adat, Wantilan*),

   A ritual place, lies in the middle zone

4. Kitchen (*Pawon*),

   The best location is in the south-west or South

5. Rice shed/granary (*Jineng*),

   The best location is in the south-west or South

6. Waterhole (*Sumur*),

   The best location is in the south-west or south-east or north-east

b. Distance

Approximations of the distance between buildings and distance from buildings to the fence were calculated by foot's size.

c. Building Orientation

The front side of the building is oriented to the centre (*natar*).

d. Circulation

Air circulation from outside to inside the area is from the downwards to the upwards zone through the centre (*natar*).

According to the *Tri Hita Karana* concept, the Balinese believe that one's soul is involved in illness and that they will become vulnerable to illness if these three factors are not in equilibrium. The Balinese believe that both natural (*e.g.*, fractures) and supernatural factors (*e.g.*, evil spirits, mistakes in ceremonies, and sins of ancestors) cause illness [2]. The above statement implies that everyday life in Bali is influenced by religion, custom and manners which are kept eternal from several centuries ago. *Tri Hita Karana* is a way of life for the Balinese people and it makes an equilibrium in their daily-lives. Therefore, in order to understand and improve Balinese culture, one should refer to this concept.

As an organic unit, the structure, significance, and function of the home is dictated by the same fundamental principles of belief that rule the village: blood-relation through the worship of the ancestors, rank, indicated by higher and lower levels, and orientation by the cardinal directions, the mountain and the sea (the cardinal directions also follow the sun rise and sun set).

The Balinese say that a house, like a human being, has a head (the family shrine), arms (the sleeping-quarters and the social parlour), a navel (the court yard), sexual organs (the gate), legs and feet (the kitchen and granary) and anus (the pit in the back yard where the refuse is disposed of) [7].

The principle of orientation –the relation from the mountains to the sea or the sun rise to the sun set- that constitutes the ever present Balinese rose of the winds, rules the orientation and distribution of the temple and house units.

Magic rules control not only the structure but also the building and occupation of the house. A Balinese home consists of a family or a number of related families living within one enclosure, praying at a common family temple, with one gate and one kitchen. The square plot of land (*natar*) in which the various units of the house stand is entirely surrounded by a wall of whitewashed mud, protected from rain erosion by a crude roofing of thatch.

The gate of a well-to-do family can be composed of a pair of brick and carved stone, but more often it consists of two simple pillars of mud supporting a thick roof of thatch. Behind the doorway is a small wall (*aling – aling*) that screens off the interior and stops evil spirits. The pavilions of the house are distributed around a well-kept yard of hardened earth free of vegetation except for some flowers (frangipani or hibiscus). The area between the house and the wall is planted with coconut, banana or papaya

trees. In the southern part of Bali, the place of honour, the higher north-east corner of the house towards the mountain was occupied by the family temple (*sanggah kemulan*) for worshipping their ancestors. Family temple is an elemental version of the formal village temple [7].

Next in importance to the family temple is the building for sleeping-quarters of the occupants (*uma meten*), built towards the mountain side of the house. This small building is of bricks or sand stone with a thick roof of thatch supported by eight posts and surrounded by four walls. There are no windows and the light comes through the narrow door. This building is the sanctuary of the home and normally where the heads of the family sleep.

The other three sides of the courtyard are occupied by three open pavilions; on the left is the nine posts building (*balé tiang sanga*) the social parlour and guest house, on the right is the four posts building (*balé sakapat*) and at the back is the six posts building (*balé sakanem*). Both four and six posts buildings are small pavilions where other relatives sleep with the children and where the women place their looms to work, respectively. In the lowest part of the land, towards to the sea, the kitchen (*paon*) and the granary (*lumbung, jineng*) were built.

The better homes often have more elaborate pavilions, by enclosing half of the pavilions with four walls, leaving the other half as an open veranda. This will provide a second sleeping-quarter for a married son. In the house of the well-to-do there is often a great square pavilion (*balé gedé*) with an extraordinarily thick thatch roof supported by twelve beautiful carved posts which is used for social life.

A well built construction is a masterpiece of simplicity, ingenuity and good taste. It consists of a platform of mud, brick or stone reached by three or four steps and covered by a cool roof of thick thatch. The roof is supported by more or less elaborate wooden posts, the number of which determines their name and function. The roof is built of grass sown on the long ribs of coconut leaves, placed close together like shingles and lashed to the bamboo skeleton of the roof with indestructible cords of sugar-palm fibre, with an extra thickness of grass added to the four corners. Such a roof, often a foot and a half in thickness, will last through fifty tropical rainy seasons. The beams that support the roof are ingeniously fitted together without nails, and are held in place with pegs made of heart of coconut wood. Generally, one or two sides of the building are protected by a low wall [7].

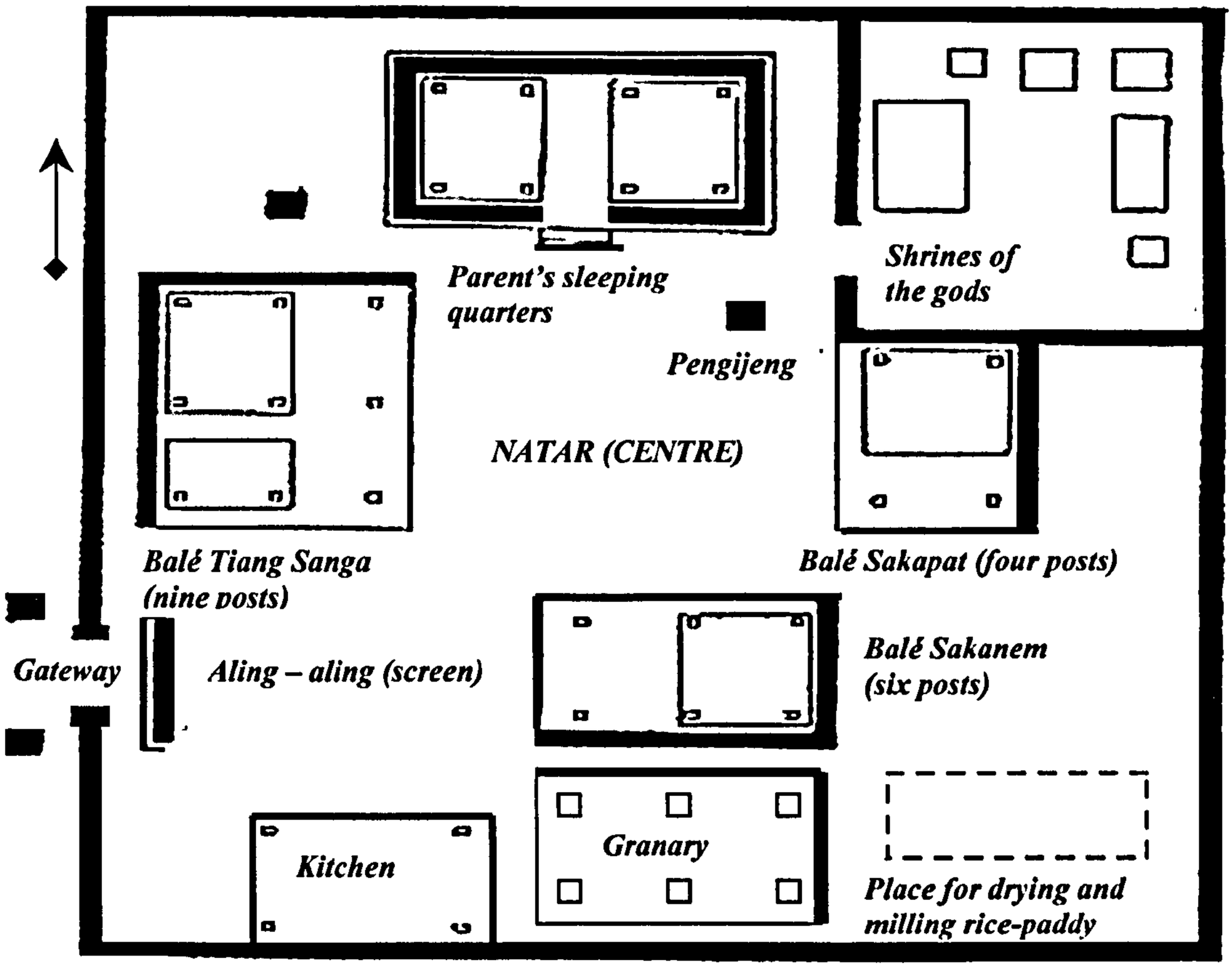

Figure 1.1.9 Plan lay out of Balinese house

(for common people)

1.1.3 Cultural Review

Culture does not simply constitute webs of significance, systems of meaning that orient humans to one another and their world. They also constitute ideologies; and so it matters to ask who has the power to enforce their views of what is to count and for what [10]. Culture may be depicted as neat and orderly and may be represented as being composed of constituent parts which articulate in a structure of logical and reassuring consistency [10]. This statement indicates that culture can be assessed, reinvestigated, improved and developed in several manners.

Culture tends to evolve with modern technology, and this often creates a conflict between the traditional and the modern. On the one hand one wants to keep traditional

values, while on the other there is a tendency to change to a modern process. To resolve these conflicts, a research study is needed which mixes modern technology in order to prove that traditional reasoning is valid and still relevant in the future.

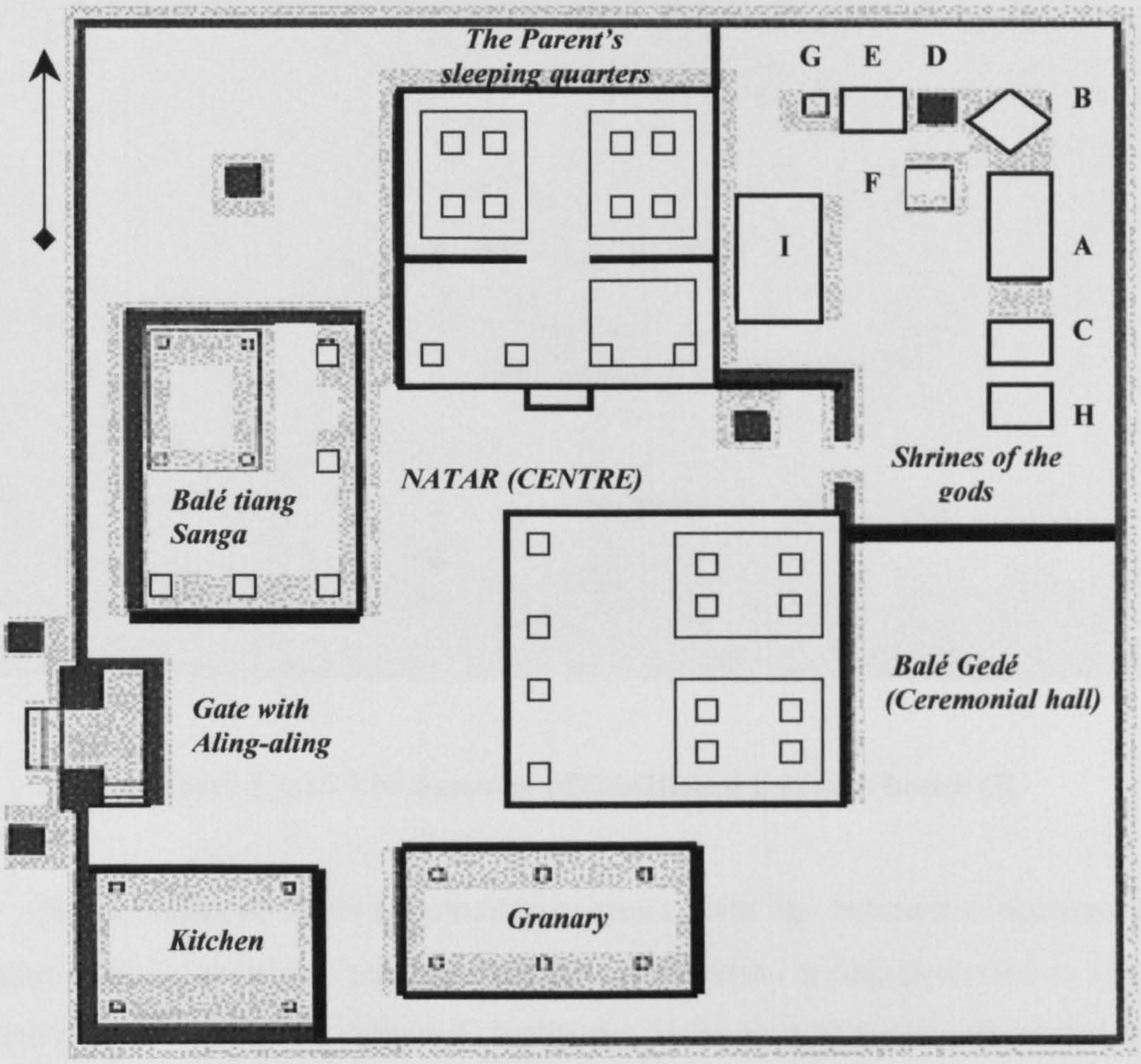

A *Kemulan*
B *Padmasana*
C *Manjangan Saluang*
D *Gedong* **for** *Gunung Agung*
E *Saren*
F *Tajok*
G *Taksu*
H *Ngrurah*
I *Bale Piasan*

Figure 1.1.10 Another example of plan lay out of Balinese house (for noble persons)

Figure 1.1.11 The gateway of traditional Balinese house [9]

Some studies on Balinese culture have been carried out, but most concentrated on anthropological aspects. Traditional Balinese architecture is only presented in a small section of these works. Although traditional Balinese architecture plays the most important part on Balinese culture and community, unfortunately none of them tried to explain this role deeper.

The present population of Bali is greater than 2.7 million in a total area of about 5300 km^2, or around 510 person/km^2. One might well wonder how an island that has so little land and whose population density is one of the largest in the world could assimilate so many new inhabitants and provide housing space to a population that more than doubled in 40 years. Besides that, per capita income is relatively low in Bali. Currently average is less than US$300-00 per year, but there are no shanty towns [2].

Bali has no changing seasons, only wet and dry seasons. The south-east monsoon, which is the dry season, is from April to November. During this time there are very heavy seas on the south coast of Bali. The wet season is from November to March, but this does not mean that the rain never ceases. Temperature average is now around 29^0C, an increase of a few degrees from the last decade. During the wet season it seems much hotter because of higher humidity and almost constant sun shine. In the mountain areas, it rains more than on the plains and at the shores [2].

Based on a traditional village, *Bayung Gede*, Bateson and Mead [11] assumed that Bali had a cultural base upon which various intrusive elements have been progressively grafted over the centuries, and that a more rewarding approach would be to study this base first (*Bayung Gede* is a traditional mountain village and now has gained fame among students of culture as a result of Bateson and Mead's detailed work in 1936-1939). Their explanation was contrasted by Suryani and Jensen [2] in 1989 who described that several traditional aspects did not change and appear to be the same as those in Bateson and Mead's work.

Those statements indicate that traditional culture in Bali did not change dramatically and is still eternal after more than 50 years. Therefore, both Bateson and Mead's and Suryani and Jensen's contributed works can be used for the study of changes in Balinese culture. This means that traditional Balinese culture has various intrusive elements which possibly change the culture, but the acculturation process itself is not dramatic.

The issue of change in Balinese culture over the last half a century is relevant for some researchers to revise Bateson and Mead's work. How different might the Balinese have been in the 1930s compared with recent years? Some cultural anthropologists concur that a few decades is a relatively short time for any significant change to occur in basic aspects of a culture. In the case of Bali, Mead addressed the issue of possible change in the 40 or more years after Dutch occupation, including automobiles, tourism, etc. Two characteristics of Balinese culture are the ready acceptance of those small changes in custom and technology which can be absorbed without changing the basic premises of life, and the utter inability and unwillingness to contemplate any more drastic change [2].

Covarrubias [7] observed that the Balinese assimilate new and foreign ideas into their traditional forms. This enables the islander to create new styles constantly, to inject new life steadily into their culture, which at the same time never loses its Balinese characteristics. Ramseyer [12] stated that the Balinese absorbed material culture without a break in tradition and that the basic values shaped by religious and communal social interactions have remained remarkably intact.

Balinese culture is a living system that is dynamic and not static. In spite of surface changes, especially as evidenced by technology, it is remarkably stable in its basic elements, Suryani *et al* (1988) [13]. Therefore, it is more clear that technology is one parameter which has possibly changed Balinese culture. Another that appears to have changed surely is Balinese architecture.

A reinvestigation of Bateson and Mead's works was described by Suryani and Jensen [2]. Since the comparison study is based on *Bayung Gede* village, several plates were taken which were based on this village. Their contributed works are applied on the present study, which is correlated to traditional Balinese architecture. All Figures 1.1.12 – 1.1.18 are taken from Suryani and Jensens'works.

In Figure 1.1.12, the main intersection of roads at *Bayung Gede* village is presented. It can be seen very clearly that the building arrangement is complex and populous. Roof type, distance between buildings and their orientation are aligned. In the front view, it can be seen that the roof type varies, with some triangular, others triangular but plane at the top, etc.

Figure 1.1.13 shows a side-street in *Bayung Gede* with walls surrounding household compounds. This figure is identical to one taken by Bateson in 1939. From figure 1.1.12, it can be seen that the distance from buildings to fence is relatively short, but there is a special distance between buildings. It can also be seen that the height of the fence is nearly the same as the roof level. But, the most interesting is that there is no open surface at the roof (*e.g.* for natural ventilation).

In Figure 1.1.14, the kitchen and parents' sleeping quarters in a household compound in *Bayung Gede* is presented. This figure also noted that the architectural style is the same as that shown in Bateson's photographs in 1939. This figure shows very clearly the traditional Balinese architectural style. The only open surface is the door, and there are no windows for natural ventilation and lighting, even in the roof.

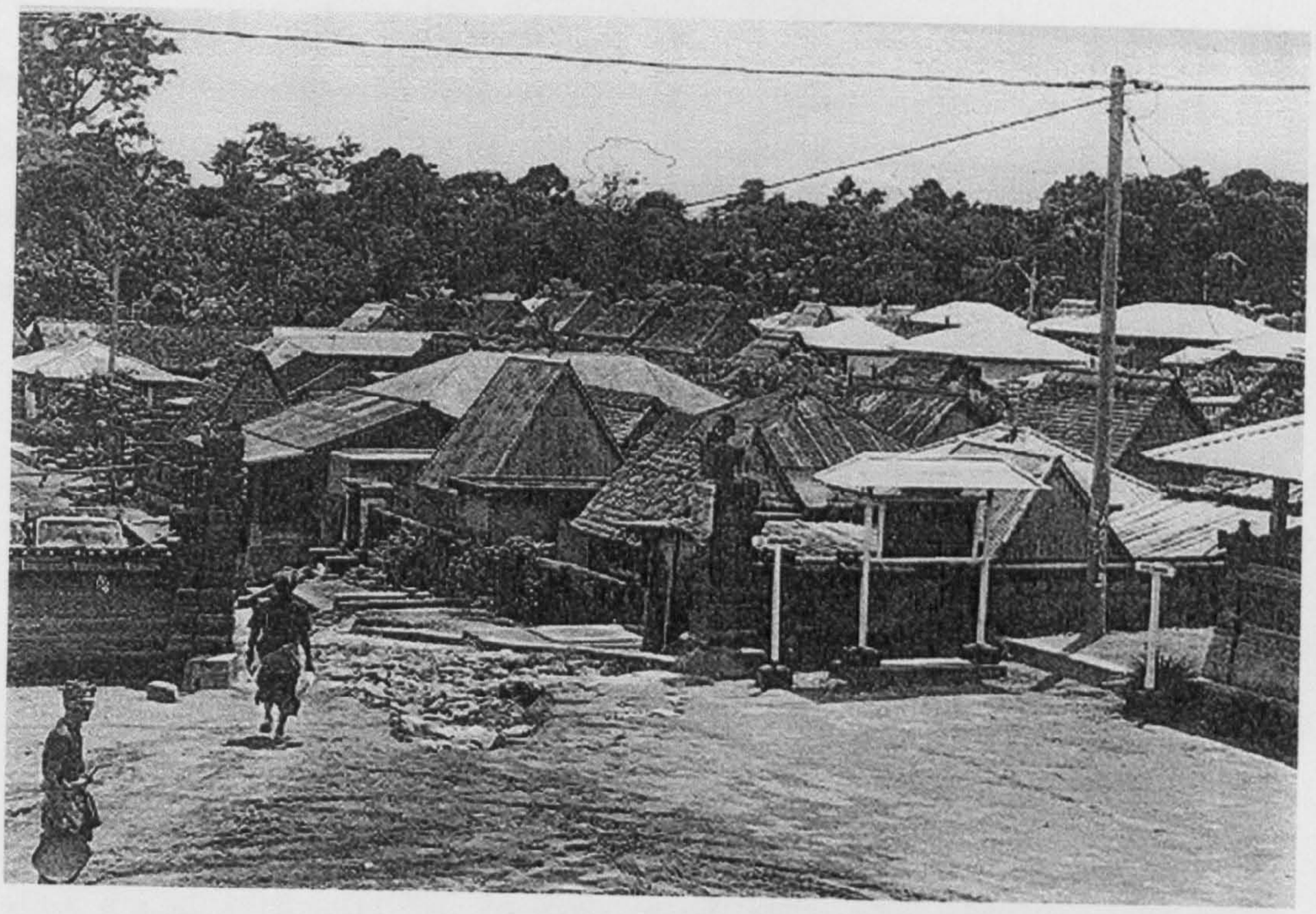

Figure 1.1.12 The main intersection of roads at *Bayung Gede* village

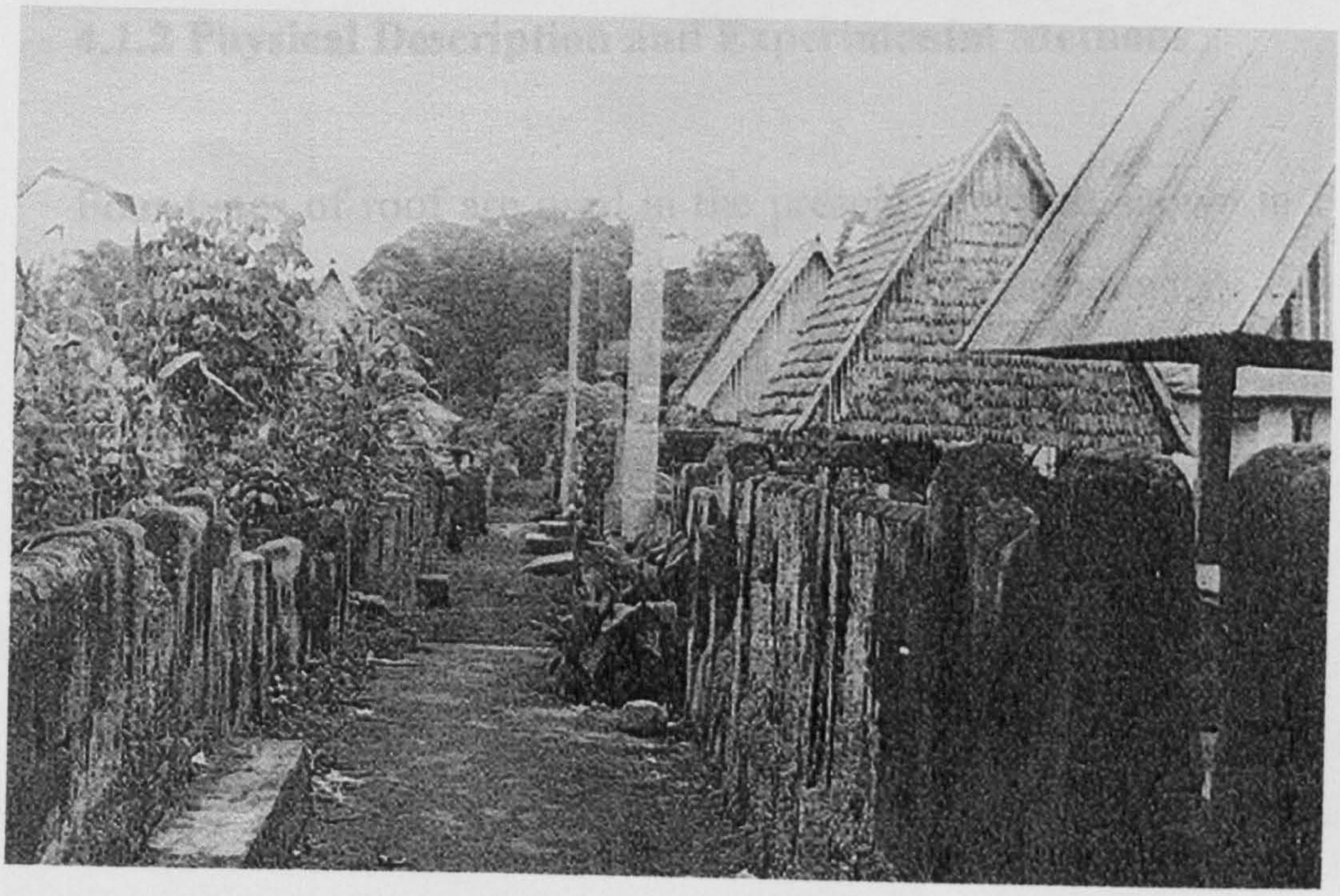

Figure 1.1.13 A side-street in *Bayung Gede*

Figure 1.1.15 shows household shrines of the gods in *Bayung Gede*. These households shrines have an open surface and lie upwards towards the mountain. In the background, a building was built with walls made of composites instead of wood. A small open surface (window-like) was built. Therefore, for several decades, the architectural style has not changed so much.

Figure 1.1.14 The kitchen and parents' sleeping quarters in a household compound in *Bayung Gede*

Figure 1.1.16 shows a view of *Bayung Gede*. It appears much the same as in photographs by Bateson more than 50 years ago. In the foreground, the roof type is triangular without an open surface for natural ventilation. The distance between buildings is very small, as well as the distance between the house to household shrines of the gods (in the left hand side).

A small snack bar is also presented in Figure 1.1.17. This bar is fully open indicating an alternative solution for better natural ventilation. A semi-naked women in

the foreground indicates that the weather is warm and heat transfer by evaporation from her body to surrounding is high.

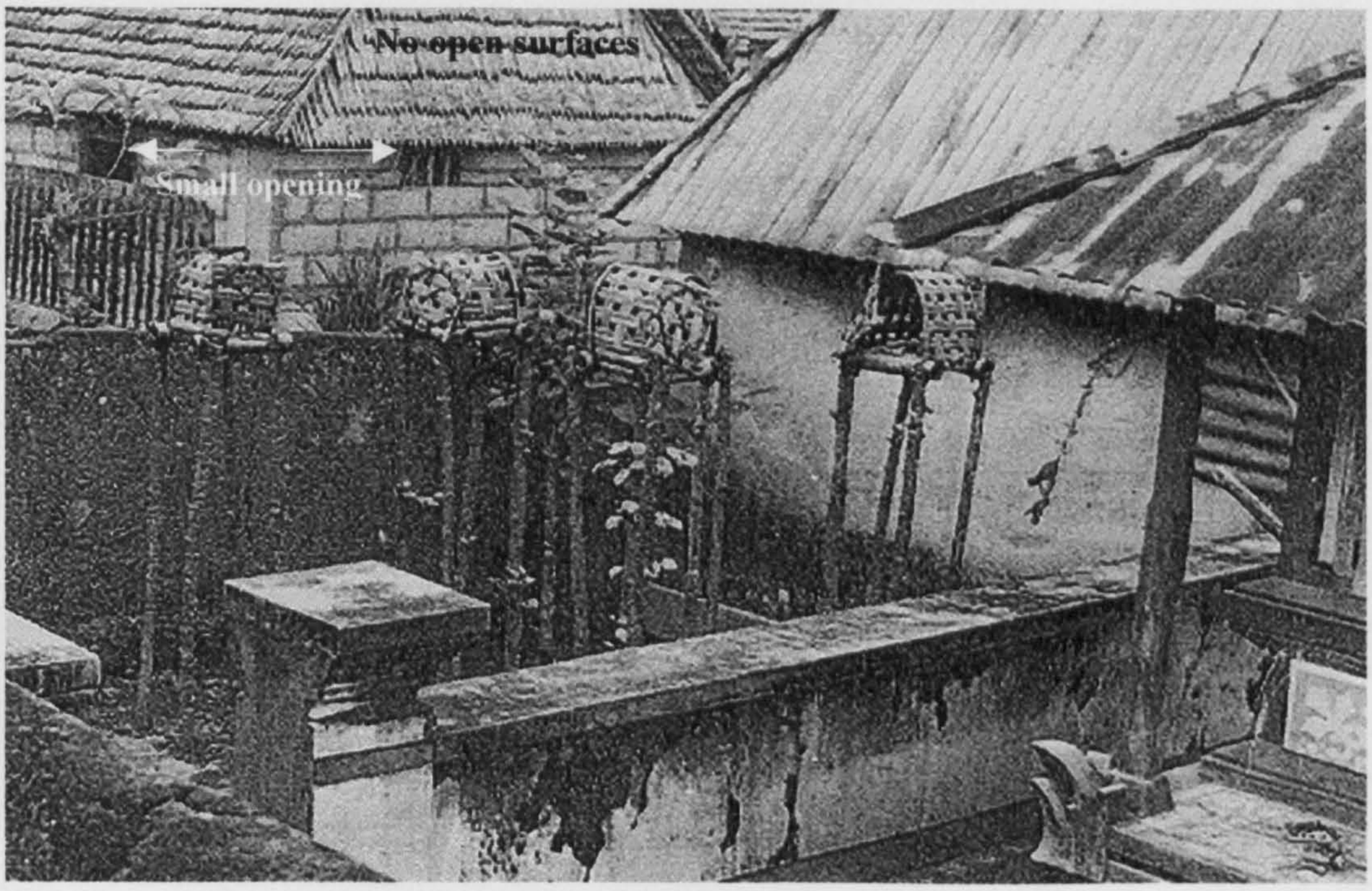

Figure 1.1.15 Household shrines of the gods in *Bayung Gede*

A government building incorporating the traditional architectural style of Bali (in the capital city of Denpasar) is presented in Figure 1.1.18. This contrasts to the original traditional Balinese architecture, as regards the building height, orientation, and distance between buildings. This traditional architectural-like style does not mean a union of separate parts of those buildings in original traditional Balinese architecture. Therefore, traditional architectural-like style is similar to those modern buildings, but covered by Balinese ornaments. In recent years, most government, hotel and public buildings are built with this style.

The figures shown here represent a statement that traditional architecture still exists. Although materials might have changed, building composition, arrangement and function have not changed much. This contrasts to that in capital/town where traditional-like buildings were developed. The traditional-like buildings are energy

consumable and most of them are very luxurious. Unfortunately, both Bateson and Mead, and Suryani and Jensen, did not explain this contradiction in their works.

Figure 1.1.16 A view of *Bayung Gede*

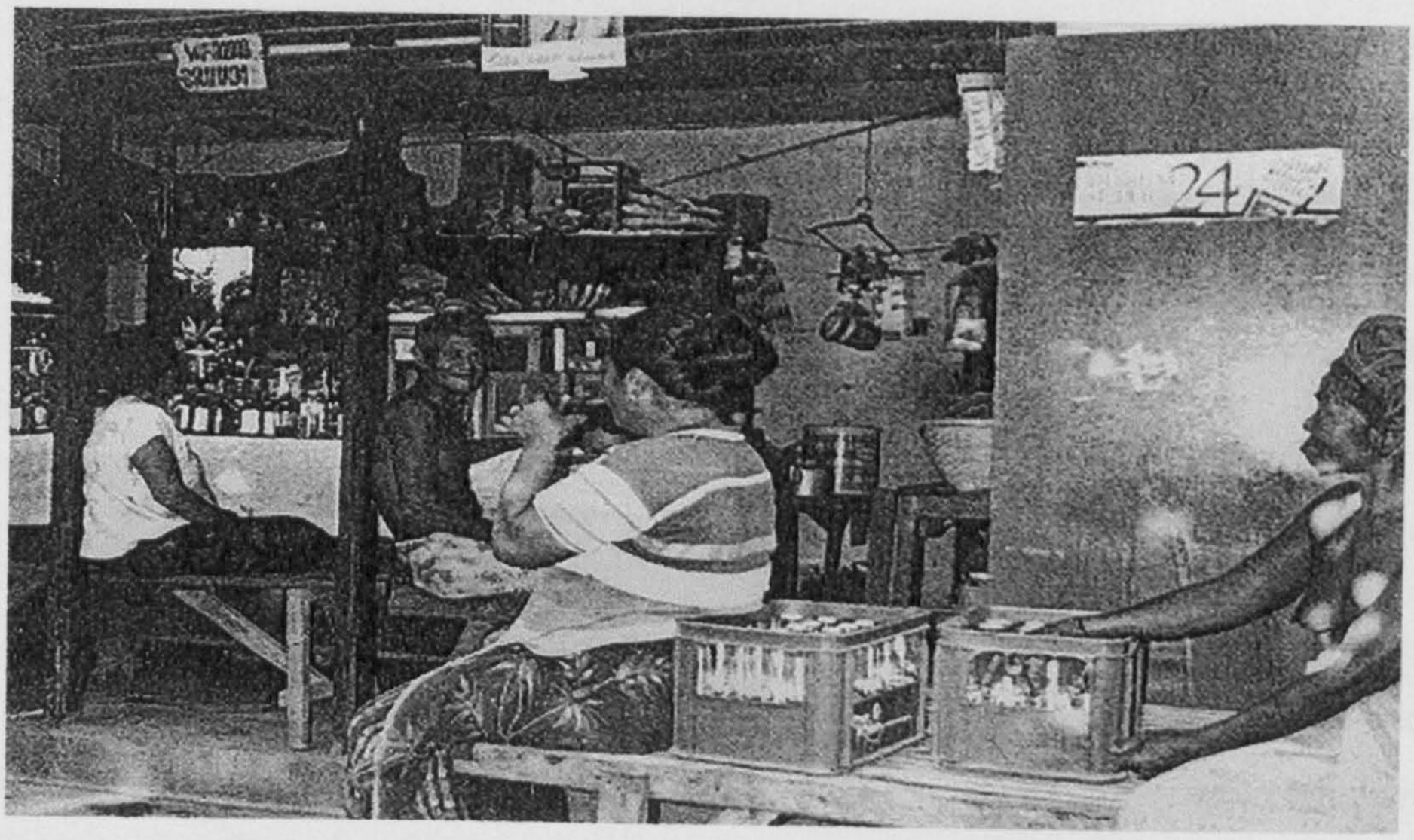

Figure 1.1.17 A small snack bar

Figure 1.1.18 A government building incorporating the traditional architectural style of Bali (in the capital city of Denpasar)

Although Suryani and Jensen concluded that there is no change on Balinese culture, several years later (in 1990s), the Balinese landscape has changed. There are many areas with hotels and building complexes, even near sacred places and temples. The development of these buildings did not consider the *Tri Hita Karana* concept. This offends most Balinese people, especially on their ritual ceremony. The *Tri Hita Karana* concept slowly but surely will disappear from Balinese life, unless some scholars can explain it.

1.1.4 Traditional Reason Review

Traditional Balinese architecture will be approached by using several parameters such as natural ventilation and thermal comfort and wind engineering/architectural aerodynamics. Therefore, several reviews are taken into consideration.

The granary and kitchen lie on the front side (poverty area). The meeting and ceremonial halls lie on the middle area. The parents' sleeping quarters lies on the

primary area. How did the traditional architects arrange this configuration? Why did not the parents' sleeping quarters lie on the middle, the granary on the primary and the halls on the poverty area? Did they have a building code for this design?

The type of roof differs from one to another building and depends on its function. For instance, a triangular roof is used as granary, as shown in Figure 1.1.19. How did they learn this phenomenon?

Building orientation and distance between buildings are also parameters to be considered in traditional Balinese architecture. Posts (or pillars) and open surfaces are also taken into account. Therefore, further questions were addressed here;

- If heat transfer was well-known several centuries ago, why this knowledge did not seem to be improved?
- If building design has a correlation to architectural aerodynamics, why do we not have a Balinese wind code for building design?
- Did traditional architects (*undagi*) learn the knowledge of traditional Balinese architecture as a part of culture and/or as a dogma that cannot be changed or improved? We suggest that traditional architects learned traditional reason as part of culture but without a strict dogma. This can be seen from the building model itself, where each area/village has a different style, but traditional reasons such as *Tri Hita Karana* and *Sanga Mandala* concepts are exactly the same.

In accordance to cultural reviews, most traditional Balinese villages are not changing so much. Some traditional buildings for instance may not be suitable for inhabitants health, since the only open surface is a small door for lighting and air re-circulation. Therefore, these conditions are possible to create several diseases *i.e.* dermatitis (see Suryani and Jensen for further reviews, but unfortunately, Suryani who is a physician did not explain the relationship between these diseases and building condition).

In order to increase the heat transfer rate and air re-circulation between the building and its surrounding, some buildings should have a very large open surface at the windward side. Traditional architects might have considered this option, especially for buildings which are used as convention halls. This can be seen in Figure 1.1.20. Again, if traditional architects have considered health and comfort parameters, another

question to be addressed here is why did this basic knowledge not apply to all buildings? Or, why terms of comfort and health are considered only for a special building? The parent's sleeping quarters which inhabitants used all the time do not have a good natural ventilation and lighting.

In Figure 1.1.21, a semi-modern version of parents' sleeping quarters is presented. It is shown that a semi-modern parents' sleeping quarters has a small modification where natural ventilation is now considered.

Figure 1.1.22 shows a modern Balinese architecture, where the household shrines of gods were built on the roof. This case is unusual in Balinese architecture. The figure indicates that people adopt traditional reasons in several ways according to land size and their own idea.

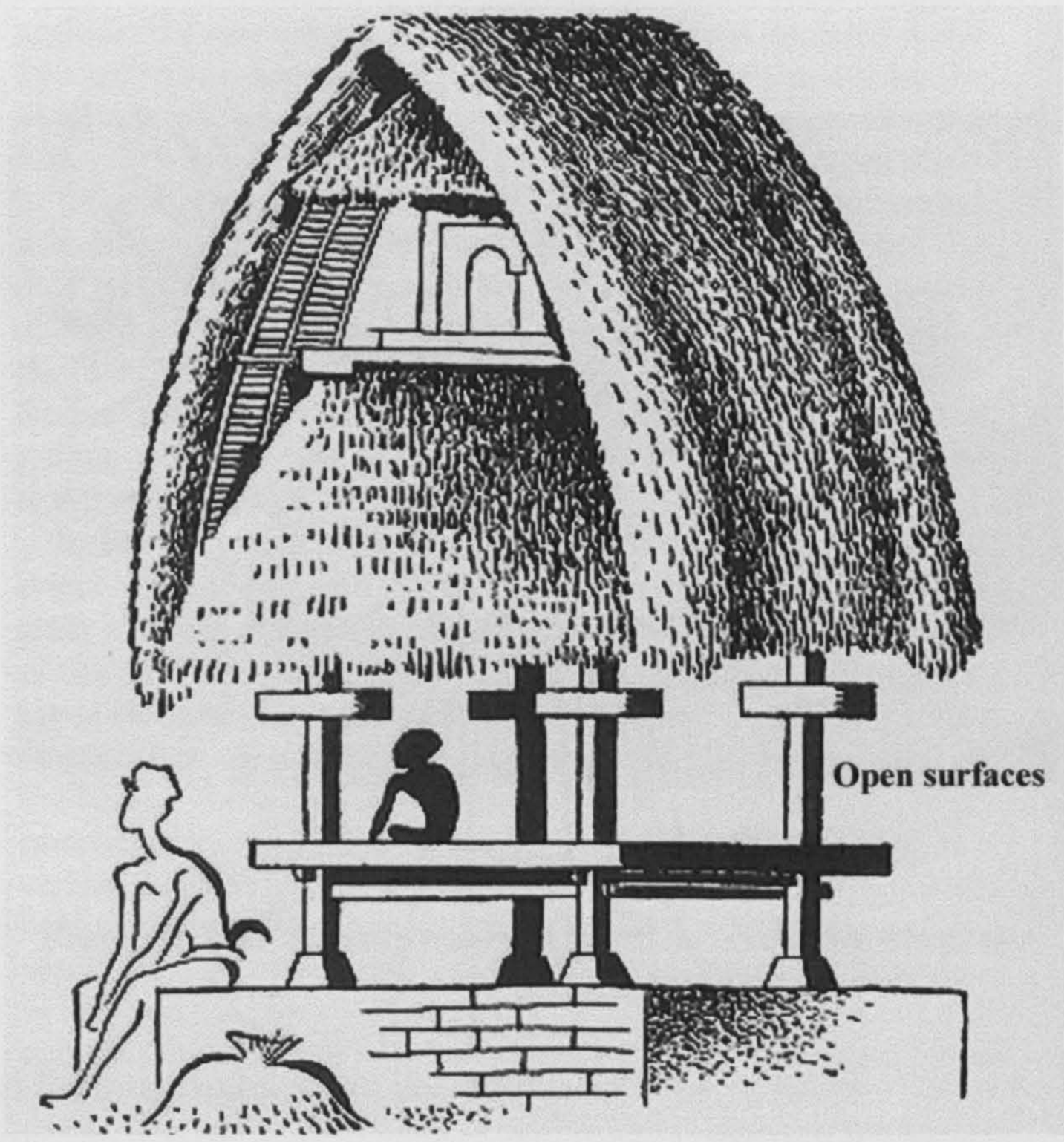

A Granary (*Lumbung*)

Figure 1.1.19 An example of roof type and its function, a granary to store rice-paddies (taken from Covarrubias [7])

Figure 1.1.20 Traditional Balinese building for a convention or meeting

Figure 1.1.21 A semi-modern parents' sleeping quarters

The traditional Balinese architecture has been correlated to magic rules, *i.e.*, evil spirit, illness, etc. Hence traditional reason becomes less attractive in the modern age since it is difficult to explain the exact meaning. Some studies about traditional Balinese architecture usually explained architectural changes in recent years, but definition and

meaning of traditional reason itself are not clear. Therefore, one can interpret traditional meaning in several ways.

Figure 1.1.22 An unusual shrine of gods in traditional Balinese architecture

Figure 1.1.23 A view from a tourist area near a temple

Building hotels near the sacred place or temple has offended many Balinese people. This can be seen in Figures 1.1.23 and 1.1.24. In Balinese communities, the distance between the sacred place and public buildings has been fixed, but it now tends to change. The rule fixing the distance between the first building to the temple/sacred place in a Balinese community should be made very clear. On the other hand, traditional Balinese architecture itself does not seem to consider health and comfort conditions. Therefore, research should link the need to protect the Balinese landscape or community to improving traditional Balinese dwellings.

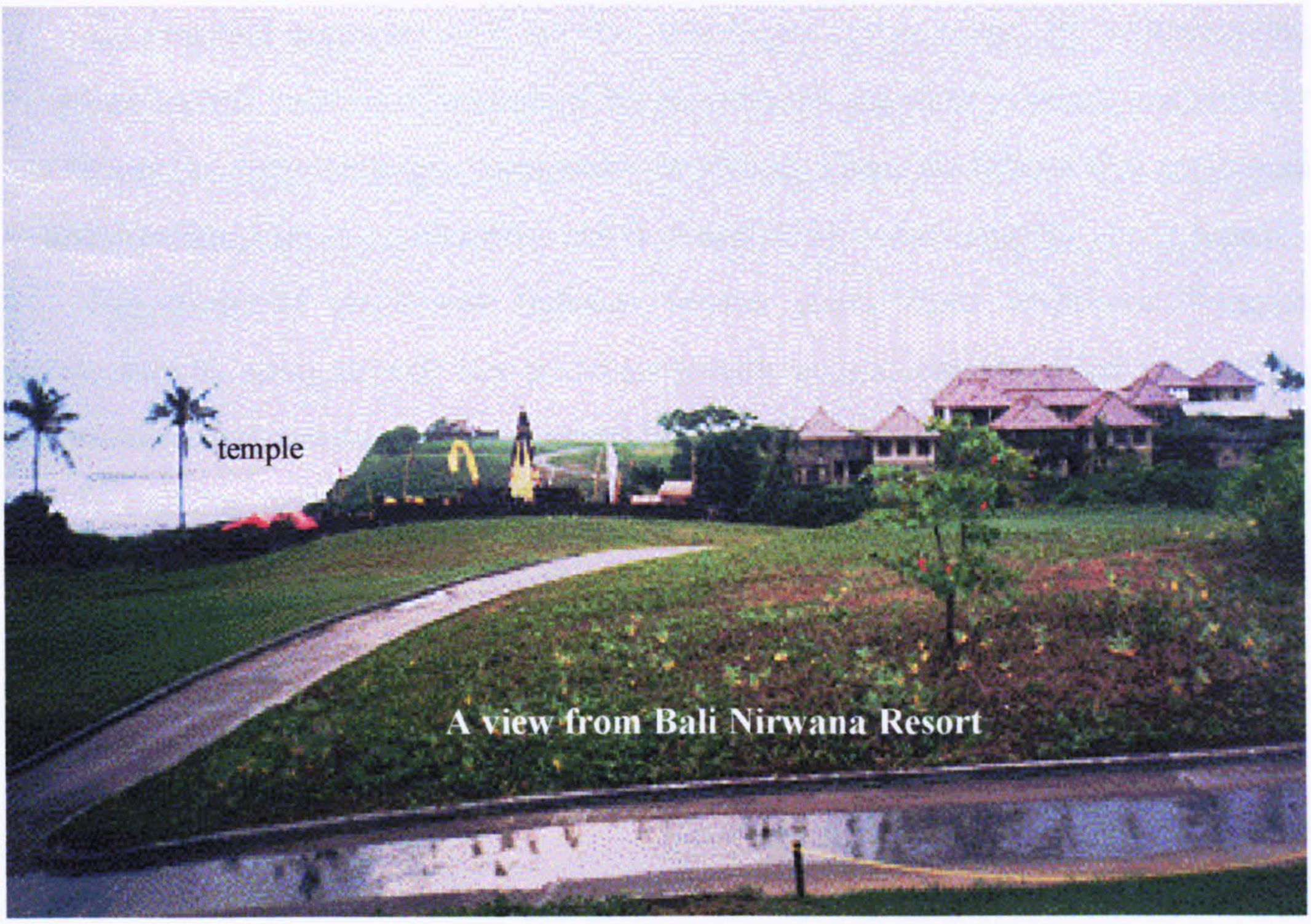

Figure 1.1.24 A view from a hotel near a temple

The population of Bali (especially in the capital) has substantially increased in the last two decades and this increases the energy demand, but unfortunately Bali does not have its own energy sources to support this request. The building arrangements in recent years are multifarious, do not consider environmental conditions and are sometimes unusual. The governmental code for buildings [14] should be revised in order to control emission of carbon dioxide, energy demand, population growth and land availability, impact of tourism and migration, and local climate changes. According

to these problems, going back to traditional Balinese community is an alternative suggestion for urban planning in Bali island. The suggestion is realistic since traditional villages and towns produce better living conditions than that in cities and the capital.

Some parts of traditional Balinese architecture (*e.g.* small openings) perhaps should be reviewed to improve thermal comfort of occupants. Before changing these parts, the meaning, concepts and conventions of traditional Balinese community as experienced by the people should be understood. Therefore, traditional Balinese architecture can be improved without loss of identity.

As an organic unit, the structure, significance, and function of the house have the same fundamental principles of belief that rule larger communities. By understanding the structure and function of traditional Balinese house, the same principle and analogy can be used to improve larger community or village. Then, we believe that traditional Balinese architecture and community can be modified by considering the above aspects.

The study of traditional Balinese reason starts from traditional Balinese architecture by using several key parameters such as heat transfer, wind engineering and architectural aerodynamics, as presented and used in several countries. The new rule of building arrangement and urban planning in Bali will not only consider the several aspects above but also take into account traditional reason, *Tri Hita Karana*.

1.2 Architectural Aerodynamics

1.2.1 Definition

Architectural aerodynamics is basically the relationship between wind and buildings. These relationships are generally regarded as including two main areas - structural and environmental. Structural considerations are wind loading and building motions due to wind.

The term 'architectural aerodynamics' was presented in 1977 by Aynsley *et al* [15], and concerns wind effects on and around buildings since the design of many ancient towns was influenced by wind effects. Without the aid of wind tunnel techniques or instruments, early planners had to learn from the errors of past planning.

1.2.2 Early Attempts to Design for Wind

The influence of wind effects on planning has been observed in the remains of the town of Kahan, founded about 2000 BC under the 12^{th} dynasty in ancient Egypt as shown in Fig.1.2.1. Its layout reveals divisions between the workmen's district in the west, with very small houses, and the 'notables' district in the north. The large houses of the 'notables' face the pleasant north wind, while those of the workmen in the west are exposed to the hot desert wind [15 and 16].

Ancient Chinese dynasties after the Chou dynasty had principles for town development laid down in the *Feng-shui* (*feng* - wind, floods of heaven ; *shui* - water, floods of earth) doctrine which treats the integration of human works into the pattern of the universe [15 and 17]. Rules governing the design of houses were concerned with spirits and forces within the house that could be controlled by arrangements to encourage the entry of air and light, and shelter from the wind and cold, as shown in Fig.1.2.2.

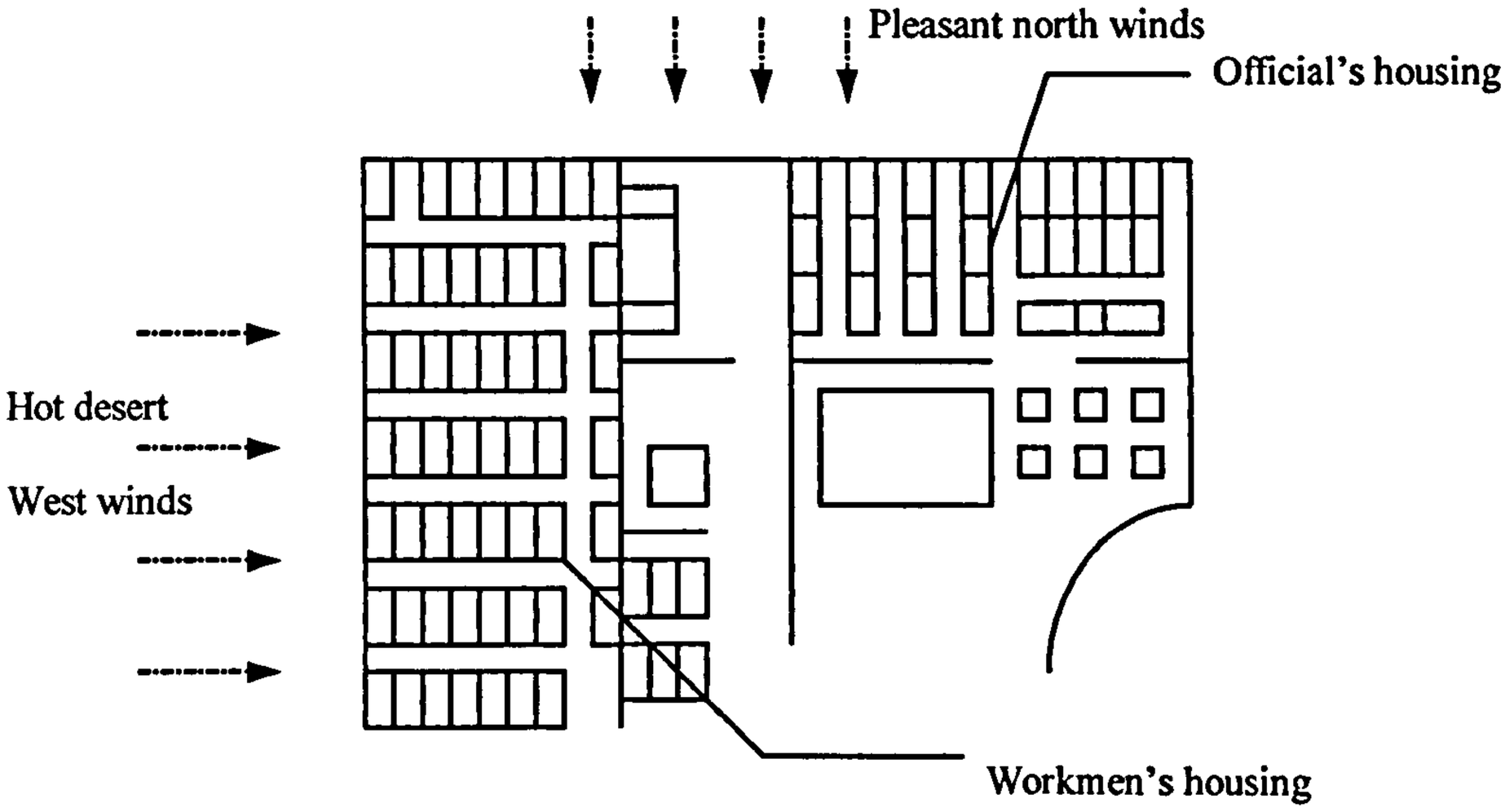

Figure 1.2.1 Sketch of housing layout at Kahan, Egypt, around 2000 BC

Aristotle was the first to write in length about the mysterious winds in his 'Meteorological' in the fourth century BC [15 and 18]. Although his attempts at

explaining the origin of wind, based on the impossibility of a vacuum in nature, have since proved unacceptable, his suggestions on town planning for Greek cities were :

'The healthiest cities are those which stand upon a slope inclining to the east so that the winds blow from the quarter of the sun rise. The next best aspect is one that is sheltered from the north wind as cities so sheltered enjoy milder winters'.

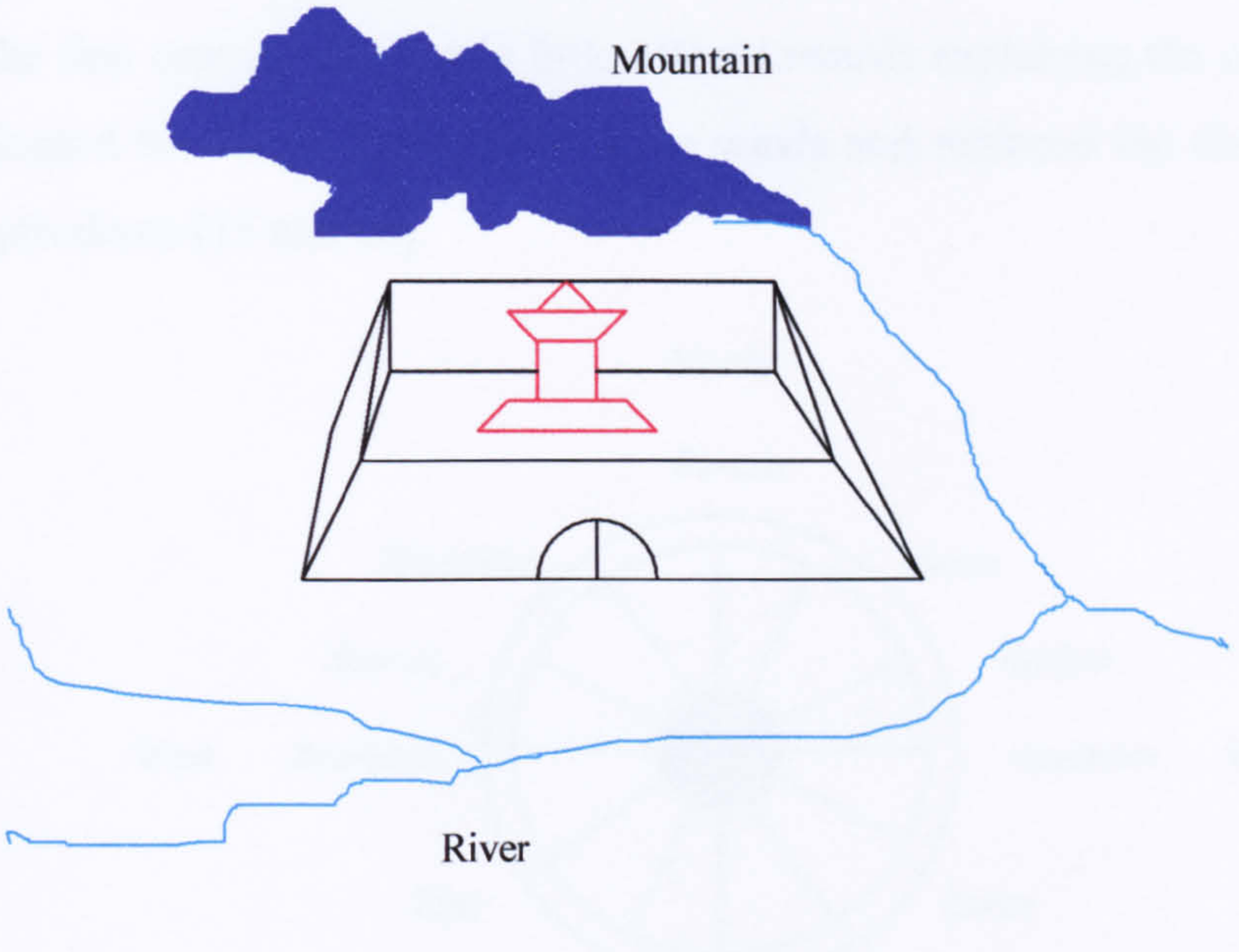

Figure 1.2.2 Sketch from a Chinese drawing showing mountains to the north, water to the south, governing the site for a town

Theophratus, a pupil of Aristotle, had fanciful ways of predicting the weather. He said that a wind could be in the offing when a dog rolled on the ground, or ducks flapped their wings, or when there was a particularly bright display of shooting stars. Wind was attributed with the ability to impregnate mares and vultures, while a whirlwind would be created by sprinkling vinegar upon the wind. More specifically, if the feet swelled there would be a change to the south wind, although this sometimes indicated a hurricane and similarly, if a man had a shooting pain in the right foot [15 and 19].

Another Greek, Xenophon, around 300 BC, suggested building to the southern side of houses higher than the northern in order to allow good sun penetration on porticos on the south wall and help keeping out the cold north winds. However,

around this time the Greeks became more occupied with the allocation of gods for the winds from various directions, such as Zephyros for the west wind. They devised a wind-rose whose points were named after the gods of those winds as shown in Fig. 1.2.3.

The Tower of the Winds erected in Athens during the second century BC has on each of its octagonal sides a sculptured motif depicting the characteristics of winds from eight points of the compass. The Romans, who flourished from the third century BC to the first century AD, made little effort towards explaining the origins of winds. They adopted the Greek knowledge of the winds and replaced the Greek names with Latin equivalents [15 and 18].

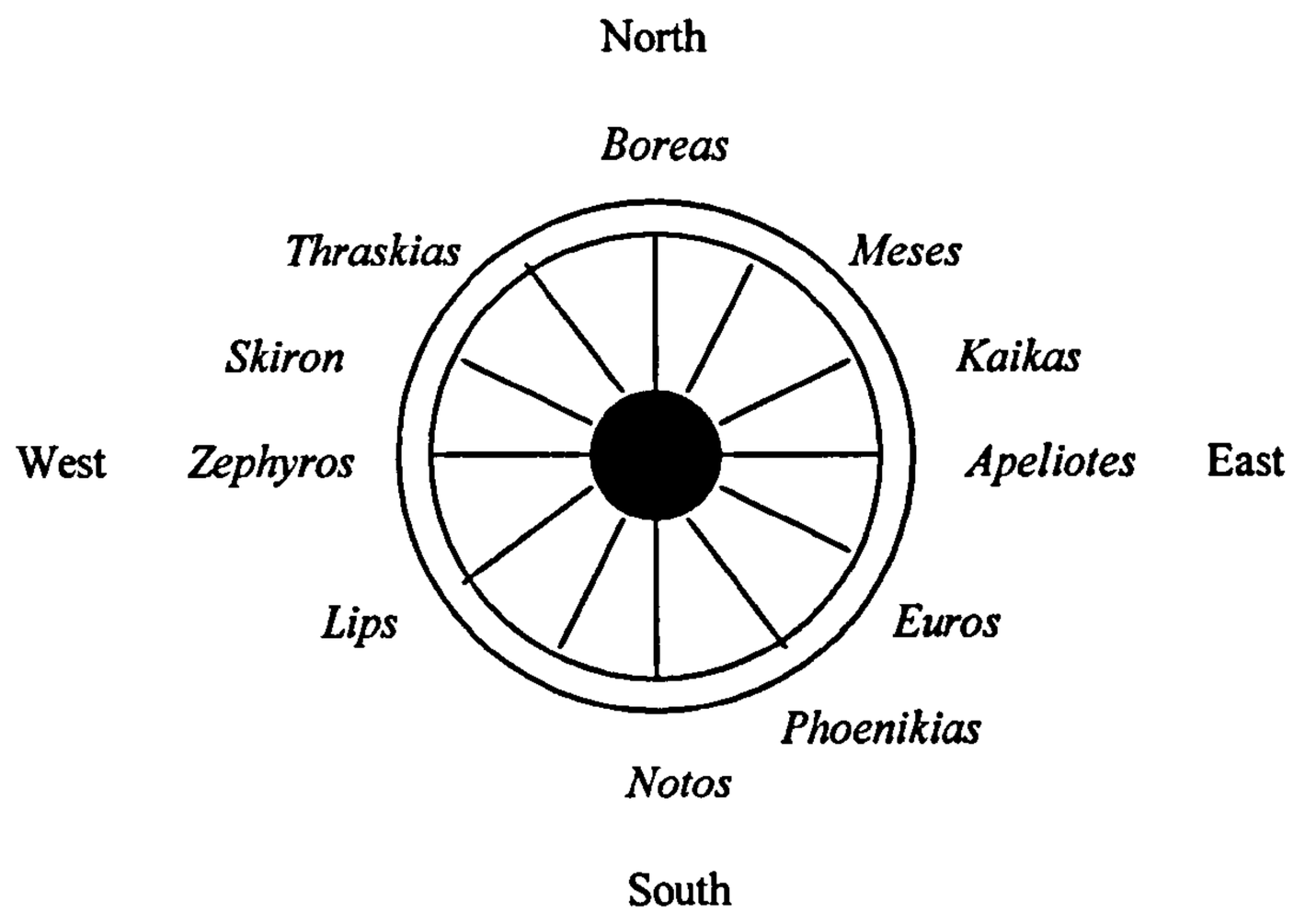

Figure 1.2.3 The Greek wind-rose of Aristotle and Theophratus

An exception was Vitruvius [15 and 20], a Roman architect and engineer of the first century BC. He wrote his 'Ten Books on Architecture', the oldest and most influential book on architecture. In this, he referred to a number of considerations given to the design of buildings and towns in relation to wind. These included the selection of the site for the fortified town, the orientations of the rectangular grid street pattern and the locations of entrances, courtyards and terraces associated with the buildings in the cities. He also observed that some industries would be better sited with careful consideration to wind.

Vitruvius' principles [20] were taken up in the fifteenth century by Leon Batista Alberti, an Italian, who was influential in spreading these ideas from Italy to France, Germany, Spain and the rest of Europe including Russia [15 and 21].

In 1573 town planning laws were established for Spanish towns in South and Central America [15 and 22]. New inland towns, according to these laws, were to be located on the eastern or western slopes of hills or mountains to shelter them from undesirable winds. Another provision urged that inlaid towns be exposed only in the north or south winds. Coastal towns were to avoid open water south or west of the settlement. This was a practical regulation because the prevailing winds along the Gulf Coast are south-easterly and would hinder the approach of sailing vessels to ports with channels leading into the wind.

Other cultures designed their buildings and towns to suit the local winds [15 and 23]. The direction of the prevailing winds or storms governed the location of openings and entries in Japanese houses. It is still customary in Japan to consult a specialist on local climate when one wishes to build a traditional house. Small openings on the northern side allow a minimal air current to pass through from north to south during colder months. Traditional houses are normally built with sliding screens for summer but problems do occur in winter when cold winds penetrate the many cracks and crevices between these sliding door panels. The idea of this design is to give warmth in winter and coolness in summer as shown in Fig.1.2.4.

Hyderabad, a city in India, is characterised by numerous tall air shafts and wind scoops projecting from the roofs of buildings. These rectangular chimneys have large flat panels over them which are inclined into the prevailing wind to deflect the roof top breezes down into the buildings. The induced airflow escapes through small windows into the narrow streets and alleys.

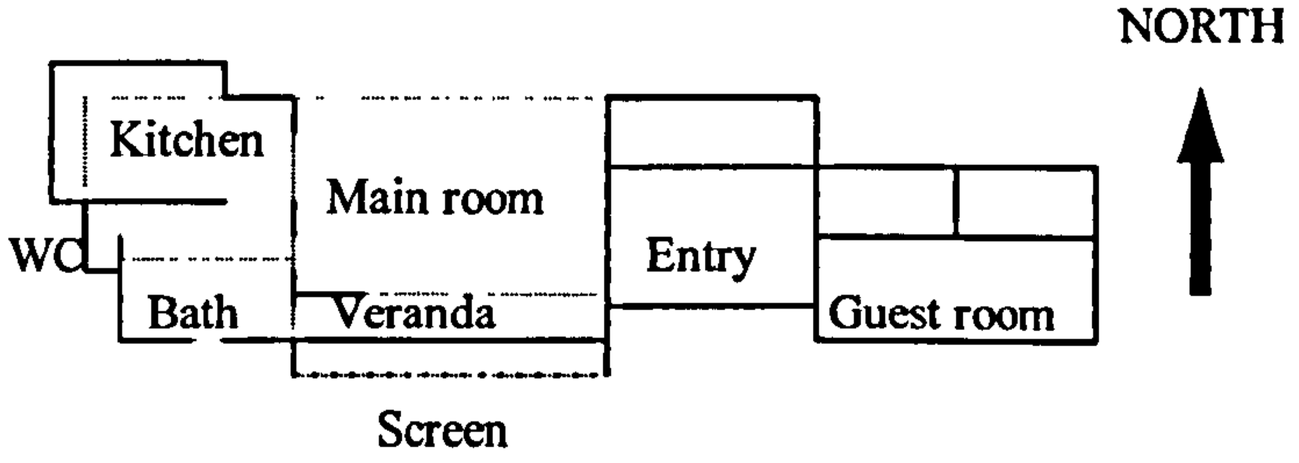

Figure 1.2.4 Plan of Japanese house indicating wall openings

A similar technique is evident in traditional Egyptian houses which use the *Mulguf*, a pair of roof ventilators in the form of triangular prisms. The windward ventilator deflects breeze down into the house while the leeward ventilators act as an exhaust [15 and 24].

From the description above, we can conclude that wind direction is as equally important as wind speed measurement. Early Chinese and Egyptian civilisations observed the wind direction from wind vanes. The Greeks also used wind vanes, one being mounted on their tower of the winds.

1.3 Aims and Objectives of this Research Work

The aims of the research work are to protect, improve and develop traditional Balinese reason by using a scientific point of view. To describe and develop traditional Balinese ideas in relation to the present and future in order to improve health, safety and comfort of occupants, and the harmony between humans and their environment as described in the *Tri Hita Karana* concept.

The research work described in this thesis is focused on traditional Balinese architecture in order to understand its meaning, concepts and conventions as experienced by the people. The *Tri Hita Karana* concept indicates the relationship between humans and their environment, therefore, to understand this traditional reason needs unification of several fields of sciences, such as engineering, physics, psychology and anthropology.

From engineering science, architectural aerodynamics, wind engineering and heat transfer are some methods that can be used to approximate this concept, in accordance to energy transfer from building, wind effects and thermal comfort of inhabitants.

The first objective of the research work is to understand the building arrangement of traditional Balinese architecture including the distance between buildings, distance between buildings and the fence and type of roof in association with heat transfer, wind load on the building envelope and thermal comfort of occupants. From this, we will understand whether traditional arrangement improves heat transfer and thermal comfort of occupants and reduces wind loads on building's surfaces.

The second objective is to justify the building position in accordance to its function. As an example, the granary which has triangular roof is located in the

windward side (poverty area), the nine posts building (for meeting and ceremonial) lies in the middle area, and the parent's sleeping quarters (twelve posts) has been placed in the leeward side (primary area). We expect that this traditional arrangement has been correlated to heat transfer, thermal comfort of inhabitants and reduction of the wind effects on buildings.

The third objective of this study is to understand the building materials in relation to building's function. Traditional buildings are composed by traditional material, but now they have been changed to modern processes. To improve the heat transfer rate, surface roughness on building surfaces are considered. From this view, the maximum surface roughness on building surfaces will be examined and the materials correlated to the surface roughness.

The fourth objective of the work is to know some traditional definitions such as centre (*natar*), shrines of the gods which is placed on the primary area, orientation of all buildings to the centre (*natar*) and distance between building to the shrines of gods. These traditional definitions are considered in association to building's function, thermal comfort of inhabitants, and wind effects on building surfaces.

The fifth objective of the work is to understand the magic rule of traditional Balinese buildings. The screen behind the gateway (*aling – aling*) has been considered in relation to wind load on building surfaces. From this study, we hope to understand if the screen reduces energy transfer and wind loads on building surfaces and affects inhabitants comfort.

The sixth objective of this study is to understand the rule of gateway in traditional Balinese building in relation to occupant's comfort. The gateway is examined at several directions in order to find the relationship between the energy transfer and wind load on building surfaces. From this view, we will understand whether traditional reason reduces energy transfer and wind loads on building surfaces.

The seventh objective of the research work is to propose some arguments which have not yet been explained in traditional reason (*e.g.* placing shrine of gods on the roof) in relation to heat transfer, wind engineering, architectural aerodynamics and thermal comfort of occupants.

The eighth objective of the research study is to propose several parameters which should be considered on building design, combination of traditional reason, present and future problems in Bali.

The ninth and last objective of the research work is to propose future work in relation to urban and town planning in Bali, involving a combination of traditional reason, present and future problems.

The analysis of those problems will be done by considering Balinese topography, therefore, the results will be representative and valid for all Balinese community.

1.4 Outline of Thesis

This thesis is organised into seven chapters. Introduction to traditional Balinese architecture, general background to the areas of study and aims and objectives of the work are presented in Chapter One. Chapter Two presents a broad literature survey and review on the subject of wind engineering and architectural aerodynamics in order to understand parameters that should be taken into account and also some ideas which have correlation to this study.

Chapter Three describes several test cases of numerical problems on two-dimensional models by using a commercial code Fidap, based on the finite element method. According to Chapter Two, several parameters have been taken into consideration, and comparison with published results has been done in order to verify and validate the models. Results of these tests are used on traditional Balinese simulation.

Numerical tests and discussion of traditional Balinese building arrangement is presented in Chapter Four. Different building parameters such as type of roof, distance between buildings and distance between buildings and the fence have been examined, in order to understand whether the traditional arrangement improves heat transfer and thermal comfort of occupants and reduces wind effects on building surfaces. Building position in accordance to building's function has been investigated in order to understand if traditional arrangement does control wind effects on building surfaces and thermal comfort of inhabitants. Building materials in relation to building's function has been considered by applying surface roughness on building surfaces.

Chapter Five describes numerical tests of three-dimensional models by using a commercial code CFX, based on the finite volume method. Several parameters have been considered, as described in Chapters Two, Three and Four. To verify and validate the results, comparison with published papers has been done.

Numerical tests and discussion of three-dimensional building arrangements are presented in Chapter Six. Three dimensional building arrangements have been simulated in order to verify some traditional definitions such as centre (*natar*), shrines of the gods, orientation of all buildings to the centre (*natar*) and distance between buildings to the shrines of gods. A unique feature of this research work is that either building arrangement or type of building does not exactly match that in traditional rule. This new idea is based on the concept that traditional rule can be explained by using modern building arrangements. Therefore, in modern buildings arrangement, one should refer to traditional rule. Traditional rule is not only magic, but contains several terms that should be understood from a scientific point of view. This is examined, for example, for the screen behind the gateway (*aling – aling*) when considering its relation to wind load on building surfaces, energy transfer and inhabitants comfort. The sentence is also examined where the gateway is placed at several directions in order to find the relationship between energy transfer and wind load on building surfaces. Therefore, some definitions of traditional reason in relation to heat transfer, wind engineering, architectural aerodynamics and thermal comfort of occupants are proposed.

Several parameters which should be considered on building design -combination of traditional reason, present and future problems in Bali- are proposed. Based on the work done in this thesis, the major conclusions and recommendations for future work to be carried out in relation to urban and town planning in Bali are presented in Chapter Seven.

REFERENCES

1. I.N. Gelebet, I.W. Meganada, I.M. Yasa Negara, I.M. Suwirya, Arsitektur Tradisional Daerah Bali (*Traditional Balinese Architecture*), Departemen Pendidikan dan Kebudayaan Proyek Inventarisasi dan Dokumentasi Kebudayaan Daerah, 1986.
2. L.K. Suryani and G.D. Jensen, The Balinese People: A Reinvestigation of Character, Oxford University Press, Singapore, 1992.
3. Anonymous, Asta Kosala, BIC Collection, Bali.
4. Anonymous, Asta Kosali, BIC Collection, Bali.
5. Anonymous, Asta Patala-Asta Patali, BIC Collection, Bali.
6. Anonymous, Swakarman, BIC Collection, Bali.
7. Miguel Covarrubias, Island of Bali, Oxford University Press, Singapore, 1972.
8. Kaler, *et al.*, *Penuntun Pembangunan Rumah Transmigran asal Bali*, 1976.
9. A. Daniel, Bali Behind the Mask, Alfred A Knopf, New York, 1981.
10. U. Wikan, Managing Turbulent Hearts: A Balinese Formula for Living, University of Chicago Press, Chicago, 1990.
11. M. Mead and G. Bateson, Balinese Character: A Photographic Analysis, Vol. II, New York Academy of Sciences, New York, 1942.
12. U. Ramseyer, The Art and Culture of Bali, Oxford University Press, Singapore, 1977.
13. L.K. Suryani, T.A.K. Adnyana, D. Thong, T.I.R. Mink, I.D.K.W. Putra, W. Widjana, D.W. Tama and G.D. Jensen, The Physical and Mental Health of Elderly in a Balinese Village, Journal of Cross-cultural Gerontology 3 (1988) 105-120.
14. I.G.M. Putra, Nilai-nilai Tata Letak Bangunan dalam Rumah Tradisional Bali, University of Udayana, 1985.
15. R.M. Aynsley, W. Melbourne and B.J. Vickery, Architectural Aerodynamics, Architectural Science Series, Applied Science Publisher Ltd., London, 1977.
16. L. Hilberseimer, The Nature of Cities, Paul Theobold & Co., Chicago, 1955.
17. A. Cotterell and D. Morgan, China: Integrated Study, Harrap, London, 1975.
18. S. Brown, World of the Wind, Bobbs-Merrill Co., Indianapolis, 1961.

19. School of Civil Engineering, University of Sydney'Post Graduate Course', The Structural and Environmental Effects of Wind on Buildings and Structures, Sydney, 1975.
20. Vitruvius, The Ten Books of Architecture, translated by Morris Hickey Morgan, Dover, New York, 1960.
21. R. Wittkower, Architectural Principles in the Age of Humanism, 2nd ed., Alec Tiranti Ltd., London 1952.
22. F. Violich, Cities of Latin America; Housing and Planning to the South, Reinhold, New York, 1944.
23. J. Harada, The Lessons of Japanese Architecture, Studio Vista, London, 1936.
24. V. Olgyay, Design with Climate, Princeton University Press, Princeton, New Jersey, 1963.

CHAPTER TWO

LITERATURE REVIEW

2.1 Wind Engineering around Buildings or Bluff Bodies

In this work, computational fluid dynamics is used as a tool for predicting wind loads on traditional Balinese architecture by numerical simulation. By this method, analyses can be done more quickly and less expensive than with wind tunnel experiments. This method is also capable of delivering more detailed and comprehensive information about the flow structure.

In 1958 Jensen [1] showed that, in wind-tunnel testing, it is important to model the building as correctly as modelling the wind. This lesson must surely carry over into the relatively new field of computational wind engineering. For many wind engineering applications only the lower 200 m or less of the atmospheric boundary layer are of interest. Ludwig and Sundaram [2] set down the basic conditions for simulating the atmospheric surface layer where any flow that is fully aerodynamically rough, horizontally homogeneous, and relatively free from any pressure gradients, constitutes a suitable model for the atmospheric surface layer. For computational modelling purposes fully aerodynamic roughness implies that the shear stresses should be dominated by the Reynolds stresses. Castro and Robins [3] described an experimental investigation of the flow around surface-mounted cubes in both uniform, irrotational and sheared, turbulent flows. The shear flow was a simulated atmospheric boundary layer. They concluded that the measurements in the wake of a surface-mounted cube in uniform and turbulent upstream flows, coupled with pressure measurements on the cube itself, have led to a fairly clear picture of the nature of the flow. Hunt [4] generated two wind-tunnel simulations on a scaled model in a boundary layer wind tunnel. The variation of the pressure field on the cube was discussed in relation to the incident flow-field parameters and he concluded that insight has been gained into the aerodynamic processes operating.

Hoxey and Richards [5], in order to adequately model the atmospheric surface layer, concluded that the turbulence model and associated constants must be consistent with each other. Full scale measurements at Silsoe have led to an evaluation of von Karman's constant K = 0.42 ± 0.01, and their measurements also suggested that $C\mu = 0.013$ and σ_ε should be increased to 3.22 for consistency.

The pressure distribution generated by wind over a cluster of buildings is determined principally by the shape of the buildings. Hoxey *et al.* [6] analysed the effects of height, span, length and roof pitch on two-dimensional structures by CFD and concluded that the pressure distribution over roofs of traditional building shapes is significantly non-uniform and dependent on geometric parameters such as eaves height, span, and roof pitch. Their research used not only CFD but also full-scale measurement.

Hoxey and Richards [7] described measurements of flow patterns and pressure fields around a low-rise portal framed building on which extensive full-scale wind load measurements have been made and compared to a CFD model. They concluded that several aspects influence the flow around a building, where the building structure influences the static pressure at the 5 % level.

Holmes [8] presented the characteristics of wind pressure acting on the walls and roofs of gable-roofed tropical houses, based on wind tunnel model experiments. The effects of elevation, roof pitch, wind direction and grouping of buildings on the external pressures were discussed with some characteristics of internal pressures when there are dominant openings in a wall. The effect of elevation is to increase the external wind pressures significantly while the roof pitch has large effects on the roof pressures when there is a significant wind component normal to the ridge. The shielding effects of upwind buildings are strongly dependent on the ratio of building spacing to height. This looks similar to traditional Balinese buildings, where the distance between buildings has a relation with the height. Although the research did not use a CFD model, since the building conditions are close to the traditional Balinese architecture, our model will start by following these results.

Hoxey and Robertson [9] continued their previous research on surface pressures of a single span by full-scale measurements. They used a quasi-steady approach for analysing full-scale data. Full-scale measurements indicated the importance of the

geometric parameters of building height, span and roof slope in the assessment of wind loads. Approximating the non-uniform wind load over a roof slope by an area-averaged pressure coefficient leads to acceptable predictions of stresses and deflections. For a closed building this is acceptable but dynamic effects may be significant if the building has a dominant opening and a dynamic magnification factor may then be required.

Another research which has correlation with Balinese architecture was presented by Ferreira *et al.* [10]. They presented a study of turbulent isothermal flow around two-dimensional sinusoidal hills. The experimental results were obtained from a simulation carried out in two wind tunnels for a Reynolds number, based on the hill's height, ranging from 1.8×10^4 to 2.5×10^5 and compared to a turbulent flow modelled with a modified low-Reynolds number k-ε model. The results indicate that the extension of the recirculating region is strongly dependent on the hill shape. The transition to a supercritical regime occurred at $Re = 9 \times 10^4$, where the non-dimensional flow characteristics are independent of the Reynolds number.

Hoxey *et al.* [11] described full-scale and numerical data for wind loads on free-standing walls. There are widely varying design net pressure coefficient values contained in different designs of free-standing walls which are not conducive to efficient design. The results from full-scale measurements suggest that the recent wind-tunnel based data underestimate the loads over the main central region away from the ends. CFD results indicate that higher or lower net loading can arise on a free-standing wall when a downwind wall is present, depending on the proximity and relative height of the downwind wall.

Another research of Hoxey and Richards [12] presented a quasi-steady approach which predicted that mean pressure coefficients (combined with peak wind dynamic pressure) are the most reliable estimate of extreme loads on buildings. The maximum (or minimum) measured pressure coefficients, which are susceptible to higher experimental error, generally underestimate the maximum values expected from quasi-steady analysis.

Hoxey *et al.* [13] presented full-scale testing to determine the wind loads on free-standing walls. The versatile modular construction enabled studies to be made of the effect of wall length, the presence or absence of return corners, and the introduction of a gap in a wall. The results illustrate the severity of loads which arise at the end of a

long wall and the dependence loads have on wind direction, wall length, position along wall, and the presence of a return corner.

Another research on buildings by computational fluid dynamics was done by Baskaran and Kashef [14]. Although not directly related to traditional Balinese architecture, it is very useful to validate the model. They concluded that CFD is emerging as a powerful tool for investigation of building air flow applications and that it can provide very detailed and qualitative predictions of air velocities around buildings. Their research on bluff bodies was compared to animation contour images.

Murakami [15] described a comparison of various turbulence models applied to a bluff body. In this research, several methods were used such as wind tunnel experiment, k-ε, EVM, ASM, and LES turbulence models. The results of this research are that both DSM and ASM were applied successfully when the flow field was highly anisotropic. For producing surface pressure and turbulence statistics, analysis by ASM, DSM or LES is effective. LES provides greater estimation accuracy than the other turbulence models but requires much more CPU time.

Still in the bluff body analysis, Murakami *et al.* [16] predicted flow around a building with various turbulence models. Similar to the above research, they concluded that LES models agree well with experimental data in terms of distributions of mean velocity, mean pressure, and turbulence energy k. Significant inaccuracies in the results of k-ε EVM are improved remarkably in ASM. Some discrepancies still exist in the result of ASM in the reproduction of the anisotropic properties of turbulence around the front corner of the building.

Selvam [17] simulated flow and pressure around a building, using hybrid upwind and streamline upwind procedures. The conclusion is that the separation length behind the leeward wall using the streamline procedure is longer than for the hybrid procedure.

Stathopoulos and Zhou [18] applied the two-layer method for the evaluation of wind effects on a cubic building. They compared the computational results to experiments. The comparison showed that neither the k-ε model nor the modified k-ε model-based two-layer method can represent the flow separation above the roof surface and near the side walls, while the one-equation model based on the two-layer approach is effective in predicting the separation.

Fusegi [19] computed the turbulent diffusion in a thermally-stratified channel with obstruction. This research concluded that the turbulence intensity and the heat transfer rate are strongly affected by the stratification in the field, in the regions near the block.

Stathopoulos and Zhou [20] computed wind pressures on L-shaped buildings. They concluded that for oblique wind cases, the k-ε model and special boundary conditions applied on the surface can be used with reservations; in particular, the computed suctions on stepped roofs may be underestimated near the windward edges.

For building arrangements, Stathopoulos and Baskaran [21] presented computer simulations of wind environmental conditions. The importance of this research is for the assessment of pedestrian comfort and dispersion of pollutants. Validation of the computed results has been carried out by using data from experiments conducted in a boundary layer wind-tunnel. Both computed and measured data indicated that the most significant features of the wind environmental conditions around buildings can be predicted with reasonable accuracy. A similar computation for the flow field around buildings in an urban area was reported by Takakura *et al.*[22].

Since traditional Balinese architecture normally includes a front and a back fence for each group of buildings, it is necessary to study the effect of the fence (or wind break) on the airflow around the buildings. Mattingly and Peters [23] described the influence of trees on wind flow, where they used experimental methods. They discussed the stagnant flow on the windward wall of the house, the flow over the lip of the roof to the roof peak, and the wake flow region adjacent to the leeward roof and wall surfaces. Another research was done by Gandemer [24] who used empirical design rules in the aerodynamic characteristics of windbreaks, as an aid to town planning.

Wilson [25] presented numerical studies of flow through a windbreak which used a porous windbreak and the k-ε model. Satisfactory estimates of the pattern of turbulent kinetic energy behind the fence were observed. Design aids for isolated windbreaks have been generated from the prediction of the second-order closure model, which gives the velocity reduction to be expected in the near wake of the fence.

Crosby *et al.* [26] described the numerical prediction of air flow through and around permeable windbreaks and over buildings. They used turbulent two-dimensional flow simulation to investigate wind-induced pressure loads on buildings, from where they developed a new model for flow through porous media. They compared the

computational results to experiments. The conclusion is that the use of a permeable wind break does not reduce the wind loads on a building.

A similar technique was developed by Raine and Stevenson [27] who presented wind protection by model fences in a simulated atmospheric boundary layer, using permeability values of 0 %, 20 %, 34 % and 50 %. They concluded that the 20 % permeable fence gave the best overall reduction in leeward mean velocity.

Jaeger and Dhatt [28] presented computations for incompressible flows. They concluded that their model was valid for high and low Reynolds numbers, and validated the model parameter for near wall boundary conditions for a flow with measured values. They found that the numerical convergence is slow and oscillatory for k-ε models.

Delaunay *et al.*[29] described a numerical approach for wind loads on buildings and structures. They concluded that the standard k-ε model is not particularly adapted to recirculating flows: besides that, the use of wall functions is erratic in non-developed boundary layers, and the inflow conditions of the wind tunnel cannot always be reproduced exactly, particularly when the generated boundary layer is not in equilibrium.

2.2 Numerical Methods

Conventionally, the wind environmental conditions around buildings and wind-induced pressures on buildings were examined either in full-scale tests or in experiments carried out in boundary-layer wind tunnels. In recent years, computational fluid dynamics has been applied for the evaluation of wind effects on buildings. Most numerical studies have dealt with rectangular buildings by using the Navier-Stokes equations with either a k-ε turbulence model or the Large Eddy Simulation model. Large Eddy Simulation can only be applied to time-dependent conditions and large-scale motion of turbulent flow, and it also needs finer grid arrangements. Moreover, it takes much more CPU time than the k-ε model. For this reason, the k-ε model is more attractive to wind engineers since it needs less computational power [18 and 30].

Experience has shown that the convergence characteristics of most turbulent flows are considerably improved when non-zero fields are used as initial guess. The

solution strategy is probably the most important factor in simulations of turbulent flows. For most three-dimensional problems, a non-fully coupled algorithm should be used. If iterative linear equation solvers are to be employed, it is recommended that the iterative solvers be used with relatively tight tolerances (say, 10^{-6}) to ensure good overall convergence behaviour and solution quality.

Relaxation of the numerical solution is a very important factor in the iterative solution of the non-linear turbulent flow equations when using implicit algorithms. With a fully coupled algorithm, this value may range from its default value of zero for very simple unidirectional and confined flows to about 1 for highly complex re-circulating flows with strong inter-coupling effects due to buoyancy or swirl or both. However, a more typical range is between 0.6 and 1.0. The relaxation factors typically used for this algorithm are about 0.6 to 0.7 for velocities, 0.9 to 1.0 for pressure, 0.9 to 1.0 for temperature and species concentration, and 0.6 to 0.7 for k and ε [31, 32 and 33].

2.2.1 Finite Element Method

There are three main sources of instability that if left untreated will seriously affect typical turbulent flow simulations. These instabilities manifest themselves in terms of non-physical negative turbulence values, and/or highly unrealistic turbulence time and length scales resulting from very small turbulence values in flow regions where turbulence levels have practically collapsed [34].

The first of these instabilities is associated with the dissipation (or sink) terms in the turbulence model equations. Physically, these terms act to maintain finite levels of k and ε. In the absence of these terms, k and ε levels will grow uncontrollably (and exponentially) due to the generation (or source) terms of the k and ε equations. During the course of a typical numerical solution, while the temporary solution field is significantly different from the fully converged solution, the dissipation terms may strongly dominate the generation terms and can momentarily produce unstable negative nodal values of k and ε. These negative values are unstable since they change the polarity of some important processes in the k and ε equations. For example, for where the turbulent viscosity becomes negative, it will cause highly unstable negative

diffusion, the source and sink terms will change polarity (*e.g.* the turbulent generation terms) instead of extracting turbulence energy from the mean flow process and will extract energy from the turbulence field and relate it to the mean flow. Similarly the sink terms, instead of dissipating turbulence energy, will generate turbulence energy (a physical impossibility).

The second source of instability is associated with the advection terms in the k and ε equations. It is well known that at large Reynolds numbers these terms will produce streamwise oscillations in the corresponding flow variables if they are approximated using accurate non-diffusive discretisation operators (*e.g.* such operators automatically result from the application of the Galerkin finite element method to the flow equations).

The third source of instability arises when the k-ε model is used in the prediction of flows containing both turbulent and laminar regions. A typical example of this is in external aerodynamic problems where the free-stream flow is not fully turbulent but the flow surrounding the body is fully turbulent. The k and ε equations of the standard high-Reynolds-number k-ε turbulence model become anomalous in the turbulence-free regions. These equations contain terms involving ratios between k and ε (*i.e.* k^2/ε, k/ε, ε/k and ε^2/k) which are clearly indeterminate in laminar flow regions where turbulence is not present. Numerically, these ratios become ultra sensitive to clatter level variations in k and ε and begin to oscillate uncontrollably from one nodal point to another. This will affect the numerical stability of the computation (as this unstable behaviour quickly spreads to the fully turbulent flow regions and in a matter of a few iterations totally contaminates the numerical solution) [34].

To avoid and/or suppress the instabilities described above, streamline upwinding are introduced. Streamline upwinding is a numerical technique which introduces stabilising false numerical diffusion along the streamwise direction. This technique helps to suppress the streamwise oscillations in the various flow variables (including k and ε) that occur in advection dominated flow regions [35].

Standard finite element methods employ the Galerkin formulation for which the shape and test functions are the same discrete subspace of the functional space. For stability, the Petrov-Galerkin-upwind approximation must be used. [36].

2.2.2 Finite Volume Method

If the function sought is not regular enough, than the remainder of Taylor's formula is not smaller than the first terms. Most modern finite-difference methods are applied through a mapping of the computational domain into the physical one, therefore, this mapping also has to be regular enough to allow truncated Taylor formulas to be sufficiently accurate. In view of this, these methods are not suitable to model discontinuous functions.

The finite volume method introduces the integral formulations expressing conservation laws in a rather simple way in the physical domain, and that allows the computation of discontinuous functions. The physical domain is considered to be divided into cells and the discrete conservation laws are introduced following the notation of flux. For high Peclet number, the central finite volume schemes may suffer instabilities, therefore, upwinding or artificial viscosities are often introduced for stabilisation.

Theories establishing finite volume convergence and accuracy have not yet been developed, except through the Essentially Non-Oscillatory developments [Harten and Osher, 1987] for higher order. The choice of cell form is also a rather important and controversial question. In cell-centred methods, primal meshes give the partition. In vertex-centred methods, a dual partition is used for flux derivation [37].

In finite element methods, fully coupled systems are solved via Newton-Raphson and Gaussian elimination, but finite volume methods evolve the simple geometry of finite difference methods in which uncoupled equations and iterative solution methods dominated the solution algorithms. The advantages of the uncoupled/iterative methods are;

- Reduced computational cost (memory and accuracy)
- A significantly larger radius of convergence.

The disadvantage is a significant increase in the number of iterations to achieve convergence, and in some cases even the ability to converge to a tight tolerance. It is thus interesting to note that a current trend in the finite volume community is towards coupled iterative solution methods, because of the disadvantage noted above. However, this is a very misleading way of comparing the relative costs, particularly in

the case of non-linear problems in which additional issues such as accuracy and convergence rates are considered [35].

A comparison between finite element and finite volume methods begins with the principal and most-oft-stated advantage of the latter over the former: the linear conservation laws implied by the governing partial differential equations are always and inherently satisfied. Hence, the discrete equations are always amenable to simple physical interpretation because the resulting stencils are also simple [35 and 38].

Schneider and Raw (1986) explained that one reason for the increasing popularity of finite volume methods is that they combine the intrinsic geometric flexibility of finite element methods together with the desirable, direct physical invocation of a conservation principle to clearly identified and delineated control volumes comprising the domain [39].

The above statements are true and local conservation is an asset, but it is also true that the stencils are far from simple and not so easy to interpret physically when the finite volume method is applied to complex geometry with its mappings, Jacobians, metrics and transformation equations, and that local conservation does not necessarily imply local accuracy [35].

There are actually more similarities than differences between finite element and finite volume methods; since both methods are members of the family of weighted residual methods, both methods rely more on integration than divided differences to generate the discrete equations, and both methods treat complex geometry via a mapping [35].

All arguments above are based on theory. In practice, the advantage of using CFX is the CPU time which is much less than Fidap. A proper convergence criterion for finite volume methods has not yet been developed, therefore, the equations are said to converge for a typical value of 0.1 percent and tolerances of about 10^{-6}. Although CFX takes smaller disk space, it takes much more machine memory than Fidap. Therefore, a large machine is needed for a particularly large model.

2.2.3 Solution Algorithms for Pressure-Velocity Coupling in Steady Flows

In Fidap which is based on the finite element method, pressure algorithms for steady flows are **continuous** or **discontinuous** and **mixed** or **penalty** formulation.

In the **continuous pressure - mixed formulation,** the pressure degrees of freedom are located at the corner nodes of each element. The **discontinuous pressure - penalty or mixed formulation** is more complex due to the fact that the pressure degrees of freedom of an element are no longer located at the nodal points but rather at points within the element. In addition, for certain elements; *e.g.* the biquadratic velocity-discontinuous linear pressure element, the pressure degrees of freedom are not directly related to pressure values, but are the coefficients of the linear polynomial approximating the pressure on the element. In this case, the pressure value output is for each element rather than nodal values. For each element, the pressure at the centroid of the element is the output. In the penalty approach (used with fully-coupled solvers), the pressure is discretized in an identical manner to that employed in the mixed approach, but is eliminated from the global system of equations before solving for the other unknowns. This significantly reduces the total number of unknowns that must be solved for and as a result the total cost of the simulation is substantially reduced. In general, the penalty approach is recommended because of its reduced cost. The penalty approach is inherently discontinuous [34].

The penalty function approach to the approximation of the pressure is a very cost-effective procedure as it eliminates the pressure as an unknown from the system of equations to be solved. In practical computations, the selection of the value of the penalty parameter can be of crucial importance. To get an accurate solution, the penalty parameter must be chosen small enough to approximate incompressibility well.

In CFX, which is based on control volume methods, the solution algorithm is a variant of SIMPLE (Semi-Implicit Method for Pressure Linked Equations), *e.g.* SIMPLER (SIMPLE Revised), SIMPLEC (SIMPLE-Consistent) and PISO (Pressure Implicit with Splitting of Operators).

The SIMPLE algorithm was originally put forward by Patankar and Spalding (1972) and is essentially a guess-and-correct procedure for the calculation of pressure on the staggered grid arrangement. Therefore, velocities are obtained by solving the

momentum conservation equations using the most recent estimate of the pressure field and then the pressure field is corrected by using the imbalances in the mass conservation equations. The method is iterative and when other scalars are coupled to the momentum equations, the calculation needs to be done sequentially [40].

The SIMPLER algorithm of Patankar (1980) [40] is an improved version of SIMPLE. In this algorithm the discretised continuity equation is used to derive a discretised equation for pressure, instead of a pressure correction equation. Thus, the intermediate pressure field is obtained directly without the use of a correction. Velocities, however, are still obtained through the velocity corrections of SIMPLE.

The SIMPLEC algorithm of Van Doormal and Raithby (1984) [40] follows the same steps as the SIMPLE algorithm, with the difference that the momentum equations are manipulated so that the SIMPLEC velocity correction equations omit terms that are less significant that those omitted in SIMPLE.

The PISO algorithm of Issa (1986) [40] is a pressure-velocity calculation procedure developed originally for the non-iterative computation of unsteady compressible flows. It has been adapted successfully for the iterative solution of steady-state problems.

The SIMPLE algorithm is relatively straightforward and has been successfully implemented in numerous CFD procedures. The other variations of SIMPLE can produce savings in computational effort due to improved convergence. In SIMPLE, the pressure correction is satisfactory for correcting velocities but not so good for correcting pressure. Hence, the improved procedure SIMPLER uses the pressure corrections to obtain velocity corrections only. Consequently, this method is highly effective in calculating the pressure field correctly. SIMPLEC and PISO have proved to be as efficient as SIMPLER in certain types of flows but it is not clear whether it can be categorically stated that they are better than SIMPLER [40].

2.2.4 Staggered Grid

The term staggered grid does not have relevancy to the grid structure. Staggered grids are associated to the pressure correction, indicating algorithms for pressure-velocity coupling in steady flows. Staggered and non-staggered grid systems have been adopted

for pressure correction, *i.e.* SIMPLE as described above. Staggered grids provide much more accurate numerical predictions.

The solution procedure for the transport of a general property will be enlisted to solve the momentum equations. The finite volume method starts with the discretisation of the flow domain and of the relevant transport equations. Therefore, the need to store the velocities is the most important followed by pressure and temperature. However, if the velocities and pressures are both defined at the nodes of an ordinary control volume, a highly non-uniform pressure field can act like a uniform field in the discretised momentum equations.

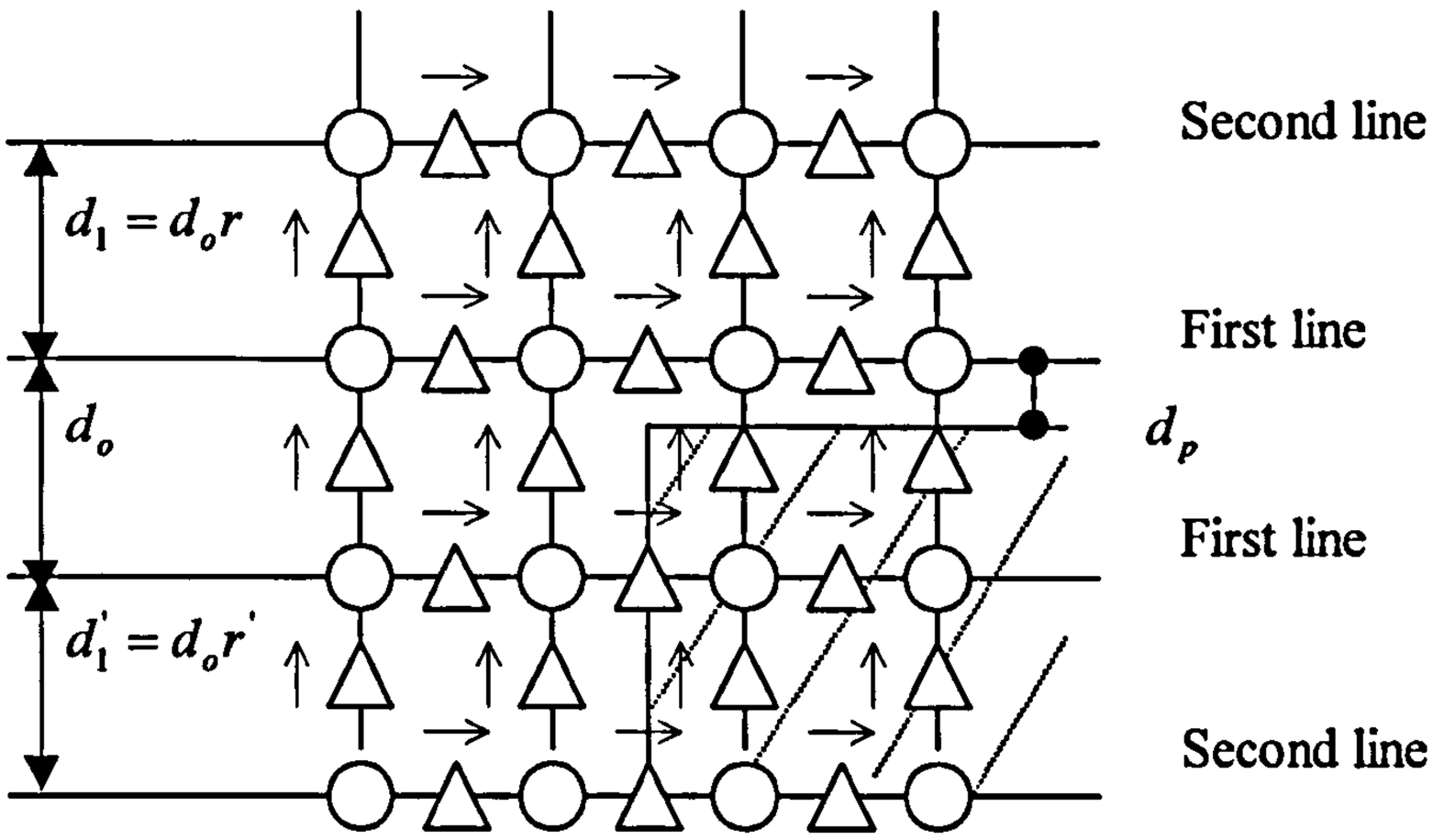

Figure 2.2.1 Staggered grid with uniform (without grading) grid arrangement

For simplicity, a staggered grid system with uniform grid arrangement is shown in Figure 2.2.1. Grid systems are usually generated with dense grid lines near solid boundaries and relatively coarse grid lines far from solid boundaries. When generating a grid system, the distance d_p will be read in the first time, then successive grid lines are generated at the specific expanding factor (r) defined for each region starting from the solid boundaries. In Figure 2.2.1, ○ denotes nodes for P, k and ε, △ represents nodes for velocity components, and → indicates direction of velocity components.

If the velocities are defined at the scalar grid nodes, the influence of pressure is not properly represented in the discretised momentum equations, therefore it can be refined by using a staggered grid for the velocity components. The staggering of the

velocity avoids the unrealistic behaviour of the discretised momentum equation for spatially oscillating pressures. A further advantage of the staggered grid arrangement is that it generates velocities at exactly the locations where they are required for the scalar transport –convection-diffusion- computations. Therefore, no interpolations are needed to calculate velocities at the scalar cell faces.

2.2.5 Grid Arrangement

The numerical simulation of wind flow needs special care in the arrangement of the computational grid nodes, especially near the building and the ground surfaces. The main practical difficulty is the construction of meshes. Actually, there are two types of grid, **structured** (regular, with or without grading) and **unstructured** (irregular).

2.2.5.1 Structured Grid

In a regular mesh, one overlays the region with a mesh of constant size (uniform/without grading) or different sizes (non-uniform with grading). This particular type of mesh provides a crude representation of the boundary. Therefore, structured grids without grading are not recommended when boundary layer effects are important. A structured grid with grading gives more realistic solutions.

2.2.5.2 Unstructured Grid

The technique is closely related to the way finite element meshes are constructed. Boundary layer effects get a better representation but are still not very accurately reproduced. Unstructured grids produce less accurate results, and are only recommended for special problems *e.g.* geometry is small but the surface is complicated.

Generally, a denser computational grid should be employed for a k-ε simulation as compared to the mesh of the corresponding laminar or zero-equation type simulation. This is because, in a typical flow problem, the k-ε fields undergo much sharper spatial

variations and involve considerably more detailed features than the mean flow variables (*i.e.* the velocity and temperature fields).

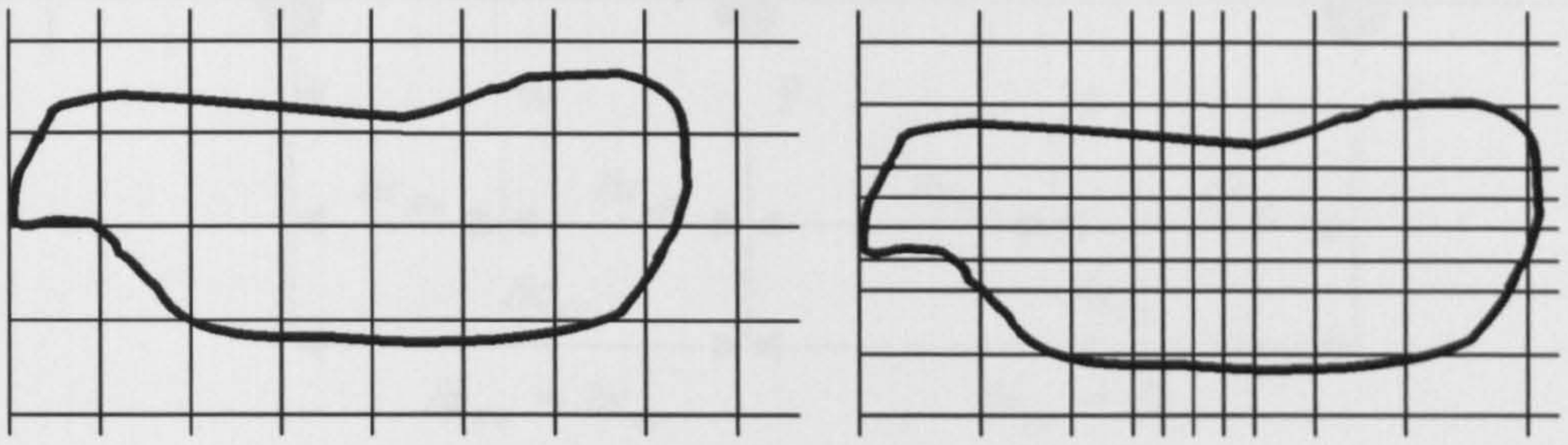

a. without grading (uniform) b. with grading

Figure 2.2.2 Structured grid

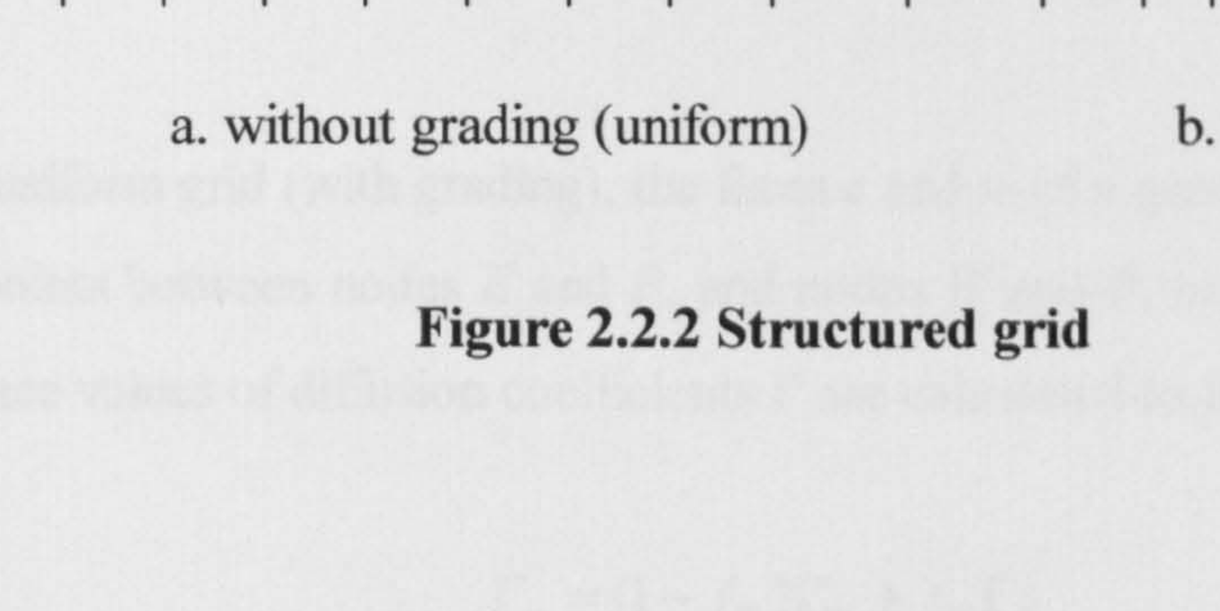

Figure 2.2.3 Unstructured grid

Thus, if a grid-independent solution to the mean flow field is to be obtained, the computational mesh must be fine enough to resolve the details of the k and ε fields. Care must also be exercised in the design of the computational mesh to ensure a smooth spatial distribution of nodal points throughout the flow domain. Abrupt jumps in mesh density, especially if these occur along the direction of the flow in regions where the grid Reynolds numbers are large, may lead to spurious spatial oscillations in the flow variables. In extreme cases these so-called "wiggles" will cause the numerical solution to diverge [41 and 42].

2.2.5.3 Non-Uniform Grid

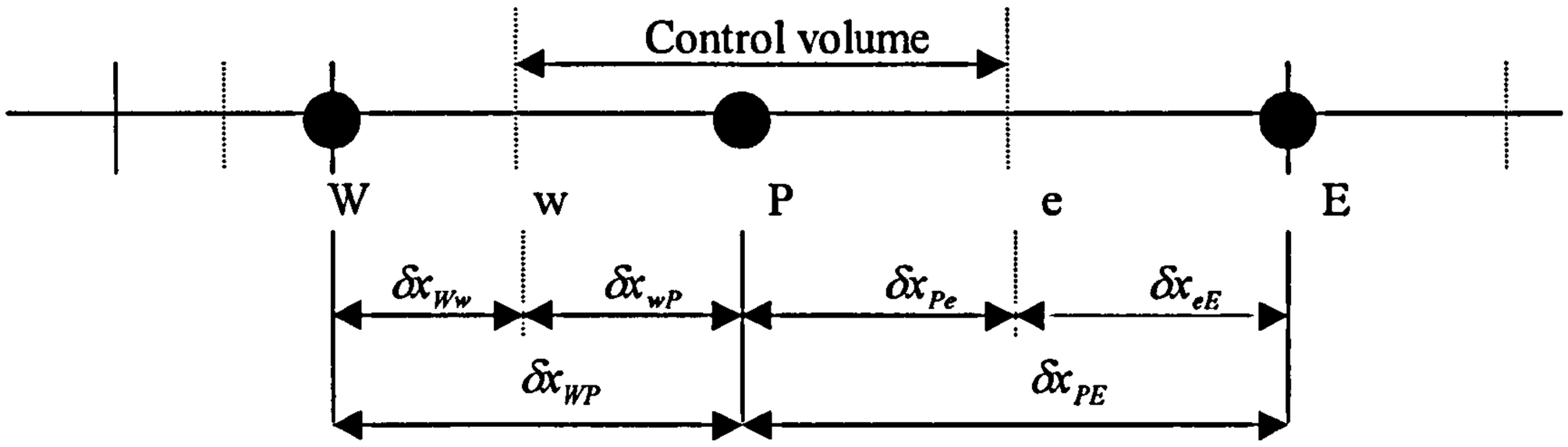

$$\delta x_{Ww} = \delta x_{wP} \qquad \delta x_{Pe} = \delta x_{eE}$$

In a non-uniform grid (with grading), the faces *e* and *w* of a general node may not be at the mid-points between nodes *E* and *P*, and nodes *W* and *P*, respectively. In this case, the interface values of diffusion coefficients Γ are calculated as follows;

$$\Gamma_w = (1 - f_W)\Gamma_W + f_W\Gamma_P$$

The interpolation factor f_W is given by

$$f_W = \frac{\delta x_{Ww}}{\delta x_{Ww} + \delta x_{wP}}$$

Similarly

$$\Gamma_e = (1 - f_P)\Gamma_P + f_P\Gamma_E$$

where

$$f_P = \frac{\delta x_{Pe}}{\delta x_{Pe} + \delta x_{eE}}$$

For a uniform grid, $f_W = f_P = 0.5$, therefore $\Gamma_w = (\Gamma_W + \Gamma_P)/2$ and $\Gamma_e = (\Gamma_P + \Gamma_E)/2$.

2.6 Boundary Conditions

Employing the k-ε turbulence model significantly increases the required CPU resources for the solution of a given flow problem compared to the corresponding simulation using zero-equation type models. Moreover, owing to the significantly stronger non-

linear and inter-coupled problems of flow equations, convergence of the solution becomes more difficult to obtain.

Generally, the convergence characteristics of k-ε simulations are less stable and also sensitive to the numerical and physical parameters involved in the numerical solution. One important aspect of a k-ε simulation is that equations are set for k and ε separately from the corresponding zero-equation model (zero-equation model is the pure Navier-Stokes equation where the energy term does not consider turbulent kinetic energy and its dissipation rate). Therefore, appropriate boundary conditions must be prescribed for k and ε on the boundaries of the computational domain.

2.6.1 Inlet Boundary Conditions

Dirichlet (*i.e.* prescribed or essential) boundary conditions for k and ε must be employed on inlet boundaries. The levels and the shapes of the profiles of k and ε at the inlet plane will be unique for each and every flow problem and these should ideally be obtained from experimental measurements. It is of course recognised that such experimental data will rarely be available for typical simulations. A precise set of laws does not exist from which appropriate profiles for k and ε can be arrived at for all possible flow scenarios.

The inlet plane is typically positioned upstream of the regions of interest in an area where the flow field is not disturbed by any nearby obstacles. The two most commonly occurring situations are external flows and fully or partially confined flows. In some shear-free situations, as is often the case in wind tunnel flows, the value of the turbulence intensity –typically between 1% and 7% of the free stream is available from experimental measurements [43].

2.6.2 Outlet Boundary Conditions

The Neumann (*i.e.* the zero-gradient or zero-flux, except pressure) boundary condition is the most appropriate one at the outlet for k and ε model with obstructions. A cautionary remark relating to the proper imposition of the outflow boundary in a computational domain is important. In design of the computational mesh, it must be

ensured that the outflow boundary is placed in a downstream location which is sufficiently far from regions of the flow where large perturbations occur in the flow field.

2.6.3 Wall Boundary Conditions

The wall is the most common boundary encountered in fluid flow. In wall-boundary turbulent flows, the near-wall modelling methodology must be invoked along those portions of the computational boundary which coincide with the solid walls. The remaining requirement is that one should apply the appropriate boundary conditions for those mean flow equations (*e.g.* momentum, temperature) that are being solved as part of the flow model.

In an isothermal flow with a stationary solid wall, zero values for velocity components need to be assigned at the wall. An important point to remember while prescribing non-zero velocity boundary conditions along wall boundaries is that the velocity components on any node lying on these boundaries should be entered in terms of the global coordinate system.

Additionally, if heat transfer is present, an appropriate boundary condition for the temperature equation is needed, such as a prescribed temperature, a prescribed heat flux, etc. In the case of a conjugate heat transfer problem, where the boundary between the fluid and solid regions is internal to the computational domain, no explicit boundary conditions need to be applied at this interface for the energy or species equations, since the values of temperature at this interface will be computed as part of the numerical solution.

In a wall boundary condition, a boundary unit normal vector is used to compute the characteristic cross-flow widths of the special near-wall elements. On external boundaries of the computational domain, the direction of the unit normal vector is uniquely defined as it points away from the computational domain. However, on internal boundaries the direction of this normal vector is not uniquely defined and one must provide a direction.

The no-slip boundary condition ($u = v = w = 0$) is the appropriate condition for the velocity components at solid walls. The implementation of wall boundary

conditions in turbulent flows starts with the evaluation of y^+. If the value of y^+ is greater than 11.63, then the first node (from walls) is considered to be in the logarithmic-law region of a turbulent boundary layer. In this region, wall functions associated with the logarithmic-law are used to calculate shear stress, heat flux, etc.

2.6.4 The Constant Pressure Boundary Condition

The constant pressure condition is used in this simulation since exact details of the flow distribution are unknown but the boundary values of pressure are known. Typical problems where this boundary condition is appropriate are external flows around buildings and buoyancy-driven flows such as natural ventilation.

2.6.5 Parameters Considered on Simulation

Boundary conditions for velocity and turbulence properties at free boundaries are fixed at the initial power-law velocity profile. The turbulent intensity at the roof level is 6.2%, according to Davenport terrain roughness classification number 4, for suburban terrain [44]. On the truncation walls and on building surfaces, the wall treatment used here is a combination of logarithmic and no-slip boundary conditions. To minimise undesired re-coupling effects, the computational domain is sufficiently wide, high and long. The Reynolds number of the main flow based on the velocity at roof level is around $2.3x10^5$. At the outlet, the constant pressure boundary condition is applied.

REFERENCES

1. M. Jensen, The model law for phenomena in natural wind, Ingenioren 2 (1985) 121.
2. G.R. Ludwig and T.R. Sundaram, On the laboratory simulation of small-scale atmospheric turbulence, CAL Report No VC-2741-S-1, 1969.
3. I.P. Castro and A.G. Robins, The flow around a surface mounted cube in uniform and turbulent stream, Journal of Fluid Mechanics 79 (1977) 307-335.
4. A. Hunt, Wind tunnel measurements of surface pressures on cubic building models at several scales, Journal of Wind Engineering and Industrial Aerodynamics 10 (1982) 137-163.
5. R.P. Hoxey and P.J. Richards, Appropriate boundary conditions for computational wind engineering models using the k-ε turbulence model, J. Wind Engineering and Industrial Aerodynamics, 46-47 (1993) 145-153.
6. R.P. Hoxey, A.P. Robertson and B.A. Younis, Geometric parameters that affect wind loads on low-rise buildings: full scale-and CFD experiments, J. Wind Engineering and Industrial Aerodynamics 50 (1993) 243-252.
7. R.P. Hoxey and P.J. Richards, Flow patterns and pressure field around a full-scale building, J. Wind Engineering and Industrial Aerodynamics 50 (1993) 203-212.
8. J.D. Holmes, Wind pressures on tropical housing, J. Wind Engineering and Industrial Aerodynamics 53 (1994) 105-123.
9. R.P. Hoxey and A.P. Robertson, Pressure coefficients for low-rise building envelopes derived from full-scale experiments, J. Wind Engineering and Industrial Aerodynamics 53 (1994) 283-297.
10. A.D. Ferreira, A.M.G. Lopes, D.X. Viegas and A.C.M. Sousa, Experimental and numerical simulation of flow around two-dimensional hills, J. Wind Engineering and Industrial Aerodynamics 54-55 (1995) 173-181.
11. R.P. Hoxey, A.P. Robertson and P.J. Richards, Design code, full-scale and numerical data for wind loads on free-standing walls, J. Wind Engineering and Industrial Aerodynamics 57 (1995) 203-214.

12. R.P. Hoxey and P.J. Richards, Full-scale wind load measurements point the way forward, J. Wind Engineering and Industrial Aerodynamics 57 (1995) 215-224.
13. R.P. Hoxey, A.P. Robertson, J.L. Short, W.A. Ferguson and S. Osmond, Full-scale testing to determine the wind loads on free-standing walls, J. Wind Engineering and Industrial Aerodynamics 60 (1996) 123-137.
14. Baskaran and A. Kashef, Investigation of air flow around buildings using computational fluid dynamics techniques, Engineering Structures 18 (1996) 861-875.
15. S. Murakami, Comparison of various turbulence models applied to a bluff body, J. Wind Engineering and Industrial Aerodynamics 46-47 (1993) 21-36.
16. S. Murakami, A. Mochida, R. Ooka, S. Kato and S. Iizuka, Numerical prediction of flow around a building with various turbulence models: comparison of k-ε EVM, ASM, DSM, and LES with wind tunnel test, ASHRAE Transactions 102 (1996) 741-753.
17. R.P. Selvam, Numerical simulation of flow and pressure around a building, ASHRAE Transaction 102 (1996) 765-772.
18. Y.S. Zhou and T. Stathopoulos, Application of two-layer methods for the evaluation of wind effects on a cubic building, ASHRAE Transaction 102 (1996) 754-764.
19. T. Fusegi, A computational study of turbulent diffusion in a thermally-stratified channel with obstruction, J. Wind Engineering and Industrial Aerodynamics 58 (1995) 19-32.
20. T. Stathopoulos and Y.S. Zhou, Computation of wind pressure on L-shaped buildings, Journal of Engineering Mechanics 119 (1993) 1526-1541.
21. T. Stathopoulos and B.A. Baskaran, Computer simulation of wind environmental conditions around buildings, Engineering Structures 18 (1996) 876-885.
22. S. Takakura, Y. Suyama and M. Aoyama, Numerical simulation of flow field around buildings in an urban area, J. Wind Engineering and Industrial Aerodynamics 46-47 (1993) 765-771.
23. G.E. Mattingly and E.F. Peters, Wind and trees: air infiltration effects on energy in housing, Journal of Industrial Aerodynamics 2 (1977) 1-19.

24. J. Gandemer, The aerodynamic characteristics of windbreaks, resulting in empirical design rules, J. Wind Engineering and Industrial Aerodynamics 7 (1981) 15-36.
25. J. D. Wilson, Numerical studies of flow through a windbreak, J. Wind Engineering and Industrial Aerodynamics 21 (1985) 119-154.
26. C.P. Crosby, E.H. Mathews and J.P. du Plessis, The numerical prediction of airflow through and around permeable windbreaks and over buildings, in Numerical Methods in Laminar and Turbulent Flow, Proceedings of the Sixth International Conference, Editors C. Taylor, P. Gresho, R.L. Sani and J. Hauser, Volume 6, Part 1, pp. 643-653, Pineridge Press, Swansea, UK, 1989.
27. J.K. Raine and D.C. Stevenson, Wind protection by model fences in a simulated atmospheric boundary layer, J. Wind Engineering and Industrial Aerodynamics 2 (1977) 159-180.
28. M. Jaeger and G. Dhatt, A k-ε finite element model for 3-D incompressible flows, in Numerical Methods in Laminar and Turbulent Flow, Proceedings of the Sixth International Conference, Editors C. Taylor, P. Gresho, R.L. Sani and J. Hauser, Volume 6, Part 1, pp. 259-327, Pineridge Press, Swansea, UK, 1989.
29. D. Delaunay, D. Lakehal and D. Pierrat, Numerical approach for wind loads prediction on buildings and structures, J. Wind Engineering and Industrial Aerodynamics 57 (1995) 307-321.
30. Y.S. Zhou and T. Stathopoulos, A new technique for the numerical simulation of wind flow around buildings, J. Wind Engineering and Industrial Aerodynamics 72 (1997) 137-147.
31. R.P. Selvam, Computation of pressures on Texas Tech Building, J. Wind Engineering and Industrial Aerodynamics 43 (1992) 1619-1627.
32. R.P. Selvam and D.A. Paterson, Computation of conductor drag coefficients, J. Wind Engineering and Industrial Aerodynamics 50 (1993) 1-8.
33. R.P. Selvam, Computation of flow around Texas Tech building using k-ε and Kato-Launder k-ε turbulence model, Engineering Structures 18 No. 11 (1996) 856-860.
34. Fluid Dynamics Analysis Package, FIDAP 7.0, Theory Manual, Fluid Dynamics International Inc., 1st ed., 1993.

35. P.M. Gresho and R.L. Sani, Incompressible Flow and the Finite Element Method, Advection-Diffusion and Isothermal Laminar Flow, John Wiley and Sons Ltd., Chichester, England, UK, 1998.
36. T.J.R. Hughes, Finite Elements in Fluids, Vol. 7, John Wiley and Sons Ltd., Chichester, England, 1988.
37. A. Harten and S. Osher, Uniformly High-Order Accurate Nonoscillatory Schemes, SIAM Journal on Numerical Analysis 24 No. 2 (1987) 279-309.
38. E. Onate and S.R. Idelsohn, A Comparison between Finite Element and Finite Volume Methods in CFD, Computational Fluid Dynamics Vol. 1, Editors Ch. Hirsch *et al.*, Elsevier Science Publishers B.V., 1992.
39. G.E. Schneider and M.J. Raw, A skewed, positive influence coefficient upwinding procedure for control-volume based-finite-element convection-diffusion computation, J. Numerical Heat Transfer 9 (1986) 1-26.
40. H.K. Versteeg and W. Malalasekera, An Introduction to Computational Fluid Dynamics: The Finite Volume Method, Longman Scientific & Technical, England, 1995.
41. P.M. Gresho and R.L. Lee, Don't suppress the wiggles-they're telling you something!, Computers and Fluids 9 (1981) 223-253.
42. B.P. Leonard, Survey of finite differences of opinion on numerical muddling of the incompressible defective-confusion equation, American Society of Mechanical Engineers, Applied Mechanics Division 34 (1979) 1-17.
43. Q.S. Li and W.H. Melbourne, Experimental investigation of the effects of free-stream turbulence on streamwise surface pressures in separated and reattaching flows, J. Wind Engineering and Industrial Aerodynamics 54-55 (1995) 313-323.
44. J. Wieringa, Updating the Davenport roughness classification, J. Wind Engineering and Industrial Aerodynamics 41-44 (1992) 357-368.

CHAPTER THREE

TWO-DIMENSIONAL MODEL

3.1 Model Validation

Model validation is very important when using computational fluid dynamics. The validation test must produce similar results using different kinds of packages and methods. As discussed in Chapter One, we do not know which parameters have been used in the design of traditional Balinese architecture in its relation to wind engineering, heat transfer and thermal comfort. However, there are many parameters that would influence the arrangement.

Several research projects have been carried out with isothermal conditions (uniform surface temperature) but only a few tried to perform simulations with uniform surface heat flux. For flow dominated heat transfer, the Nusselt number has a correlation with Reynolds and Prandtl numbers. For large Nusselt number with constant Reynolds number, the Prandtl number is also large, increasing the convective heat transfer coefficient. For this condition, the energy transfer will also be greater. So, the heat exchange between the building and its surroundings will also be greater. In reality of Balinese architecture, the condition is not isothermal and a surface heat flux has to be imposed to consider the solar radiation absorbed by building surfaces.

Second, the existence of turbulent flow can be advantageous in the sense of providing increased heat transfer rates. Since the motion is extremely complicated and difficult to describe theoretically, numerical solutions are the most popular to approach this flow. There are many numerical approaches to model turbulent flow so, to validate the model, the most popular numerical approach which is the k-ε model is adopted. Although this is a standard model, special boundary conditions should be used with reservations; for

instance, the computed suctions on surfaces may be underestimated near the windward edges.

Third, the numerical method to solve turbulent flow around traditional Balinese buildings is the finite element method. This numerical method can produce near-optimal approximate solutions to the initial-boundary value problem with a small approximation error.

Most researchers on bluff bodies give their results in terms of pressure loads. The influence of the wind on the building itself is not normally available. From the building arrangement, the maximum velocity that will occur should be taken into account. The maximum velocity is very important since it influences the heat transfer rate. Another important parameter is the pressure drop over the arrangement, which will be affected by the distance and the inter-building area. The model validation for a building will start from isothermal conditions, and will then be continued by a combination of isothermal and surface heat flux conditions.

3.2 Initial Tests

The initial simulation will be performed with a simple square obstacle as shown in Figure 3.1. Models of this building were presented by many researchers as discussed in Chapter Two.

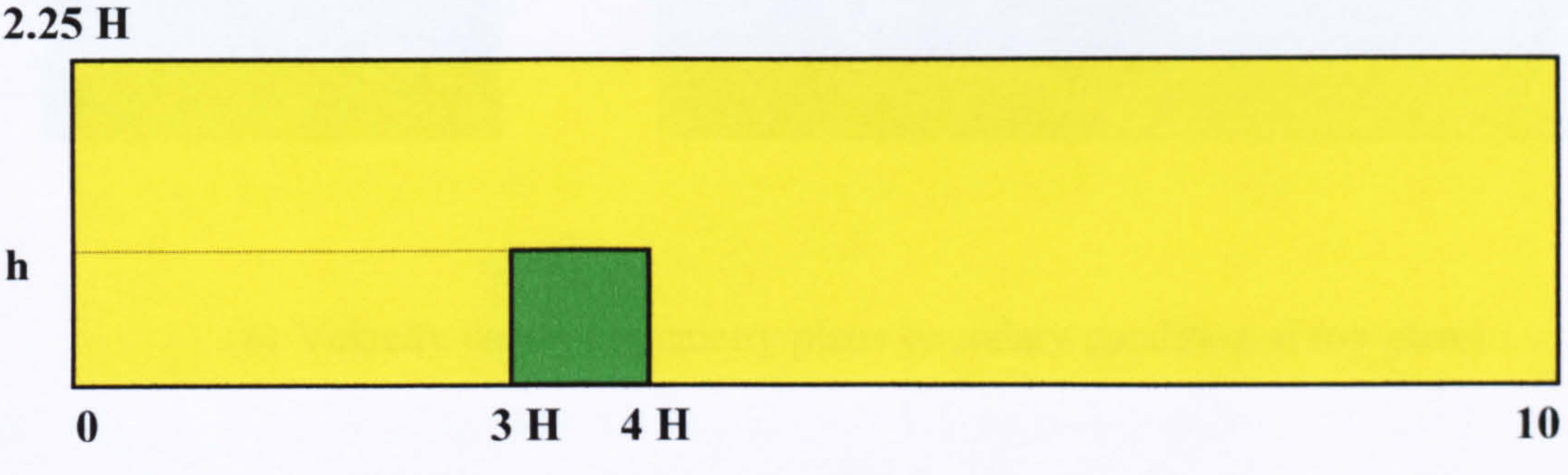

Figure 3.1 Physical description

3.2.1 Test of Boundary Condition at Upper Plate

To simulate atmospheric flow, the boundary condition at the upper plate plays an important role. A symmetry boundary condition is applied on the upper plate in order to take into account the fact that only a small portion of an infinite domain is being modelled. It seems that there is no difference for the flow pattern results between no-slip condition and symmetry plane on upper plate as presented in Figure 3.2.

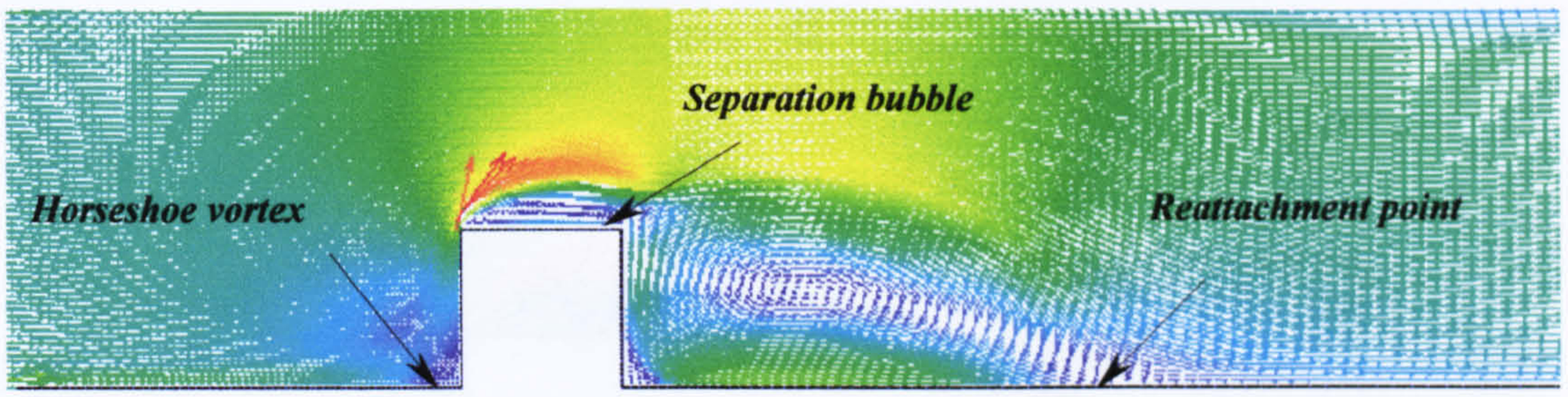

(a) Velocity vector (stationary boundary condition at top plate)

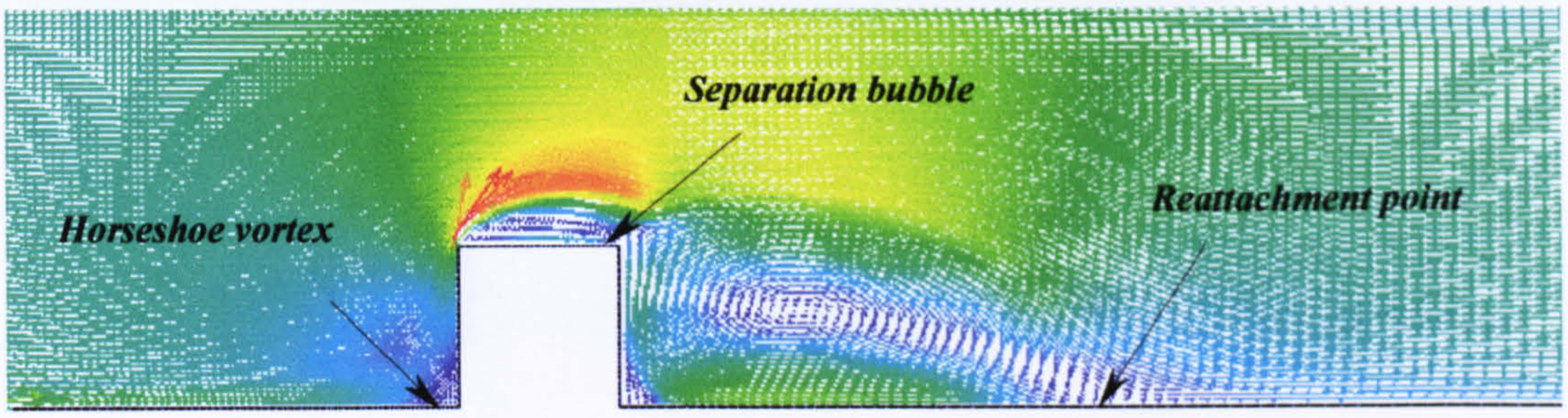

(b) Velocity vector (symmetry plane boundary condition at top plate)

Figure 3.2 Comparison between no slip boundary condition and symmetry plane at the upper plate

3.2.2 Test of Boundary Condition at Outlet

The boundary condition at the outlet is set to zero for pressure or vertical velocity. Since we assumed that the flow was fully developed at the inlet, first of all, we do not impose any boundary conditions at the outlet and the results are given as shown in Figure 3.2. The default condition at the outlet prescribed by Fidap is that all normal derivatives are zero (the so-called Neumann boundary condition). To better understand the influence of the boundary condition at the outlet, results for pressure set to zero are presented in Figure 3.3 and vertical velocity set to zero are presented in Figure 3.4.

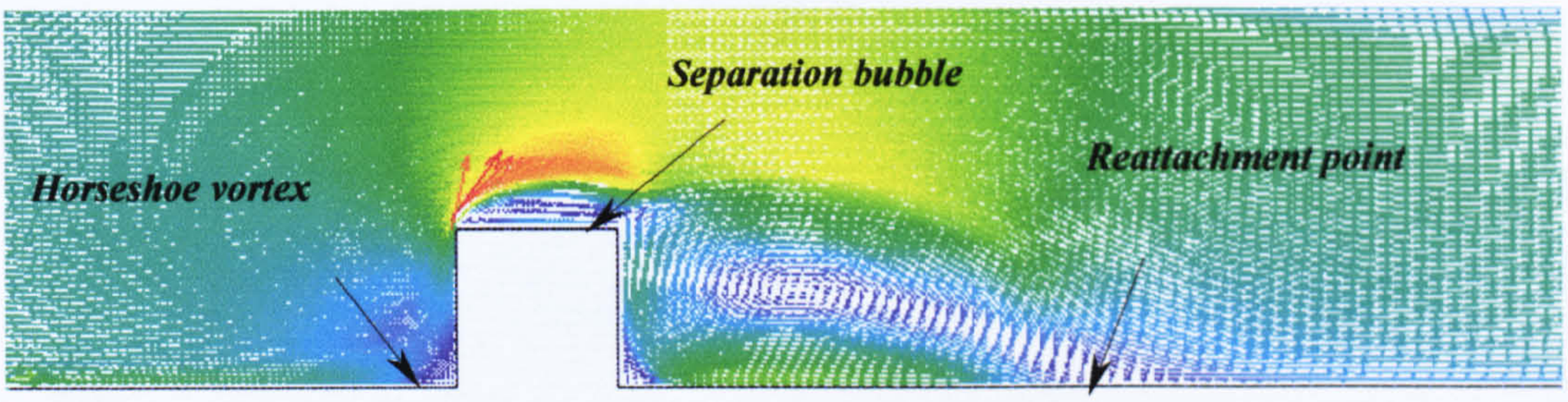

Figure 3.3 Result for zero pressure boundary condition at outlet

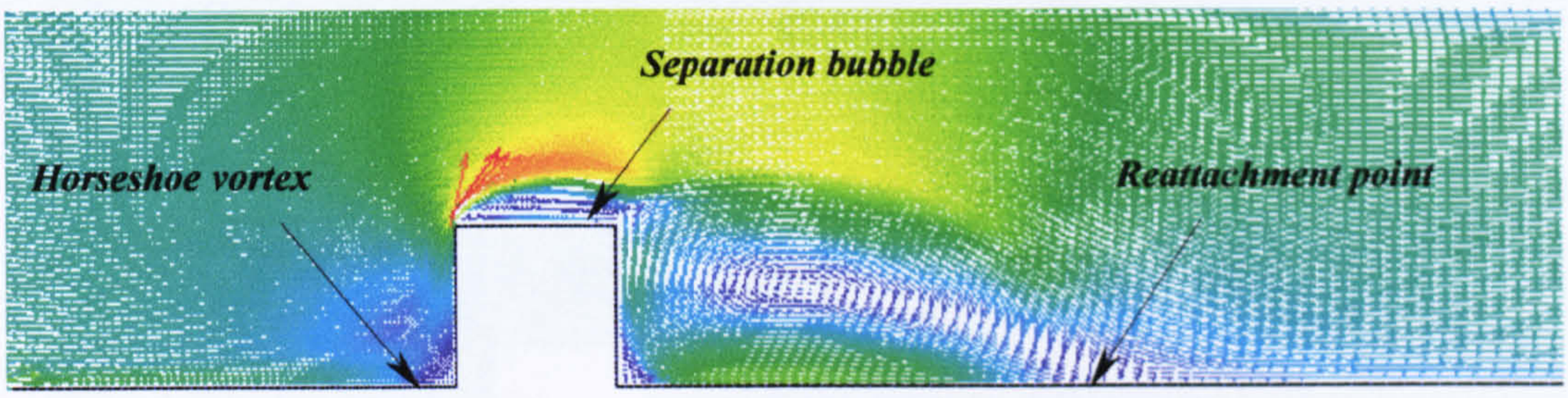

Figure 3.4 Result for zero vertical velocity boundary condition at outlet

From Figures 3.3 and 3.4 above, it seems that the boundary condition at the outlet does not have any effect on the results. The only difference is that the CPU time of these two boundary conditions at the outlet is a bit faster than when imposing the Neumann boundary condition.

3.2.3 Test of Tunnel Height

The flow is classified as external, thus the Reynolds number is computed based on the size of the object and not by the tunnel size. Since the position of the upper plate plays an important role on the model and to better understand about modelling by CFD, the distance between the plates (lower and upper plates) is now changed with reference to the step height of the obstacle. Results for this parameter variation are presented in Figures 3.5 to 3.7.

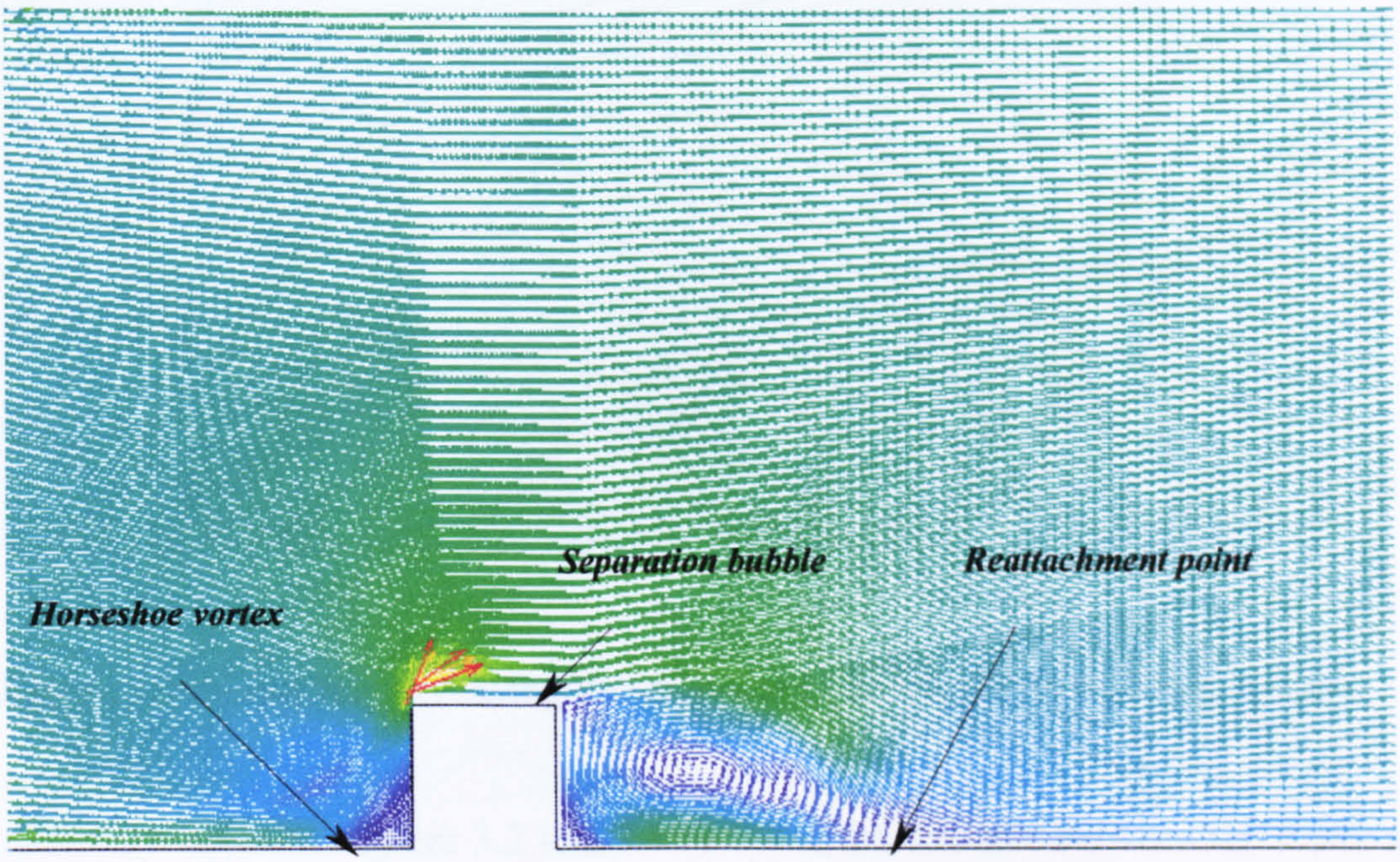

Figure 3.5 Result for increasing the distance between plates to 6 step heights

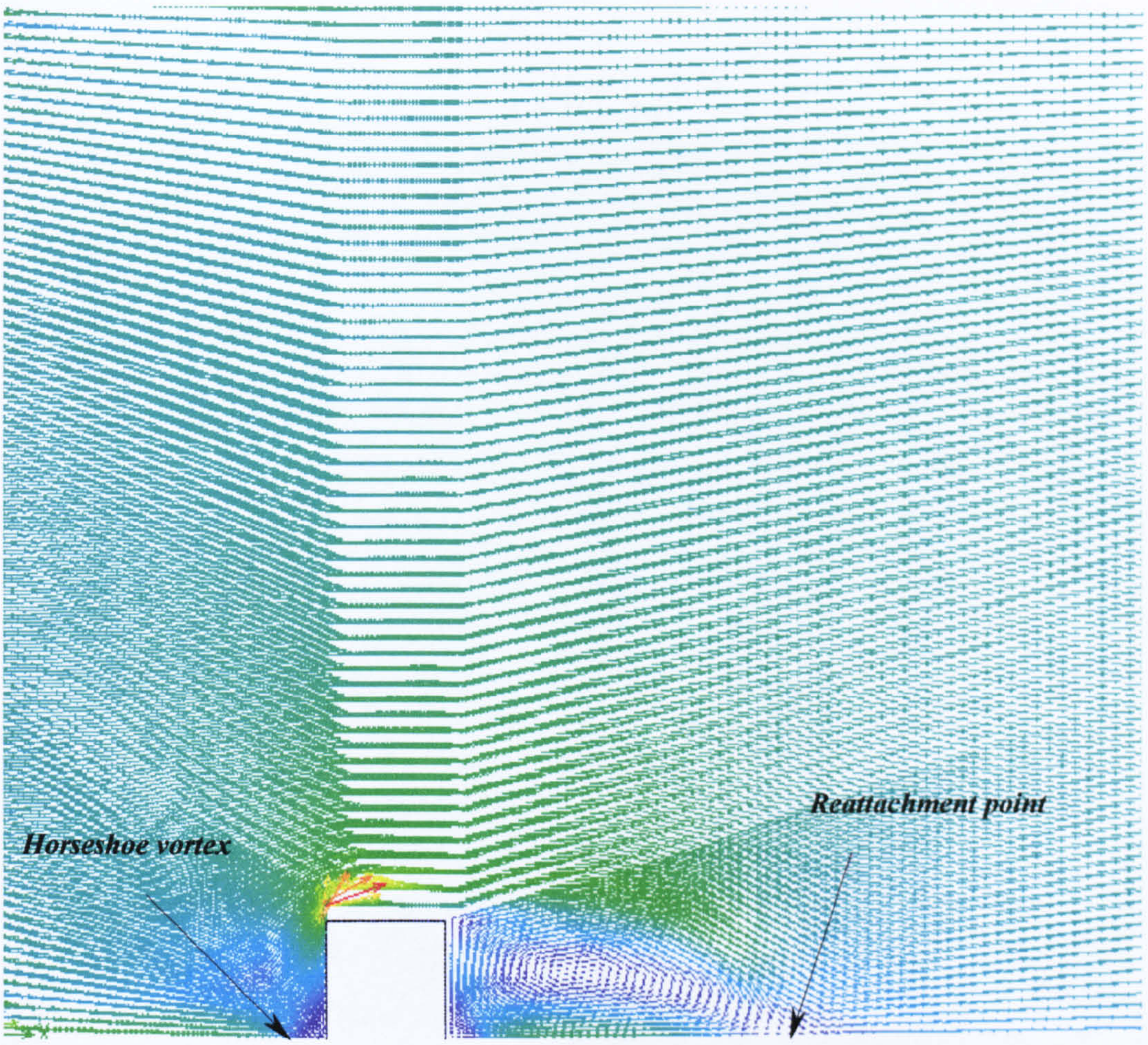

Figure 3.6 Result for increasing the distance between plates to 9 step heights

The difference between Figures 3.2 and 3.5 to 3.7 is the distance between the lower and upper plates. From the velocity vector it can be seen that the maximum velocity for all models occurs on the windward side of the obstacle, and re-circulation appears at the top and the leeward sides of the obstacle. Since the model in Figure 3.2 gives better results (*e.g.* separation bubbles at the top side is clearer) to that of Figures 3.5 to 3.7, it appears that a distance of 2.25 H between plates is considered on the next modelling.

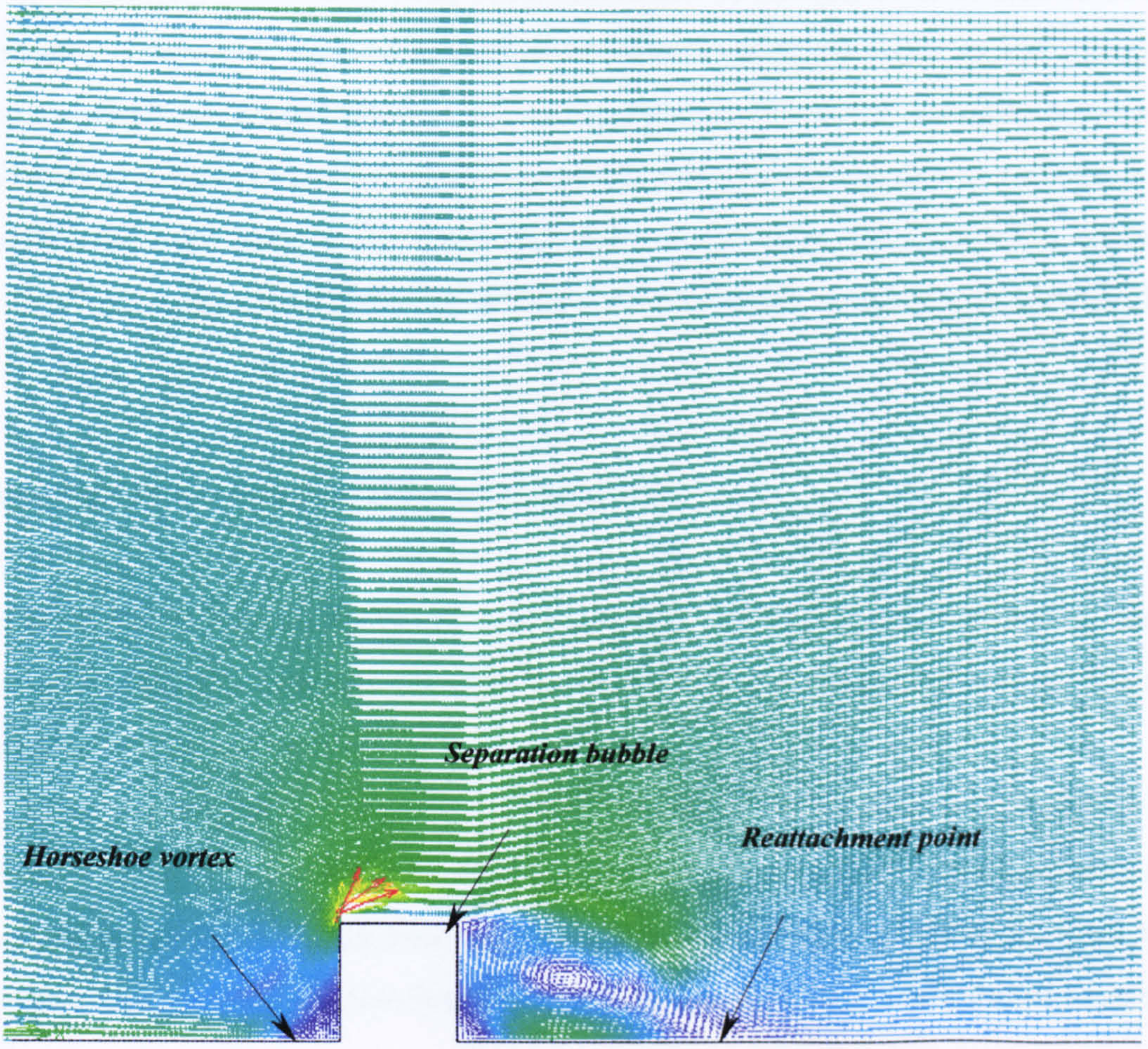

Figure 3.7 Result for increasing the distance between plates to 9 step heights (refining the mesh of Figure 3.6)

3.2.4 Test of k-ε Values

We now consider the properties of k and ε (turbulent kinetic energy and energy dissipation, respectively) and their boundary values which are imposed in the modelling.

In a turbulent flow, the velocity components can be thought of as a mean value and a fluctuating component, and such analysis produces additional terms in the momentum equation which can be modelled as additional stresses. There are analogies between the modification to the momentum equations and the energy equation due to turbulence. The velocity values are taken to be those that apply at the inlet, then the initial values are calculated from an assumed value of turbulence intensity (I), which ranges between 1 and 7%.

a. Multiplying the k and ε values by a thousand

Results shown in Figures 3.2 to 3.7 use low initial k and ε values or turbulent intensity around 1%. We now consider this value becomes 31%, for typhoon condition. The result changes as shown in Figure 3.8.

Increasing turbulent intensity value of 31% reduces the reattachment length by 31%. Therefore, there is a significant correlation between k-ε values and turbulent intensity. It notes that increasing turbulent intensity reduces the reattachment length by the same value. The horseshoe vortex at the windward side of the obstacle is larger than that in Figure 3.2.

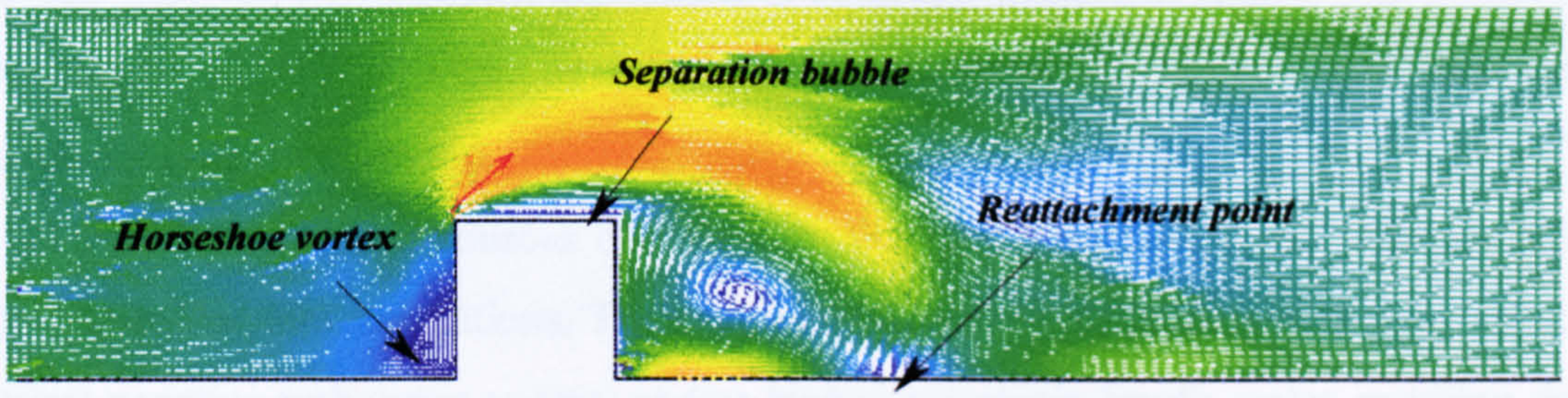

Figure 3.8 Result for initial values of k-ε multiplied by a thousand

This indicates that increasing turbulent intensity will increase the eddy vortex at the stagnation point but reduces the reattachment length at the separation region.

b. No imposed initial and boundary values

To better understand the influence of the initial values of k and ε, we now do not impose any initial or boundary conditions for k-ε at the inlet. Fidap produces default values for k and ε if no boundary values are imposed. These values are based on the inlet velocity and characteristic length scale of the flow. If no value is specified, the globally computed value of characteristic length scale is assumed by Fidap. A non-zero value of characteristic length scale overrides the global value. This creates a strange result, as can be seen in Figure 3.9.

From Figure 3.8, it can be seen that increasing the values of k and ε will reduce the maximum velocity, but imposing no boundary values will increase the maximum velocity. Increasing the values of k and ε will increase the velocity length scale and reduce the mixing length. This leads to reduced eddy viscosity and velocity at the stagnation point. The default boundary values created by Fidap generate results with increased mixing length and eddy viscosity, and lead to an increase in the maximum velocity at the stagnation point.

Figures 3.8 and 3.9 show that increasing a thousand times or imposing no boundary values of k-ε will reduce the flow pattern and reattachment length at the leeward side. This confirms that the default values created by Fidap are based on characteristic length scale and inlet velocity. The non-imposition of boundary conditions for k-ε will reduce the reattachment length by 44%, or the reattachment length is smaller than that when multiplying k-ε by a thousand.

There are two main sources of instability that if left untreated will seriously affect typical turbulent flow simulations. These instabilities manifest themselves in terms of non-physical negative turbulence values, and/or highly unrealistic length scales resulting from very small turbulence values in flow regions where turbulence levels have practically collapsed.

The first of these instabilities is associated with the dissipation (or sink) terms in the turbulence model equations. In the absence of these terms, k and ε levels will grow uncontrollably (and exponentially) due to the generation (or source) terms of the k and ε equations. These negative values are unstable since they change the polarity of some important processes in the k and ε equations. If the turbulent viscosity becomes negative, it will cause highly unstable negative diffusion, the source and sink terms will change polarity (*e.g.* the turbulent generation terms) instead of extracting turbulence energy from the mean flow process and will extract energy from the turbulence field and relate it to the mean flow.

The second source of instability arises when the k-ε model is used in the prediction of flows containing both turbulent and laminar regions. A typical example of this is in external aerodynamic problems where the free-stream flow is not fully turbulent but the flow surrounding the body is fully turbulent. The k and ε equations of the standard high-Reynolds-number k-ε turbulence model become anomalous in the turbulence-free regions. This will affect the numerical stability of the computation, since this unstable behaviour quickly spreads to the fully turbulent flow regions and in a matter of a few iterations totally contaminates the numerical solution. This leads to reducing eddy viscosity and reattachment length at the leeward side of building.

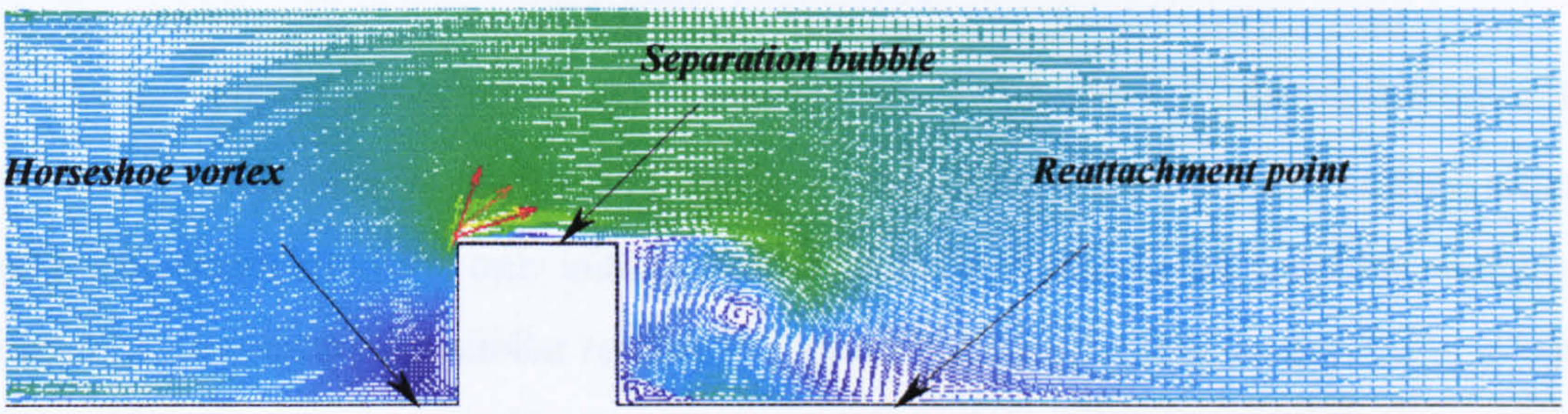

Figure 3.9 Result without imposing initial and boundary condition values of k-ε

To avoid the instabilities described above, streamline upwinding should be introduced. Streamline upwinding is a numerical technique which introduces stabilising

false numerical diffusion along the streamwise direction. This technique helps to suppress the streamwise oscillations in the various flow variables (including k and ε) that occur in advection dominated flow regions.

c. No boundary values of k-ε, initial values the same as in Figures 3.2 to 3.7

We now consider a simulation with no boundary values of k and ε but imposing their initial values to be the same as in Figures 3.2 to 3.7. This is important since we want to ensure that both initial and boundary values in Figures 3.2 to 3.7 are satisfactory. The results of this simulation are presented in Figure 3.10 and depict the same results to that of Figures 3.2 to 3.7.

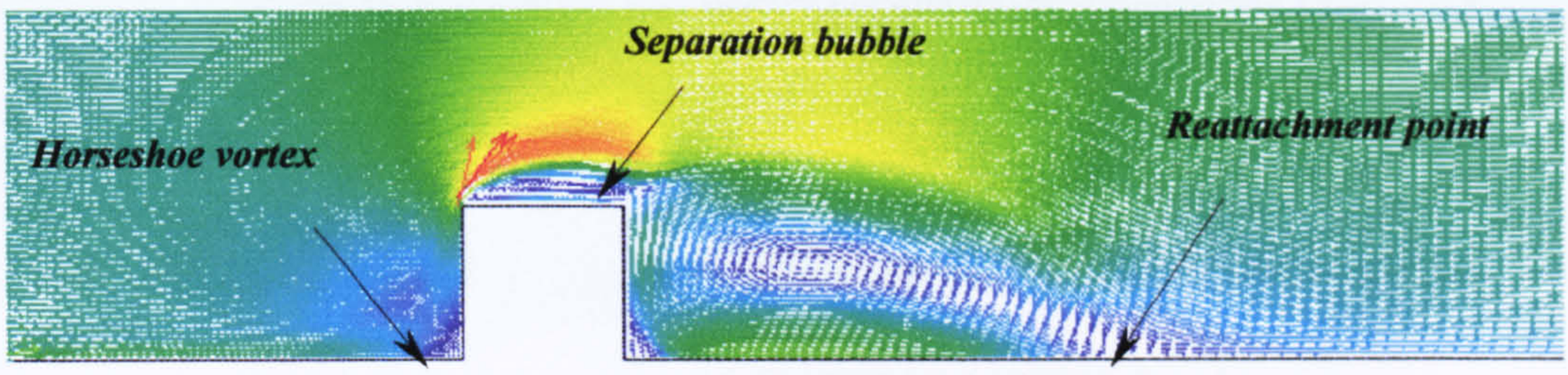

Figure 3.10 Result for no boundary value of k-ε but initial condition the same as in Figures 3.2 to 3.7

The non-imposition of initial and boundary values of k and ε, as shown in Figure 3.9, gives very strange results. Multiplying the k-ε values by a thousand also gives strange results. But, when imposing only initial values of k and ε similar to the previous ones (as in Figure 3.2), the results are similar to that in Figures 3.2 to 3.7. This indicates that if initial values of k and ε are very small, adequate boundary values will be created by Fidap based on the inlet velocity. This condition will produce very low velocity length scale but increased mixing length, and leads to an increase in the reattachment length, similar to that in Figure 3.2.

d. Both initial and boundary values reduced by a thousand

To verify if the previous values (Figures 3.2 to 3.7) are still satisfied, we now consider reducing the initial and boundary values of k-ε by a thousand. Results for this simulation are presented in Figure 3.11.

Here we note that both initial and boundary conditions of k-ε play important roles in the modelling and are different from other physical properties. Since reducing both k-ε values by a thousand does not change the results, this also indicates that the values which have been imposed in Figures 3.2 to 3.7 are satisfactory. From all of the models, the reattachment length from Figures 3.2 to 3.12 changes by around 40%.

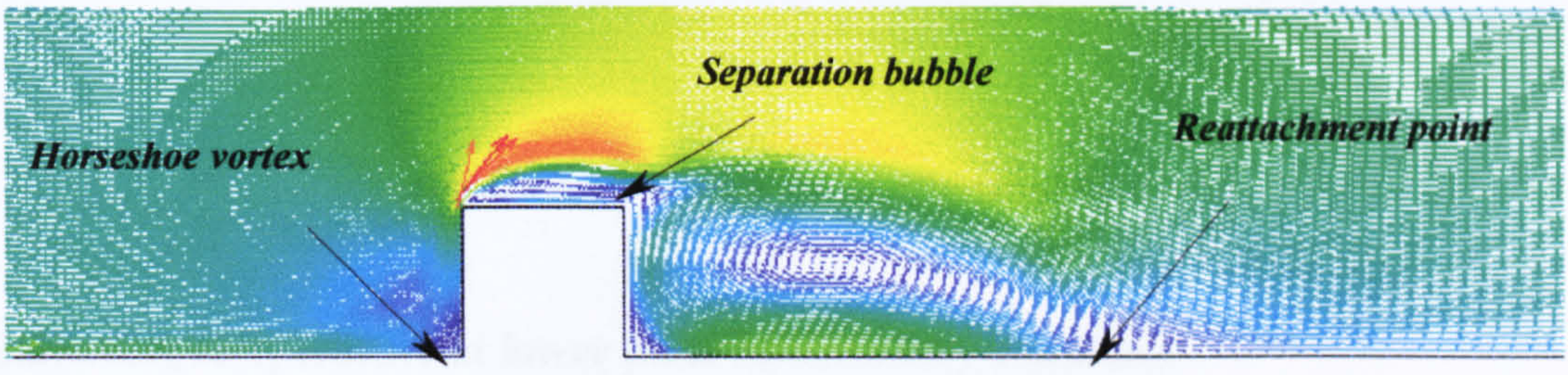

Figure 3.11 Result for k-ε values of Fig. 3.2 reduced by a thousand

3.2.5 Test of Temperature and Heat Flux Boundary Conditions

When modelling incompressible viscous flow, momentum and continuity equations are used to calculate the velocity components and the static pressure of the fluid. The relation between the flow variables and a property related to the heat flow in the fluid is important, and is obtained by using an energy equation derived from the first law of thermodynamics.

a. Isothermal flow

For isothermal flow, the velocity field does not seem to be influenced by temperature since the results of isothermal flow as presented in Figure 3.12 are more or less the same as that of Figure 3.2.

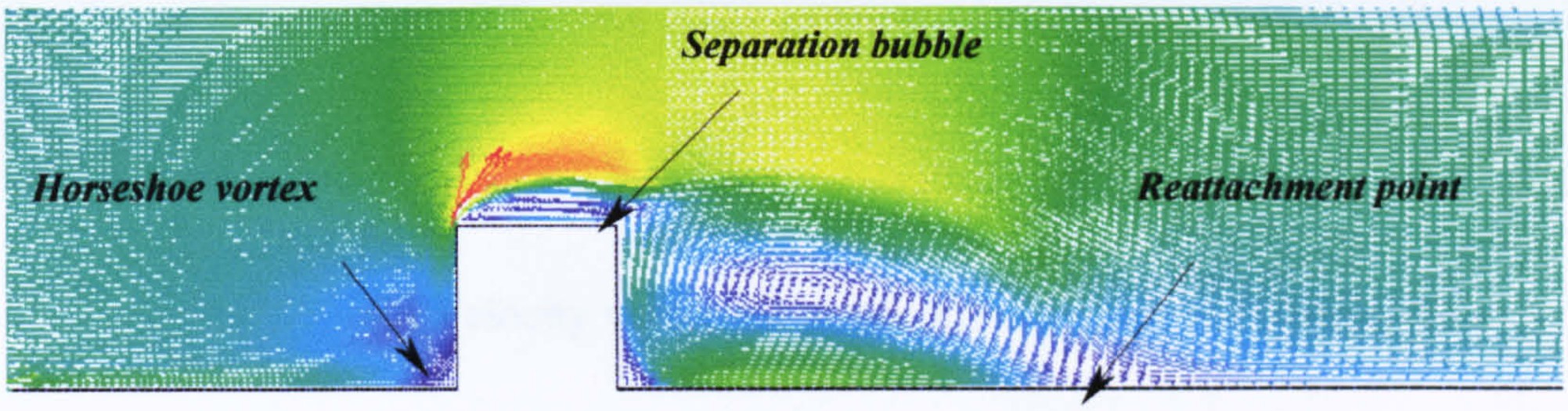

Figure 3.12 Result for isothermal flow

b. Imposing temperature at lower plate as boundary condition

Now, we assume T is not zero at y = 0 and T is the same as at the inlet at y = h. By applying this boundary condition, the results are more or less the same to that in isothermal condition. If physical properties of the fluid depend on the temperature, we notice here that the flow pattern is affected by the Peclet number (Re * Pr). Since physical properties of the fluid do not change, then the flow pattern with heat at the bottom plate is the same as isothermal flow, as shown in Figure 3.13.

Prandtl's analogy states that the fluid temperature is related to the flow velocity and some physical properties of the fluid (or Peclet number). It can be seen that temperature distribution descends at the separation region, but after reattachment point, the free-stream temperature tends to ascending. The boundary conditions are likely to be the specification of the temperature on a boundary or the specification of the normal derivative of temperature. In some circumstances these will be known directly, but often heat fluxes will have to be found from experimental data. Prandtl's and Reynolds' analogies are valid in

the region of thermal and velocity boundary layers. After these layers, the temperature will match that at the inlet.

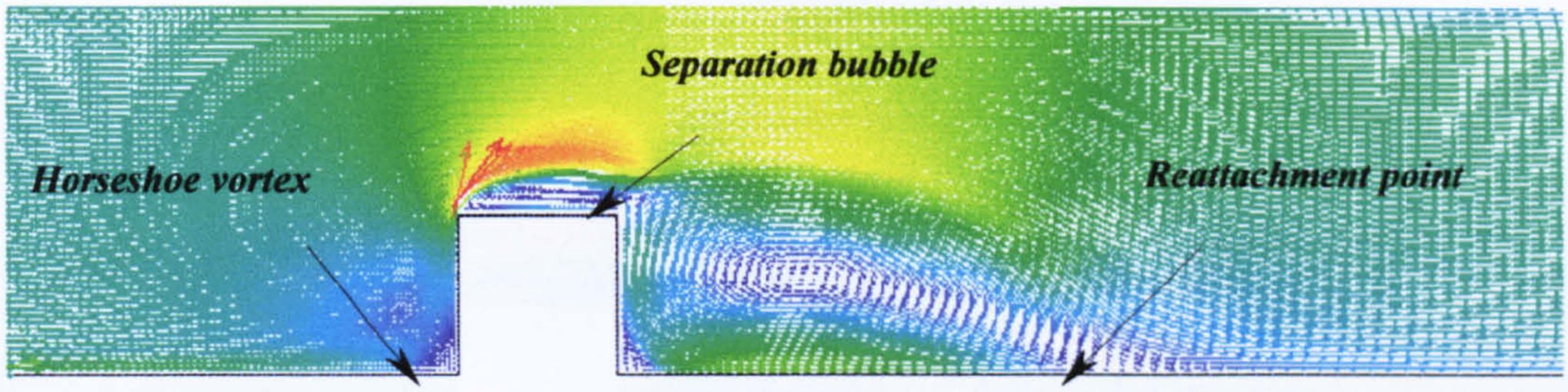

(a) Velocity vector for temperature imposed at bottom plate

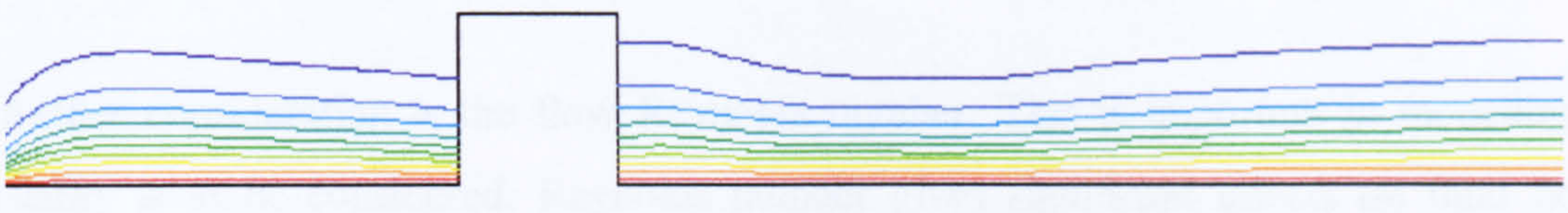

(b) Temperature plot for temperature imposed at bottom plate

Figure 3.13 Several views for temperature constant at bottom plate

c. Imposing constant heat flux at the obstacle as boundary condition

Since in the real case the condition is not isothermal, we now consider a constant surface heat flux imposed on the obstacle. Results of this condition are shown in Figure 3.14.

From the results shown in Figures 3.13 and 3.14 we note that there is no difference between isothermal and surface heat flux on the flow pattern. Comparing the results above, we suggest that one known parameter (temperature or surface heat flux) can be

used on the modelling and it will produce a valid (and similar) result. But, if temperature and surface heat flux are known at different surfaces, it is better to impose both parameters on the simulation.

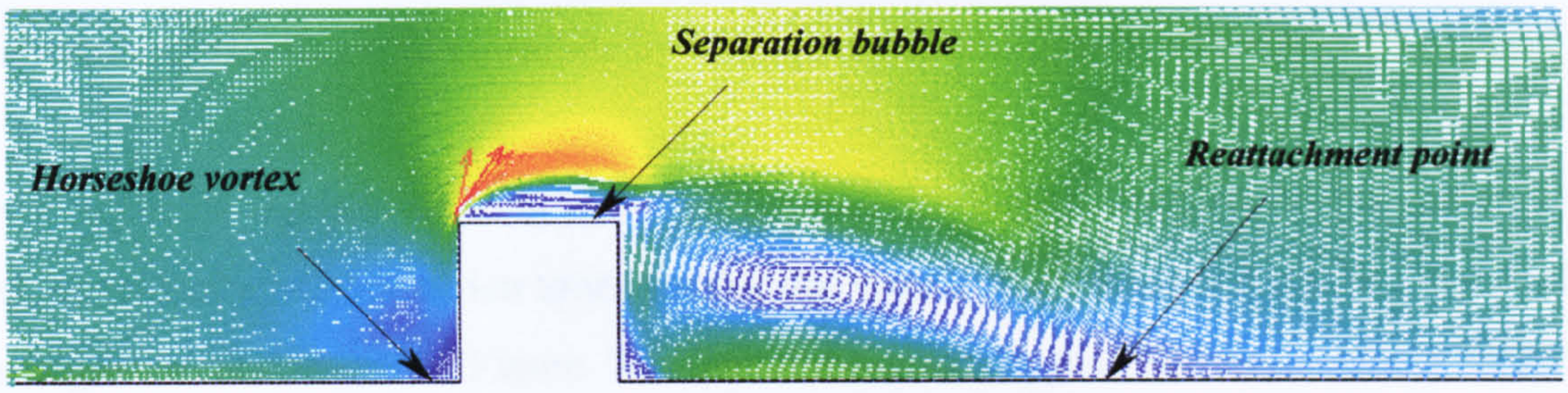

Figure 3.14 Result for constant surface heat flux at the object

3.2.6 Test of Reynolds Number

A further consideration is the flow Reynolds number. This is important in modelling if similarity is to be considered. Reynolds number gives significant effects on fluid flow, especially on scale-model.

a. Reducing the Reynolds number by decreasing the velocity

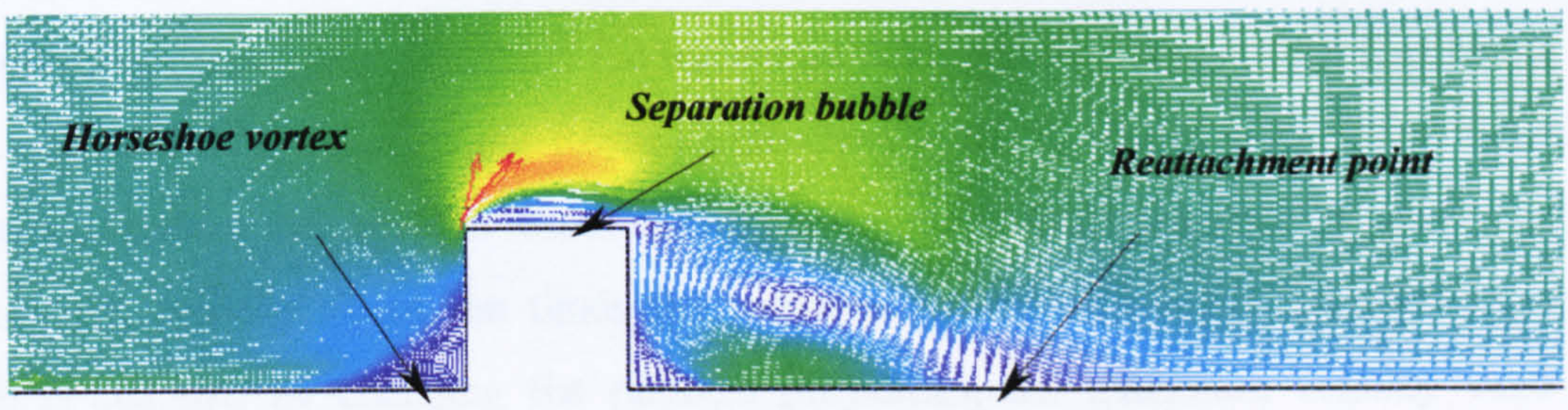

Figure 3.15 Result for Reynolds number decreased by ten

For a Reynolds number reduced by ten (velocity decreased by a factor of ten), the static pressure decreases a hundred times ($p = \frac{1}{2}\rho v^2$) compared to the previous result (Figure 3.2). An important result is that the reattachment length is about 3/4 of the previous value (Figure 3.2), as shown in Figure 3.15.

b. Increasing the Reynolds number by changing the physical properties

For a Reynolds number which is increased by ten (multiplying the physical properties by ten), the velocity will not be ten times greater and the static pressure will not be a hundred times greater than those in Figure 3.2. The main result is that the reattachment length increases by about 17 % of the previous result (Figure 3.2) as presented in Figure 3.16.

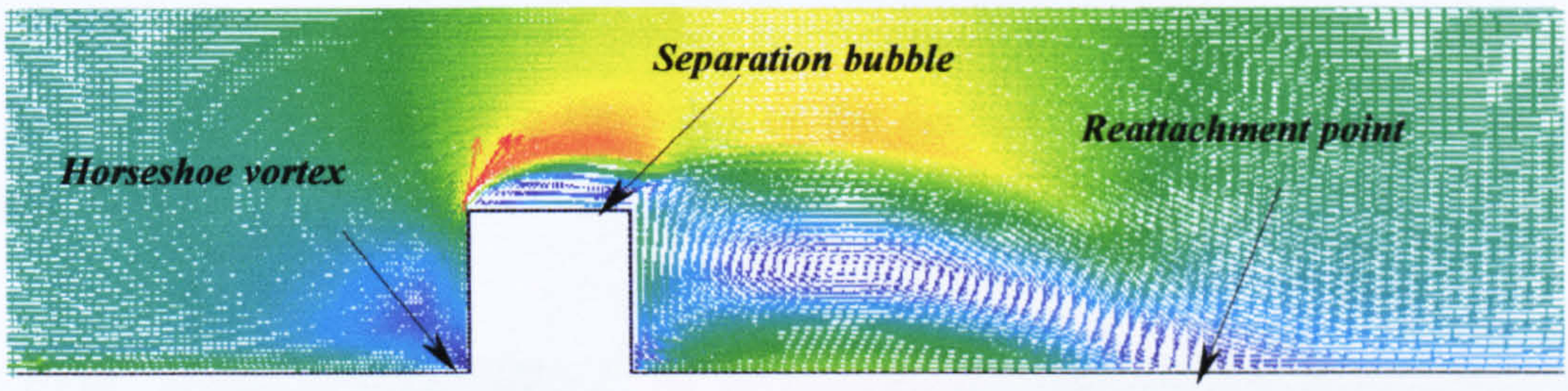

Figure 3.16 Result for Reynolds number multiplied by ten

From the results shown in Figures 3.2, 3.15 and 3.16 we note that if the Reynolds number is changed by changing the velocity, the maximum velocity value depends on the change of scale being used (*e.g.* decreasing Reynolds number by ten produces a maximum velocity about one tenth of the previous result, and in reverse condition, increasing by ten produces a maximum velocity about ten times the previous result). But for a Reynolds number which is changed by changing the physical properties, the maximum velocity value is independent of the change of scale being used (*e.g.* increasing Reynolds number by multiplying the physical properties -and keeping the velocity constant- the maximum

velocity does not change by the scale factor being used, but remains similar to the previous result).

3.2.7 Test of Roughness Factor

The main idea of this test is to improve the heat exchange between the building surface and its surrounding. The amount of heat exchange between the building surface and its surrounding is affected by the building surface condition. The smoother the surface, the lower the heat exchange between the surface and its ambient is. In reverse, the rougher the surface, the greater its heat exchange is. Although we know that a rougher surface will produce a greater heat exchange, for an external flow, the surface roughness should have an optimum value in order to optimise heat exchange. To prove this hypothesis, the effects of surface roughness are now considered on the simulation. Results of imposing a value of 5% of the obstacle height for the surface roughness on the building surface are presented in Figure 3.17, and increasing the value of the surface roughness coefficient by ten in Figure 3.18.

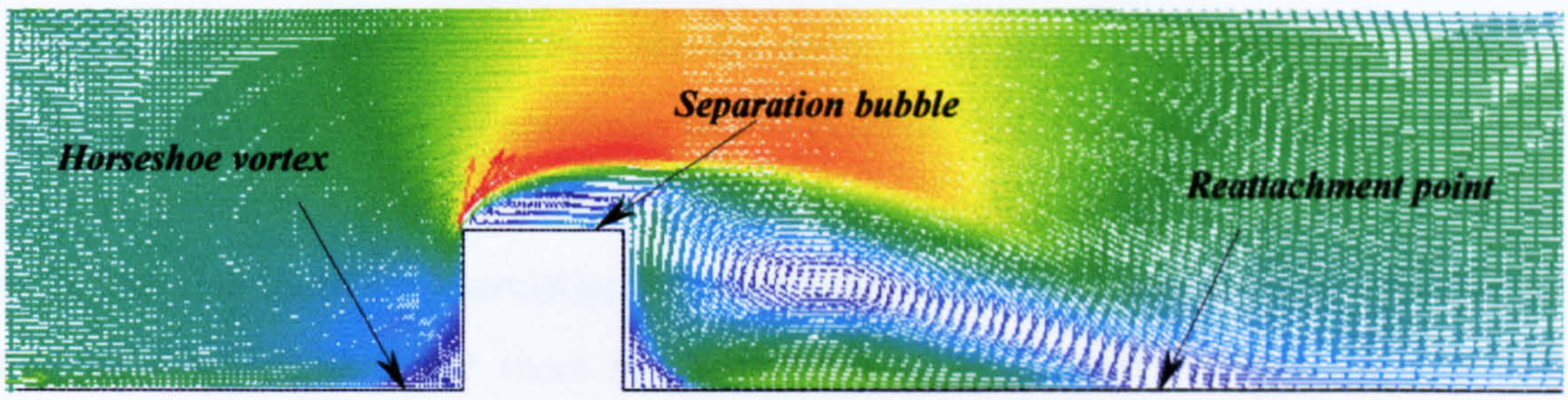

Figure 3.17 Result for imposing surface roughness on building surface

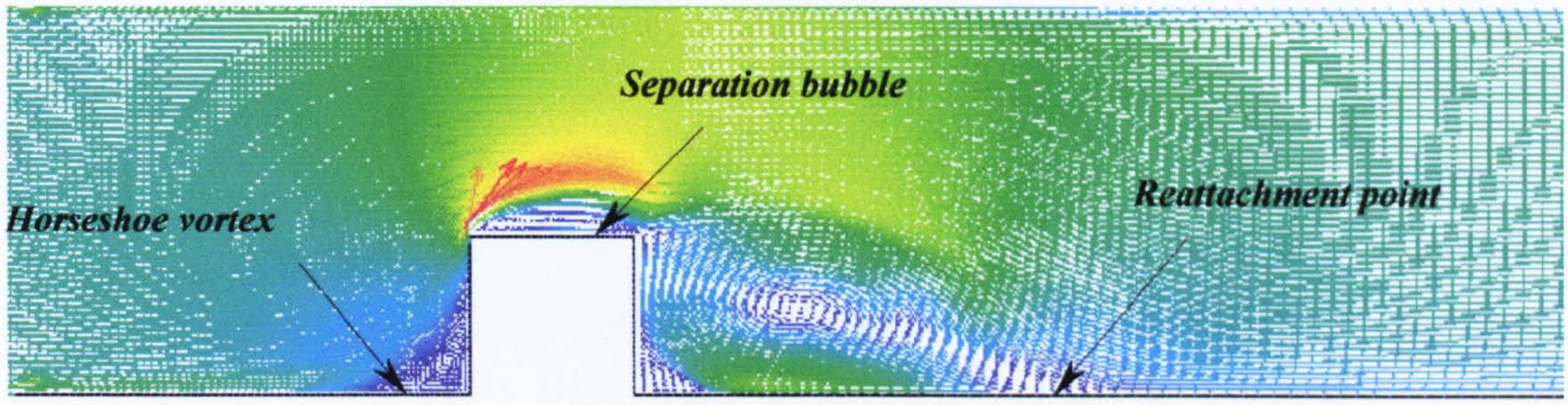

Figure 3.18 Result for imposing surface roughness on building surface (multiplied by ten)

From Figure 3.17 it can be seen that imposing surface roughness on building surface will increase the maximum velocity, pressure distribution and reattachment length. It indicates that the flow over the building increases and the heat transfer between the building surface and its surrounding also increases. But, increasing the value of surface roughness does not always increase the maximum velocity, as shown in Figure 3.18. In other words, increasing the value of surface roughness does not always increase the heat transfer between the building surface and its surrounding since heat transfer depends on velocity. This agrees with our hypothesis that in external flow there is an optimum value of surface roughness in order to obtain the optimum heat exchange. However, this initial test gives an idea that there is a correlation between the surface roughness and the velocity and reattachment length, and that there is a maximum value of surface roughness that will increase the heat exchange between the building and its surrounding.

So far, only a rectangular block has been tested but it gives many ideas for the next step of the simulation. The standard k-ε turbulence model was used in this simulation since it is possible to compare results with other published researches. For a rectangular obstacle, the main result that can be compared is the pressure distribution on the building surface. The drawback of this comparison is that none of the researchers give the physical properties of their simulation. From our simulation, it can be seen that different results are obtained for different conditions. For instance, for the same Reynolds number it appears

that the results vary depending on the parameters being used (*e.g.* results for different k-ε properties varies with the same Reynolds number).

In Figure 3.19 (g), it can be seen that all experimental pressure coefficients are very high at the top side of the windward face. The numerical results show a pressure coefficient at this corner close to that near the ground. The experimental results shown here are based on three-dimensional problems, the same as Zhou and Stathopoulos [1] who use LES on their transient simulation. This indicates that the geometry does affect the pressure coefficient, especially at the windward corner. Pressure coefficient of three-dimensional problem along the centre lines (45^0 azimuth) is similar to two-dimensional. At the top side of the obstacle, the pressure coefficient is nearly the same for all researches. At the leeward side, the pressure coefficient for all models tends to the same value, around -0.2 [2, 3, 4, 5, 6 and 7].

Another important result that can be compared is the reattachment length at the leeward side of the obstacle. Again, the same Reynolds number did not give the same reattachment length. As presented by Ruck [8], imposing different boundary conditions also changes the reattachment length. For isothermal flow, the present results can be compared to Qasim *et al* [9], and for several turbulent conditions this can be compared to Zhang *et al* [10].

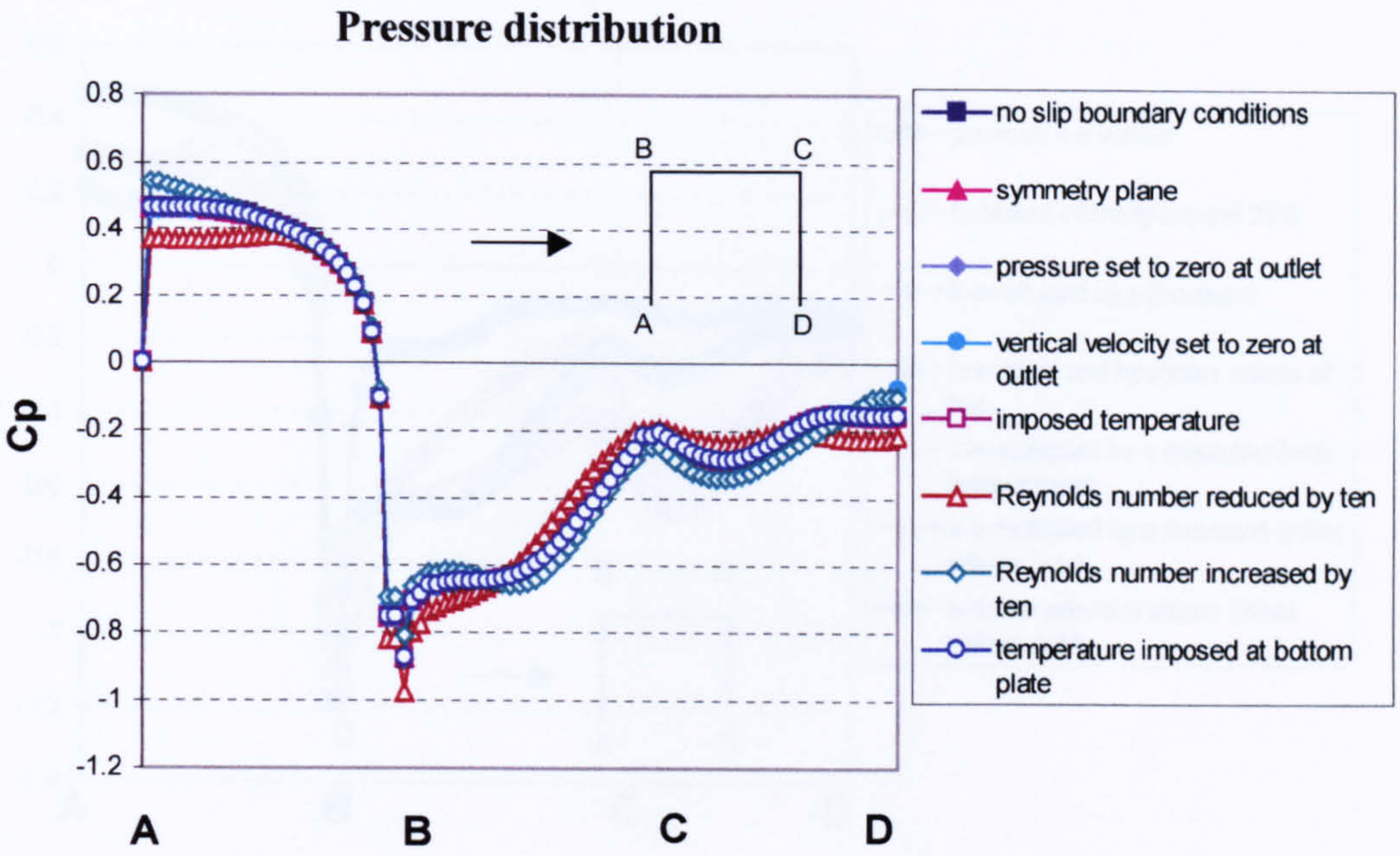
Pressure distribution
0.8
0.6
0.4
0.2
0
-0.2
-0.4
-0.6
-0.8
-1
-1.2
Cp
A
B
C
D
no slip boundary conditions
symmetry plane
pressure set to zero at outlet
vertical velocity set to zero at outlet
imposed temperature
Reynolds number reduced by ten
Reynolds number increased by ten
temperature imposed at bottom plate

(a)

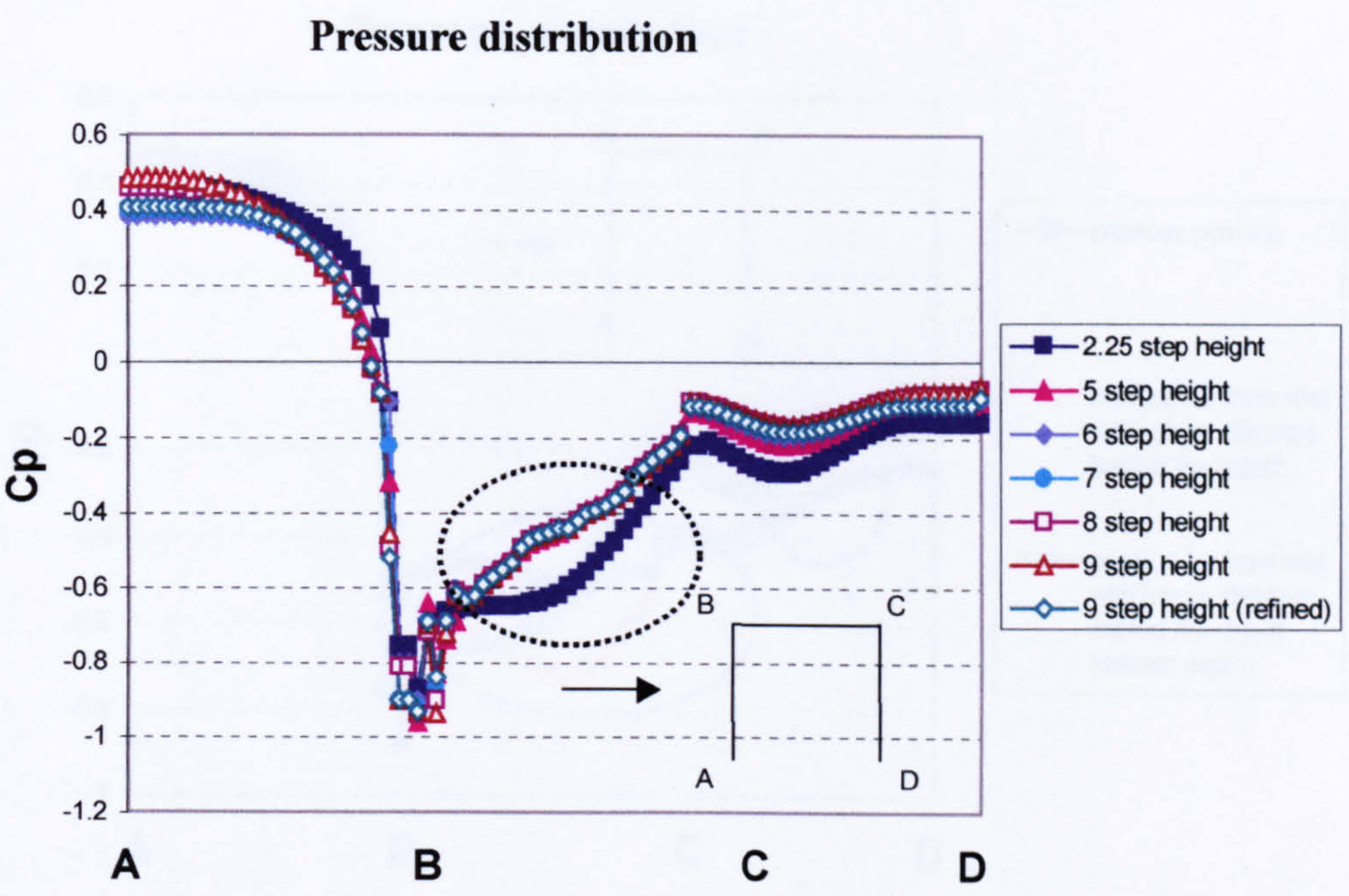
Pressure distribution
0.6
0.4
0.2
0
-0.2
-0.4
-0.6
-0.8
-1
-1.2
Cp
A
B
C
D
2.25 step height
5 step height
6 step height
7 step height
8 step height
9 step height
9 step height (refined)

(b)

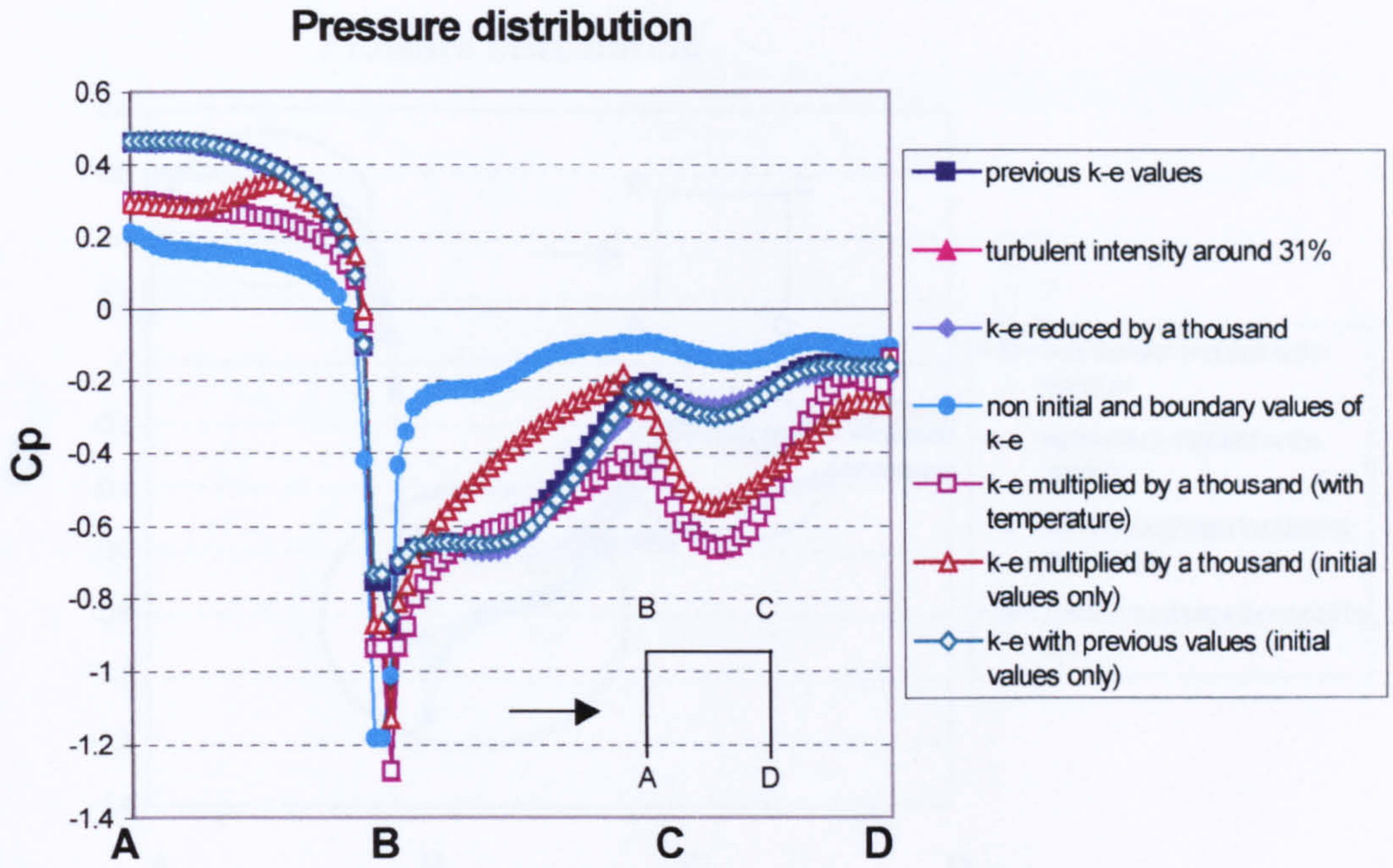
Pressure distribution
Cp
0.6
0.4
0.2
0
-0.2
-0.4
-0.6
-0.8
-1
-1.2
-1.4
A
B
C
D
previous k-e values
turbulent intensity around 31%
k-e reduced by a thousand
non initial and boundary values of k-e
k-e multiplied by a thousand (with temperature)
k-e multiplied by a thousand (initial values only)
k-e with previous values (initial values only)

(c)

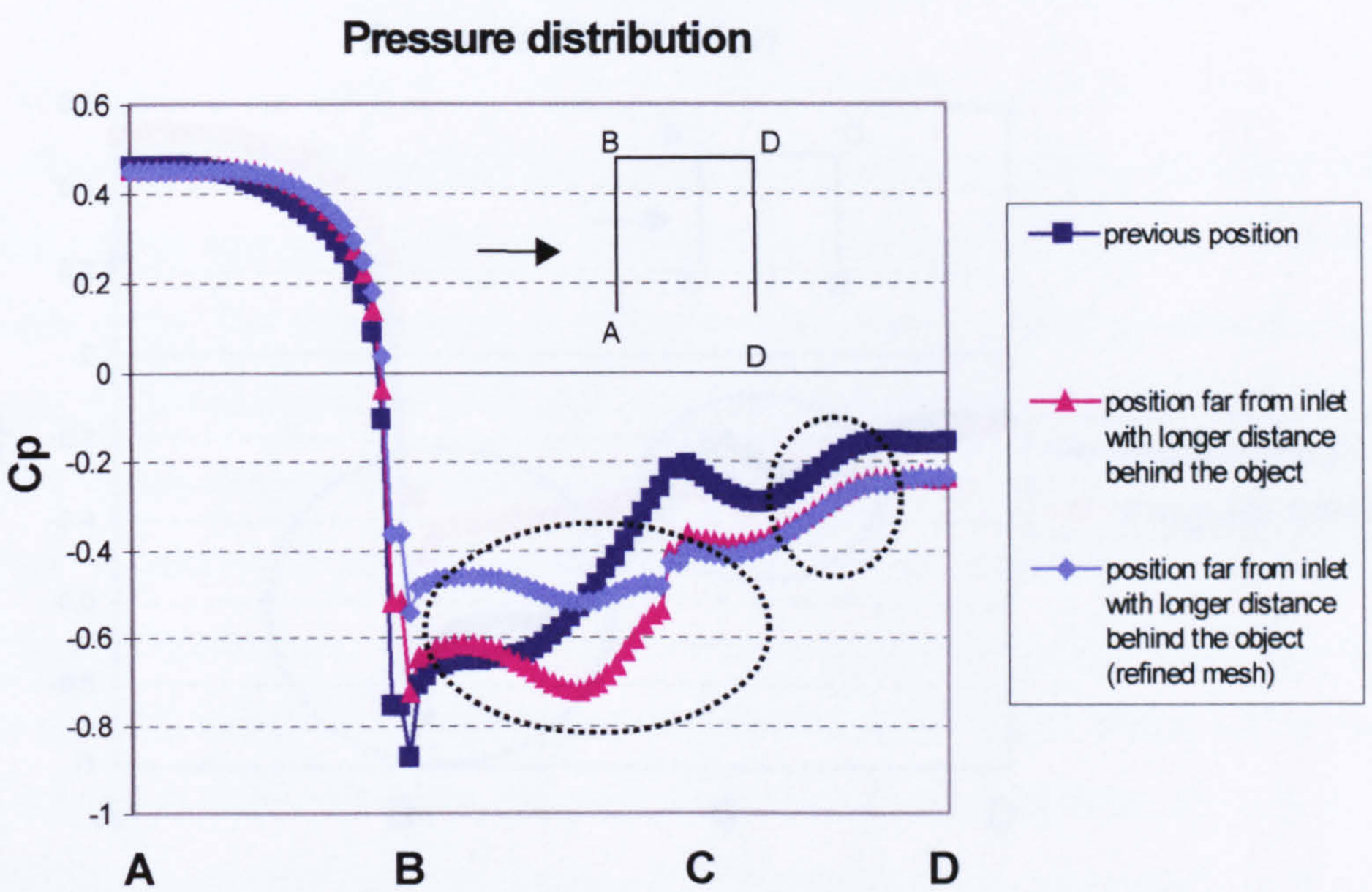
Pressure distribution
Cp
0.6
0.4
0.2
0
-0.2
-0.4
-0.6
-0.8
-1
A
B
C
D
previous position
position far from inlet with longer distance behind the object
position far from inlet with longer distance behind the object (refined mesh)

(d)

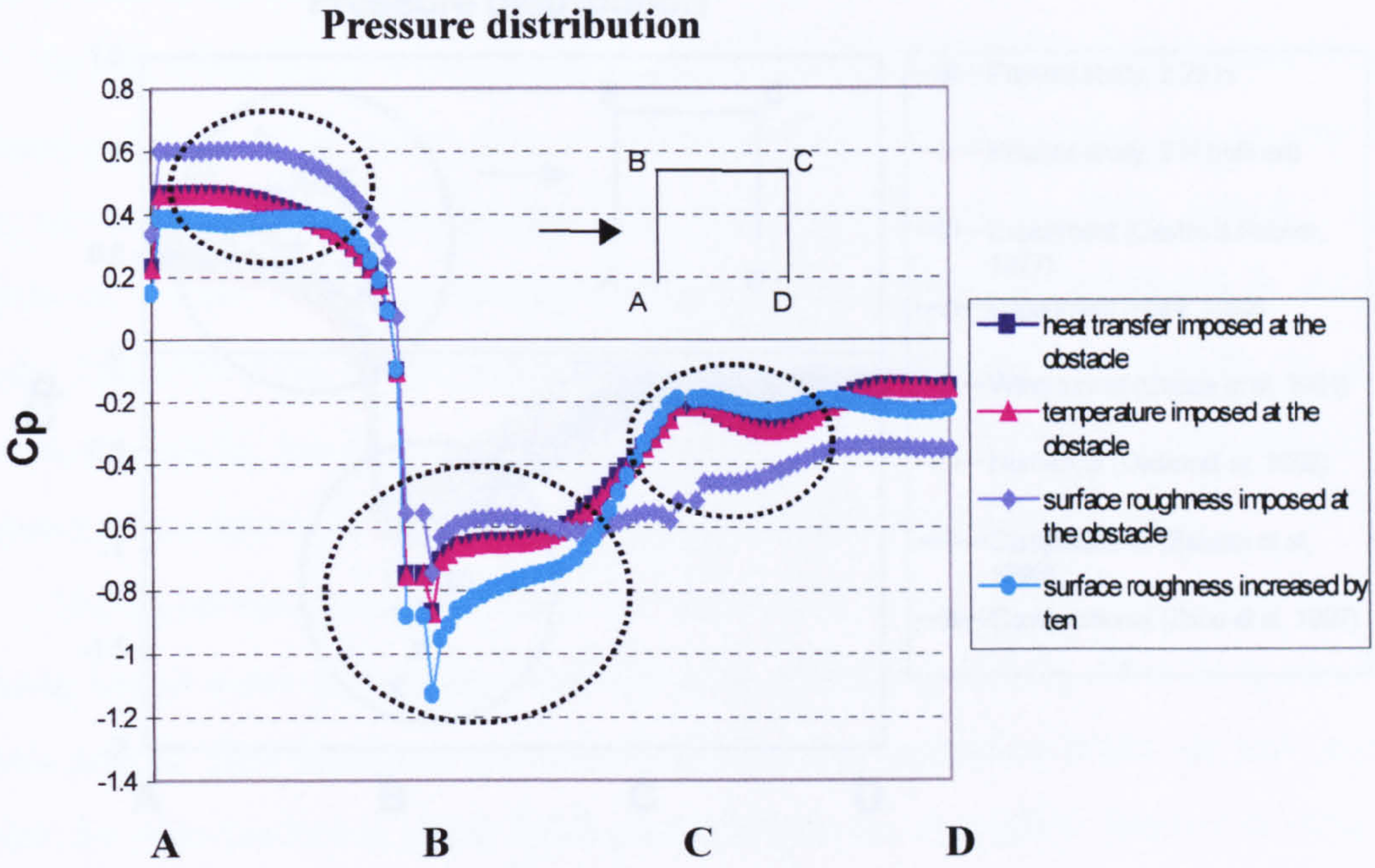
Pressure distribution
Cp
0.8
0.6
0.4
0.2
0
-0.2
-0.4
-0.6
-0.8
-1
-1.2
-1.4
A
B
C
D
heat transfer imposed at the obstacle
temperature imposed at the obstacle
surface roughness imposed at the obstacle
surface roughness increased by ten

(e)

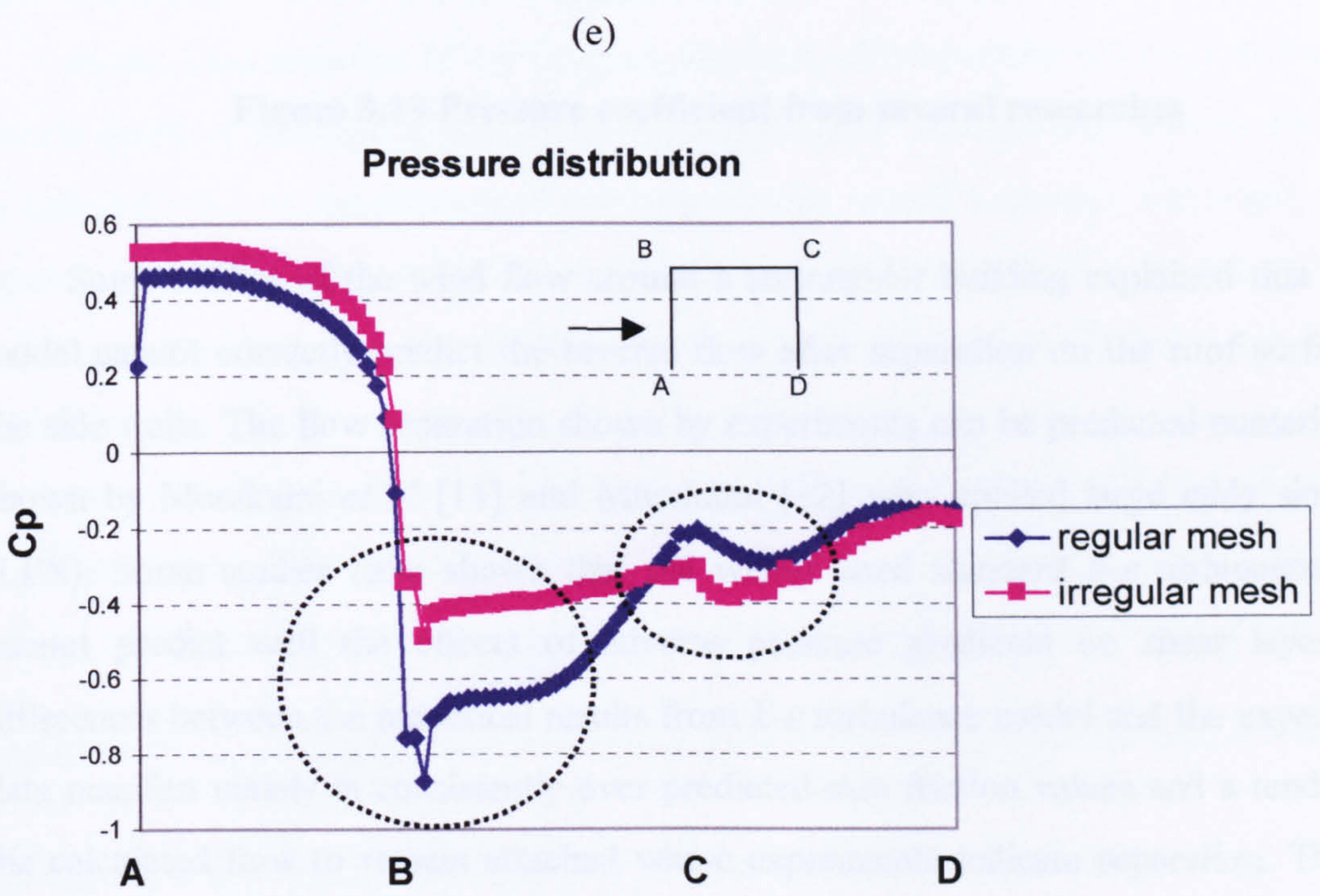
Pressure distribution
Cp
0.6
0.4
0.2
0
-0.2
-0.4
-0.6
-0.8
-1
A
B
C
D
regular mesh
irregular mesh

(f)

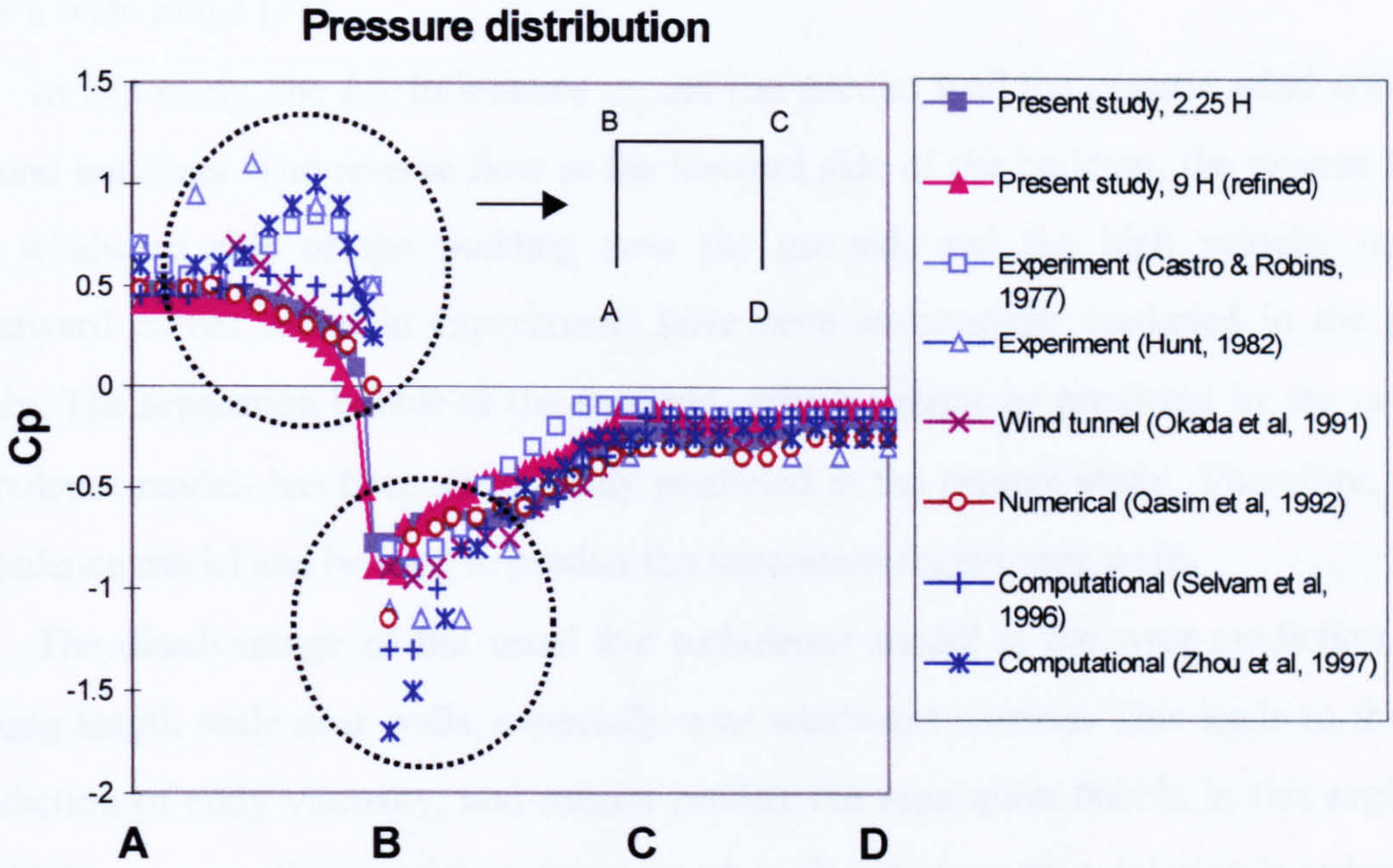

(g)

Figure 3.19 Pressure coefficient from several researches

Some studies of the wind flow around a rectangular building explained that the k-ε model cannot correctly predict the reverse flow after separation on the roof surface and the side walls. The flow separation shown by experiments can be predicted numerically as shown by Murakami *et al* [11] and Murakami [12] who applied large eddy simulation (LES). Some studies have shown that the widely used standard k-ε turbulence model cannot predict well the effects of adverse pressure gradients on shear layers. The differences between the numerical results from k-ε turbulence model and the experimental data manifest mainly in consistently over predicted skin friction values and a tendency of the calculated flow to remain attached where experiments indicate separation. The poor prediction can be attributed to the fact that the length scale determined by the ε-equation rises steeper near the wall than in the case of zero pressure gradient, whereas experimental

data suggest that the length-scale gradient is virtually independent of the pressure gradient over a wide range [13].

In this study, the k-ε turbulence model can predict well the general wind conditions around buildings. The reverse flow at the leeward side of the building, the reverse flow at the windward side of the building near the ground, and the high velocity near the windward corner found in experiments have been successfully predicted in the present study. The separation bubble at the top side –which cannot be predicted by the usual k-ε turbulence model- has been successfully predicted in the present study. Therefore, the k-ε turbulence model can be used to predict the separation region near walls.

The disadvantage of the usual k-ε turbulence model is the over-prediction of the mixing length scale near walls, especially near windward corners. This leads to the over-prediction of eddy viscosity, and cannot predict the separation bubble in this region. To avoid the over-prediction of the mixing length scale, an alternative solution is reducing the k-ε turbulence values. These conditions lead to reduced eddy vortex and turbulent production near solid walls, especially at the top of the building.

As the main objective of our research, the heat transfer coefficient plays an important part to avoid or minimise the use of air conditioning systems. The heat transfer coefficient is fully affected by the maximum ambient velocity where a greater maximum velocity produces a greater heat transfer coefficient. A ratio between the maximum ambient velocity and the mean velocity for the rectangular obstacle is known to be around 2.29 [14 and 15].

From our results, the ratio between the maximum ambient velocity and the mean velocity of the 2.25H model agrees very well with that of other researches. Increasing the tunnel height tends to increase this factor. The mixing length scale (l_m) at the inlet is expressed by $l_m = \frac{\kappa y}{C_\mu^{0.75}}$ where y is half the inlet height. The higher the tunnel, the greater the mixing length scale at the inlet. The eddy viscosity is described as $\upsilon_t = C_\mu k^{0.5} l_m$, then the higher the tunnel height, the greater the eddy viscosity at the inlet.

At the building top, a lower tunnel height produces higher pressure as can be seen in Figure 3.19 (b), where the augmented pressure is denoted by $P = \frac{\bar{p}}{\rho} + \frac{2}{3}k$. This also leads to increased turbulent kinetic energy and dissipation rate. Increasing the tunnel height reduces these values over the building but not at the stagnation point, as presented in Figure 3.20. It can be clearly seen that increasing the tunnel height tends to increase turbulent kinetic energy and dissipation rate. Since turbulent kinetic energy is related to the velocity length scale, the higher the tunnel height, the greater the velocity at the stagnation point. It should be noted that the results are fully affected by mesh density, since refining the grid reduces these values.

Increasing the tunnel height reduces turbulent kinetic energy and dissipation rate at the building top and also leads to a reduced pressure distribution. The maximum velocity is reached when $dp/dx = 0$ and decelerates as a result of the adverse pressure gradient ($du/dx<0$ when $dp/dx>0$). Then, the tunnel with 2.25 step height produces the greatest pressure distribution at the building top, as can be seen in Figure 3.19 (b).

The rule for the ratio between the maximum ambient velocity and the mean velocity is, the higher the building the lower this value. This indicates that increasing the tunnel height should be followed by refining the mesh. Due to CPU time, the tunnel with 2.25 times the step height is considered in the next simulation.

An important result shown here is that the k-ε properties affect the ratio between the maximum ambient velocity and the mean velocity. Increasing the k-ε values will increase this ratio, which means that there is a relation between the turbulence intensity and the ratio between the maximum ambient velocity and the mean velocity. From our results, the previous k-ε properties are reasonable and acceptable in accordance to the expected value.

Another important result is the effect of the Reynolds number on the ratio between the maximum ambient velocity and the mean velocity. Modifying the Reynolds number by changing the velocity increases the ratio between the maximum ambient velocity and the mean velocity more than by changing the physical properties. This point should be very carefully taken into consideration, especially for similarity and scaling problems.

Results of a comparison study of the reattachment length and the ratio between the maximum ambient velocity and the mean velocity are presented in Tables 3.1(a) and 3.1(b). From Table 3.1 (a), it can be seen that the reattachment length of the tunnel with 2.25 H agrees well with Qasim *et al* [9]. For higher turbulent intensity, the reattachment length also agrees well with Zhang *et al* [10]. It can be seen from Table 3.1 (b) that the ratio between the maximum ambient velocity and the mean velocity agrees well with Kato *et al* [14] and Murakami *et al* [15]. The results indicate that the atmospheric boundary layer simulation can be performed well by using a lower tunnel height with appropriate boundary conditions. This also concludes that the tunnel with 2.25 H can be used in the next simulation.

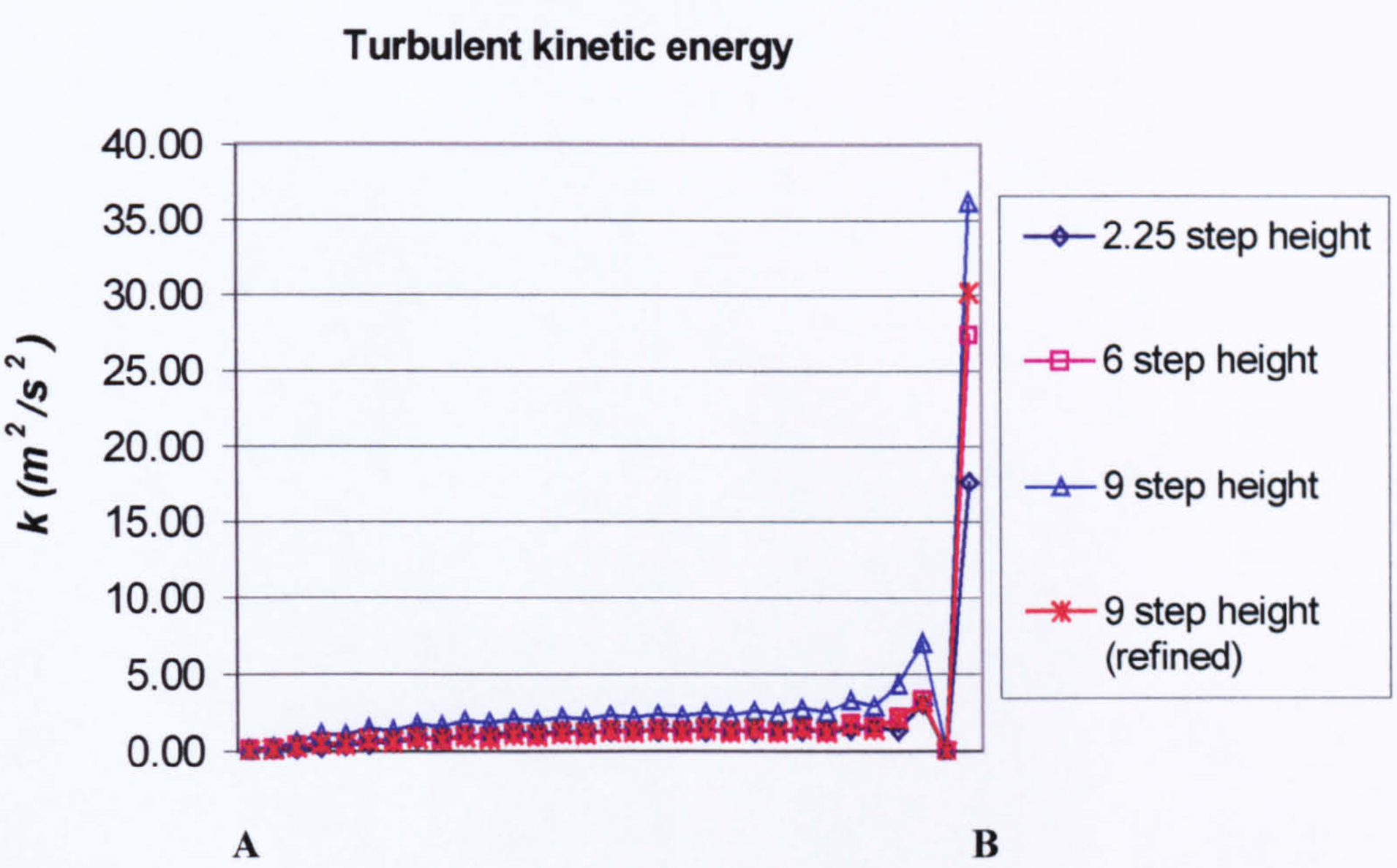

Figure 3.20 Turbulent kinetic energy at the windward side of building

Table 3.1 (a) Comparison of reattachment length from several researches

	1	2	3	4	5	6	7	8
(i)	3.1	3.1	3.1	3.1	2.95	2.4	2.81	2.3
(ii)	1.73	1.9	1.3	3.1	3.1			
(iii)	3.1	3.1	3.1					
(iv)	2.1	3.5						
(v)	3.6	2.5						
(vi)	3.1	1.9						

(i) previous values of physical and k-ε properties

1 symmetry plane at top plate

2 stationary condition at top plate

3 zero pressure and vertical velocity at outlet

4 regular mesh with stationary condition at top plate

5 irregular mesh with stationary condition at top plate

6 tunnel height with 6 times the step height

7 tunnel height with 9 times the step height

8 tunnel height with 9 times the step height (refined)

(ii) test of k-ε properties

1 increasing turbulent intensity by 31%

2 non initial and boundary values of k-ε

3 only initial values of k-ε (with a thousand of (i))

4 only initial values of k-ε (the same to that of (i))

5 both initial and boundary values of k-ε reduced by a thousand

(iii) test of temperature and heat flux

1 isothermal flow

2 temperature imposed at lower plate

3 heat flux imposed at the obstacle

(iv) test of Reynolds number

1 Reynolds number reduced by velocity

2 Reynolds number increased by physical property

(v) test of surface roughness

1 surface roughness applied

2 surface roughness multiplied by ten

(vi) Comparison to published research

1 Qasim *et al*, 1992 [9]

2 Zhang *et al*, 1993 (with a higher turbulence at inlet) [10]

Table 3.1 (b) Comparison of the ratio between the maximum ambient velocity and the mean velocity from several researches

Gu	1	2	3	4	5	6	7	8
(i)	2.24	2.24	2.24	2.24	2.25	2.94	2.95	2.96
(ii)	2.74	2.64	2.41	2.24	2.24			
(iii)	2.24	2.24	2.24					
(iv)	2.57	2.34						
(v)	2.24	2.29						
(vi)	2.24	2.29						

(i) previous values of physical and k-ε properties

1 symmetry plane at top plate

2 stationary condition at top plate

3 zero pressure and vertical velocity at outlet

4 regular mesh with stationary condition at top plate

5 irregular mesh with stationary condition at top plate

6 tunnel height with 6 times the step height

7 tunnel height with 9 times the step height

8 tunnel height with 9 times the step height (refined)

(ii) test of k-ε properties

1 increasing turbulent intensity by 31%

2 non initial and boundary values of k-ε

3 only initial values of k-ε (with a thousand of (i))

4 only initial values of k-ε (the same to that of (i))

5 both initial and boundary values of k-ε reduced by a thousand

(iii) test of temperature and heat flux

1 isothermal flow

2 temperature imposed at lower plate

3 heat flux imposed at the obstacle

(iv) test of Reynolds number

1 Reynolds number reduced by velocity

2 Reynolds number increased by physical property

(v) test of surface roughness

1 surface roughness applied

2 surface roughness multiplied by ten

(vi) Comparison to published research

1 Kato *et al*, 1992 [14]

2 Murakami *et al*, 1996 [15]

3.3 Summary

From the various results obtained in this chapter, there are many points to be considered in our modelling.

1. Boundary condition

The simplest and most common boundary condition at solid walls is no-slip, *i.e.* the normal and tangential velocity components must agree with those at the wall. **Symmetry** is sometimes present and can be used to significantly reduce the cost of a simulation via the application of appropriate boundary conditions at the symmetry plane (or line) and solving the problem in the appropriate fraction of the full domain –typically 1/2-, although there are some cases where 1/4 and 1/8 is appropriate.

The most common symmetry boundary condition is typified by vanishing normal velocity ($u_n = 0$). The viscous stress tensor on the boundary can be written as $\mu[\nabla u_n + \partial u / \partial n - 2n\partial u_n / \partial n] = 0$. This can be simplified via $\mathbf{u} = u_t + \mathbf{n}u_n$ and $\nabla = \nabla_t + \mathbf{n}(\partial / \partial n)$ to be $\mu(\nabla_t u_n + \partial u_t / \partial n) = 0$, where u_t is the component of **u** in the tangent plane, u_n is the outward normal velocity and ∇_t is the gradient operator in the tangent plane. Since $u_n = 0$ on the boundary, this finally produces $\partial u_t / \partial n = 0$. The boundary condition at the upper plate , however, can be either the no-slip condition or a symmetry plane, and produces similar results on building surfaces.

The normal force is defined as $F_n = 2\mu \frac{\partial u_n}{\partial n} - P = 0$. By applying this boundary condition at the symmetry line, the pressure distribution along the object is similar to that with no-slip boundary condition at the upper plate, since $\partial u_t / \partial n = 0$ along symmetry line leads $\partial u_n / \partial n = 0$. This condition leads to $P = 0$.

At the inlet, if v = 0, incompressibility requires that the flow must always be parallel to the boundary. This so-called Dirichlet boundary condition is very common for the inlet flow. Therefore, the inlet position is not significant since the flow is considered to be fully developed turbulent.

For two-dimensional problems, the boundary condition **at the outlet** can be expressed as $2\mu\frac{\partial u_n}{\partial n} - P = n \cdot F = F_n$ in the normal direction and $\mu\left(\frac{\partial u_t}{\partial n}\right) = \tau \cdot F \equiv F_t$ in the tangential direction. These boundary conditions can be simplified by using $\partial(*)/\partial n = 0$. Thus, we can assume that $\partial u_n / \partial n = 0$ and $\partial u_t / \partial n = 0$. The Neumann boundary condition yields to $\mu\frac{\partial u_n}{\partial n} - P = f_n$ and $\mu\frac{\partial u_t}{\partial n} = f_t$. If the average pressure at the outlet is now set to zero, the normal and tangential components of the traction forces (f_n and f_t) are zero since $\partial u_n / \partial n = 0$ and $\partial u_t / \partial n = 0$.This leads to reducing the convergence and CPU times and avoiding oscillations, even by using a coarse mesh [16].

2. Tunnel height

From pressure distribution results shown in Figure 3.19, it seems that the pressure distribution of 2.25 H is more appropriate than 9 H with refinement. From several comparisons, pressure at the top and at the leeward side agrees with other researches. Pressure distribution of 2.25H agrees very well with Qasim *et al* [9], and also agrees with Hunt [3], Okada and Okabe [4], Selvam [5] and Stathopoulos and Zhou [6].

Results for imposing a higher turbulence at the inlet agrees very well with Zhang *et al* [10], where for a high turbulence at the inlet the reattachment point is about 1.7-1.9, the same as when we multiply the turbulence properties by a thousand. However, the reattachment length varies and depends on the boundary condition.

From Figure 3.5, it can be seen that horseshoe vortex at the windward side of the obstacle is longer than that in Figure 3.2. The separation bubble at the top side is not as clear as that in Figure 3.2. This can be improved by refining the grid above and at the rear side of the obstacle, but it will take longer CPU time and greater machine memory.

Since the flow is external, the effects of height and size of channel should not influence the results. To save CPU time during computation, one should use the smallest possible channel size. Therefore, the channel height of 2.25 times the object height is sufficient.

3. Different values of k-ε at the inlet

Since the kinetic and dissipation energies are not properties of the fluid but indicate a condition of the velocity profile, where

$$k \equiv \frac{1}{2}\left(\overline{u'^2 + v'^2 + w'^2}\right) \tag{3.1}$$

and the exact boundary-layer form of the k-equation at high Reynolds numbers is described as,

$$\rho\frac{Dk}{Dt} = -\frac{d}{dy}(\rho\overline{v'k'} + \overline{v'p'}) - \rho\overline{u'v'}\frac{du}{dy} - \mu\sum\left(\frac{\overline{du_i'}}{dx_j}\right)^2 \tag{3.2}$$

convective flux = diffusion + production - dissipation

where p' denotes fluctuating pressure and k' denotes the instantaneous value of turbulent energy, then if different values are imposed for the above properties, they will influence the fluctuating component of u' (at inlet, $v = w = 0$). Larger values of k-ε will produce greater fluctuating components. From equation (3.2) above, as larger values are imposed, the convective flux will be smaller than in the case of smaller values.

There is a relationship between convective heat flux and Nusselt number. If the convective heat flux becomes smaller, the Nusselt number will also be smaller. There is a correlation between Nusselt number and point of separation. For a fully developed turbulent flow, the Nusselt number becomes smaller at the point of separation. An earlier point of separation will produce a greater Nusselt number.

Lower values of turbulent kinetic energy and its dissipation rate produce better results, especially for reverse flow at the top side of building. This separation which has not been predicted well by other researchers is now clearly shown. Lower values of turbulent kinetic energy and its dissipation rate increase the convective term at the separation region since the local element Reynolds number increases. This convective term can be reduced by reducing the truncation error at the separation regions, *i.e.* by

using multi-blocks grid near solid walls, and will be examined in Chapters Four and Five.

4. Isothermal and constant surface heat flux

Under isothermal condition, it is possible to produce a heat flux which is greater than the real surface heat flux. But under the surface heat flux condition, it is impossible to produce surface temperatures which are greater than in the isothermal condition. Although the flow pattern is similar, application of a constant surface heat flux (often heat fluxes will have to be found from experimental data) is more reasonable than the isothermal condition when the temperature distribution is being considered.

5. Reynolds number

The Reynolds number plays an important role in the simulation, especially for similarity and scaling problems. For higher Reynolds number, both pressure and viscous terms of the Navier-Stokes equation can be neglected. This may be true in certain cases, but since the pressure was scaled in a rather subjective manner, it is not clear that the magnitude of its dimensionless gradient will remain of order unity in this limit. To allow for this occurrence, the pressure should be re-scaled by introducing the new dimensionless variable

$$\hat{\hat{p}} = \frac{p}{\rho U^2} = \frac{1}{\mathrm{Re}}\hat{p} \tag{3.3}$$

and work as previously to the Navier-Stokes equation. By introducing this new term, the viscous term becomes small. This also reduces the order of the Navier-Stokes equation, from two to one. This occurrence has important implications, not only on the number of required boundary conditions, but also on the structure and properties of the solution.

Similarity problems may be exploited to study the flow of a particular fluid in a certain domain by studying the flow of another fluid in a similar, larger or smaller domain. This may be achieved by adjusting the properties of the second fluid so as match the same values of Reynolds number. Miniaturisation of a domain of flow is

important in the study of large-scale flows. Similarity of structure means that the velocity or pressure field of one fluid may be found from those of another fluid (with different physical properties) by multiplying by an appropriate factor [18].

6. **Surface roughness**

From various results of surface roughness, we conclude that there are significant effects of the roughness on the results. This is important since the objective of this research is to improve the heat exchange between building surface and its surrounding. We will discuss these conditions in the next chapter.

REFERENCES

1. Y.S. Zhou and T. Stathopoulos, A new technique for the numerical simulation of wind flow around buildings, J. Wind Engineering and Industrial Aerodynamics 72 (1997) 137-147.
2. I.P. Castro and A.G. Robins, The flow around a surface mounted cube in uniform and turbulent stream, Journal of Fluid Mechanics 79 (1977) 307-335.
3. A. Hunt, Wind tunnel measurements of surface pressures on cubic building models at several scales, J. Wind Engineering and Industrial Aerodynamics 10 (1982) 137-163.
4. H. Okada and M. Okabe, Wind tunnel tests to determine the wind forces on roof blocks for existing buildings, J. Wind Engineering and Industrial Aerodynamics 38 (1991) 393-403.
5. R. P. Selvam, Numerical simulation of flow and pressure around a building, ASHRAE Transaction 102 (1996) 765-772.
6. T. Stathopoulos and Y.S. Zhou, Application of two-layer methods for the evaluation of wind effects on a cubic building, ASHRAE Transaction 102 (1996) 754-764.
7. D. Delaunay, D. Lakehal and D. Pierrat, Numerical approach for wind loads prediction on buildings and structures, J. Wind Engineering and Industrial Aerodynamics 57 (1995) 307-321.
8. B. Ruck, Wind-tunnel measurement of flow field characteristics around a heated model building, J. Wind Engineering and Industrial Aerodynamics 50 (1993) 139-152.
9. A. Qasim, T.T. Maxwell, S. Parameswaran, Computational predictions of flow over a 2-D building, J. Wind Engineering and Industrial Aerodynamics 44 (1992) 2839-2840.
10. Y.Q. Zhang, A.H. Huber, S.P.S. Arya and W.H. Snyder, Numerical simulation to determine the effects of incident wind shear and turbulence level on the flow around a building, J. Wind Engineering and Industrial Aerodynamics 46-47 (1993) 129-134.
11. S. Murakami, A. Mochida, Y. Hayashi, Examining the k-ε model by means of a wind tunnel test and large-eddy simulation of the turbulence structure around a cube, J. Wind Engineering and Industrial Aerodynamics 35 (1990) 87-100.

12. S. Murakami, Computational wind engineering, J. Wind Engineering and Industrial Aerodynamics 36 (1990) 517-538.
13. W. Rodi, G. Scheuerer, Scrutinising the k-ε turbulence model under adverse pressure gradient conditions, Trans. ASME 108 (1986) 174-179.
14. N. Kato, T. Ohkuma, J.R. Kim, H. Marukawa, and Y. Niihori, Full scale measurements of wind velocity in two urban areas using an ultrasonic anemometer, J. Wind Engineering and Industrial Aerodynamics 41 (1992) 67-78.
15. S. Murakami *et al*, Investigation on statistical characteristics of wind at ground level and criteria for assessing wind induced discomfort part-2, characteristics of turbulence of city wind at ground level, Trans. Of the Arch. Inst. Of Japan, 314 (1982) 112-120.
16. P.M. Gresho and R.L. Sani, Incompressible Flow and the Finite Element Method, Advection-Diffusion and Isothermal Laminar Flow, John Wiley and Sons Ltd., Chichester, 1998.
17. B.E. Launder and D.B. Spalding, Mathematical Models of Turbulence, Academic Press, New York, 1972.
18. C. Pozrikidis, Introduction to Theoretical and Computational Fluid Dynamics, Oxford University Press, New York, 1997.

CHAPTER FOUR

TWO-DIMENSIONAL MODELLING OF TRADITIONAL BALINESE BUILDINGS

In Chapter One, it has been described that a community in Bali is an organic unit, the structure, significance, and function of the home is dictated by the same fundamental principles of belief that rule the village. The principle of orientation –the relation from the mountains to the sea or from the sun rise to the sun set- that constitutes the ever present Balinese rose of the winds rules the orientation and distribution of the temple and house units.

Modelling and analysing environments that can be used for generating the principal rules of traditional Balinese buildings is very difficult in view of the orientation principle, magic rules and the shrine of gods.

Several key technologies must be exploited, adapted and integrated in order to build such environments successfully: atmospheric boundary layer, the temporal and spatial distribution of velocity, pressure and temperature fields around buildings.

The above parameters are used to simulate the rules of traditional Balinese buildings. Building parameters such as type of roof, distance between buildings, fence height and distance between buildings and the fence will be examined, in order to understand whether the traditional arrangement provides thermal comfort to occupants and reduces wind effects on building surfaces. Traditional materials such as thatch and brick stones -which have high surface roughness- are examined in order to reduce the cooling loads on buildings.

4.1 Effects of the Roof Type on Wind Motion around Traditional Balinese Buildings

4.1.1 Introduction

In a tropical country with a warm climate and high relative humidity, natural ventilation proves to be a realistic alternative technique for energy conservation and thermal comfort of occupants. Therefore, we start this study with a hypothesis that there is a relation between roof type of traditional Balinese buildings with energy conservation and thermal comfort of occupants. If so, this strategy aims to reduce the cooling loads of buildings and improve the indoor thermal comfort by modifying the roof type of buildings.

The aim of this study is to find a correlation between roof type and air motion around buildings, therefore the effects of orientation, infiltration, ventilation and size of buildings are not considered.

4.1.2 Physical Description and Mathematical Model

Four types of roof are used in the present study, as shown in Figure 4.1.1. Since the flow region is unbounded, an upper truncation boundary is artificially placed at a height of 2.25 H, where H is the height of the houses' eaves (Figure 4.1.2); this value was arrived at by trial and error (see Chapter Three). The tunnel height is also examined in order to ensure that the imposed boundary conditions are correct. Boundary conditions appertaining to fully developed flow are imposed at the inlet. A uniform heat flux $q^{"}$ is applied at the houses and fences, so that thermal stratification is established in the field. Since temperature changes on the ground are mainly caused by heat conduction, a uniform temperature T_s is applied on the ground. This value was measured daily at the peak time, in the dry season. Surface roughness of the walls is also considered in the modelling.

The following assumptions and conditions are introduced:

1. The atmosphere and the soil layers are plane parallel and can be treated two-dimensionally.

2. The region of the atmospheric boundary layer from the ground up to 500 m above the Earth's surface is considered in this simulation. The surface boundary layer at an altitude 10 m is supposed to be the layer of constant vertical momentum, heat and mass fluxes, then Monin-Obukhov's similarity theory is applied [1].
3. The horizontal distance of 100 m is considered in this simulation.
4. Radiation heat transfer for clear and non-clear sky conditions are considered in the surface heat flux boundary conditions at the buildings.
5. The atmosphere is assumed to be in hydrostatic equilibrium. The Boussinesq approximation is adopted [2].

Boundary Conditions

The boundary conditions for the atmospheric boundary layer model are those for a homogeneous boundary layer with the following characteristics:

(a) **Inlet**

- The boundary conditions for the inlet velocity are fixed with the profile $\frac{u_y}{\overline{u_{10m}}} = \frac{\log(y/y_0)}{\log(10/y_0)}$, where $\overline{u_y}$ and $\overline{u_{10m}}$ are the mean velocities at height y and 10 m, respectively, y_0 is a surface roughness length of 0.010 m for a cut grass fetch, and $v = w = 0$ [3]. The turbulent intensity was evaluated to be 6.2% according to Davenport's terrain roughness classification number 4 for a suburban terrain [4], and the inlet temperature (T_0) is 301 K.
- The shear stress is constant and given by

$$(\mu_l + \mu_t)\frac{\partial u}{\partial y} = \tau_w = \rho u_\tau^2 \qquad (4.1.1)$$

where τ_w is the solid surface shear stress and u_τ is the friction velocity.

- The turbulent kinetic energy k and its dissipation rate ε satisfy their respective conservation equations which reduce to

$$\frac{\partial}{\partial y}\left[\frac{\mu_t}{\sigma_k}\frac{\partial k}{\partial y}\right] + \mu_t G_k - \rho\varepsilon = 0 \qquad (4.1.2)$$

and

$$\frac{\partial}{\partial y}\left[\frac{\mu_t}{\sigma_\varepsilon}\frac{\partial \varepsilon}{\partial y}\right]+C_1\mu_t G_k\frac{\varepsilon}{k}-C_2\rho\frac{\varepsilon^2}{k}=0$$

where

$$G_k=\left[\frac{\partial u}{\partial y}\right]^2 \tag{4.1.3}$$

$\sigma_k, \sigma_\varepsilon, C_1$ and C_2 are constants of the model, with $\sigma_k = 1.0, \sigma_\varepsilon = 1.3, C_1 = 1.44$ and C_2=1.92

- The above equations are satisfied by using

$$u=\frac{u_\tau}{K}\ln\left[\frac{y+y_0}{y_0}\right] \tag{4.1.4}$$

$$\kappa=\frac{u_\tau^2}{\sqrt{C_\mu}} \tag{4.1.5}$$

$$\varepsilon=\frac{u_\tau^3}{\kappa(y+y_0)} \tag{4.1.6}$$

where κ is von Karman's constant ($\cong 0.41$) and $C_\mu = 0.09$.

(b) **Solid Boundaries**

Velocity is zero on the ground, the fence and the buildings. Temperature is constant and equal to 305 K on the ground. Heat fluxes were assumed to be constant but having different values along the fences, the building walls, ceiling and roof; these values are estimated from the measured peak-time temperatures, and change according to building location and orientation. The heat flux absorbed by the building (by solar radiation) has been imposed as boundary conditions. Surface roughness (*e*) varies between 0.05% and 0.10% of the houses' height (*H*), and is applied for all wall surfaces. On the truncated walls and building surfaces, the wall treatment is a combination of logarithmic and no-slip boundary conditions. The no-slip boundary condition (u = v = w = 0) is the appropriate condition for the velocity components at solid walls.

(c) **Outlet**

At the outlet, homogenous Neumann boundary conditions are applied for all variables.

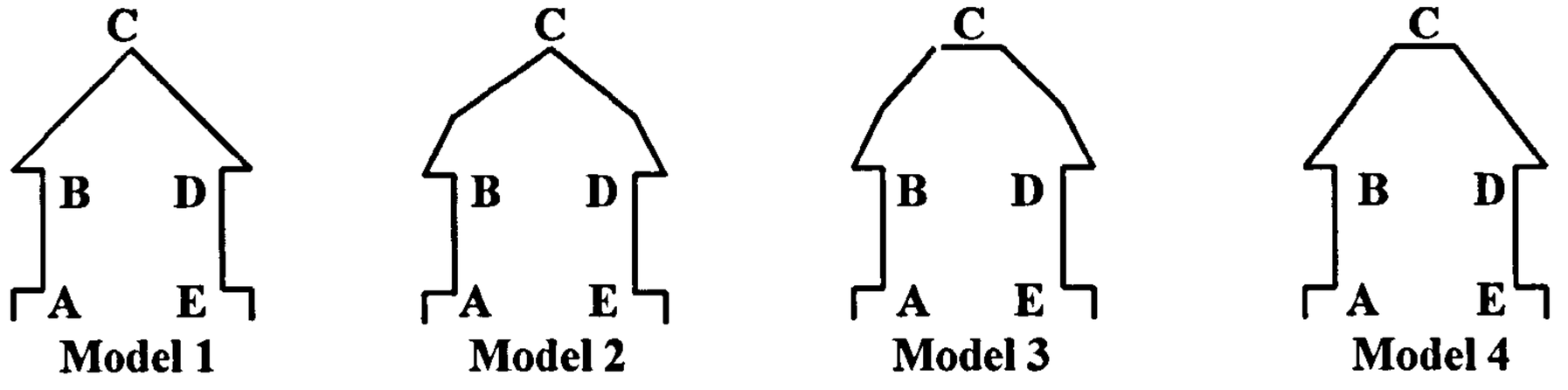

Figure 4.1.1 Geometry of roof

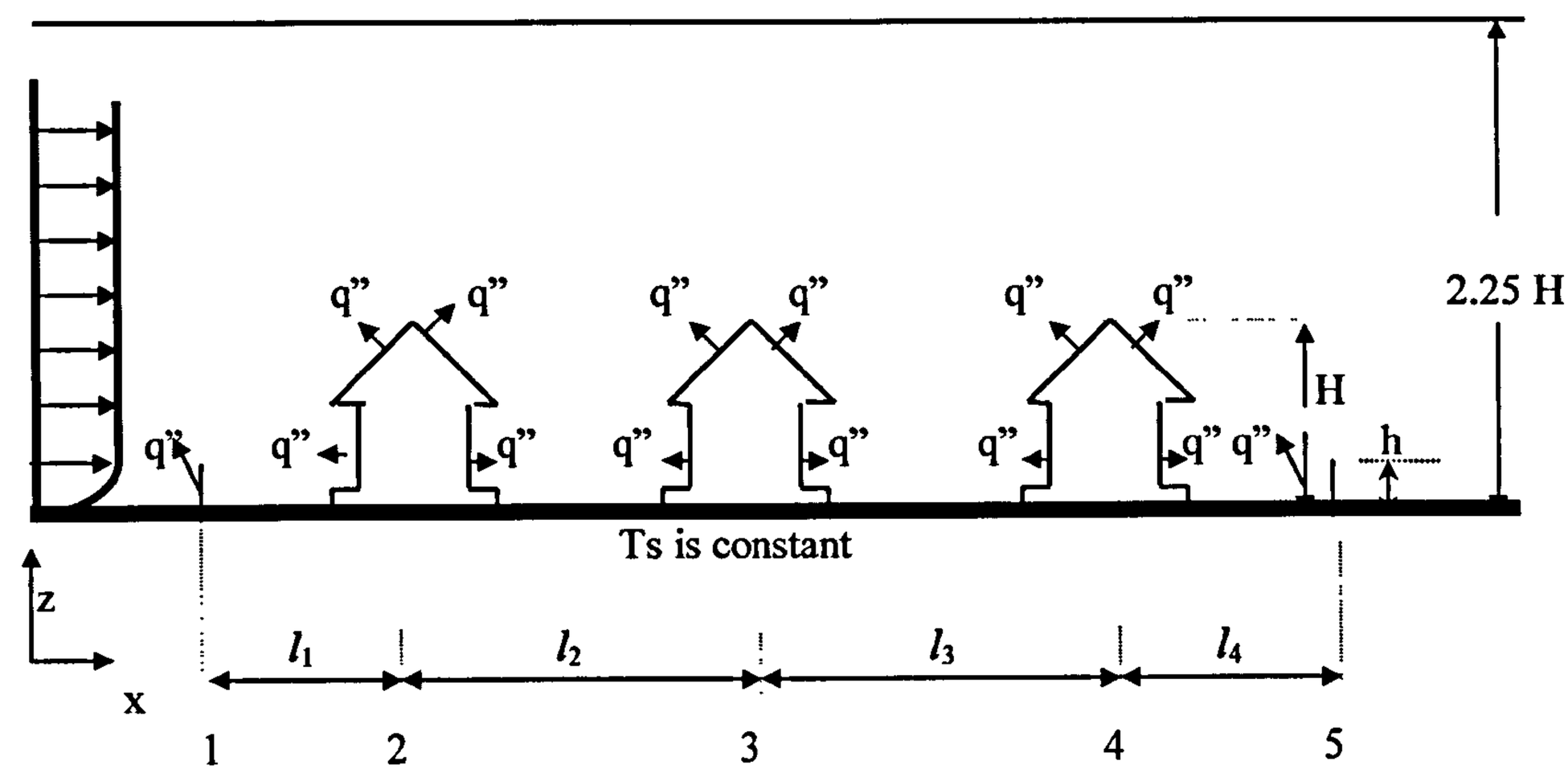

1 = front fence
2 = first house
3 = second house
4 = third house
5 = back fence
l_1 = distance between the front fence and first house
l_2 = distance between first and second house
l_3 = distance between second and third house
l_4 = distance between third house and the back fence
H = height of the house
q" = heat flux on the surface

Figure 4.1.2 Geometry of the problem and boundary conditions for computations

4.1.3 Numerical Procedures

The conservation equations are written in terms of the primitive variables, with pressure removed through a penalty function formulation. The turbulence model is a standard $k-\varepsilon$ with a logarithmic-law near-wall closure scheme. The set of differential equations is solved iteratively using Picard's iteration, with relaxation.

Since the solution procedure is iterative, a criterion has been used to decide when a convergent solution has been reached. A suitable convergence criterion is to require that the sum of residuals over the whole domain should be less than a small specified tolerance (10^{-6}). This convergence criterion will be examined for accuracy of the results.

4.1.4 Results of Grid-Independence Tests

Grid-independence tests play an important role on numerical simulations, especially if the wall shear stresses need to be calculated accurately. For simple problems as described in Chapter Three, it was shown that a coarse grid -at the leeward side of the building- gave reasonable results for both regular and irregular meshes. Grid refinement is the main tool at the disposal of CFD simulations for improvement of the accuracy of results. Simulations will be started by using a coarse mesh to get an idea of the overall features of the solution. Subsequently, the grid will be refined in stages until no significant differences of results occur between successive grid refinement stages, the so-called grid-independent results.

For the grid-independence tests, the chosen grids are non-uniform and regular. Multiple-blocks have been used in order to reduce the truncation error. Three initial models proposed are shown in Figure 4.1.3. In Figure 4.1.3 (a), 20 nodes with ratio 1.2 are used between the first and second buildings, and between the second and third buildings. In Figure 4.1.3 (b), 30 nodes are used with ratio 1.2, and in Figure 4.1.3 (c), 40 nodes are used with ratio 1.05. A ratio of 1 means that the grid is uniform. A ratio of 1.2 means that the size of each element is the previous one divided by 1.2. Therefore, the second element has 1/1.2 the first element size, the third element has 1/1.2 the second element size, and so on.

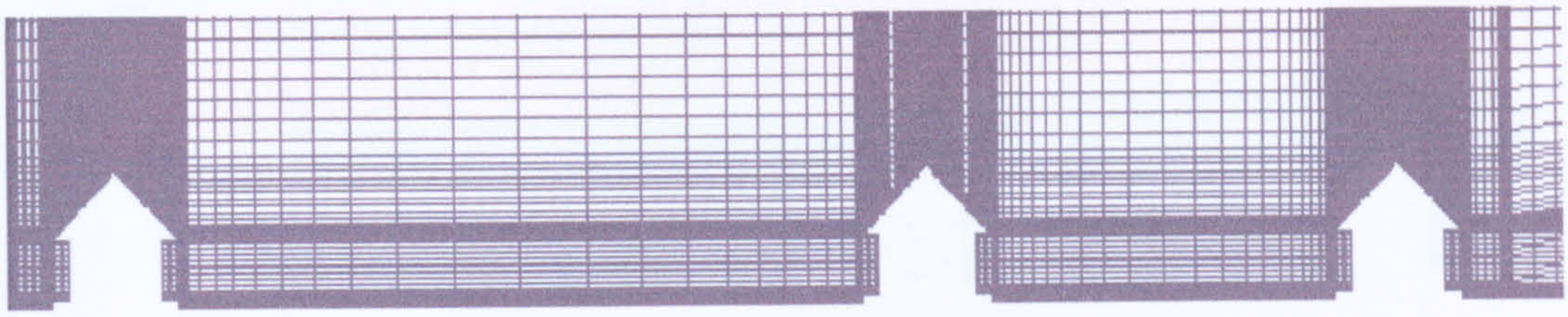

(a)

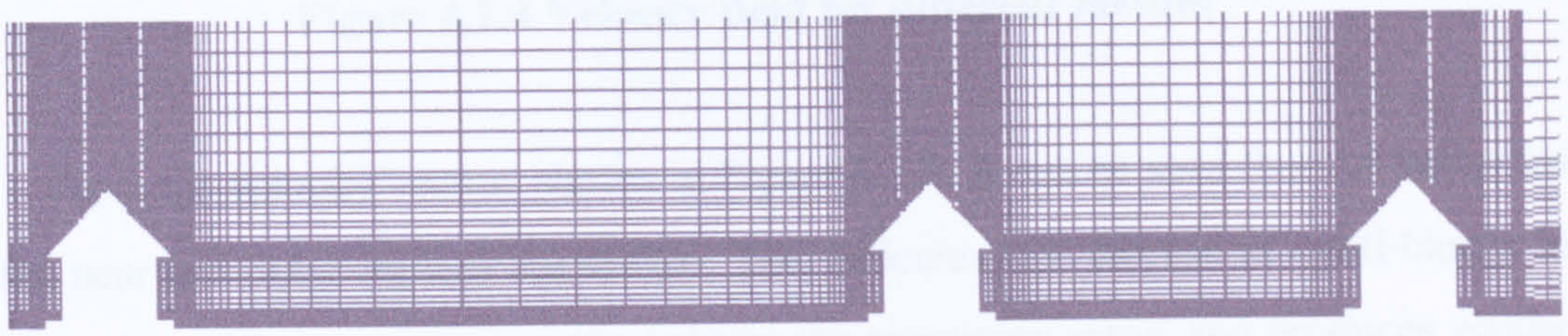

(b)

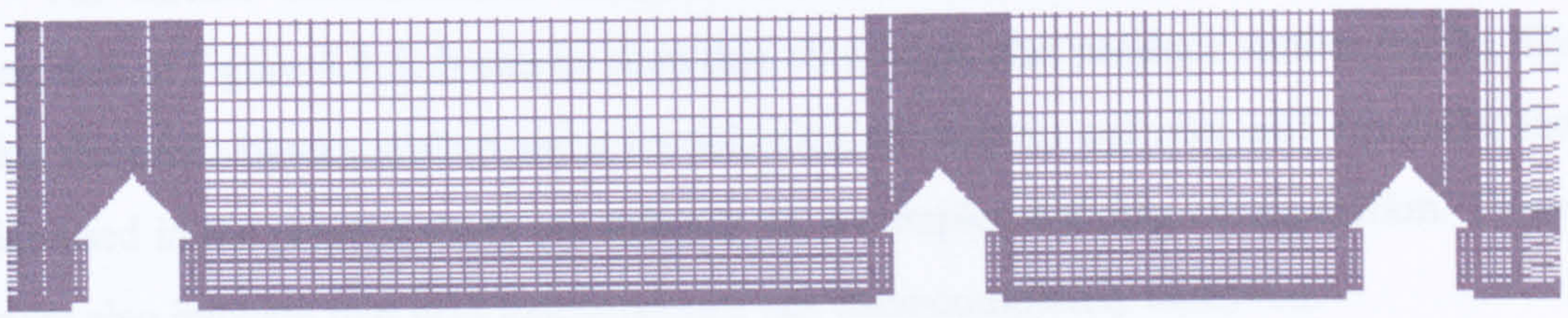

(c)

Figure 4.1.3 Typical meshes

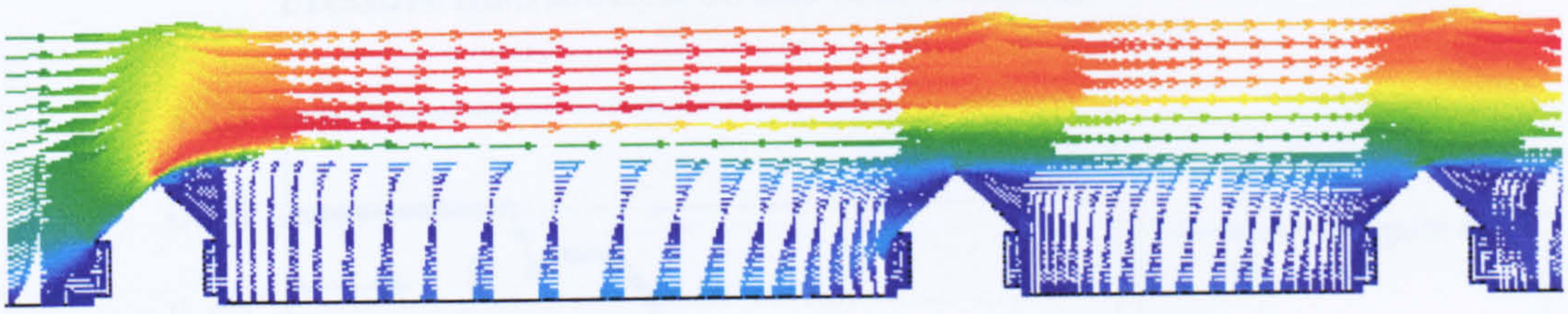

(a)

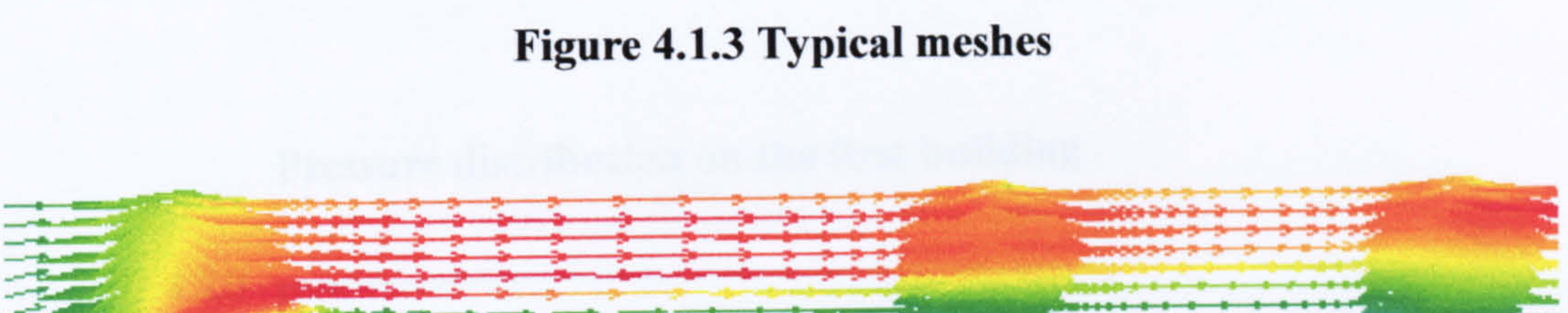

(b)

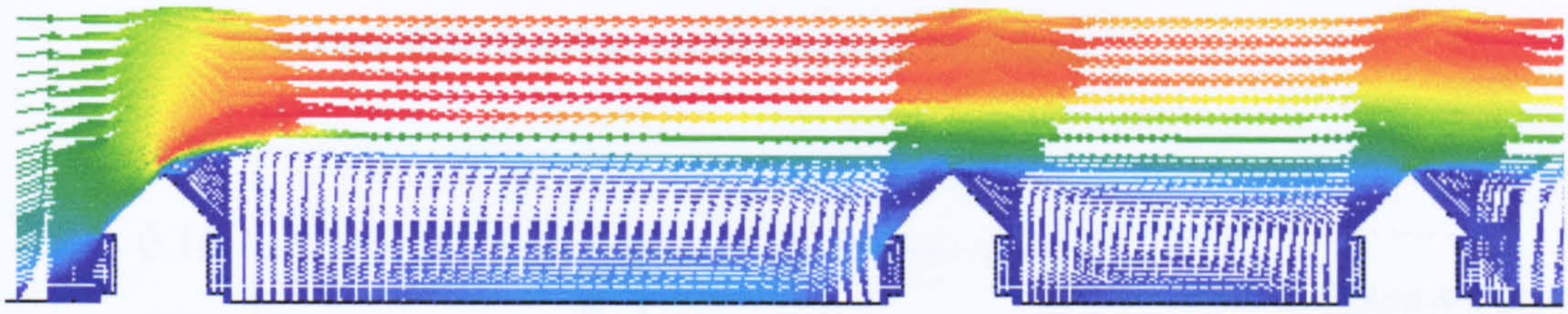

(c)

Figure 4.1.4 Velocity field for different meshes

From the velocity vectors shown in Figure 4.1.4, it can be seen that the velocities in the near and outer regions are similar. This indicates that the use of multi-blocks in combination with non-uniform grids reduces the truncation error, and produces similar results for all models.

For further consideration, the pressure distribution on the building surfaces is presented in Figure 4.1.5. It can be seen that all models also produce similar results. By using the multi-blocks system and a combination of uniform and non-uniform grids, the grids used in the present study are suitable for a complex building configuration. These results also indicate that grid independence has been completely observed.

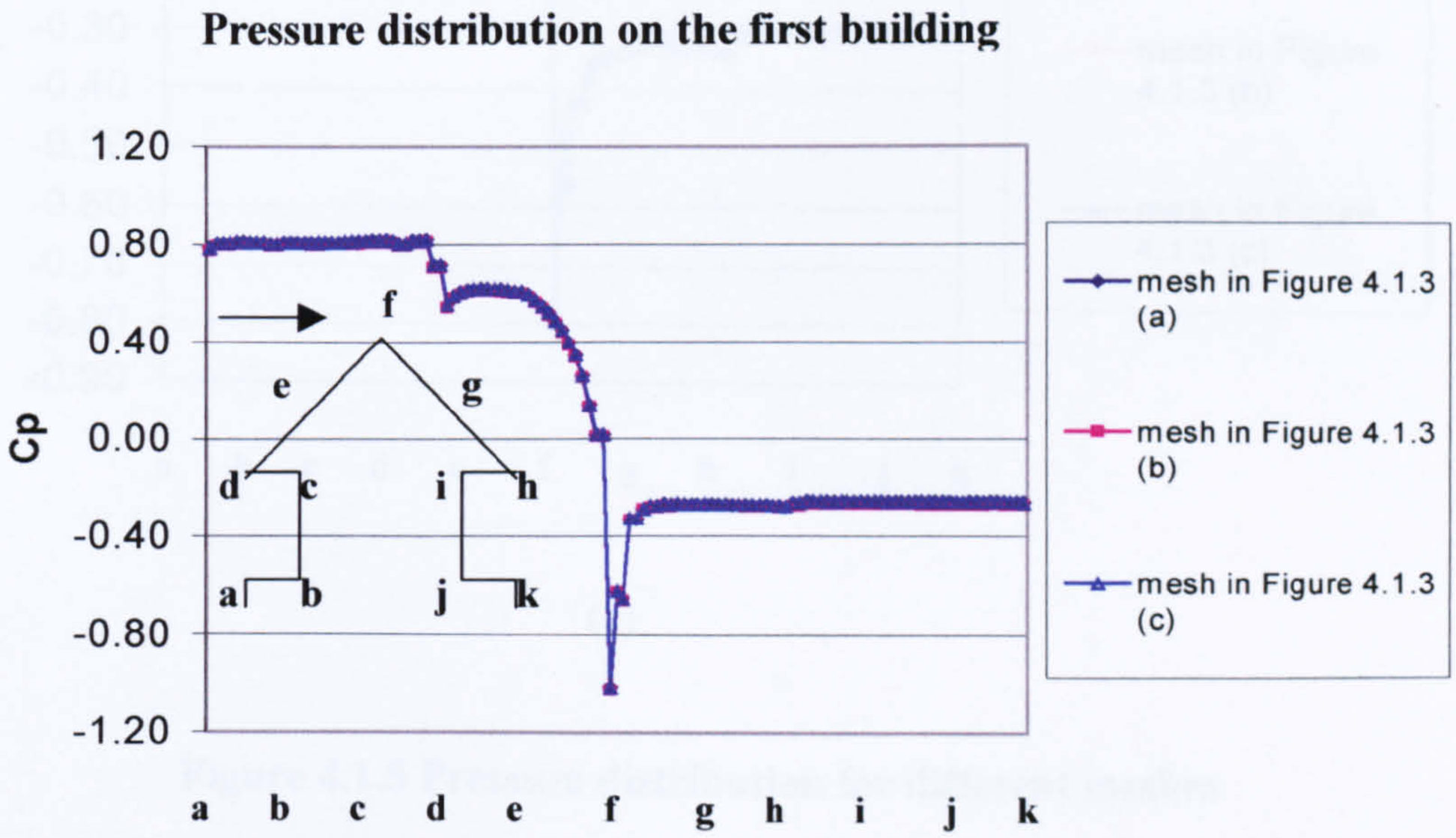

(a)

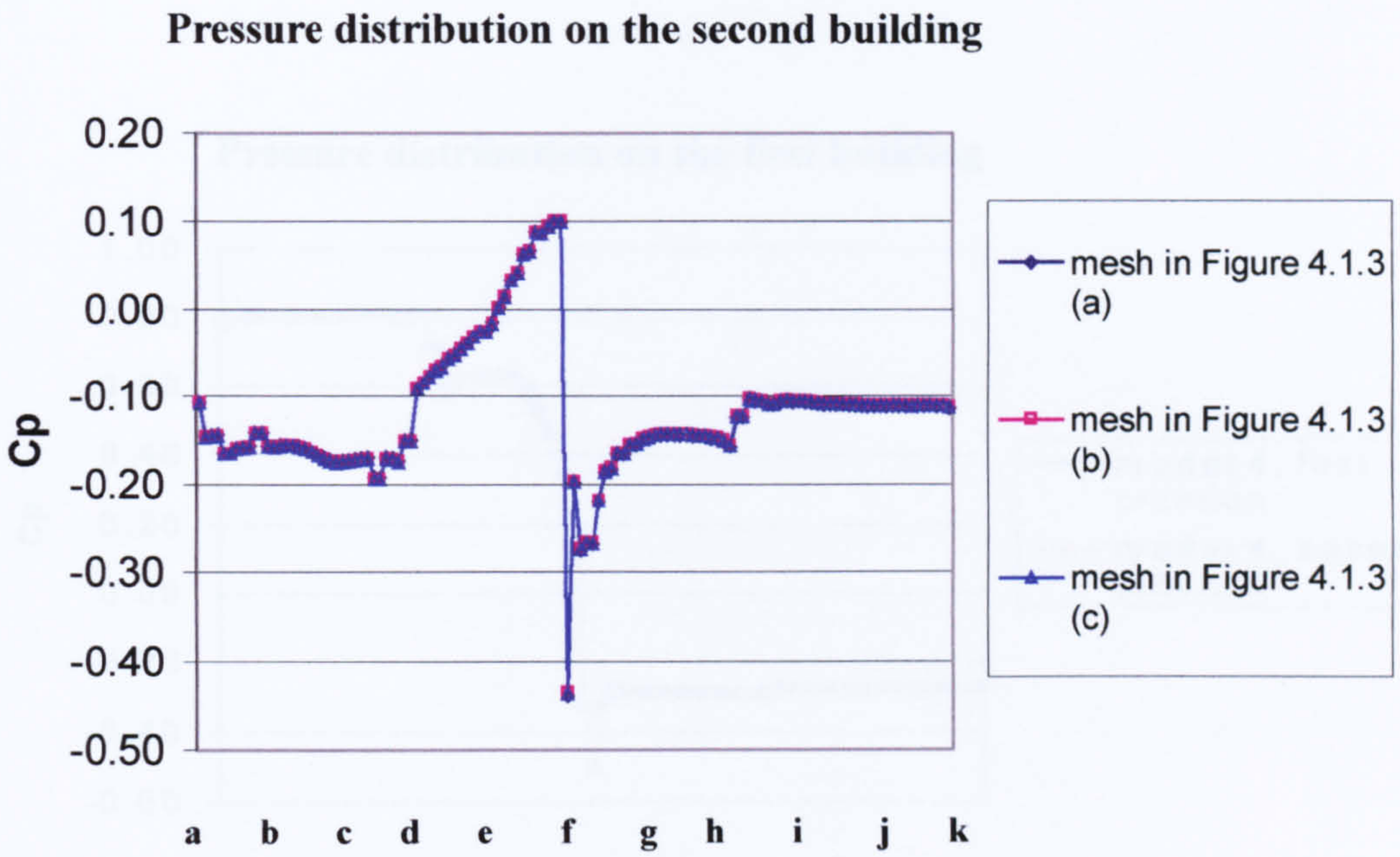

(b)

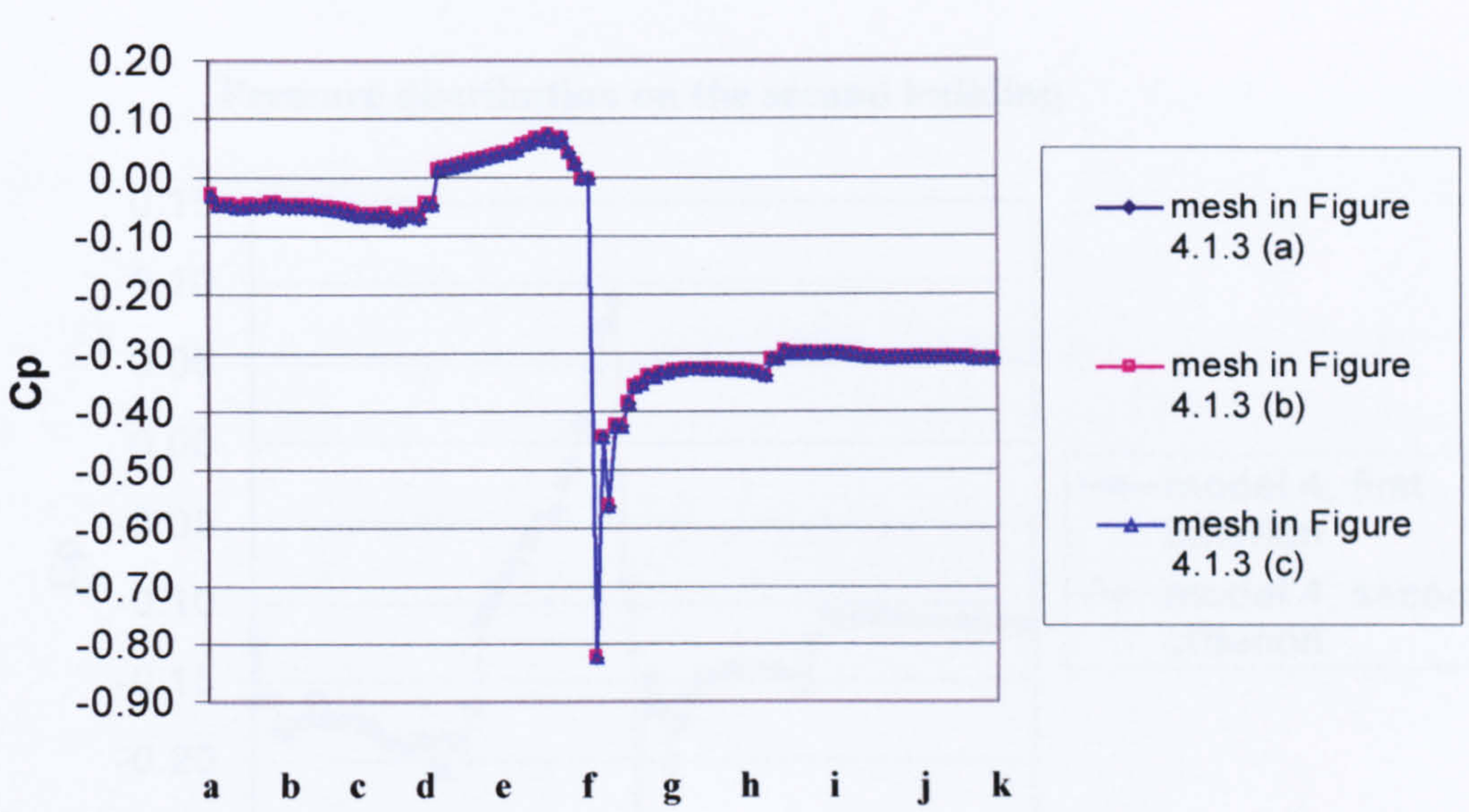

(c)

Figure 4.1.5 Pressure distribution for different meshes

4.1.5 Results for Different Convergence Criteria

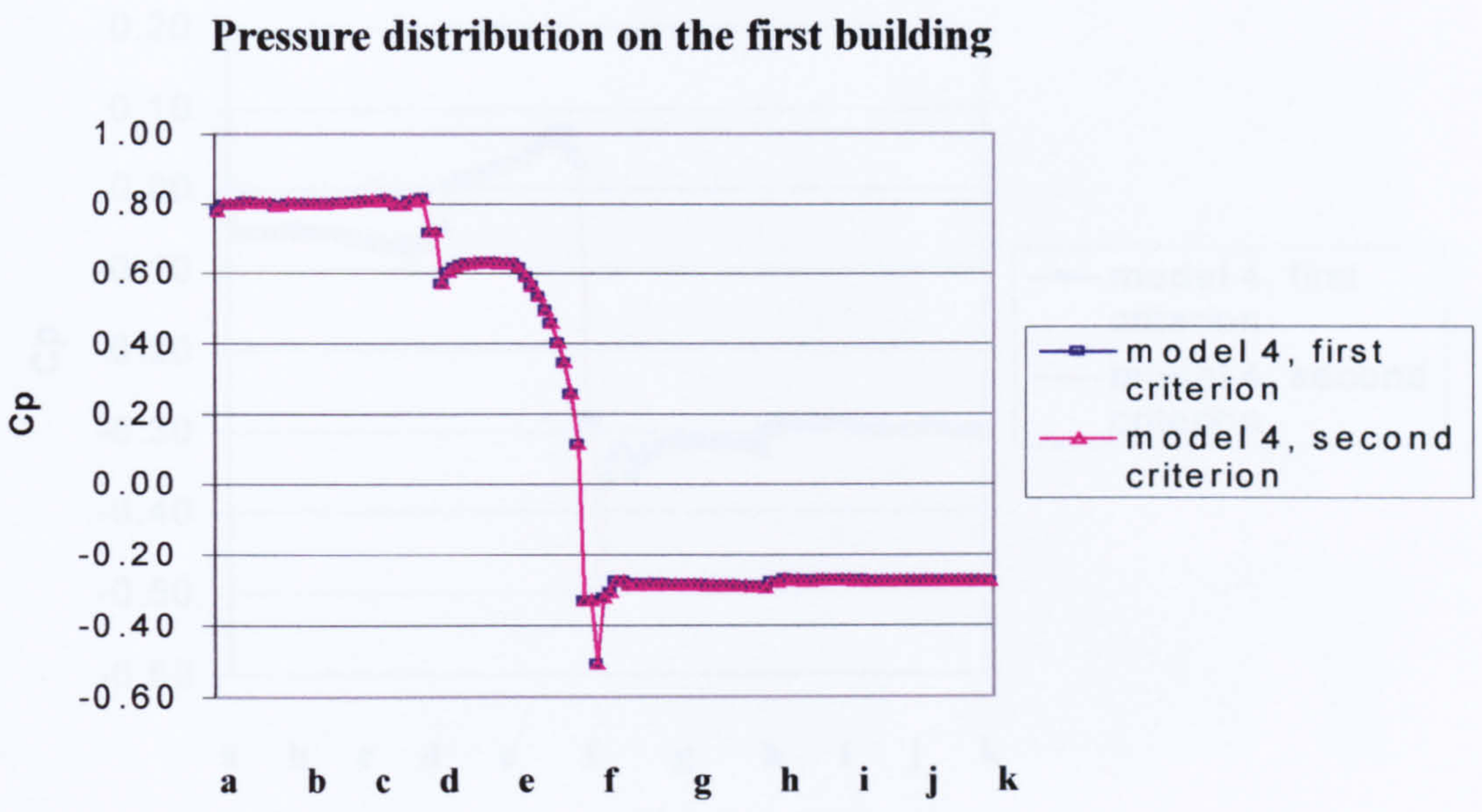

(a)

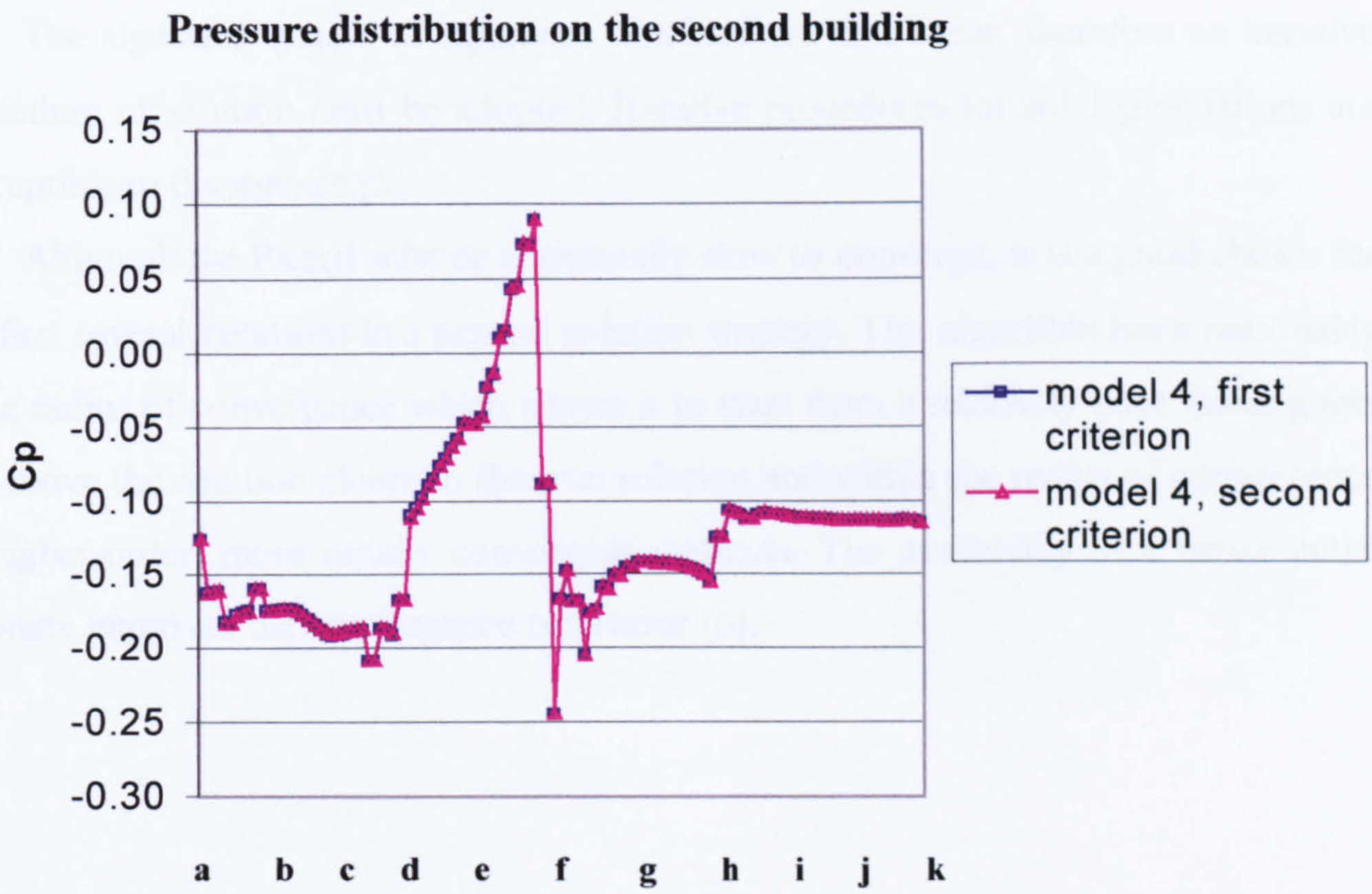

(b)

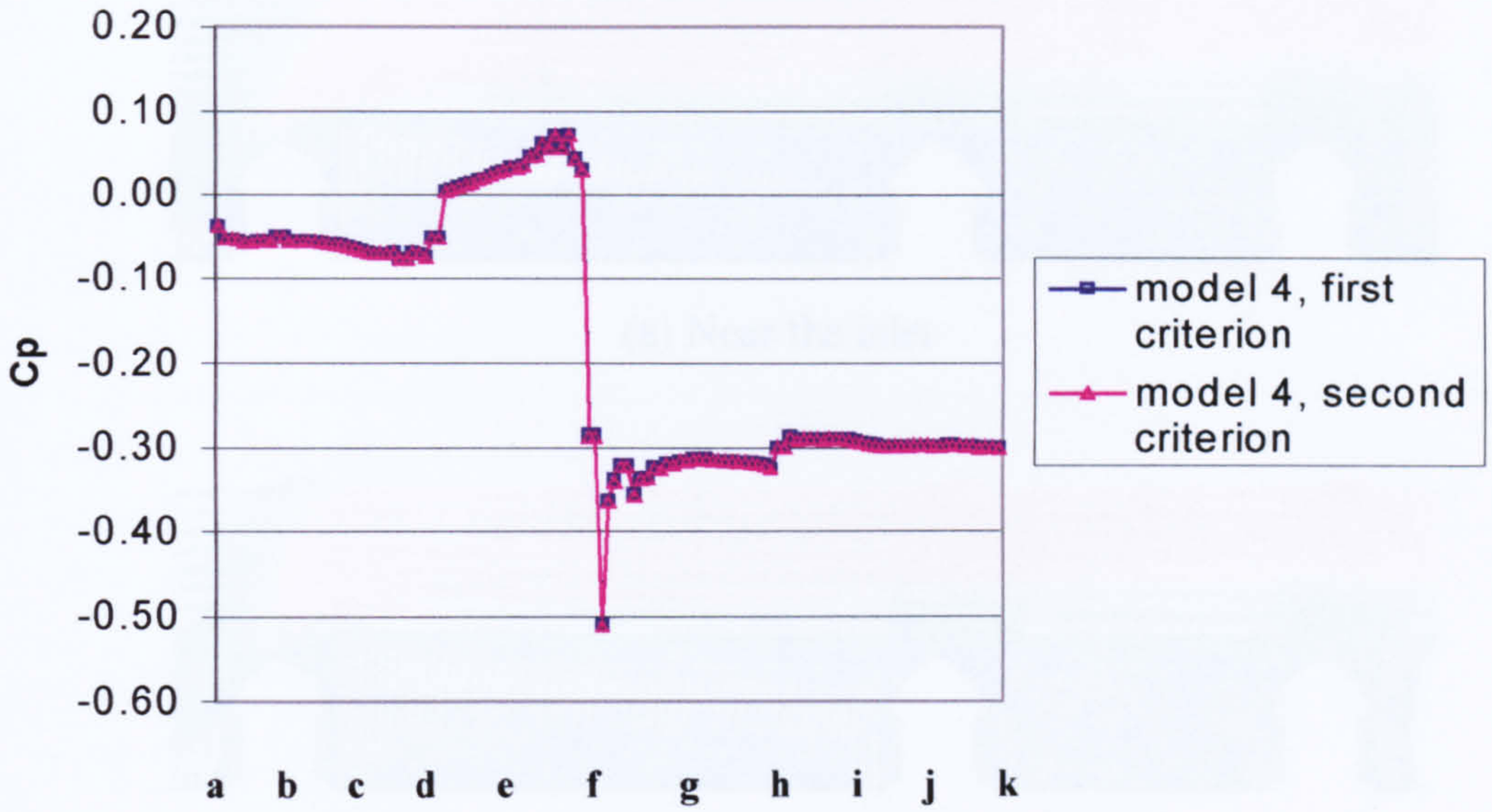

(c)

Figure 4.1.6 Pressure distribution for different convergence criteria

The algebraic system of equations obtained are non-linear, therefore an iterative procedure of solution must be adopted. Iterative procedures for solving equations are susceptible to divergence [5].

Although the Picard scheme is generally slow to converge, it is a good choice for the first several iterations in a general solution strategy. This algorithm has a reasonably large radius of convergence which allows it to start from a relatively poor initial guess and move the solution closer to the true solution and within the radius of convergence of higher-order, more rapidly convergent methods. The availability of a better initial estimate improves the convergence behaviour [6].

4.1.6 Results for Different Distances to the Inlet

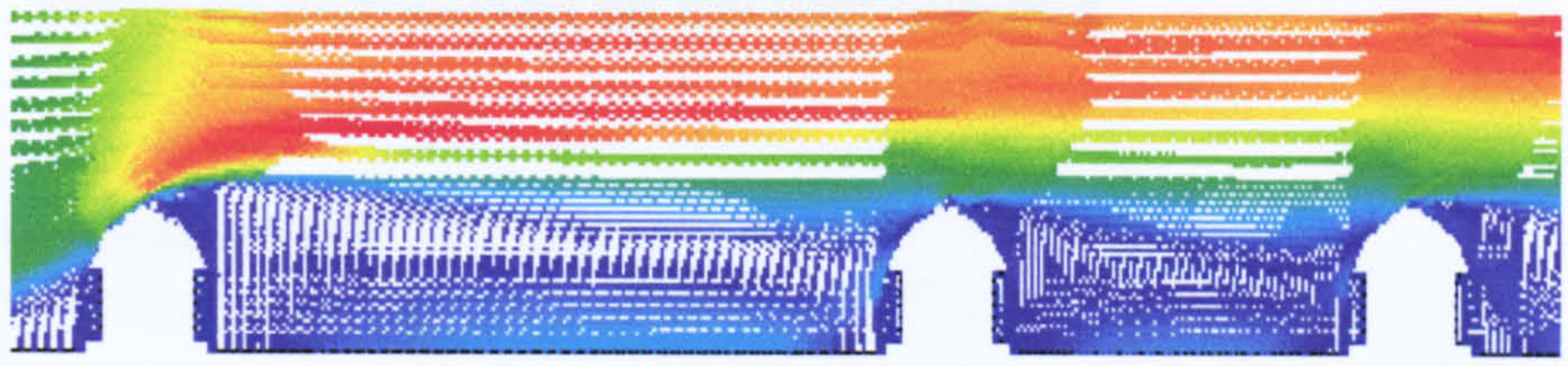

(a) Near the inlet

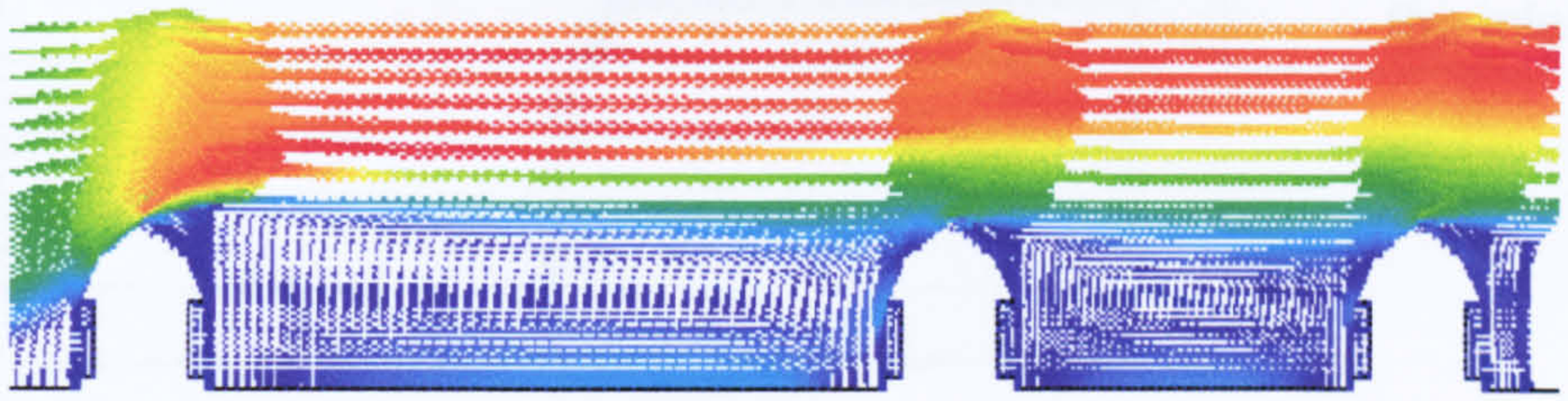

(b) Far from the inlet

Figure 4.1.7 Velocity vector for different distances to the inlet

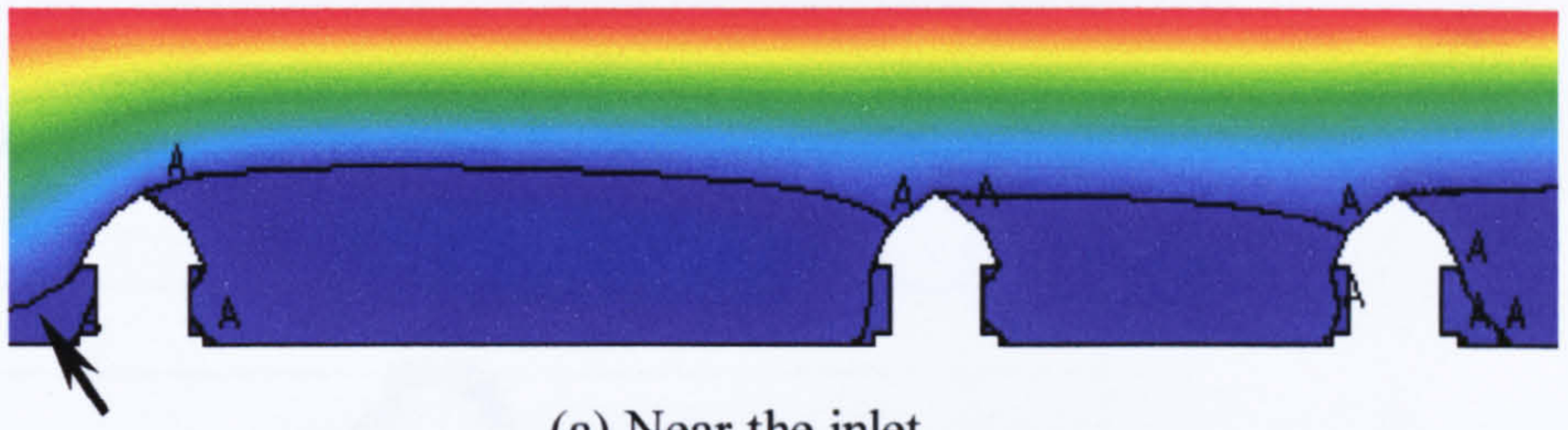

(a) Near the inlet

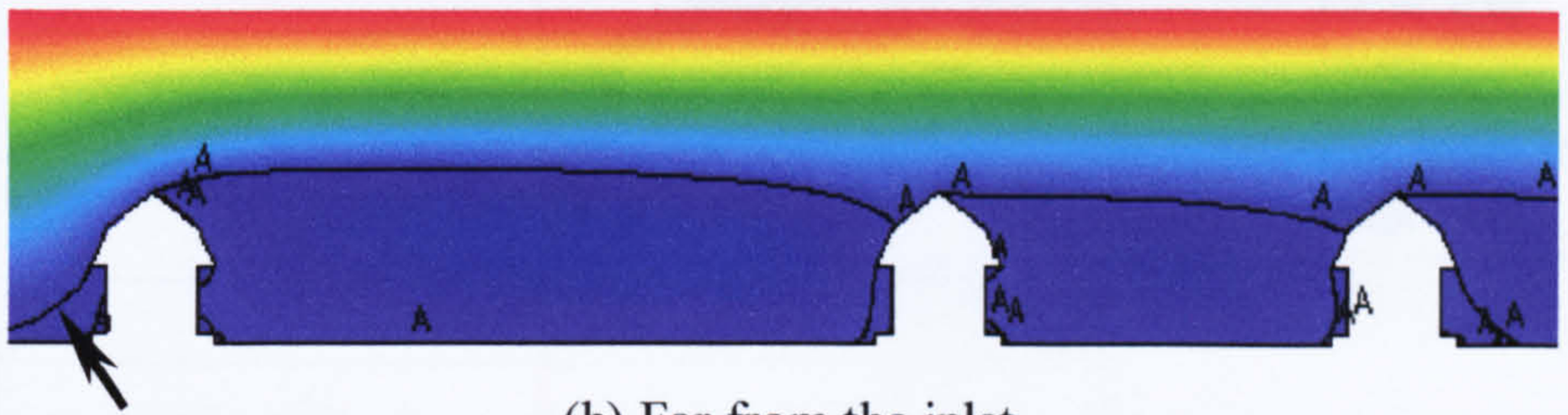

(b) Far from the inlet

Figure 4.1.8 Streamline plots for different distances to the inlet

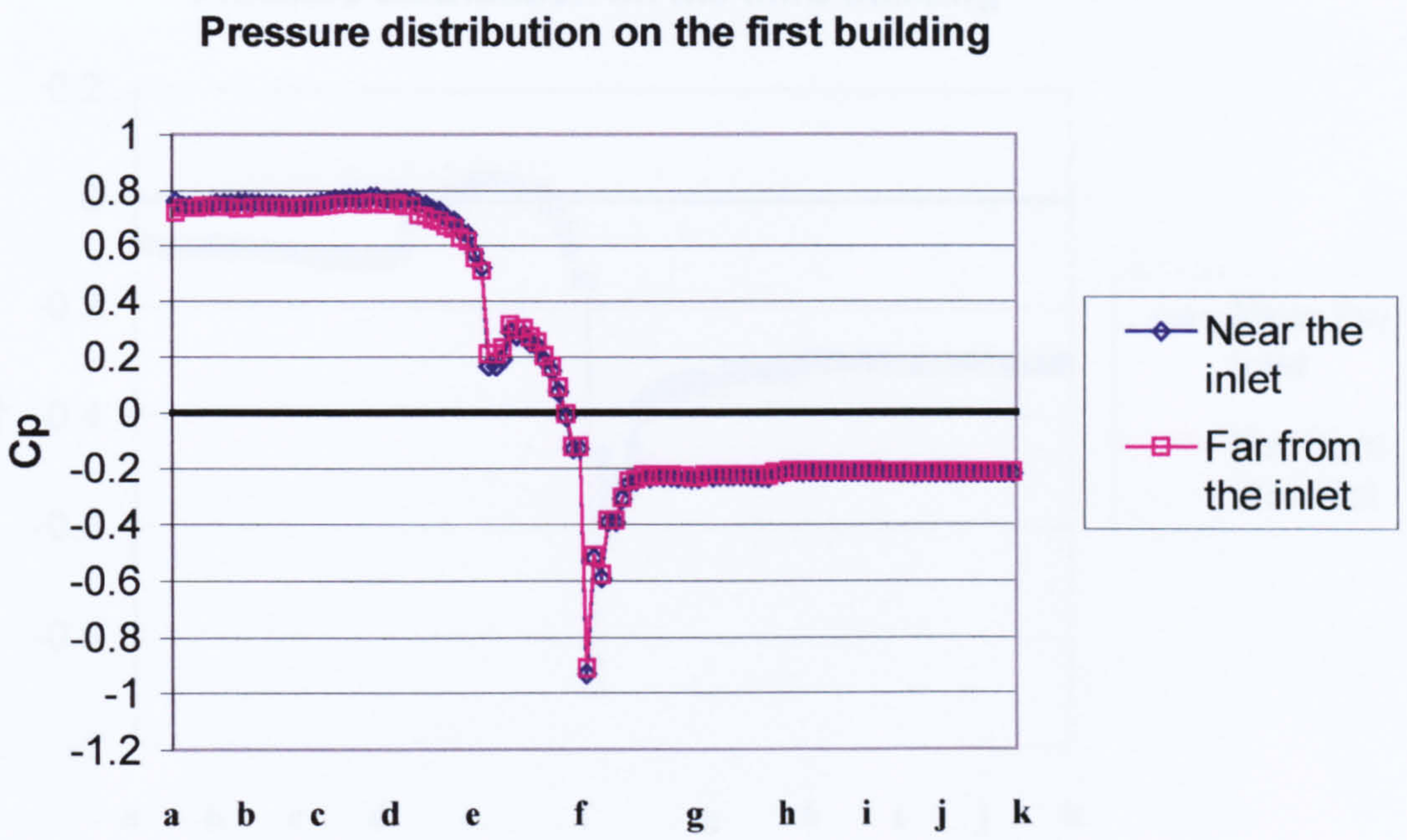
Pressure distribution on the first building
1
0.8
0.6
0.4
0.2
0
-0.2
-0.4
-0.6
-0.8
-1
-1.2
Cp
a b c d e f g h i j k
Near the inlet
Far from the inlet

(a)

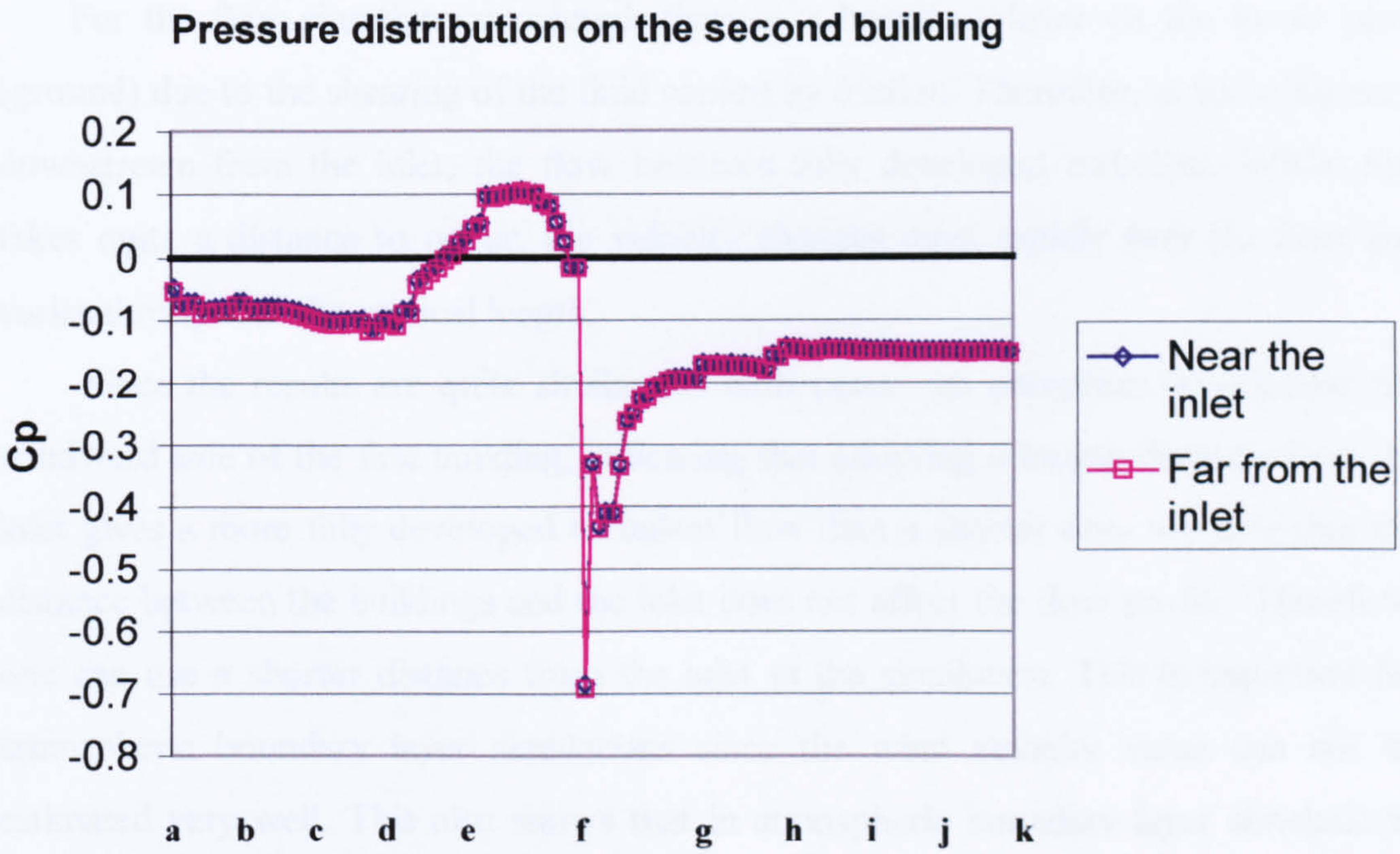
Pressure distribution on the second building
0.2
0.1
0
-0.1
-0.2
-0.3
-0.4
-0.5
-0.6
-0.7
-0.8
Cp
a b c d e f g h i j k
Near the inlet
Far from the inlet

(b)

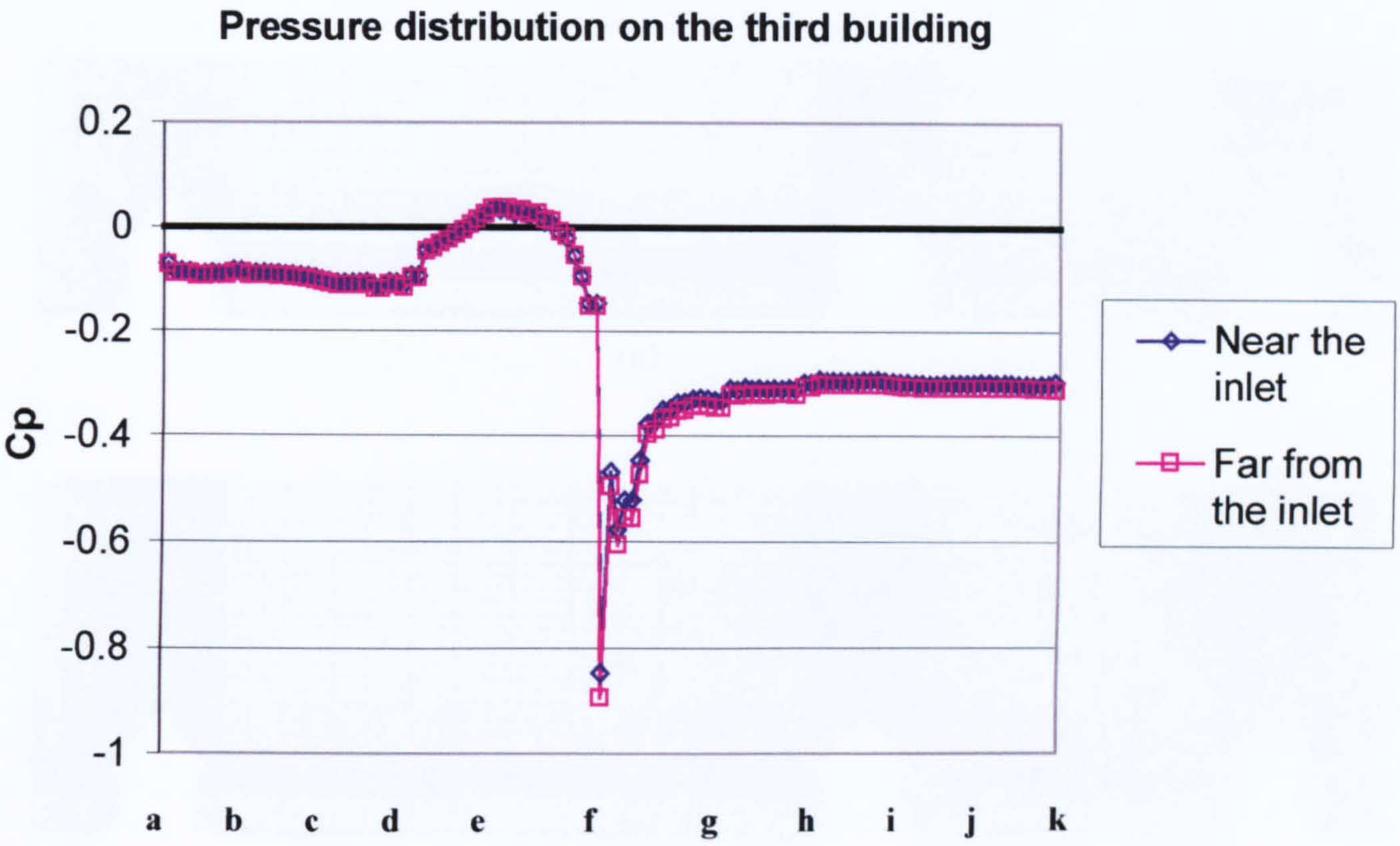

(c)

Figure 4.1.9 Pressure distribution for different distances from the inlet

For the flow situation considered, there is a boundary layer on the lower plate (ground) due to the shearing of the fluid caused by friction. Therefore, at some distance downstream from the inlet, the flow becomes fully developed turbulent. Whilst this takes quite a distance to occur, the velocity changes most rapidly near the inlet and varies throughout the vertical length.

Since the results are quite similar for both cases –an exception occurs near the windward side of the first building, indicating that adopting a longer distance from the inlet gives a more fully developed turbulent flow than a shorter one- we note that the distance between the buildings and the inlet does not affect the flow profile. Therefore, one can use a shorter distance from the inlet in the simulation. This is important for atmospheric boundary layer simulations since the wind velocity value can not be estimated very well. This also shows that in atmospheric boundary layer simulations, the ground boundary layer thickness is small.

4.1.7 Results for Different Tunnel Heights

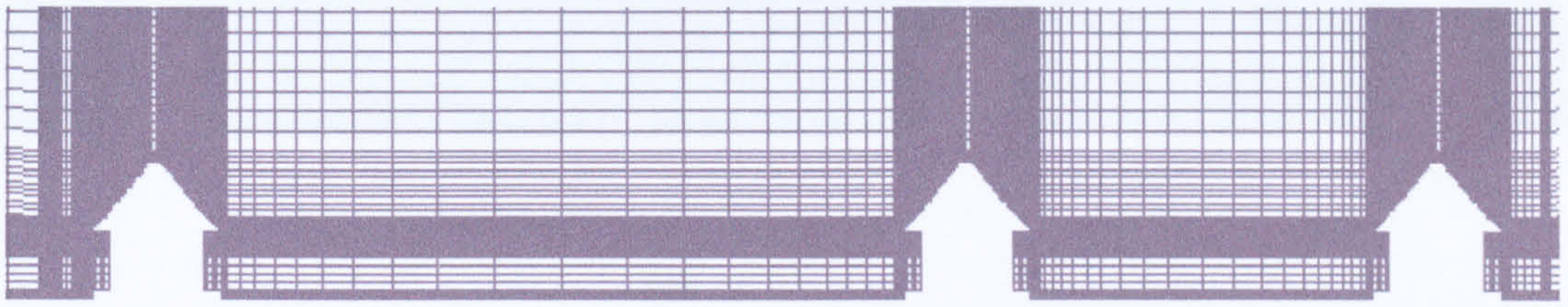

(a)

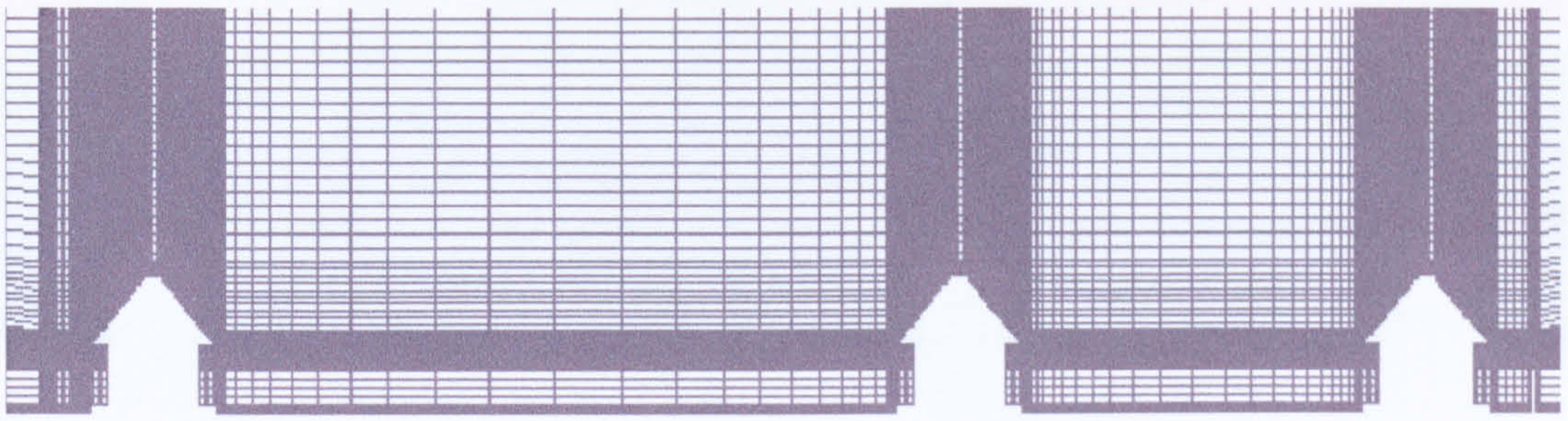

(b)

Figure 4.1.10 Typical meshes

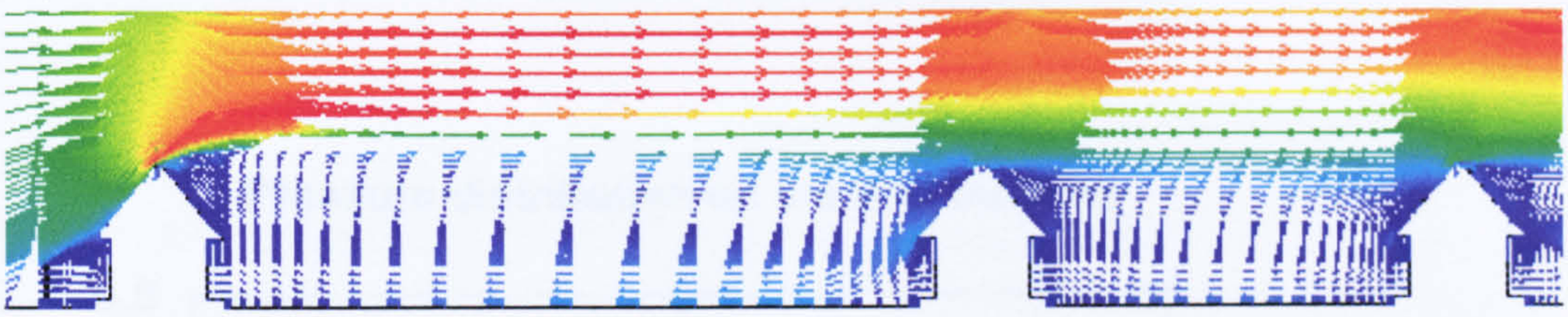

(a)

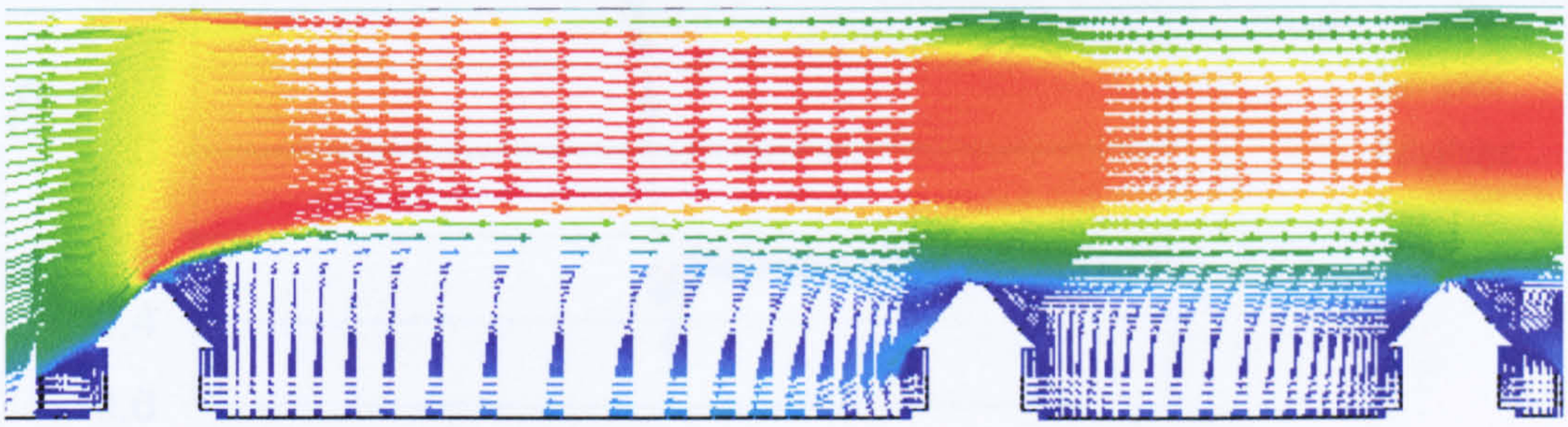

(b)

Figure 4.1.11 Velocity vector for different tunnel heights

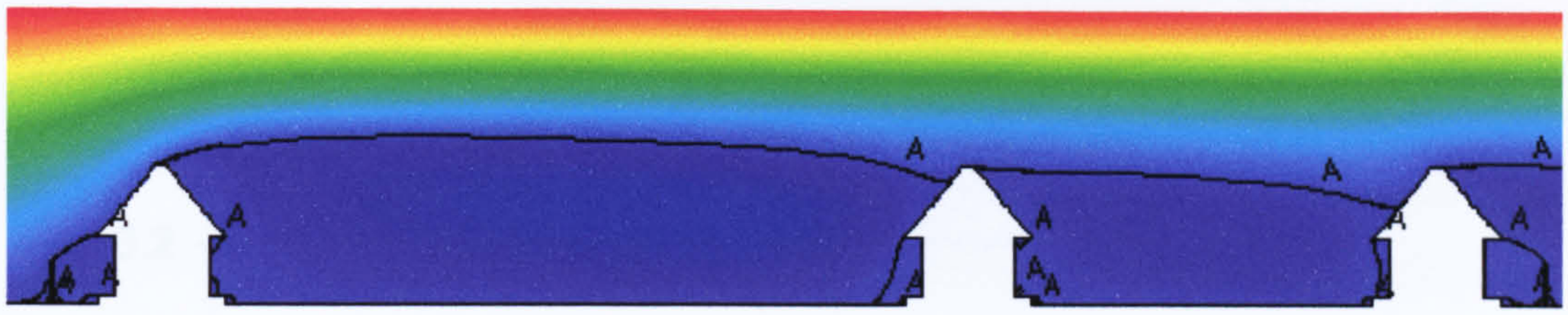

(a)

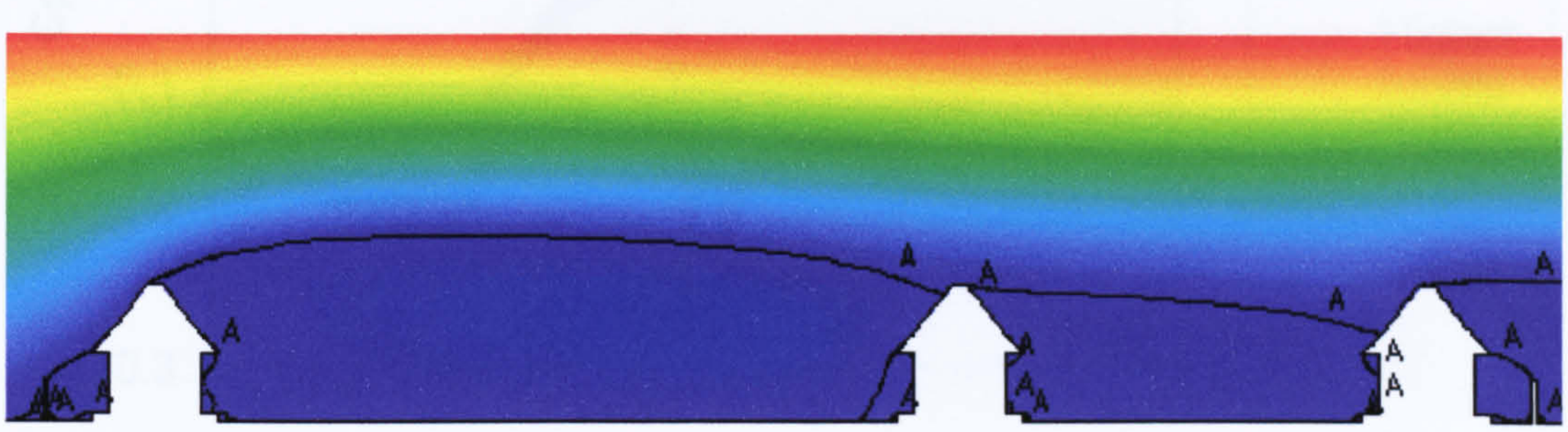

(b)

Figure 4.1.12 Streamline plots for different tunnel heights

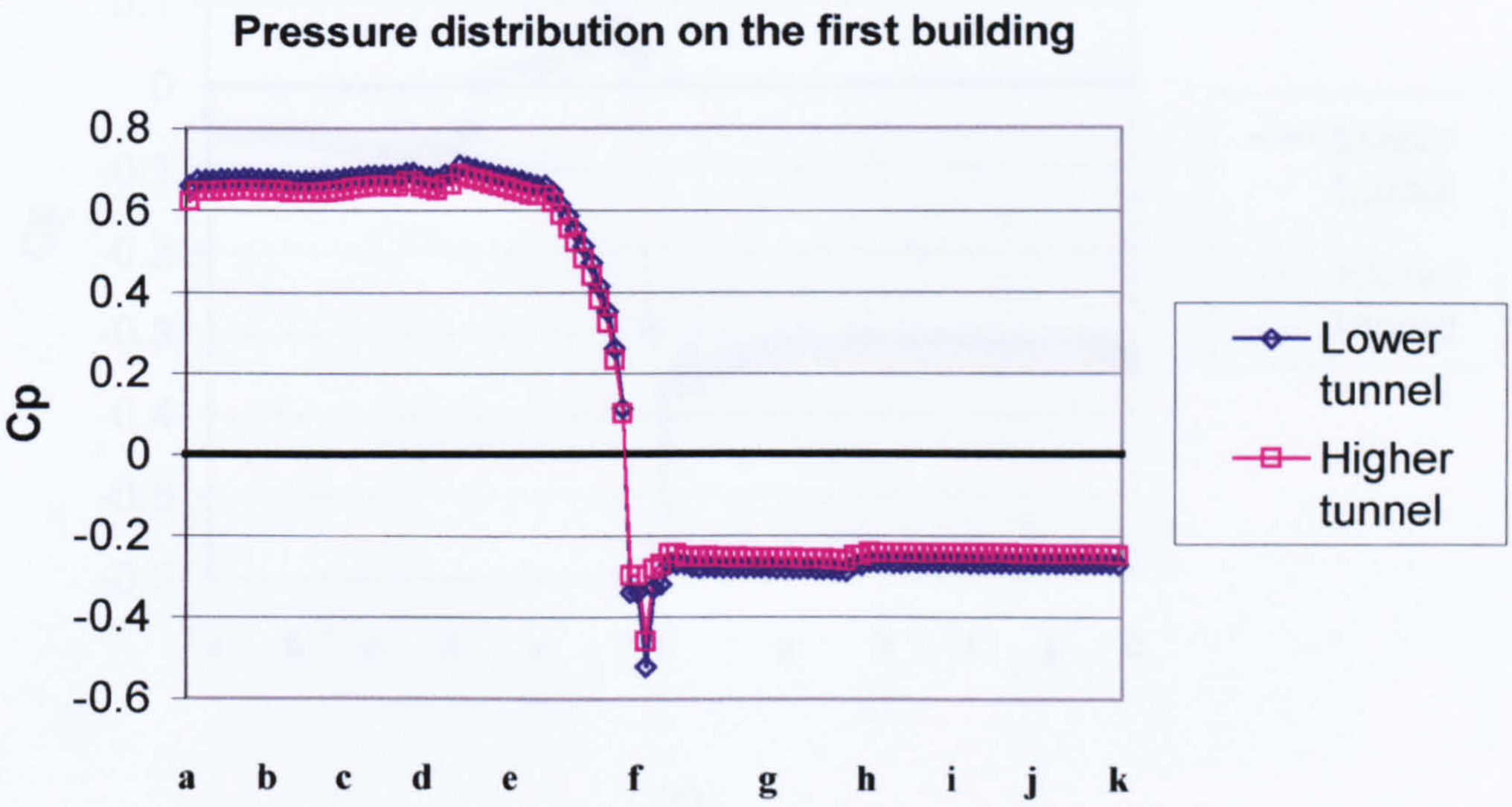

(a)

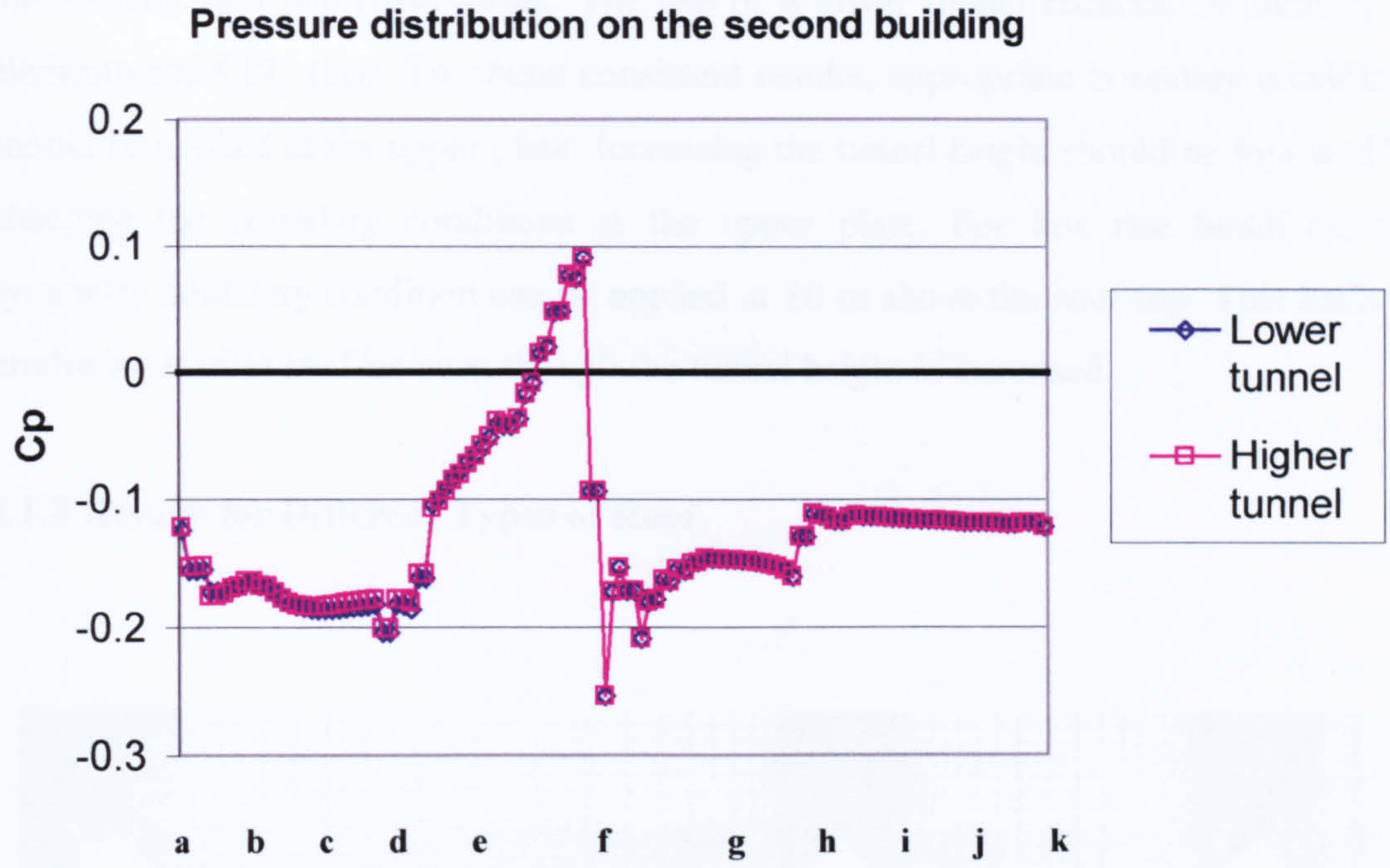

(b)

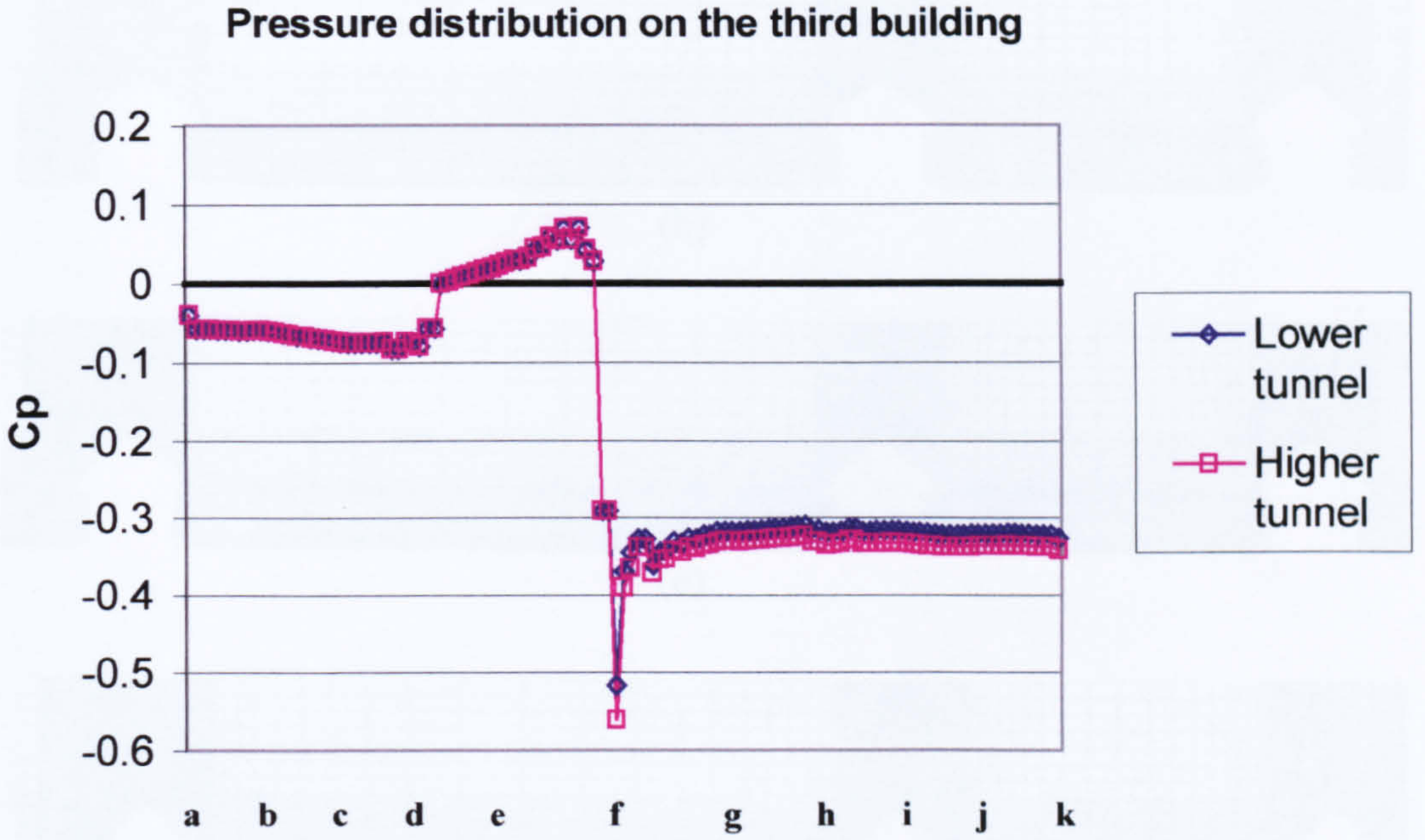

(c)

Figure 4.1.13 Pressure distribution for different tunnel heights

The surface boundary layer ($0 \leq y \leq 10$ m) is supposed to be at constant vertical momentum, heat and mass fluxes. The use of a lower tunnel reduces the number of elements and CPU time. To obtain consistent results, appropriate boundary conditions should be applied at the upper plate. Increasing the tunnel height should be followed by changing the boundary conditions at the upper plate. For low rise buildings, the symmetry boundary condition can be applied at 10 m above the roof top. This leads to producing similar profiles even though the tunnel height is increased.

4.1.8 Results for Different Types of Roof

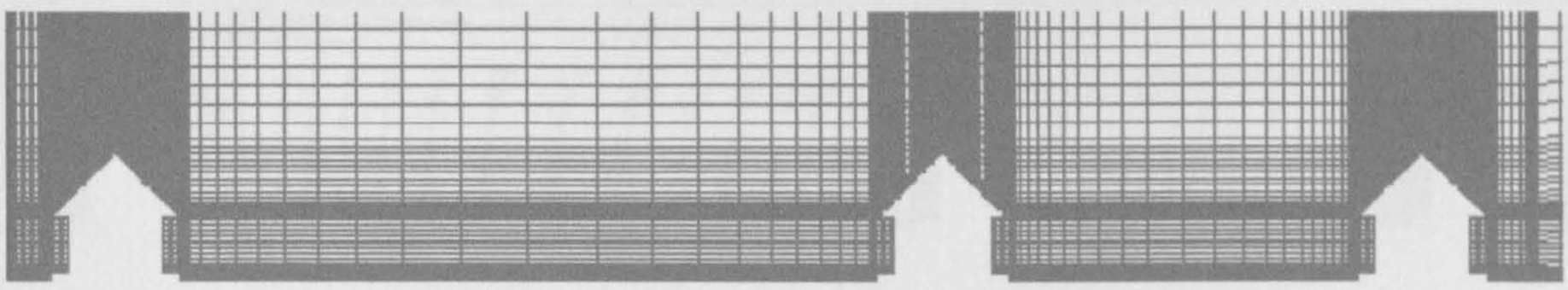

(a)

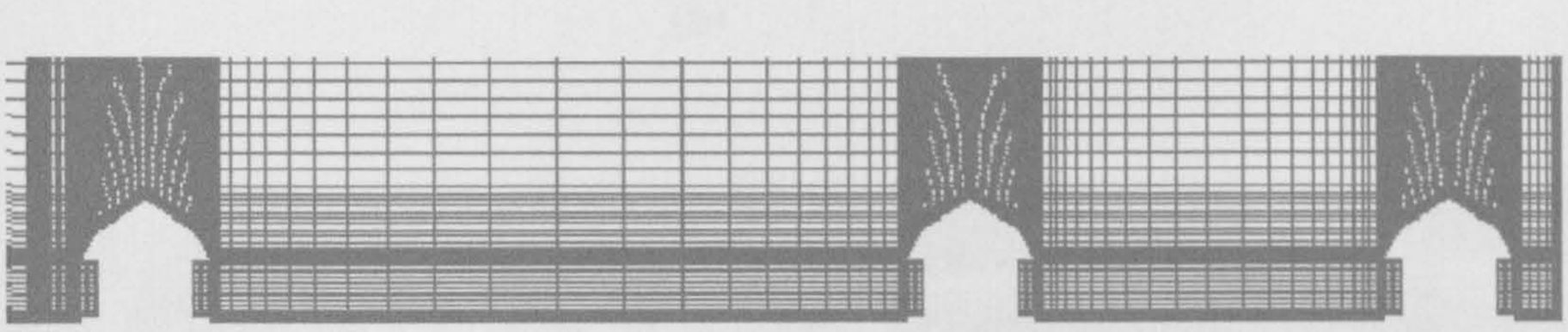

(b)

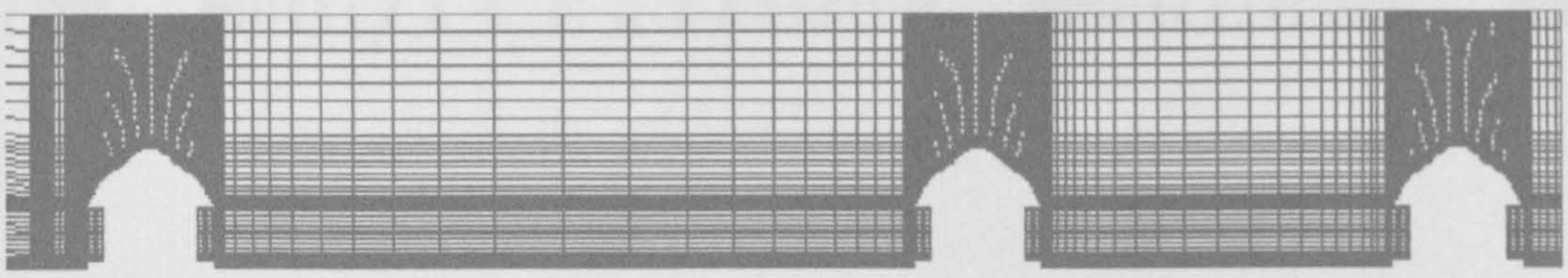

(c)

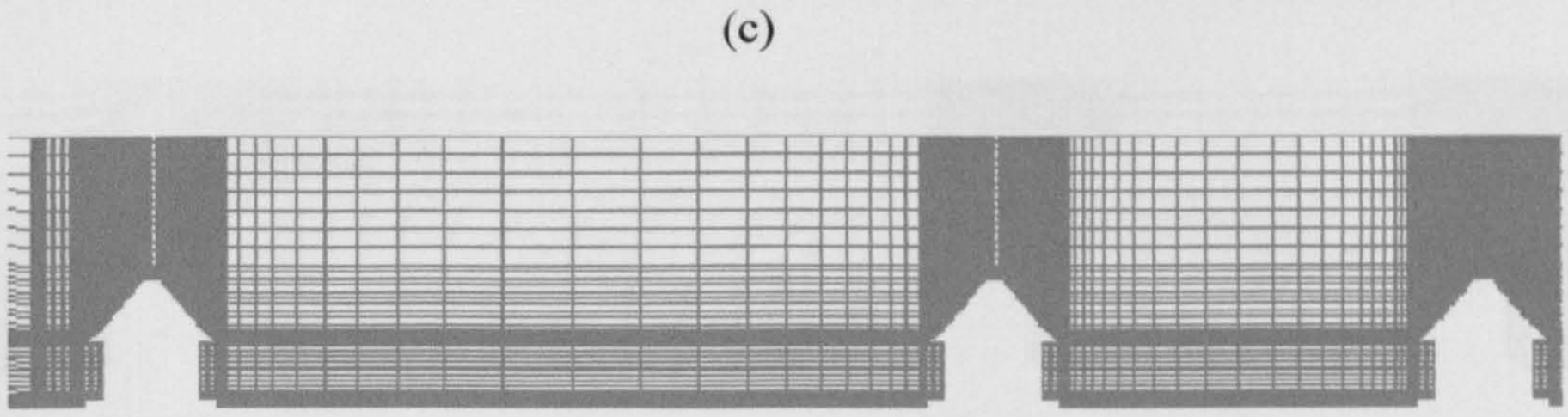

(d)

Figure 4.1.14 Typical meshes

Velocity Vector

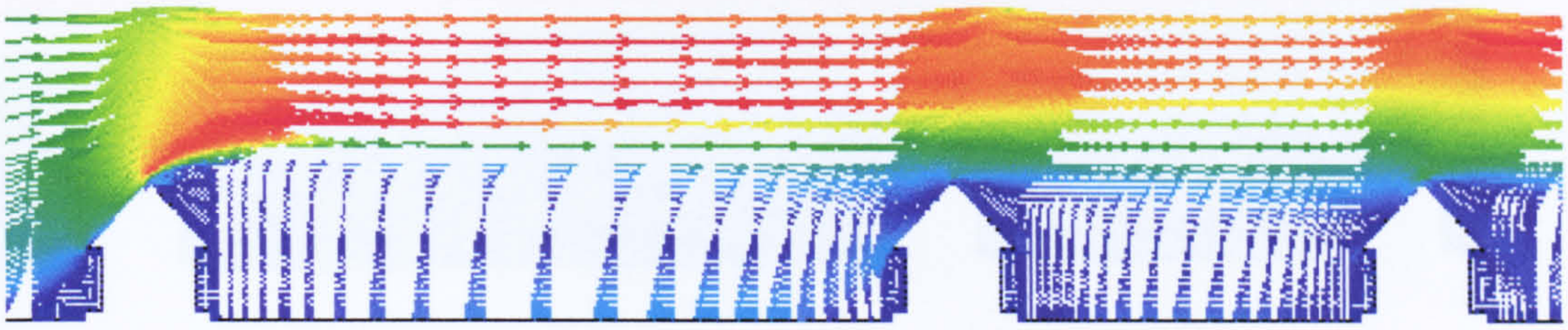

(a)

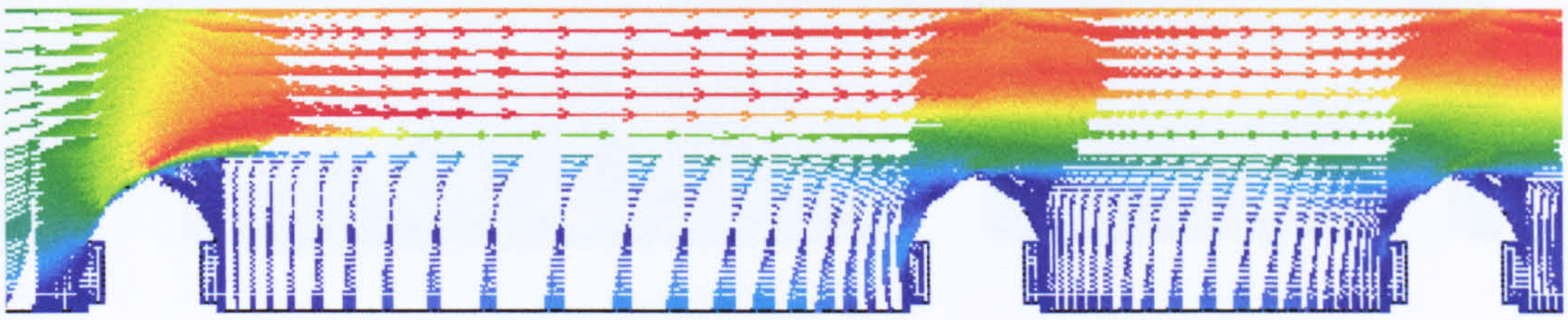

(b)

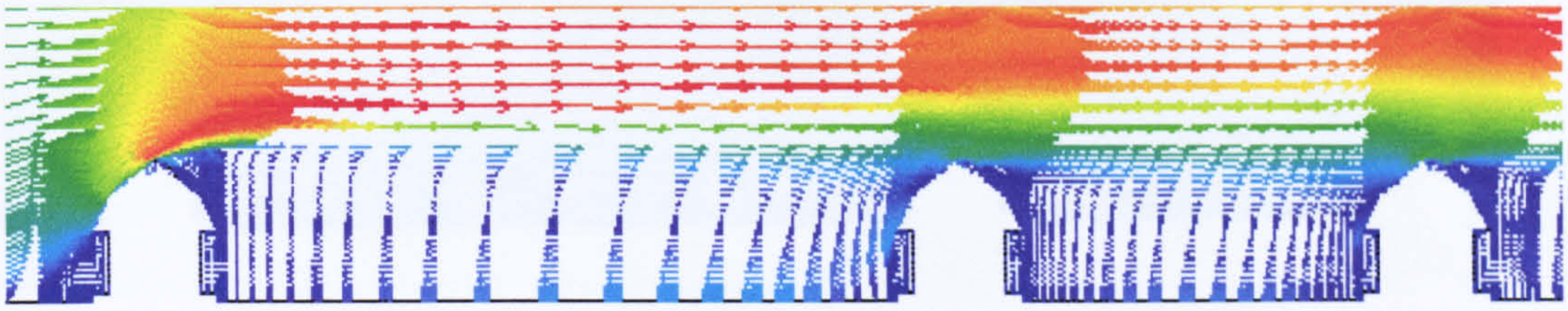

(c)

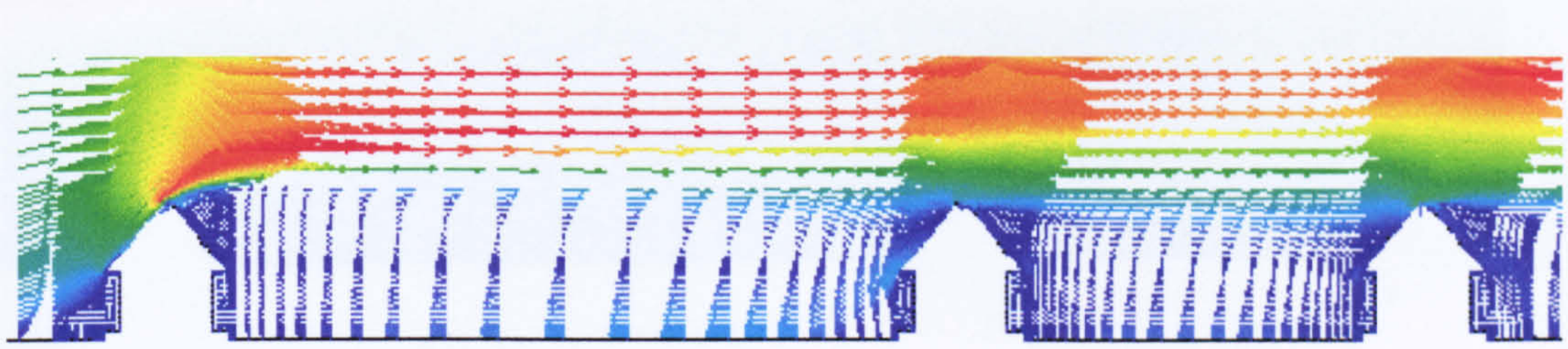

(d)

Figure 4.1.15 Velocity field around a cluster of buildings for different roof types

Streamline Plot

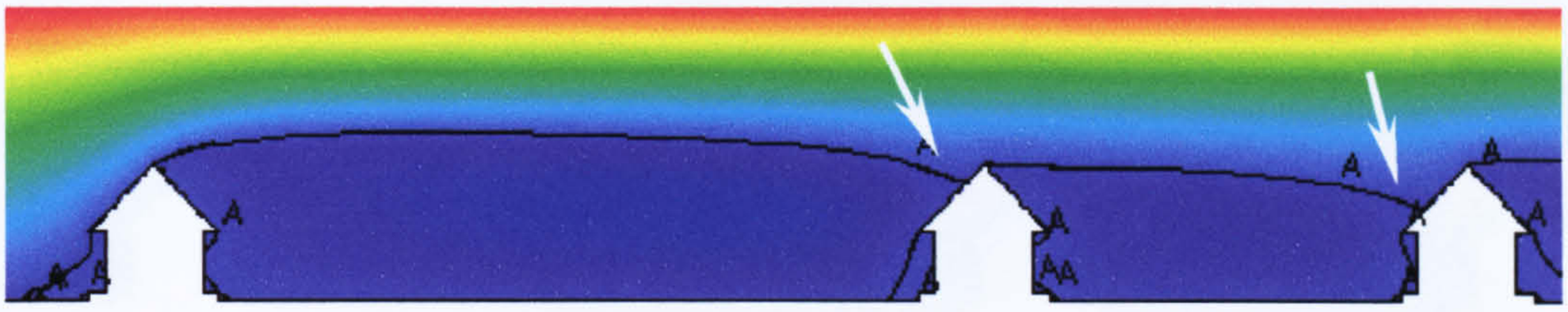

(a)

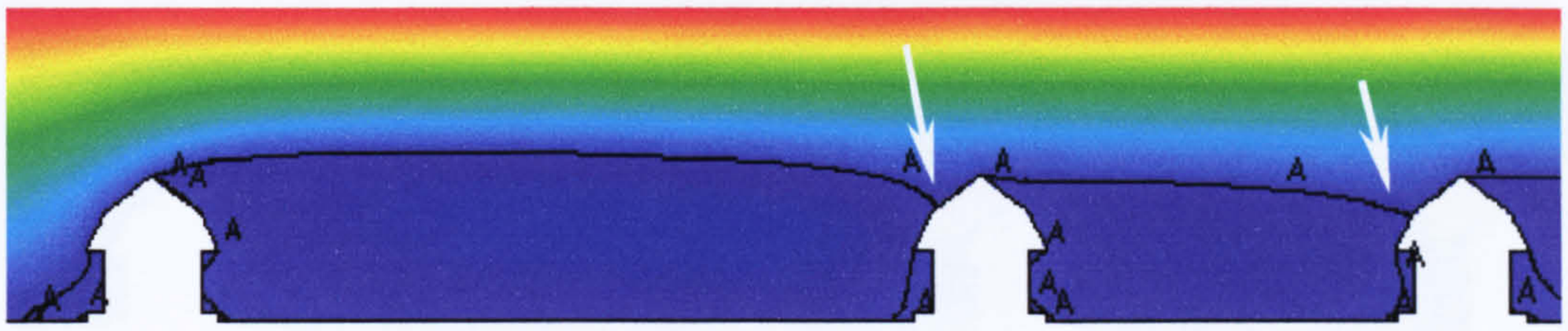

(b)

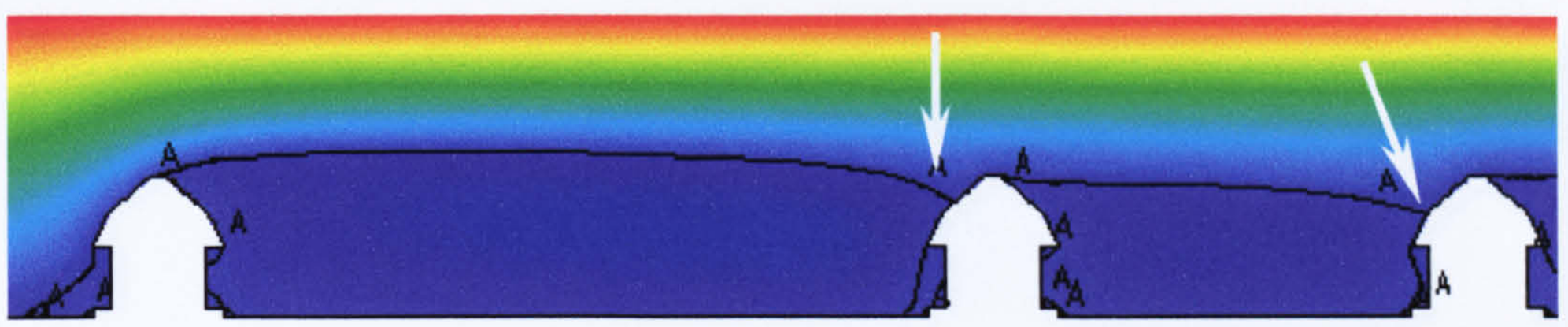

(c)

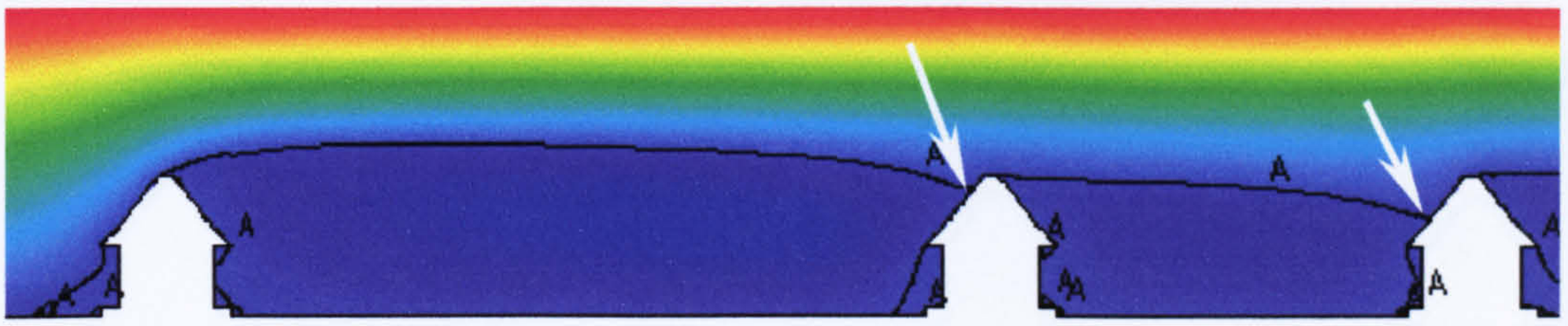

(d)

Figure 4.1.16 Streamline plots for a cluster of buildings with different roof types, arrows indicating the reattachment point

Turbulent Kinetic Energy Plot

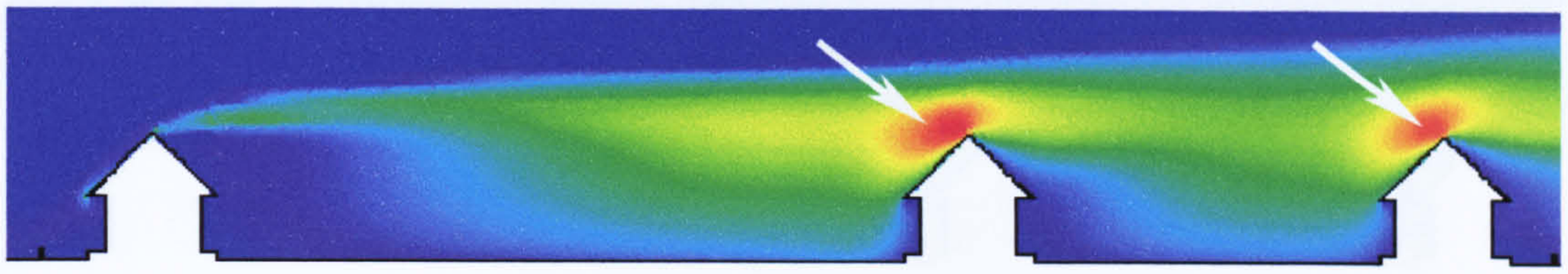

(a)

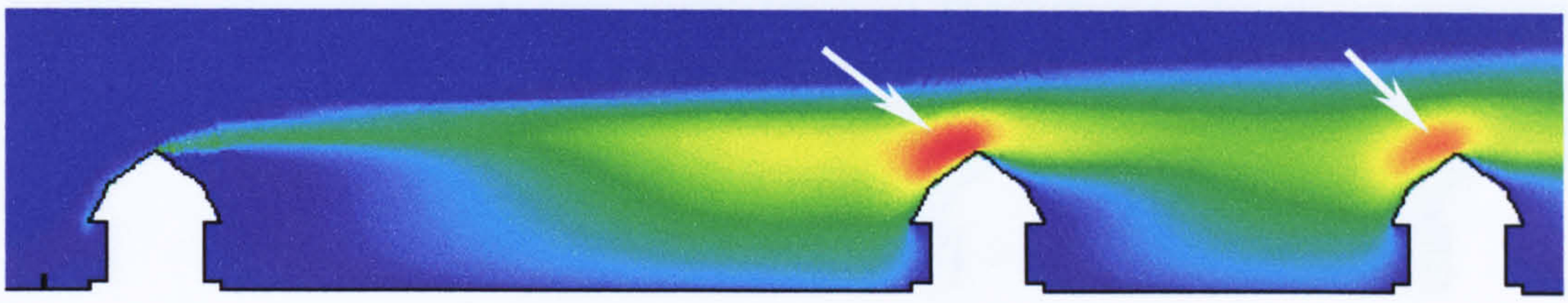

(b)

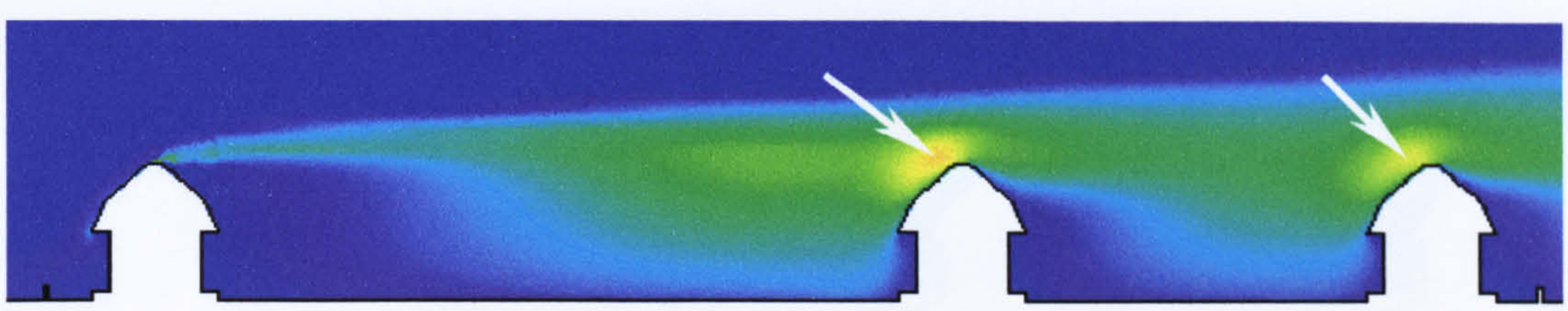

(c)

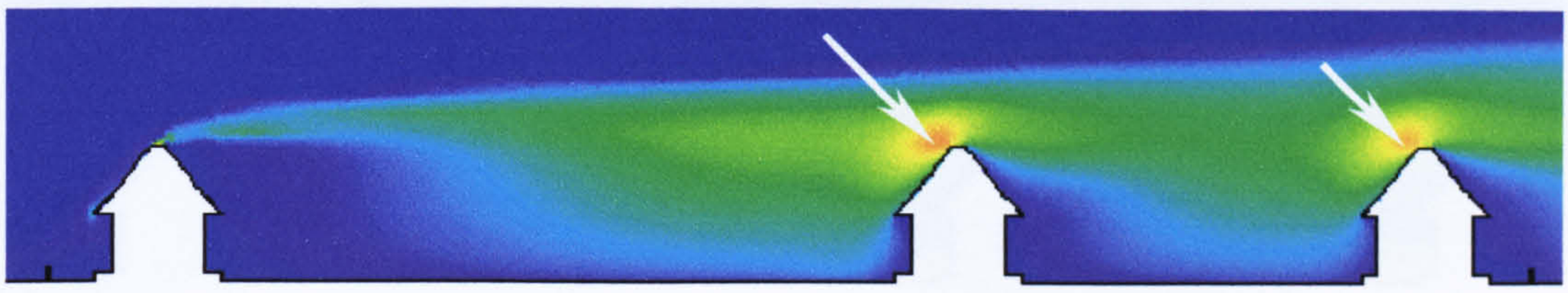

(d)

Figure 4.1.17 Turbulence kinetic energy plots for a cluster of buildings with different roof types, arrows indicating different results

Temperature Plot

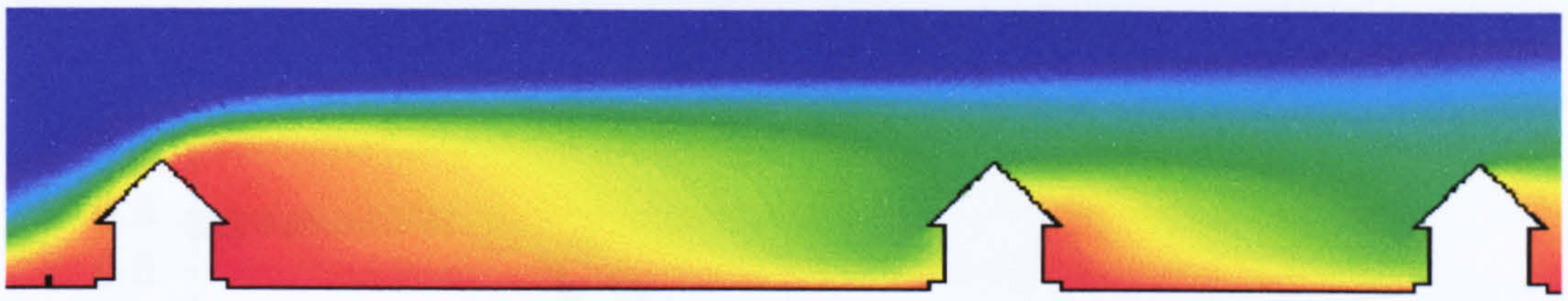

(a)

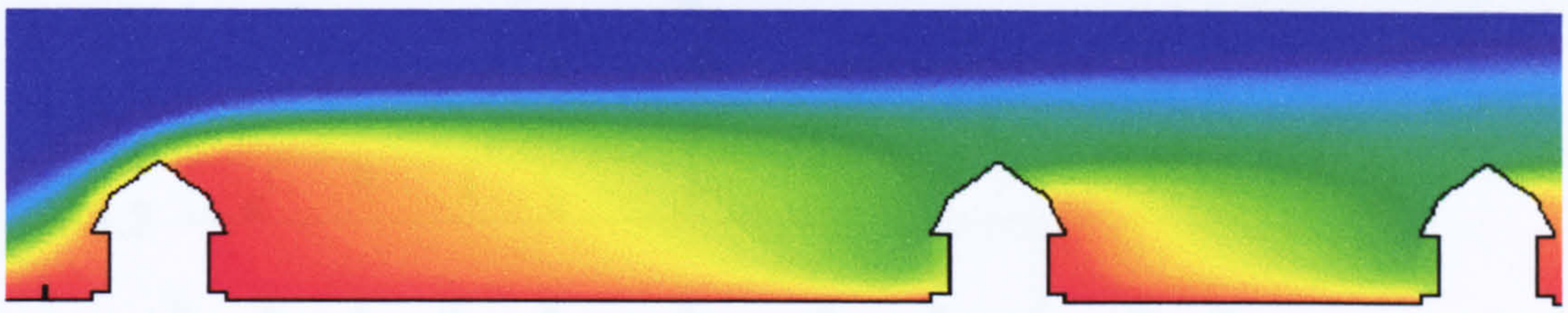

(b)

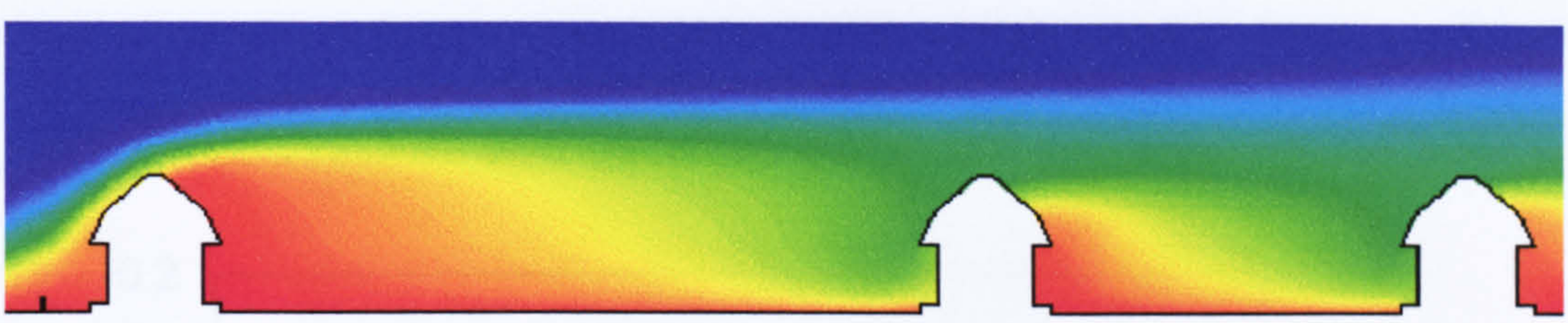

(c)

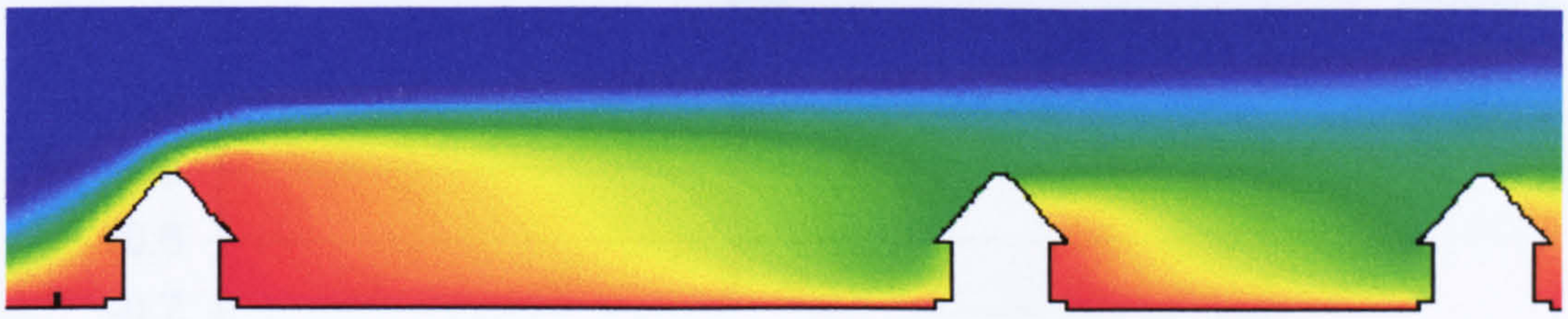

(d)

Figure 4.1.18 Temperature plot for a cluster of buildings for different roof types

Pressure Distribution

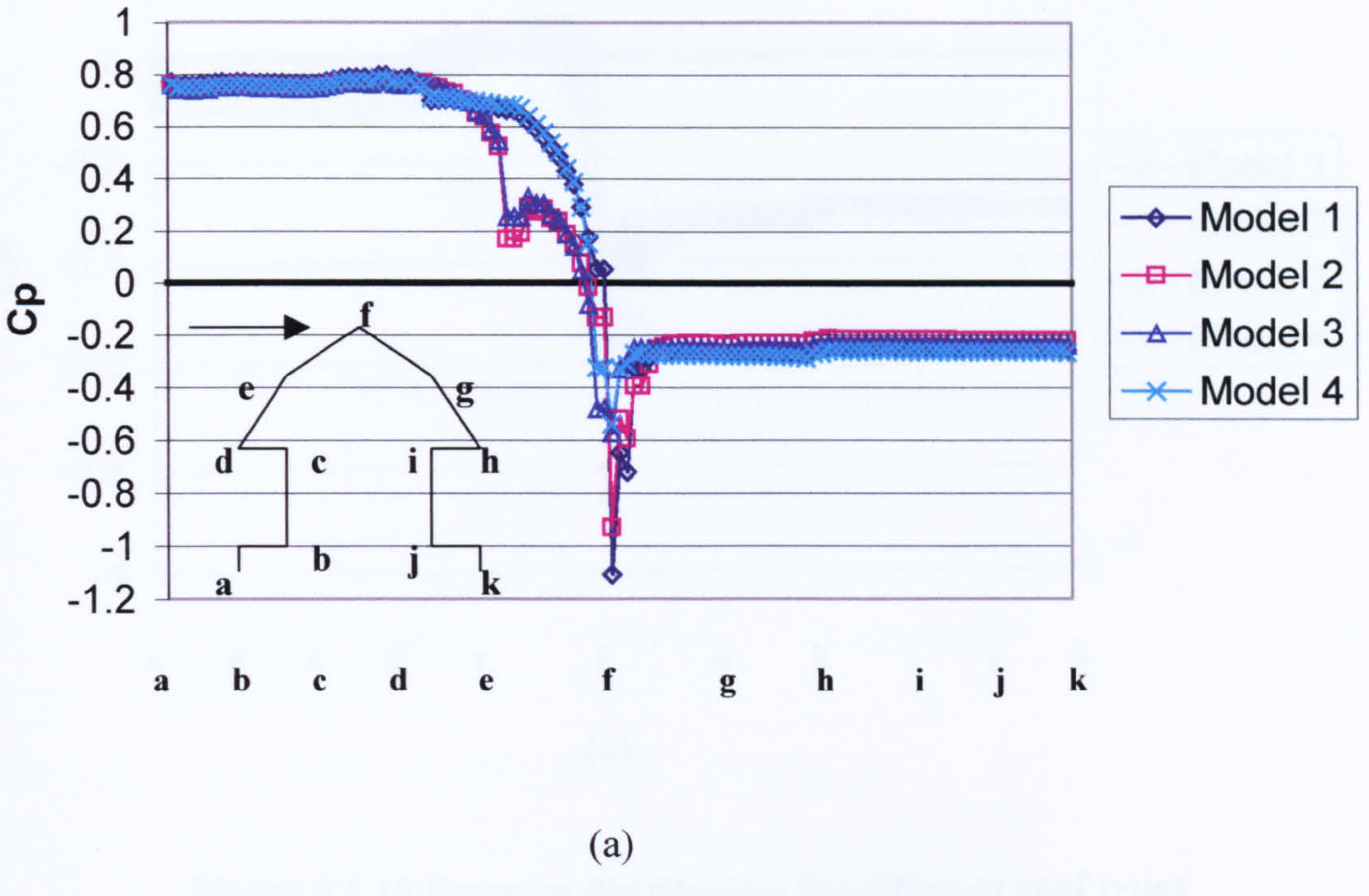

(a)

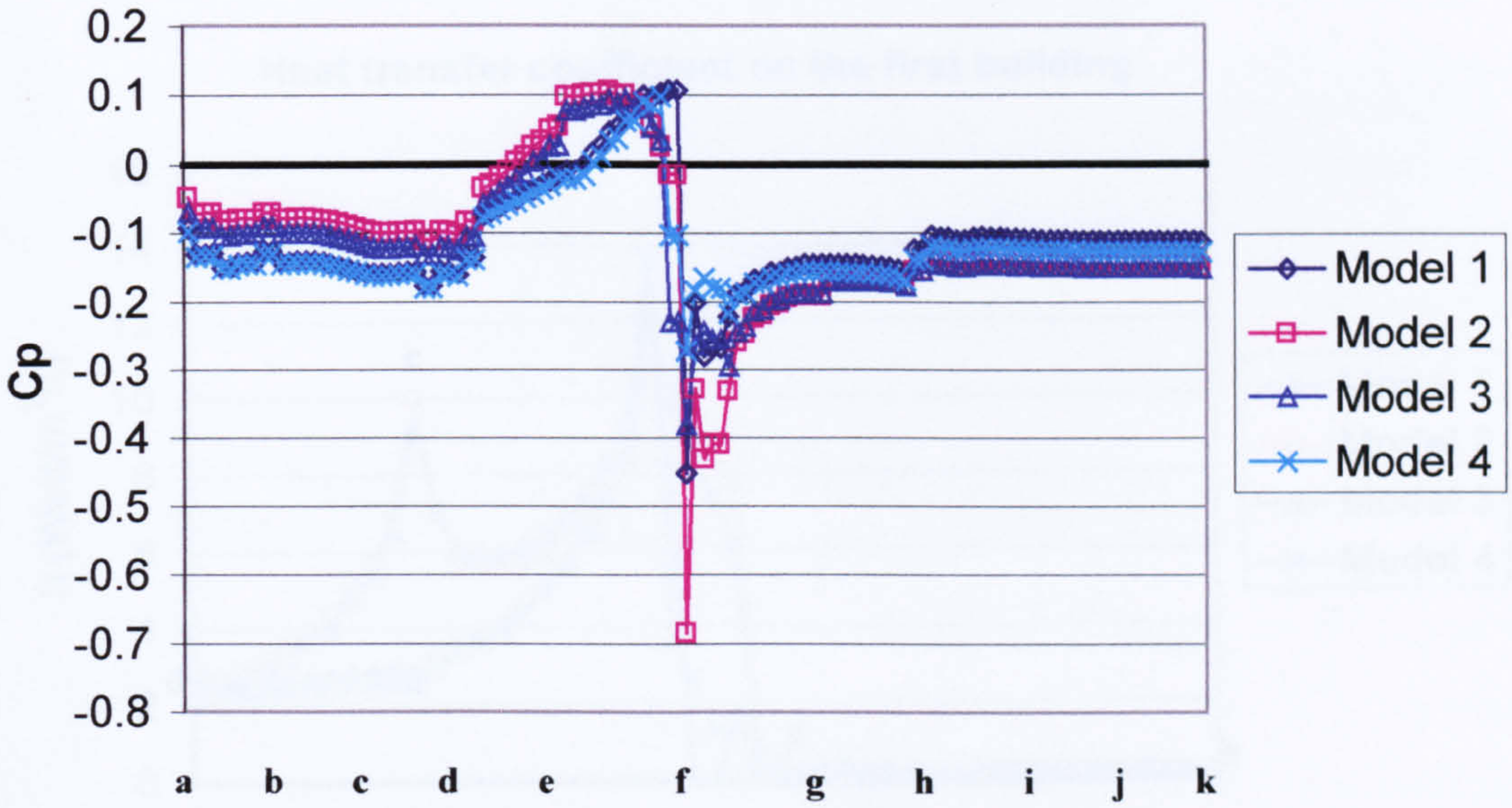

(b)

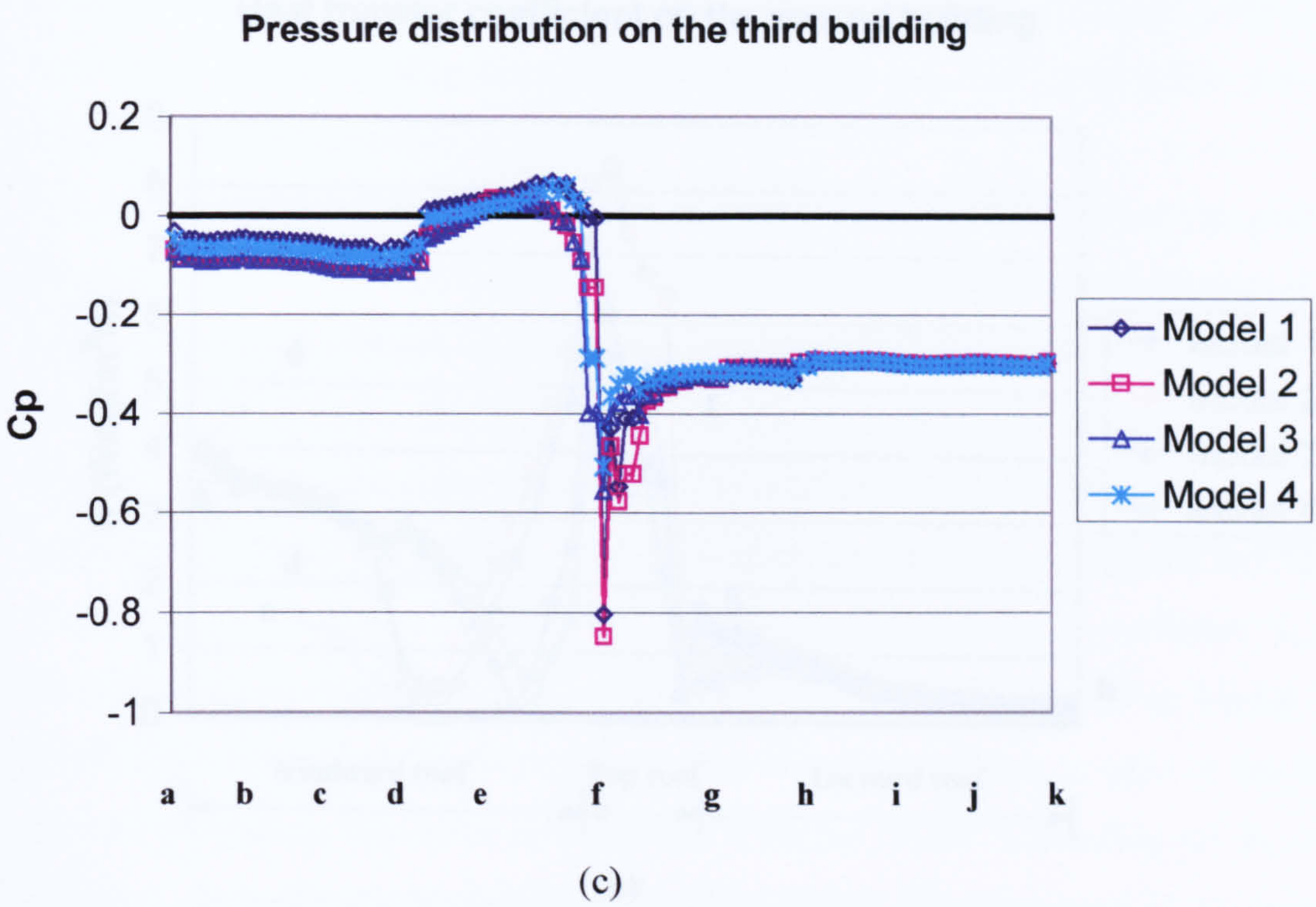

(c)

Figure 4.1.19 Pressure distribution for different roof types

Heat Transfer Coefficient

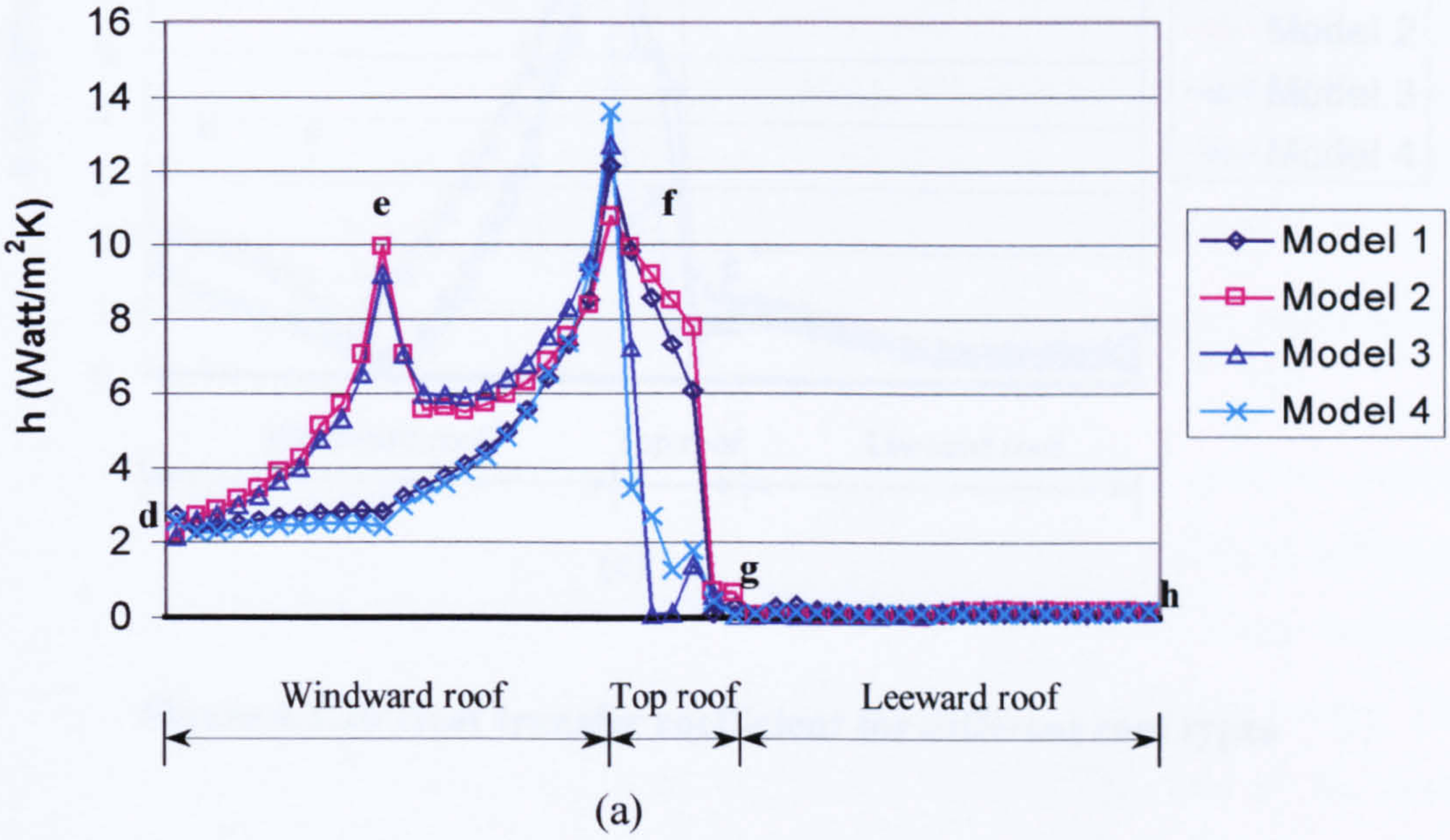

(a)

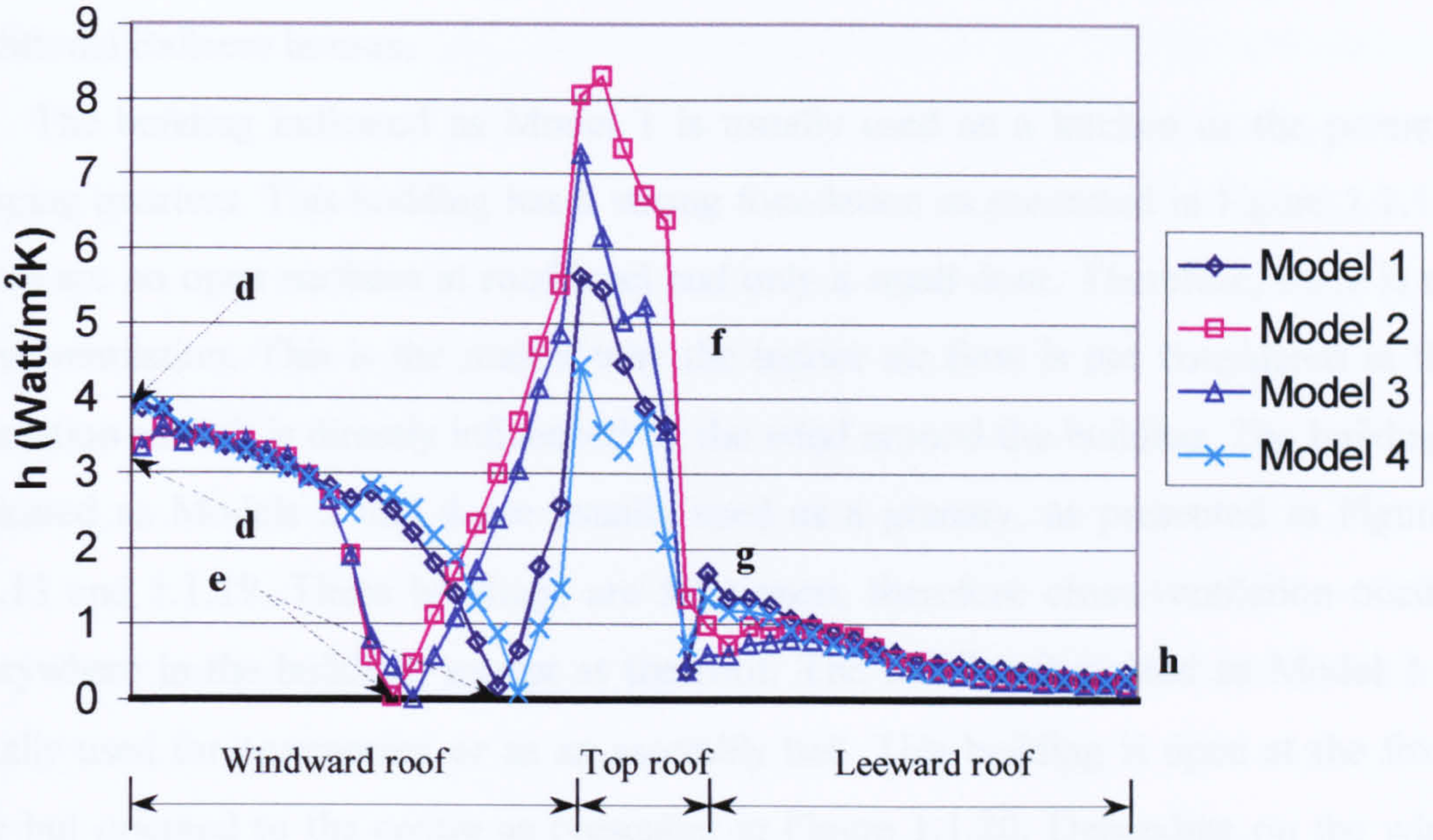

(b)

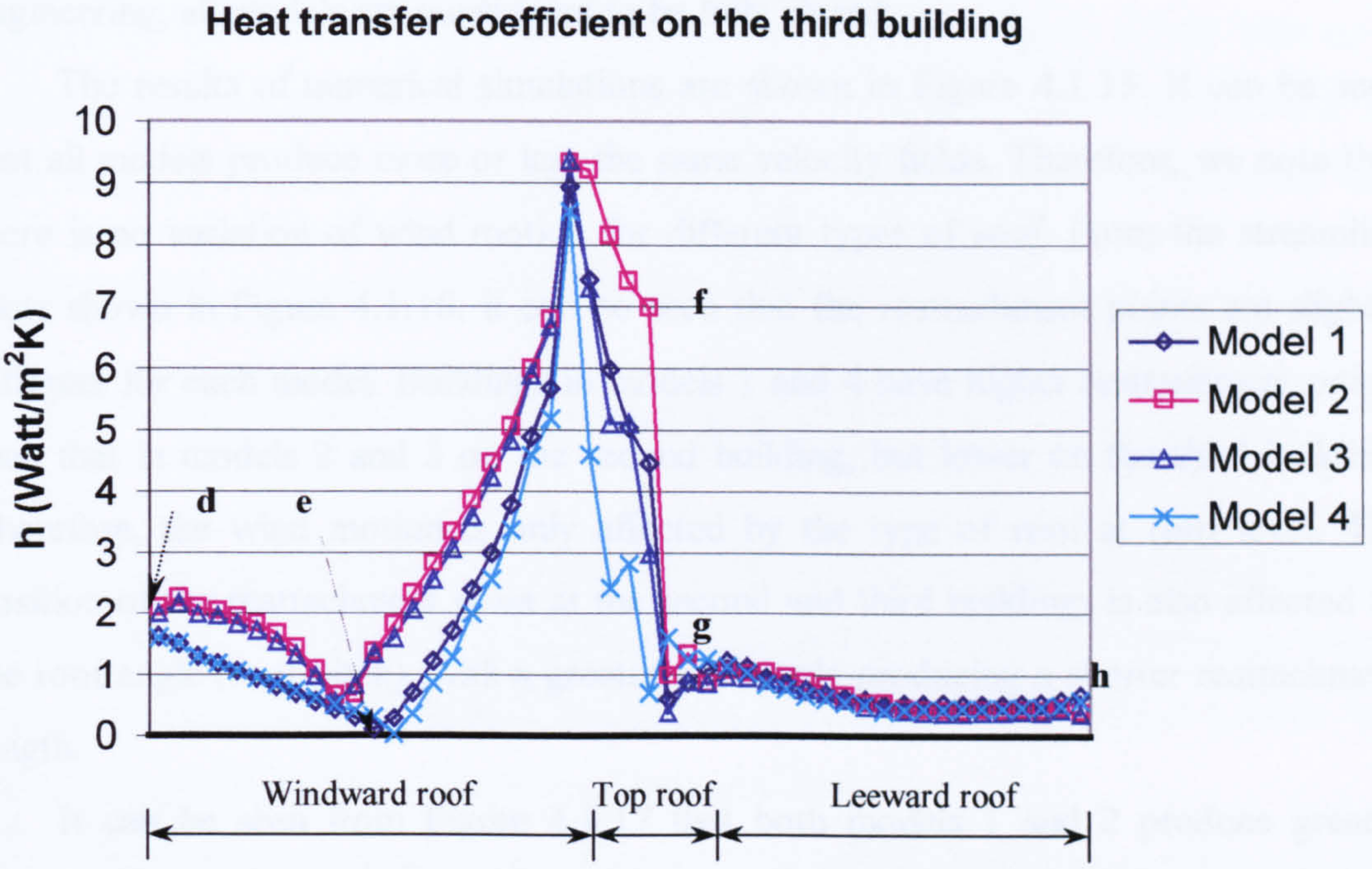

(c)

Figure 4.1.20 Heat transfer coefficient for different roof types

Wind is regarded as a popular passive cooling resource in hot and humid summer climates. Traditional houses in hot and humid climate zones are designed to utilise the wind as a natural cooling source. However, there are few quantitative data on traditional Balinese houses.

The building indicated as Model 1 is usually used as a kitchen or the parent's sleeping quarters. This building has a strong foundation as presented in Figure 1.1.14. There are no open surfaces at roof level and only a small door. Therefore, there is no cross-ventilation. This is the reason why the indoor air flow is not considered in the simulation since it is directly influenced by the wind around the building. The buildings indicated as Models 2 and 4 are usually used as a granary, as presented in Figures 1.1.13 and 1.1.19. These buildings are fully open, therefore cross-ventilation occurs everywhere in the building, except at the roof. The building indicated as Model 3 is usually used for ceremonies or as an assembly hall. This building is open at the front side but oriented to the centre as presented in Figure 1.1.20. Depending on the wind direction, the walls are considered to be fully closed. Since we want to understand whether traditional reasoning can be correlated to architectural aerodynamics and wind engineering, all models are considered to be fully closed.

The results of numerical simulations are shown in Figure 4.1.15. It can be seen that all models produce more or less the same velocity fields. Therefore, we note that there is no variation of wind motion for different types of roof. From the streamline plots shown in Figure 4.1.16, it can be seen that the reattachment points are slightly different for each model. Buildings in models 1 and 4 have higher reattachment points than that in models 2 and 3 on the second building, but lower on the third building. Therefore, the wind motion is only affected by the type of roof at roof level. The position of the reattachment point at the second and third buildings is also affected by the roof angle (roof pitch), with a greater roof angle producing a shorter reattachment length.

It can be seen from Figure 4.1.17 that both models 1 and 2 produce greater turbulent kinetic energy values than models 3 and 4, on the second and third buildings. This result also indicates that a roof which is flat at the top produces lower turbulent kinetic energy, and that a longer flat roof top reduces the turbulent kinetic energy. The highest turbulent kinetic energy occurs at the second building, followed by the third. The second building is used for ceremonies or as an assembly hall and the third building

is the parent's sleeping quarters. This indicates that there may be a relation between turbulent kinetic energy and building's function, indicated by the number of pillars (*saka*). The nine posts building (*balé tiang sanga*) used for meetings receive the highest turbulent kinetic energy. The use of nine pillars in this building will minimise the momentum effects and avoid the damage caused by the kinetic energy, since pressure distribution becomes lower at the second and third buildings. The parent's sleeping quarters (the third building), which has eight posts, received a lower turbulent kinetic energy than the second building. From this point of view, the use of pillars appears to indicate the need to protect the building to avoid possible damage, and correlates the traditional Balinese architecture to architectural aerodynamics.

There is no variation of temperature with type of roof as shown in Figure 4.1.18, in which all models produced similar temperature distributions. The non-dimensional similarity temperature for each building, $T^* = (T_s - T_g)/(T_o - T_g)$, is also presented in Figure 4.1.21.

Heat transfer by conduction and convection on building surfaces is strongly affected by the temperature distribution. Heat transfer by convection is also strongly affected by the velocity field. The distributions shown in Figure 4.1.21 indicate a similarity to the atmospheric boundary layer of low speed and forced-convection flows. This similarity is useful if the building size is to be modified (enlarged) since the heat transfer on the building can be directly related as $\dot{q}'' = \frac{k_f}{\Delta x}\frac{dT^*}{dy^*}$, where $y^* = y/H$, Δx is the material thickness in the heat transfer direction, and k_f is the thermal conductance of the material.

It can be seen in Figure 4.1.21 that the non-dimensional similarity temperature at the first building is the lowest one. This leads to the first building producing the lowest heat transfer to the surrounding. The highest cooling loads due to heat transfer will occur at the third building followed by the second building.

The greatest heat transfer occurs on the third building and this condition is needed for the parent's living quarter [7]. The lowest heat transfer happens on the first building indicating cooler but drier condition. This condition is good to store food. Therefore, it appears that there is a strong relation between buildings function and position in

traditional Balinese architecture and thermal comfort of occupants. Traditional Balinese design, therefore, can be related to thermal comfort.

From the pressure distributions presented in Figure 4.1.19, it can be seen that models 1 and 4 produce similar profiles, as well as models 2 and 3. Both models 2 and 3 produce lower pressure distributions at the windward roof (points d, e and f) of the first building. Therefore, there is a correlation between reattachment point and pressure distribution at the roof, higher reattachment points indicating higher pressure distributions. Point *d* of the first building can be assumed as the forward stagnation point with an accompanying rise in pressure.

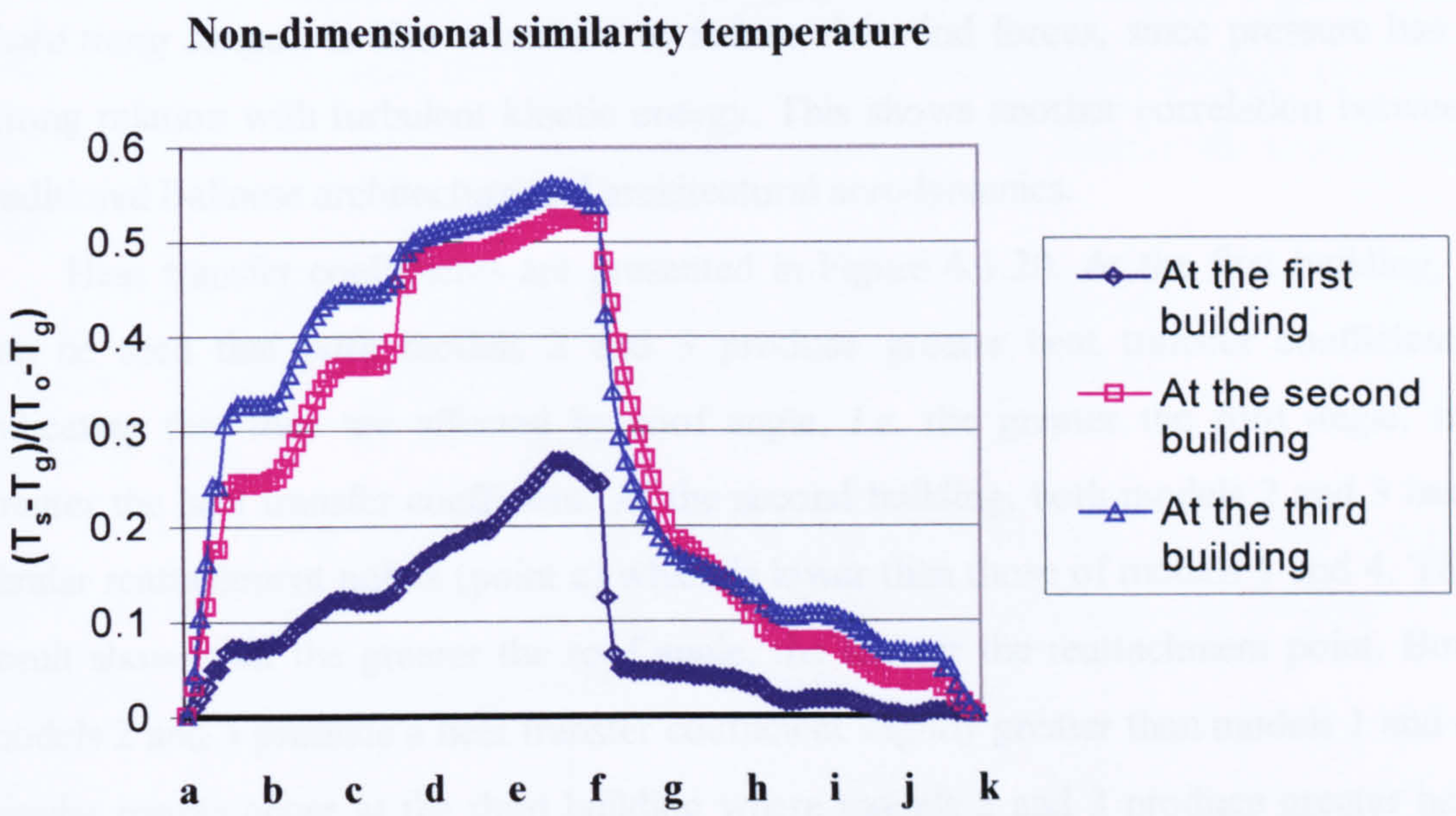

Figure 4.1.21 Non-dimensional similarity temperature on building surfaces

From this point, the pressure decreases with increasing *x*, the streamline co-ordinate, and the boundary layer develops under the influence of a favourable pressure gradient ($dp/dx<0$). At point *f*, the pressure reaches a minimum towards the rear building, and further boundary layer development occurs in the presence of adverse pressure gradient ($dp/dx>0$). From the streamline plot in Figure 4.1.16, it can be seen that the boundary layer at the windward roof is very thin indicating that the flow is turbulent. From point *d*, the fluid accelerates because of the favourable pressure gradient ($du/dx>0$ when $dp/dx<0$), reaches a maximum velocity when $dp/dx = 0$, and decelerates as a result of the adverse pressure gradient ($du/dx<0$ when $dp/dx>0$).

As the fluid decelerates, the velocity gradient at the surfaces becomes zero, at the so-called separation point. Since the Reynolds number is the same for all models, the separation point at the roof top is more or less the same for all models.

Air motion around the buildings strongly influences the drag force acting on the surface. The greater the roof angle (as indicated by models 2 and 3), the lower the pressure, but the higher the skin friction.

In the second building, model 2 produces higher pressures than the others, thus greater drag force. At the third building, models with a greater roof angle (models 2 and 3) produce greater skin friction.

From this point of view, it appears that the use of pillars, *e.g.* nine posts buildings (*balé tiang sanga*), is also a method to reduce the wind forces, since pressure has a strong relation with turbulent kinetic energy. This shows another correlation between traditional Balinese architecture and architectural aerodynamics.

Heat transfer coefficients are presented in Figure 4.1.20. At the first building, it can be seen that both models 2 and 3 produce greater heat transfer coefficients, indicating that they are affected by roof angle, *i.e.* the greater the roof angle, the greater the heat transfer coefficient. At the second building, both models 2 and 3 have similar reattachment points (point e) which is lower than those of models 1 and 4. This result shows that the greater the roof angle, the shorter the reattachment point. Both models 2 and 3 produce a heat transfer coefficient slightly greater than models 1 and 4. Similar results occur at the third building where models 2 and 3 produce greater heat transfer coefficients than models 1 and 4.

It appears that buildings with greater roof angles produce greater heat transfer coefficients. This also indicates greater friction at building surfaces leading to increased force at the roof. Therefore, buildings as indicated by models 2 and 3 are subjected to greater skin friction which leads to an increased lift force.

According to the above discussion, we propose that buildings in models 2 and 3 will increase the heat transfer to the surrounding. This is the reason why these models are used as granaries, as presented in Figure 1.1.19, since rice paddies and any other foods should be stored in a dry and cool place.

4.2 Effects of the Fence Height on Wind Motion around Traditional Balinese Buildings

4.2.1 Introduction

Windbreaks such as plants and fences provide protection against glare and dust but desirable air movement can be drastically reduced or directed away from the building. There is a difference between the shelter offered by windbreaks composed of plants and that offered by solid screens, as the extent of shelter depends not only on height but also on the degree of permeability. Plant material, which permits a certain amount of air to pass through, causes less turbulence than solid screens and produce a greater total area of shelter. The zone just behind the windbreak itself has the greatest protection from the wind. The more impenetrable the windbreak, the shorter the reattachment length.

In traditional Balinese architecture, the fence is relatively high, as presented in Figures 1.1.11, 1.1.12 and 1.1.13 and the distance between buildings and the fence is relatively short.

The aim of this study is to find a correlation between fence height and distance between fence and buildings with the air motion around buildings, and whether these parameters affect the thermal comfort of occupants.

4.2.2 Physical model

Two types of fence are used in the present study, as shown in Figure 4.2.1. The boundary conditions used are the same as that in Section 4.1. Therefore, the study only focus on the effects of the fence height and distance between fence and buildings on air flow patterns. All figures denoted by (a) indicate models with a lower fence height, $\mathbf{h_1}$, and (b) indicate models with a higher fence height, $\mathbf{h_2}$, where $\mathbf{h_1}$ is 0.1 **H** and $\mathbf{h_2}$ is 0.3 **H.**

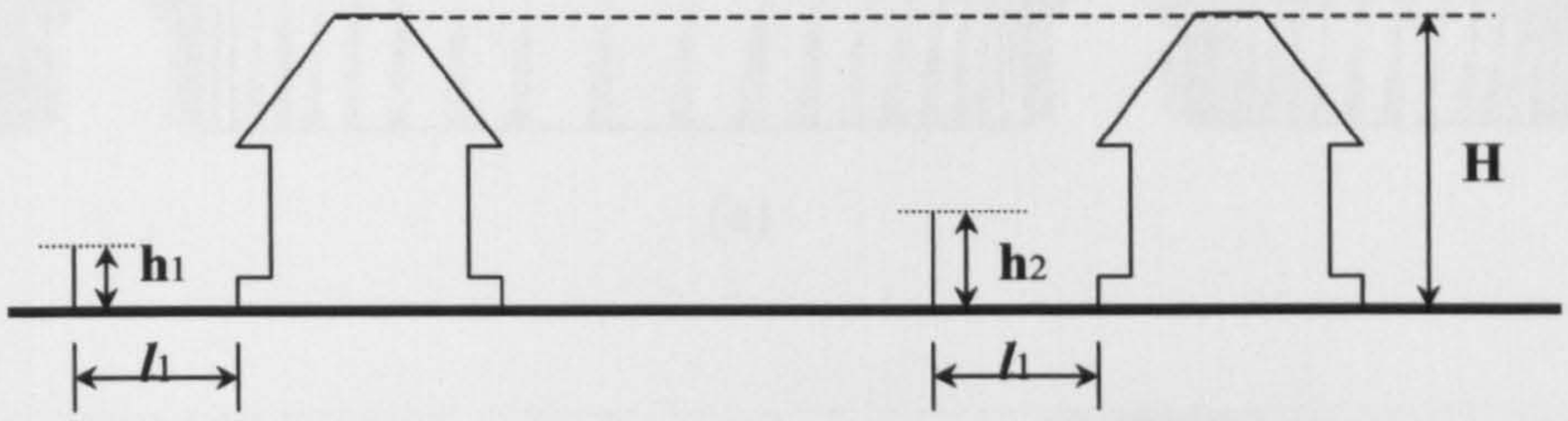

Figure 4.2.1 Physical model

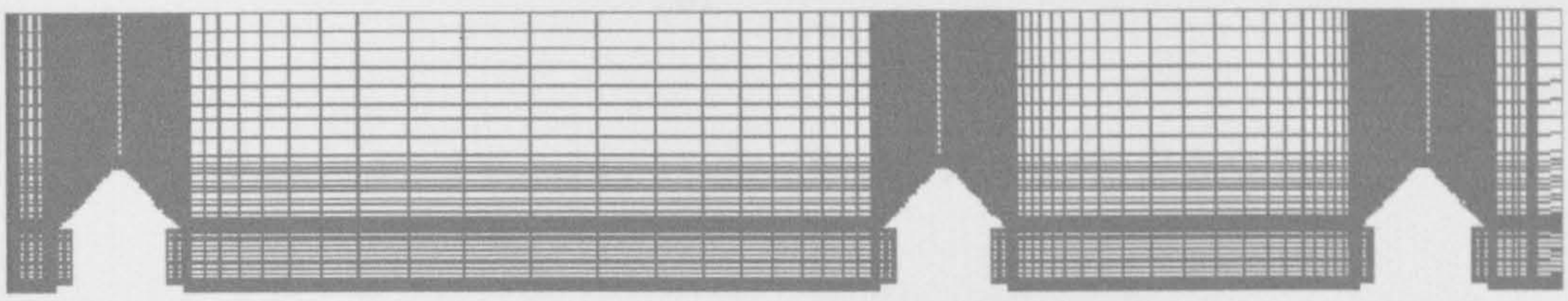

(a)

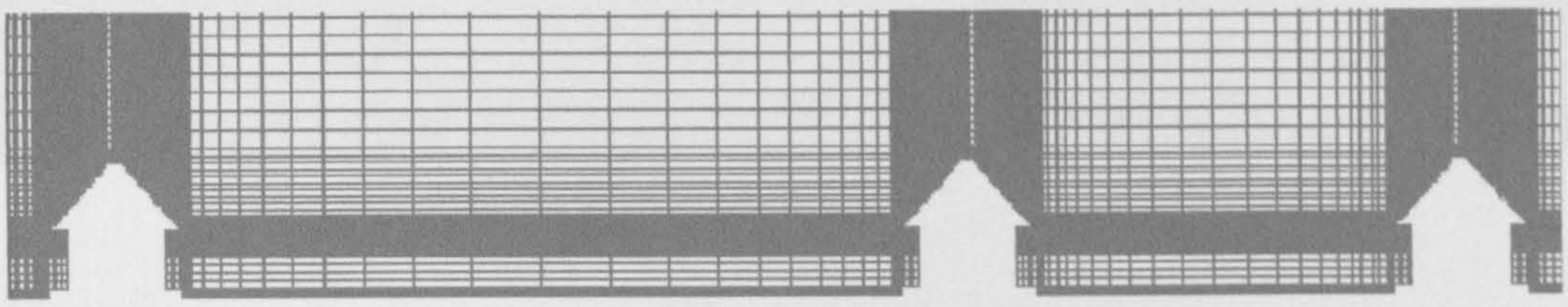

(b)

Figure 4.2.2 Typical meshes

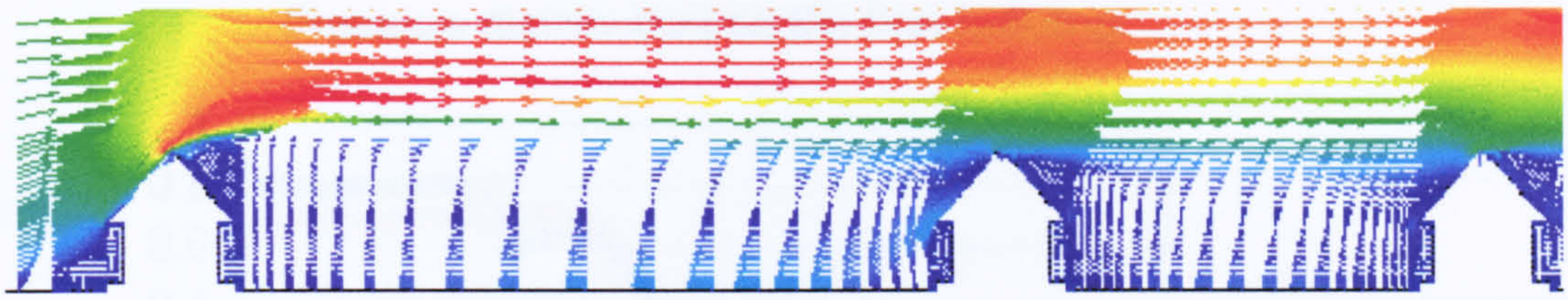

(a)

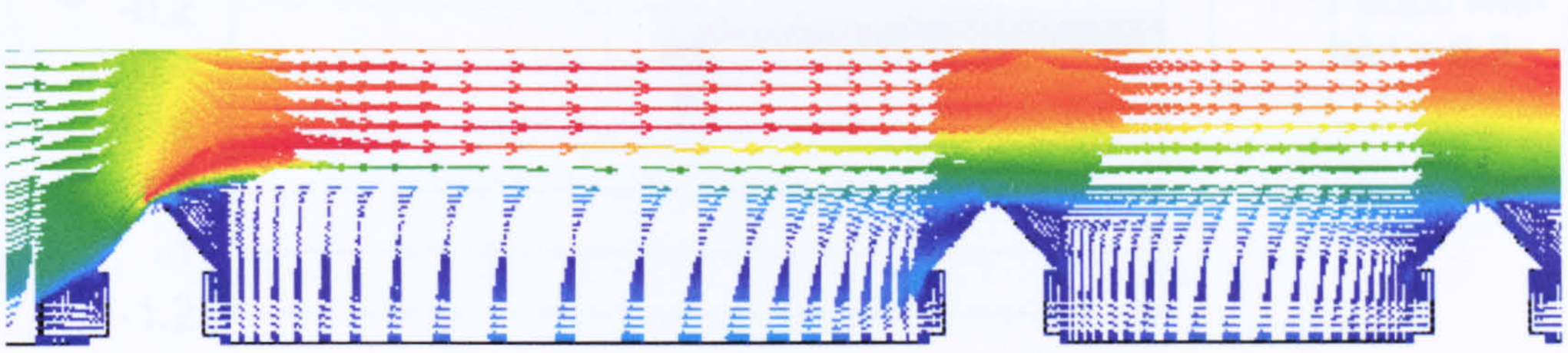

(b)

Figure 4.2.3 Velocity vectors for different fence heights

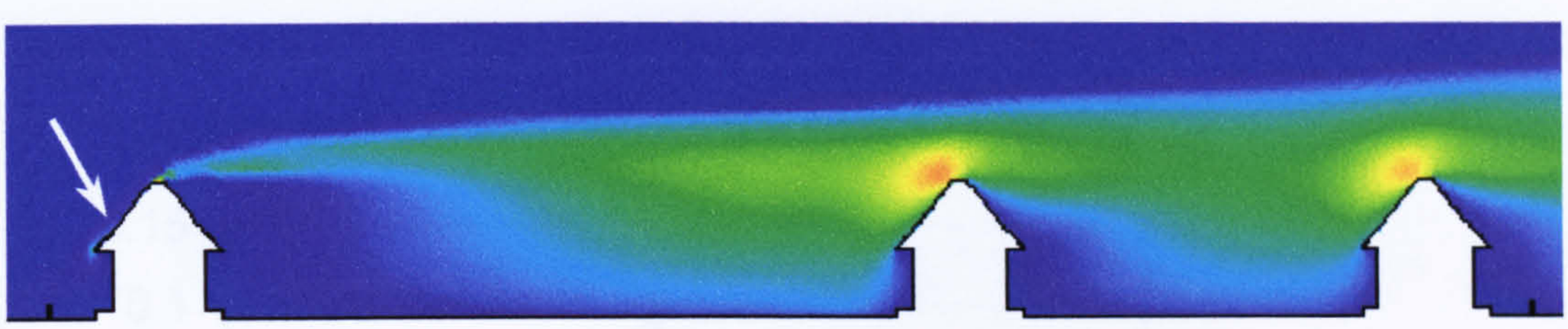

(a)

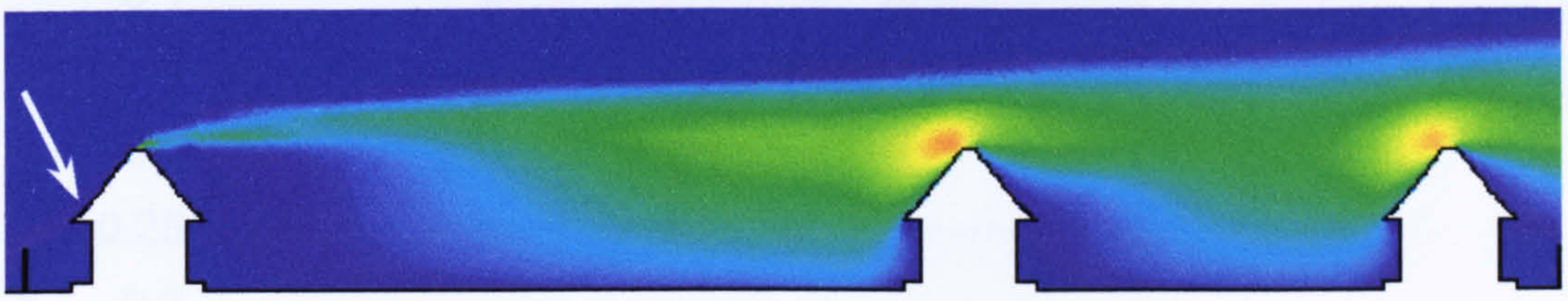

(b)

Figure 4.2.4 Turbulent kinetic energy plots for different fence heights

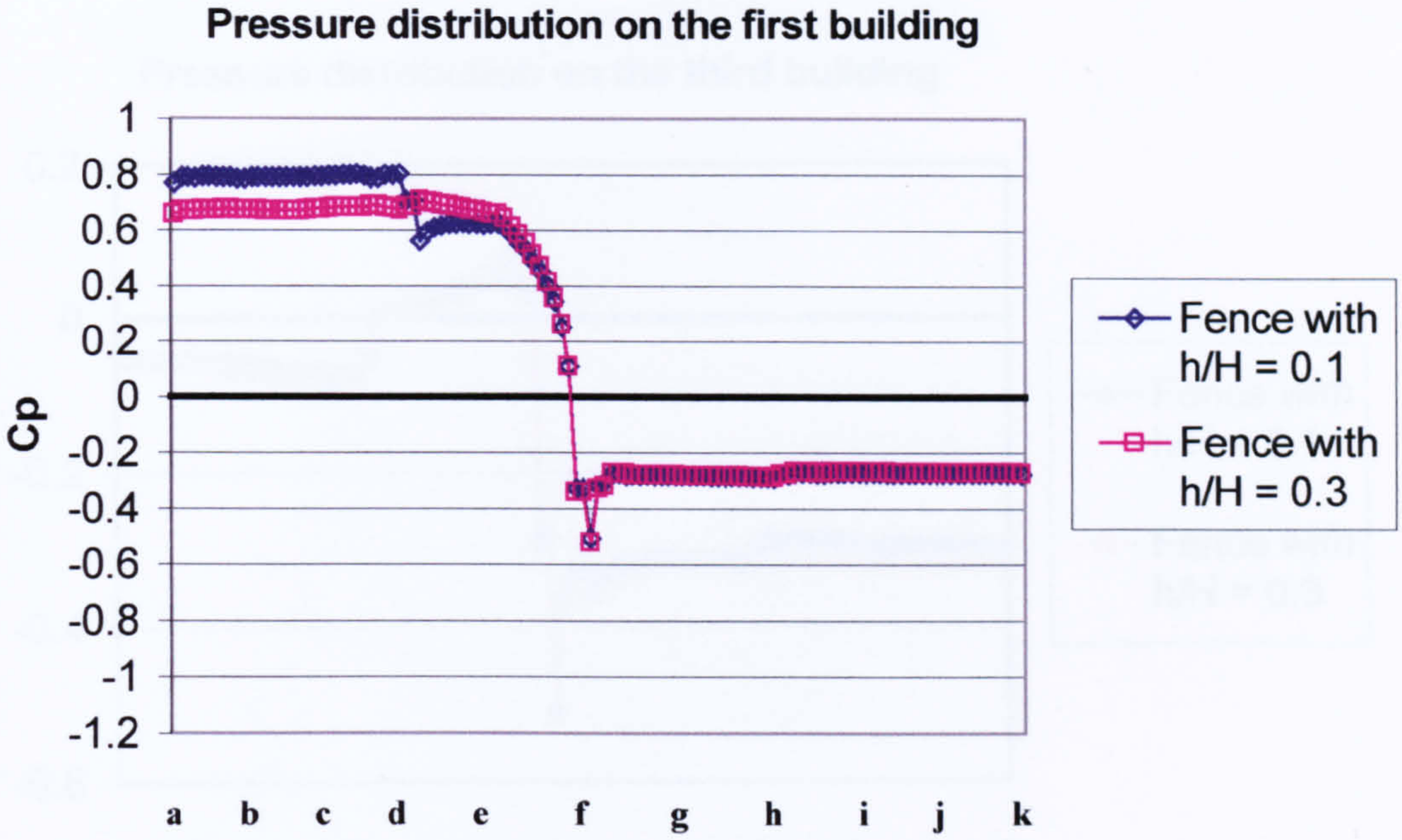
Pressure distribution on the first building
1
0.8
0.6
0.4
0.2
0
-0.2
-0.4
-0.6
-0.8
-1
-1.2
Cp
a b c d e f g h i j k
Fence with h/H = 0.1
Fence with h/H = 0.3

(a)

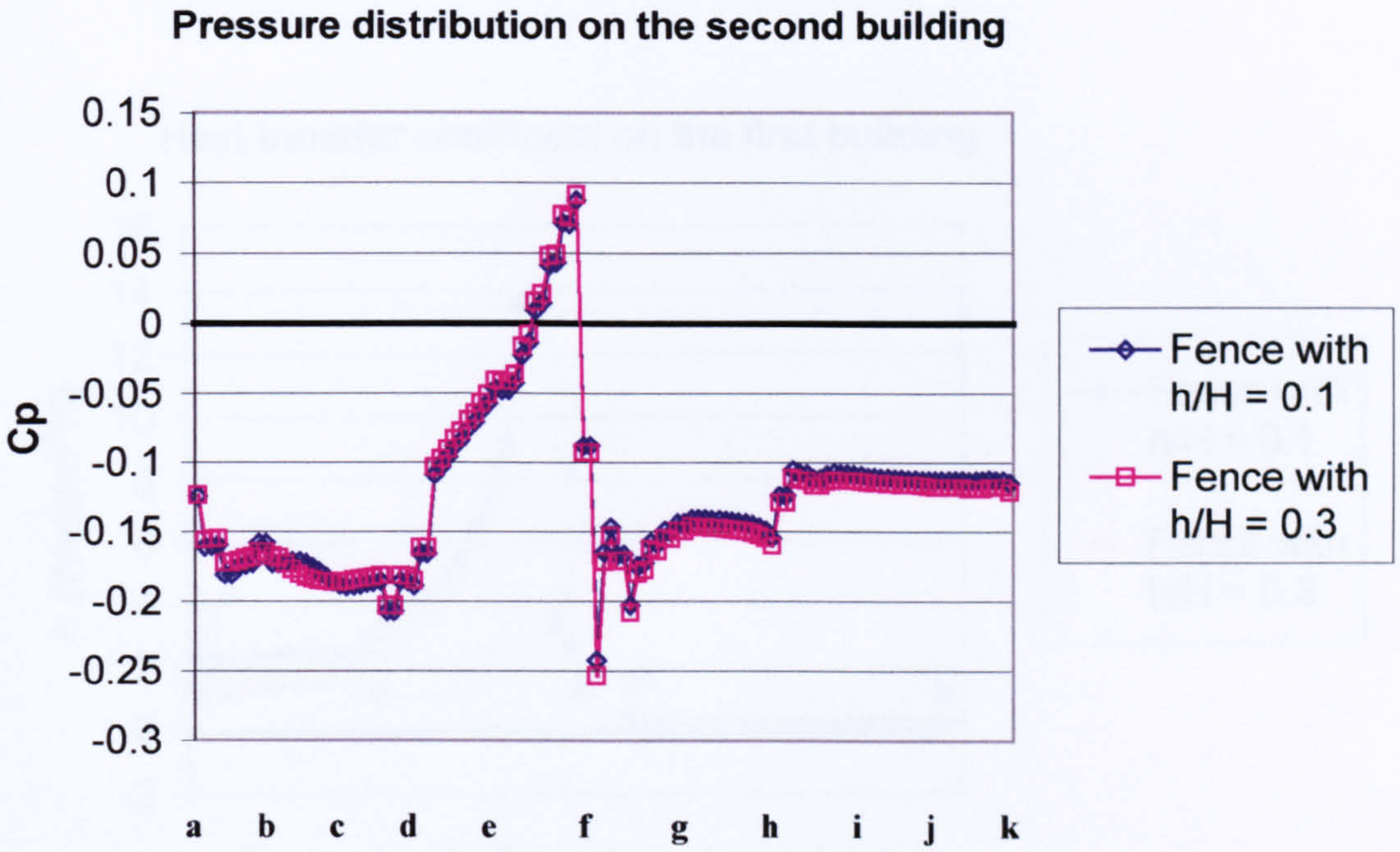
Pressure distribution on the second building
0.15
0.1
0.05
0
-0.05
-0.1
-0.15
-0.2
-0.25
-0.3
Cp
a b c d e f g h i j k
Fence with h/H = 0.1
Fence with h/H = 0.3

(b)

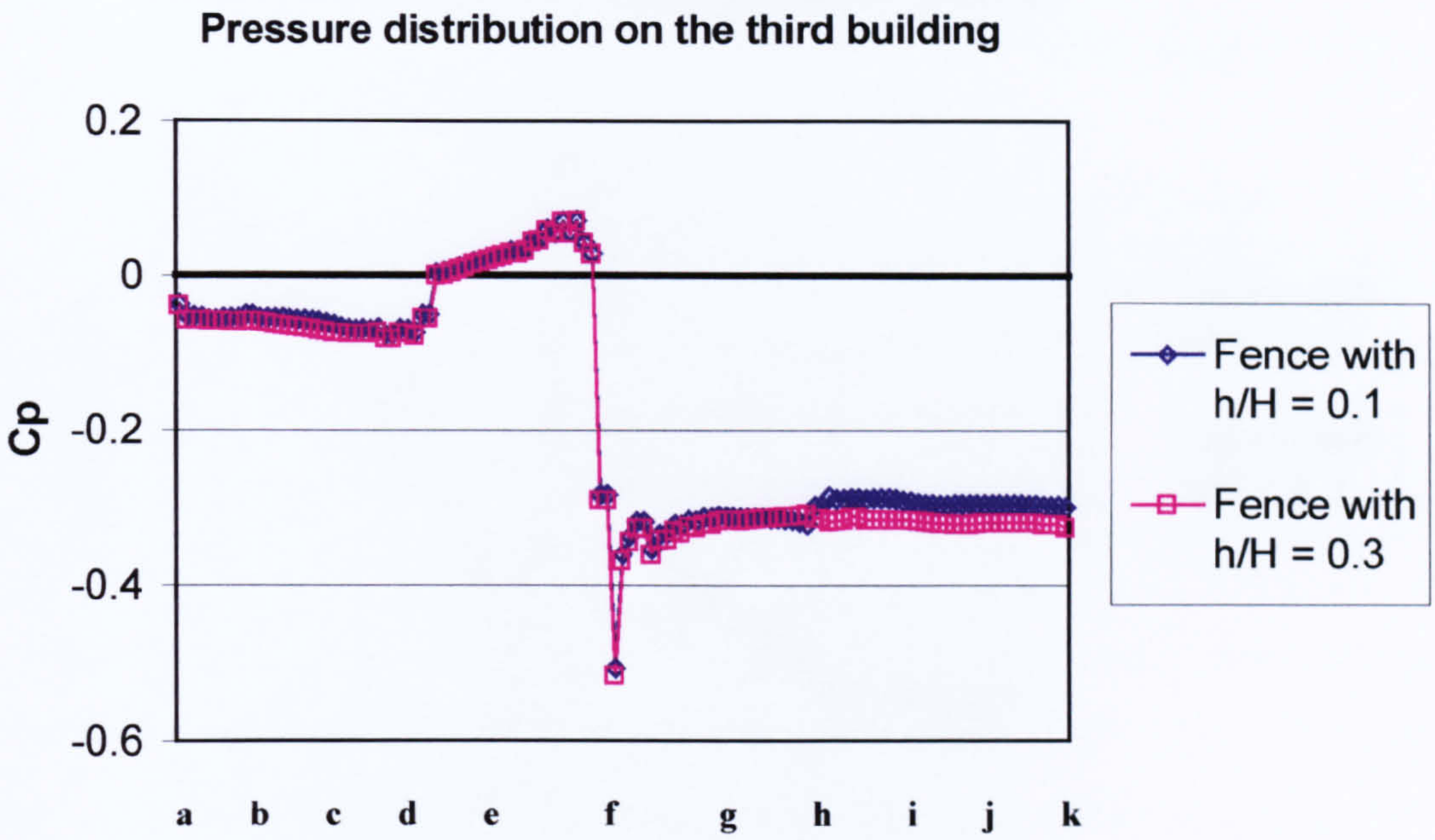

(c)

Figure 4.2.5 Pressure distributions for different fence heights

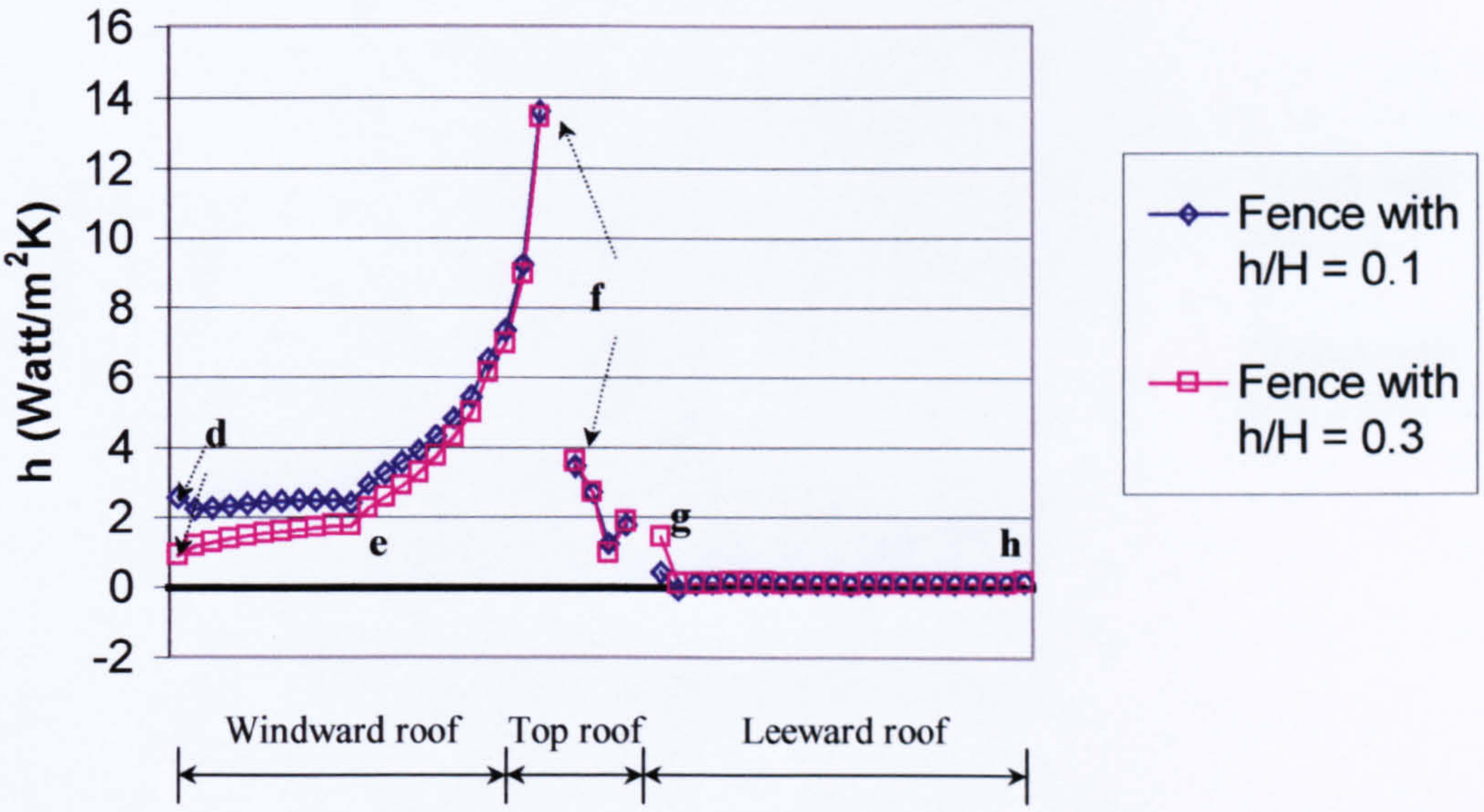

(a)

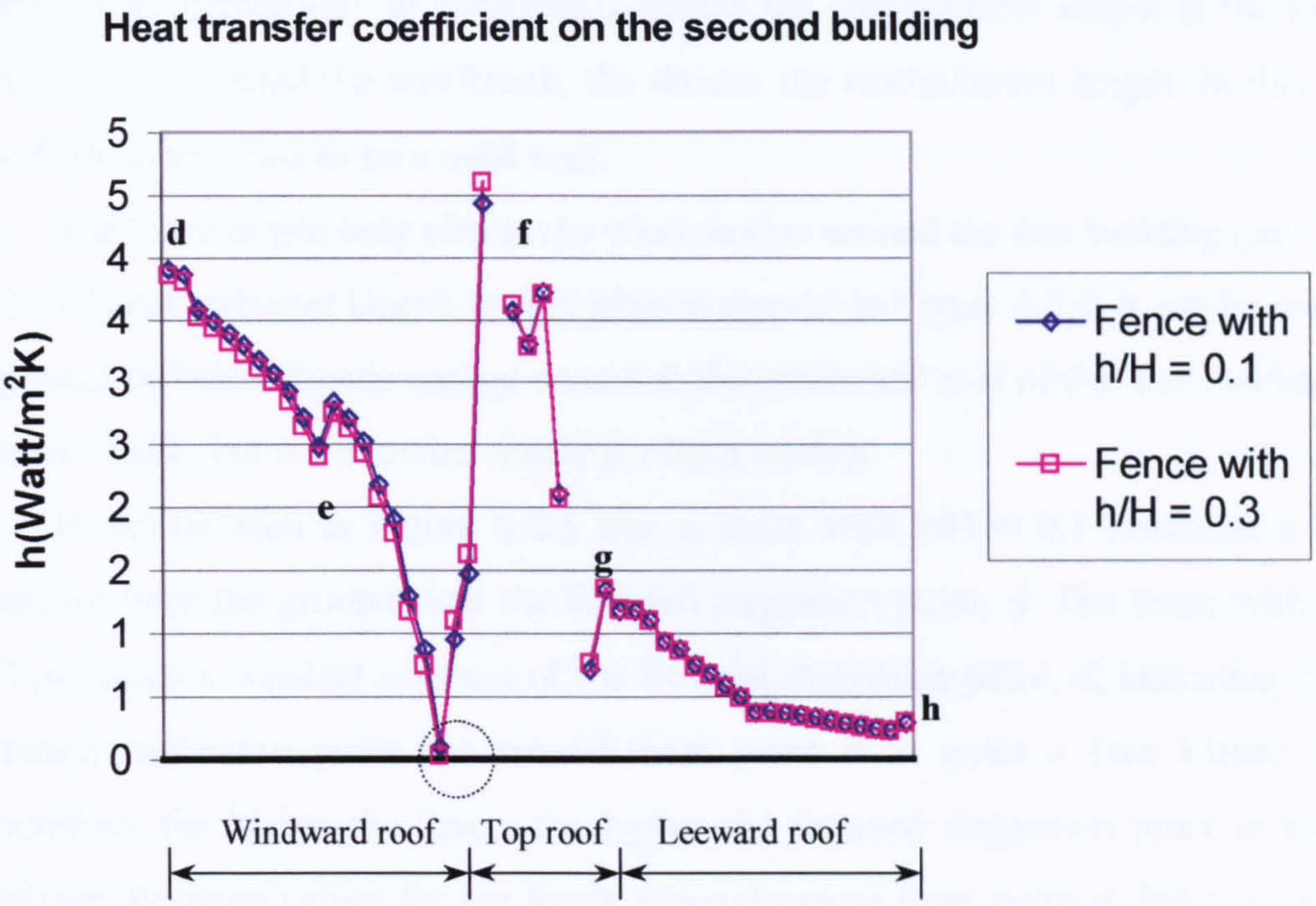

(b)

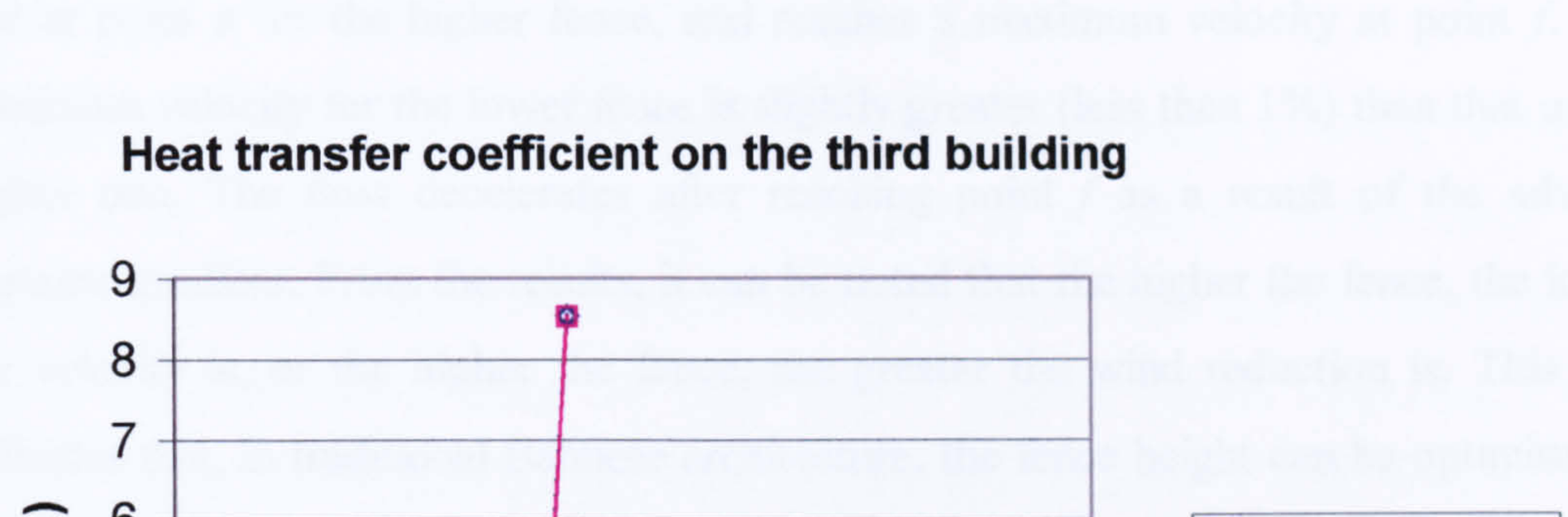

(c)

Figure 4.2.6 Heat transfer coefficients for different fence heights

Windbreaks are most effective when placed perpendicularly to the prevailing winds. The permeability of windbreaks affects the reattachment length at the leeward side. The more solid the windbreak, the shorter the reattachment length. In this study, the fence is assumed to be a solid wall.

The fence height only affects the wind motion around the first building (see Figure 4.2.3). From turbulent kinetic energy plots presented in Figure 4.2.4, it can be seen that a greater turbulent kinetic energy occurs at the windward roof of the first building with a lower fence, but is otherwise similar for both models.

It can be seen in Figure 4.2.5 that a fence with h/H = 0.1 produces a higher pressure from the ground until the forward stagnation point, *d*. The fence with h/H = 0.3 produces a constant pressure at the forward stagnation point, *d*, indicating that the forward stagnation point has moved from point *d* to point *e* (see Figure 4.1.5). Therefore, the higher the fence, the higher the forward stagnation point at the first building. Pressure values for the lower fence decrease from point *d*, but from point *e* for the higher fence. Both models reach a minimum pressure at point *f*. The fluid then accelerates because of the favourable pressure gradient at point *d* for the lower fence and at point *e* for the higher fence, and reaches a maximum velocity at point *f*. The maximum velocity for the lower fence is slightly greater (less than 1%) than that of the higher one. The flow decelerates after reaching point *f* as a result of the adverse pressure gradient. From the results, it can be noted that the higher the fence, the lower the velocity is, or the higher the fence, the greater the wind reduction is. This also indicates that, in traditional Balinese architecture, the fence height can be optimised as a windbreak/shelter, especially for the first building.

It was shown in Section 4.1 that the granary (the first building as indicated by models 2 and 3) has a possibility of receiving a greater momentum and lift force due to wind effects. Therefore, a higher front fence will lower the velocity and wind load in this building.

Heat transfer coefficients are presented in Figure 4.2.6. The fact that a solid wall reduces the reattachment length at the leeward side of the fence can be seen from the heat transfer coefficient results, where both models produce the same heat transfer coefficient at point *f* of the first building. A higher fence produces lower heat transfer coefficients. On one hand, this reduces the lift force due the boundary layer surface shear stress; on the other hand, this also reduces the heat transfer rate between the

building surface and its surrounding. Based on this result, the fence height (h) at the front side of a cluster of buildings should not be very high since this will reduce the heat transfer rate on the building surfaces. A fence with h/H = 0.3 is a good value, since it reduces the wind force at the first building but does not affect the heat transfer rate at the second and third buildings, as shown in Figure 4.2.6.

We propose that the fences in traditional Balinese architecture have a strong relation with windbreaks/shelters, especially at the first building. The fence heights shown in Figures 1.1.12 and 1.1.13 represent a good design in order to reduce wind forces at the first building without reducing the heat transfer rate at the other buildings. The fence height in Figure 1.1.11 should be reduced in order to optimise the heat transfer rate on the building surfaces. This will improve wind protection, heat transfer rate and thermal comfort of occupants.

4.3 Effects of Building Surface Roughness on Wind Motion around Traditional Balinese Buildings

4.3.1 Introduction

In traditional Balinese architecture, the square plot of land (*natar*) in which the various units of the house stand is entirely surrounded by a wall of whitewashed mud, protected from rain erosion by a crude roofing of thatch. This can be composed of a pair of brick and carved stone, but more often it consists of mud supporting a thick roof of thatch. A well built construction consists of a platform of mud, brick or stone reached by three or four steps and covered by a cool roof of thick thatch. The roof is supported by more or less elaborate wooden posts, the number of which determines their name and function. The roof is built of grass sown on the long ribs of coconut leaves, placed close together like shingles and lashed to the bamboo skeleton of the roof with indestructible cords of sugar-palm fibre, with an extra thickness of grass added to the four corners. Such a roof, often a foot and a half in thickness, will last through fifty tropical rainy seasons. The beams that support the roof are ingeniously fitted together without nails, and are held in place with pegs made of heart of coconut wood. Generally, one or two sides of the building are protected by a low wall [8].

Traditional materials such as those described above have a high surface roughness, while new materials produced by modern processes tend to reduce this surface roughness. In order to increase heat transfer rate between buildings and their surroundings, their surface roughness is now examined.

For internal flows inside pipes, increasing the relative roughness increases the friction factor and leads to increased the heat transfer coefficients. For external flows, the heat transfer coefficient is strongly affected by the separation point. At the stagnation point, the heat transfer coefficient decreases due to laminar boundary layer development. At the separation point, the heat transfer coefficient increases due to the mixing associated with vortex formation in the wake. Therefore, the key parameter in order to increase the heat transfer is where the separation point occurs. In section 4.1, it was shown that the boundary layer at the forward stagnation point, *d*, is turbulent. The higher the separation point, the greater the heat transfer coefficient and heat transfer rate.

4.3.2 Mathematical Model

The simulation of surface roughness is done by using specialised near-wall elements. The surface roughness imposed in this study is defined in terms of the height of the roughness elements and their distribution, such as pitch and mesh. Therefore, two types of surface roughness are described as a comparison of the height of material/element to the height of the building, **e/H** in percent, where **e** is surface roughness height and **H** is building height. A surface roughness of **e/H** = 0.05% is typical of a new material and **e/H** = 0.45% denotes a traditional material. All boundary conditions are similar to those in Section 4.1. All figures denoted by (a) indicate models with a lower relative surface roughness, **e/H = 0.05%**, and (b) indicate models with a higher relative surface roughness, **e/H = 0.45%.**

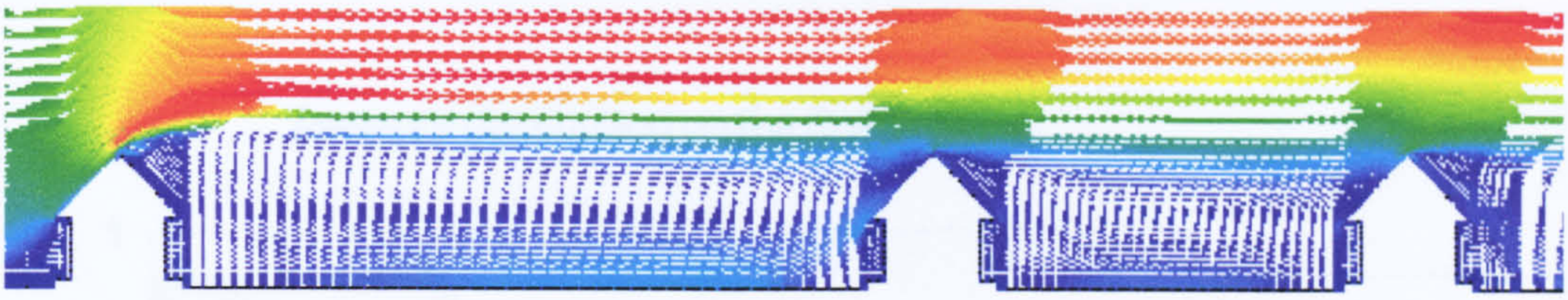

(a)

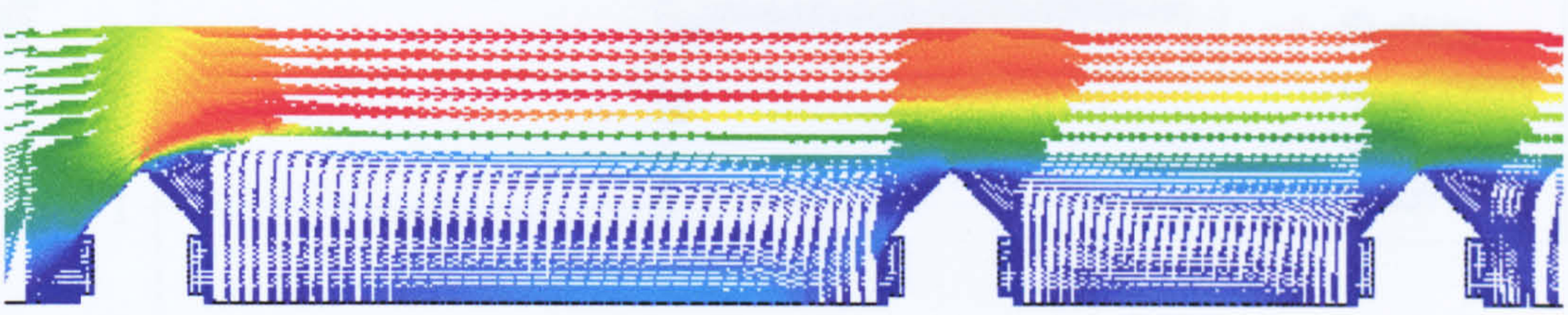

(b)

Figure 4.3.1 Velocity vectors for different surface roughness

(a)

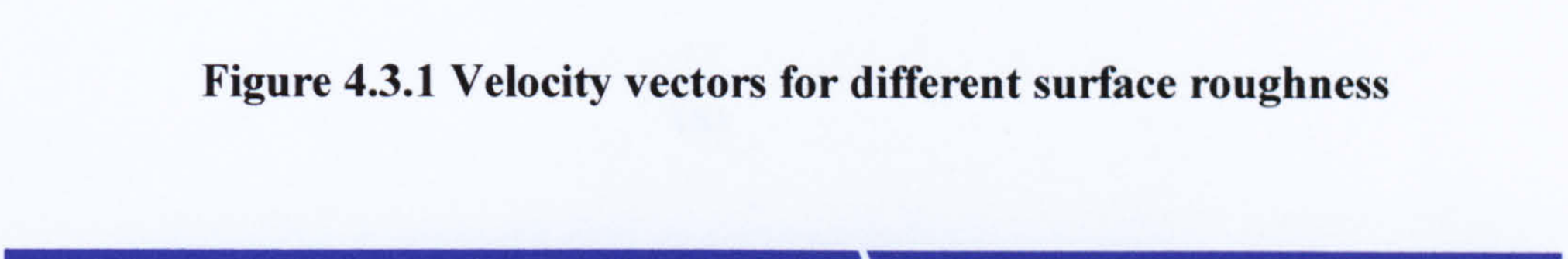

(b)

Figure 4.3.2 Turbulent kinetic energy plots for different surface roughness

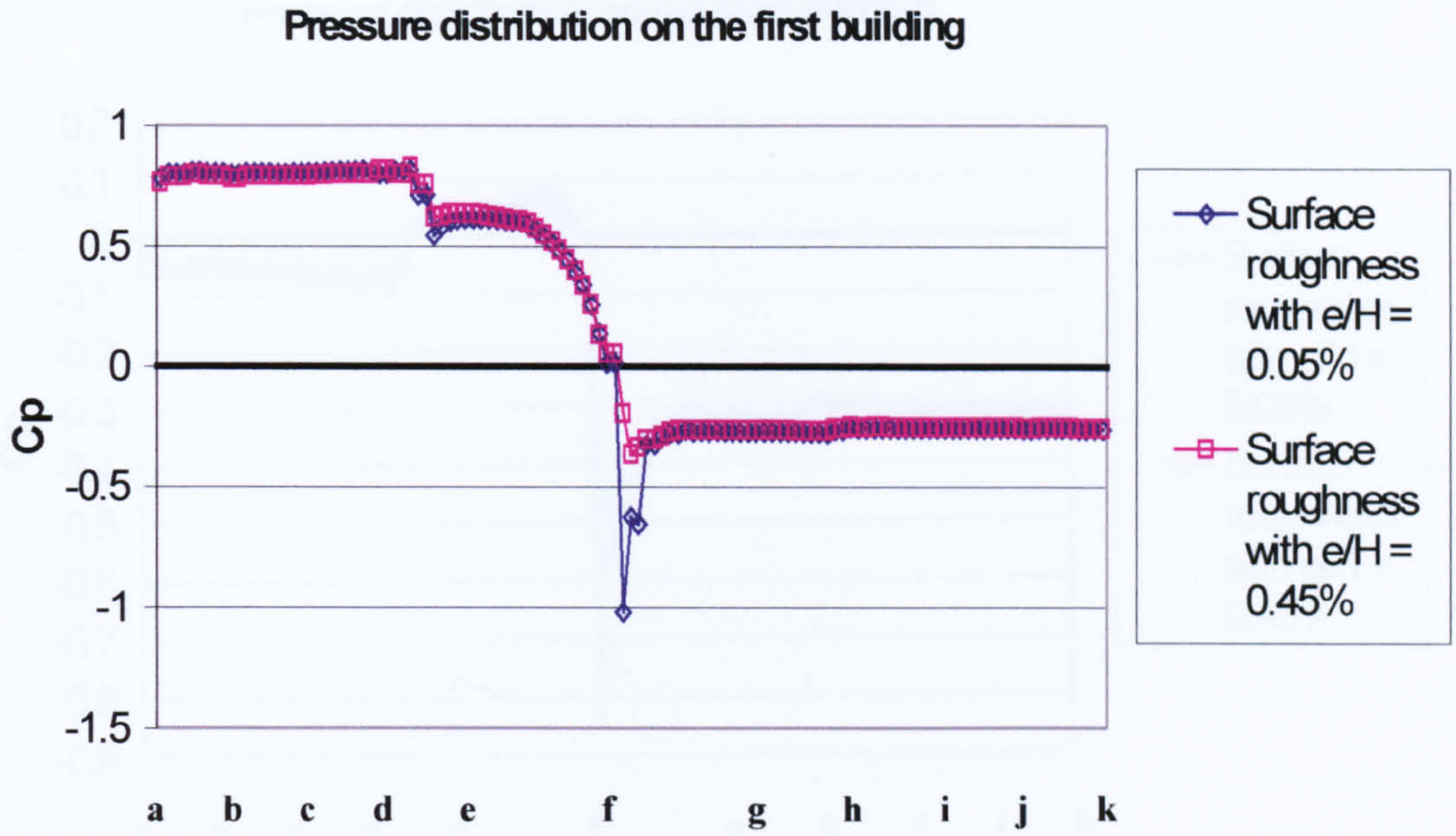
Pressure distribution on the first building
1
0.5
0
-0.5
-1
-1.5
Cp
a
b
c
d
e
f
g
h
i
j
k
Surface roughness with e/H = 0.05%
Surface roughness with e/H = 0.45%

(a)

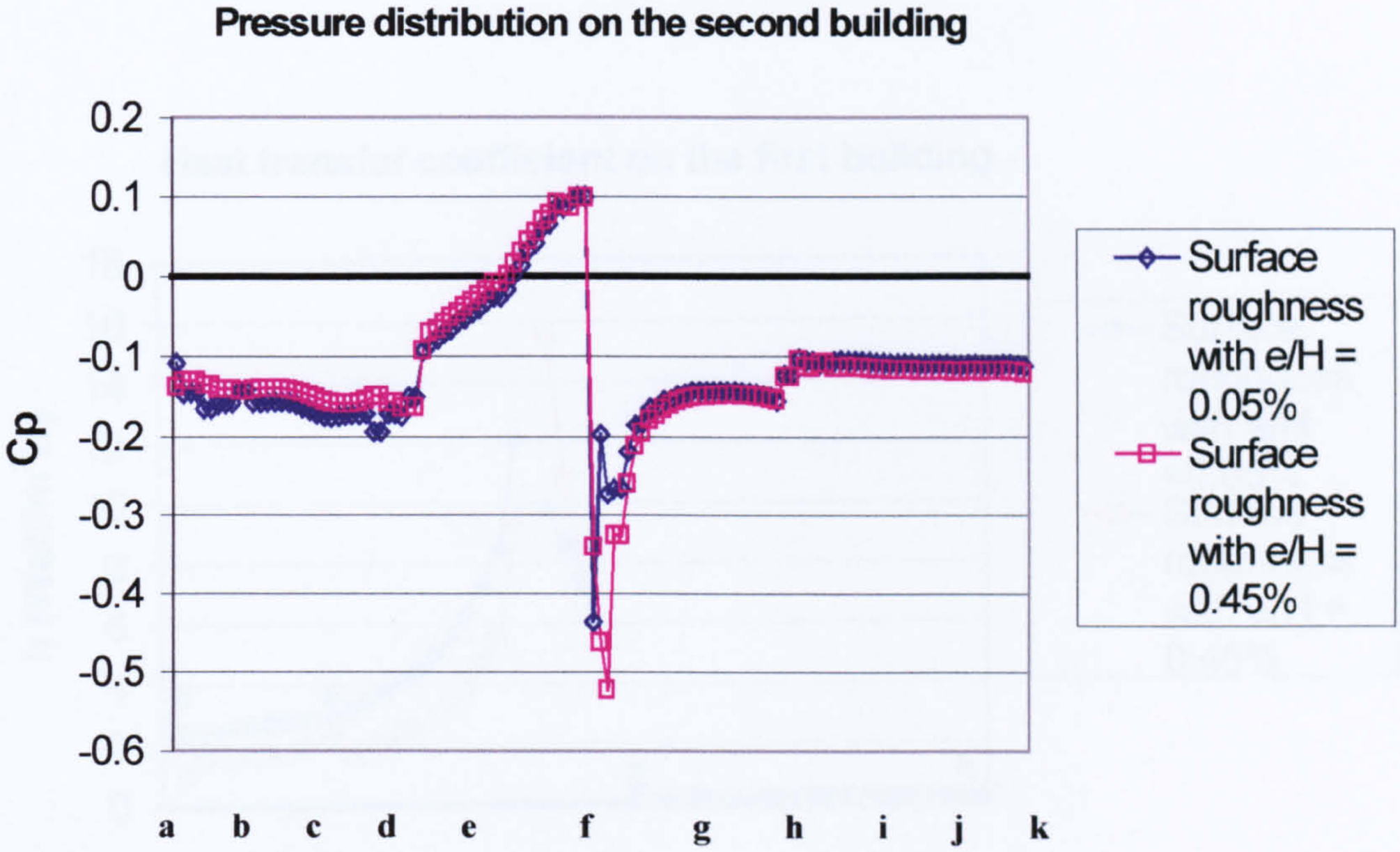
Pressure distribution on the second building
0.2
0.1
0
-0.1
-0.2
-0.3
-0.4
-0.5
-0.6
Cp
a
b
c
d
e
f
g
h
i
j
k
Surface roughness with e/H = 0.05%
Surface roughness with e/H = 0.45%

(b)

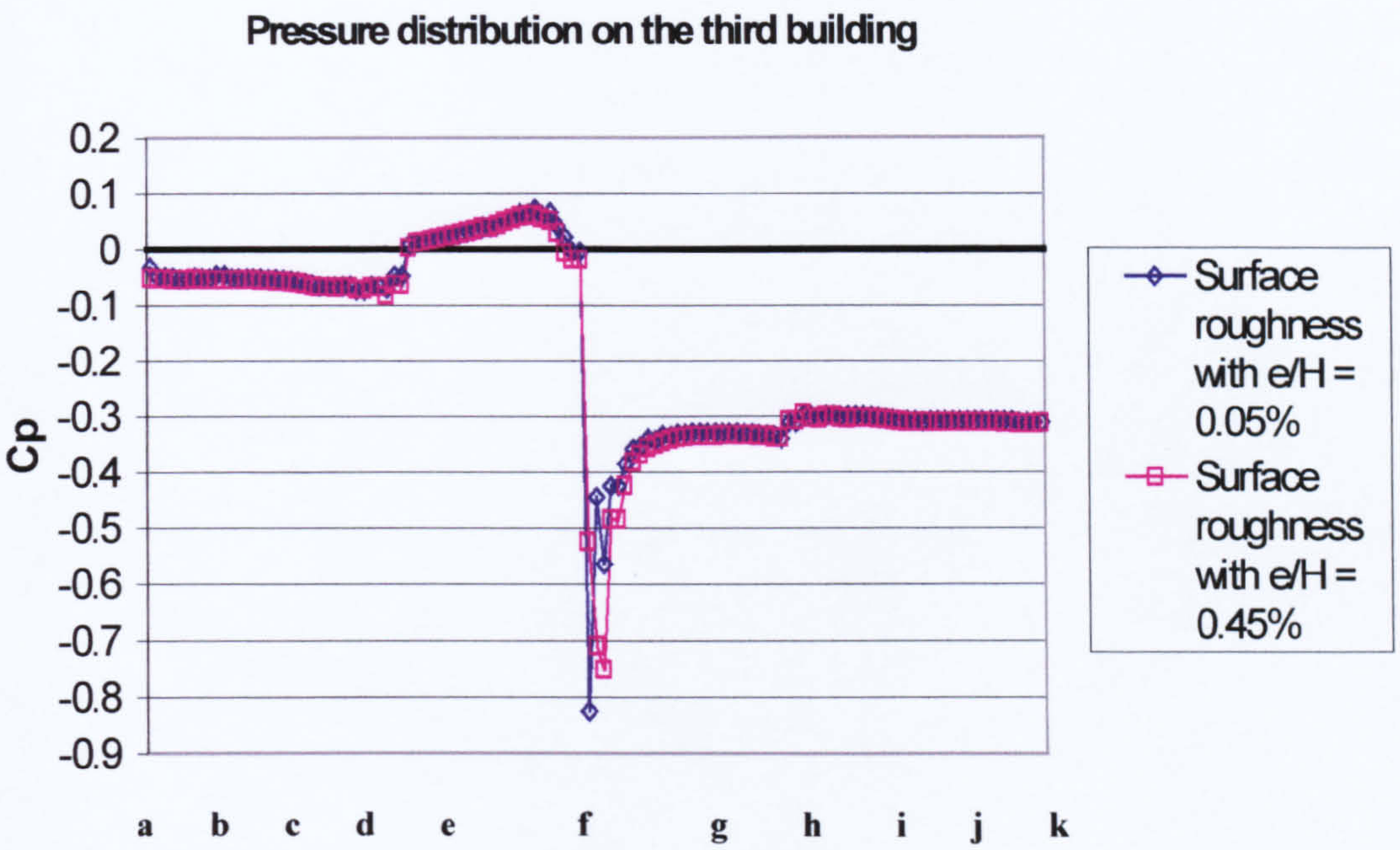

(c)

Figure 4.3.3 Pressure distributions for different surface roughness

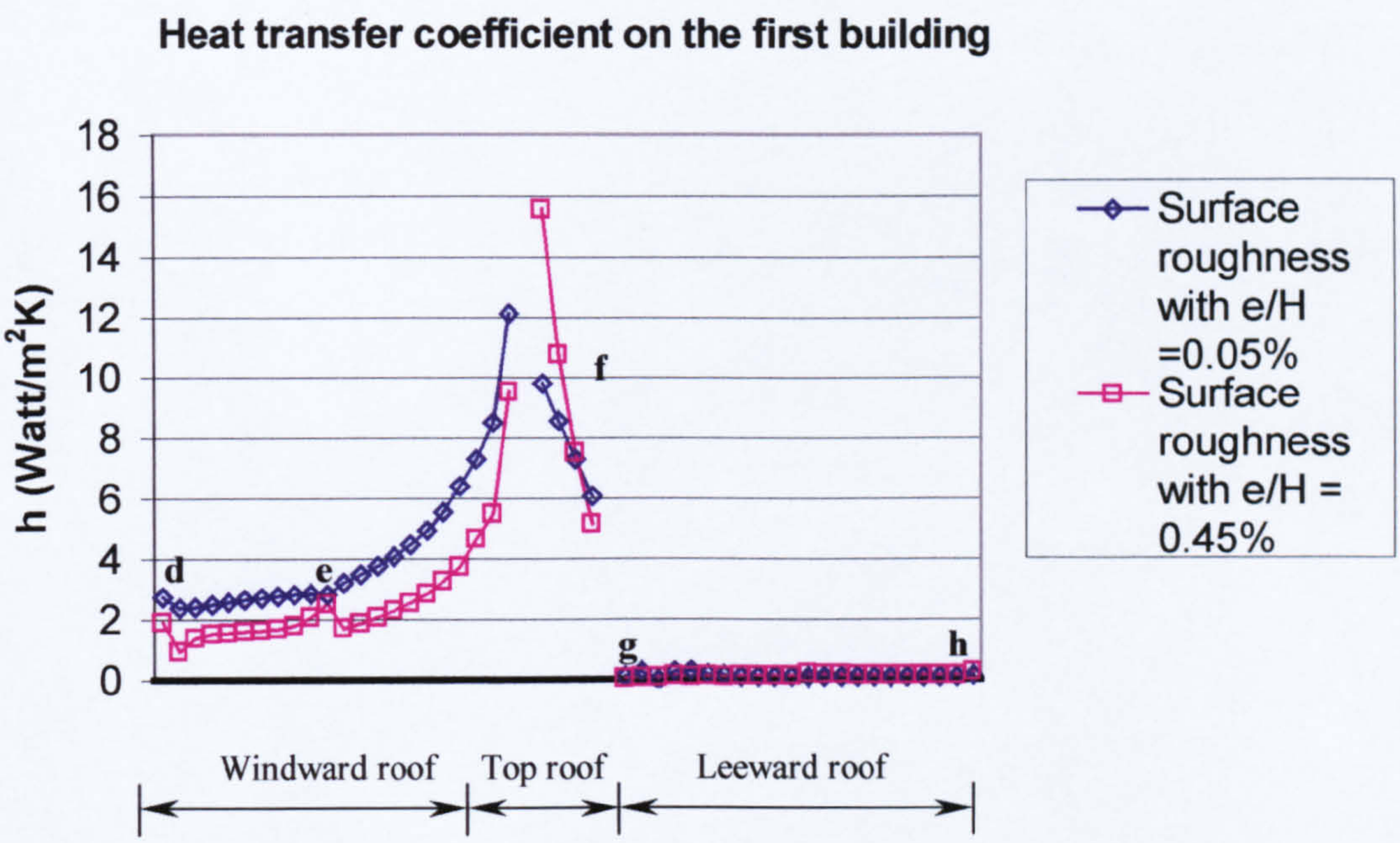

(a)

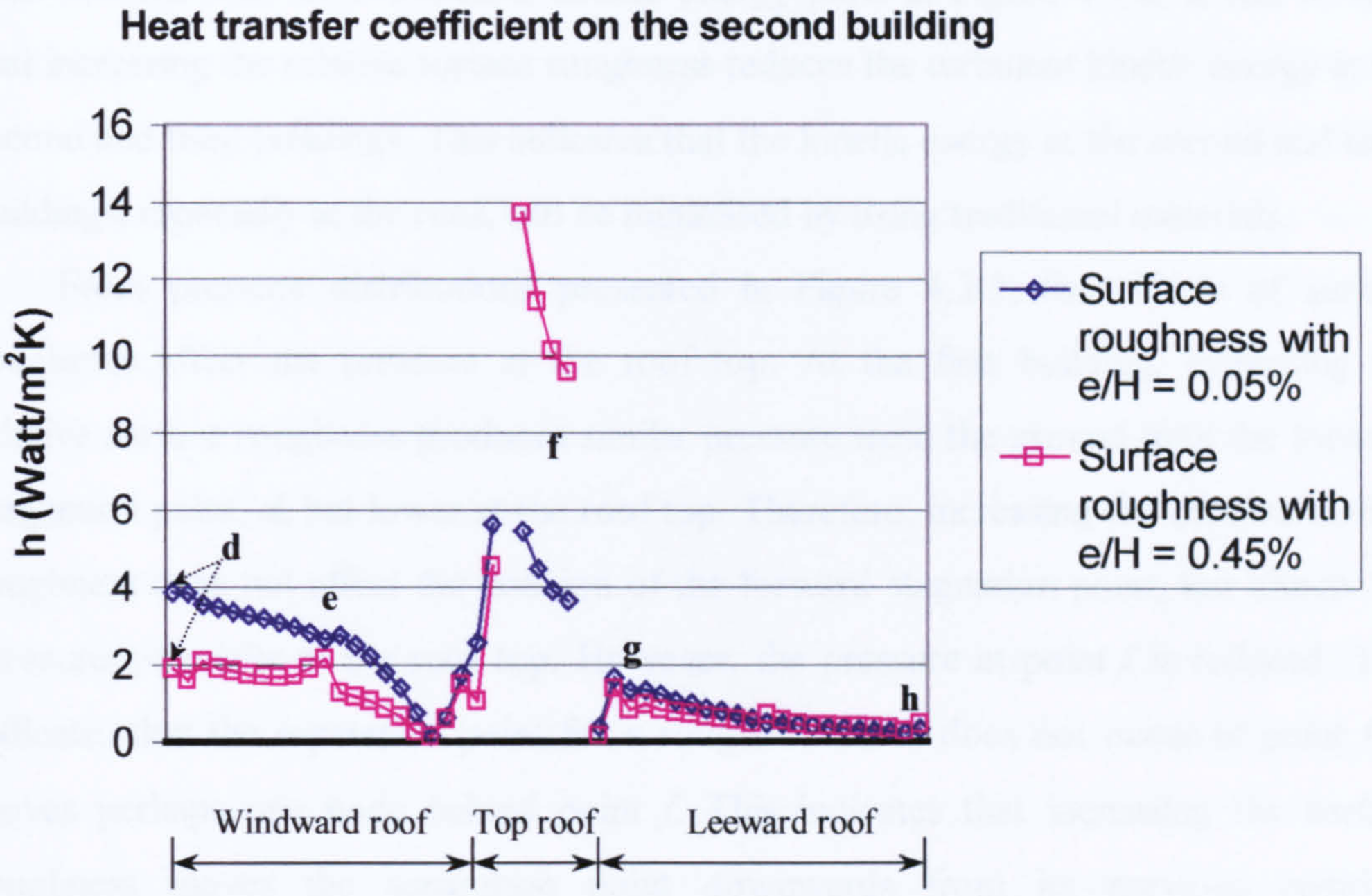

(b)

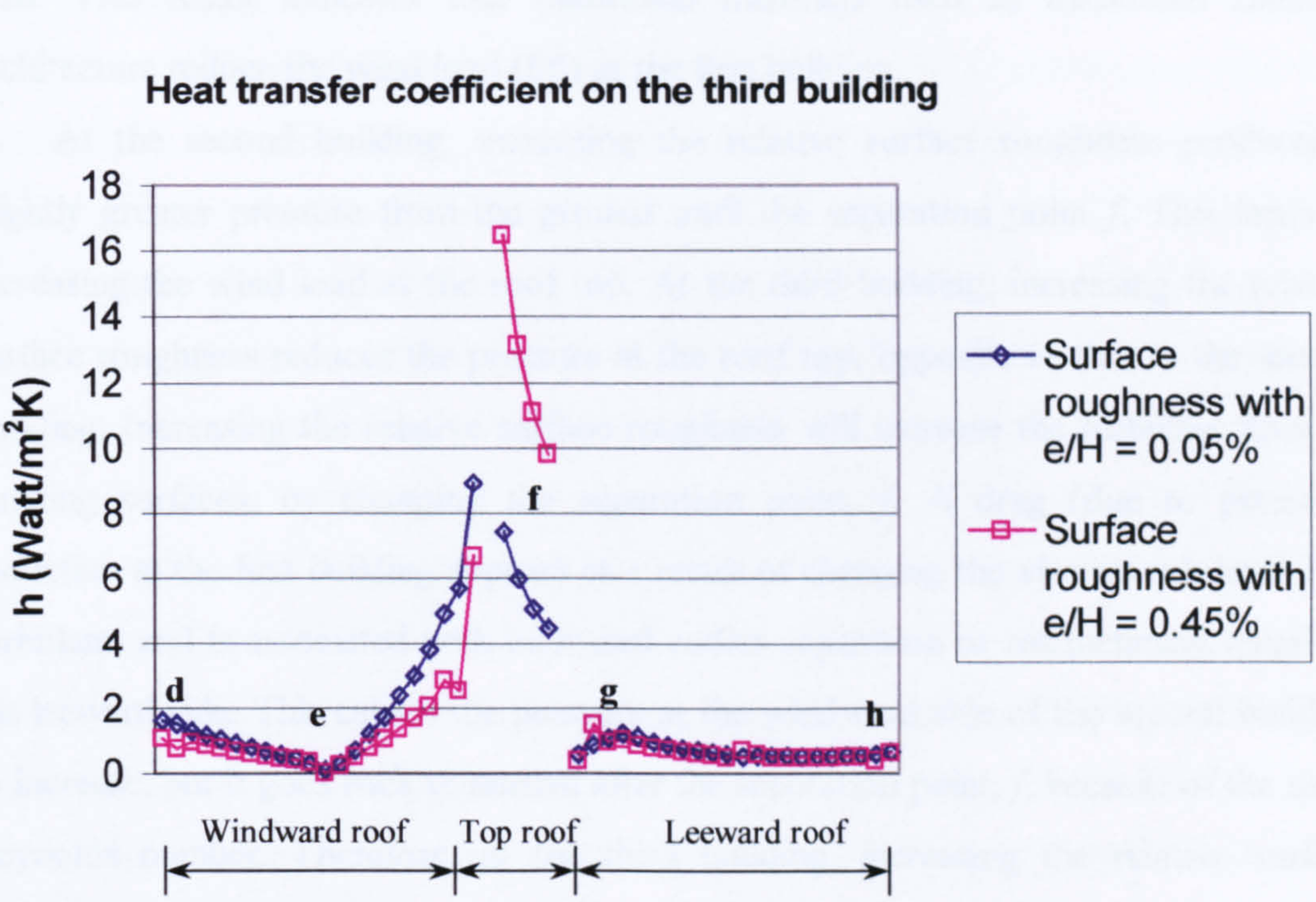

(c)

Figure 4.3.4 Heat transfer coefficients for different surface roughness

The velocity vectors in Figure 4.3.1 show no differences in the flow patterns for both models. But, from turbulent kinetic energy plots in Figure 4.3.2, it can be seen that increasing the relative surface roughness reduces the turbulent kinetic energy at the second and third buildings. This indicates that the kinetic energy at the second and third buildings, especially at the roof, can be minimised by using traditional materials.

From pressure distributions presented in Figure 4.3.3, the effects of surface roughness affect the pressure at the roof top. At the first building, increasing the relative surface roughness produces similar pressure from the ground until the forward stagnation point, *d*, but lower at the roof top. Therefore, increasing the relative surface roughness does not affect the position of the forward stagnation point, but affects the pressure especially at the roof top. However, the pressure at point *f* is reduced. This indicates that the separation point for a rougher surface does not occur at point *f*, it moves perhaps one node behind point *f*. This indicates that increasing the surface roughness moves the separation point downwards from its previous position. Therefore, the maximum velocity for a smooth surface is slightly greater than that for a rougher one, because of the change on its separation point, producing a higher wind load. This result indicates that traditional materials used in traditional Balinese architecture reduce the wind load (lift) at the first building.

At the second building, increasing the relative surface roughness produces a slightly greater pressure from the ground until the separation point *f*. This leads to increasing the wind load at the roof top. At the third building, increasing the relative surface roughness reduces the pressure at the roof top, opposite to that at the second building. Increasing the relative surface roughness will increase the turbulent flow on building surfaces, by changing the separation point, *f*. A drag (due to pressure) reduction at the first building appears as a result of changing the viscous sub-layer into turbulent, and is associated with increased eddies separation or reattachment length at the leeward side. This causes the pressure at the windward side of the second building to increase, but it goes back to normal after the separation point, *f*, because of the same Reynolds number. Therefore, at the third building, increasing the relative surface roughness reduces the pressure at the roof top. From the above results, it can be noted that increasing the relative surface roughness will decrease the transport of momentum and reduce the eddy viscosity and the velocity gradient at the roof top, as seen from the

turbulent kinetic energy plots. Increasing the relative surface roughness increases the eddies separation.

Heat transfer coefficients are presented in Figure 4.3.4. It can be seen in Figures 4.3.4 (a, b and c) that the heat transfer coefficient for rougher surface increases at nodes after point *f*. Therefore, it is clear that increasing the surface roughness moves the separation point downwards from its previous position, increasing the heat transfer rate.

From the forward stagnation point, *d*, until the leading edge of the roof top, the rougher the surface, the lower the heat transfer coefficient. This reduces the lift force due to the skin friction, but also reduces the heat transfer rate between the building surface and its surrounding with corresponding reduction of the cooling loads. A relatively low surface roughness should be used at the roof top since the heat transfer rate increases for a rough surface. This can also be solved by placing transverse rectangular grooves or longitudinal v-grooves at the roof top, the so-called *pemugbug* in Balinese architecture, since they reduce the flow separation, and lead to reduced drag forces.

We propose that the use of traditional materials in traditional Balinese architecture has a strong relation to architectural aerodynamics, wind engineering, heat transfer and thermal comfort of occupants. The use of traditional materials with a relatively high surface roughness reduces the heat transfer rate from outdoor to indoor, at all buildings; reduces turbulent kinetic energy at the second and third buildings, and also reduces the wind load at the first building. In order to reduce the pressure at the second building, the distance between the first and second buildings should be increased.

The surface shear stress and friction velocity depend on the Reynolds number or the wind velocity. Wind velocities are very strong and increase the surface shear stress at the shores and plains. Therefore, the heat flux generated at these areas become very high. Very rough traditional materials as shown in Figures 1.1.11 and 1.1.19 are good in order to reduce cooling loads on building surfaces. Due to lower pressure and temperatures at mountains and hills, traditional materials (smoother than in the previous figures), presented in Figures 1.1.12, 1.1.13, 1.1.14, 1.1.15 and 1.1.16, should be used in order to reduce cooling loads on building surfaces.

4.4 Summary

In general terms, if the accuracy of numerical results is to be satisfactory, the distance between grid points must be very small. One possibility of achieving this is by merely increasing the fineness of the grid until the solution is substantially independent of it. When the spacing between the grid lines –which lie in the same direction as the wall- is not uniform, divergence may occur. Therefore, near the wall, the ratio of the intervals between the nodes should be kept as close to unity as possible. The accuracy which can be obtained is closely tied up with the truncation error. The truncation error has the effect of introducing an additional false diffusion [5 and 9]. To control false diffusion, two methods are suggested; refining the grid and the choice of a co-ordinate system for which one set of grid lines will be very nearly parallel to the streamlines. The second choice can be realised if the grid follows the shape of the object. This leads to the use of body-fitted grids. Multi-blocks is also a good strategy to reduce this false diffusion since not only it follows the shape of the object but also reduces the mesh size near the walls. From results described in this Chapter, it can be seen that the use of multi-blocks and grid refinement near the buildings reduces false diffusion and leads to reduced truncation errors.

Iterative methods of solution can be susceptible to round-off errors, which arise because computers only carry out calculations to a limited number of significant figures. The CPU time is proportional to the number of iterations which must be executed before the change affected by an iteration cycle is acceptably small. The rate of convergence of an iterative procedure can be improved by over-relaxation, as in this study. The Picard schemes have a reasonably large radius of convergence. The wide radius of convergence allows them to start with a relatively poor initial solution guess and move the solution closer to the true solution and within the radius of convergence of higher-order, more rapidly convergent methods. It is obvious that the closer the initial guess the fewer the iterations required to reach the solution.

Traditional houses in hot and humid climate zones are designed to utilise the wind for natural cooling. The type of roof affects the wind motion, especially at roof level. In a cluster of buildings, the reattachment point at the second and third buildings is affected by the roof angle (roof pitch).

A flat-top roof reduces turbulent kinetic energy. In this study, the highest turbulent kinetic energy occurs at the second building, followed by the third. The use of pillars in these buildings will minimise the momentum effects. There appears to be a relation between the buildings' name given in traditional Balinese architecture, *e.g.*, *Sakapat*, *Sakanem*, *Balé Tiang Sanga* and *Balé Sakutus*, the four posts building, the six posts building, the nine posts building and the eight posts building, respectively, and the need to protect them against the damage caused by turbulent kinetic energy. Therefore, the building arrangement should be in the following order: four posts building at the front followed by six posts building, with the nine posts building in the middle and the eight posts building at the rear.

Similarity temperature at the first building is generally the lowest, and it is relatively high at the second and third buildings. According to the heat transfer rate from building to the surrounding, this can be directly related to thermal comfort of occupants, since suggested thermal comfort for residences, apartments, convalescent homes and homes for the aged (third building, the parent's sleeping quarters) is higher than that for conference rooms, meeting rooms or auditoriums (second building). The suggested thermal comfort for kitchens and stores is the lowest (the first building). Therefore, there is a relation between the position of buildings and their function, with the thermal comfort of occupants. Storage rooms and kitchens should lie at the front side, ceremonial and meeting halls should lie in the middle and the parent's sleeping quarters should lie at the rear of the site.

The fence height only affects the wind motion around the first building. A lower fence produces a greater turbulent kinetic energy at the windward roof of the first building. A higher fence changes the forward stagnation point. A higher front fence reduces the velocity, wind loads and heat transfer at the first building. The use of fences in traditional Balinese architecture has a strong relation with windbreak/shelter, especially for the first building. The fence model presented in Figures 1.1.12 and 1.1.13 represents a good design in order to reduce wind forces at the first building without reducing the heat transfer rate at the second and third buildings.

Increasing the relative surface roughness (*e.g.* by using traditional materials) reduces the turbulent kinetic energy at the second and third buildings, and moves the separation point. The maximum velocity for smoother surfaces is slightly greater than for rougher ones because of this change of position of the separation point. Therefore,

to increase the heat transfer rate on building surfaces, a relatively high surface roughness should be used.

It appears that traditional Balinese architecture has a relation with wind engineering, heat transfer and thermal comfort of occupants. Numerical investigations in this chapter provide a better understanding of traditional Balinese architecture and some design modifications to improve thermal comfort. Some aspects discussed include air circulation, sun lighting and heat transfer.

In an area with temperature around 30^0C and relative humidity between 70 and 90%, the wind plays an important role for natural ventilation. The suggested building design is elongated in the east-west direction. Design objectives are to:

1. Reduce penetration of solar radiation
2. Remove inside heat of the occupants
3. Improve evaporative cooling conditions by natural ventilation

To remove heat by cross-ventilation, a ventilated roof is needed. Rough materials are used to reflect solar radiation and to reduce heat transfer and cooling loads on the building. Very rough materials with high permeability are also needed on the roof in order to allow wind flows through these media. An elevated floor is used to allow air circulation under the structure. To achieve beneficial air motion, inlet openings should be located to intercept prevailing wind, but the outlets should be larger than the inlet area. A lower inlet provides a better natural ventilation since the air motion is directed towards the living room. A cantilever overhang is also needed for better natural ventilation since the heat transfer rate is very low in this region. A longer flat at the top is considered in order to reduce the turbulent kinetic energy on the roof top. Solar radiation must be reduced before it penetrates the building surfaces. The use of glass panels in the windows is avoided to reduce solar radiation or cooling loads.

From the above aspects, suggested building design is shown in Figure 4.4.1 (a). The granary should be let with fully-open surfaces since it can be used for other functions, as shown in Figure 4.4.1 (b).

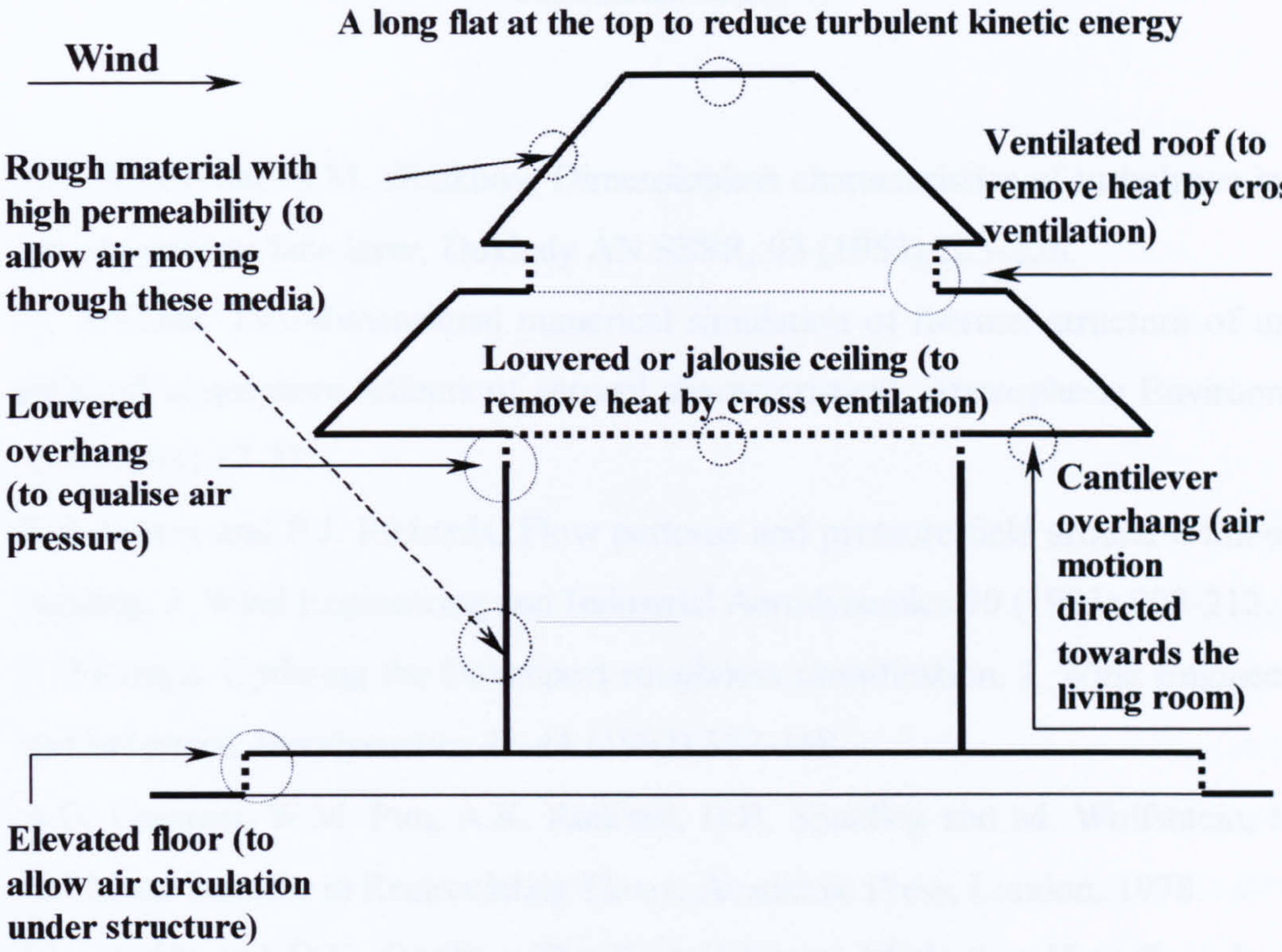

Figure 4.4.1 (a) Modified building design

Figure 4.4.1 (b) The first building with fully-open surfaces and its alternative functions

REFERENCES

1. A.S. Monin and A.M. Obukhov, Dimensionless characteristics of turbulence in the atmospheric surface layer, Doklady AN SSSR, 93 (1953) 223-226.
2. A. Yoshida, Two-dimensional numerical simulation of thermal structure of urban polluted atmosphere (effects of aerosol characteristics), Atmospheric Environment 25B (1991) 17-23.
3. R.P. Hoxey and P.J. Richards, Flow patterns and pressure field around a full-scale building, J. Wind Engineering and Industrial Aerodynamics 50 (1993) 203-212.
4. J. Wieringa, Updating the Davenport roughness classification, J. Wind Engineering and Industrial Aerodynamics 41-44 (1992) 357-368.
5. A.D. Gosman, W.M. Pun, A.K. Runchal, D.B. Spalding and M. Wolfshtein, Heat and Mass Transfer in Recirculating Flows, Academic Press, London, 1978.
6. J.N. Reddy and D.K. Gartling, The Finite Element Method in Heat Transfer and Fluid Dynamics, CRC Press, Boca Raton, Florida, 1994.
7. M.D. Egan, Concepts in Thermal Comfort, Prentice-Hall Inc., New Jersey, 1975.
8. M. Covarrubias, Island of Bali, Oxford University Press, Singapore, 1972.
9. H.K. Versteeg and W. Malalasekera, An Introduction to Computational Fluid Dynamics: The Finite Volume Method, Longman Scientific & Technical, England, 1995.

CHAPTER FIVE

THREE-DIMENSIONAL MODEL OF THE FLOW AROUND A CUBIC BUILDING

5.1 Introduction

In this chapter, numerical simulations of the flow around a cubic building are investigated for incompressible, three-dimensional, viscous and turbulent fluids.

The flow patterns around a cubic building have been studied by many researchers, not only experimentally but also numerically. In the last two decades, many numerical algorithms were introduced in order to validate the results, not only by introducing new turbulence models but also by developing improved schemes for numerical stability during computation. The validity of results for a cubic building, therefore, can be compared either with experimental or numerical results.

In our two-dimensional model, the commercial package Fidap has been used. For three-dimensional simulations using a very coarse mesh, Fidap took more than 2 GB disk space. Therefore, if one needs to refine the grid (*e.g.* for grid independence tests), the disk space of a normal workstation would quickly be exceeded. Therefore, another commercial package has been used which took smaller disk spaces and provided better stability. The commercial package used here is CFX, based on finite volume methods.

An experimental investigation of the flow around surface-mounted cubes in both uniform, irrotational and sheared turbulent flow was described by Castro and Robins [1] in 1977, and became a benchmark to validate numerical models. The practical importance of bluff-body aerodynamics has increased over the past few decades, with an enormous increase in the literature concerning laboratory simulations, full-scale measurements, and more recently, numerical calculations and theoretical predictions of a wide variety of bluff-body flows. The flows around full-scale or model buildings have been investigated much less thoroughly, despite the obvious practical implications regarding, say, effluent

dispersion or wind loads on buildings. There is little experimental data available even for the simple case of surface-mounted bodies in a uniform upstream flow (by 'uniform upstream flow', it is meant one in which the mean velocity is uniform and the turbulence intensity is very low –less than, say, 0.5 % - except in the thin boundary layer which must exist on the surface even if the body is mounted on a false floor) [1]. Wind tunnel simulation of the atmospheric boundary layer has been generated and evaluated by some researchers. The variations of the pressure field on the cube have been discussed in relation to the incident flow-field parameters. The velocity profile at the model position and the local surface roughness, largely determine the pressure on the windward side. This is specific to each building scheme and cannot be estimated from general tests of a building shape [2].

5.2 Initial Tests

5.2.1 Grid Tests

Computational fluid dynamic methods based on Cartesian or cylindrical co-ordinate systems have certain limitations for irregular geometries. In practice, the boundary geometries can be complex and often irregular. They can be approximated in Cartesian and cylindrical co-ordinate systems by treating surfaces in a stepwise manner.

The use of body-fitted co-ordinate systems in CFD procedures can be seen in Figure 5.2.1. To calculate the flow past a cylinder by using a Cartesian co-ordinate system, the cylindrical surface may be represented by a step approximation and cells inside the solid part of the cylinder are blocked in the calculation. This has considerable disadvantages since the approximate boundary description is tedious to set up and introduces errors, especially if the wall shear stresses need to be calculated. Further disadvantages of the Cartesian/cylindrical co-ordinate system include a wastage of computer storage and resources due to

- blocking of the cells in solid regions
- the introduction of a fine Cartesian mesh in one region of particular interest could imply unnecessary refinement in another region of minimal interest.

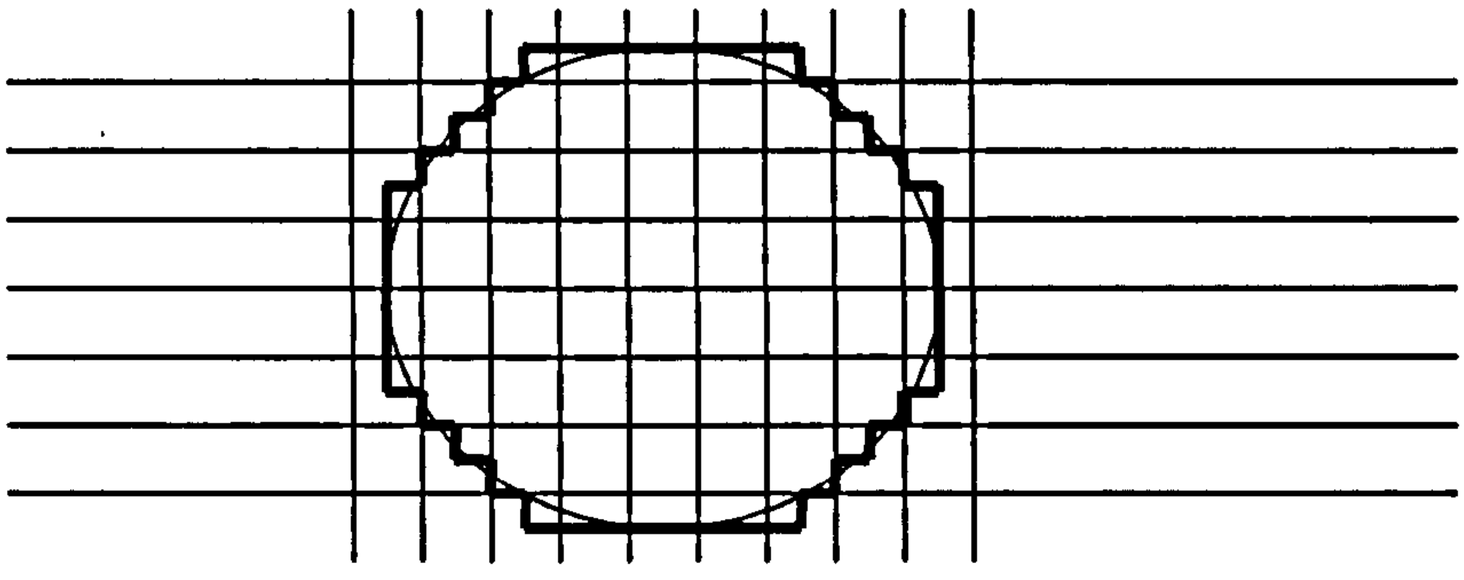

Figure 5.2.1 Cartesian grid arrangement for a cylinder

Methods based on body-fitted grid or non-orthogonal grid systems have been developed to solve the limitations referred to in the explanation above as presented by Rhie and Chow [3], Peric [4], Demirdzic [5], Shyy and Vu [6] and Karki and Patankar [7].

Majumdar and Rodi [8] applied a cylindrical polar grid and k-ε model to the calculation of wind flow around a cylindrical structure. The cylindrical-polar grid could be considered as a body-fitted grid for such structure. Body-fitted grid systems are usually designed by using a body-fitted co-ordinate which is transformed from a Cartesian co-ordinate by an appropriate mapping function. However, with the exception of some simple geometries, the transformation from Cartesian to body-fitted co-ordinates is very complicated especially for three-dimensional problems [9]. Han [10] applied a body-fitted grid for wind flow around a vehicle-like body, Kot [11] applied body-fitted co-ordinates to simulate the stratified air flow around a three-dimensional hill and Deng *et al* [12] for a prolate spheroid [9].

Figure 5.2.2 shows a body-fitted grid for the cylinder problem. The geometrical flexibility offered by body-fitted grid techniques is useful in the modelling of practical problems involving irregular geometries because

- all geometrical details can be accurately incorporated
- the grid properties can be controlled to capture useful features in regions of interest.

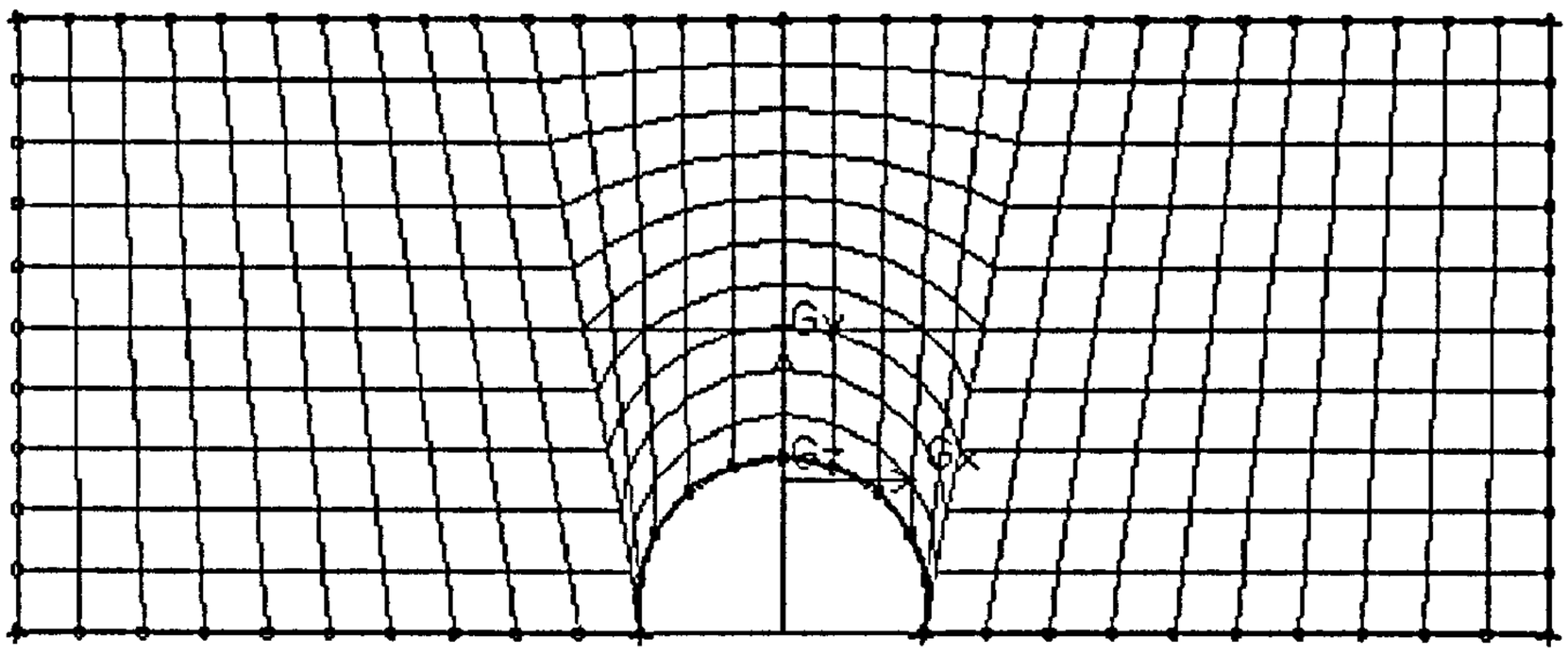

Figure 5.2.2 Body-fitted grid for half of cylinder

The governing equations in body-fitted coordinates are much more complex than the Cartesian ones, especially the momentum equations. The structured grid method uses a curvilinear body-conforming mesh [13]. This approach is very suitable for simulating high Reynolds number viscous flow fields (as in the present study), therefore most of the current CFD results for the Navier-Stokes equations employ structured grid systems.

However, for realistic three-dimensional configurations, body-fitted grid generation sometimes becomes a seriously difficult task. The common strategy to use a body-fitted grid for a complex body is to employ multiple zone and multiple grid methods, such as the multi-blocks method. The multi-blocks method was also shown to be a very powerful approach for complex configurations. The procedure to generate the grid requires multi-blocks zoning of the flow field.

From the above description, body-fitted grids are used for complex geometries and spatial discretization although most researchers still use rectangular grid systems to simulate problems with simpler geometries such as a cubic building [13].

A grid arrangement for a cubic building can be seen in Figure 5.2.3. The multi-blocks method is used since it is possible to develop the two-layers method which most researchers suggest produces better results than a single-layer.

This Chapter discusses numerical methods for wind flow around a cubic building considering different grid systems, rectangular and body-fitted. Results of pressure distribution are compared to other published results.

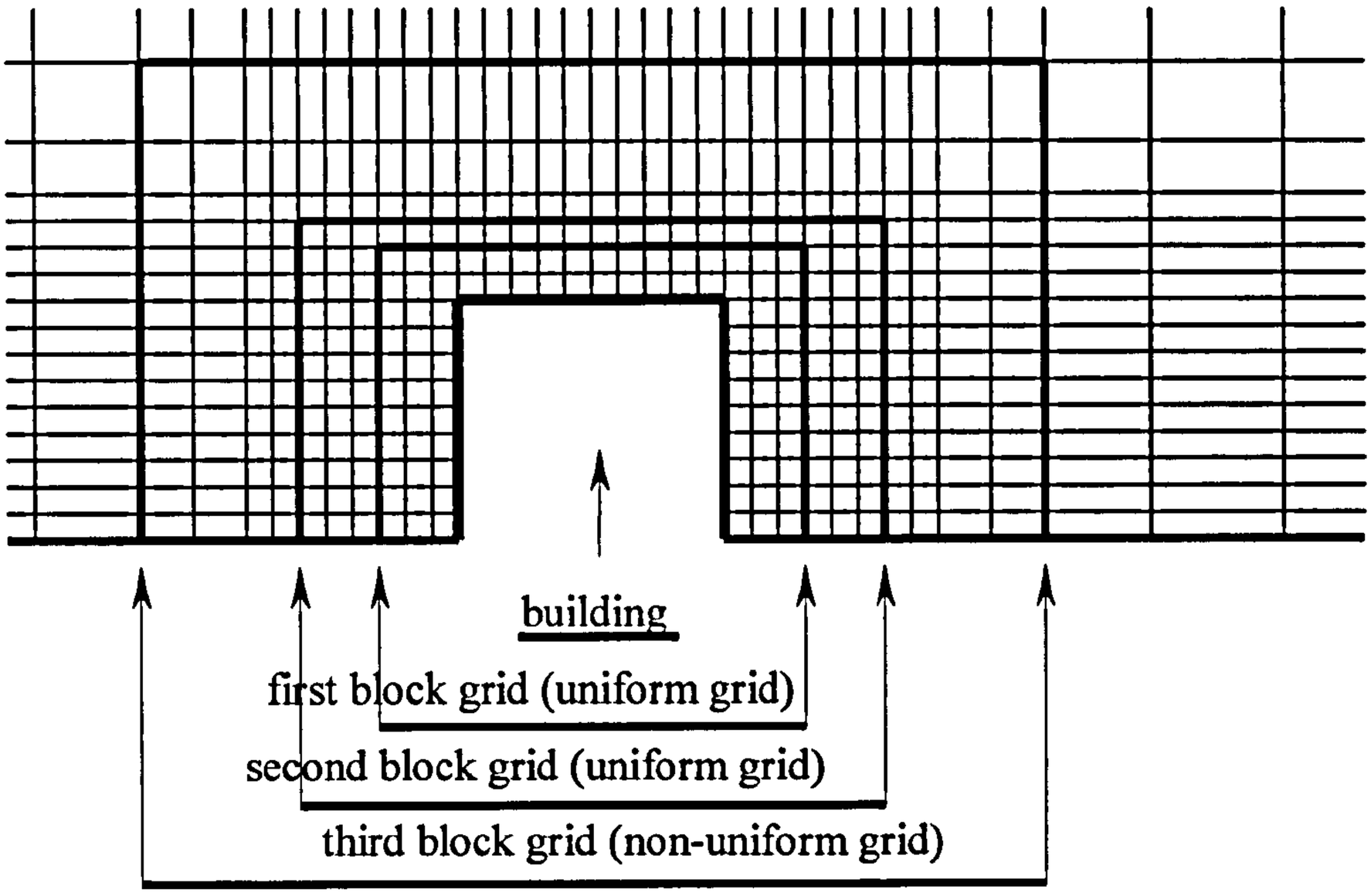

Figure 5.2.3 (a) Grid arrangement in the present study

outer region (two equations of turbulence model, k-ε)

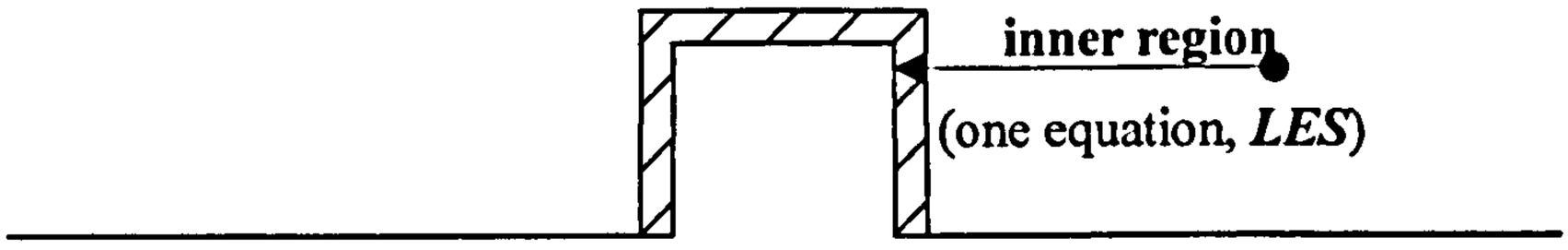

Figure 5.2.3 (b) A two-layers method

A cubic building has been used as an initial test for three-dimensional problems. The flow around the building is modelled by using the Navier-Stokes equations and the k-ε turbulence model. Rectangular and body-fitted grid systems have been used. A uniform grid system has been applied at the building surfaces, first and second blocks, but a non-uniform grid system has been used at the third block and outer region. The staggered grid

thus used avoids the evaluation of boundary condition for pressures (Patankar, 1980) and also provides much more accurate predictions (Selvam and Paterson, 1991) [13].

The momentum, k and ε turbulence model equations are solved by successive over relaxation point iteration with an under-relaxation parameter of 0.7 for each cycle. To satisfy mass and momentum conservation simultaneously, the SIMPLE procedure is used.

The boundary conditions for the inlet velocity are fixed at the initial power-law velocity profile $u/u_g = (z/z_g)^{0.25}$, where u and u_g are mean velocities at height z and at a reference point at height z_g, respectively, with $v = w = 0$. The turbulent intensity was evaluated to be 6.2% according to Davenport's terrain roughness classification number 4, for a suburban terrain [14]. The inlet flow profile can be seen in Figure 5.2.4 (a) and can be compared to other published profile in Figure 5.2.4 (b). The grid used has 112 x 92 x 59 nodes for the x, y and z directions, respectively.

On the truncated walls and building surfaces, the wall treatment is a combination of logarithmic and no-slip boundary conditions. The no-slip boundary condition (u = v = w = 0) is the appropriate condition for the velocity components at solid walls. The implementation of wall boundary conditions in turbulent flows starts with the evaluation of y^+, where a near-wall flow is taken to be laminar if $y^+ \leq 11.63$. If the value of y^+ is greater than 11.63, the first node (from solid walls) is considered to be in the logarithmic-law region of a turbulent boundary layer. The relationship can be described as follows

$$u^+ = \frac{1}{\kappa}\ln(Ey^+)$$

and

$$T^+ = \sigma_{T,l}\left(u^+ + \left[9.24\left[\left(\frac{\sigma_{T,l}}{\sigma_{T,t}}\right)^{0.75} - 1\right]\times\left\{1+0.28\exp\left[-0.007\left(\frac{\sigma_{T,l}}{\sigma_{T,t}}\right)\right]\right\}\right]\right)$$

where κ is von Karman's constant (0.4187), E is an integration constant which for smooth walls with constant shear stress has a value of 9.793, $\sigma_{T,l}$ is the laminar Prandtl number (0.707) and $\sigma_{T,t}$ is the turbulent Prandtl number (≈ 0.9).

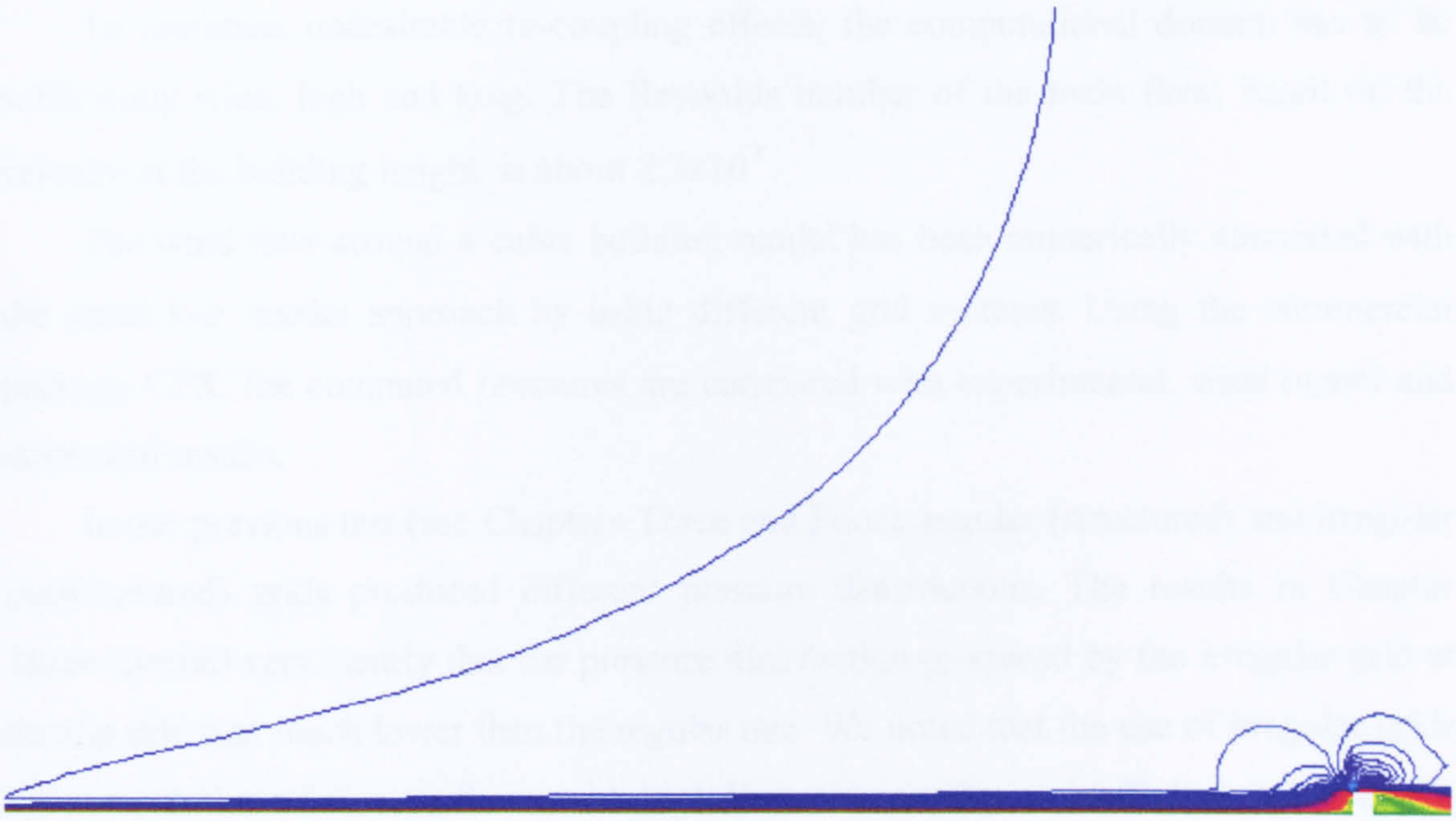

Figure 5.2.4 (a) Flow profile in the present study

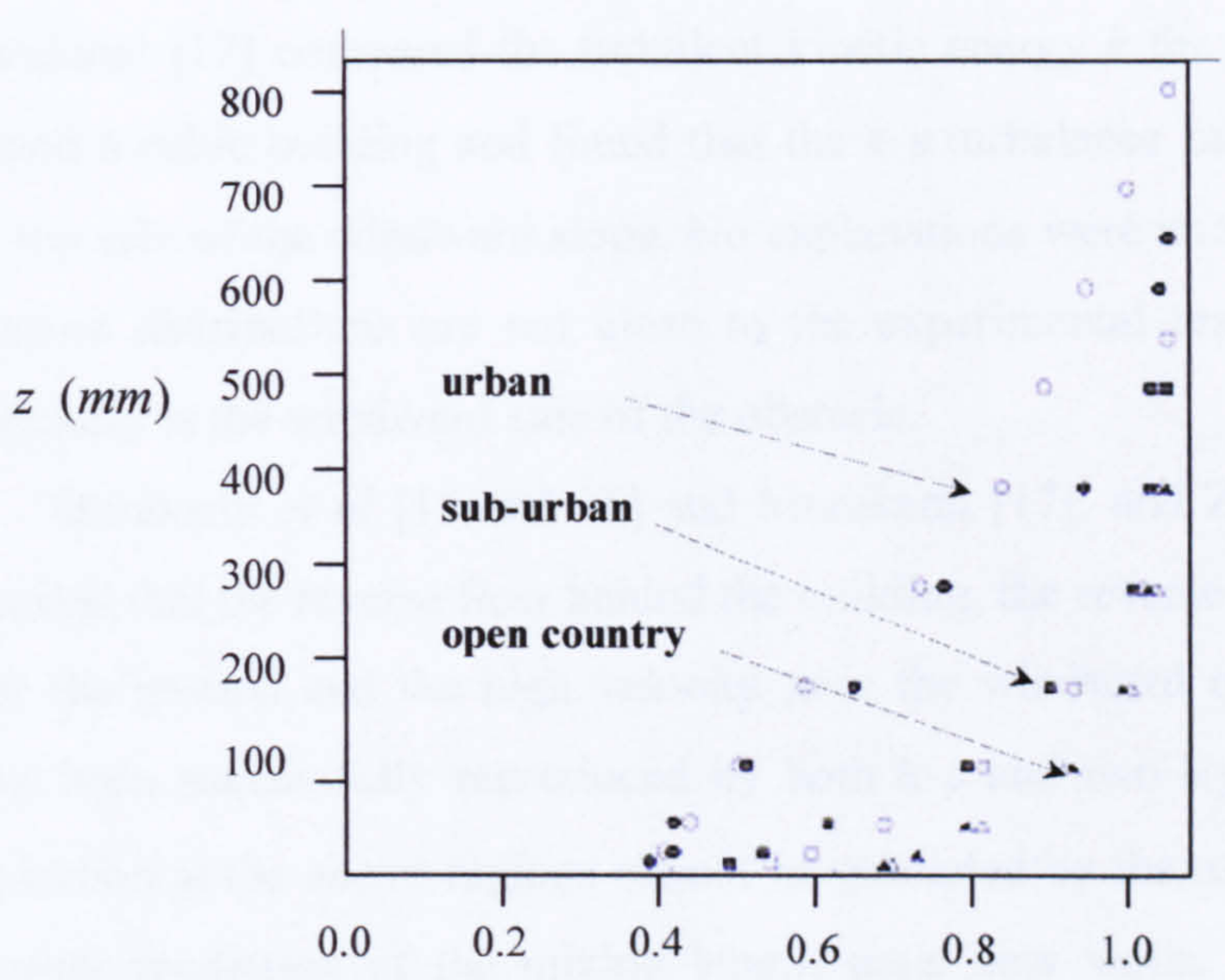

Figure 5.2.4 (b) Flow profile from published results

To minimise undesirable re-coupling effects, the computational domain has to be sufficiently wide, high and long. The Reynolds number of the main flow, based on the velocity at the building height, is about $2.3x10^5$.

The wind flow around a cubic building model has been numerically simulated with the usual k-ε model approach by using different grid systems. Using the commercial package CFX, the computed pressures are compared with experimental, wind tunnel and numerical results.

In our previous test (see Chapters Three and Four), regular (structured) and irregular (unstructured) grids produced different pressure distributions. The results in Chapter Three showed very clearly that the pressure distribution produced by the irregular grid at the top side was much lower than the regular one. We noted that the use of irregular grids for computation of viscous flows with high-Reynolds number is inefficient, but irregular grids can be used for small and complex geometries.

The pressure distribution around a square obstacle (two-dimensional) was computed by using the k-ε turbulence model. The computed pressures were in good agreement with field results except at the top side of the windward slope. Murakami *et al* [15 and 16] and Murakami [17] compared the turbulent kinetic energy k for different turbulence models around a cubic building and found that the k-ε turbulence model over-estimates the k in the top side of the windward slope. No explanations were attempted for this problem, and pressure distributions are not close to the experimental results of Castro and Robins, especially at the windward side of the obstacle.

Murakami *et al* [15 and 16] and Murakami [17], and Zhou and Stathopoulos [18], reported that the reverse flow behind the building, the reverse flow in front of the building near the ground and the high velocity near the windward corner found in experiments have been successfully reproduced by both k-ε and two-layers methods. However, the separation at the above regions cannot be predicted by the usual k-ε model since there is an over prediction of the mixing length scale near walls, especially at the windward corner, as shown in Figure 5.2.5.

Regarding our previous studies (two-dimensional problems), separation at the above regions actually has been successfully computed by using lower initial values for the k-ε parameters (see Chapter Three). Although the results are not similar to the experimental,

they agreed well with those of Qasim *et al* [19] who also used a two-dimensional model. We also noted that the geometry of the model (two or three-dimensional) may influence the results. The results are presented in Figures 5.2.6 and 5.2.7.

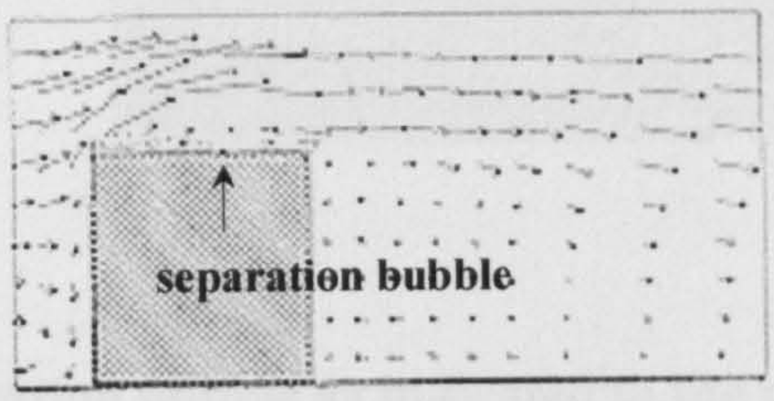

experiment (Murakami, 1990)

k-ε model (published results)

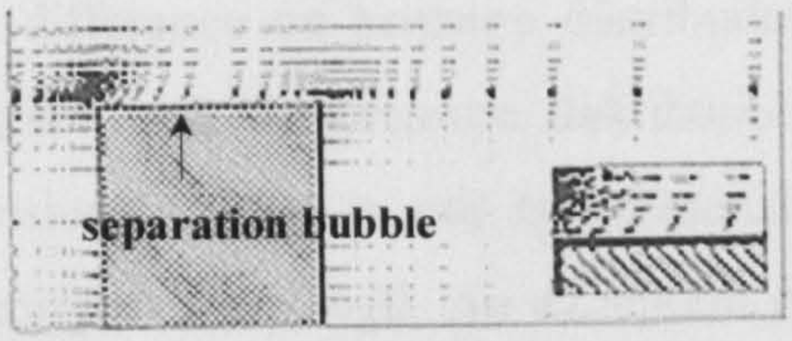

two-layers model

Figure 5.2.5 Mean velocity vector field around the building

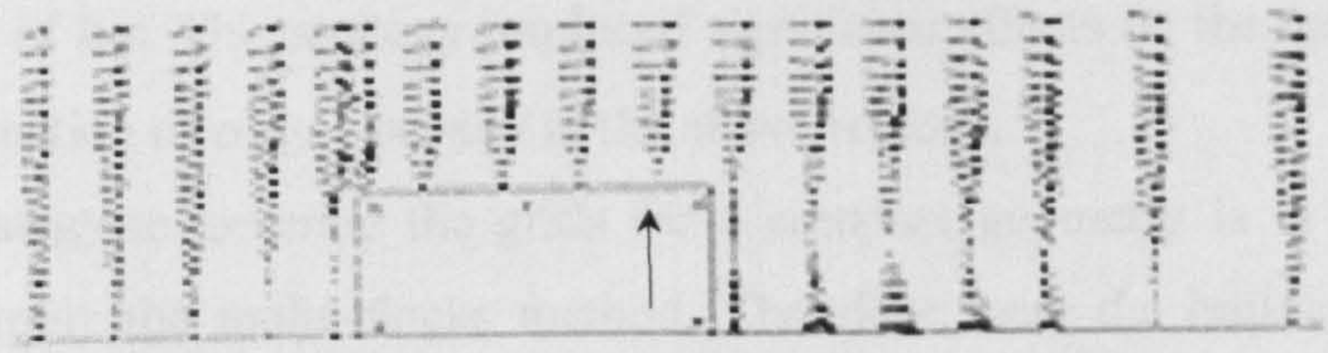

Figure 5.2.6 Separation bubble as indicated in Qasim *et al* [19] results

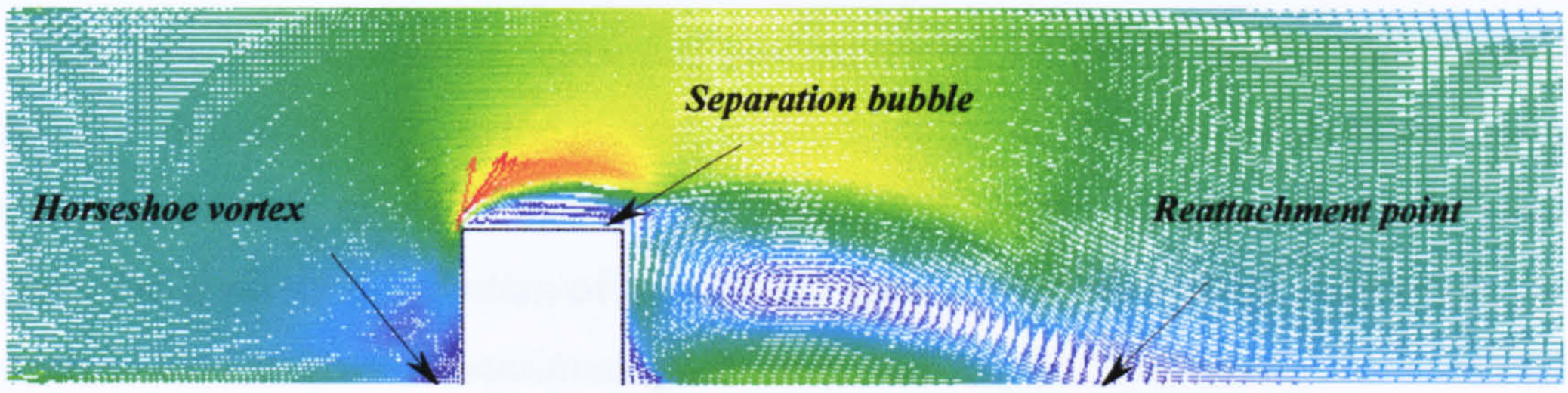

Figure 5.2.7 Separation bubble as indicated in the present study

In the present study, the same turbulence values (as in the two-dimensional model) have been used. The computed pressure coefficients along the centre line of the obstacle are plotted in Figure 5.2.8. The computed pressures for both rectangular and body-fitted grids produce the same results and agree well with Castro and Robins results [1]. First, this indicates that there is no difference on pressure distributions between the use of rectangular and body-fitted grids, and the pressure distributions are affected by the geometry (two or three-dimensional) since in our two-dimensional model, results of pressure distribution did not compare very well. An exception occurs at the windward side near the ground -where our results are a bit lower- and at the leeward side -where our results are higher- compared to that of Castro and Robins [1]. From the results, it can be seen that the pressure distribution at the windward side (for the three-dimensional model) are closer than that in the two-dimensional model. Second, this also indicates that the over-prediction of mixing length scale at the windward corner has been reduced by using lower values of k-ε. This strategy produced significant effects on the results and reduced the over estimation of eddy viscosity in the above regions.

The strategy to generate the grids for a complex geometry is to employ multiple zones, *e.g.* apply the multi-blocks method. Therefore, near the building surfaces, both rectangular and body-fitted grids produce the same flow profiles. Second, by using the multi-blocks system and a combination of uniform and non-uniform grids around the

obstacle, the grid method used in the present study is suitable and can be used for a complex building configuration.

As described above, the numerical procedures for the three-dimensional model are correlated to Selvam [20]. In the present study, it can be seen that pressure distributions at the windward side given by Selvam are lower than our results. But, at the windward corner, the pressure distribution of Selvam are greater than our results. According to our previous section (two-dimensional problems), the higher the turbulence values, the greater the pressure distribution at the windward corner. Since Selvam produced a larger pressure distribution at this point, we suggest that the turbulence values used in his simulation are relatively high. Selvam's results for the non-dimensional turbulent kinetic energy at the building surfaces are very high, around 2.5 at the windward side, 4.5 at the top and 0.41 at the leeward side. Our maximum non-dimensional turbulent kinetic energy is 0.27 at the windward side, around 0.1 at the top and 0.05 at the leeward side. It seems that Selvam used very high turbulence values and/or the thickness sub-layer at the windward corner was not sufficiently refined (*e.g.* ≤ 11.63).

For another comparison, Zhou and Statophoulus [21] applied a two-layers method, combining the k-ε model in fully turbulent regions with a one-equation model in the near wall (inner) region. They divided the layer into two sections, inner and external regions (similar to our model which was divided into four blocks). The wind flow in all external regions (the third and fourth blocks) is computed with the standard k-ε model, but the flow near the building surfaces (the first and second blocks) is simulated with the one-equation model.

Although their pressure distributions at the windward side agree very well (better than our results) with the experimental results of Castro and Robins [1], the pressure distribution at the windward corner is very high (far away from our numerical and the experimental results). At the leeward side, all numerical results produce the same pressure distribution. From the comparison study, it is noted that although the two-layers method was used for the simulation, the boundary condition for turbulence values in the external region should have a reduced value.

For flows dominated by heat transfer, the energy dissipation of the k-ε turbulence model produces greater turbulent kinetic energy. Therefore, one-equation models in the

inner region should be associated with lower turbulence values in the external region. However, Zhou and Stathopoulos [20 and 21] demonstrated that the two-layers model provides a better result at the windward side, but not at the windward corner.

A standard k-ε turbulence model has been used to simulate the flow profile around a cubic building. It seems that the pressure distribution around the building surfaces is not affected by the grid system since both rectangular and body-fitted grids produce the same results. The multi-blocks grid system is also a good strategy to minimise grid effects on the results. This result also explains our hypothesis in Chapter Three, that the reattachment length at the separation region can be examined by using multi-blocks grids arrangement. In order to reduce the over-predicted eddy viscosity, lower turbulence values of k-ε are provided to use. This produces better results and agrees well with experimental results of Castro and Robins [1]. A single-layer method is also sufficient for computation. For multi-layer models, we suggest that lower turbulence values of k-ε should be assigned in the external region.

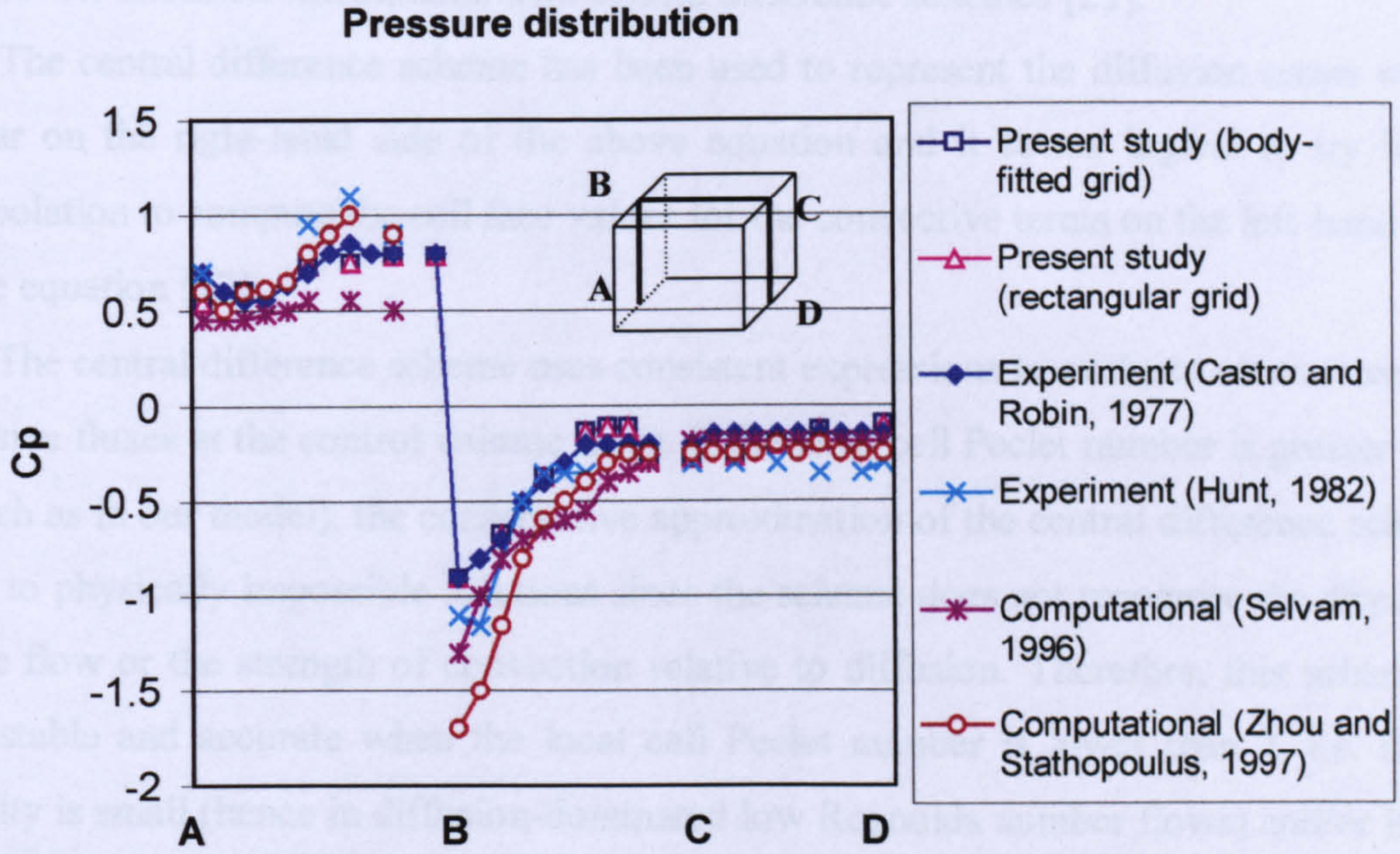

Figure 5.2.8 Pressure distribution around a cubic obstacle

5.2.2 Test of Numerical Schemes for Stabilisation

The steady convection-diffusion equation can be derived from the transport equation as follows,

$$div(\rho u\phi) = div(\Gamma grad\phi) + S_\phi$$

This equation represents the flux balance in a control volume. The left-hand side gives the net convective flux and the right-hand side contains the net diffusive flux and the generation or destruction of the property ϕ within the control volume [22].

The main problem in the discretisation of the convective terms is the calculation of the value of transported property ϕ at control volume faces and its convective flux across the boundaries. The diffusion process affects the distribution of a transported quantity along its gradients in all directions, whereas convection spreads influence only in the flow direction. This crucial difference appears in an exacting upper limit to the grid size, that is dependent on the relative strength of convection and diffusion, for stabilisation of convection-diffusion calculations with central difference schemes [22].

The central difference scheme has been used to represent the diffusion terms which appear on the right-hand side of the above equation and it seems logical to try linear interpolation to compute the cell face values for the convective terms on the left-hand side of the equation [22].

The central difference scheme uses consistent expressions to evaluate convective and diffusive fluxes at the control volume faces. If the local cell Peclet number is greater than 2 (such as in our model), the conservative approximation of the central difference scheme leads to physically impossible solutions since the scheme does not recognise the direction of the flow or the strength of convection relative to diffusion. Therefore, this scheme is only stable and accurate when the local cell Peclet number is lower than 2, *i.e.* if the velocity is small (hence in diffusion-dominated low Reynolds number flows) and/or if the grid spacing is small. For high Peclet number, the central finite volume schemes may suffer instabilities, therefore, upwind schemes or artificial viscosities are often introduced for stabilisation.

Parpia [23] derived the Van Leer split-flux vectors for moving curvilinear co-ordinate systems, and successfully applied it to a fixed wing. Ferrand and Aubert [24] applied the Van Leer scheme for inviscid transonic flow, but also presented an alternative hybrid scheme to resolve the same problem. Their new approach is based on Van Leer's flux vector splitting and is called the mixed Van Leer method since it conserves the advantages of the central schemes at low Mach numbers and the advantages of Van Leer schemes elsewhere. It seems that Van Leer methods are specially suitable for transonic flows, but this scheme can also be applied for other problems.

Wilkes and Thomson [25] presented a higher-order upwind difference scheme which is robust and can be used without adding excessive under-relaxation or an especially good initial approximation. Kawamura *et al* [26] presented a new higher-order upwind scheme for incompressible Navier-Stokes flow. The stability of the first-order upwind scheme is very good but has a strong diffusive effect to the molecular viscosity. The second-order upwind scheme has worse stability properties since it caused undesirable propagation of errors. They developed a new upwind scheme which has third-order accuracy. They mention that it has a local diffusive effect, but the global effect is much smaller than the second-order. Li and Rudman [27] suggested a new generalised formulation for four-point discretization schemes of non-uniform grids. They mention that the central difference scheme, the QUICK scheme, and the second-order upwind scheme fall into this formulation. A second-order hybrid scheme was also presented for non-uniform grids. The unbounded behaviour of the generalised formulation was examined. A flux-corrected transport algorithm was then applied to the above four schemes on a uniform grid. They noted that incorporation of flux-corrected transport into the high-order schemes greatly improves the solution accuracy.

Choi and Yoo [28] presented numerical approaches by using both finite element and finite volume methods for the Navier-Stokes equation. They proposed hybrid numerical methods which give accurate results and are free from the checkerboard-type of pressure distribution. A dual adaptation scheme was developed for evaluation of the viscous terms.

In the present study, a comparison of several numerical schemes to stabilise the central difference scheme of finite volume methods is performed. The QUICK difference scheme does not produce good stability, therefore, it is not used for this comparison

study. A higher upwind scheme was considered to establish its convergence and accuracy, since it has been successful to solve non-symmetric linear systems. The Van Leer scheme is also introduced since it reduces oscillations.

The upwind scheme has a major drawback when the flow is not aligned with the grid lines. It should be noted that in high Reynolds number flows the false diffusion can be large and give physically incorrect results. Therefore, grid refinement must be considered to eliminate the false diffusion. The higher upwind difference scheme is based on the backward difference formula of the upwind scheme, but it involves more neighbouring points to reduce discretisation errors.

The hybrid difference scheme is based on a combination of central and upwind difference schemes. The central difference scheme is employed for small Peclet number ($Pe < 2$) and the upwind scheme is employed for large Peclet number ($Pe > 2$). The hybrid difference scheme uses piecewise formulae based on the local Peclet number to evaluate the net flux through each control volume. This scheme produces physically realistic solutions and is highly stable when compared with the higher upwind scheme. The disadvantage is that the accuracy in terms of Taylor series truncation error is only first-order [22].

Although Wilkes and Thomson [25] noted that in the hybrid scheme it was not necessary to use excessive under-relaxation nor an especially good initial approximation, in the present study the successive over-relaxation point iteration has been used. Therefore, all schemes have the same numerical procedure with a relaxation parameter for each cycle. The solution algorithm is a variant of the SIMPLE scheme of Patankar [22], in which velocities are obtained by solving the momentum conservation equations using the pressure field and then the pressure field is corrected by using the imbalances in the mass conservation equations. A rectangular grid is applied in the simulation. In the viscous sub-layer, the thickness is determined by $y^+ \leq 11.63$. The other boundary conditions are the same as in the previous tests.

Pressure distributions for the different numerical schemes can be seen in Figure 5.2.9. From the results, it is clear that the pressure distribution for all models is similar. We note that the higher upwind difference scheme is actually suitable for high Reynolds number flows and also appears to eliminate the false diffusion. It is suggested that by

using multi-blocks grid, the spatial oscillations or "wiggles" in the flow variables are reduced, therefore the truncation error and false diffusion are eliminated.

The hybrid difference scheme produced slightly higher results at the windward corner, but at the top side, the pressure distribution is a bit lower than the others. It can be seen that both Van Leer and higher upwind difference schemes produce similar pressure distribution everywhere.

In Figure 5.2.10, it can be seen that the hybrid scheme produces slightly greater turbulent kinetic energy at the windward side. At the leeward side, the hybrid difference scheme also produces slightly higher turbulent kinetic energy. It appears that the hybrid scheme produces a slightly greater transport of turbulent kinetic energy by diffusion than the Van Leer or higher upwind difference schemes.

The rate of energy dissipation for all models can be seen in Figure 5.2.11. Similarly to the turbulent kinetic energy, the hybrid scheme produces higher values at the windward and leeward sides of the building. This confirms that the hybrid scheme produces a slightly greater transport of turbulent kinetic and its dissipation rate by diffusion than the other schemes. Since this transport can be large for high Reynolds number flows and/or very coarse grids, a hybrid difference scheme should not be used for a complex geometry problem where coarser grids may occur.

The use of the Van Leer scheme is suggested here for the following reasons. First, the turbulent kinetic energy and its dissipation rate seem to be the mean value of higher upwind and hybrid difference schemes. This indicates that in case of coarse grids, energy transport by diffusion will not increase too much. Second, the Van Leer scheme was derived for transonic or low Mach number flows. However, in general problems with high Reynolds number, the truncation and round-off errors can be minimised.

The main objective of this study is to compare the performance of several numerical schemes to stabilise the iteration procedure. Relative residues for all models can be seen in Figure 5.2.12. It can be noted that the relative residues of the hybrid scheme are larger than the other methods. After 30 iterations, the hybrid scheme seems to converge to a value just below 0.02. Its relative residue then decreases and reaches the same value of the other methods after 70 iterations.

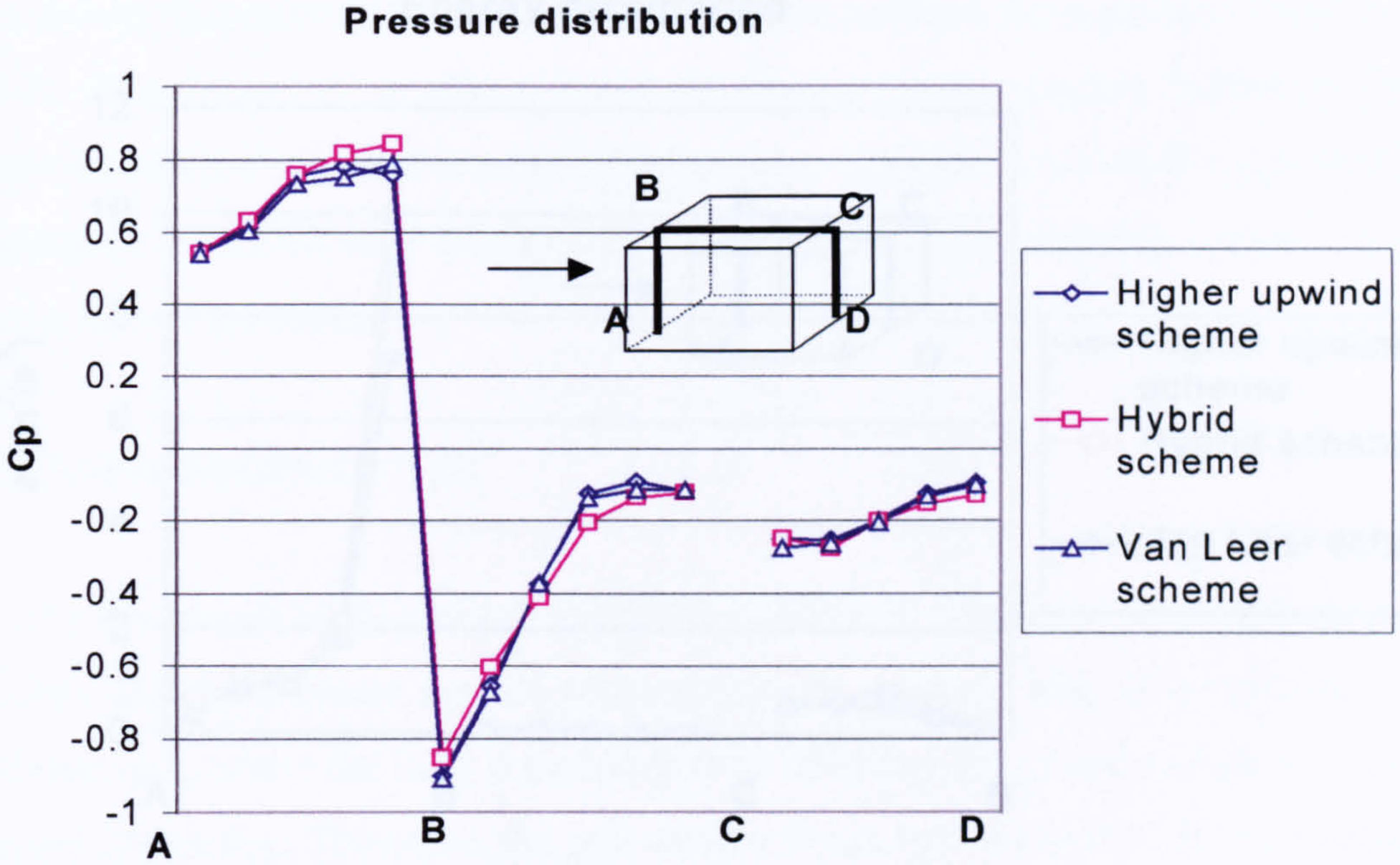

Figure 5.2.9 Pressure distribution for different numerical schemes

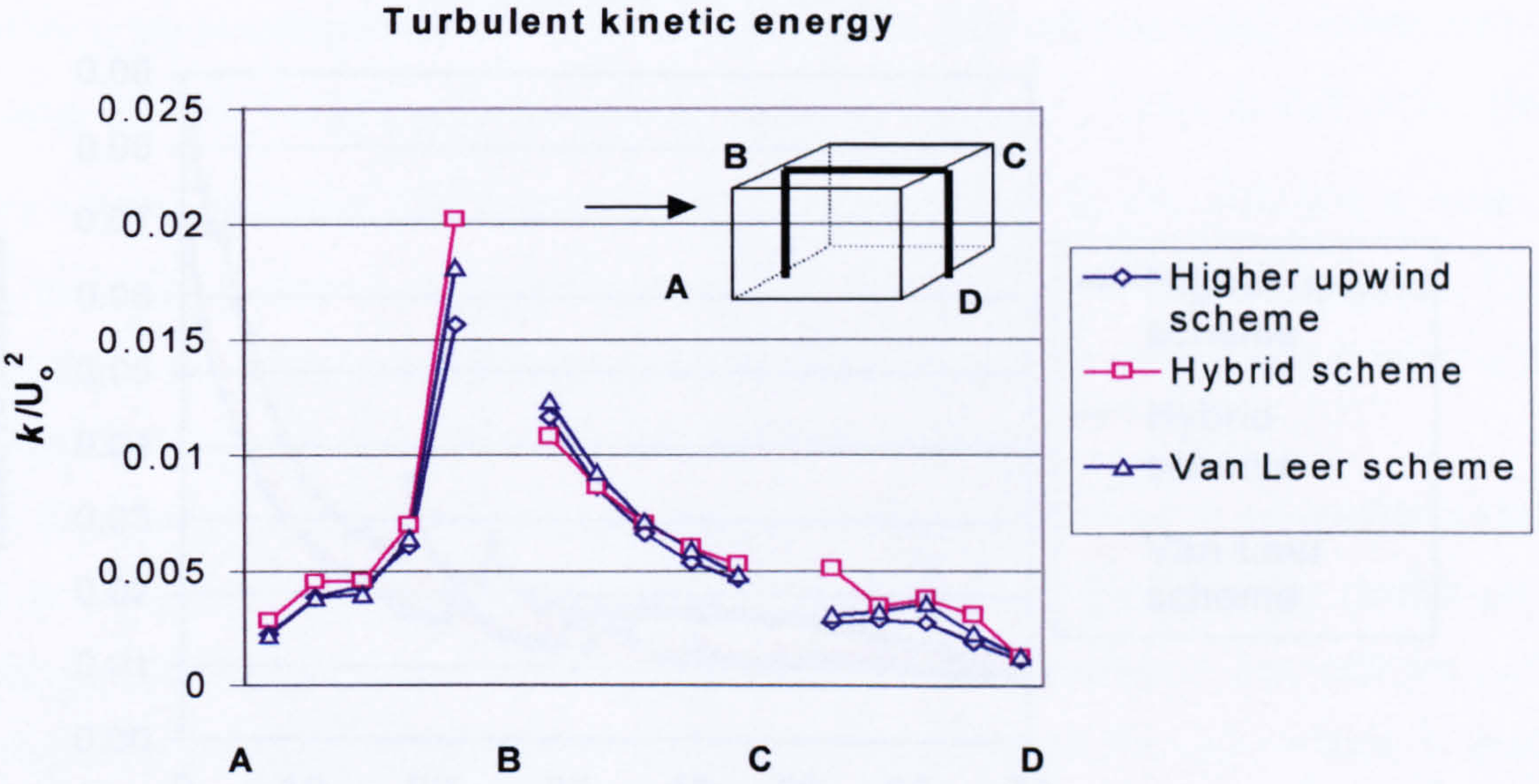

Figure 5.2.10 Turbulent kinetic energy for different numerical schemes

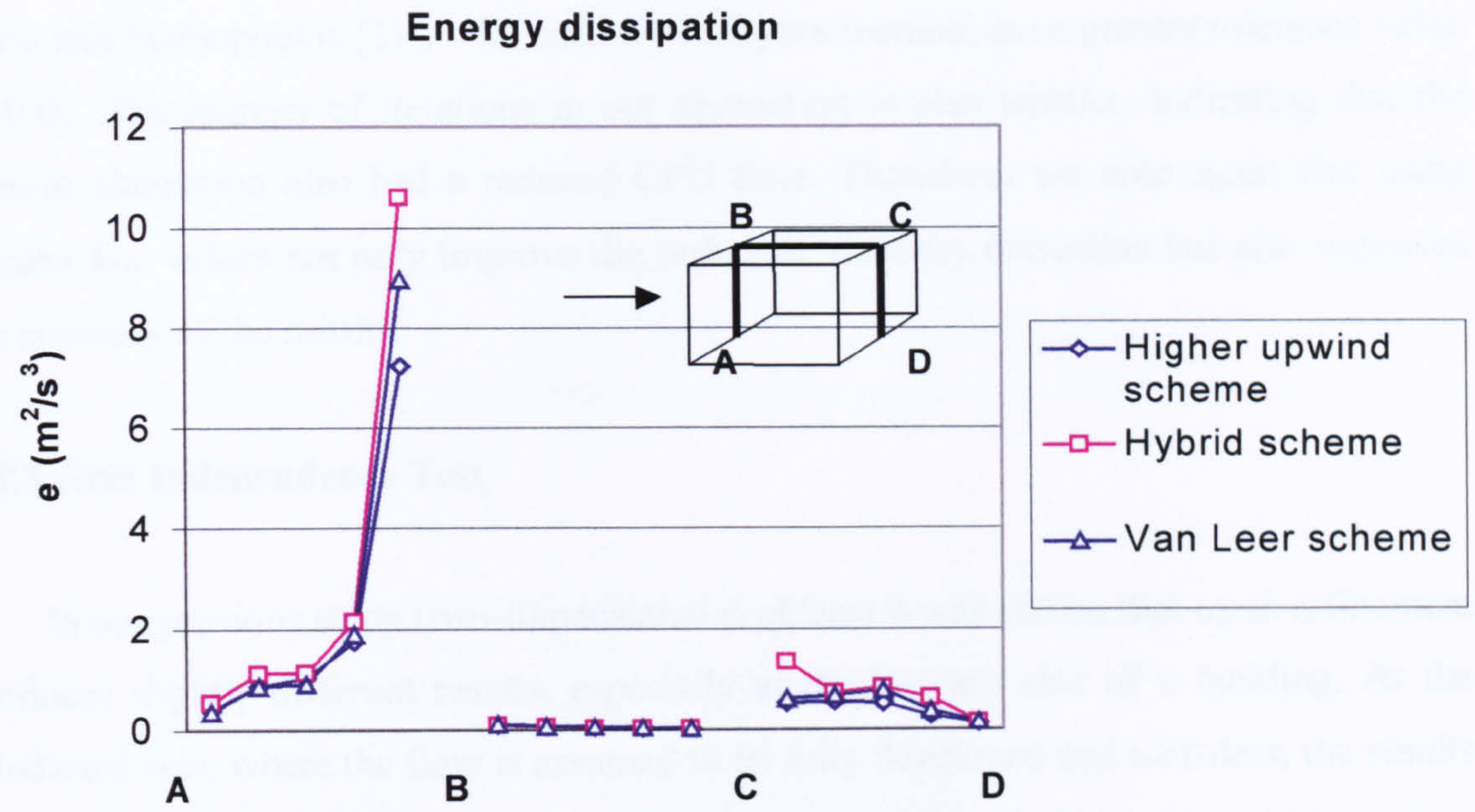

Figure 5.2.11 Turbulent energy dissipation for different numerical schemes

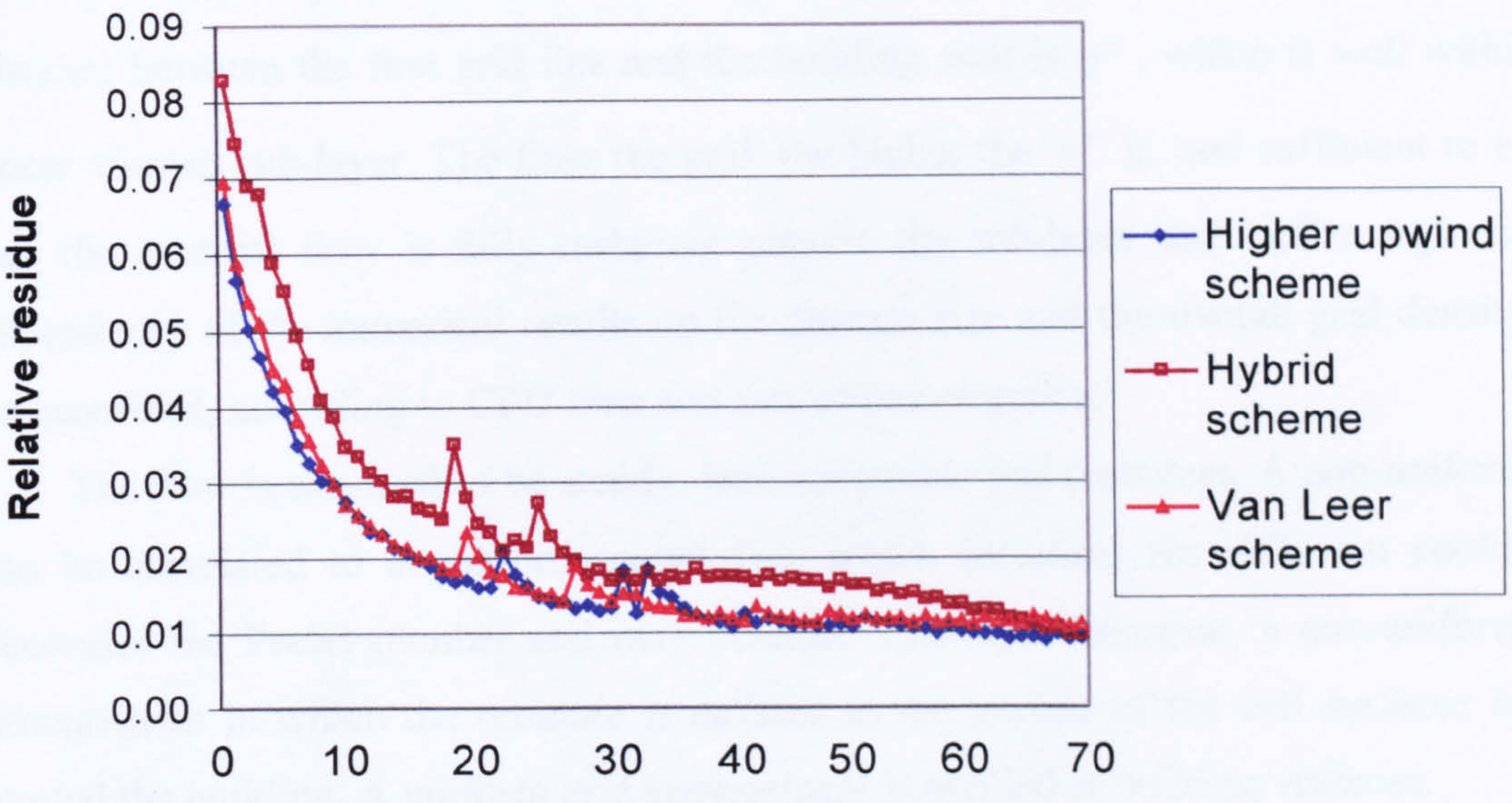

Figure 5.2.12 Relative residues for three schemes

Relative residues for convergence -as presented in this section- are around 0.01. Zhou and Stathopoulos [21], who used a two-layers method, have greater tolerance value of 0.02. The number of iterations in our simulation is also smaller, indicating that the present simulation also had a reduced CPU time. Therefore, we note again that using smaller k-ε values not only improve the turbulent viscosity correction but also improves the accuracy of the results.

5.2.3 Grid Independence Test

In our previous study (two-dimensional problem) it was shown that mesh refinement produces slightly different results, especially at the leeward side of a building. At the windward side, where the flow is assumed to be fully developed and turbulent, the results are more insensitive. Therefore, the grid density at the leeward side is the most important parameter for accuracy.

Most researchers quote that refining the grid near solid surfaces will produce better solutions, but the effects of mesh refinement on results near solid surfaces are not generally described. As far as we know, the pressure near solid surfaces can be obtained directly without extrapolation for non-staggered grids. The corresponding dimensionless distance between the first grid line and the building wall is y^+, which is well within the linear viscous sub-layer. The finer the grid, the higher the y^+ is, and sufficient to ensure that the external flow is fully turbulent outside the sub-layer and buffer regions. The dependency of the numerical results on the domain size and the overall grid density will be examined, according to CPU time and rate of convergence.

The flow is assumed to be steady, incompressible and turbulent. A non-uniform grid can be correlated to a non-orthogonal flux which increases the diffusion coefficient, decreases the Peclet number and may produce stability. Therefore, a non-uniform grid arrangement in which the pressure is defined at the middle of the cell surfaces is used around the building. A uniform grid arrangement is applied at building surfaces.

Although the grid arrangement at the leeward side of the building does affect the results and should be carefully refined, in the present study this statement is neglected. Therefore, the grid at the leeward side was reduced. Since the flow was fully developed at

the inlet, the grid at the windward side was also reduced. The total grid is the same as in the previous test, with 112 x 92 x 59 nodes in the x, y and z directions, respectively.

Van Leer's numerical scheme has been used for this test, according to our previous results. The SIMPLE pressure correction algorithm was used with relaxation 0.7 for turbulence values. The other boundary conditions are the same as in the previous tests.

From the pressure distribution in Figure 5.2.13, it seems that a more refined grid does not alter the pressure distribution at the leeward side. At the windward and top sides, the two curves also look similar.

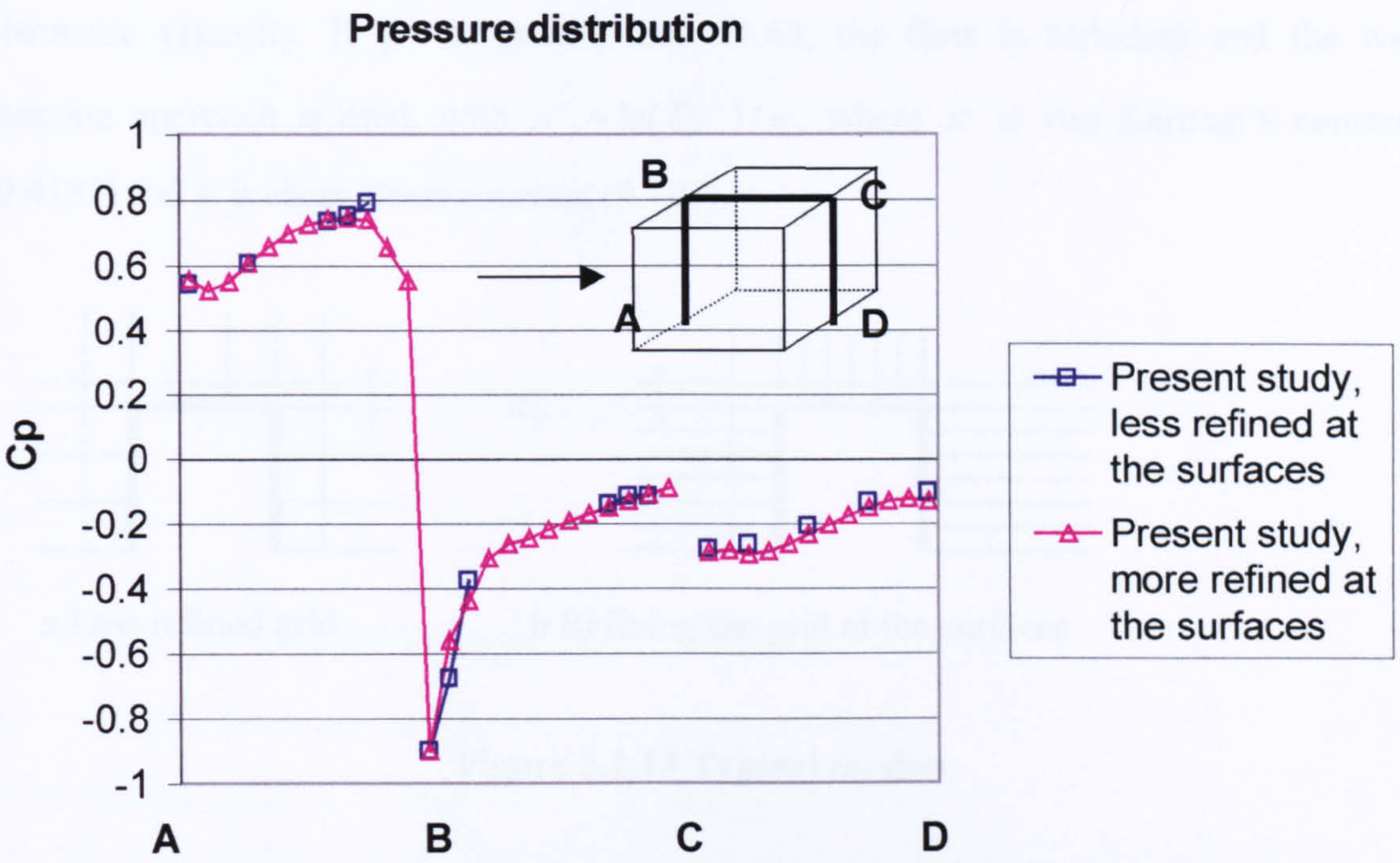

Figure 5.2.13 Pressure distribution for different meshes

In this study, the total grid is the same as in the previous test. Therefore, the local cell Reynolds number now depends on velocity only, since the area of each cell -outer region of the cube- is constant. Refining the grid at the building surfaces will reduce the area of each cell, tending to increase velocity.

The height d_p of the first cell next to the top of the building is set to a constant, as shown in Figure 5.2.14. Refining the grid at the building surfaces tends to increase the velocity at the windward and leeward sides since the local cell area is reduced. By using a mass balance equation, the local velocity in a finer grid will be greater than in a coarser one, especially at the windward and leeward sides. At the top side of the building, refining the grid reduces the local cell area but with constant thickness d_p. By using a mass balance equation, the same local velocity should occur at this side. The y^+ of building surfaces is defined as $y^+ = d_p u_\tau \upsilon^{-1}$, where u_τ is friction velocity and υ is kinematic viscosity. If y^+ is greater than 11.63, the flow is turbulent and the wall function approach is used, with $u^+ = \ln(Ey^+)/\kappa$, where κ is von Karman's constant (0.4187) and E is shear stress constant (9.793).

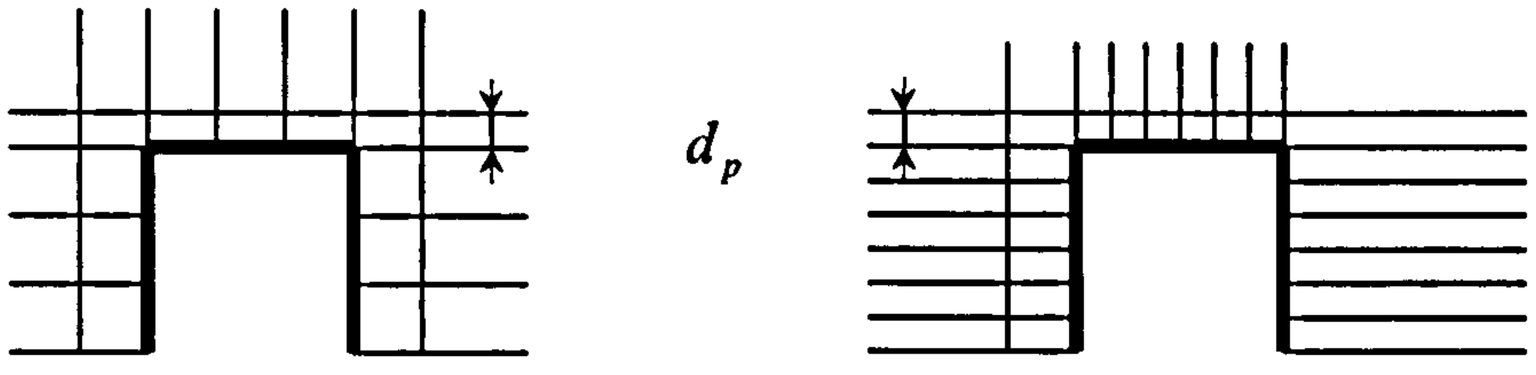

a Less refined grid b Refining the grid at the surfaces

Figure 5.2.14 Typical meshes

Adverse pressure occurs in the separation region. In this region, increasing the local velocity reduces the pressure. Therefore, at the windward and leeward sides, pressure distributions for the finer grid should be a bit lower than for the coarser one. This statement can be compared to the results in Figure 5.2.13 where a coarser grid produced a slightly higher pressure distribution at the windward and leeward corners, but with similar curves. From this statement, it can be noted that grid independence is affected by the local cell thickness, especially at the windward and leeward sides. In this study, the local cell thickness for the finer grid is one third of the coarse grid, but the pressure distributions produced are more or less the same.

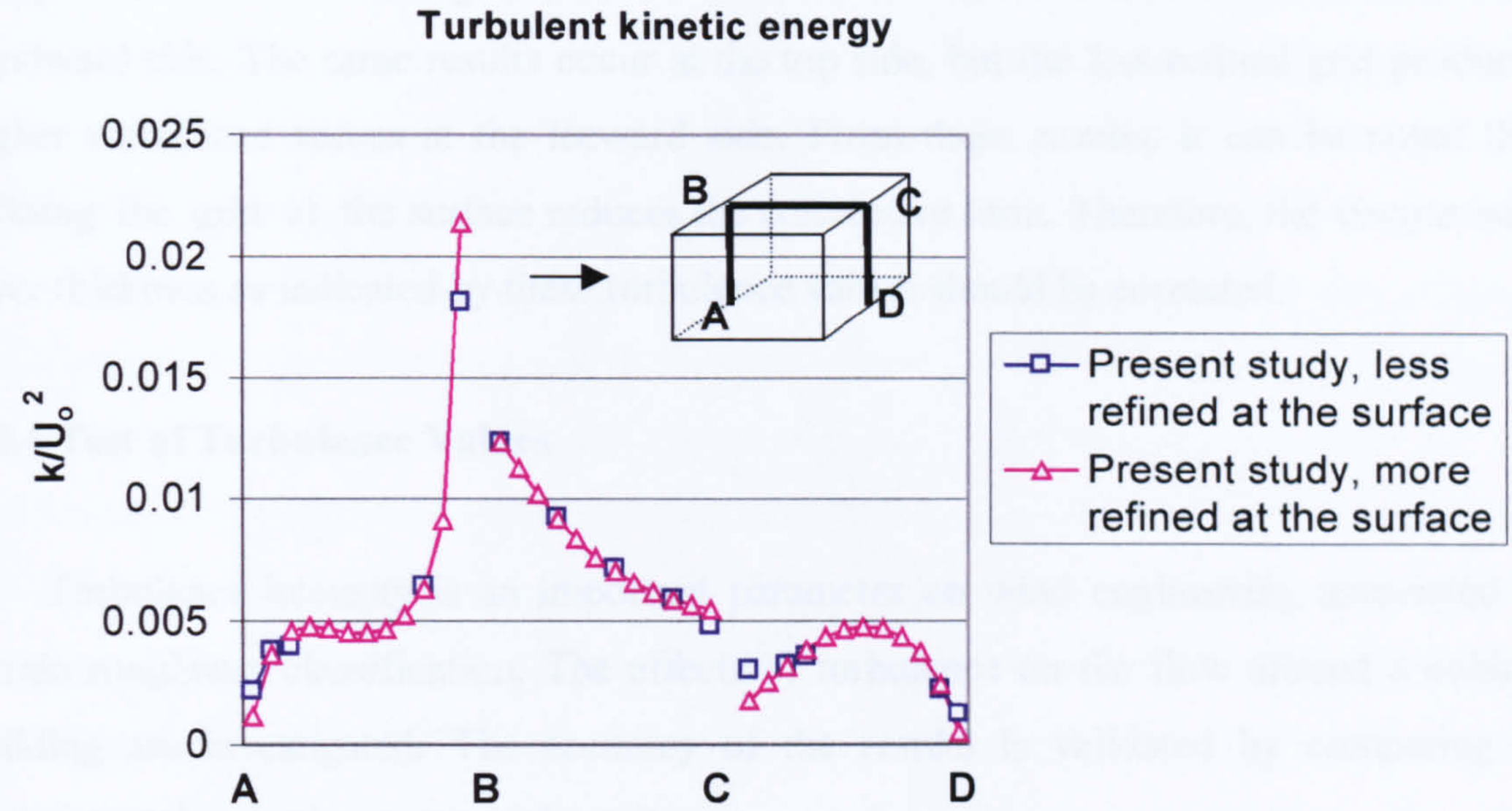

Figure 5.2.15 Turbulent kinetic energy for different meshes

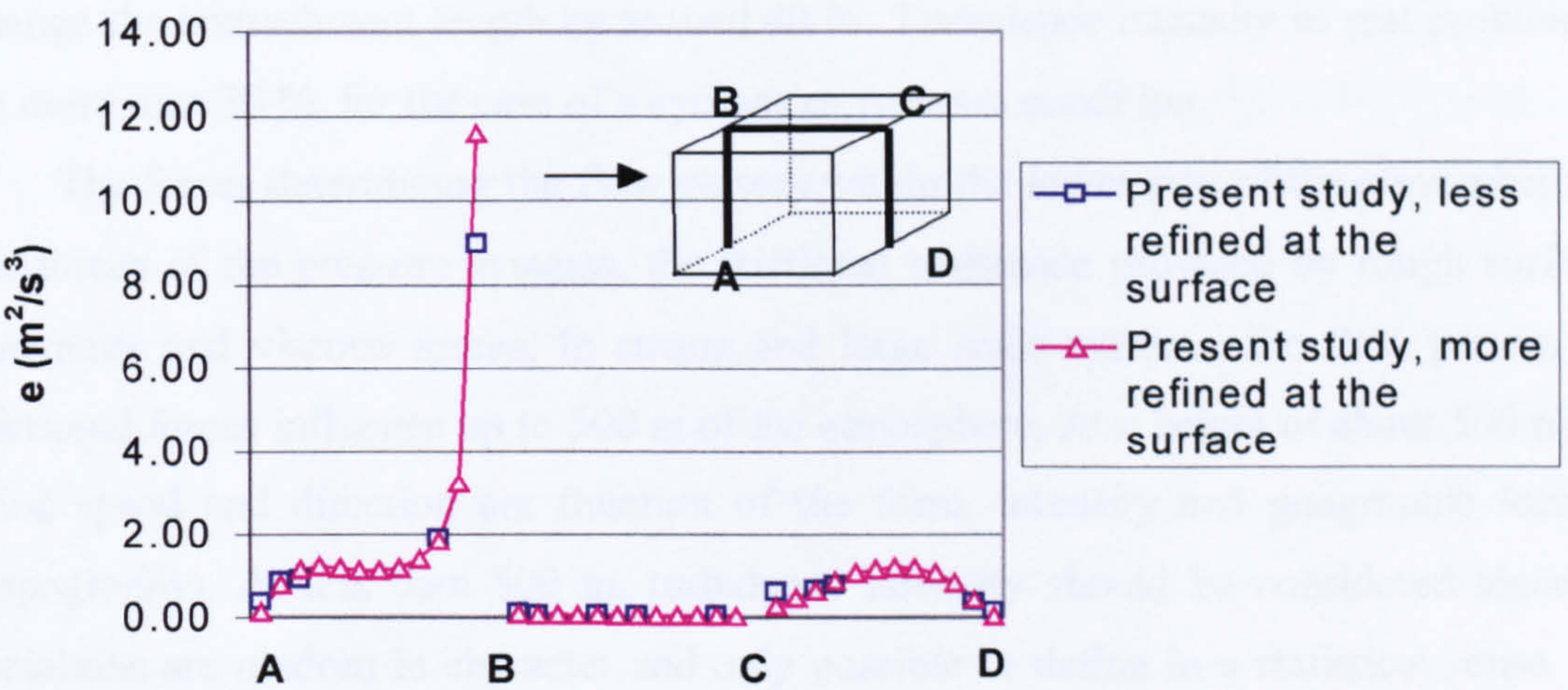

Figure 5.2.16 Turbulent energy dissipation for different meshes

It can be seen in Figures 5.2.15 and 5.2.16 that the kinetic energy and energy dissipation of a less refined grid at the surfaces are a bit lower than the refined one, at the windward side. The same results occur at the top side, but the less refined grid produces higher turbulence values at the leeward side. From these results, it can be noted that refining the grid at the surface reduces the convective term. Therefore, the viscous sub-layer thickness as indicated by these turbulence values should be corrected.

5.2.4 Test of Turbulence Values

Turbulence intensity is an important parameter on wind engineering associated to terrain roughness classification. The effects of turbulence on the flow around a cubical building are investigated. The accuracy of the results is validated by comparing to experimental and other numerical results.

Flow fields around buildings are fully affected by the nature of the upstream flow, characterised by the profiles of wind velocity, turbulence intensity, shape of the building and wind direction. The turbulence intensity of a flow field strongly depends on the terrain roughness which produces different fluctuating velocity components. In Chapter Three, the effects of turbulence values on the flow profile were investigated, and it was found that changing the turbulence values significantly (increasing or decreasing) will change the reattachment length by around 40 %. Turbulence intensity in real problems is no more than 30 %, for the case of a cyclone or typhoon condition.

The forces determining the flow pattern within the lower part of the atmosphere are the forces of the pressure systems, the frictional resistance provided by rough surfaces, buoyancy and viscous forces. In strong and large scale systems, the flow pattern and frictional forces influence up to 500 m of the atmosphere. At a height of about 500 m, the wind speed and direction are function of the form, intensity and geographic location (topography). At less than 500 m, turbulence intensity should be considered since the variations are random in character and only possible to define in a statistical sense. The intensity of turbulence differs because of the change in mean speed value and is reflected not only in the range to mean speed ratio but also in the variations in direction.

Li and Melbourne [29] presented the pressure distribution along a rod by using an experimental set up. From their results, it can be seen that an increase of free-stream turbulence intensity reduces the size of the separation length. In our previous simulation (two-dimensional flow), it was shown that increasing the free-stream turbulence intensity reduced the separation (reattachment) length. Therefore, our previous results agree with Li and Melbourne [29]. They also concluded that fluctuating pressures are dependent on turbulence intensity. The magnitude of peak pressures also increases with turbulent intensity. Although pressure distributions depend on turbulence intensity, Li and Melbourne [29] suggested that the pressure distributions for different turbulence intensity values are similar.

The effects of turbulent intensity on the flow profile around the building surface are now investigated. Two different turbulent intensity values were considered, around 2.1% and 6.7%. The flow is assumed to be steady, incompressible and turbulent. The same velocity, grid, numerical formulation, numerical scheme and relaxation factors have been used. Boundary conditions are the same as those in previous tests.

From pressure distribution in Figure 5.2.17, a higher turbulence intensity does not affect the pressure distribution at the windward and top sides. This indicates that the forces determining the flow pattern within the lower part of the atmosphere are the forces of the pressure systems, in agreement with Li and Melbourne's results where pressure distributions at the windward side do not have a significant correlation with turbulent intensity. Since pressure distributions at the windward and top sides of the building are not affected by the turbulence intensity, we note that changing the turbulence intensities by around 1 to 7% does not change pressure distributions.

Transport of turbulent kinetic energy or dissipation rate by diffusion is function of the turbulent Prandtl number and eddy viscosity. The higher the turbulent Prandtl number or the lower the eddy viscosity, the lower this transport is. Higher pressure distribution indicates lower eddy viscosity. Therefore, in cases where turbulence values are very high, eddy viscosity is reduced at the windward and leeward sides of the building.

In the previous section, we noted that in the separation region where recirculation occurs, the flow was dominated by the shear rate with reduced pressure distributions. In the present study, pressure distributions with a high turbulence intensity are similar to

those with a low one, therefore, the eddy viscosity is not affected at the windward, top and leeward sides. This can be used to reduce the over-prediction of eddy viscosity at the separation regions.

Applying the mixing length equation, an increase on the turbulence intensity at the inlet should be followed by an increase on the friction velocity. The only way to increase the friction velocity is by increasing the co-ordinate direction normal to a solid wall, y^+. By increasing this value, the linear viscous sub-layer will change into a logarithmic overlap layer, decreasing the pressure.

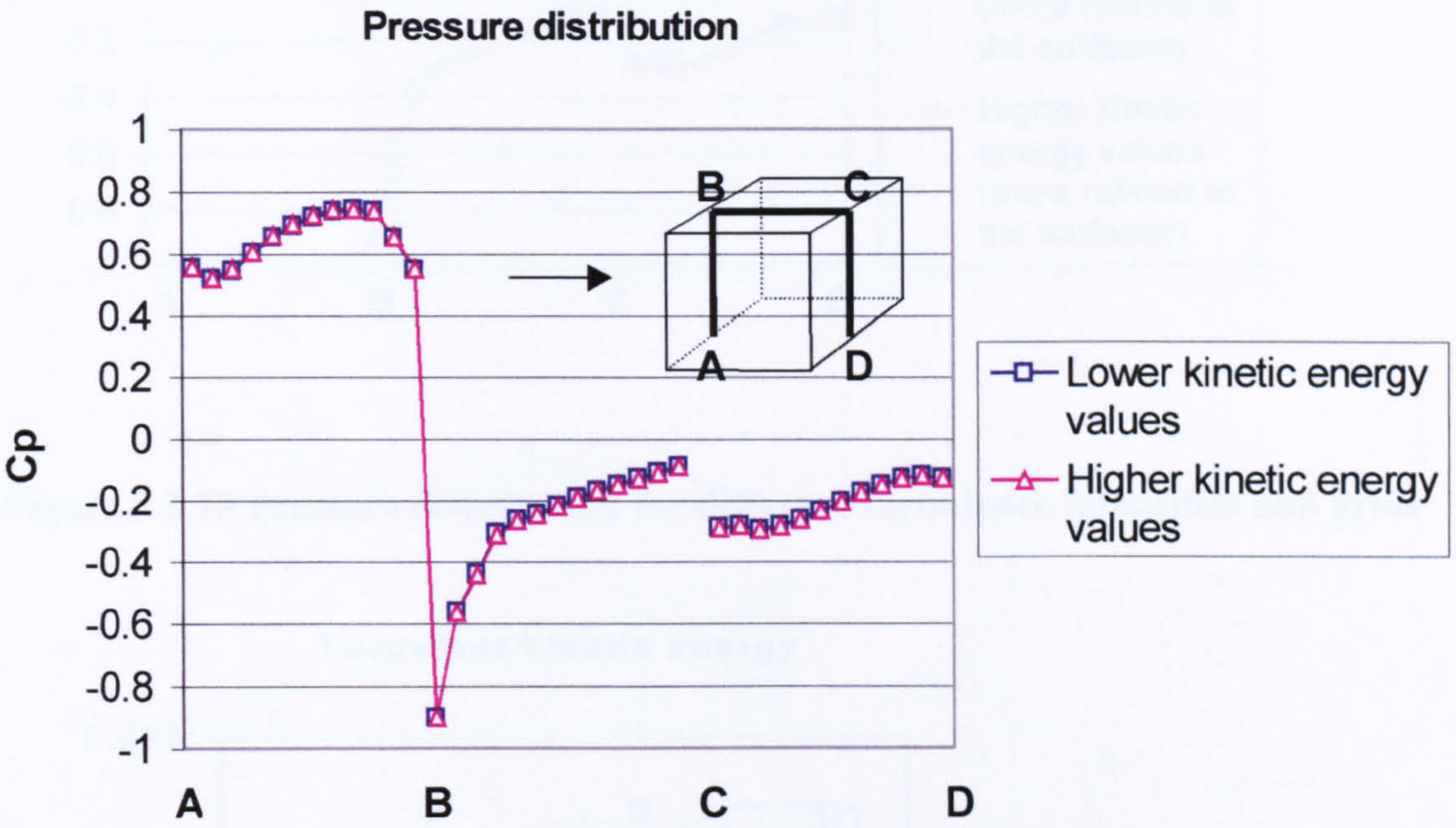

Figure 5.2.17 Pressure distribution for different turbulence intensities

To better understand the pressure distribution for higher turbulence values, results for lower turbulence values and a less refined mesh at the surface are plotted in Figure 5.2.18. It can be seen that all pressure distributions are similar. The turbulent stresses are related to the convective acceleration terms associated to y^+. In the present study, the viscous sub-layer thickness is set to constant. Since direction y normal to the wall

surfaces is constant, the convective term remains constant. Therefore, the pressure distributions on the building surface are also similar since the eddy viscosity at the separation regions does not change.

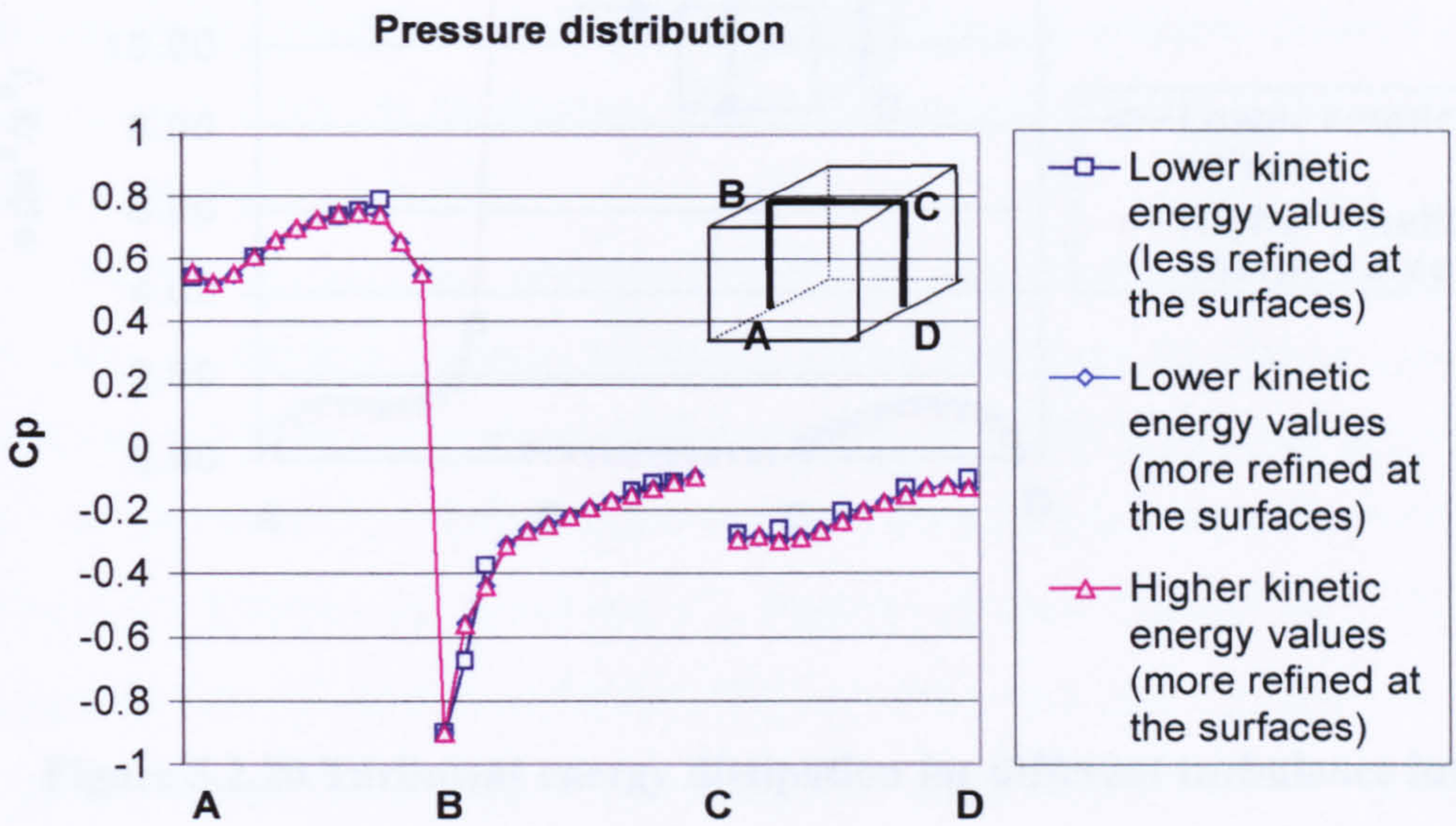

Figure 5.2.18 Pressure distribution for different turbulence intensities and grids

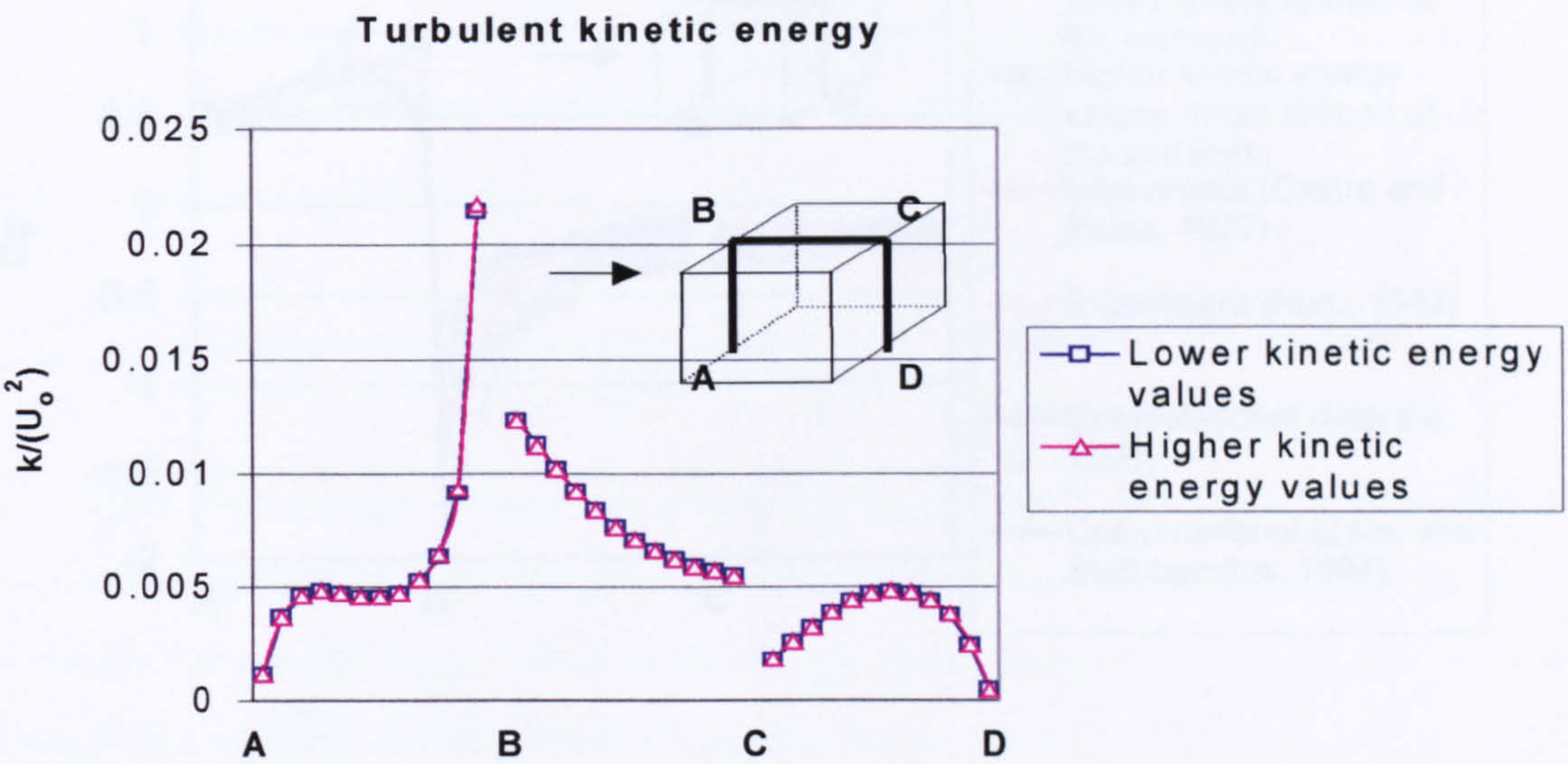

Figure 5.2.19 Turbulent kinetic energy for different turbulence intensities

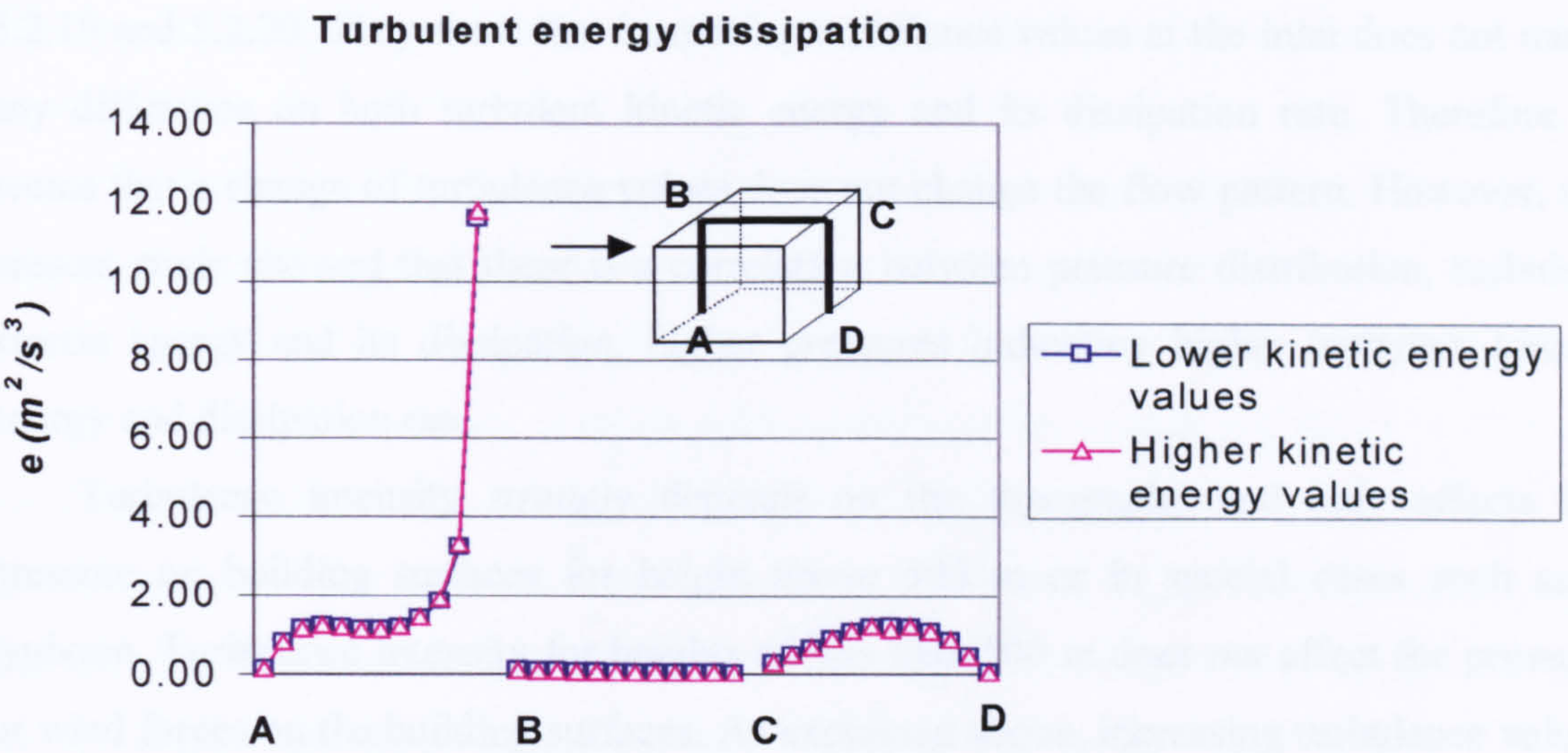

Figure 5.2.20 Turbulent energy dissipation for different turbulence intensities

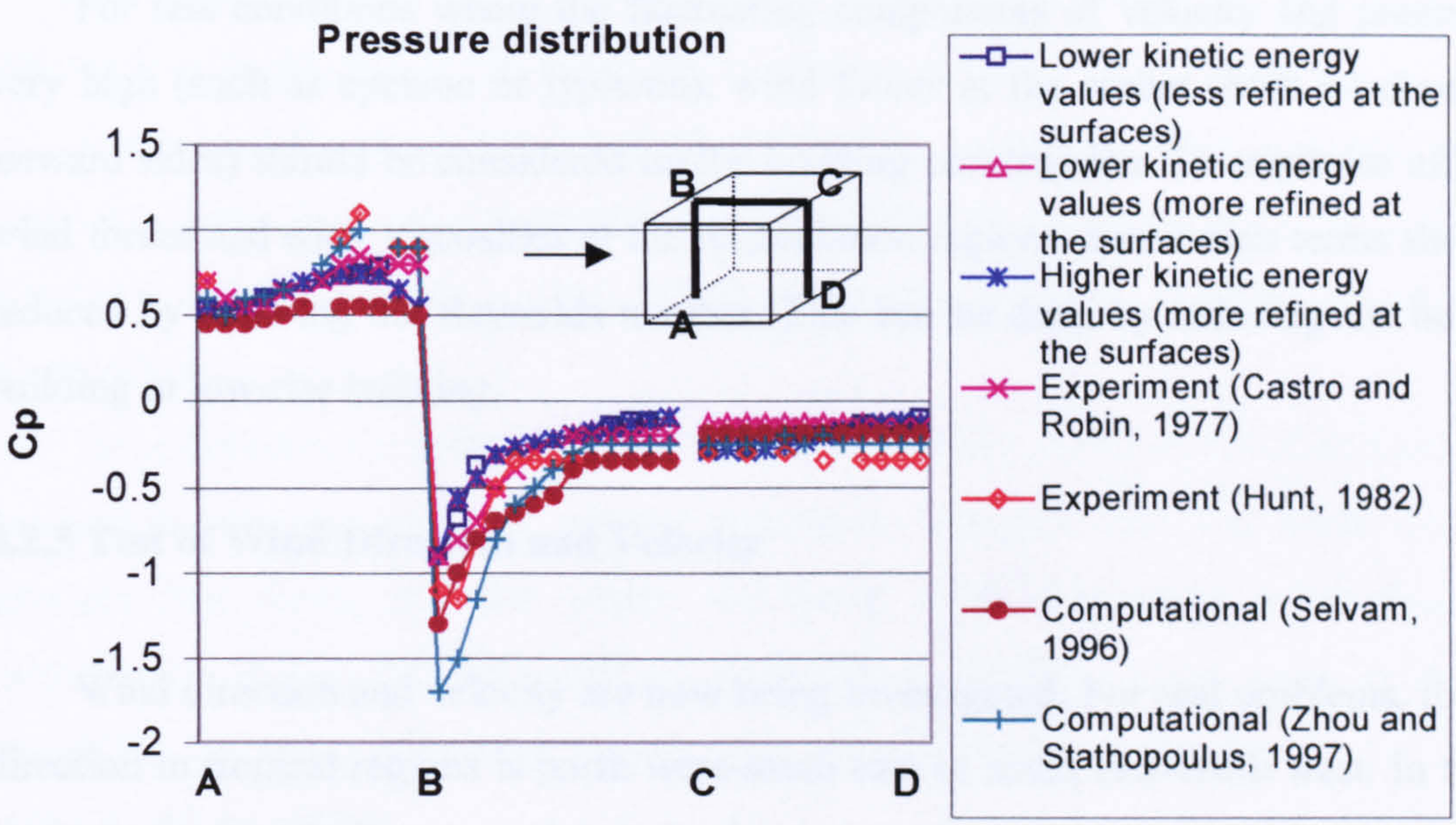

Figure 5.2.21 Pressure distribution for different turbulence intensities

Results for turbulent kinetic energy and its dissipation rate are presented in Figures 5.2.19 and 5.2.20. They show that increasing turbulence values at the inlet does not make any difference on both turbulent kinetic energy and its dissipation rate. Therefore, it seems that a change of turbulence values does not change the flow pattern. However, the present study showed that there is a correlation between pressure distribution, turbulent kinetic energy and its dissipation, higher pressures indicating higher turbulent kinetic energy and dissipation rate.

Turbulence intensity strongly depends on the topography and only affects the pressure on building surfaces for height above 500 m or in special cases such as a typhoon. Turbulence intensity for heights of less than 500 m does not affect the pressure or wind forces on the building surfaces. As explained above, increasing turbulence values should be followed by increasing y^+. From the pressure distribution in Fig. 5.2.21, it is suggested that the models of Selvam [20] and Zhou and Stathopoulos [18 and 21] used high turbulence values without increasing the sub-layer thickness y^+ at the windward corner.

For real conditions where the fluctuating components of velocity and pressure are very high (such as cyclone or typhoon), wind forces at the corner (both windward and leeward sides) should be considered on the building construction. To minimise effects of wind forces and eddy viscosities at the recirculation regions, convection terms should be reduced by reducing the Reynolds number. This can be done by reducing the height of building or low-rise building.

5.2.5 Test of Wind Direction and Velocity

Wind direction and velocity are now being investigated. For real problems, the wind direction in tropical regions is north west-south east or south east-north west. In tropical countries such as Indonesia which is the largest archipelago in the world, the wind flow changes dramatically not only in direction but also in velocity. During the wet season, the wind flow contains water vapour and produces heavy rain which always creates flooding and affects building construction. This is opposite to the dry season when the wind flow is relatively weak and dry. The dry season is the best time to analyse natural ventilation

systems since temperature and thermal radiation are very high. The wet season is the best time to analyse building construction and orientation since wind flow and precipitation are very high.

In the present study, wind direction and velocity were investigated. The effect of the buoyancy terms is negligible in this simulation and will be taken into consideration in the next section. Therefore, the flow is assumed to be steady, incompressible and turbulent.

At the inlet, the velocity is set to uniform either with straight (north) or north-west directions. Low values of k-ε are used according to the terrain roughness. A higher value of velocity is also set with the same k-ε values. Therefore, higher velocity has smaller turbulence intensity at the inlet, following our previous results. It also means that the higher velocity has lower turbulence kinetic energy as can be clearly seen in Figures 5.2.22 and 5.2.23.

It can be seen in Figure 5.2.22 that a lower velocity produces greater dimensionless turbulent kinetic energy. This occurs since turbulent values at the inlet are set to constant for both velocity values. In fact, a higher velocity with a lower turbulence value produces greater turbulent kinetic energy. Therefore, this indicates that turbulent values are fully affected by velocity, but do not affect turbulent intensity.

Similar results occur for the north-west wind direction, where a lower velocity produces greater turbulence intensity. The only difference between north and north-west directions is the magnitude of their turbulent intensity, with the straight flow producing lower values.

From turbulence kinetic energy or turbulent intensity, it can be noted that the north-west wind direction produces greater turbulence intensity than the north one. This indicates that during the wet season the heavy wind will create larger fluctuating components of velocity and pressure on building surfaces. Since there is a strong correlation between turbulence values and wind pressure, wind forces on building surfaces will be greater.

The pressure distribution can be seen in Figures 5.2.24 and 5.2.25. The pressure distribution for the north-wind direction is lower than the north-west one, at the windward side. According to turbulence values, this also denotes that pressure distribution and

turbulence values have a proportional correlation as described in the previous section. This is an interesting result which needs further analyses.

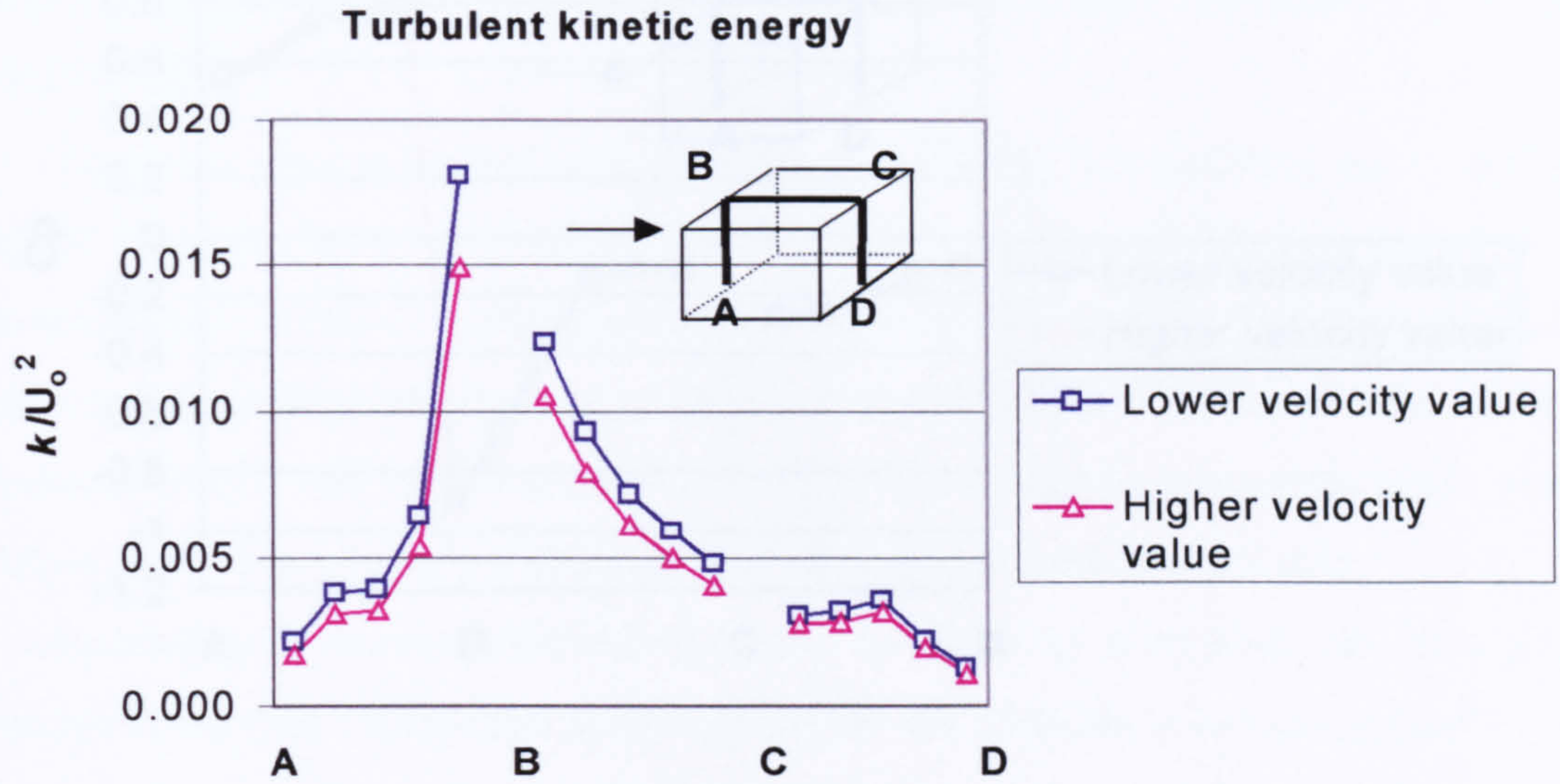

Figure 5.2.22 Turbulent kinetic energy for different velocity values (north-wind)

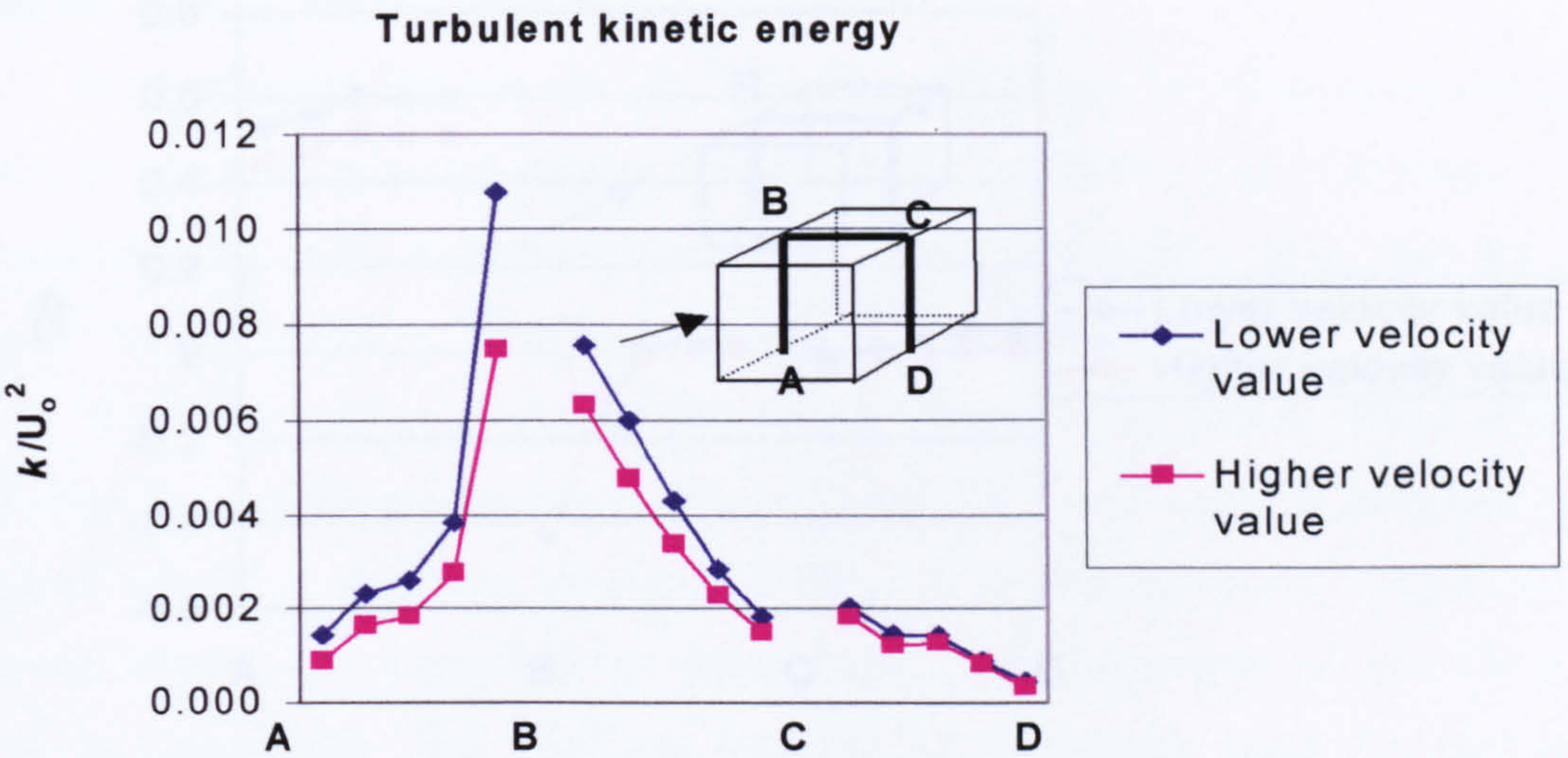

Figure 5.2.23 Turbulent kinetic energy for different velocity values (north-west wind)

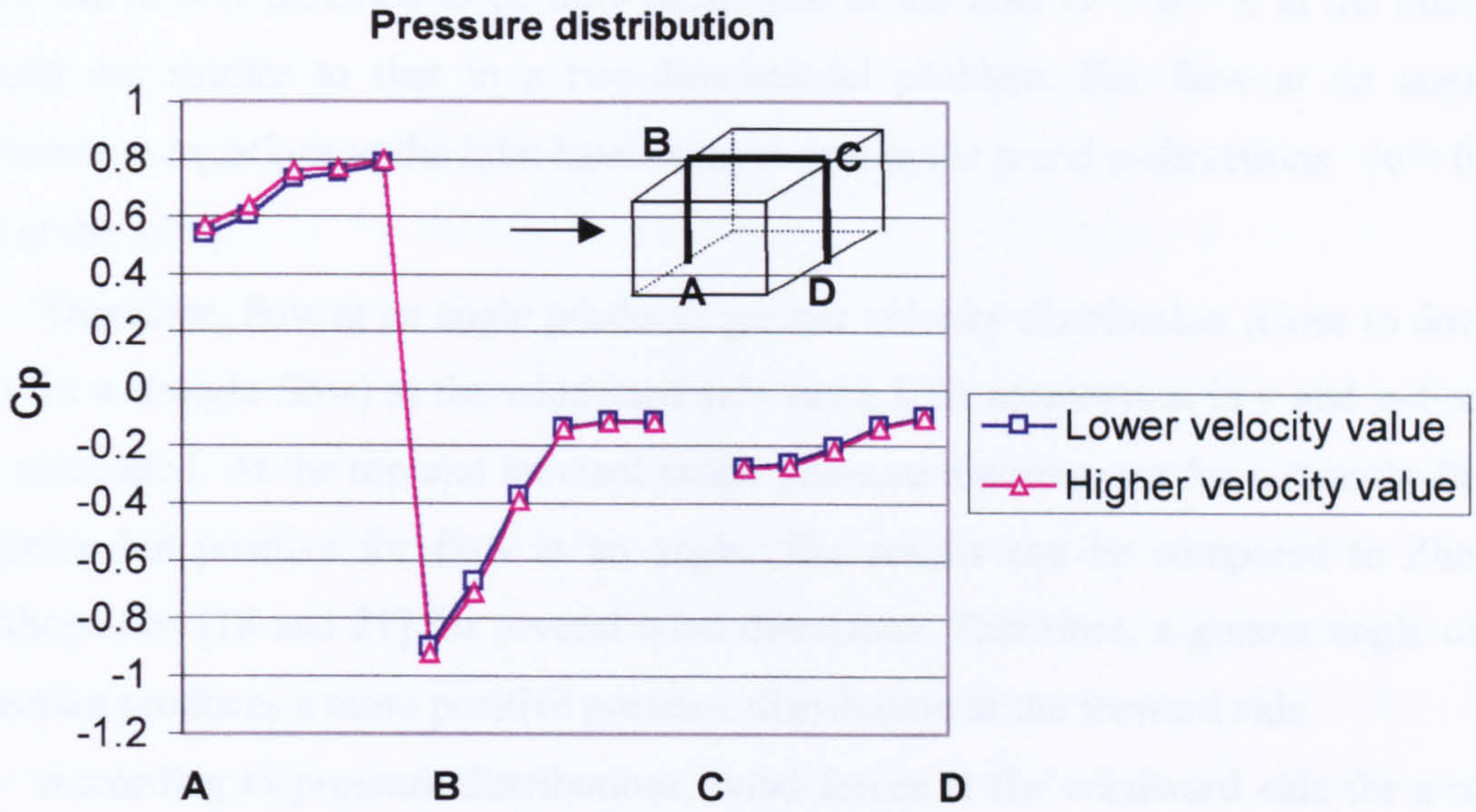

Figure 5.2.24 Pressure distribution for different velocity values (north wind)

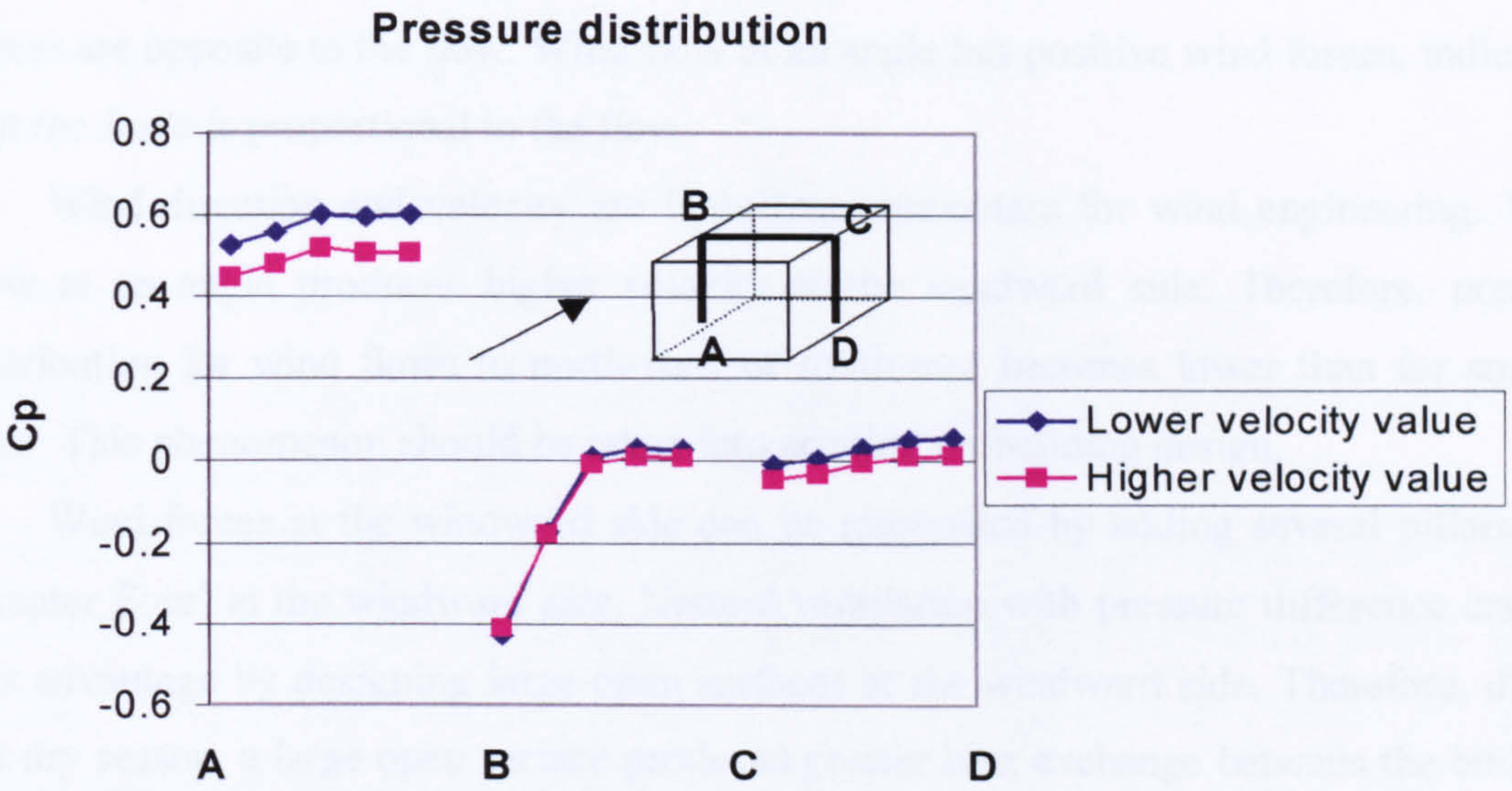

Figure 5.2.25 Pressure distribution for different velocity values (north-west wind)

For a straight flow, the momentum equations at the inlet act in the x-direction only since the flow is assumed to be fully developed at the inlet ($v = w = 0$ at the inlet). The results are similar to that in a two-dimensional problem. For flow at an angle, the momentum equations at the inlet have components in the x and z–directions ($v = 0$ but $w \neq 0$ at the inlet).

Therefore, flow at an angle produces greater velocity distribution (close to double of that for a straight flow) at the windward side since both momentum in x and z-directions are calculated. At the top and leeward sides, pressure distributions for a straight flow are negative but positive for flow at an angle. The results can be compared to Zhou and Stathopoulos [18 and 21] for several wind directions. Therefore, a greater angle of wind direction produces a more positive pressure distribution at the leeward side.

According to pressure distributions, wind forces at the windward side for a straight flow are lower than for the flow at an angle. Both wind directions produce a positive wind force. At the top side, lifting forces for a straight flow are greater than for the flow at an angle. Therefore, the greater the angle of attack of the wind, the lower the lift force is. At the leeward side, wind forces for a straight flow have a negative value indicating that the forces are opposite to the flow. Wind flow at an angle has positive wind forces, indicating that the force is proportional to the flow

Wind direction and velocity are important parameters for wind engineering. Wind flow at an angle produces higher velocity at the windward side. Therefore, pressure distribution for wind flows to north-west or south-east becomes lower than for straight ones. This phenomenon should be taken into account on building design.

Wind forces at the windward side can be minimised by adding several pillars (see Chapter Four) at the windward side. Natural ventilation with pressure difference can use this advantage by designing large open surfaces at the windward side. Therefore, during the dry season, a large open surface produces greater heat exchange between the building and its surrounding. This condition can also be realised by using louvered window openings.

5.2.6 Test of Turbulence Models

For most engineering purposes, it is unnecessary to resolve the details of the turbulent fluctuations. Only the turbulence effects on the mean flow are usually sought. For a turbulence model to be useful in general purpose CFD codes, it must have widely applicability, accuracy, be simple and economical [30].

The classical models use the Reynolds equations and form the basis of turbulence calculations in current commercial CFD codes. Large eddy simulation (LES) are turbulence models where only the largest eddies are modelled. It was argued in the previous section that the largest eddies interact strongly with the mean flow and contain most of the energy so this approach is a good model of the main effects of turbulence. At present, large eddy simulation is too costly although anticipated improvements in computer hardware may change this perspective in the future [30].

In our previous test we described that turbulence levels and turbulent stresses vary from point to point in a flow. The underlying assumption of a turbulence model is that the turbulent viscosity μ_t is isotropic, or the ratio between Reynolds stress and mean rate of deformation is the same in all directions. This assumption is not representative of many categories of flow.

Mixing length models attempt to describe the stresses by means of a simple algebraic formula for μ_t as a function of position. The k-ε model is more sophisticated and general. In Reynolds stress equation models (also known as second-moment closure models) assumptions are made about these unknown terms and the resulting partial differential equations are solved in conjunction with the transport equation for the rate of dissipation ε. This model has not been validated as widely as the mixing length and k-ε models. A much more far-reaching set of modelling assumptions reduces the partial differential equations describing Reynolds stress transport to algebraic equations to be solved alongside the k and ε equations of the k-ε model. This approach leads to the algebraic stress models that are the most economical form of Reynolds stress model able to introduce anisotropic turbulence effects into CFD simulation [30].

In our previous tests, the changes in the flow direction are always slow in shear layers. If the convection and diffusion of turbulence properties can be neglected, it is

possible to express the influence of turbulence on the mean flow in terms of mixing length. Where the convection and diffusion are not negligible (in recirculating zones), a compact algebraic prescription for the mixing length is no longer feasible.

At high Reynolds number, the rate at which large eddies extract energy from the mean flow is precisely matched to the rate of energy transfer across the energy spectrum to small, dissipating eddies. If this did not happen, the energy at some scales of turbulence could grow or diminish without limit. Production and destruction of turbulent kinetic energy are always closely linked. The dissipation rate ε increases where production of k is large. The model equation for ε assumes that its production and destruction terms are proportional to the production and destruction terms of the k equation. As described in previous tests, increasing k will increase ε but where k decreases, ε decreases sufficiently fast to avoid negative values of turbulent kinetic energy. This is the reason why pressure distribution, turbulent kinetic energy and its dissipation rate do not change for very low turbulence values (see Chapter Three for test of turbulence values).

At high Reynolds number, the standard k-ε model avoids the need to integrate the model equations right to the wall by making use of the universal behaviour of near wall flows, considering the co-ordinate direction normal to the solid wall y^+. The logarithmic-law, therefore, can be satisfied indicating that the rate of turbulence production equals the rate of dissipation.

The algebraic stress model is an economical way of accounting for the anisotropy of Reynolds stresses without going to the full length of solving the Reynolds stress transport equations. Rodi [31] proposed the idea that if the convective and diffusive transport terms are eliminated, the Reynolds stress equations reduce to a set of algebraic equation. This leads to the algebraic stress model (ASM).

The simplest method to remove those two terms is by neglecting them altogether, Naot and Rodi [32] and Demuren and Rodi [33]. A more generally applicable method is to assume that the sum of convection and diffusion terms of the Reynolds stress is proportional to the sum of the convection and diffusion terms of turbulent kinetic energy.

The algebraic stress model is not as well validated as the k-ε model but can be used in flows where the transport assumptions made do not compromise the accuracy of the

calculation. The recent development of the anisotropic k-ε model have made algebraic stress models less popular [34].

The anisotropic k-ε turbulence model is a version of the standard k-ε model that includes terms in the equation which relate to the anisotropic structure of the turbulence field. These terms, which are based on those used in differential Reynolds stress turbulence models, are intended to better predict anisotropy effects which were previously unresolveable with standard k-ε models. Such influences can be significant in flows involving strong curvature, swirl and body forces effects.

Launder [35] and Speziale [36] described equations for anisotropic turbulent viscosity based on the Boussinesq anistropic model [37]. Launder's [35] model renders the Reynolds stress tensor a cubic function of the strain rate tensor and correctly predicts the anisotropy of the turbulent normal stresses in boundary-layer type flows and qualitatively predicts the secondary flows in channels of non-circular cross-section. Additionally, Launder's model is better equipped to predict some types of swirling flows.

Speziale's [36] model renders the Reynolds stress tensor a quadratic function of the strain rate tensor. The model has been shown to correctly account for the anisotropy of the turbulent normal stresses in boundary-layer type flows and qualitatively predicts the weak secondary flows resulting from stress anisotropy in channels of non-circular cross-section. In addition to this work, Speziale and researchers at NASA Langley Research Centre have derived a variant of the algebraic stress model, Gatski and Speziale [38], that is claimed to be more computationally stable.

It is important to emphasise that the three eddy-viscosity models (Boussinesq's, Launder's and Speziale's) can be combined with any turbulence models with the exception that the anisotropic k-ε model must be used with one of the non-isotropic eddy-viscosity models. This provides a wide choice of turbulence modelling options for the expert user. The anisotropic k-ε turbulence model and the anisotropic Eddy-Viscosity models represent the first attempt to provide two-equation models capable of accurately predicting turbulence anisotropy effects.

The initial interest in the algebraic stress model arose from its ability to provide a cheap way of accounting for anisotropy of the Reynolds stresses. The statistical mechanics approach has led to new mathematical formula in conjunction with a limited

number of assumptions regarding the statistics of small scale turbulence, provide an exacting basis for the extension of eddy viscosity models. The renormalization group by Yakhot and Orszag [39] has to date attracted most interest.

This model represents the effects of the small scale turbulence by means of a random forcing fluctuation in the Navier-Stokes equation. This systematically removes the small scales of motion from the governing equations by expressing their effects in terms of larger scale motions and a modified viscosity.

This model is very similar in form to the standard k-ε turbulence models, where the turbulence model employs an additional source/sink term in the equation and employs different values for the various model coefficients. The model can be applied with the isotropic Reynolds stress equation or with the non-linear form, but still needs to be widely validated.

Employing the k-ε turbulence model significantly increases the required CPU resources for the solution of a given flow problem compared to the corresponding simulation using zero-equation type models. Moreover, owing to the significantly stronger non-linear and inter-coupled nature of the system of flow equations, securing a fully converged solution becomes harder. In general, the convergence characteristics of k-ε simulations are less stable and relatively sensitive to the numerical and physical parameters involved in the numerical solution.

This section is mainly dedicated to some aspects relating to the simulation of flows using several turbulence models. First, turbulence models tend to be employed more frequently than zero-equation type models. Second, there are considerably more physical and numerical issues involved in performing turbulent flow simulations and it is consequently more difficult for the inexperienced CFD user to obtain optimal solutions to such simulations.

Invoking the k-ε turbulence model requires the solution of two additional transport equations. This can significantly increase the CPU requirements of the numerical solution. Moreover, the introduction of the k and ε equations significantly increases the non-linearity and coupling of the overall flow equations and this in general disturbs the convergence characteristics of the numerical solution. In contrast to the above, turbulent flow simulations using zero-equation type models (where the value of the eddy viscosity

is either fixed or prescribed algebraically) exhibit relatively more stable convergence characteristics (similar to those observed in the simulation of laminar flow problems).

The simulation of turbulent flows is a specialised area within CFD. An adequate knowledge of turbulent flows and turbulence models is recommended. This study intends to contribute to a discussion of the optimum turbulence model based on accuracy requirements and available CPU resources.

Five types of turbulence models were investigated; standard k-ε model, re-normalisation group (RNG- k-ε) model, algebraic stress model (ASM), differential stress model (DSM) and differential flux model.

The ASM model is not stable and tends to diverge for very low turbulence values (turbulence intensity around 0.66%). This phenomenon is interesting since it was not described in Murakami *et al* published results [16 and 40]. Therefore, for very low turbulence values, the standard k-ε model is compared to RNG, DSM and differential flux models. For higher turbulence values (turbulence intensity around 2.1%), the standard k-ε model is compared to ASM and DSM models. The same grid arrangement, numerical procedures and boundary conditions have been used.

The pressure distribution obtained with several turbulence models is presented in Figure 5.2.26 for a low turbulence value. Both DSM and differential flux models produced exactly the same pressure distribution at the leeward side. At this point, both RNG and standard k-ε models produce the same results which are greater than those of ASM and differential flux models. All models tend to produce similar values at the top side, but at the leeward side, the standard k-ε model produces higher values than the others, especially at the corner.

The pressure distribution of the standard k-ε model seems to be the highest one, therefore, this model produces the greatest values for turbulent kinetic energy and its dissipation rate, as can be seen in Figures 5.2.27 and 5.2.28. An interesting result for the RNG model is that although it produces a similar pressure distribution at the windward side, its turbulent kinetic energy and dissipation rate are lower than for the standard k-ε model. RNG also produces the lowest turbulent kinetic energy and dissipation, indicating that the turbulence dissipation equation (which was suspected to be one of the main sources of accuracy limitation) has been properly corrected.

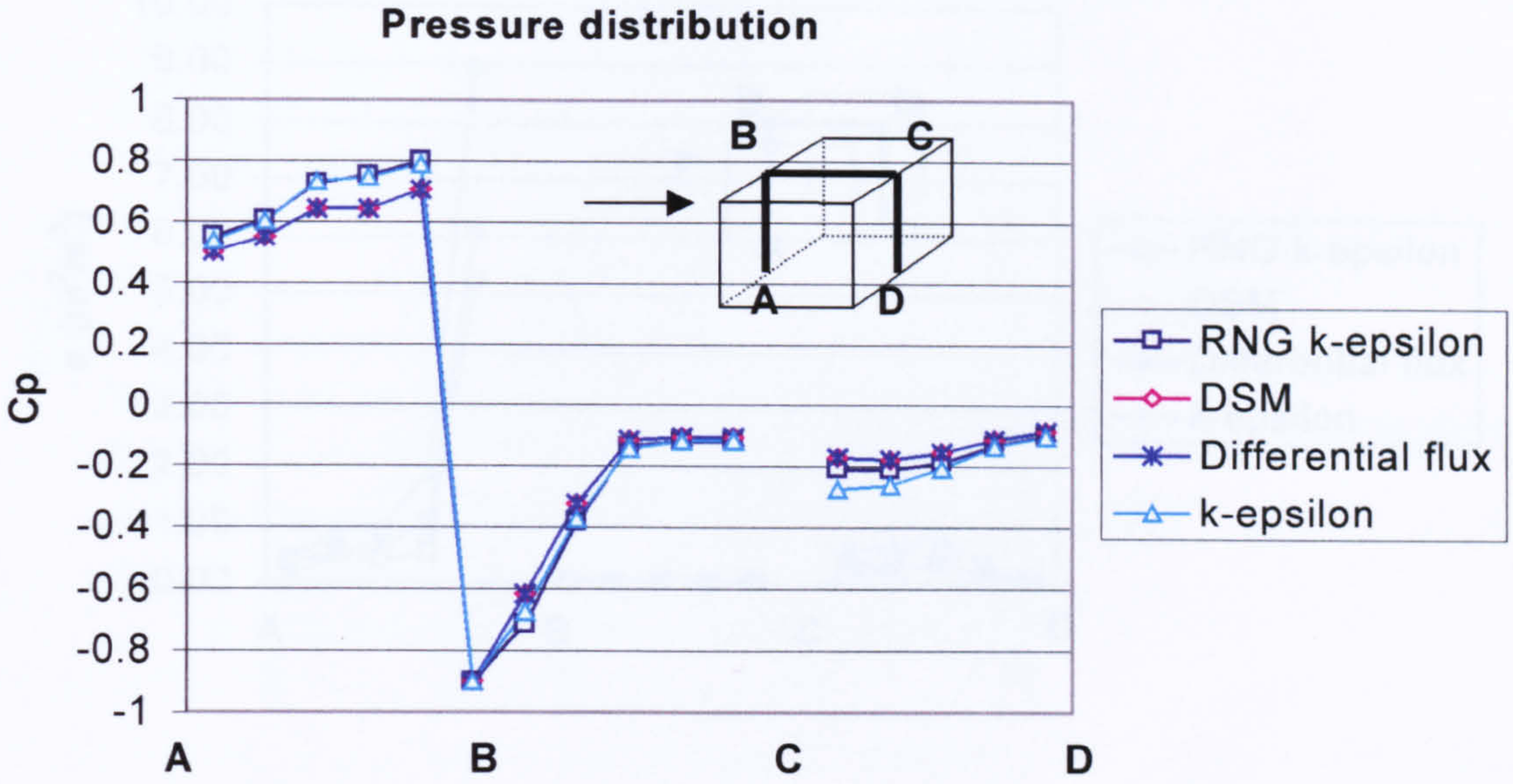

Figure 5.2.26 Pressure distribution for different turbulence models

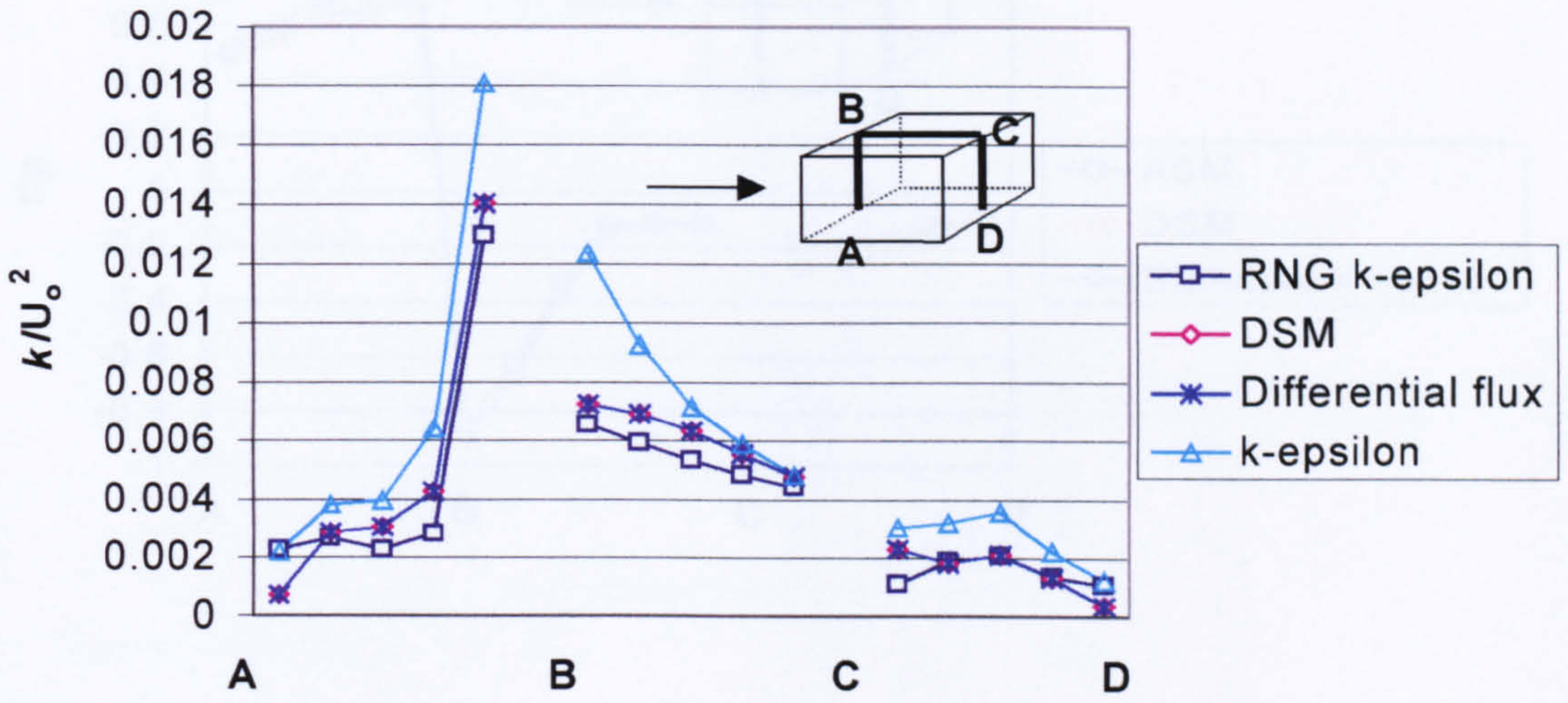

Figure 5.2.27 Turbulent kinetic energy for different turbulence models

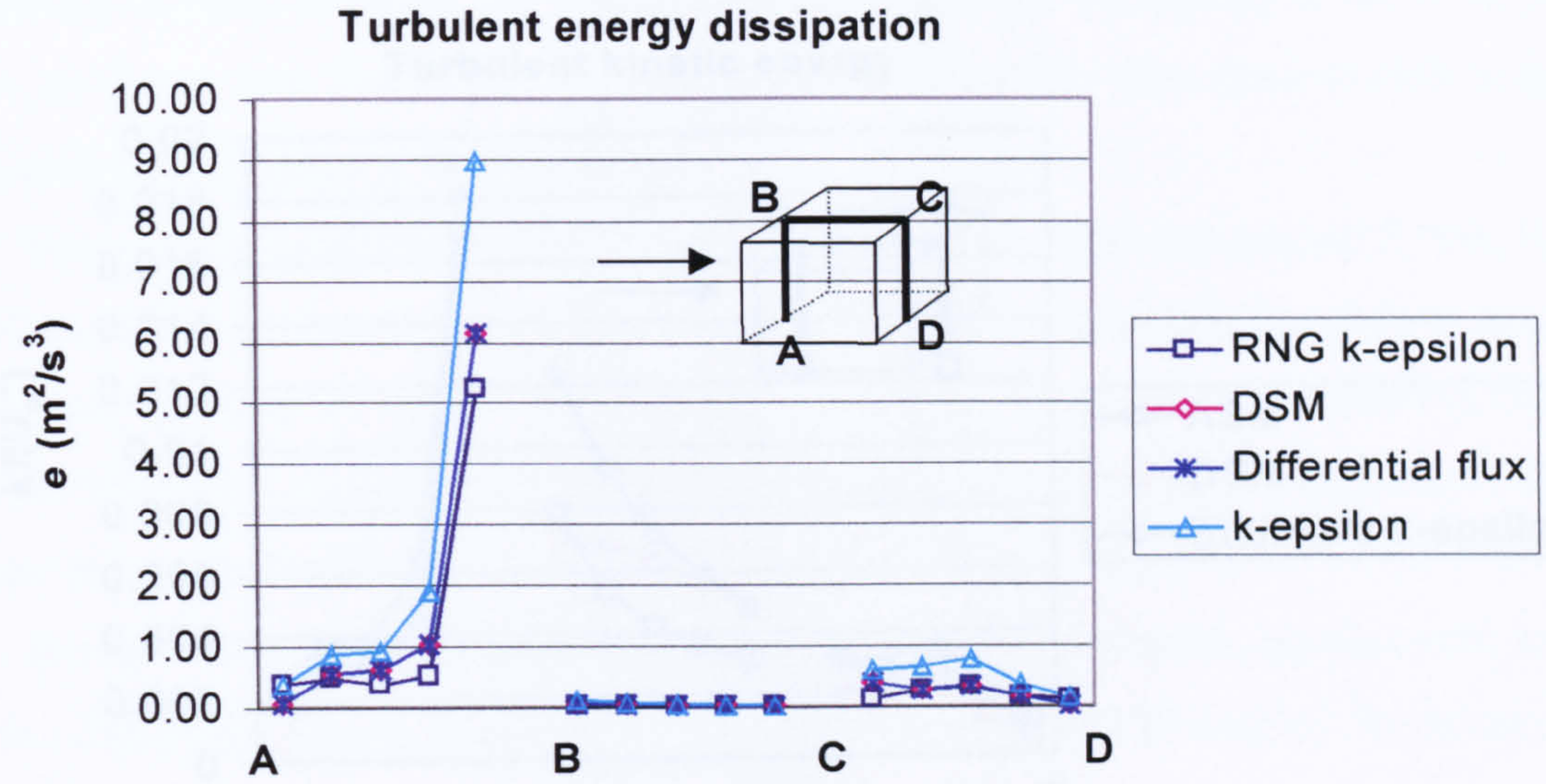

Figure 5.2.28 Turbulent energy dissipation for different turbulence models

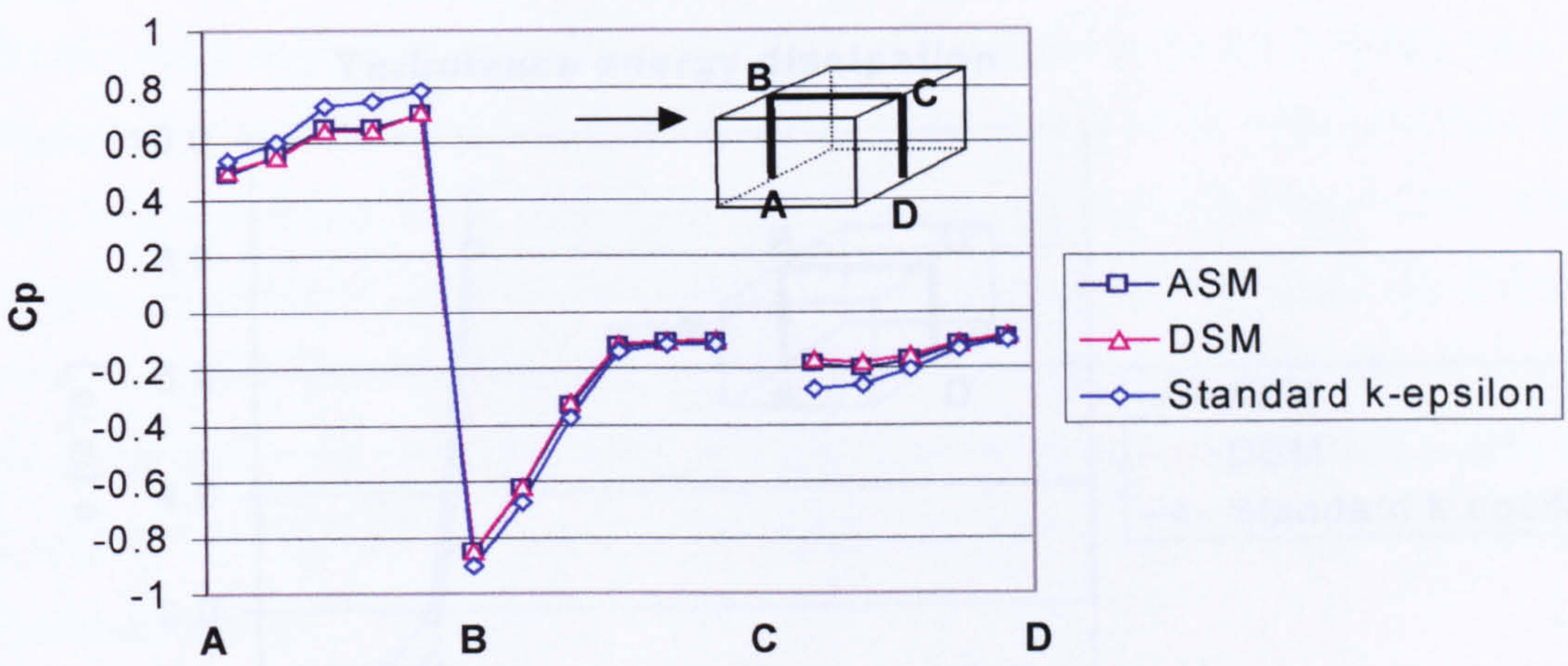

Figure 5.2.29 Pressure distribution for different turbulence models (higher turbulence value at inlet)

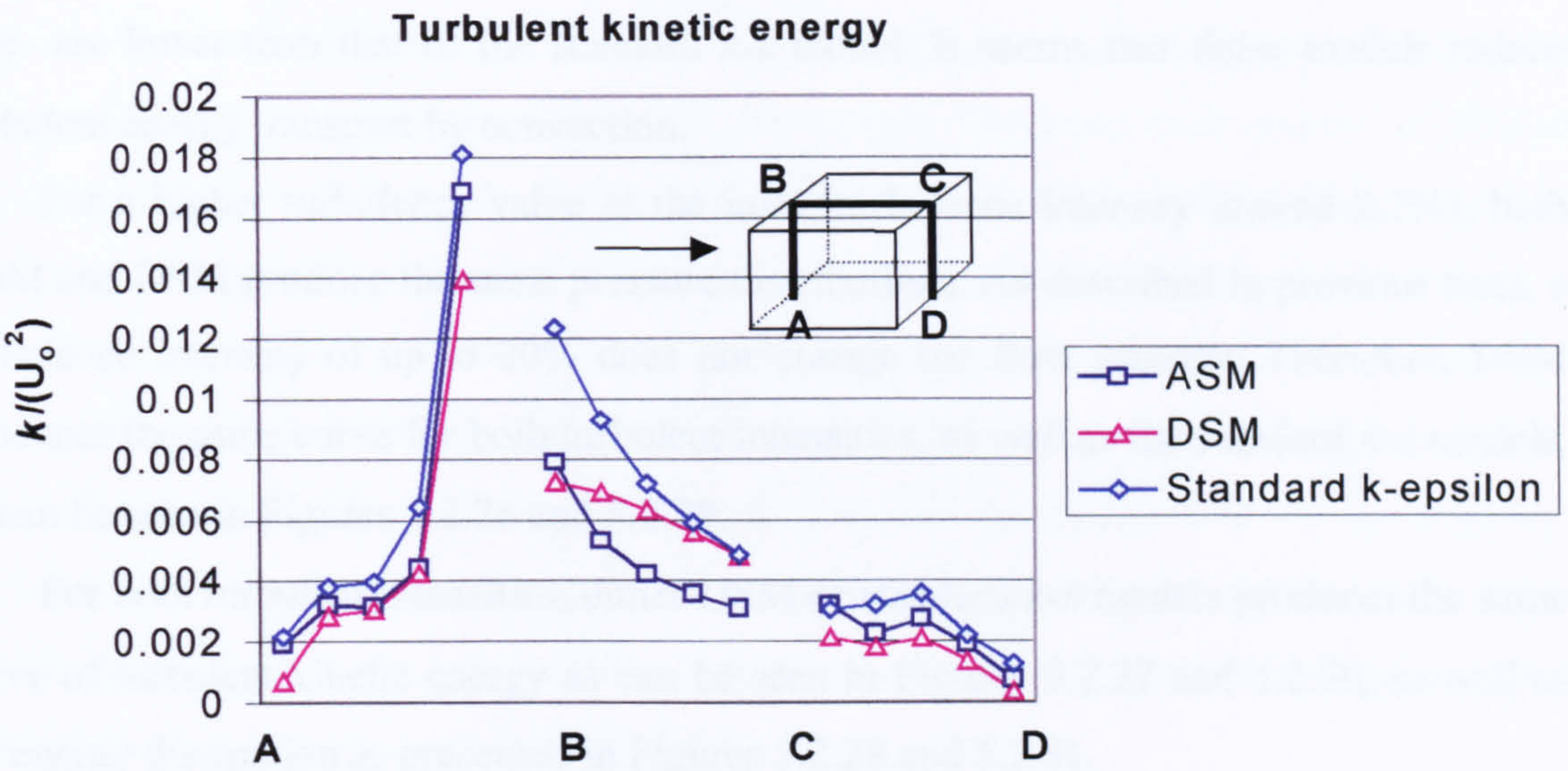

Figure 5.2.30 Turbulent kinetic for different turbulence models (higher turbulence value at inlet)

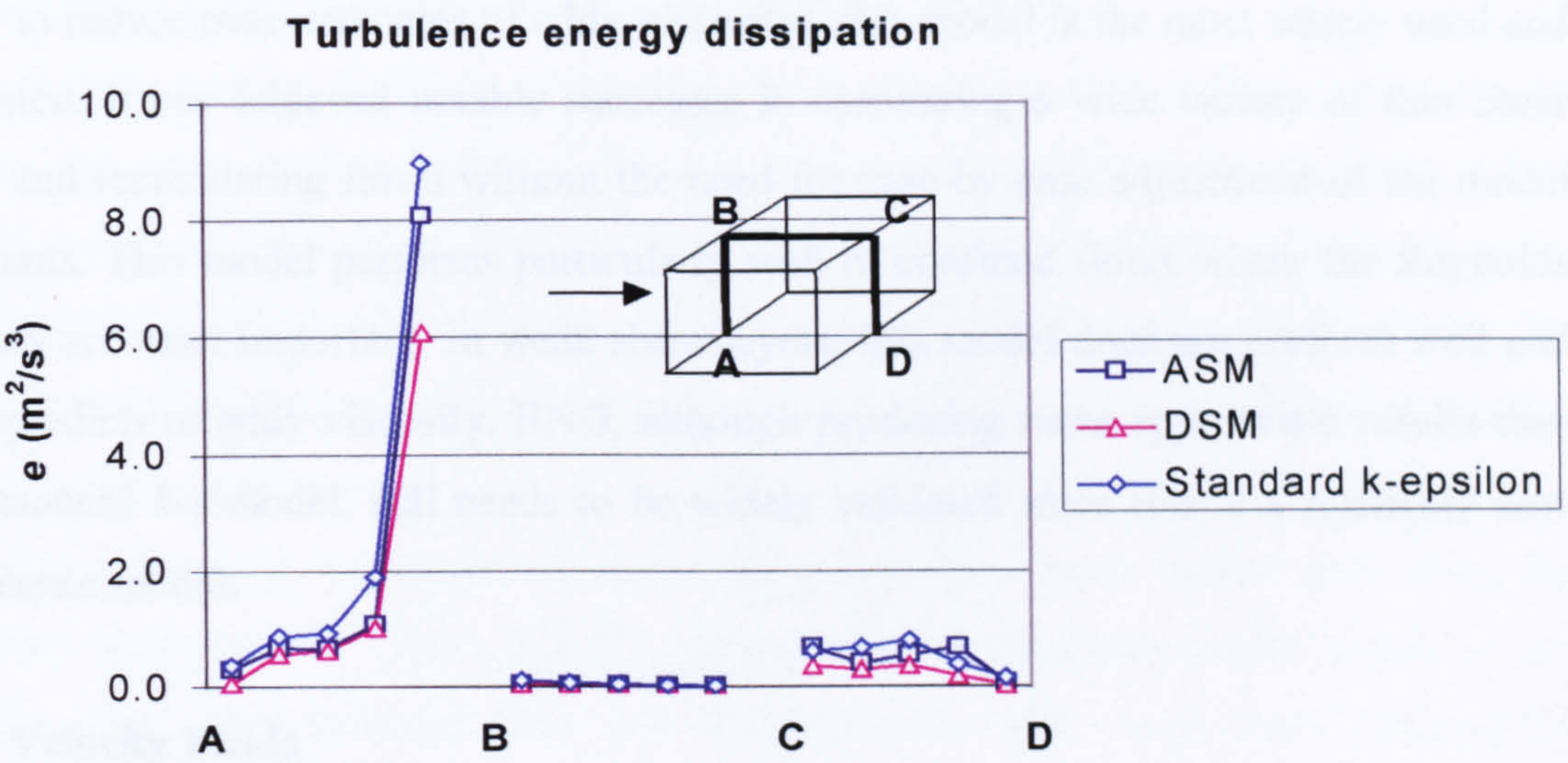

Figure 5.2.31 Turbulent dissipation for different turbulence models (higher turbulence value at inlet)

DSM and differential flux models are in good agreement to reduce the over-prediction of eddy viscosity, but their pressure distributions –especially at the windward side- are lower than that of the standard k-ε model. It seems that these models reduce turbulent energy transport by convection.

For a higher turbulence value at the inlet (turbulence intensity around 2.1%), both ASM and DSM produce the same pressure distributions. As described in previous tests, a turbulence intensity of up to 20% does not change the flow patterns. Therefore, DSM produces the same curve for both turbulent intensities, as well as the standard k-ε models, as can be seen in Figures 5.2.26 and 5.2.29.

For both turbulent intensities, either DSM or standard k-ε models produces the same curve of turbulent kinetic energy as can be seen in Figures 5.2.27 and 5.2.30, as well as for energy dissipation as presented in Figures 5.2.28 and 5.2.31.

Although ASM produces similar pressure distribution to DSM, its turbulent kinetic and dissipation are higher. This indicates that DSM is better than ASM in reducing energy transport by convection.

All models have been developed from the same governing equations which differ in the production terms only. Although the k-ε model produces a slightly greater result (in order to reduce over-estimates of eddy viscosity), this model is the most widely used and validated. It has achieved notable successes in calculating a wide variety of thin shear layer and recirculating flows without the need for case by case adjustment of the model constants. This model performs particularly well in confined flows where the Reynolds stresses are most important. In weak shear layers, this model does not perform well and over-predicts of eddy viscosity. RNG, although producing more appropriate results than the standard k-ε model, still needs to be widely validated since this is a relatively new turbulence model.

5.2.7 Velocity Fields

The velocity field showing the reattachment length at the leeward side of the building is presented in Figures 5.2.32 until 5.2.47. Since the reattachment length is an important

parameter to describe the effects of shear rate on flow, many researchers correlated their results using this parameter.

In the re-circulation zone, the effects of shear stress dominate the flow, which reduces the ability to transfer energy by convection. The local heat transfer coefficient becomes very low at this zone. At the reattachment point the convection heat transfer is the lowest, but it tends to increase thereafter.

From the velocity results, it can be seen that the non-dimensional reattachment length of a cubic building for a Reynolds number of 2.3×10^5 is 1.67 (see Figures 5.2.32-34 and 5.2.36) at the leeward side and 0.32 at the windward side of the building. According to Frank [41] who used the Large Eddy Simulation (LES) method, these reattachment lengths are comparable. Comparison of the reattachment length to other published results can be seen in Table 5.2.1.

The hybrid difference scheme produces an interesting result in that the reattachment length is about 1.42 (see Figure 5.2.35), shorter than the other methods. This indicates that the hybrid difference scheme increases convective effects in the flow direction, especially at the re-circulation zone. In problems where fluid flow plays a significant role, convection effects must be considered. Since diffusion always occurs alongside convection in nature, their combined effects should be examined.

In finite volume methods, truncation errors caused by false diffusion increase for higher Reynolds number and/or if the grid is very coarse. Since the geometry of the model is the same as seen in Figure 5.2.3 (a), it appears that the hybrid difference scheme is not appropriate to reduce this error, and give physically incorrect results. Therefore, for a complex geometry problem (which may require a coarse grid), the hybrid difference scheme is not recommended.

Regarding grid independence, it can be noted that a more refined grid along the building surfaces (see Figure 5.2.37) produces the same reattachment length as the coarser one. This indicates that grid independence tests have been successfully completed.

Higher turbulence intensity at the inlet (see Figure 5.2.38) produce more or less the same reattachment length as lower ones. This indicates that turbulent intensities varying

from 1% to 7% do not affect the flow pattern. Therefore, this turbulent intensity range can be used for atmospheric boundary layer simulations.

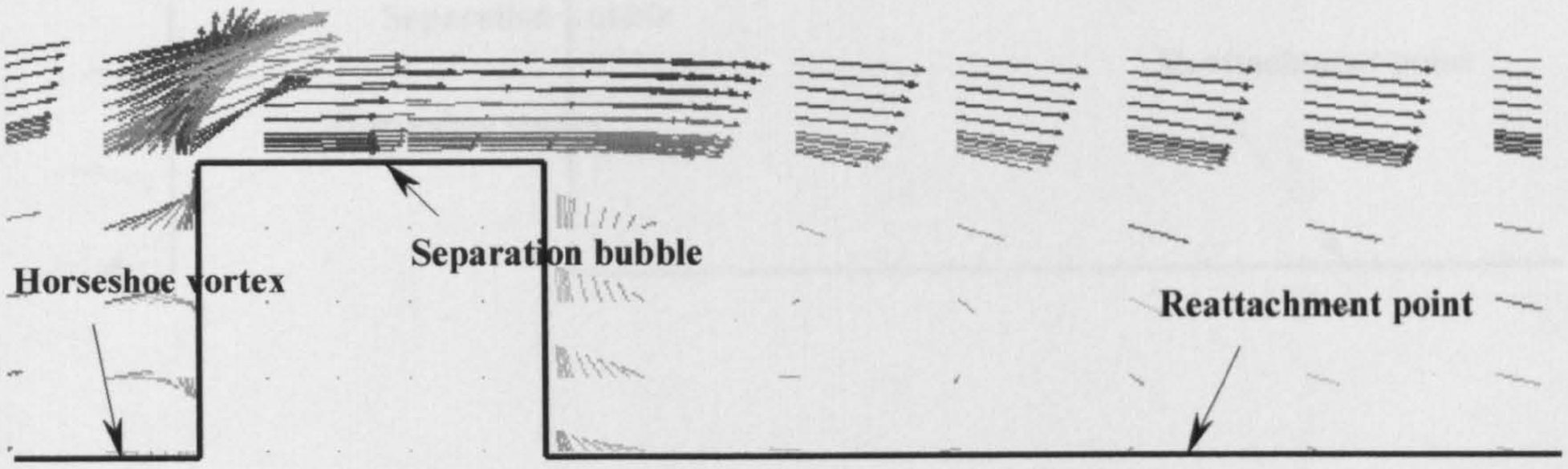

Figure 5.2.32 Velocity vector of body-fitted grid model

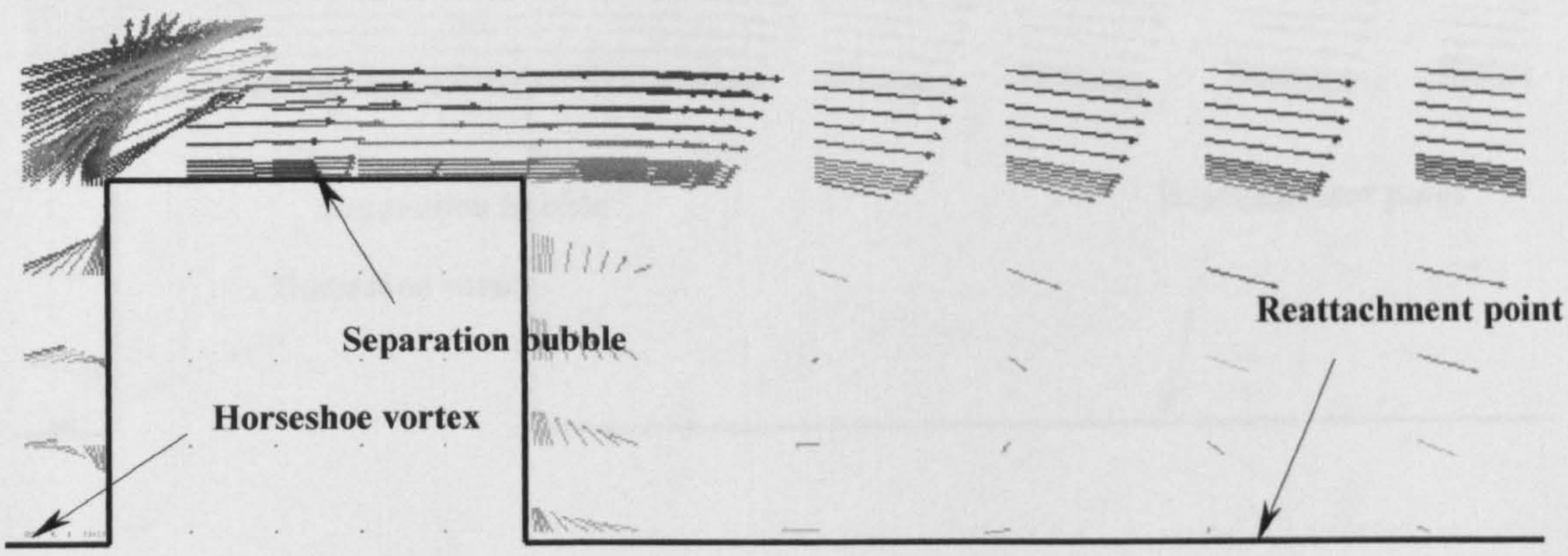

Figure 5.2.33 Velocity vector of rectangular grid model

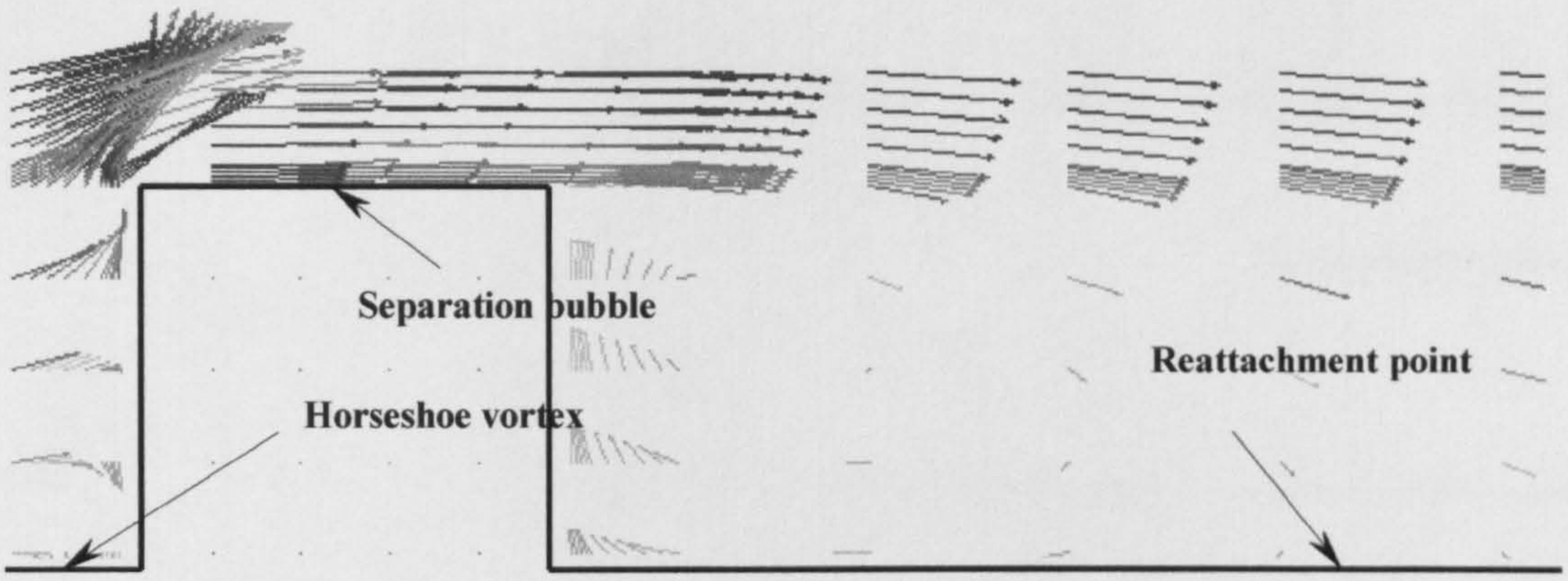

Figure 5.2.34 Velocity vector of higher upwind difference scheme model

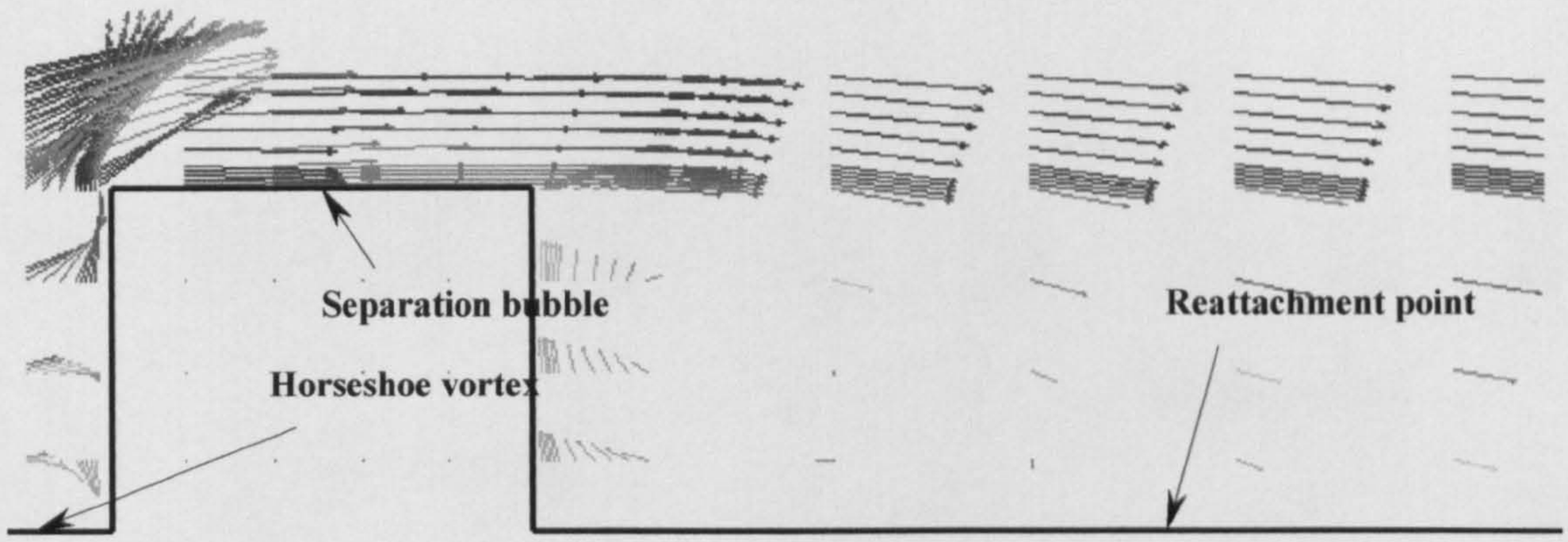

Figure 5.2.35 Velocity vector of hybrid difference scheme model

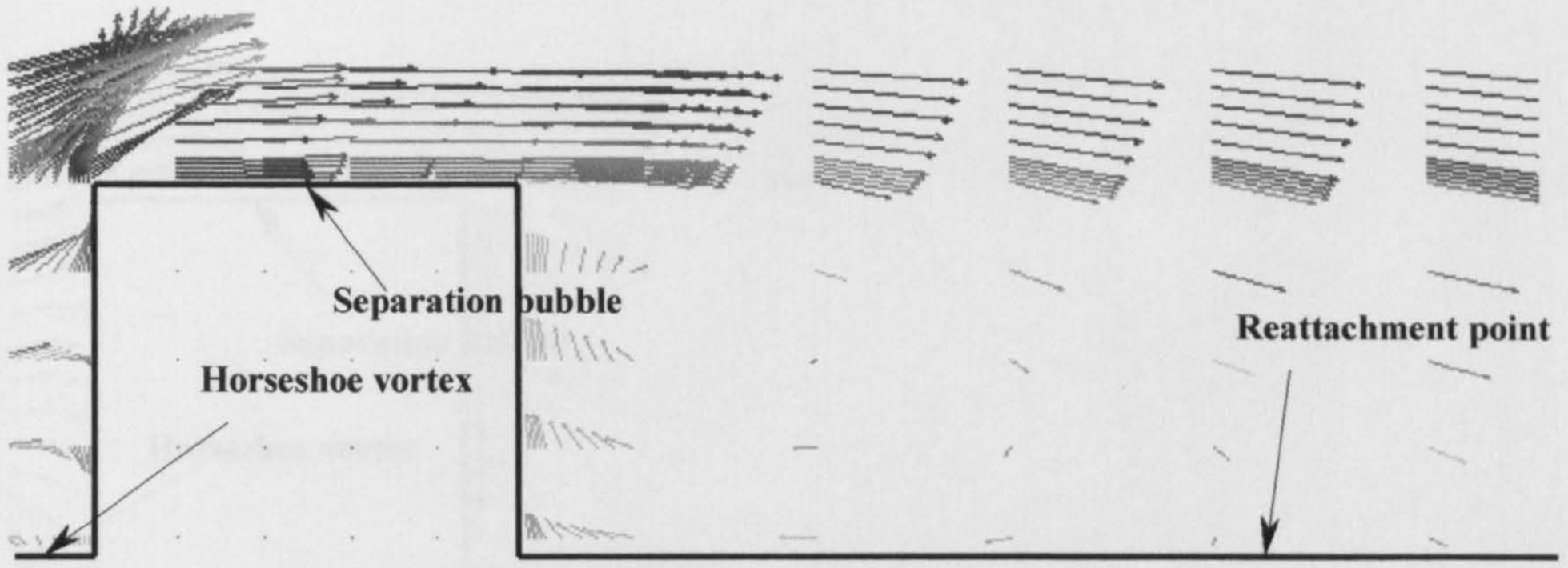

Figure 5.2.36 Velocity vector of Van Leer difference scheme model

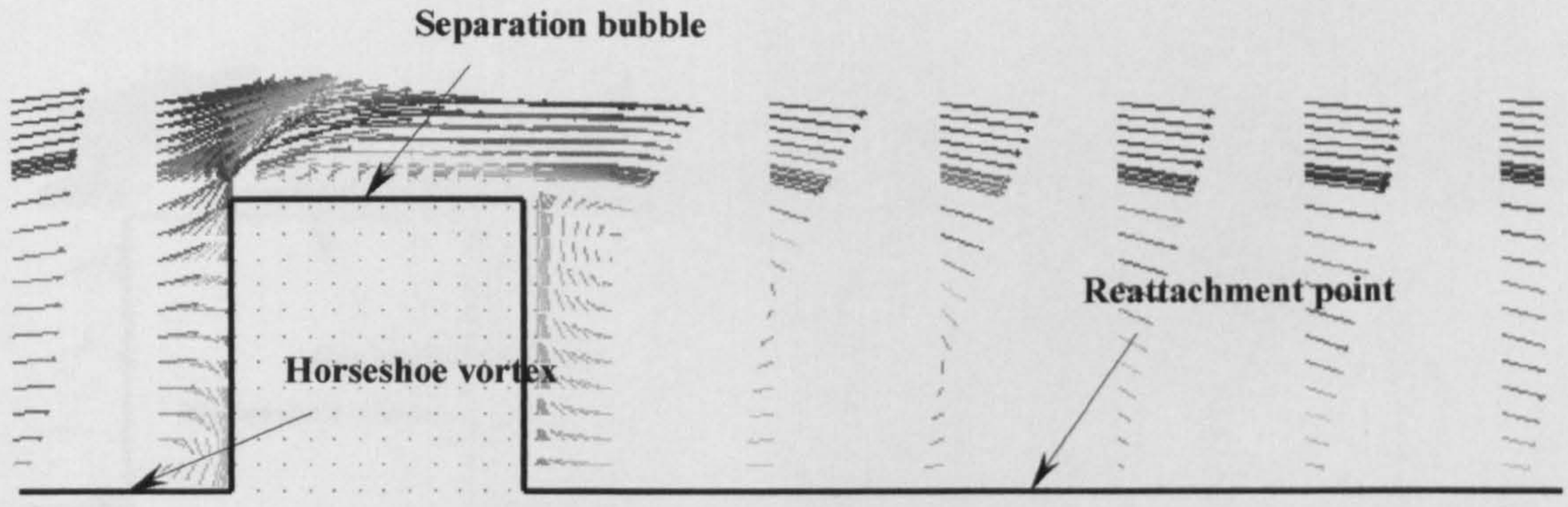

Figure 5.2.37 Velocity vector for model which is more refined on building surfaces

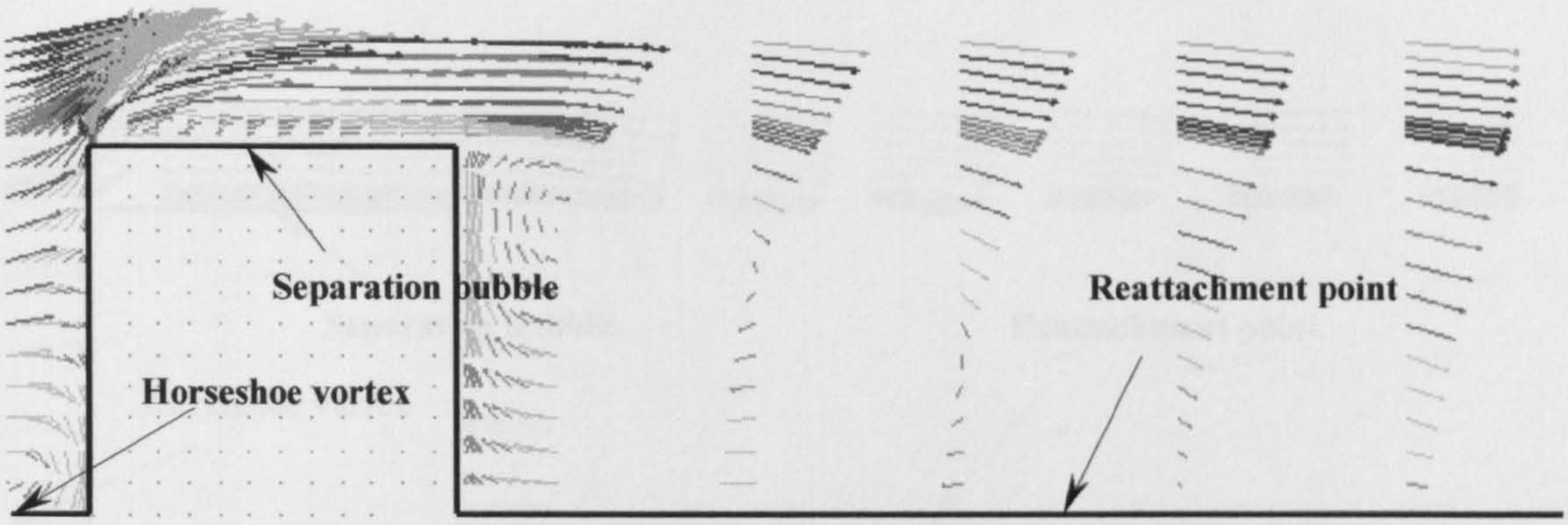

Figure 5.2.38 Velocity vector for model with higher turbulence values at the inlet and more refined on building surfaces

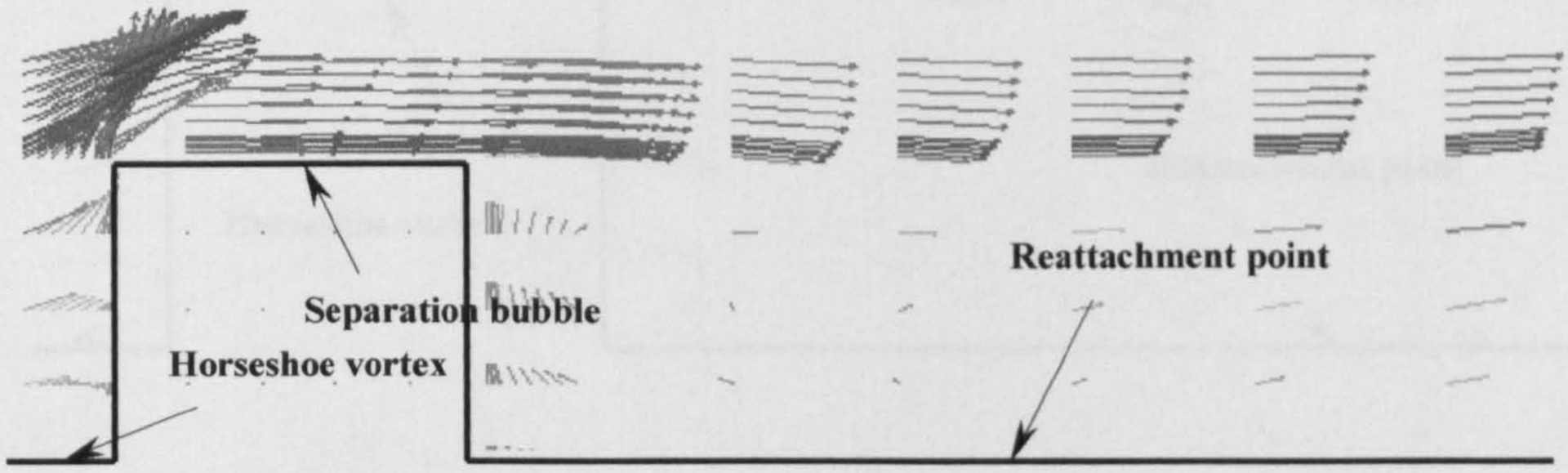

Figure 5.2.39 Velocity vector for model where wind flow at an angle (based on 3.61 m/s)

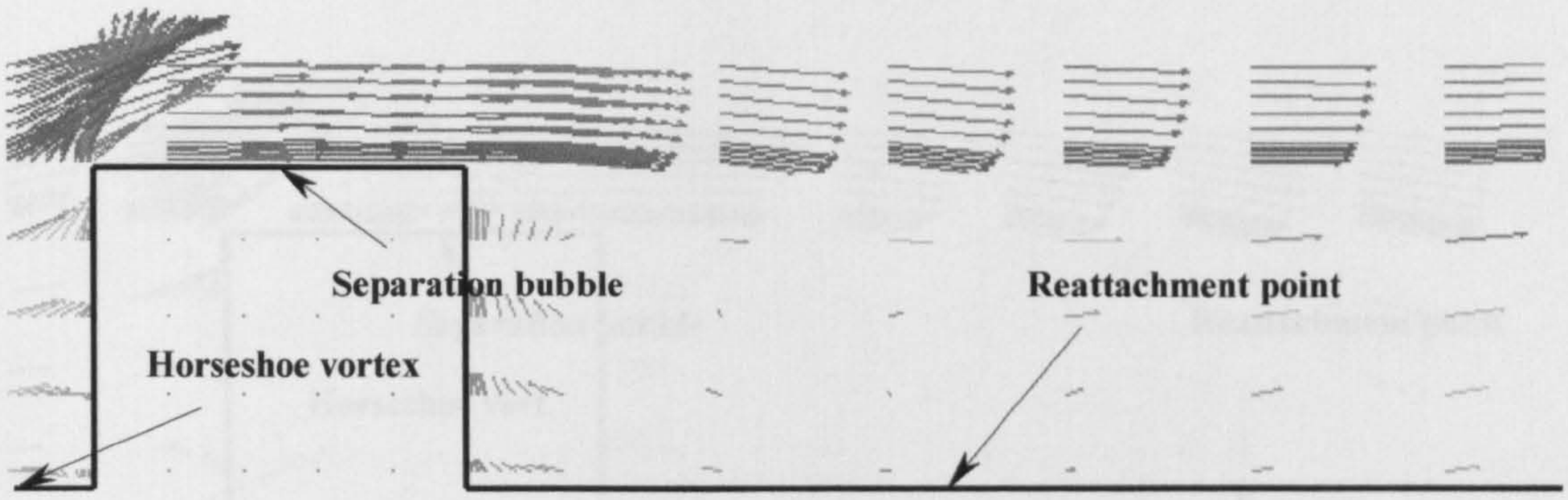

Figure 5.2.40 Velocity vector for model where wind flow at an angle (based on 13.61 m/s)

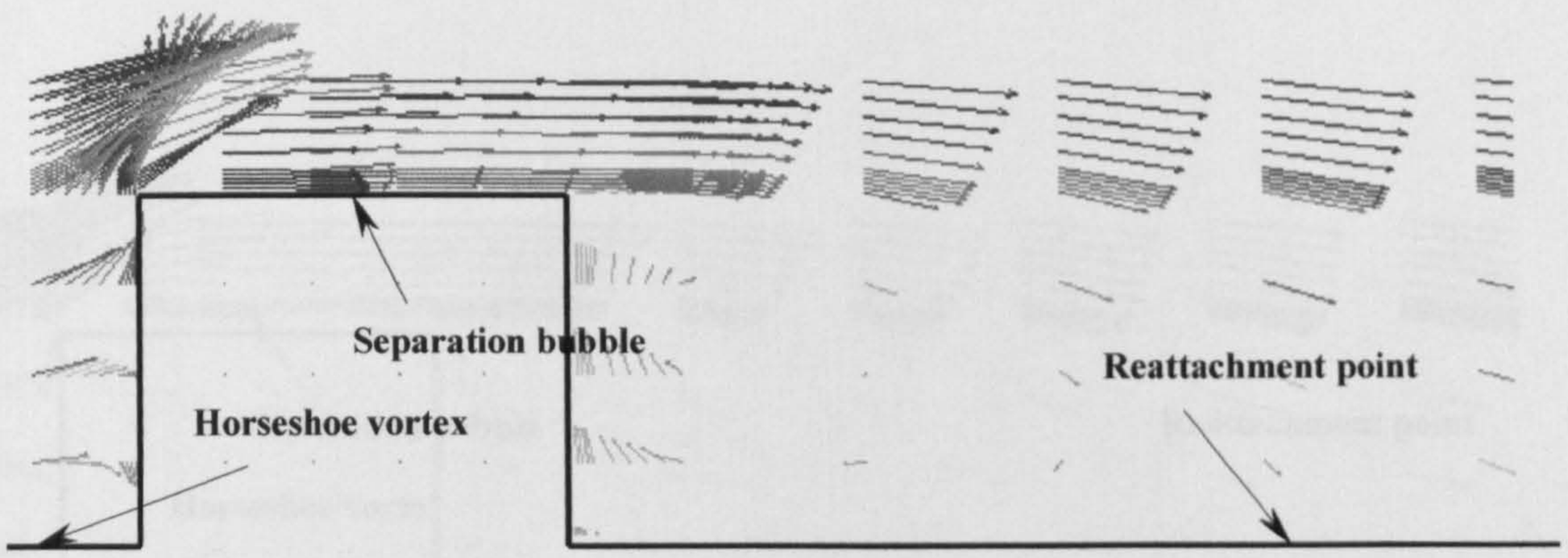

Figure 5.2.41 Velocity vector for model where wind flow has a straight direction (based on 13.61 m/s)

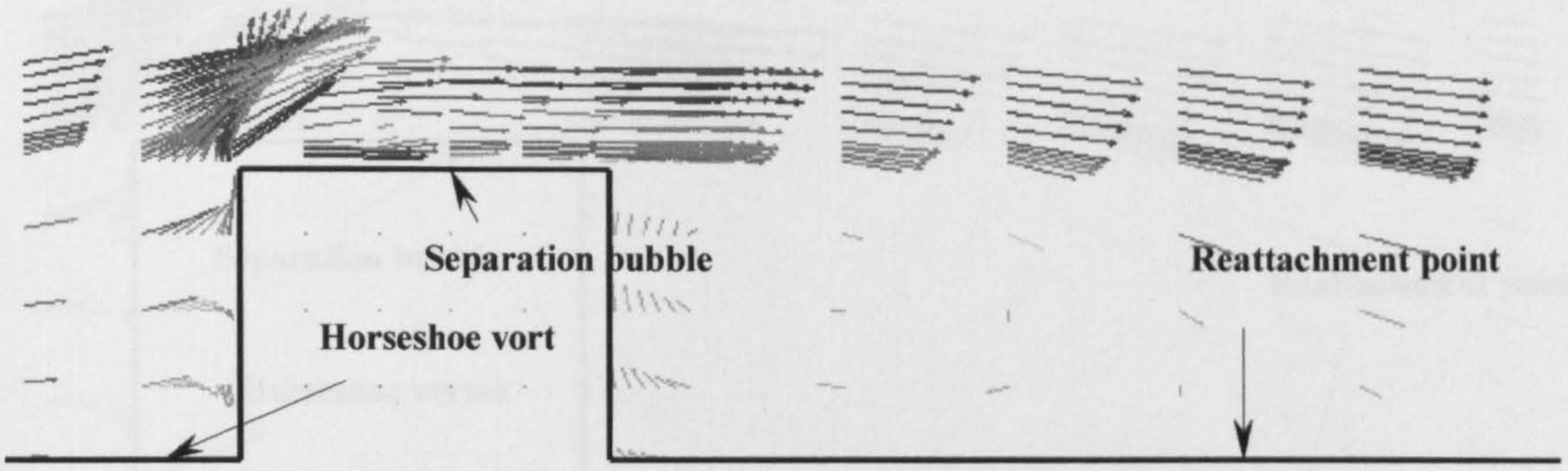

Figure 5.2.42 Velocity vector for Differential Stress turbulence model

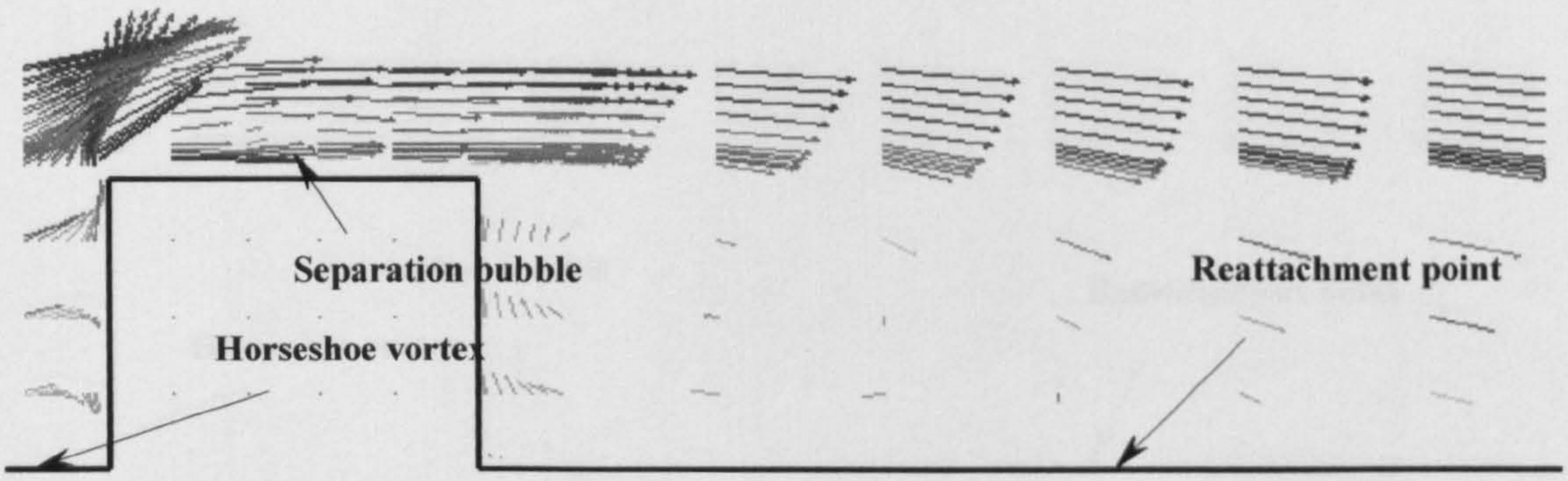

Figure 5.2.43 Velocity vector for Differential Flux turbulence model

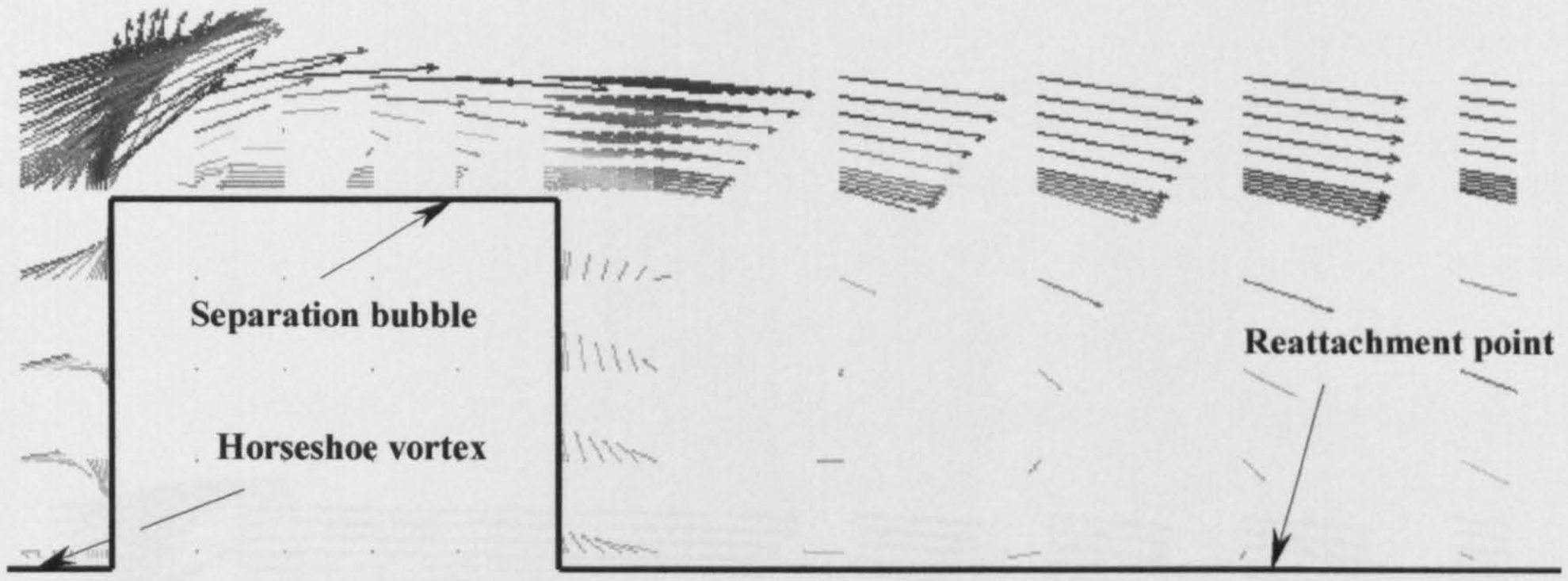

Figure 5.2.44 Velocity vector for RNG turbulence model

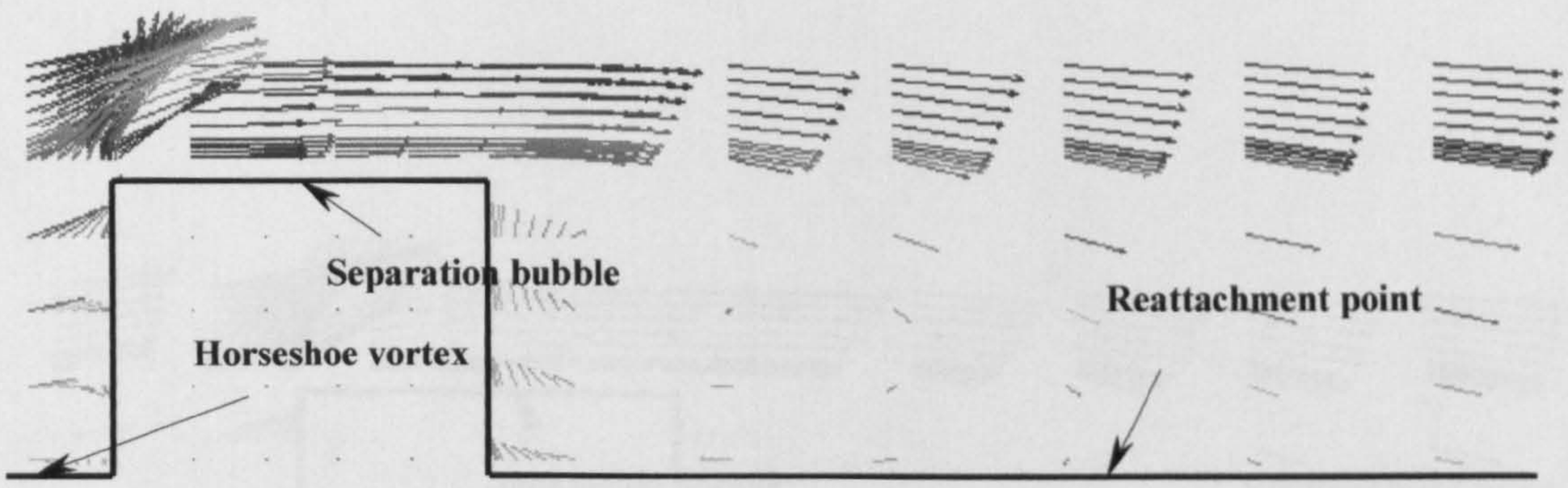

Figure 5.2.45 Velocity vector for standard k-ε turbulence model with very low turbulence values

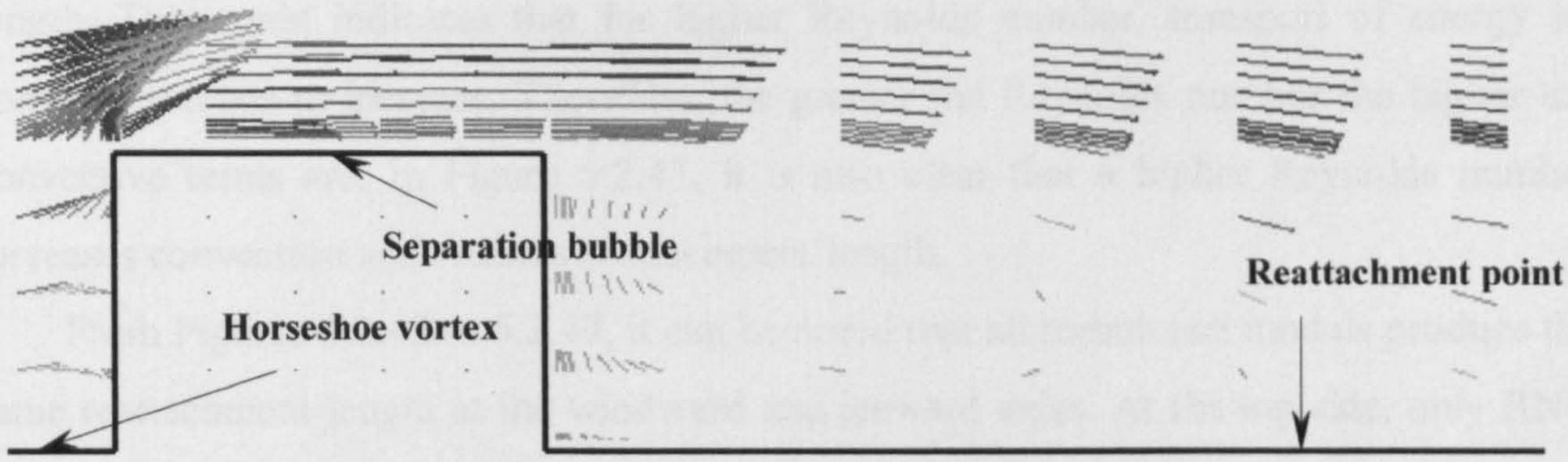

Figure 5.2.46 Velocity vector for Algebraic Stress turbulence model

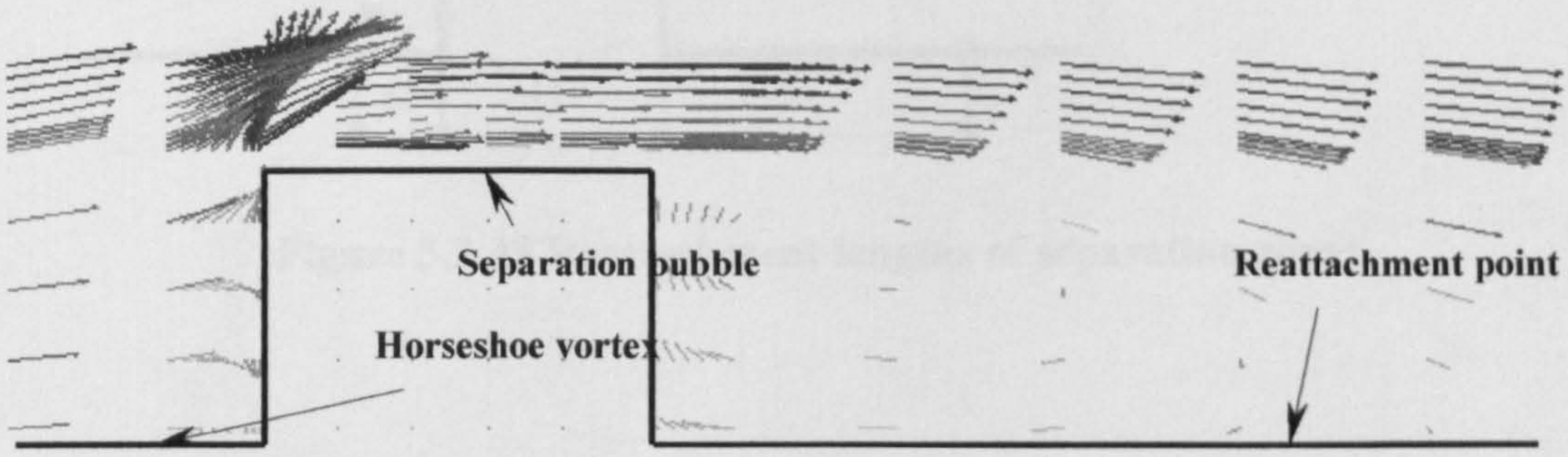

Figure 5.2.47 Velocity vector for Differential Stress turbulence model

For wind flow at an angle, it can be seen in Figure 5.2.39 that the reattachment length is shorter than for the straight flow. Wind flow at an angle produces greater velocity, increasing the Reynolds number which leads to an increased convective term. This causes the reattachment length of the wind flow at an angle to be shorter than the straight wind flow. As described in section 5.2.5, the pressure distribution at the leeward side for wind at an angle is positive which is proportional to the wind direction. There is also a relation between pressure and turbulent kinetic energy, a higher pressure distribution indicates a higher transport of turbulent kinetic energy and dissipation rate.

In Figure 5.2.40, a higher velocity value (13.61 m/s) produces a shorter reattachment length. This again indicates that for higher Reynolds number, transport of energy by convection tends to increase. Therefore, the greater the Reynolds number the higher the convective terms are. In Figure 5.2.41, it is also clear that a higher Reynolds number increases convection and reduces reattachment length.

From Figures 5.2.42 to 5.2.47, it can be noted that all turbulence models produce the same reattachment length at the windward and leeward sides. At the top side, only RNG produces a very clear reattachment, indicating that RNG is much better than the other methods to estimate eddy viscosity at separation regions. The reattachment length at the top side is 0.74 of the building height.

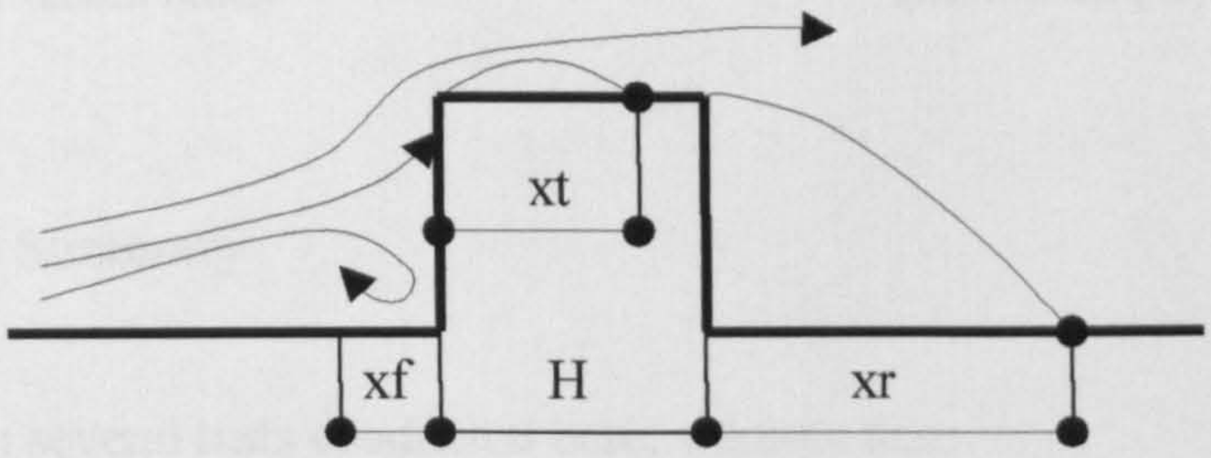

Figure 5.2.48 Reattachment lengths of separation zones

Table 5.2.1 Comparison of different numerical calculations of the separation zones

	/1/	/2/	/3/	/4/	/5/	/6/	/7/	/8/	/9/	/10/	/11/
xf/H	0.31	0.33	0.9	0.37	0.32	0.32	0.32	0.32	0.32	0.32	0.32
xt/H	0.9	-	0.75	0.78	0.55	0.78	0.57	0.55	0.55	0.55	0.57
xr/H	1.65	1.68	1.75	1.65	1.67	1.67	1.67	1.4	1.25	1.55	1.42
Re(10^5)	1	2.5	-	4.8	2.3	2.3	2.3	2.3	8.67	8.67	2.3

/1/ Larousse, Martinuzzi & Tropea [42] (experimental)
/2/ Frank [43] (experimental)
/3/ Werner & Wengle [44] (numerical)
/4/ Frank [41] (numerical, LES)
/5/ Present study (numerical, standard k-ε)
/6/ Present study (numerical, RNG)
/7/ Present study (numerical, DSM, ASM, Diff.Flux)
/8/ Present study (numerical, wind at an angle)
/9/ Present study (numerical, wind at an angle, higher Re)
/10/ Present study (numerical, straight wind, higher Re)
/11/ Present study (numerical, hybrid difference scheme)

5.2.8 Summary

From several tests conducted here, we note that:

1. There was no difference between results obtained with body-fitted and rectangular grids. For a simple geometry problem (such as a cubic building), both rectangular and body-fitted grids can be used, but the grid arrangement should be refined by using multi-blocks. A body-fitted grid is recommended for a complex geometry, since this grid follows the shape of the model. This method needs an extremely large number of grid points to resolve the viscous boundary layer on curved surfaces for computations

of high-Reynolds number (as in this study), therefore, the viscous sub-layer thickness of walls can be better resolved and the error reduced.

2. The importance of grid refinement is at the viscous sub-layer. A coarse grid at walls seems to give reasonable results with similar curves of pressure distribution. The truncation error was reduced at the windward and leeward sides of the building, but the false diffusion was not eliminated. For grid independence tests, the value of y^+ should be greater than 11.63. Therefore, the flow is turbulent and the wall function approach is used. The value of $y^+ \approx 11.81$ [45] is suggested in order to reduce the false diffusion.
3. A range of turbulence intensities between 1% and 7% can be used to simulate the atmospheric boundary layer. But it should be noted that turbulent intensity is affected by topography since the flow pattern varies in accordance with the surface roughness. In suburban areas, the above turbulent intensity values can be used without affecting the flow patterns.
4. A wind flow at an angle produces higher velocity distributions, turbulent energy and its dissipation rate than a straight wind. For building design, wind at an angle should be taken into account since it tends to create higher wind forces.
5. The use of a standard k-ε turbulence model is preferred because it needs much less computational power and has achieved notable successes in calculating a wide variety of thin shear layer and recirculating flows without the need of adjustment of the model constants. The standard k-ε turbulence model performs particularly well where the Reynolds shear stresses are most important.

The pressure distribution around a cubic building is presented in Figures 5.2.49 and 5.2.50. It is clear that the results of other researchers who also applied a k-ε model produced a higher pressure distribution at the windward corner, which has been minimised in the present study. Adopting lower values of k-ε is a good technique to reduce the over-estimation of turbulent viscosity at the separation regions.

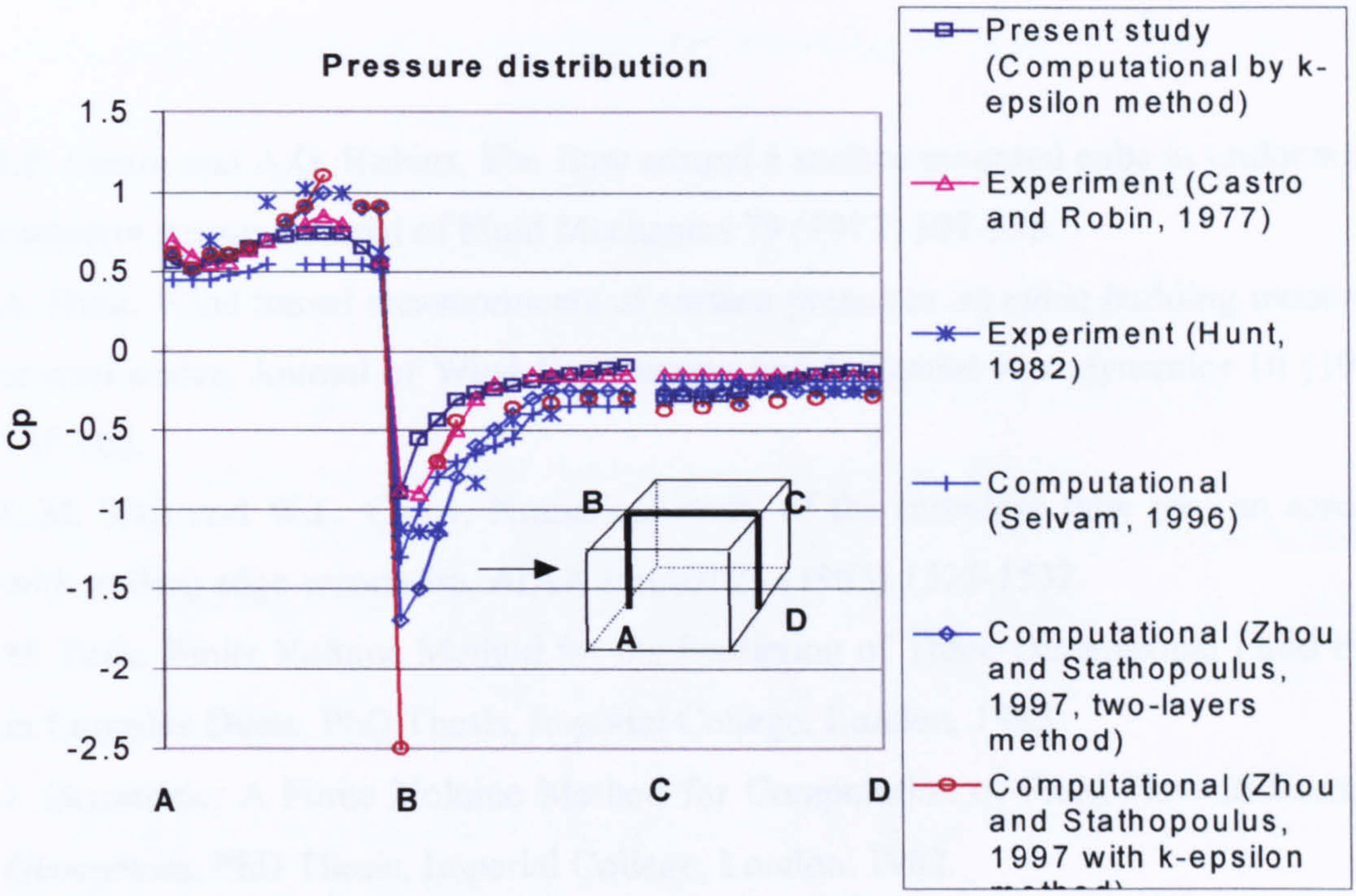

Figure 5.2.49 Pressure distributions along the centreline

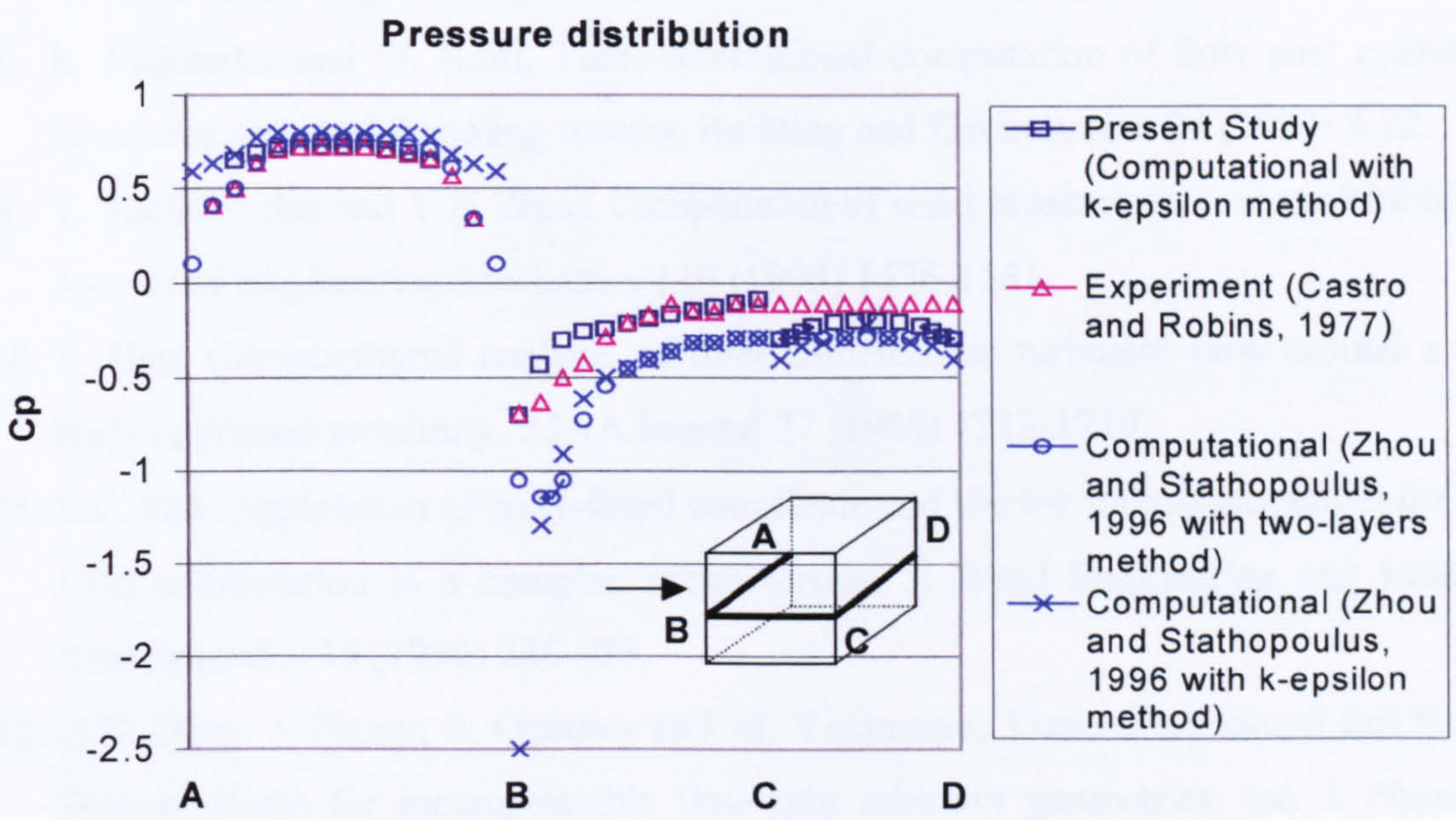

Figure 5.2.50 Pressure distributions at half-building height

REFERENCES

1. I.P. Castro and A.G. Robins, The flow around a surface mounted cube in uniform and turbulent stream, Journal of Fluid Mechanics 79 (1977) 307-335.
2. A. Hunt, Wind tunnel measurements of surface pressures on cubic building models at several scales, Journal of Wind Engineering and Industrial Aerodynamics 10 (1982) 137-163.
3. C.M. Rhie and W.L. Chow, Numerical study of the turbulent flow past an aerofoil with trailing edge separation, AIAA Journal 21 (1983) 1525-1532.
4. M. Peric, Finite Volume Method for the Prediction of Three-Dimensional Fluid Flow in Complex Ducts, PhD Thesis, Imperial College, London, 1985.
5. I. Demirdzic, A Finite Volume Method for Computation of Fluid Flow in Complex Geometries, PhD Thesis, Imperial College, London, 1982.
6. W. Shyy, and T. G. Vu, On the adaptation of velocity variable and grid systems for fluid flow in curvilinear co-ordinates, J. Comp. Phys. 92 (1991) 82-105.
7. K.C. Karki and S.V. Patankar, Calculation procedure for viscous incompressible flows in complex geometries, Numerical Heat Transfer 14 (1988) 295-307.
8. S. Majumdar and W. Rodi, Three-dimensional computation of flow past cylindrical structures and model cooling towers, Building and Environment 24 (1989) 3-22.
9. T. Stathopoulos and Y.S. Zhou, Computation of wind pressure on L-shaped buildings, Journal of Engineering Mechanics 119 (1993) 1526-1541.
10. T. Han, Computational analysis of three-dimensional turbulent flow around a bluff body in ground proximity, AIAA Journal 27 (1989) 1213-1219.
11. S.C. Kot, Application of body-fitted coordinate and the k-ε turbulence model for wind field computation in a complex urban terrain, J. Wind Engineering and Industrial Aerodynamics 35 (1990) 225-235.
12. G.B. Deng, J. Piquet, P. Queutey and M. Visonneau, Three-dimensional full Navier-Stokes solvers for incompressible flow past arbitrary geometries, Int. J. Numerical Methods in Engineering 31 (1991) 1427-1451.

13. R.P. Selvam and D.A. Paterson, Computation of pressures on and velocities near the Texas Tech. Building: using staggered and non-staggered grids, 9th ASCE Structures Congress, ASCE, New York, 1991.
14. J. Wieringa, Updating the Davenport roughness classification, J. Wind Engineering and Industrial Aerodynamics 41-44 (1992) 357-368.
15. S. Murakami, A. Mochida, Y. Hayashi, Examining the k-ε model by means of a wind tunnel test and large-eddy simulation of the turbulence structure around a cube, J. Wind Engineering and Industrial Aerodynamics 35 (1990) 87-100.
16. S. Murakami, A. Mochida, R. Ooka, S. Kato and S. Iizuka, Numerical prediction of flow around a building with various turbulence models: comparison of k-ε EVM, ASM, DSM, and LES with wind tunnel test, ASHRAE Transactions 102 (1996) 741-753.
17. S. Murakami, Computational wind engineering, J. Wind Engineering and Industrial Aerodynamics 36 (1990) 517-538.
18. Y.S. Zhou and T. Stathopoulos, A new technique for the numerical simulation of wind flow around buildings, J. Wind Engineering and Industrial Aerodynamics 72 (1997) 137-147.
19. A. Qasim, T.T. Maxwell, S. Parameswaran, Computational predictions of flow over a 2-D building, J. Wind Engineering and Industrial Aerodynamics 44 (1992) 2839-2840.
20. R.P. Selvam, Numerical simulation of flow and pressure around a building, ASHRAE Transaction 102 (1996) 765-772.
21. Y.S. Zhou and T. Stathopoulos, Application of two-layer methods for the evaluation of wind effects on a cubic building, ASHRAE Transaction 102 (1996) 754-764.
22. H.K. Versteeg and W. Malalasekera, An Introduction to Computational Fluid Dynamics: The Finite Volume Method, Longman Scientific & Technical, England, 1995.
23. I.H. Parpia, Van Leer flux vector splitting in moving coordinates, AIAA Journal 26 (1998) 113-115.
24. P. Ferrand and S. Aubert, New mixed Van Leer flux splitting for transonic viscous flow, AIAA Journal 34 (1996) 190-193.

25. N.S. Wilkes and C.P. Thomson, Evaluation of higher-order upwind differencing for elliptic flow problems, Numerical Methods in Laminar and Turbulent Flow, Proceedings of the International Conference (1983) 248-257.
26. T. Kawamura, H. Takami and K. Kuwahara, New higher-order upwind scheme for incompressible Navier-Stokes equations, Lecture Notes in Physics (1985) 291-295.
27. Y. Li and M. Rudman, Assessment of higher-order upwind schemes incorporating FCT for convection-dominated problems, Numerical Heat Transfer, Part B: Fundamentals 27 (1995) 1-21.
28. H.G. Choi and J.Y. Yoo, Streamline upwind scheme for the segregated formulation of the Navier-Stokes equation, Numerical Heat Transfer, Part B: Fundamentals 25 (1994) 145-161.
29. Q.S. Li and W.H. Melbourne, Experimental investigation of the effects of free-stream turbulence on streamwise surface pressures in separated and reattaching flows, J. Wind Engineering and Industrial Aerodynamics 54-55 (1995) 313-323.
30. U. Piomelli and J.R. Chasnov, Large-Eddy Simulations: theory and applications, in Turbulence and Transition Modeling, Editors, M. Hallbäck, D.S. Henningson, A.V. Johansson and P.H. Alfredsson, Kluwer Academic Publishers, The Netherlands, 1996.
31. W. Rodi, Turbulence models and their application in hydraulic –A state of the art review, IAHR, Delft, The Netherlands, 1980.
32. D. Naot and W. Rodi, Numerical simulation of secondary currents in channel flow, J. Hydraulic Div., ASCE 108 (1982) 948-968.
33. A.O. Demuren and W. Rodi, Calculation of turbulence-driven secondary motion in non-circular ducts, Journal of Fluid Mechanics 140 (1984) 189-222.
34. R. Abid, J. H. Morrison, T.B. Gatski and C.G. Speziale, Prediction of aerodynamic flows with a new explicit algebraic stress model, AIAA Journal 34 (1996) 2632-2635.
35. B.E. Launder, Lecture notes on "Turbulence modeling in industrial flows", Les Houches Summer School on Computational Fluid Dynamics, 1993.
36. C.G. Speziale, On non-linear k-l and k-e models of turbulence, Journal of Fluid Mechanics 178 (1987) 459-475.
37. B.E. Launder and D.B. Spalding, Mathematical Models of Turbulence, Academic Press, New York, 1972.

38. T.B. Gatski and C.G. Speziale, On explicit algebraic stress models for complex turbulent flows, J. Fluid Mech. 254 (1993) 59-78.
39. V. Yakhot, S.A. Orszag, S. Thangam, T.B. Gatski and C.G. Speziale, Development of turbulence models for shear flows by a double expansion technique, J. Physics of Fluids A 4 7 (1992) 1510-1520.
40. S. Murakami, A. Mochida, Y. Hayashi and S. Sakamoto, Numerical study on velocity-pressure field and wind forces for bluff bodies by k-ε, ASM and LES, J. Wind Engineering and Industrial Aerodynamics 44 (1992) 2841-2852.
41. W. Frank, Three dimensional numerical calculation of the turbulent flow around a sharp-edged body by means of large-eddy simulation, J. Wind Engineering and Industrial Aerodynamics 65 (1996) 415-424.
42. A. Larousse, R. Martinuzzi and C. Tropea, Flow around surface-mounted, three-dimensional obstacles, 8th Symposium on Turbulent Shear Flows, TU-Munich/ Germany, 9-11 September 1991, 14-4-1 – 14-4-6.
43. W. Frank, Building aerodynamics, in W.J. Yang (Ed.), Handbook of Flow Visualization, 637-642, Hemisphere Publishing Corporation, New York, 1989.
44. H. Werner and H. Wengle, Large eddy-simulation of turbulent flow over and around a cube in a plate channel, 8th Symposium on Turbulent Shear Flows, TU-Munich/ Germany, 9-11 September 1991, 19-4-1 – 19-4-6.
45. S. Murakami and A. Mochida, Turbulent vortex shedding flow past 2D square cylinder predicted by CFD, J. Wind Engineering and Industrial Aerodynamics 54-55 (1995) 191-211.

CHAPTER SIX

THREE-DIMENSIONAL MODELLING OF TRADITIONAL BALINESE BUILDINGS

Introduction

Numerical tests and discussion of three-dimensional buildings arrangements are presented in this chapter. Three-dimensional buildings arrangements have been simulated in order to verify some traditional definitions such as centre (*natar*), shrines of the gods, orientation of all buildings to the centre (*natar*) and distance between buildings to the shrines of gods, where those aspects cannot be achieved in two-dimensional investigations. A unique feature of this research work is that either buildings arrangement or type of building does not exactly match those in traditional architecture. This new idea is based on the concept that traditional rule can be explained by using modern buildings arrangements, since it contains several terms that should be understood from a scientific point of view. The screen behind the gateway (*aling – aling*) is considered and its position related to wind load on building surfaces, energy transfer and occupants comfort. The gate is placed at several locations in order to find a relationship between energy transfer and wind load on building surfaces.

Some traditional definitions such as centre, shrines of the gods, orientation of all buildings to the centre and distance between buildings to the shrines of gods are analysed in relation to heat transfer, wind engineering, architectural aerodynamics and thermal comfort of occupants.

Numerical simulations of traditional Balinese buildings are set as incompressible, three-dimensional, viscous and turbulent flows in accordance to results of the flow around a cubic building in Chapter Five. A body-fitted grid is now provided since the geometry is more complex. The common strategy to use a body-conforming grid for a complex body is by employing multiple zone and multiple grid methods, such as the multi-blocks method. The multi-blocks method was also shown to be a very powerful approach for complex configurations, as described in Chapter Four. The flow around buildings is modelled by using the Navier-Stokes equations and the standard k-ε

turbulence model. Low values of k-ε are applied since this was shown to produce better results. A uniform grid system has been applied on the building surfaces and on the first block outside buildings, but a non-uniform grid system has been used in the outer region. A staggered grid is used since it avoids the evaluation of pressure boundary conditions and also provides more accurate predictions.

The momentum, k and ε turbulence model equations are solved by successive over-relaxation point iteration with an under-relaxation parameter. The relaxation factors typically used for this algorithm are about 0.6 to 0.7 for velocities, 0.9 to 1.0 for pressure, 0.9 to 1.0 for temperature, and 0.6 to 0.7 for k and ε. To satisfy mass and momentum conservation simultaneously, the SIMPLE procedure is used. According to initial tests in Chapter Five, the boundary conditions for the inlet velocity are fixed at the initial power-law velocity profile $u/u_g = (z/z_g)^{0.25}$, where u and u_g are mean velocities at height z and at a reference point at height z_g, respectively, with $v = w = 0$. The turbulent intensity was set as 6.1% according to Davenport terrain roughness classification number 4, for a suburban terrain.

On the truncated walls and building surfaces, the wall treatment is a combination of logarithmic and no-slip boundary conditions. The implementation of wall boundary conditions in turbulent flows starts with the evaluation of y^+, where the value of y^+ is greater than 11.81, and the first node (from solid walls) is considered to be in the logarithmic-law region of a turbulent boundary layer. To minimise undesired re-coupling effects, the computation domain has to be sufficiently wide, high and long. The Reynolds number of the main flow based on the velocity at the building height is about 9.62×10^5. For stability, Van Leer numerical schemes are imposed to control false diffusion as explained in Chapter Five. Wind at an angle of attack is considered according to the real condition.

6.1 Balinese Architecture Model

To simulate traditional Balinese buildings, a complex arrangement is introduced in Figure 6.1.1. The first and fourth buildings are aligned, as well as the third and fifth buildings, similarly to a modern arrangement.

The roof type is the same for all buildings and similar to that in modern sites. This is different from a traditional arrangement where each building has a typical roof.

In the present study, no open surfaces at walls or roofs are considered, similar to traditional villages, therefore, natural ventilation is proposed by considering pressure distribution and temperature variations (stack effects) on building surfaces. In modern arrangements, the distance between buildings is usually uniform. This contrasts to traditional arrangements where each building has different distances depending on their function. A uniform distance equal to one building height, ***H***, is used on the simulation. The distance ***H*** is longer than that in modern sites, but shorter than the reattachment length found in Chapter Five, around 1.2-1.7, and depends on the building shape and Reynolds number. For two-dimensional problems, as described in Chapter Four, a shorter distance between buildings reduces the pressure distribution and turbulent kinetic energy at the second and third buildings. Therefore, the distance between buildings for three-dimensional models will be re-examined to verify whether it affects wind loads, heat transfer and thermal comfort of occupants.

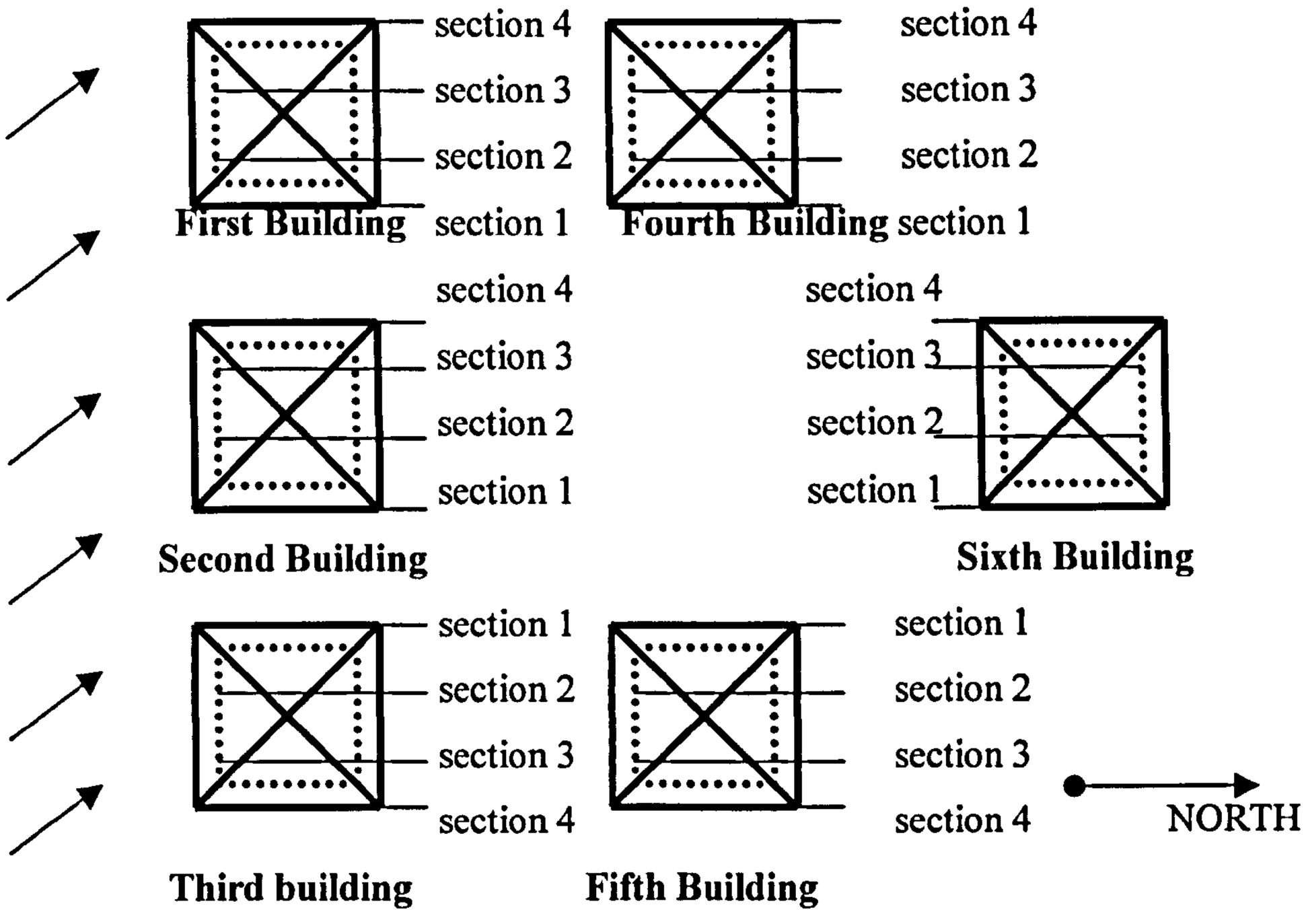

Figure 6.1.1 (a) A top view of the buildings arrangement

A body fitted-grid is used in this simulation. This grid method which has been adopted by many researchers is presented in Figure 6.1.2, which shows a body-fitted grid arrangement in the vicinity of a house, as presented by Delaunay *et al* [1].

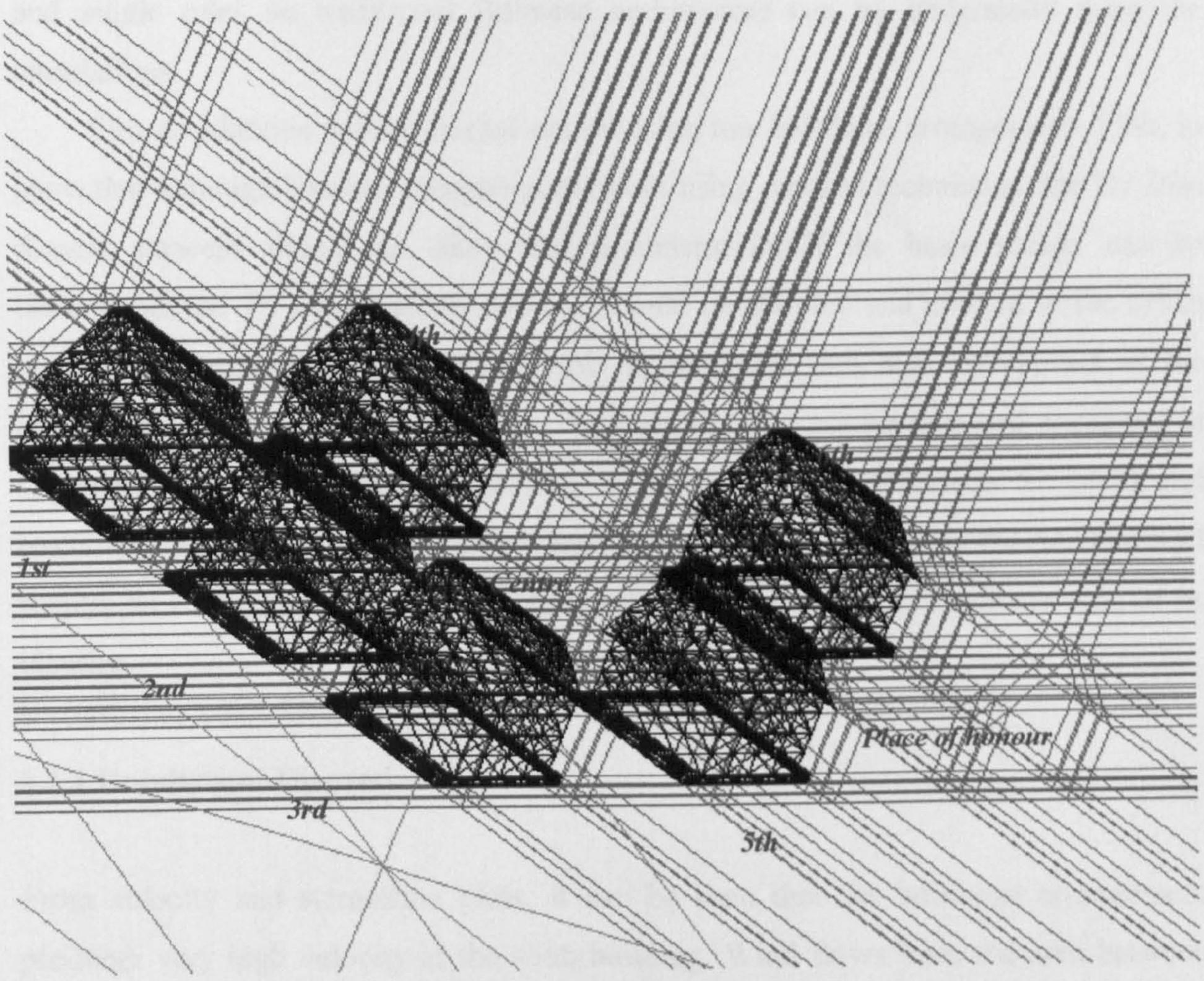

Figure 6.1.1 (b) A side view of building model

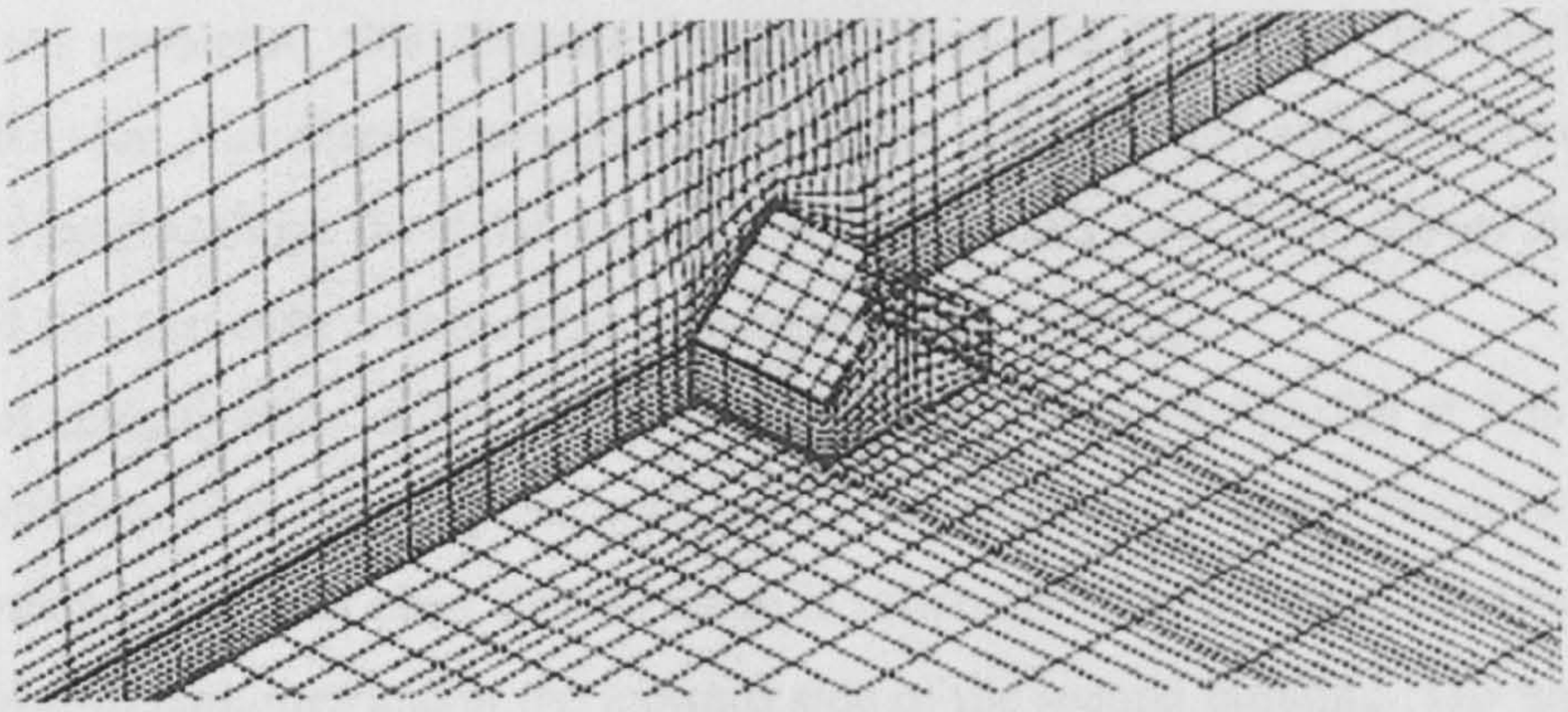

Figure 6.1.2 A body-fitted grid arrangement in the vicinity of the house

In modern sites, the windward side of buildings faces the main street, but in traditional arrangements all buildings are oriented to the centre (*natar*). Therefore, in order to better understand the buildings orientation, all buildings are facing the windward side in Figure 6.1.1 (b). Therefore, definition of *natar*, the place of honour and magic rules on traditional Balinese architecture can be understood from the simulations.

Two simulations will be carried out by using this buildings arrangement. First, to show that although housing complexes are built using modern techniques, the *Tri Hita Karana* concept should be taken into consideration. If the basic reason can be understood, the *Tri Hita Karana* concept should be adopted and applied in the urban and town planning of Bali. Second, this arrangement can also be applied to the original traditional Balinese buildings. As described in Chapter One and discussed in Chapter Four, some features of traditional buildings may not be suitable for health and comfort conditions. By using similar arrangements to modern sites, the weakness of traditional architecture can be corrected, improved and developed without loss of its identity.

6.1.1 Results and Discussion

From velocity and streamline plots, it can be seen that the buildings arrangement produces very high velocity at the sixth building. Wind flows from the area between the first and second buildings merge with wind flows from the area between the second and third buildings, at the windward side of the sixth building. For two-dimensional problems, this distance is around two and two-thirds the building's height, but for the three-dimensional model is around one and two-thirds the building's height. Since the wind direction is at an angle, both flows merge near the windward side and deflect at the rear sides of the sixth building.

From velocity plots, it can be clearly seen that the velocity profile at 8 m above roof is uniform. This result agrees well with other published results. From turbulent kinetic energy plots, it is clear that its value is relatively high in the area between the first and fourth buildings and at the leeward side of the second building. The turbulent kinetic energy is also high at the corner between the fifth and sixth buildings.

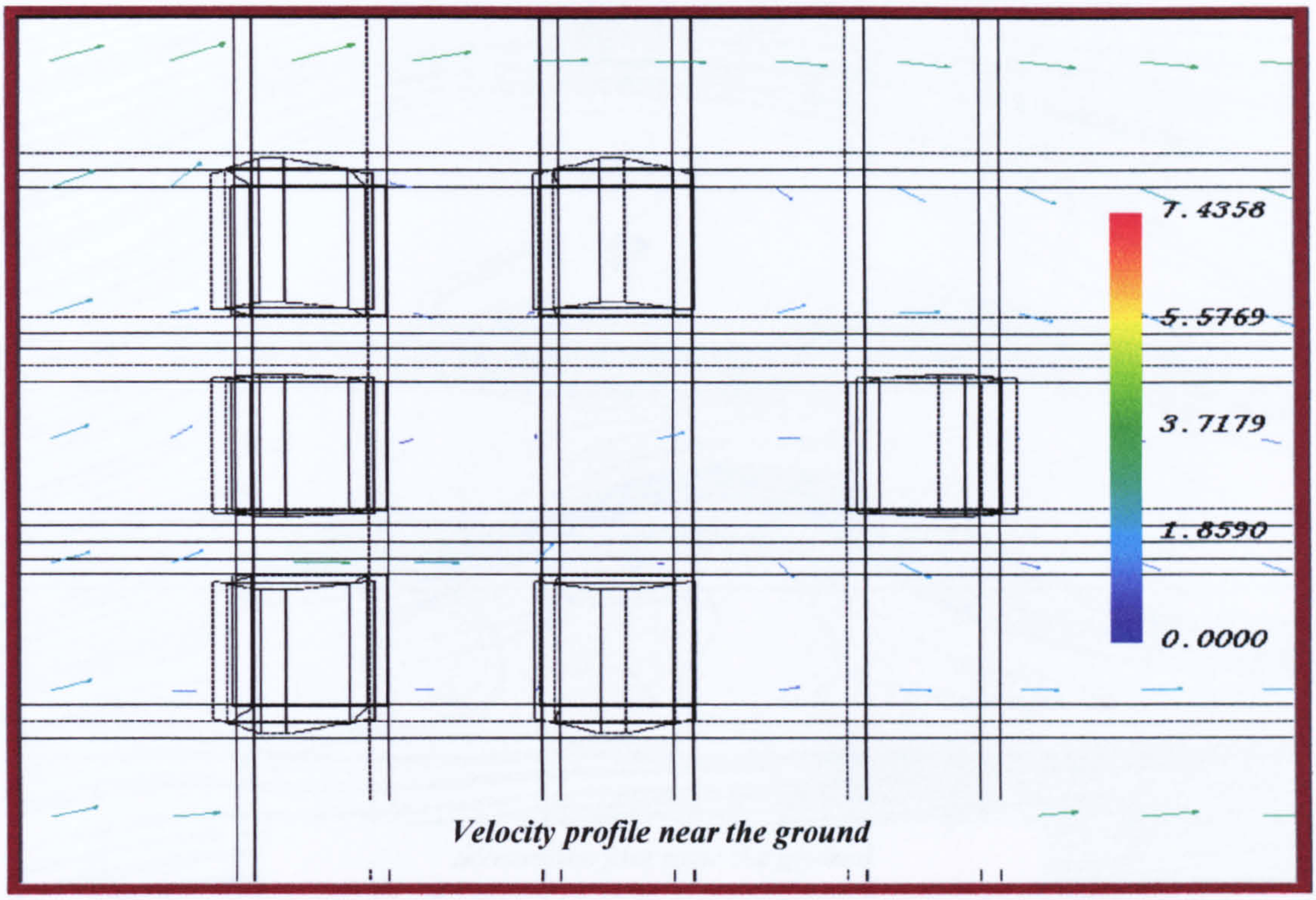

Figure 6.1.3 Velocity profile near the ground

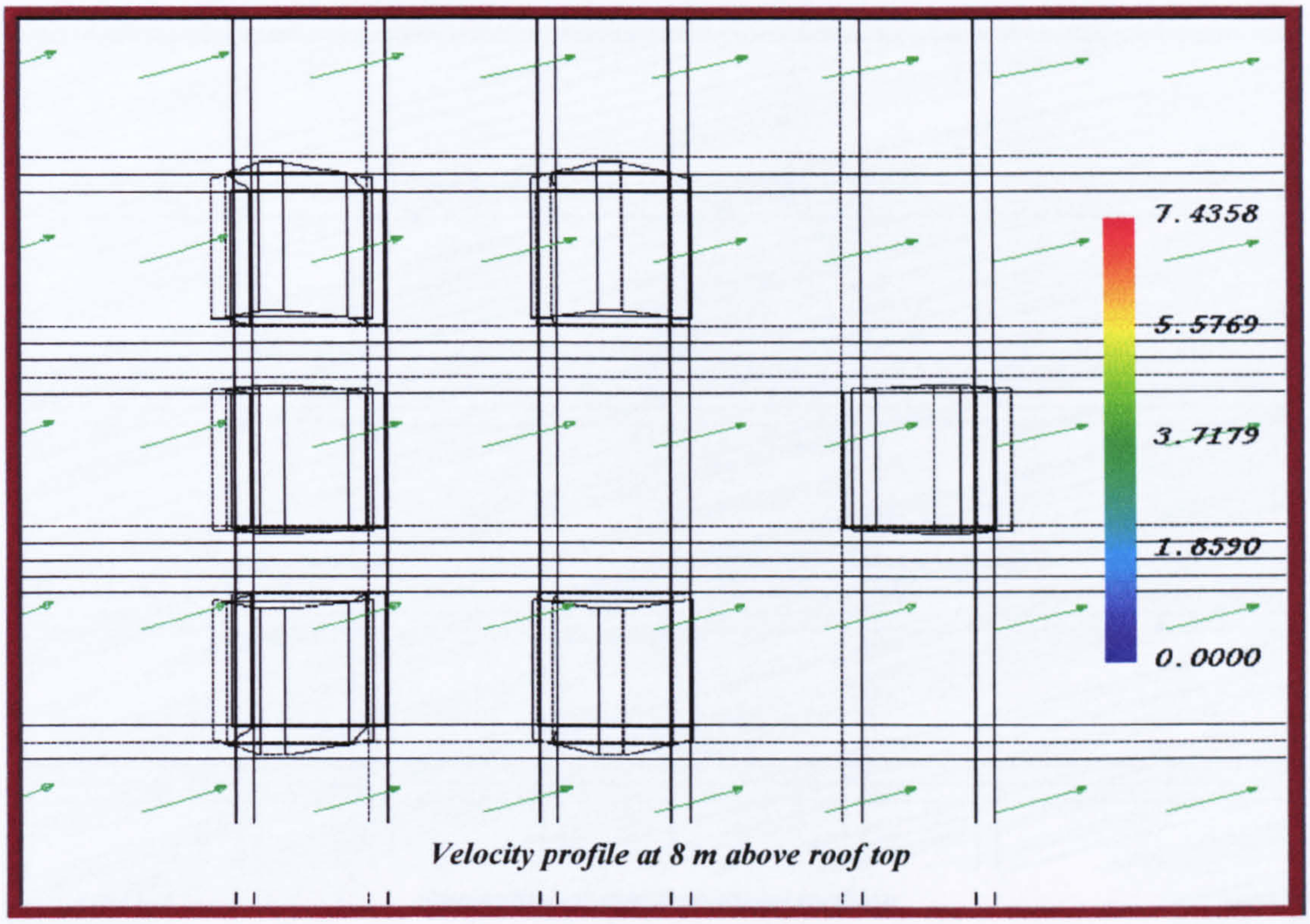

Figure 6.1.4 Velocity profile at 8 m above roof top

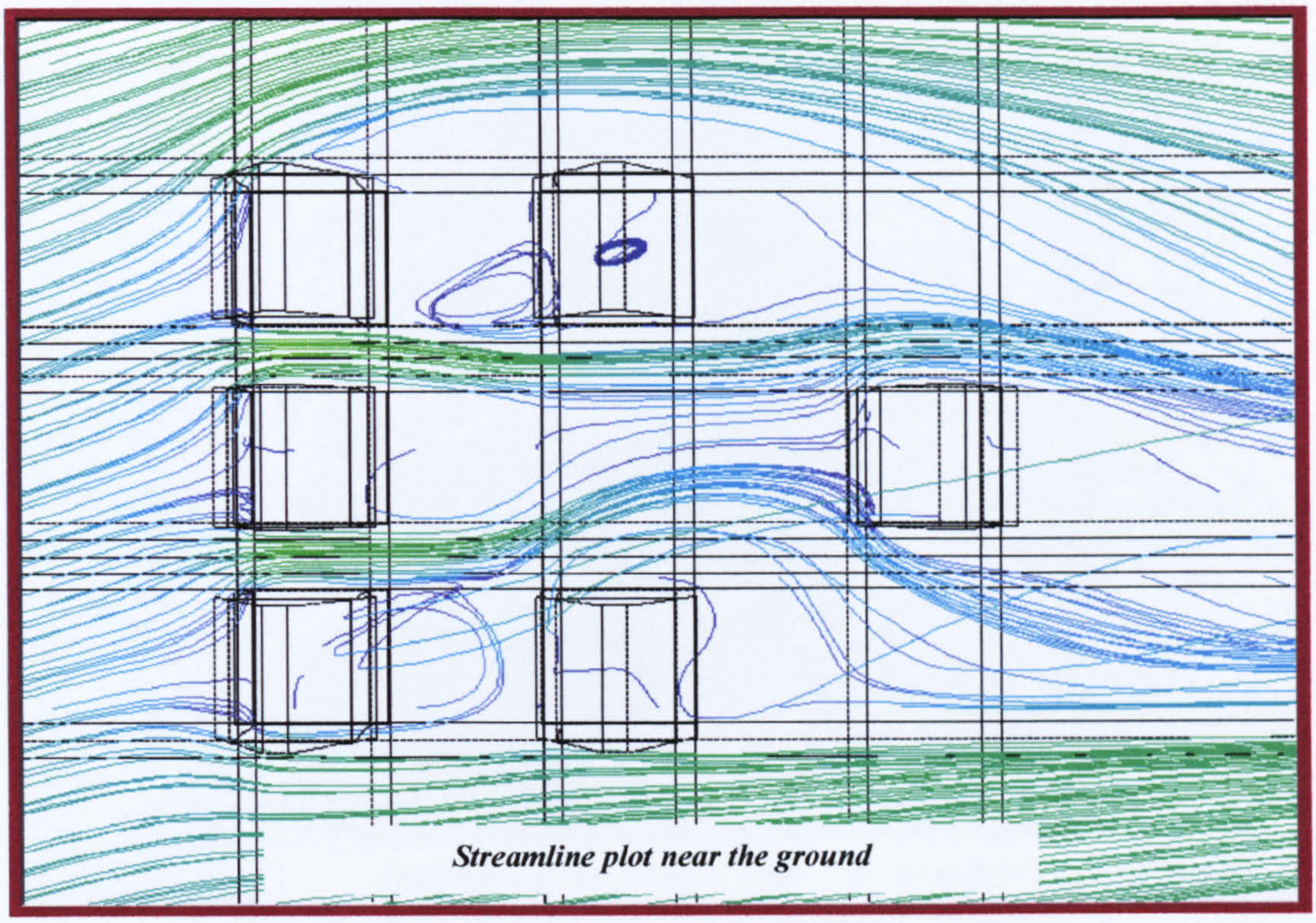

Streamline plot near the ground

Figure 6.1.5 Streamline plot near the ground

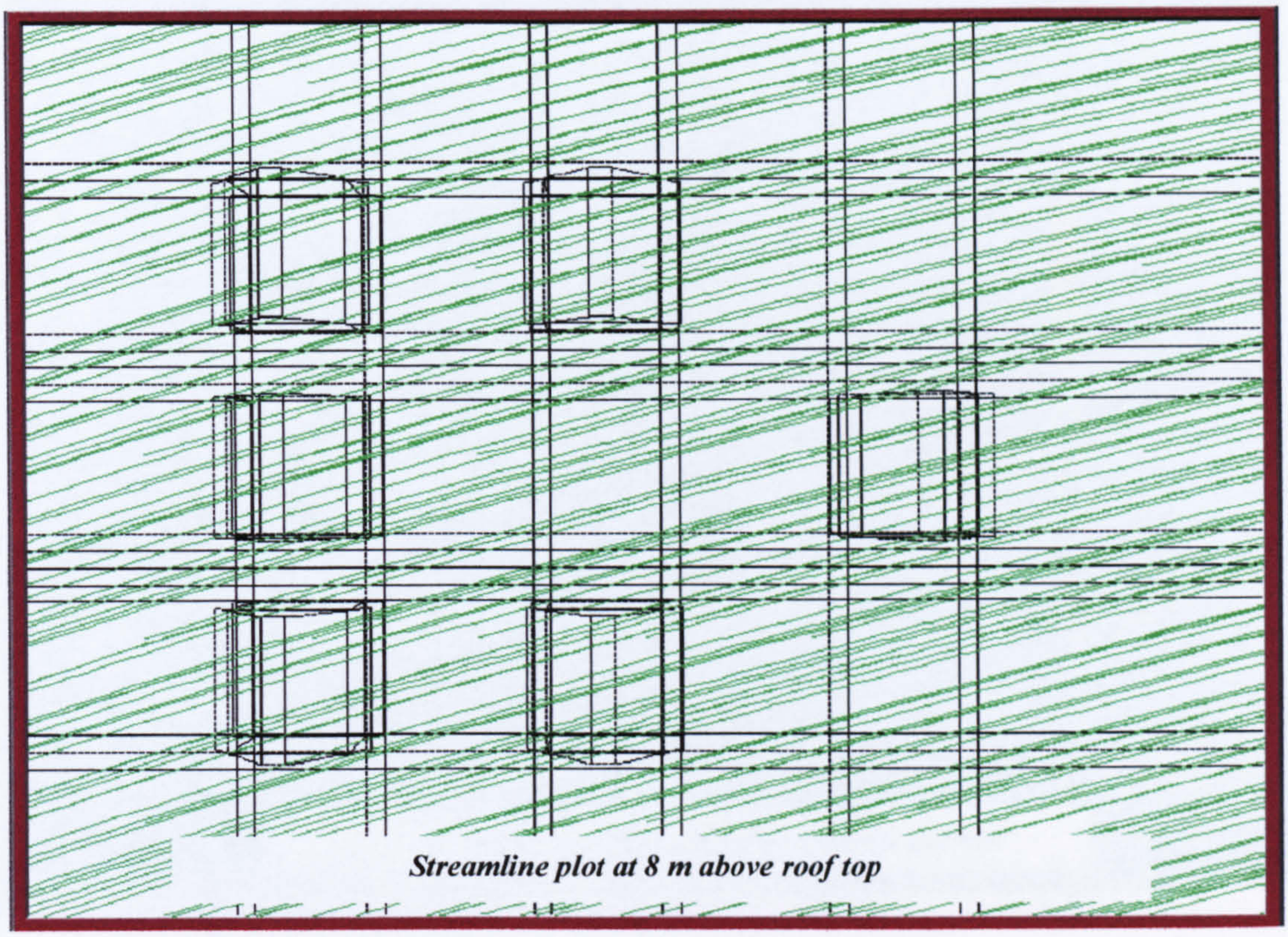

Streamline plot at 8 m above roof top

Figure 6.1.6 Streamline plot at 8 m above roof top

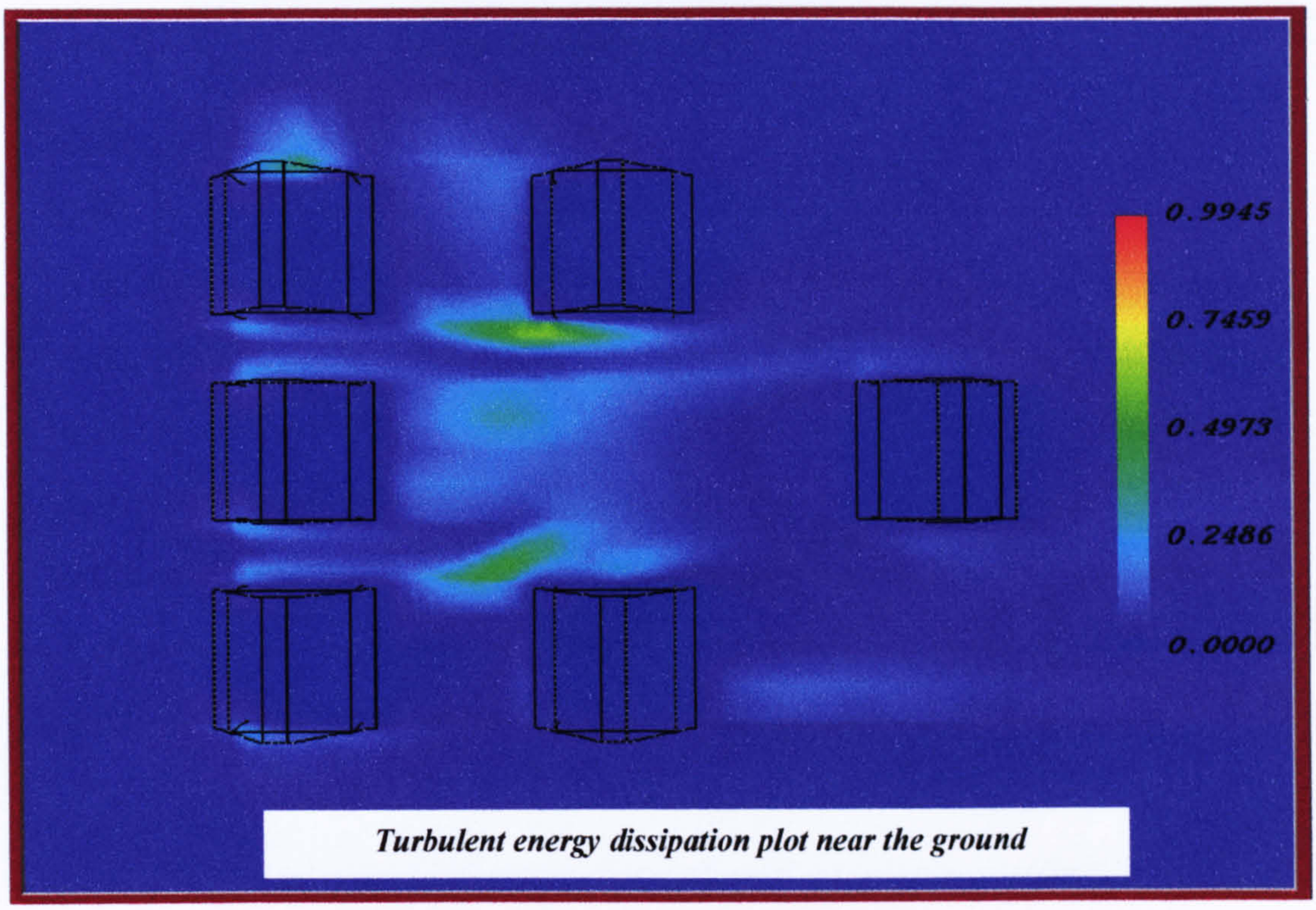

Figure 6.1.7 Turbulent energy dissipation plot near the ground

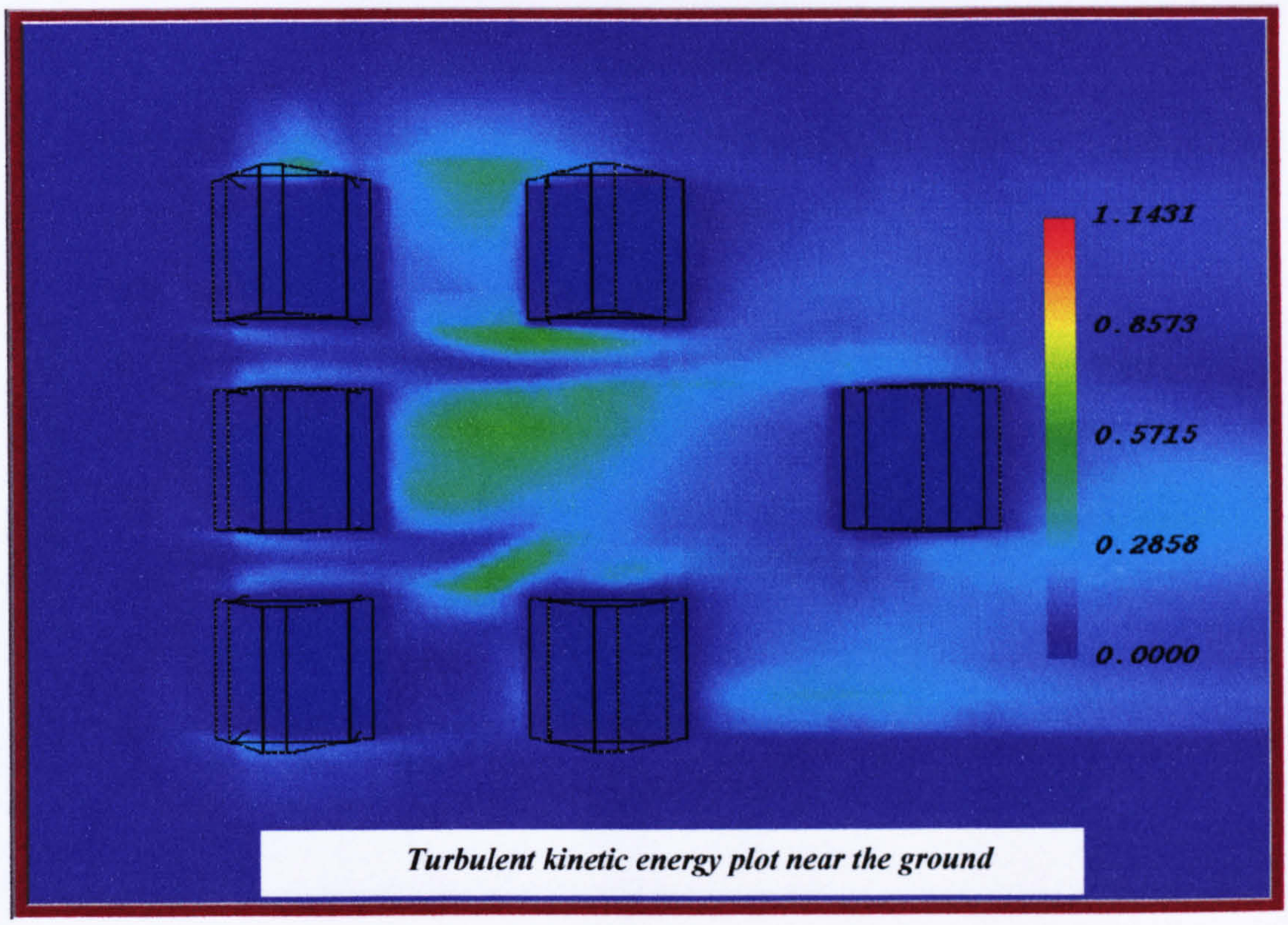

Figure 6.1.8 Turbulent kinetic energy plot near the ground

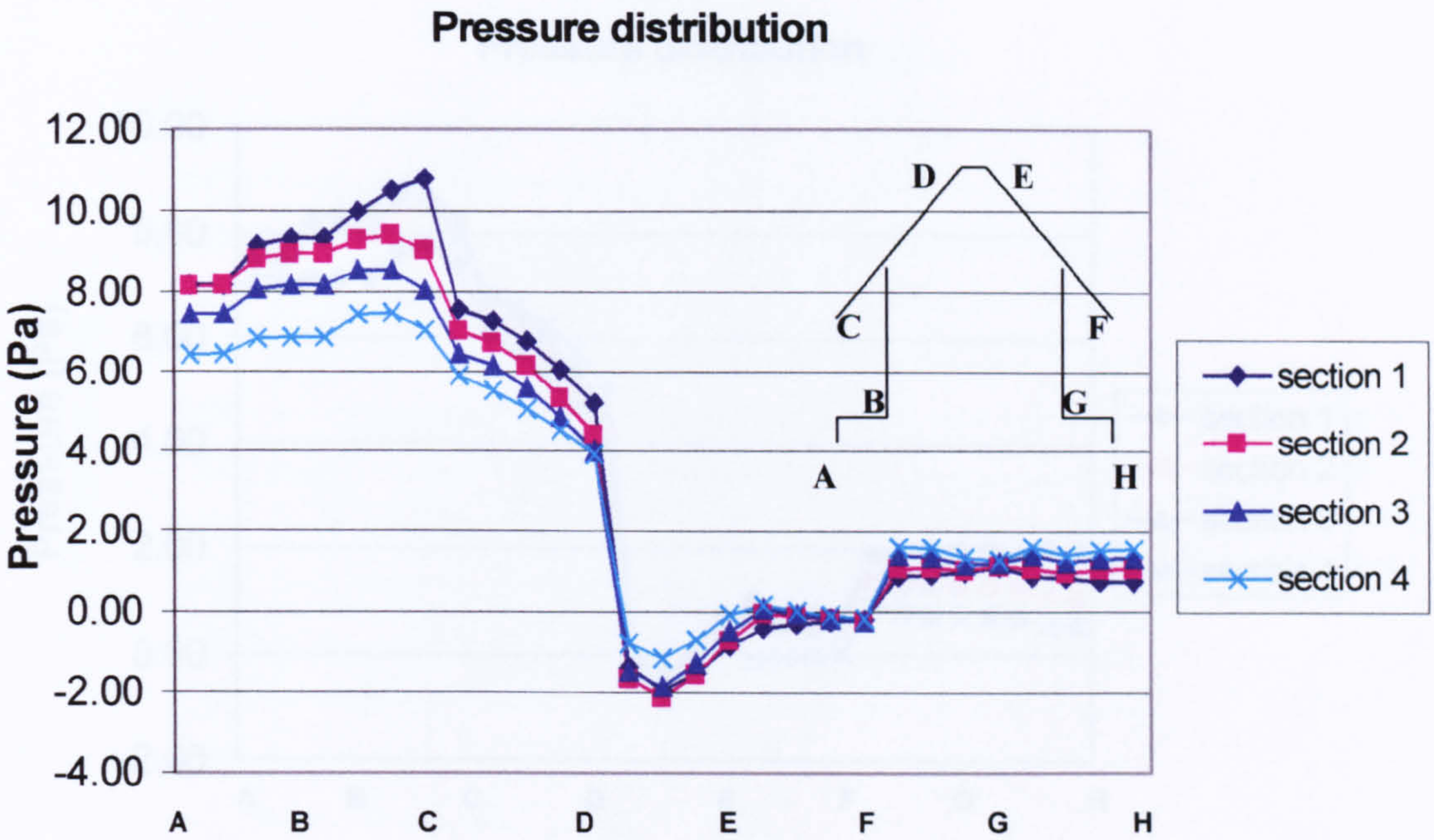

Figure 6.1.9 Pressure distribution on the first building

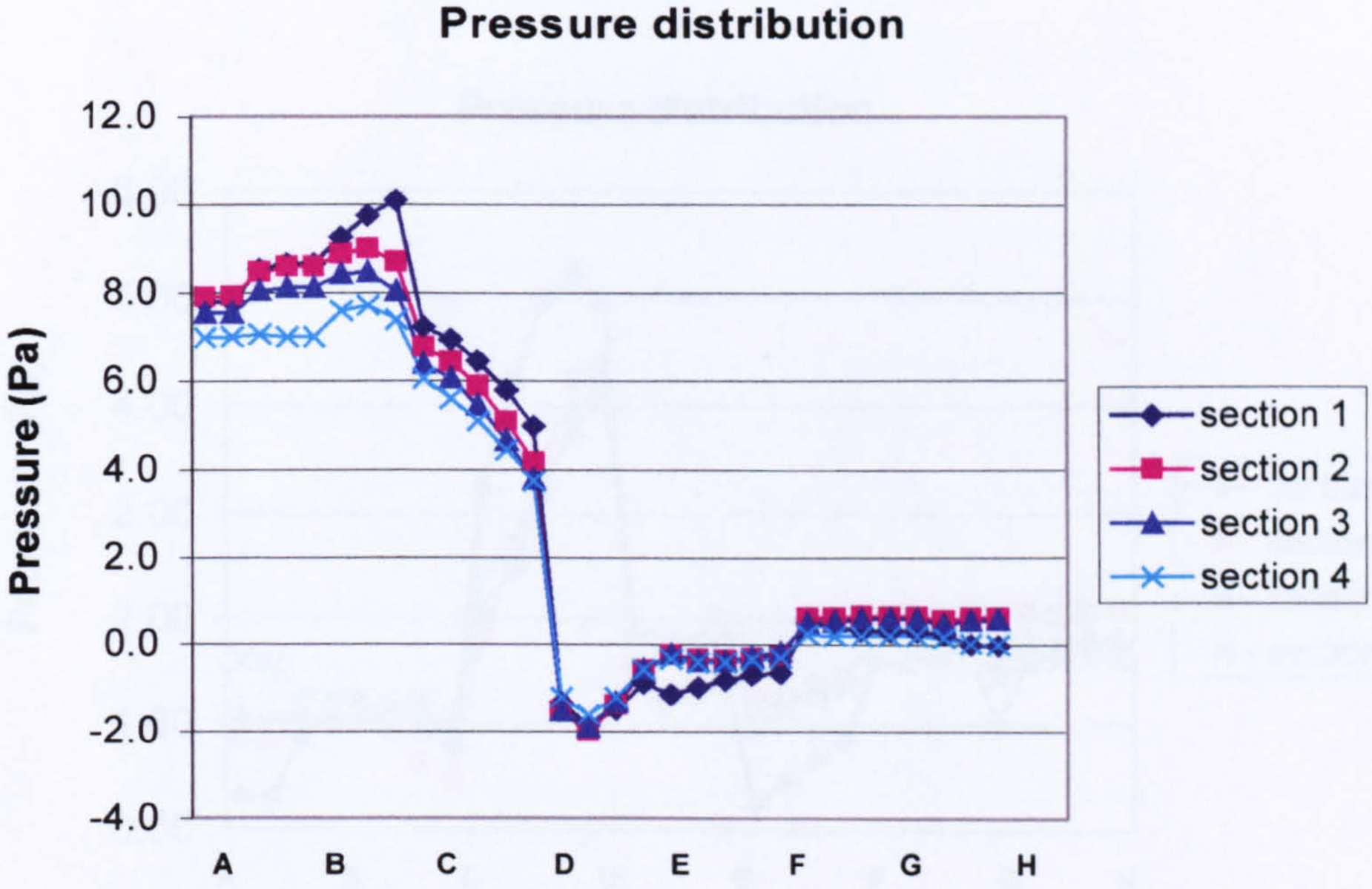

Figure 6.1.10 Pressure distribution on the second building

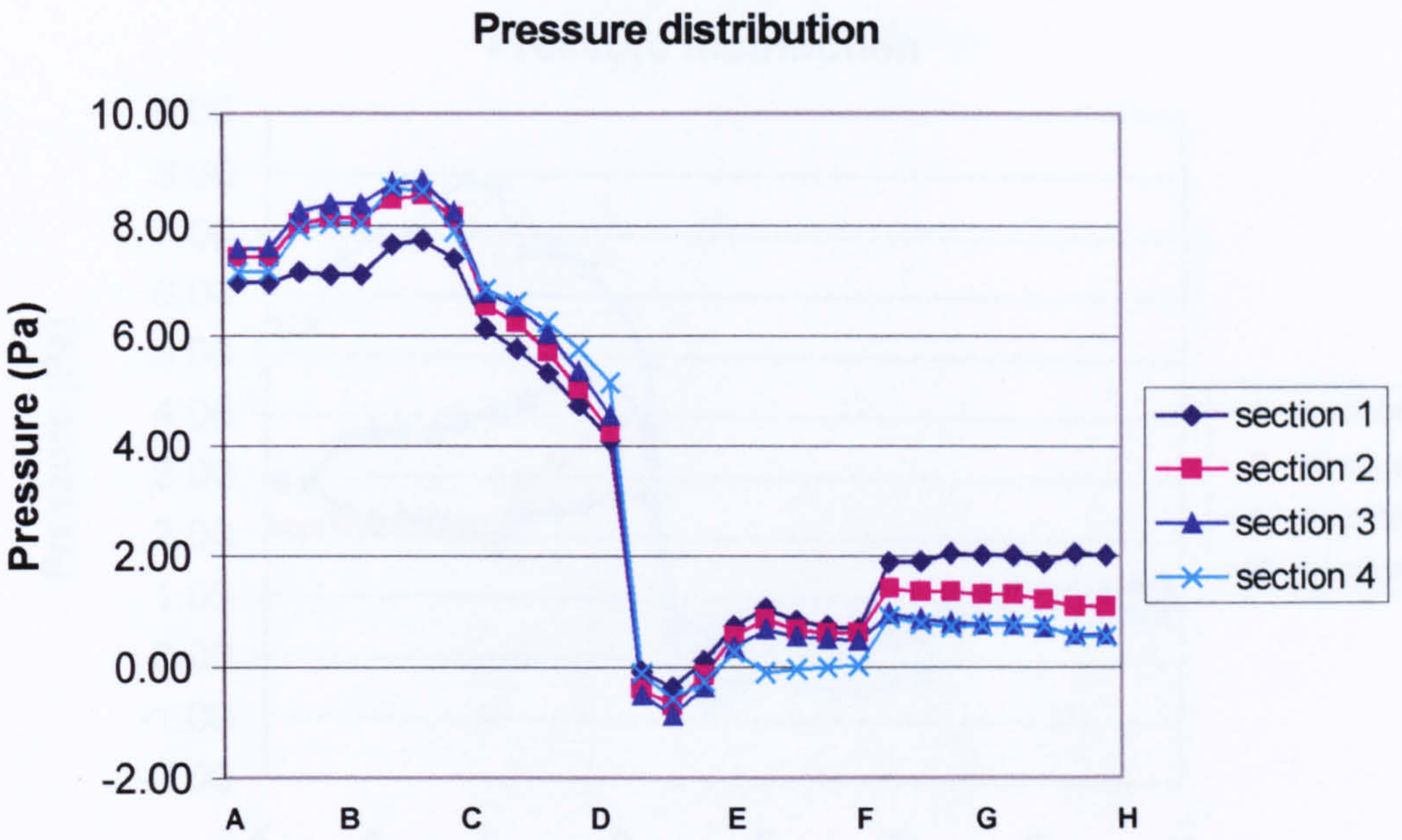

Figure 6.1.11 Pressure distribution on the third building

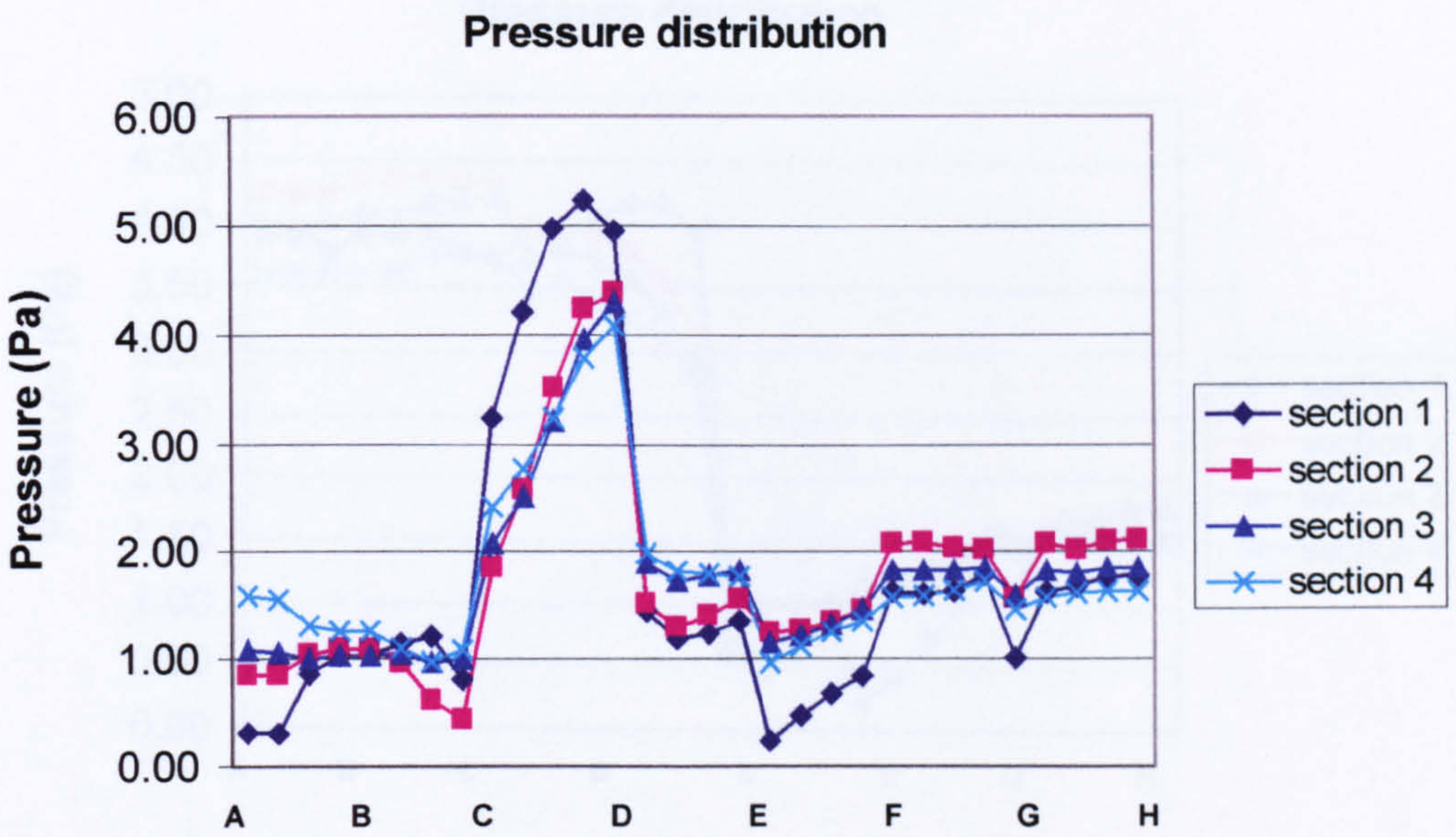

Figure 6.1.12 Pressure distribution on the fourth building

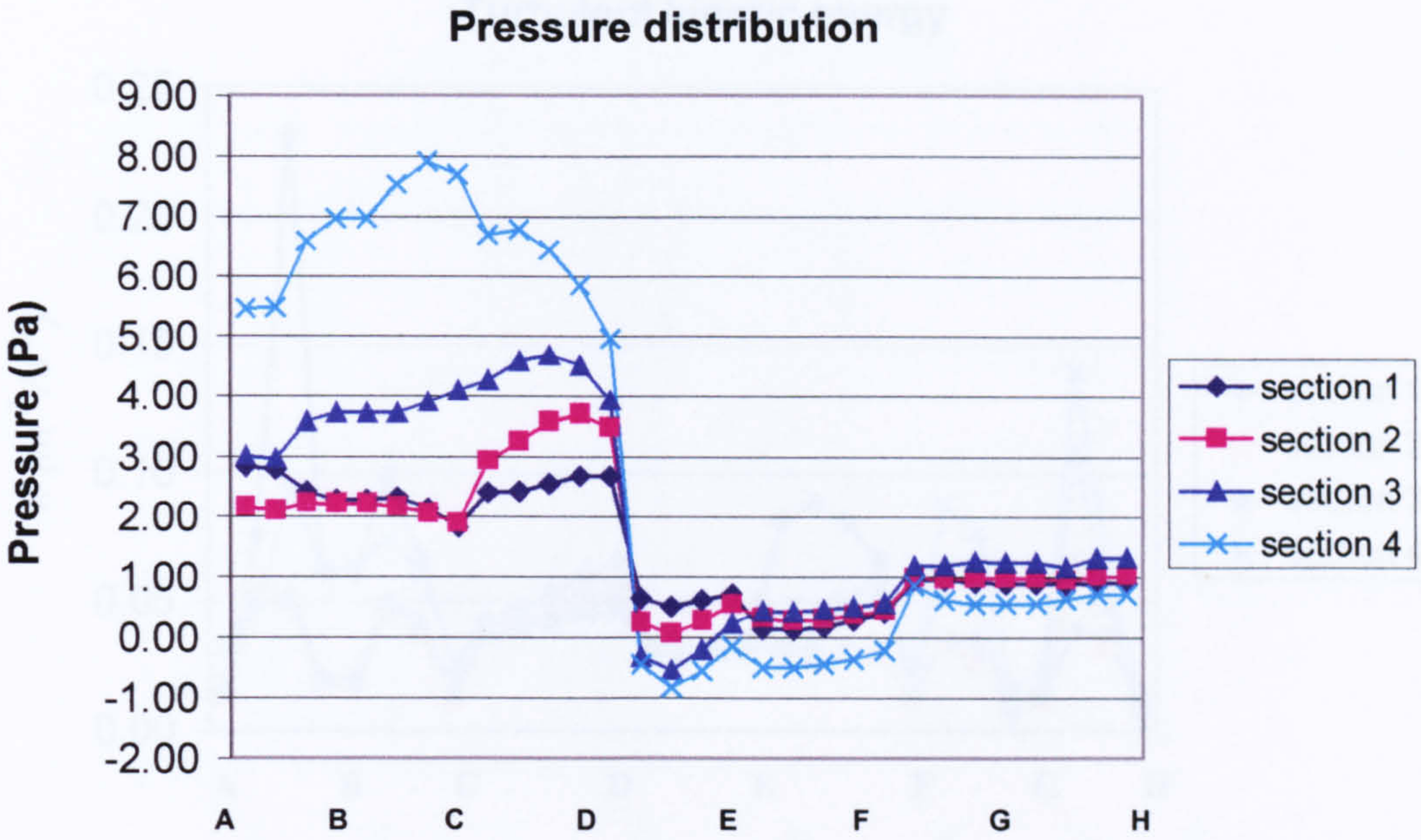

Figure 6.1.13 Pressure distribution on the fifth building

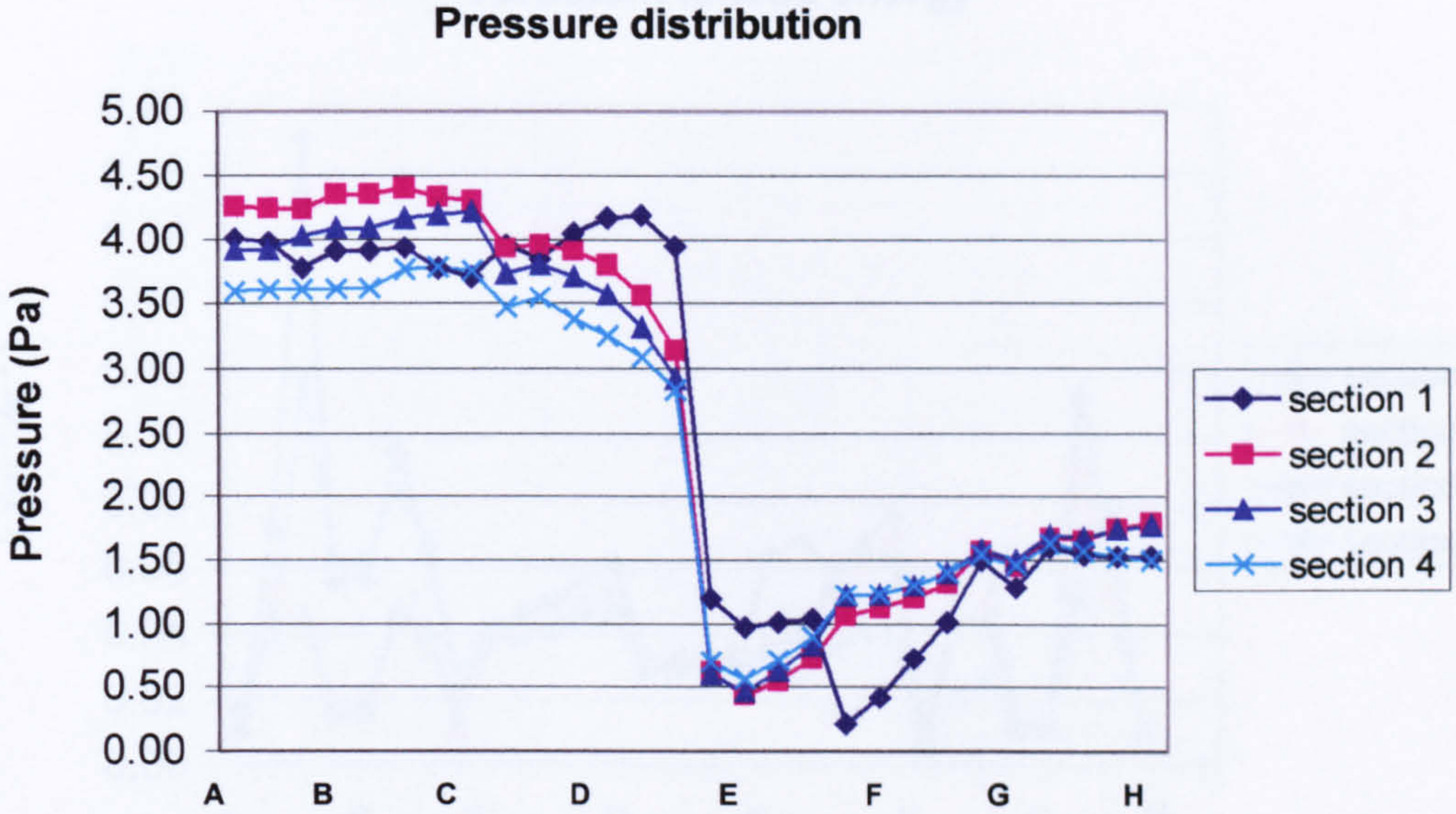

Figure 6.1.14 Pressure distribution on the sixth building

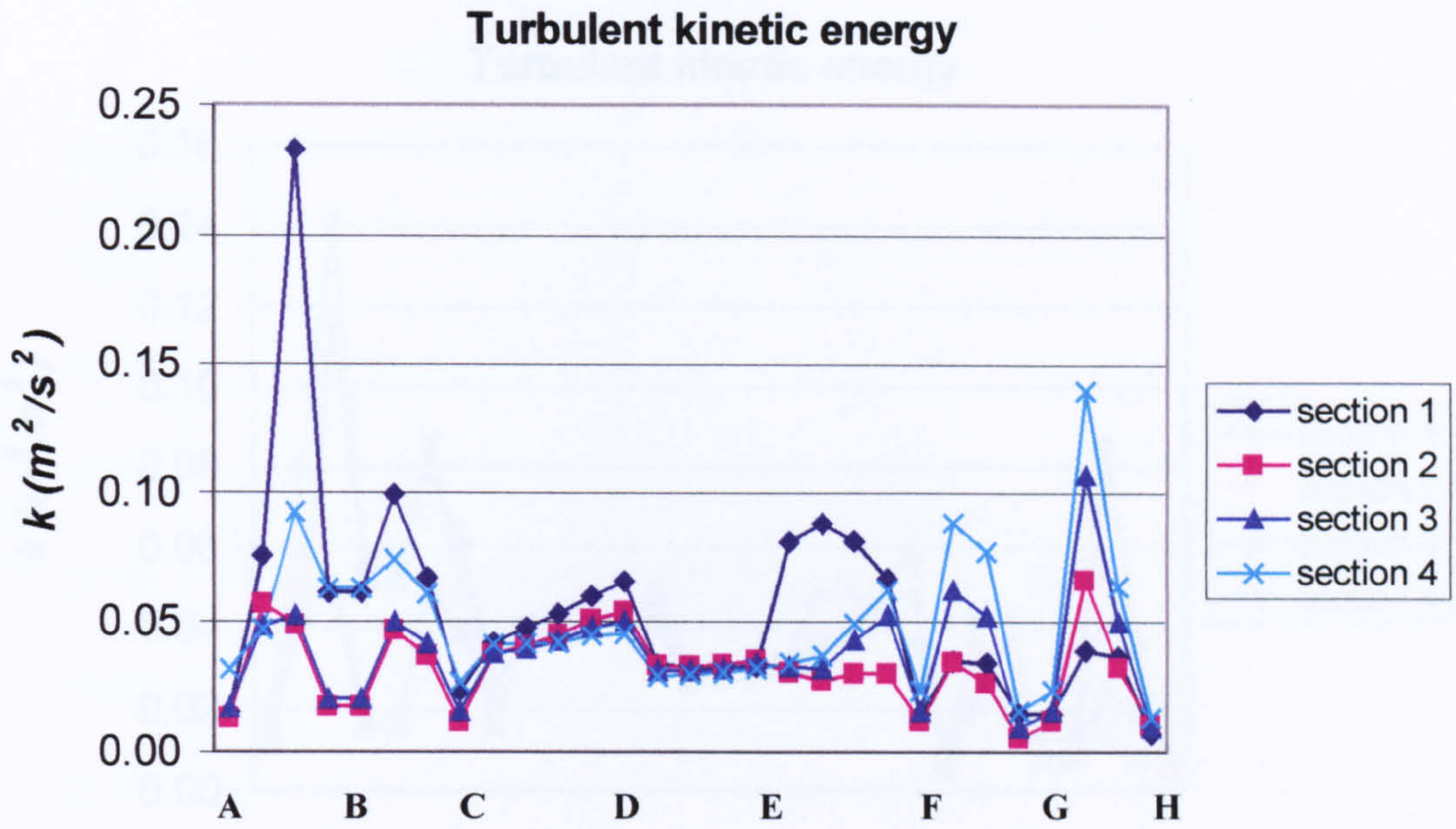

Figure 6.1.15 Turbulent kinetic energy on the first building

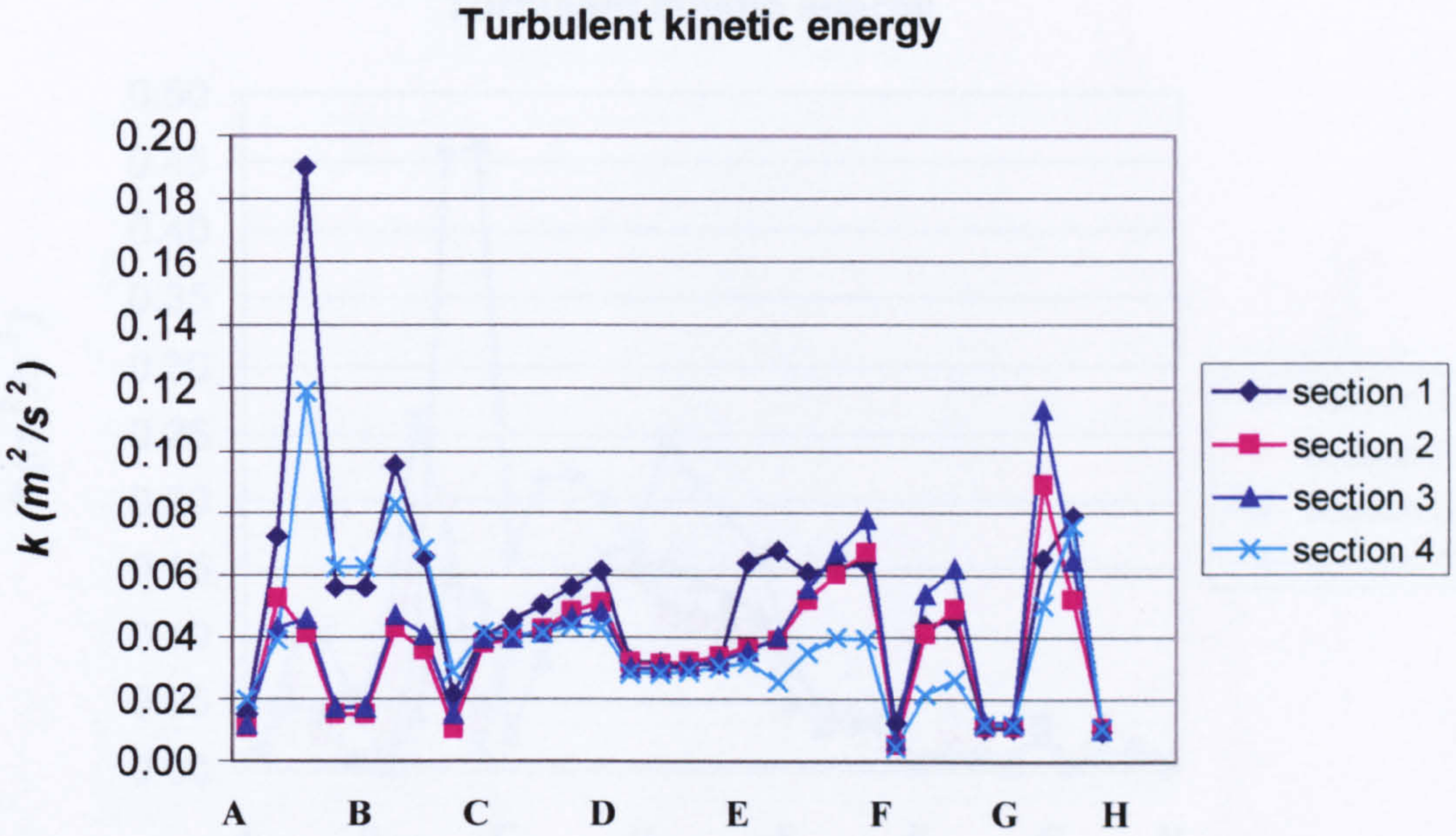

Figure 6.1.16 Turbulent kinetic energy on the second building

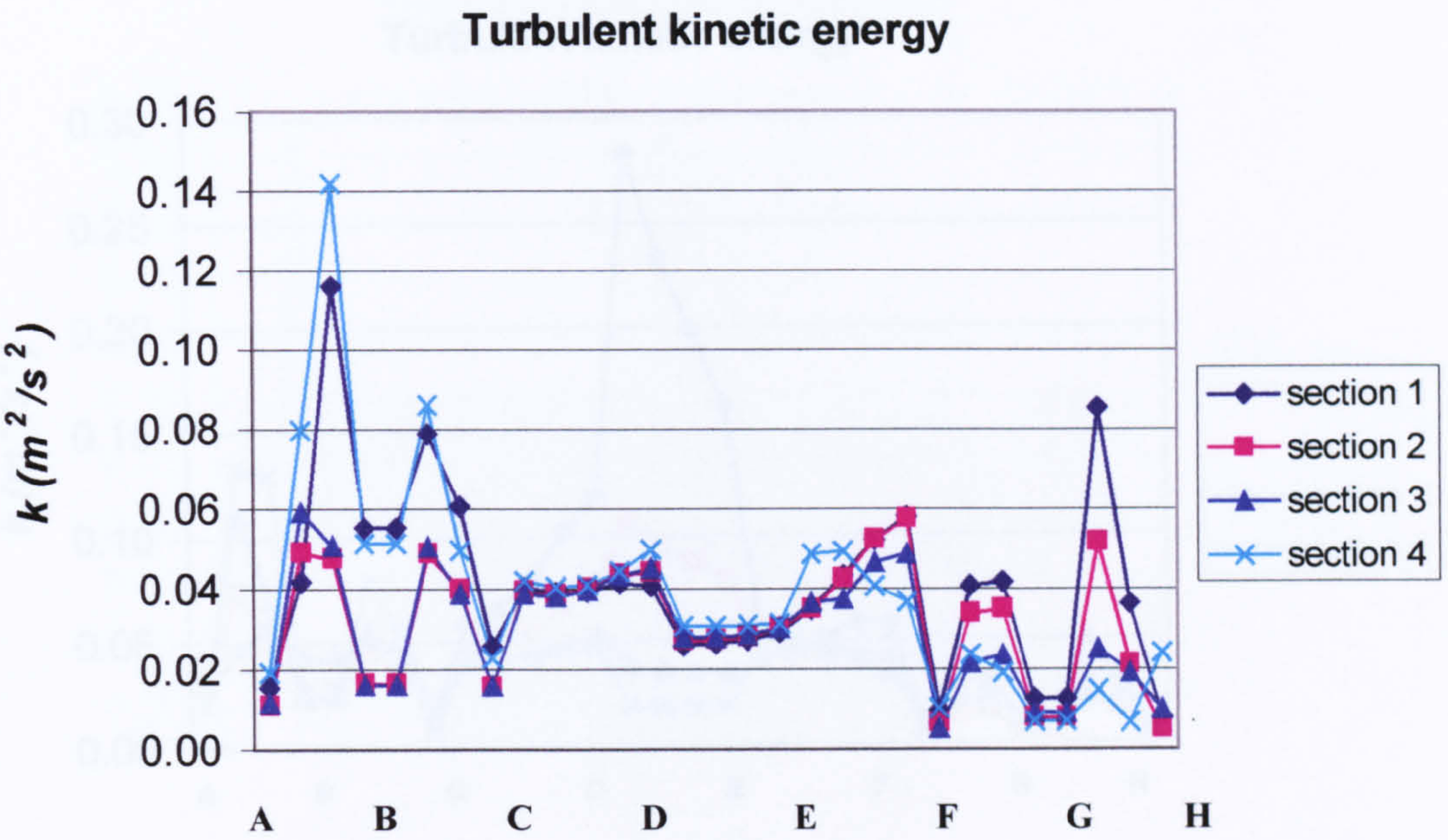

Figure 6.1.17 Turbulent kinetic energy on the third building

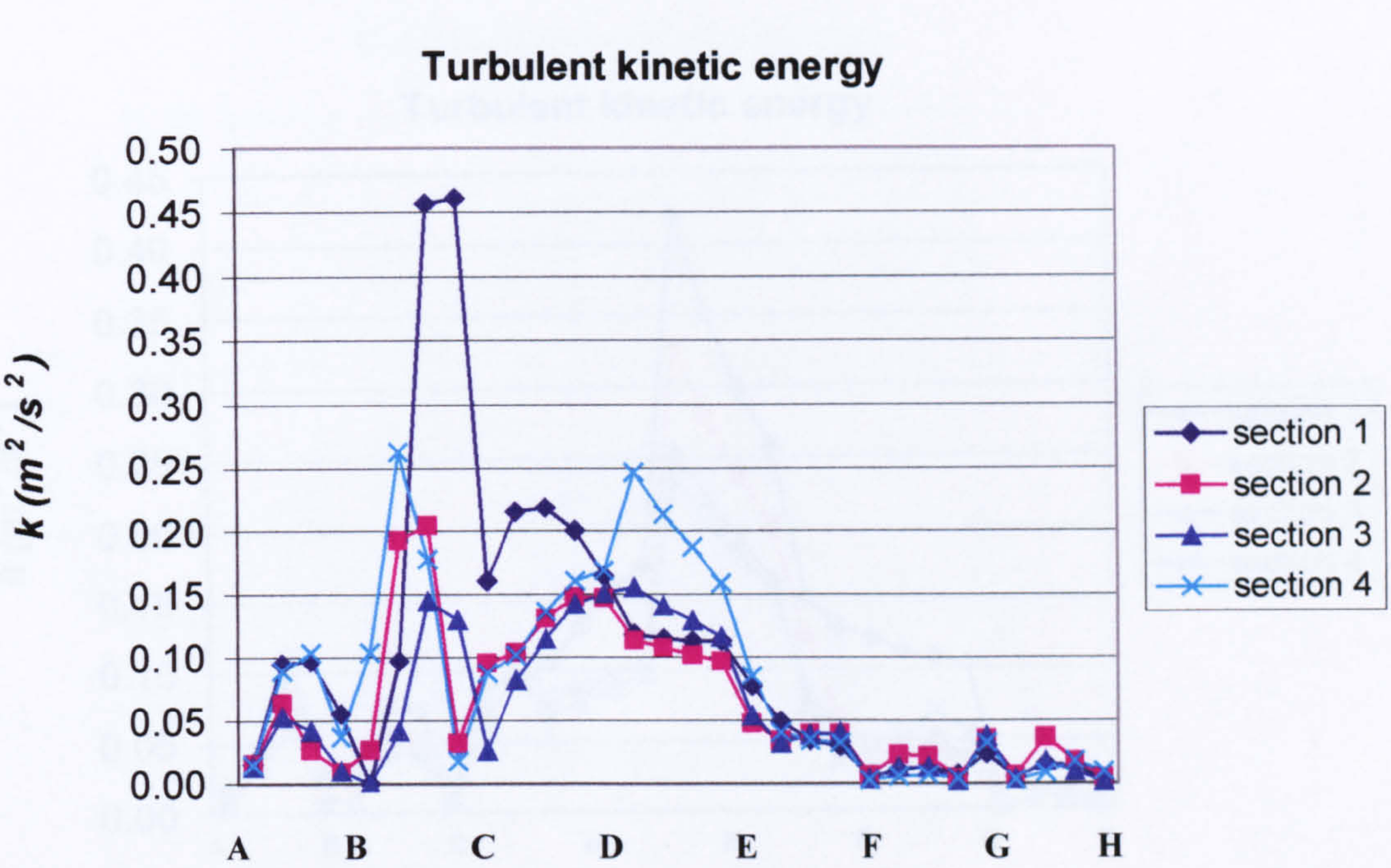

Figure 6.1.18 Turbulent kinetic energy on the fourth building

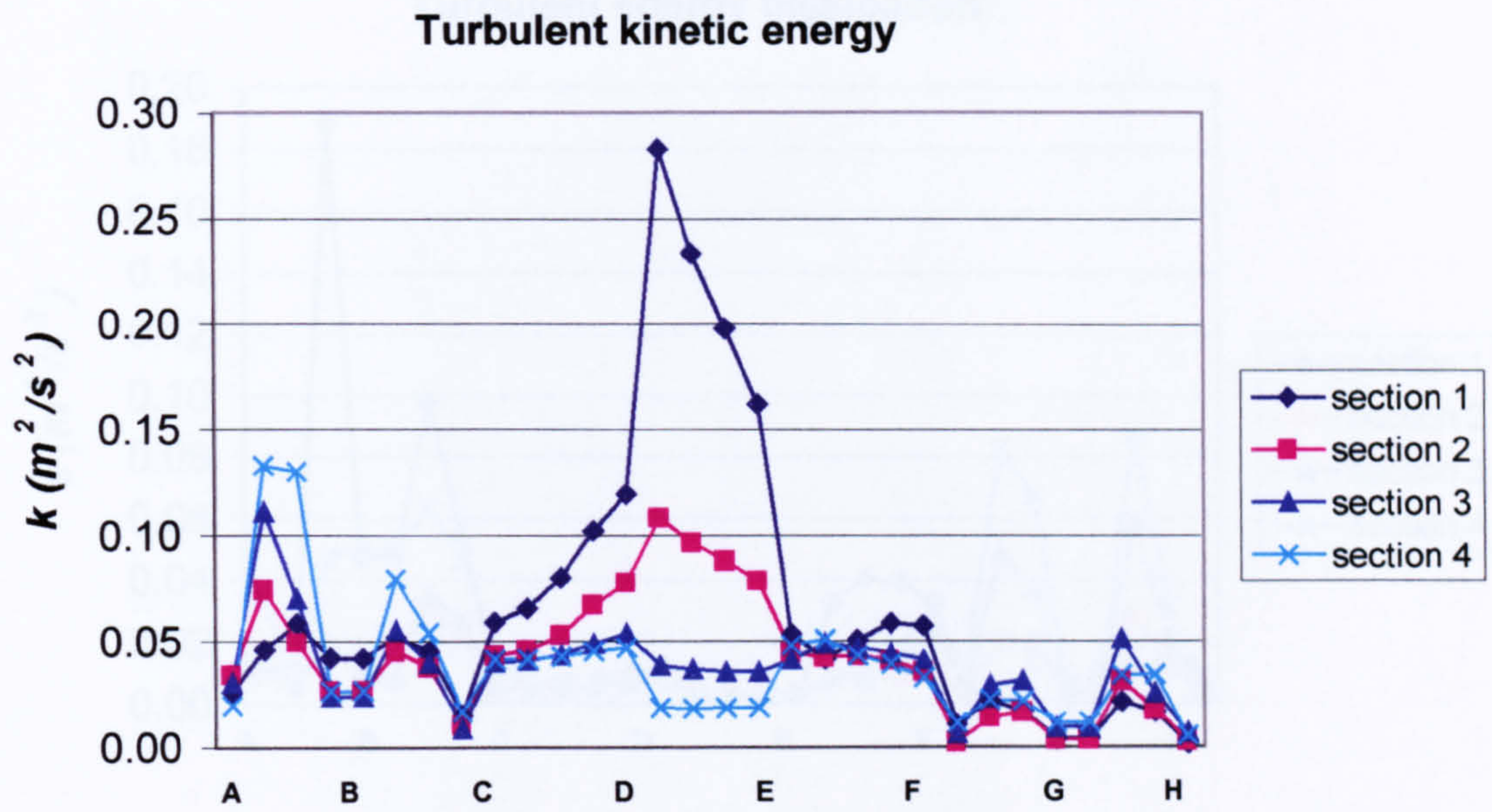

Figure 6.1.19 Turbulent kinetic energy on the fifth building

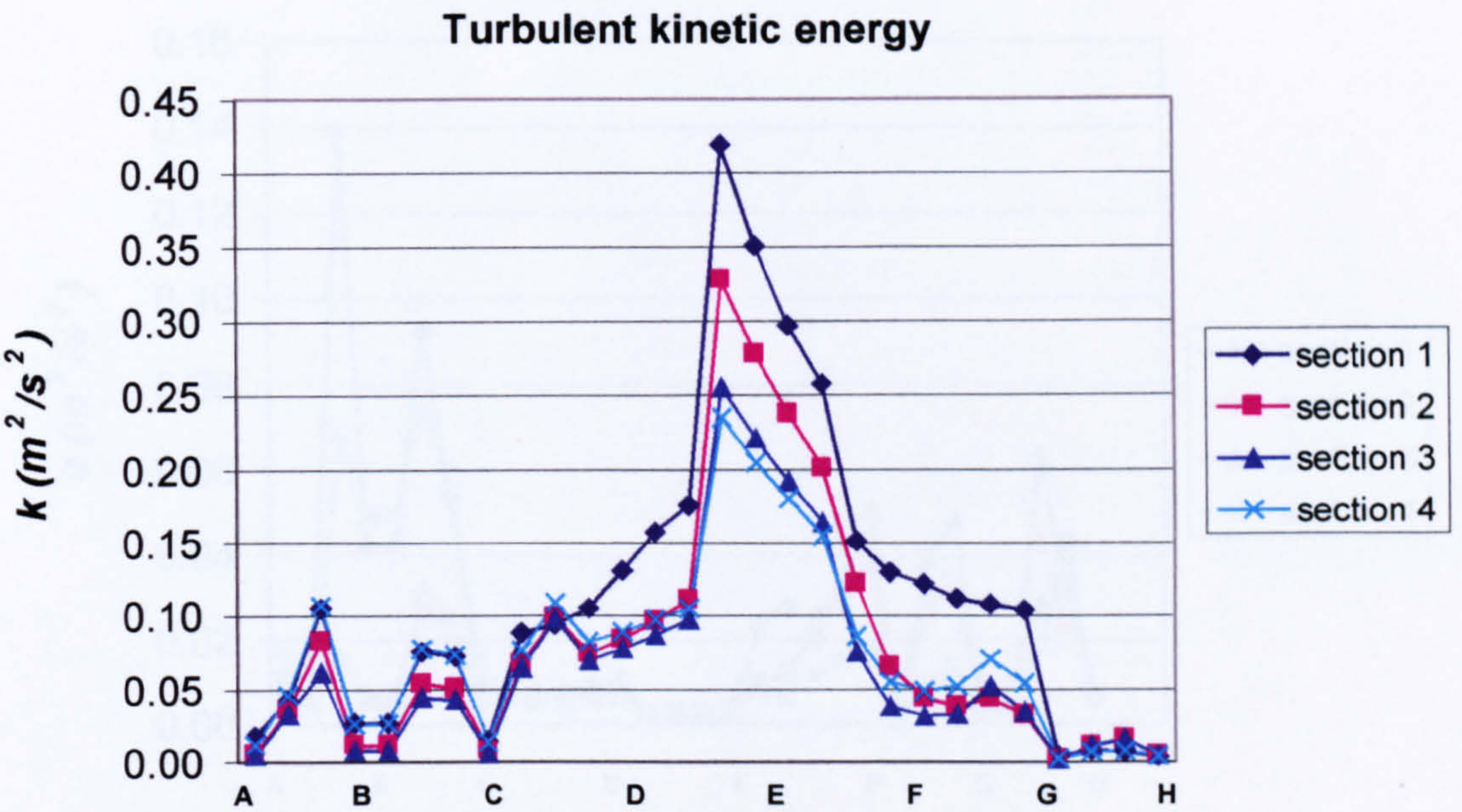

Figure 6.1.20 Turbulent kinetic energy on the sixth building

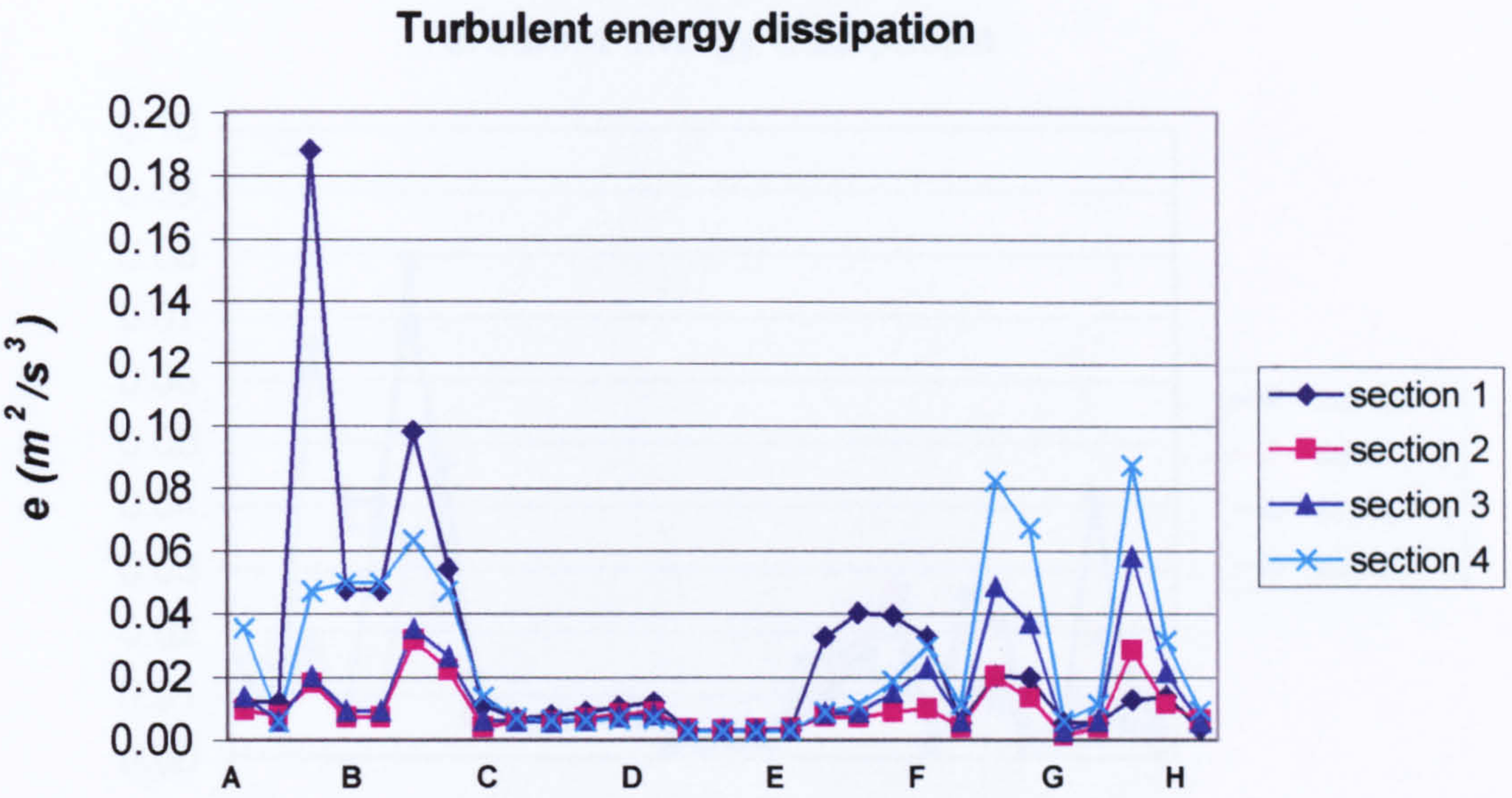

Figure 6.1.21 Turbulent energy dissipation on the first building

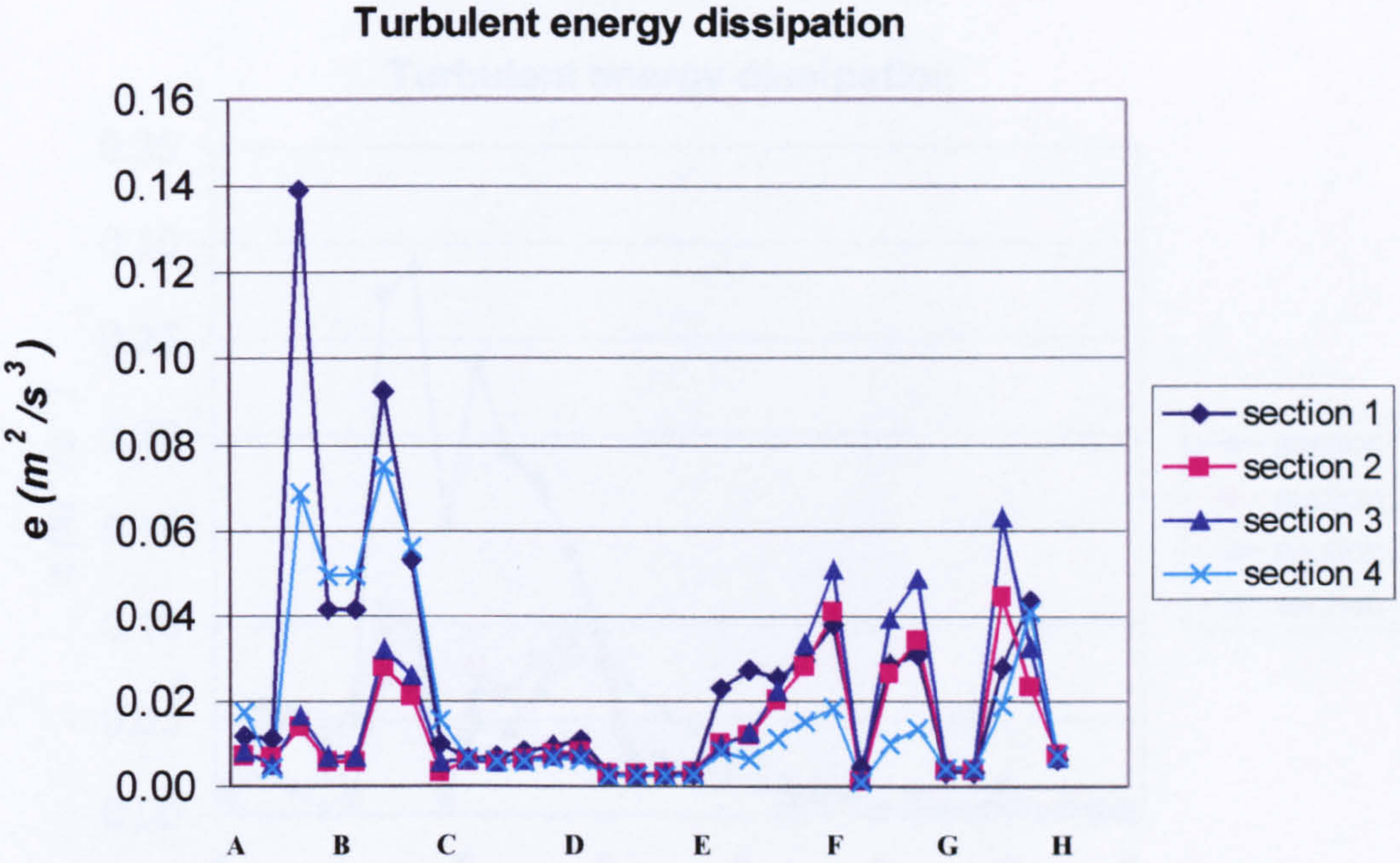

Figure 6.1.22 Turbulent energy dissipation on the second building

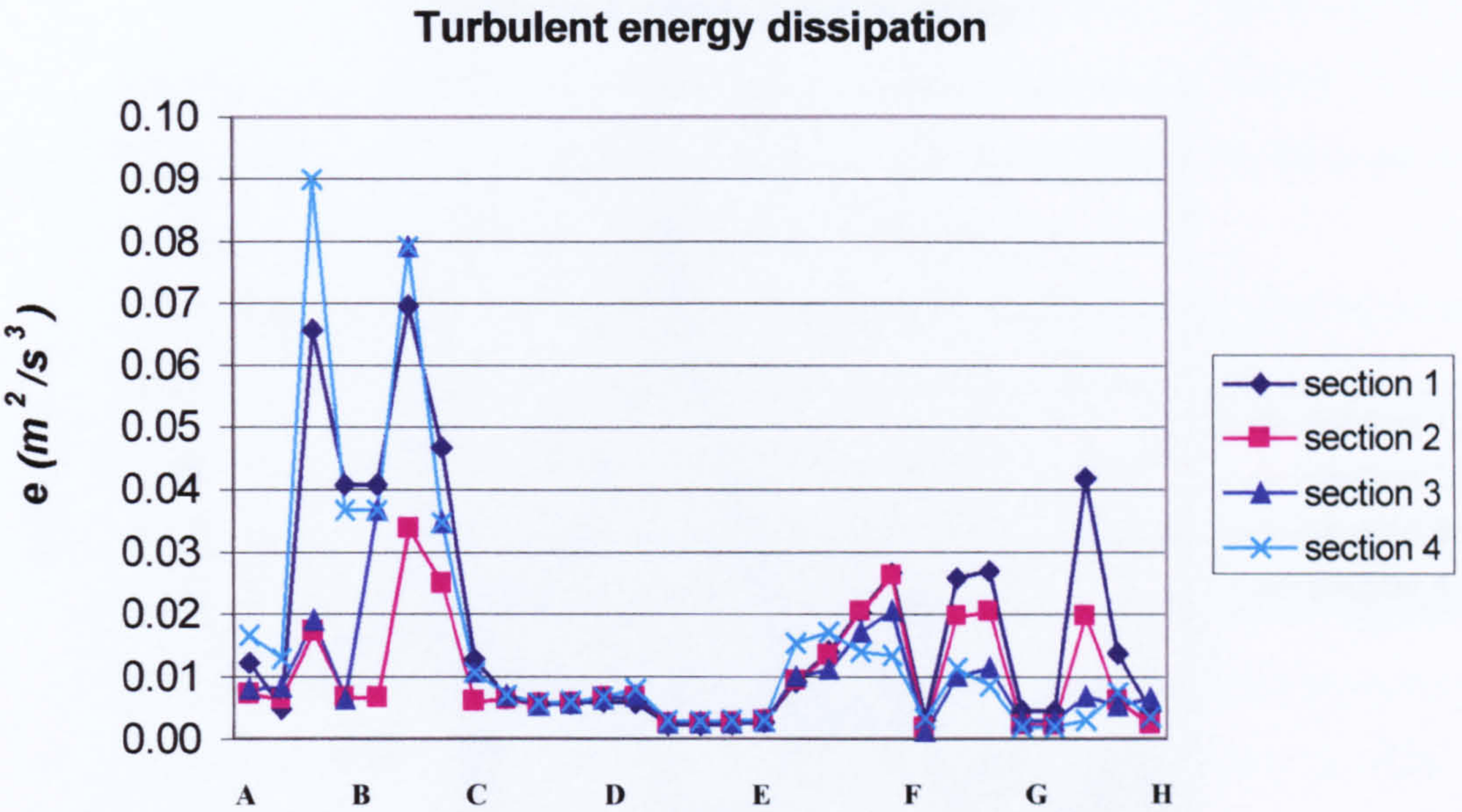

Figure 6.1.23 Turbulent energy dissipation on the third building

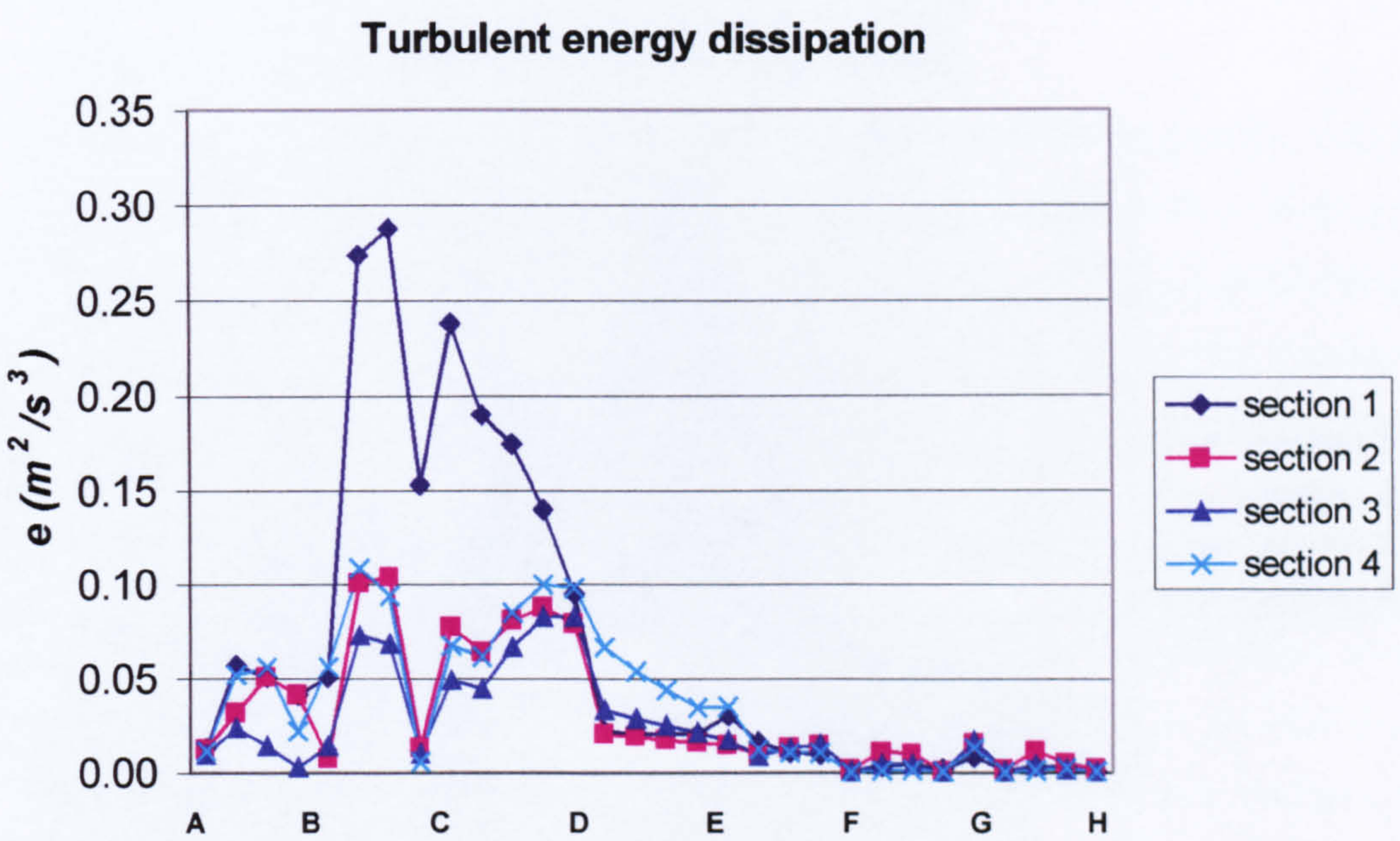

Figure 6.1.24 Turbulent energy dissipation on the fourth building

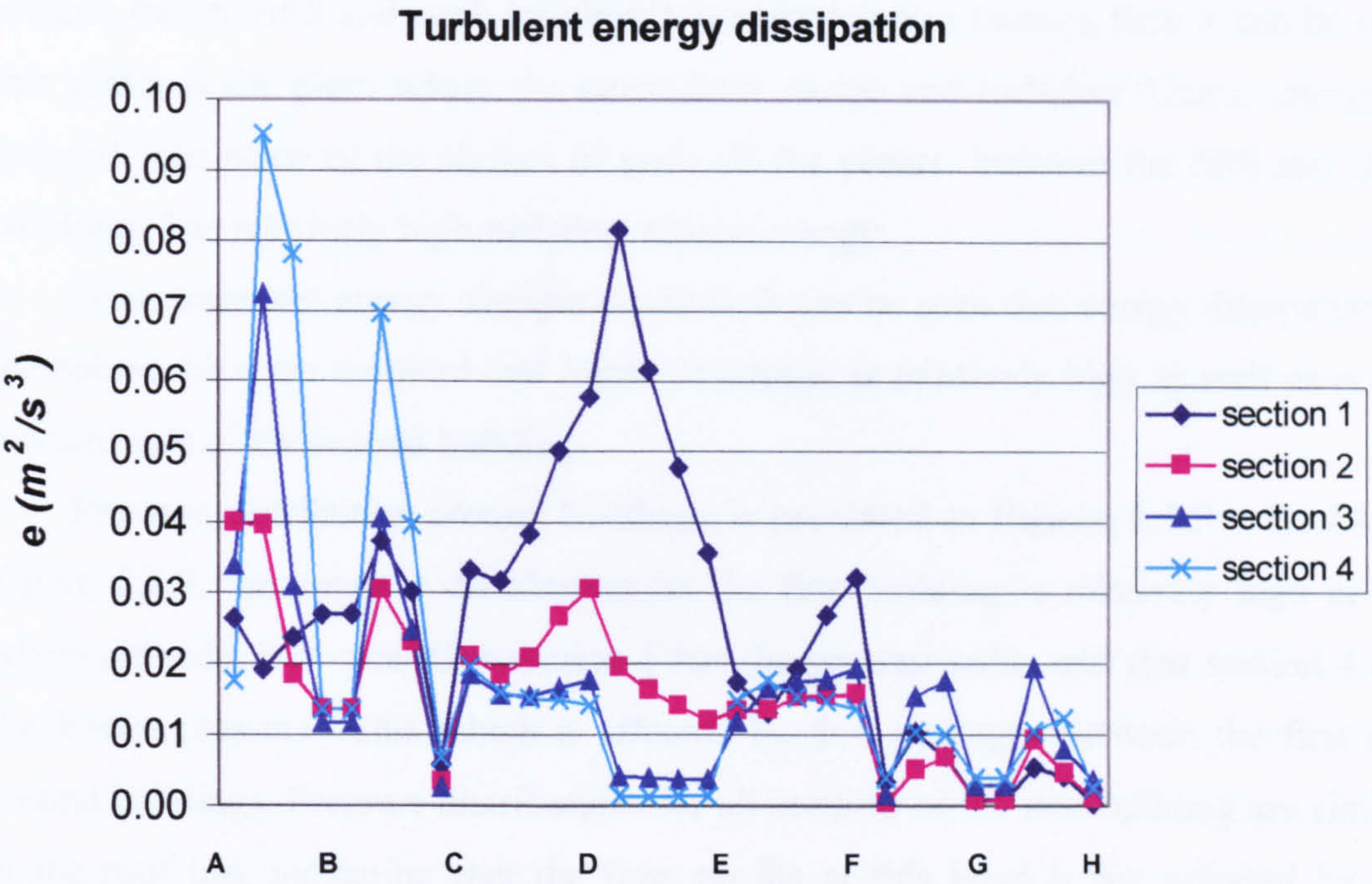

Figure 6.1.25 Turbulent energy dissipation on the fifth building

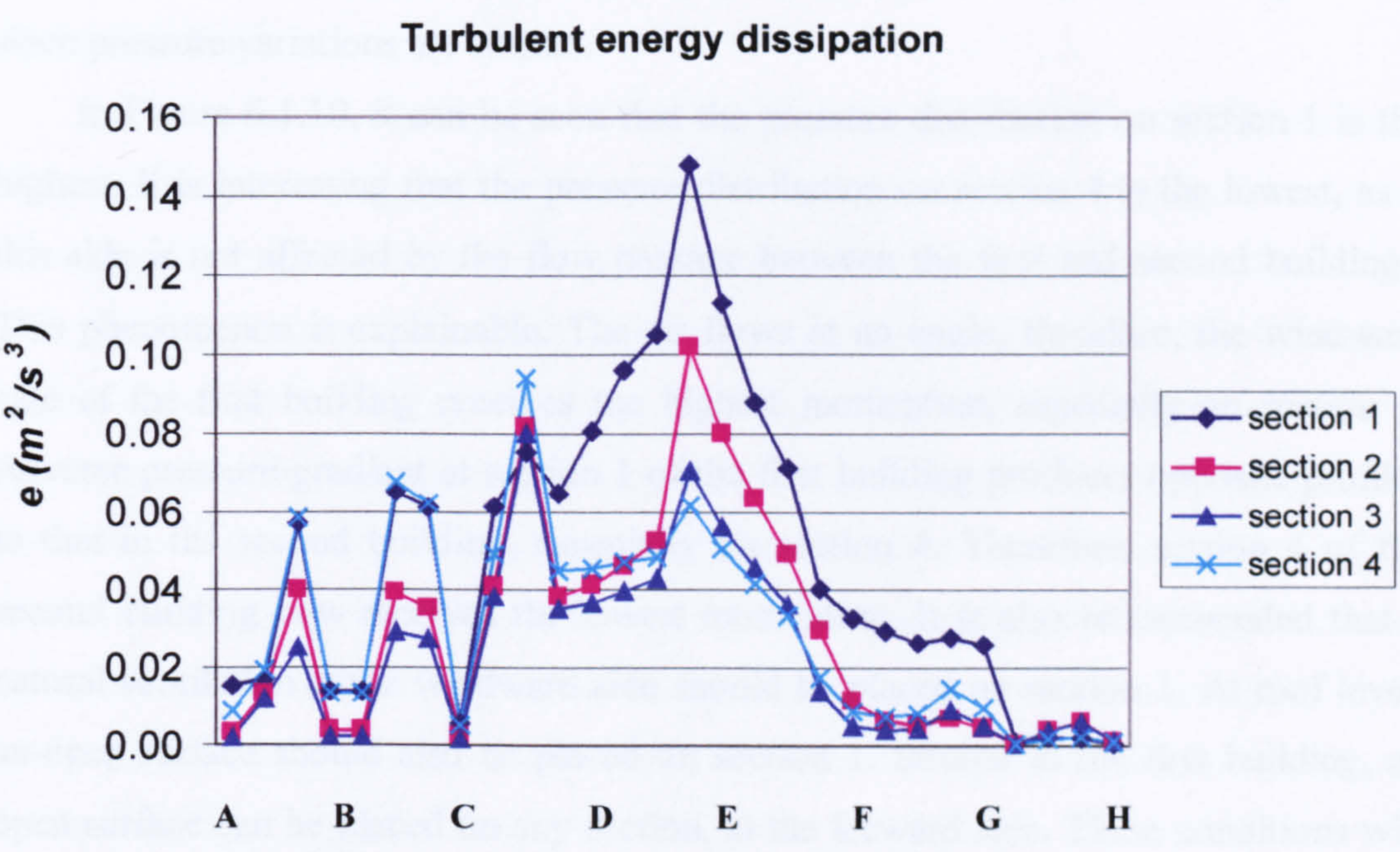

Figure 6.1.26 Turbulent energy dissipation on the sixth building

If the area at the leeward side of the second building (or the area between the second, fourth, fifth and sixth buildings) is named centre (*natar*), then it can be seen that centre is the place where the streamlines merge and turbulent kinetic energy is reduced. The place of the shrines of gods (in the corner, between the fifth and sixth buildings) has relatively high turbulent kinetic energy.

From turbulent energy dissipation plots, it can be seen that energy dissipation at the corner, between the third and fourth buildings, is relatively high as well as at the leeward side of the second building.

Pressure distribution around buildings is presented in Figures 6.1.9 – 6.1.14. In Figure 6.1.9, the pressure distribution on the first building is relatively high at the windward side. It is clear that section 1 has the greatest value and that section 4 has the lowest pressure value which is affected by flow passages between the first and second buildings. Pressure distributions for all sections of the first building are similar at the roof top, indicating that the flow profile at this level is not affected by the buildings arrangement. Since pressure variations on section 1 are relative high at the windward side, it is recommended that an open surface is placed on section 1 for natural ventilation. At roof level, an open surface can also be placed on section 1. At the leeward side of the first building, an open surface can be placed on any section since pressure variations are similar.

In Figure 6.1.10, it can be seen that the pressure distribution on section 1 is the highest. It is interesting that the pressure distribution on section 4 is the lowest, as if this side is not affected by the flow passage between the first and second buildings. This phenomenon is explainable. The air flows at an angle, therefore, the windward side of the first building receives the highest momentum, especially on section 1. Adverse pressure gradient at section 1 of the first building produces opposite profiles to that in the second building, especially on section 4. Therefore, section 4 of the second building now receives the lowest momentum. It is also recommended that a natural ventilation at the windward side should be placed on section 1. At roof level, an open surface should also be placed on section 1. Similar to the first building, an open surface can be placed on any section, at the leeward side. These conditions will minimise the wind load effects on the building but produce good natural ventilation to the occupants.

The same explanation is valid for the third building. From Figure 6.1.11, it can be seen that the pressure distribution on section 1 is the lowest one (note: section

numbers of the third building are opposite to that in the first and second buildings). An open surface at the windward side should be placed on section 3, but an open surface at roof level is recommended on section 4. At the leeward side, a natural ventilation should be placed on section 3.

As shown in Figure 6.1.12 for the fourth building, the pressure distribution on section 1 is very low at the windward side. Since the pressure distribution at the windward side is lower than at the leeward side, open surfaces at this side are not necessary. At roof level, we recommend an open surface on section 1. Since the pressure variation on section 1 is a bit lower than on the other sides, an open surface on section 1 is preferred at the leeward side.

It is clear in Figure 6.1.13 that the pressure distribution on section 4 is the highest one at the fifth building. Therefore, an open surface on section 4 is recommended for better natural ventilation. The maximum pressure is lower than that in the third building, indicating that air momentum decreases after hitting the first obstacle (*i.e.*, the third building). The pressure distribution on section 1 is also different from that on section 1 of the fourth building. It can be noted that the flow pattern on section 1 of the fourth building tends to be fully developed, but not in the fifth building. This phenomenon leads to producing high momentum (and turbulent kinetic energy) on the fourth building.

From Figure 6.1.14, it can be seen that the pressure distribution at the windward side of the sixth building is high on section 2. It can be noted that the flow at the windward side also tends to be fully developed. Theoretically, the flow at the leeward side of the first obstacle should be fully developed after one and a half reattachment lengths (or about two and two-thirds the building's height). Since the wind direction is at an angle, it affects the flow pattern near the windward side of the sixth building and does not produce a fully develop turbulent flow, similar to the fourth building. On the sixth building, an open surface on section 2 is recommended at the windward side. An open surface at roof level is recommended on section 1. At the leeward side, an open surface on section 1 will produce a higher pressure difference between the room and its surrounding.

The highest pressure distribution is received at the windward side of the first and second buildings. Therefore, drag forces at the windward side of these buildings should be taken into consideration on the building design. Similarly to the discussion

in Chapter Four, adding several posts at the windward side will minimise the wind load effects on the building surfaces.

Turbulent kinetic energy plots are presented in Figures 6.1.15 – 6.1.20. The highest turbulent kinetic energy occurs at the fourth and sixth buildings. In the two-dimensional simulations discussed in Chapter Four, the maximum turbulent kinetic energy occurred at the second building, followed by the third building. Therefore, the second row of buildings receives the highest turbulent kinetic energy, whatever the distance between buildings is. The results agree well with our suggestion above, indicating that air momentum increases after separation. The separation point occurs at the first line of buildings (in this case at the second building), where the fluid near surfaces lacks sufficient momentum to overcome the pressure gradient and produces wakes at the separation regions. The interesting phenomenon is the maximum turbulent kinetic energy moves from the fourth to the sixth building, indicating the changes of direction at the separation region, especially at the centre. After separation, the flow tends to be fully developed but it depends on the Reynolds number. This phenomenon indicates that the flow at the centre is not fully developed turbulent, according to our result in Chapter Five, Figures 5.2.37-5.2.40 which showed a strong correlation between pressure distribution and turbulent kinetic energy. A greater pressure distribution usually produces a greater turbulent kinetic energy. Since the flow produces high turbulent kinetic energy but low pressure, it is suggested that the flow at the centre is not fully developed turbulent.

This phenomenon can also be understood from the streamline plots. It is clear that there is a high eddy vortex at the windward side of the fourth building which tends to produce higher turbulent kinetic energy. Turbulent kinetic energy on the sixth building also increases because of the jet flows merging and producing high energy at the windward side of the sixth building. Since the highest turbulent kinetic energy occurs at the fourth building, the flow is not turbulent at the centre.

As seen in Figure 6.1.15, the turbulent kinetic energy on the first building is relatively high at the windward side, especially on section 1 and near the ground. Therefore, a strong foundation is needed to minimise these effects on building surfaces.

On the second building, it also clear that the turbulent kinetic energy near the ground is relatively high, as well as in the third building. These are clear in Figures

6.1.16 and 6.1.17. Similarly to the first building, the second and third buildings should be designed with a strong foundation.

The turbulent kinetic energy on the fourth building is relatively high at the roof level, on section 1. According to the pressure distribution, an open surface on section 1 is a good strategy to minimise this turbulent kinetic energy. The transition flow can be changed by increasing the surface roughness, thus reducing the critical Reynolds number. Therefore, in order to minimise the effects of turbulent energy, the surface roughness at the roof should be increased, or the distance between the second and the fourth buildings increased, at least to one and a half the reattachment length. This phenomenon was discussed in Chapter Four.

Turbulent kinetic energy on the fifth building is presented in Figure 6.1.19 where it shows a greater value at the roof top. At the fourth building, the turbulent kinetic energy is very high at the windward side. Although the distance between the first and the fourth buildings and the third and the fifth buildings is the same, it can be seen that the maximum value of both buildings occurs on section 1 (near the centre). This indicates that the separation width at the centre is affected by the wind direction through the passages in the first line of buildings. A method to reduce the effects of turbulent kinetic energy on the building surface is by moving the surface from section 1 to section 2, since it appears that the turbulent kinetic energy on section 2 is much lower than on section 1.

Turbulent kinetic energy on the sixth building has a high value at the leeward roof. From Figure 6.1.20, it can be seen that the greatest turbulent kinetic energy occurs on section 1. Since the turbulent kinetic energy on section 4 is much lower than that on section 1, we argue that the sixth building should be moved. From the turbulent kinetic energy plot, it can also be seen that its value at the corner between the fifth and sixth buildings is relatively high. Therefore, we propose that the sixth building is moved away from the corner (between the fifth and sixth buildings), at least one and a half the separation width at that corner.

Turbulent energy dissipation results are presented in Figures 6.1.21 – 6.1.26. The maximum turbulent energy dissipation occurs at the fourth building. Therefore, the fourth building receives the highest turbulent kinetic energy and its dissipation rate.

In Figure 6.1.21, it can be seen that turbulent energy dissipation near the ground is relatively high on the first building. Since pressure distribution is low but turbulent kinetic and its dissipation rate are relatively high, one method to reduce these effects

is by using a floating foundation. In this case, the surface area near the ground is minimised, therefore both momentum and energy will be reduced. The same condition occurs on the second building, where the turbulent energy dissipation is relatively high near the ground. In order to reduce turbulent kinetic energy and its dissipation near the ground, a floating foundation should be considered.

As presented in Figure 6.1.23, the turbulent energy dissipation near the ground is also relatively high in the third building. Similarly to the first and second buildings, a floating foundation should be considered in order to minimise the effects of turbulent kinetic energy and its dissipation rate. Therefore, all buildings in the first line should be designed with floating foundations.

As described above, the turbulent energy dissipation at the windward side of the fourth building is the highest one. The turbulent energy dissipation on section 1 is relatively high at the windward roof, but low near the ground. Therefore, the distance to the centre should be increased in order to minimise the effects of energy dissipation on the fourth building.

From the pressure distribution, turbulent kinetic energy and its dissipation rate, it can be stated that the distance to the centre should be increased by moving the fourth building to a distance where the two flows -at the centre- merge, the so-called reattachment point. At this point, the pressure distribution reaches the minimum and both turbulent kinetic energy and dissipation rate become very low. Therefore, by placing the fourth building after the reattachment point the effects of wind loads due to pressure distribution and energy can be minimised. The fourth building does not need a floating foundation since these values become low.

Turbulent energy dissipation on the fifth building is presented in Figure 6.1.25. It can be seen that the turbulent energy dissipation is relatively high near the ground, on section 4. This indicates that the fifth building should have a strong foundation on this section. Similar to the fourth building, we suggest that by moving the fifth building after the reattachment length, the effects of turbulent energy dissipation can be minimised. This procedure will also reduce the effects of turbulent kinetic energy on the building surfaces.

Turbulent energy dissipation on the sixth building is also high, the greatest value occurring at the leeward side of the roof. The maximum turbulent energy dissipation always occurs on section 1 but the lowest value is on section 4. Therefore, in order to reduce the pressure, turbulent kinetic energy and its dissipation rate, it is suggested to

increase the distance between the sixth building and the corner (between the fifth and sixth buildings), by at least one and a half times the separation width at the corner. The separation width is the length of the separation region before the flow merges, which depends on building shape. An object in this region will receive high momentum (turbulent kinetic energy and dissipation) but low pressure. Therefore, the distance between two buildings should not only consider the reattachment length but also the separation width. A typical building design is proposed in Figure 6.1.27. The fourth, fifth and sixth buildings are moved from their previous positions by considering the reattachment length and separation width at the centre. By changing this position , it is expected that the streamlines will change, producing a fully developed turbulent flow at the centre and reducing drag forces on the buildings.

A summary of results for pressure distribution, turbulent kinetic energy and its dissipation rate is presented in Table 6.1.1.

Table 6.1.1 A summary of results for a cluster of buildings without gate

Building number	**I**	**II**	**III**	**IV**	**V**	**VI**
Maximum pressure (Pa) position	11 windward wall	10 windward wall	9 windward wall	5.5 windward roof	8 windward wall	4.5 windward wall
Maximum turbulent kinetic energy (m^2/s^2) position	0.23 near ground	0.19 near ground	0.14 near ground	0.46 windward roof	0.28 top roof	0.42 leeward roof
Maximum turbulent energy dissipation (m^2/s^3) position	0.19 near ground	0.14 near ground	0.09 near ground	0.28 windward wall	0.09 near ground	0.15 leeward roof

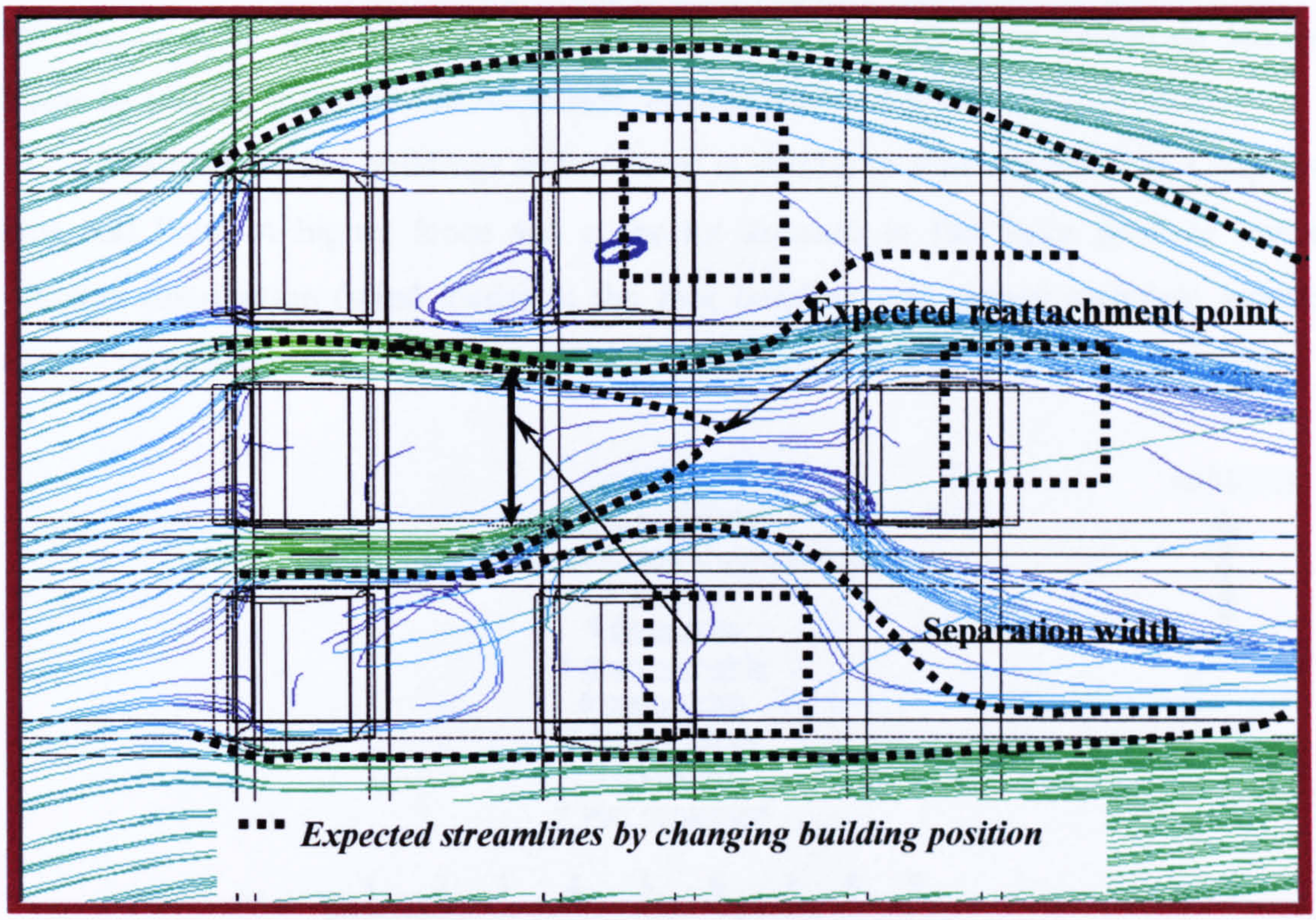

Figure 6.1.27 Expected streamlines by changing building position

6.2 The Gate of a Well to-do Family House

The gate of a well-to-do family house can be composed of brick and carved stone, but more often it consists of two simple mud pillars supporting a thick roof of thatch, and lies on the west side of the site. In Balinese manuscripts (*lontar*), it has a similar description to the gateway as presented in Figure 6.2.1, with a few differences in their meaning (Putra *et al*, 1985) [2].

6.2.1 Gate at the South-West Side

From Figure 6.2.1, it can be seen that the location of the gate will affect the occupant. This traditional meaning cannot be explained but is believed by the people of Bali. This is the reason why people in Bali carefully consider the gate's position.

In several published works, the gateway is correlated to the magic rule, therefore, in order to understand this phenomenon, the gate position is considered in the present

investigation. In this study, we start to investigate the gate of a well-to-do family house by placing it at the south-west side, as presented in Figure 6.2.2.

Distance between buildings to the fence is similar to that explained in Chapters One and Four. A higher fence and a shorter distance to the fence produce lower pressure distribution (wind loads) at the first building and reduce turbulent kinetic energy at the second and thirds line of site. Therefore, this condition is now applied.

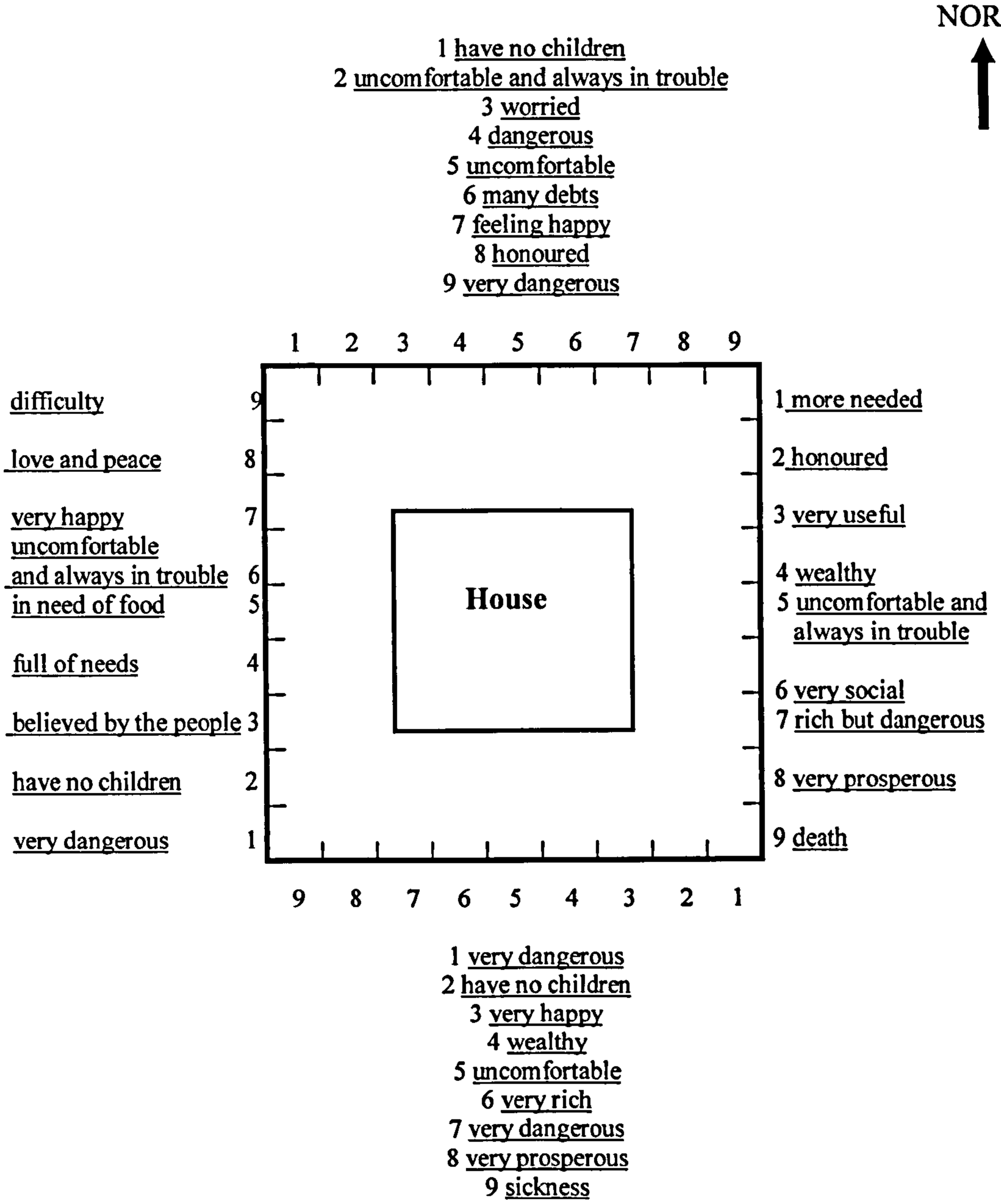

Figure 6.2.1 Traditional meaning of a gateway location

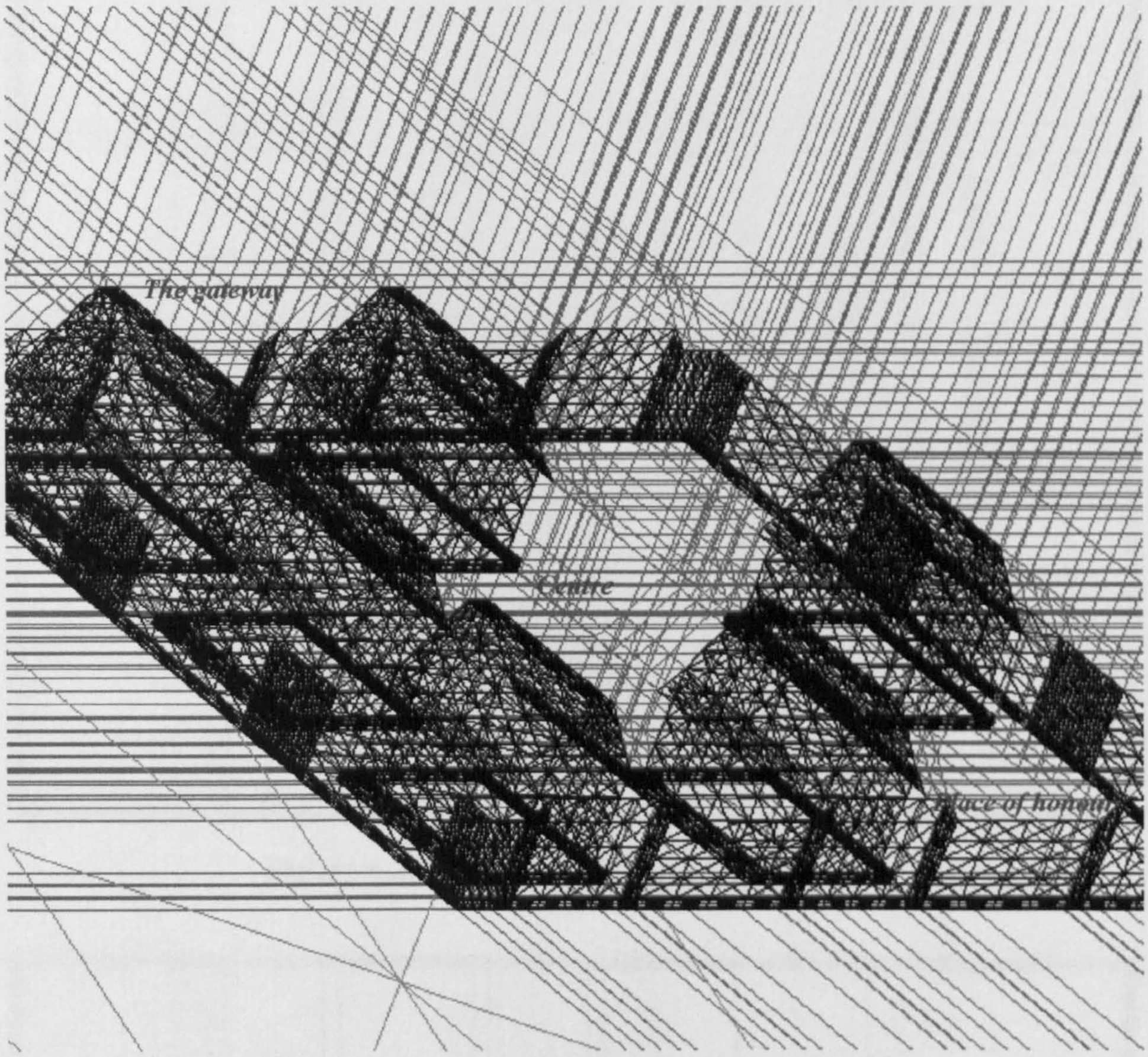

Figure 6.2.2 Side view of buildings arrangement with gate on the south-west side

6.2.1.1 Results and Discussion

In traditional Balinese architecture, the gate of a well-to-do-family house is normally built on the south-west side, therefore, we consider this position in the first simulation.

In Figure 6.2.3, it can be seen that velocity values are relatively high near the ground at the leeward side of the second building, as well as at the corner between the fifth and sixth buildings. At a height 8 m above roof, the velocity profile is uniform indicating that it is not influenced by the building configuration.

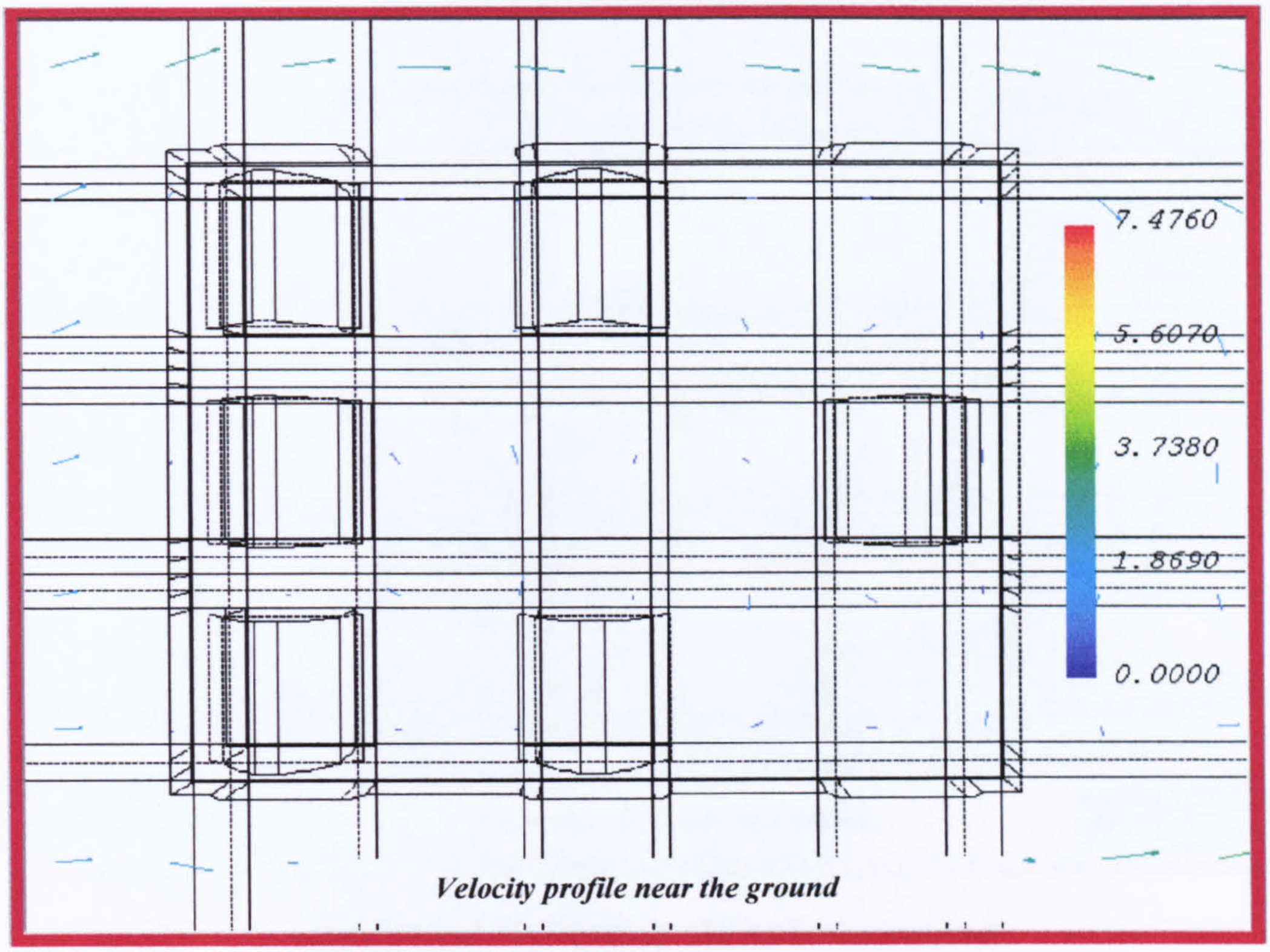

Velocity profile near the ground

Figure 6.2.3 Velocity profile near the ground

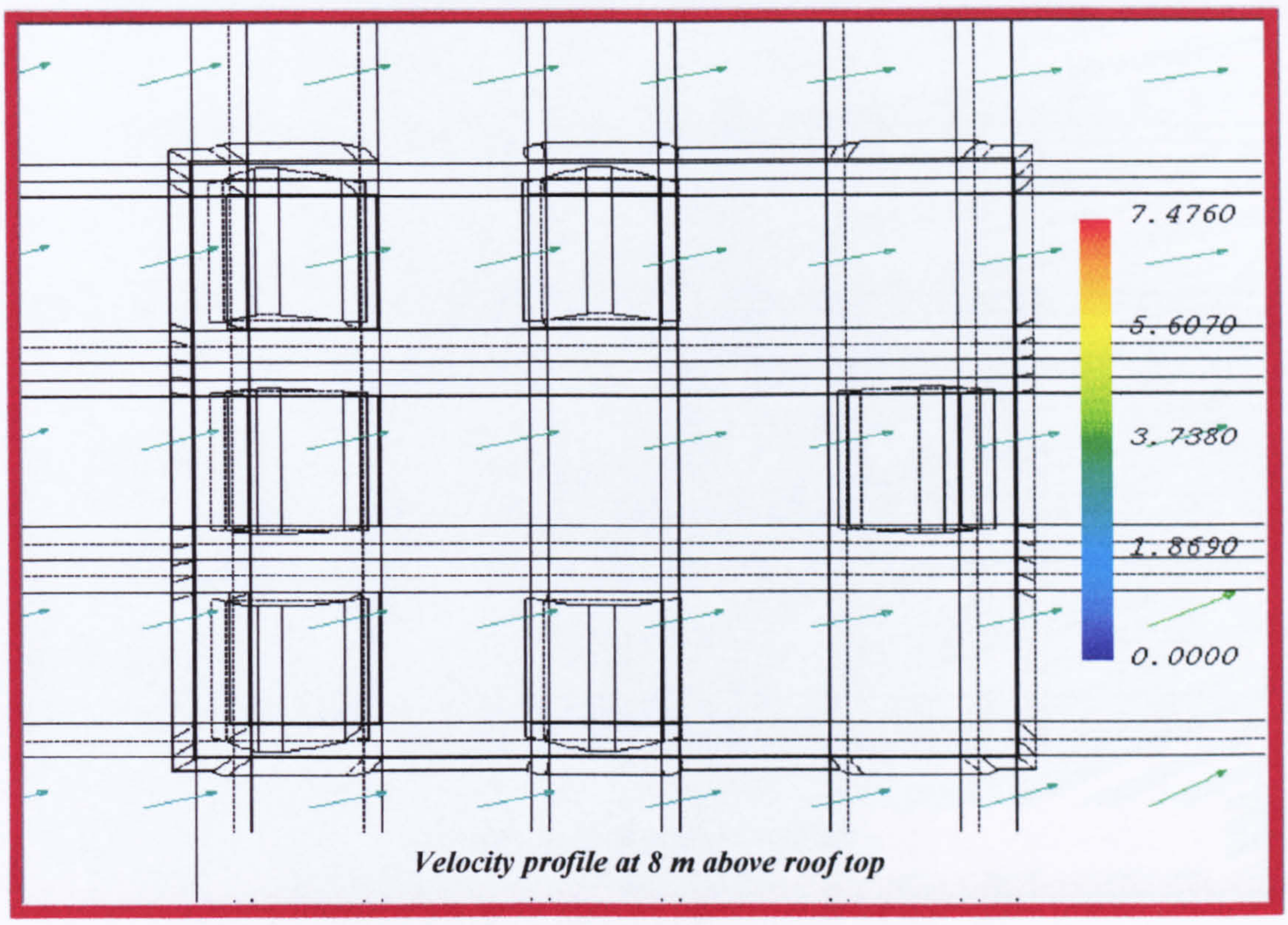

Velocity profile at 8 m above roof top

Figure 6.2.4 Velocity profile at 8 m above roof top

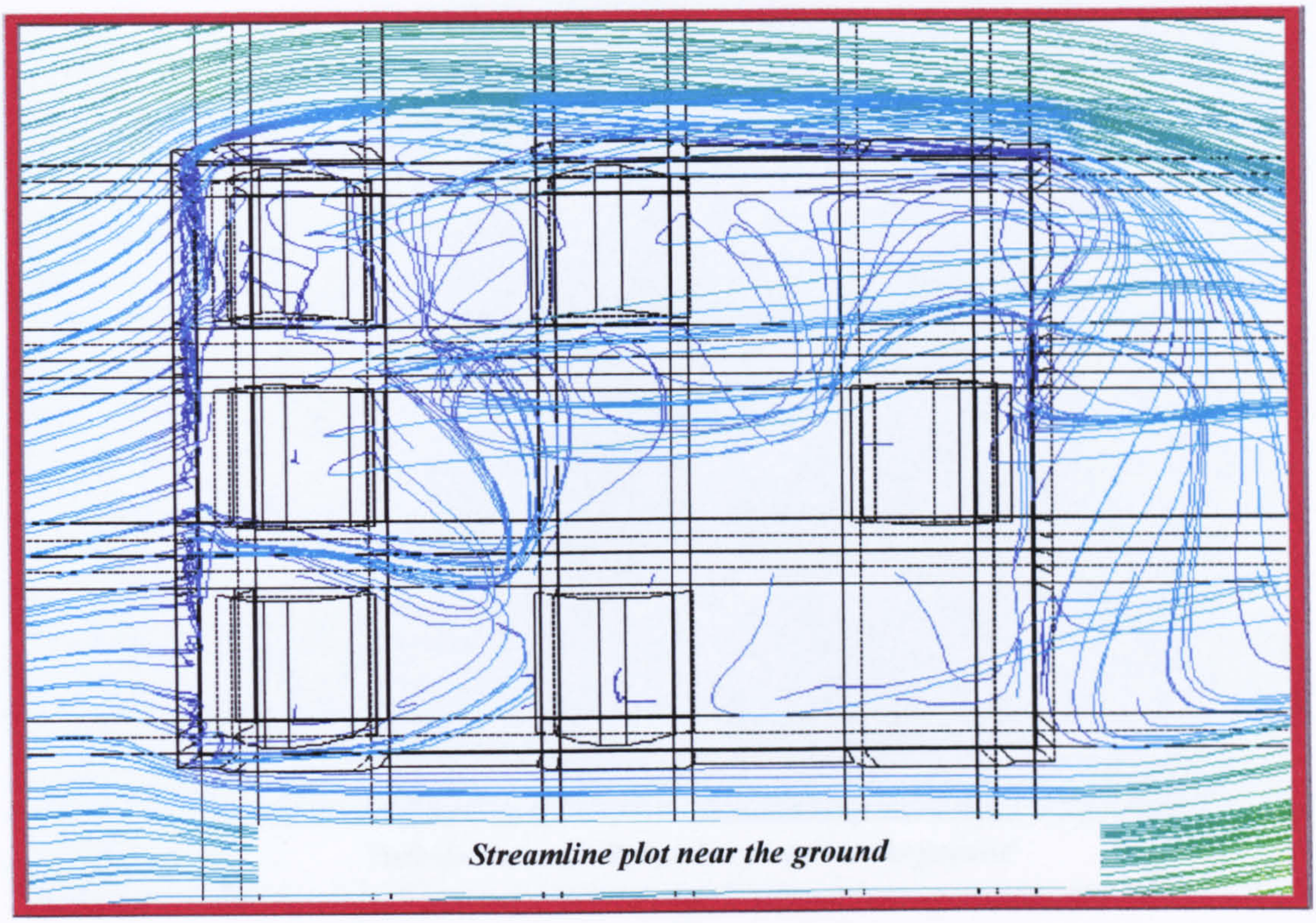

Figure 6.2.5 Streamline plot near the ground

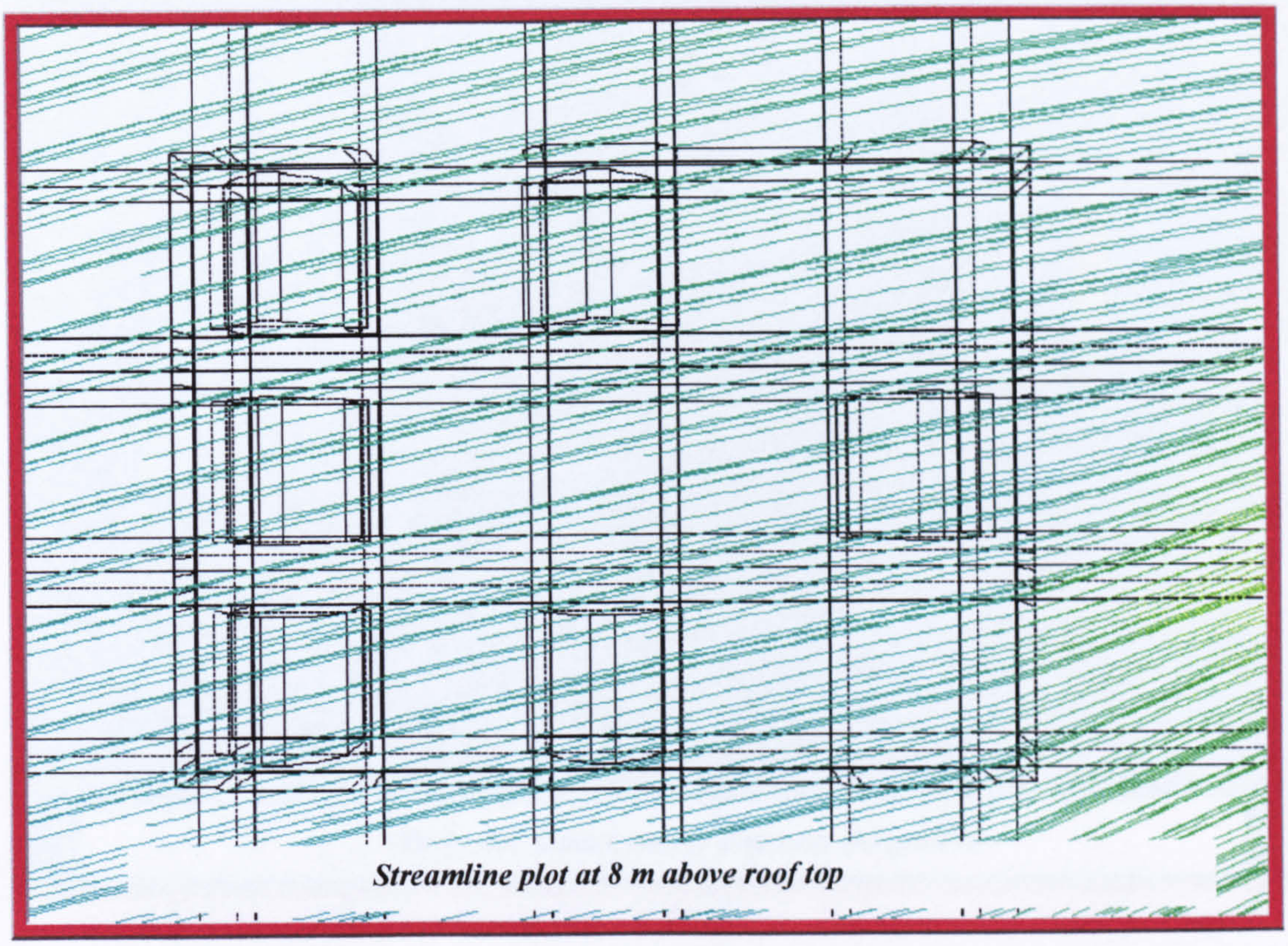

Figure 6.2.6 Streamline plot at 8 m above roof top

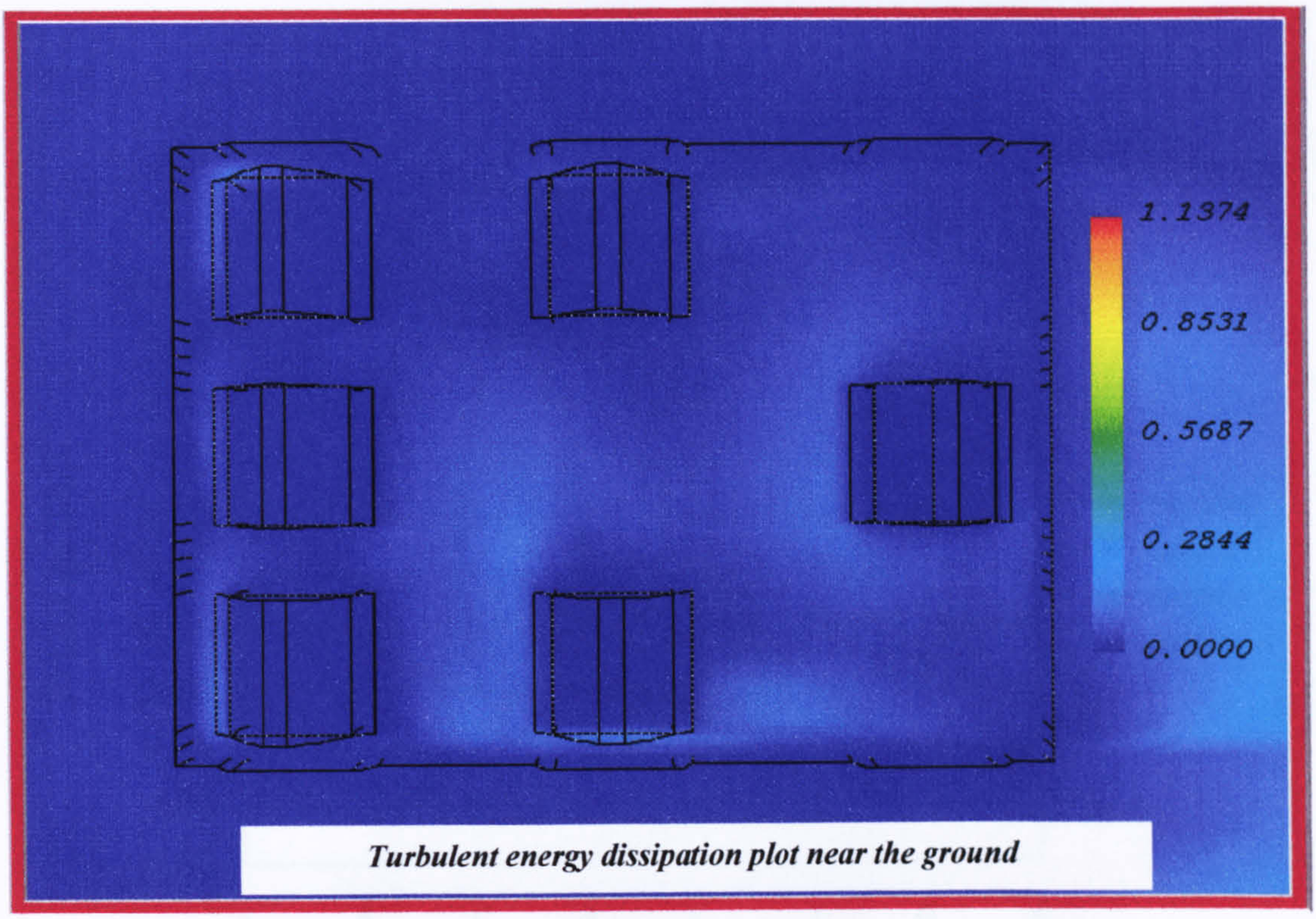

Turbulent energy dissipation plot near the ground

Figure 6.2.7 Turbulent energy dissipation plot near the ground

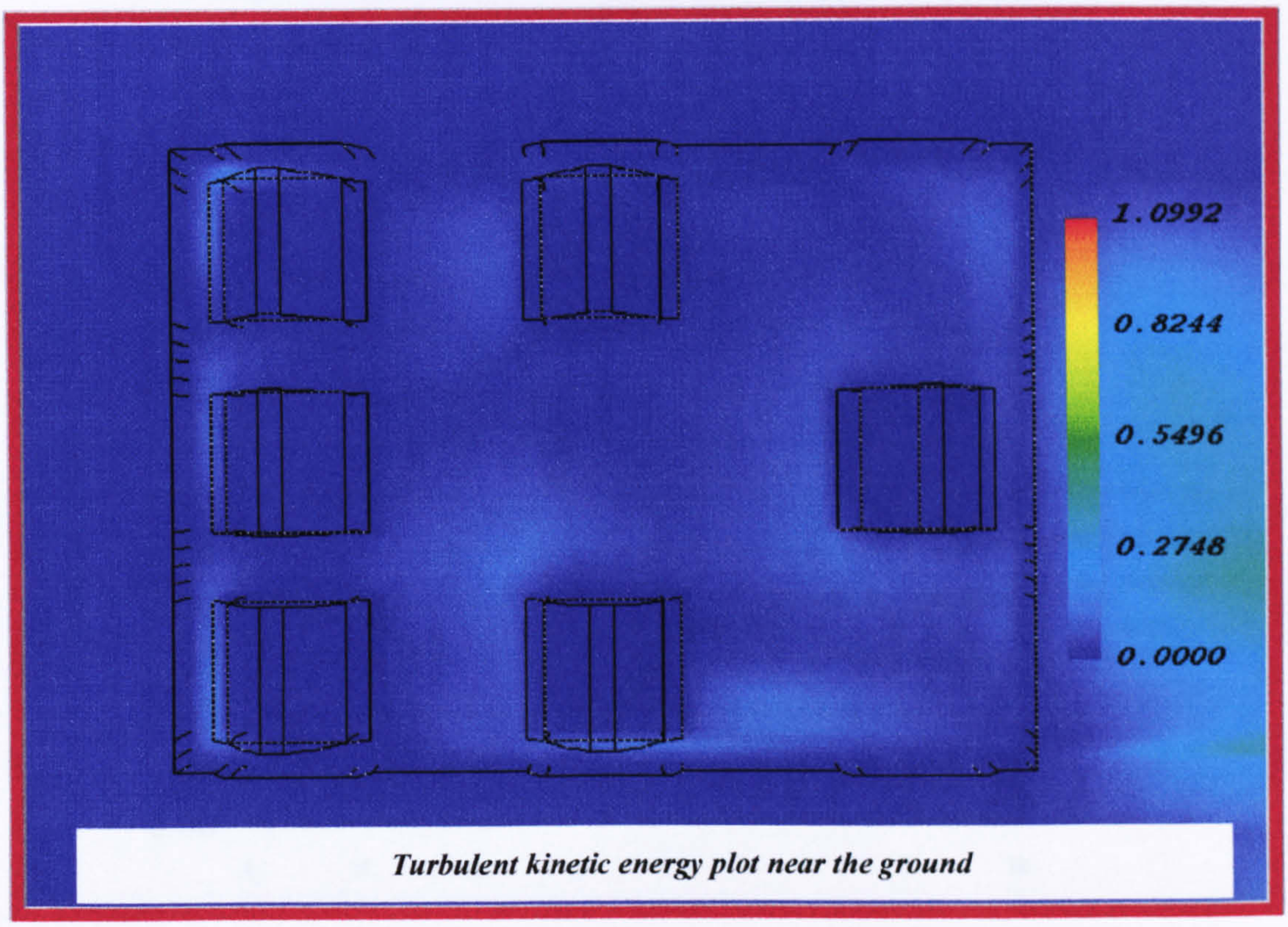

Turbulent kinetic energy plot near the ground

Figure 6.2.8 Turbulent kinetic energy plot near the ground

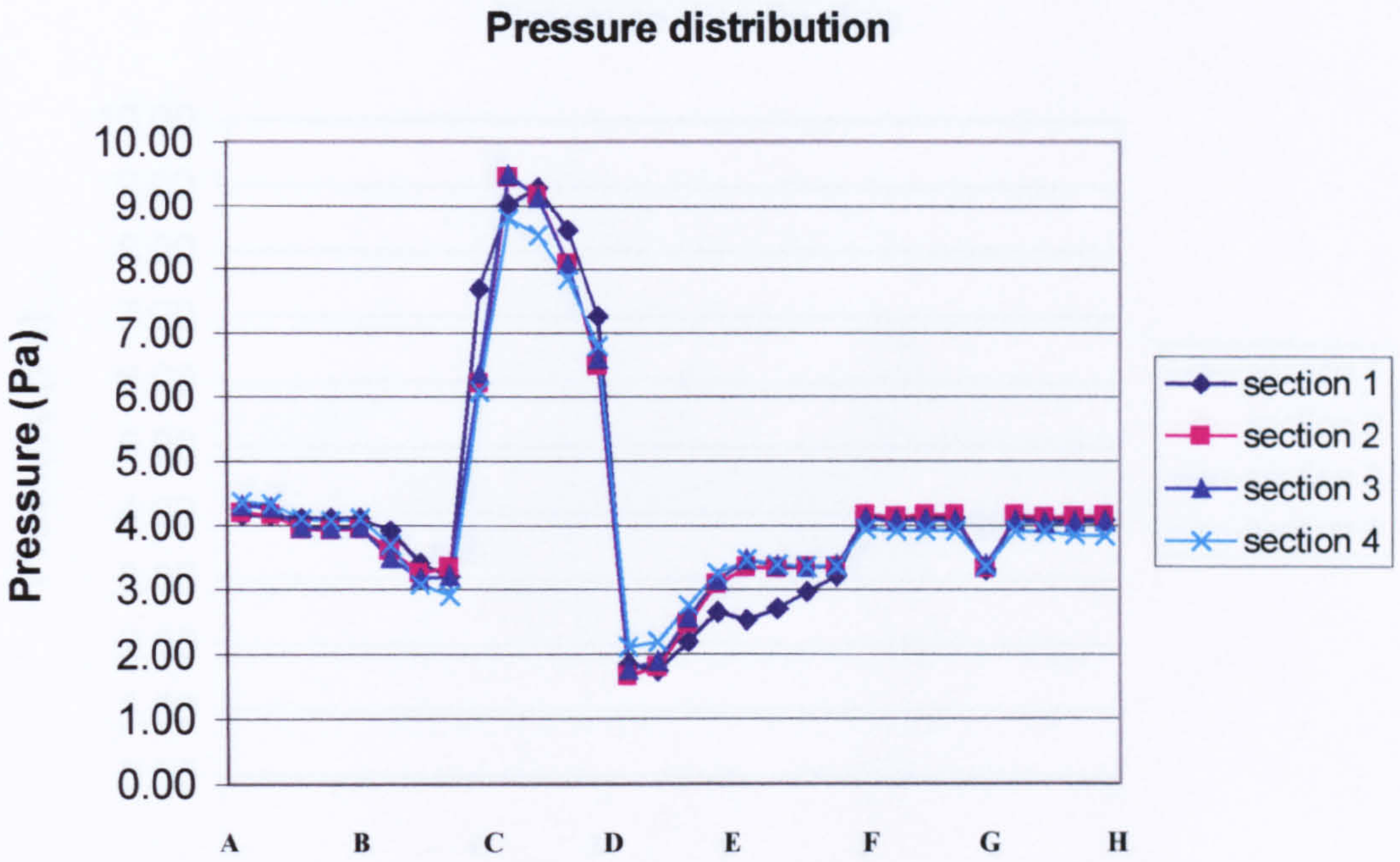

Figure 6.2.9 Pressure distribution on the first building

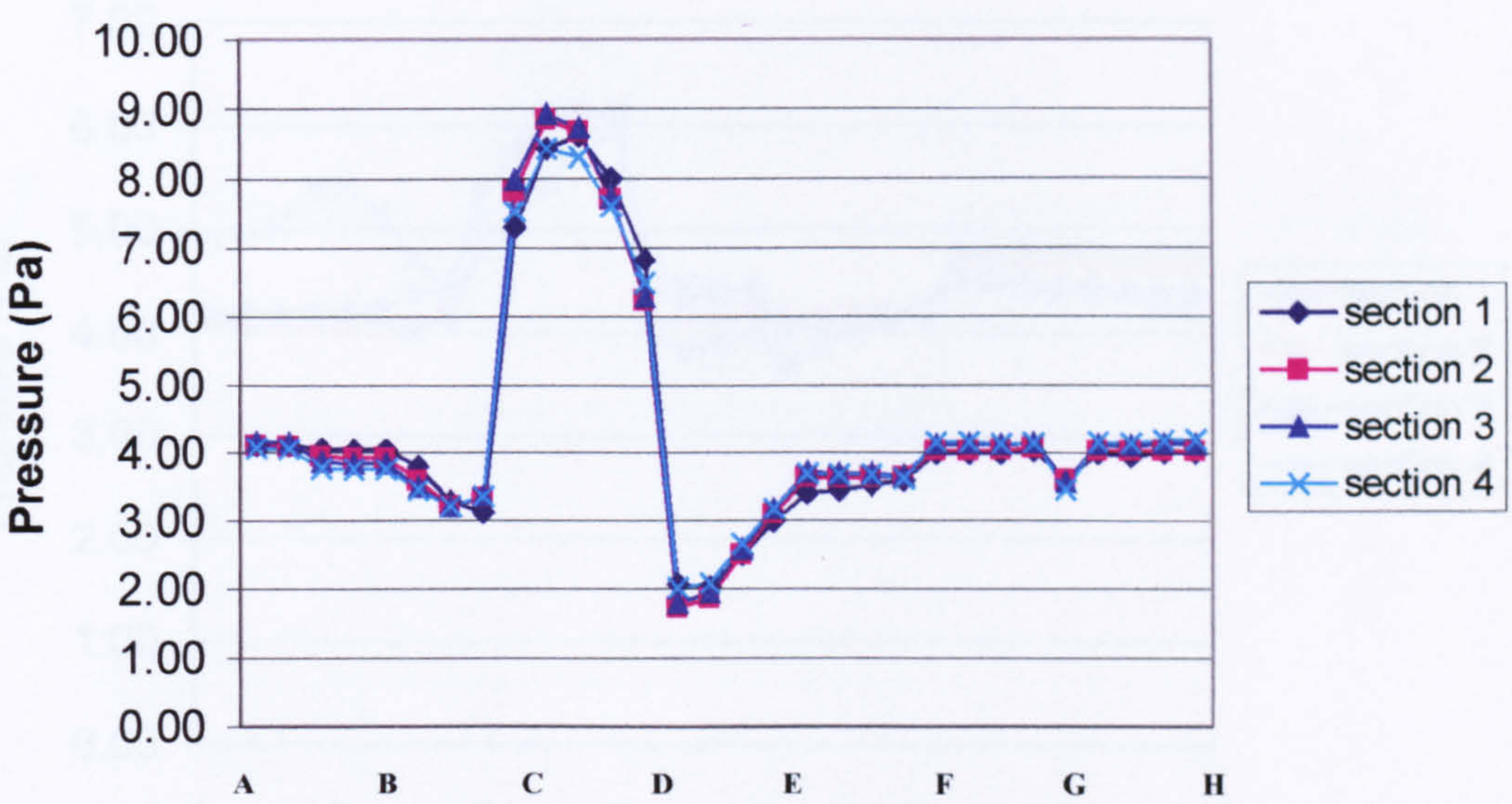

Figure 6.2.10 Pressure distribution on the second building

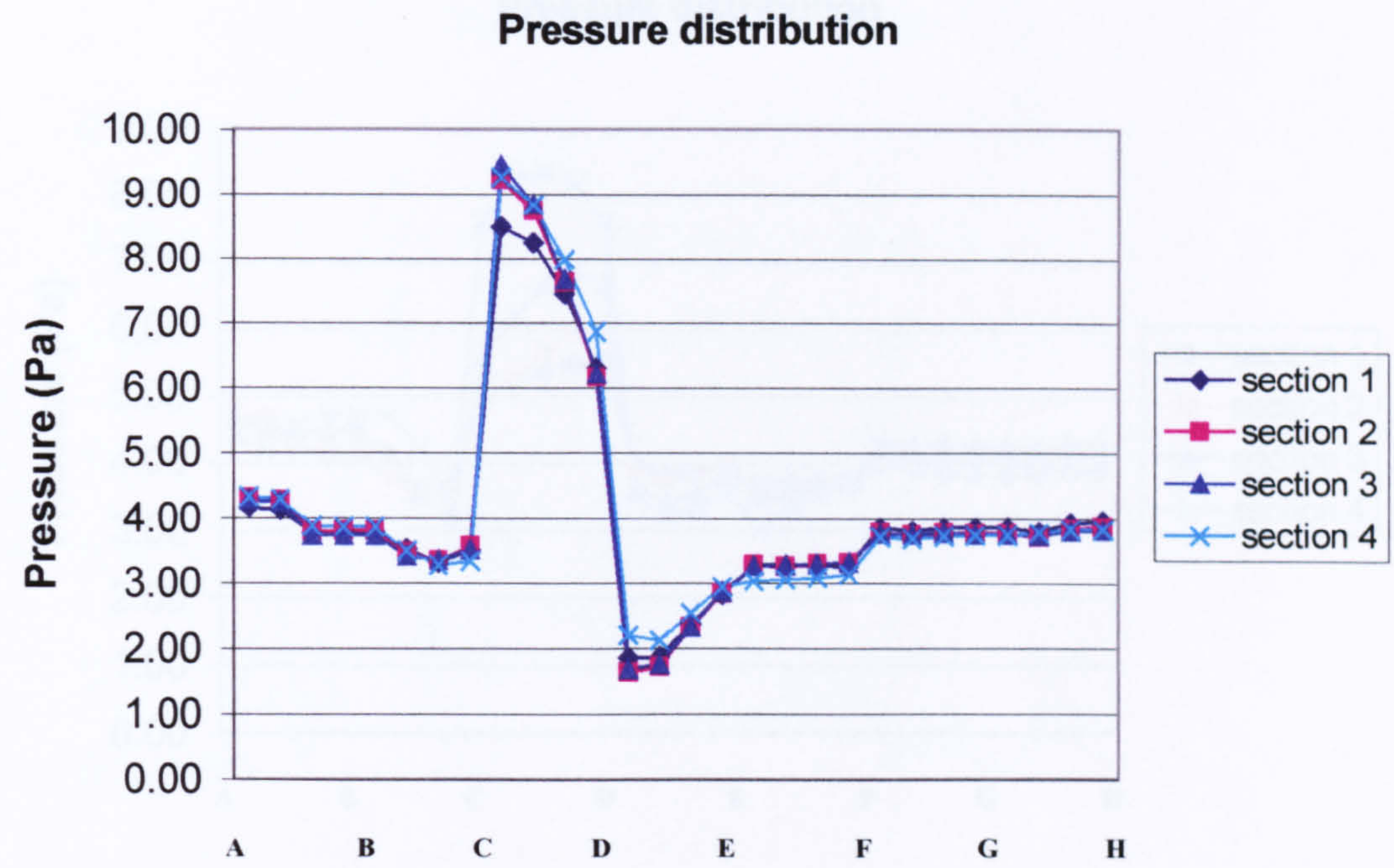

Figure 6.2.11 Pressure distribution on the third building

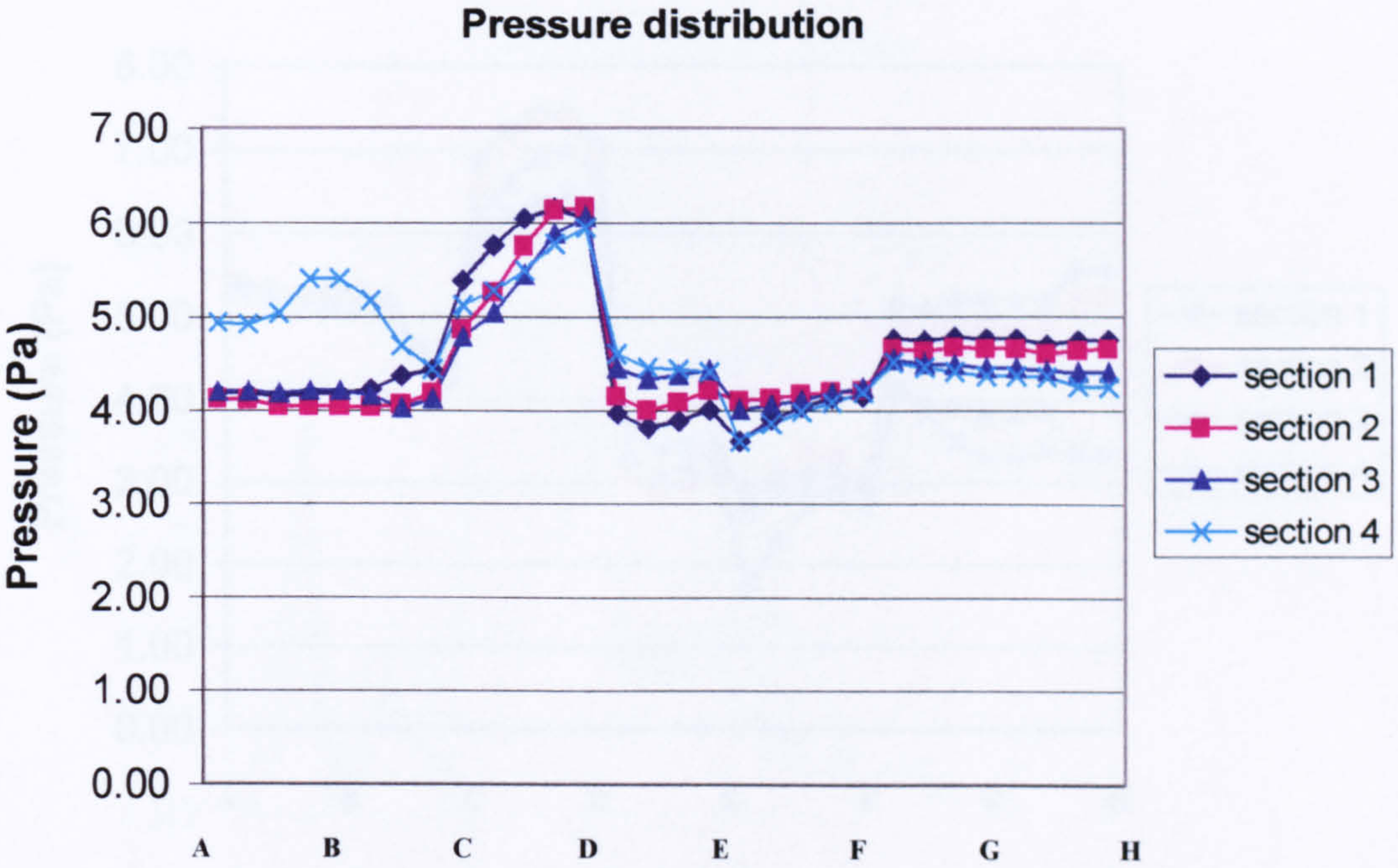

Figure 6.2.12 Pressure distribution on the fourth building

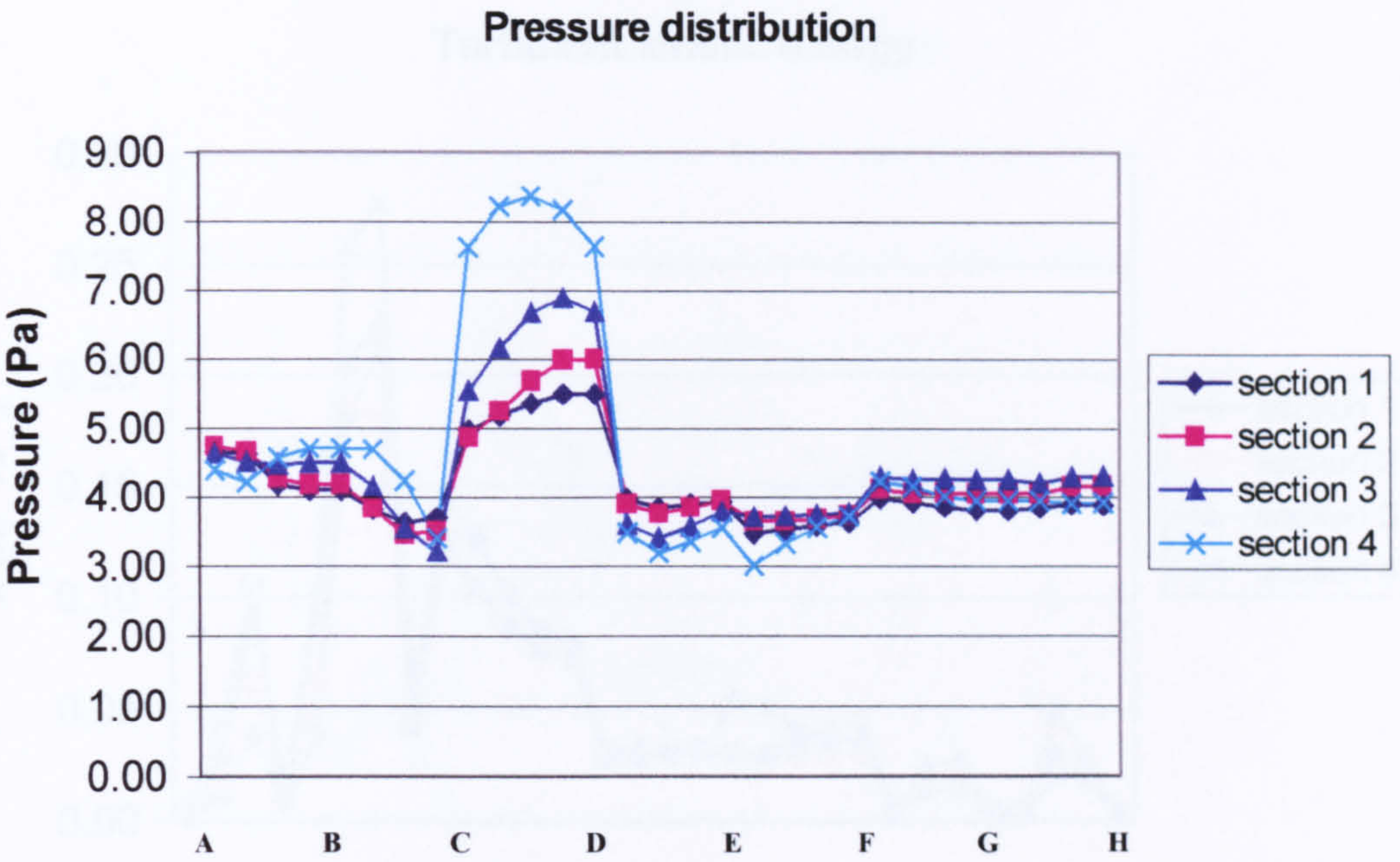

Figure 6.2.13 Pressure distribution on the fifth building

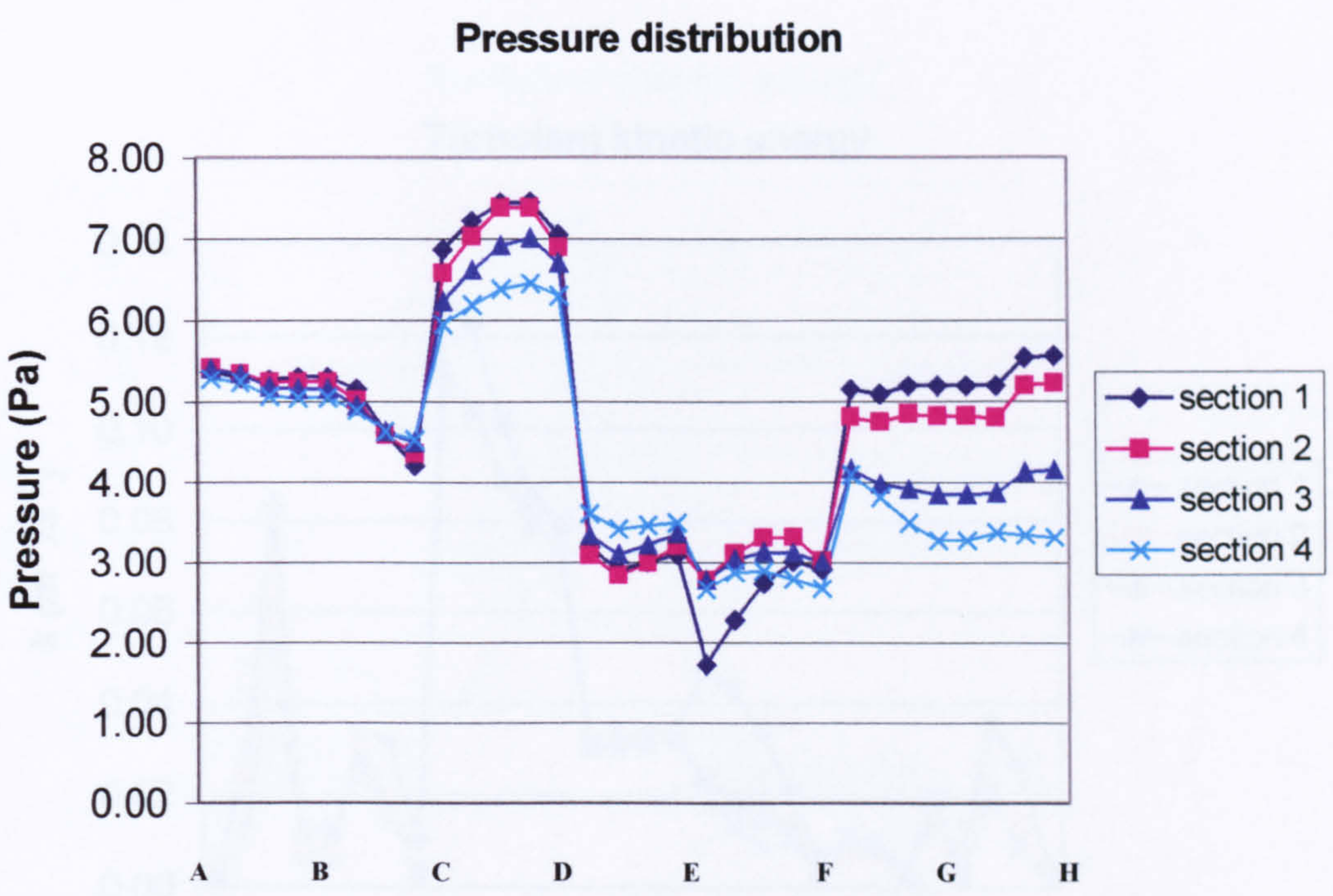

Figure 6.2.14 Pressure distribution on the sixth building

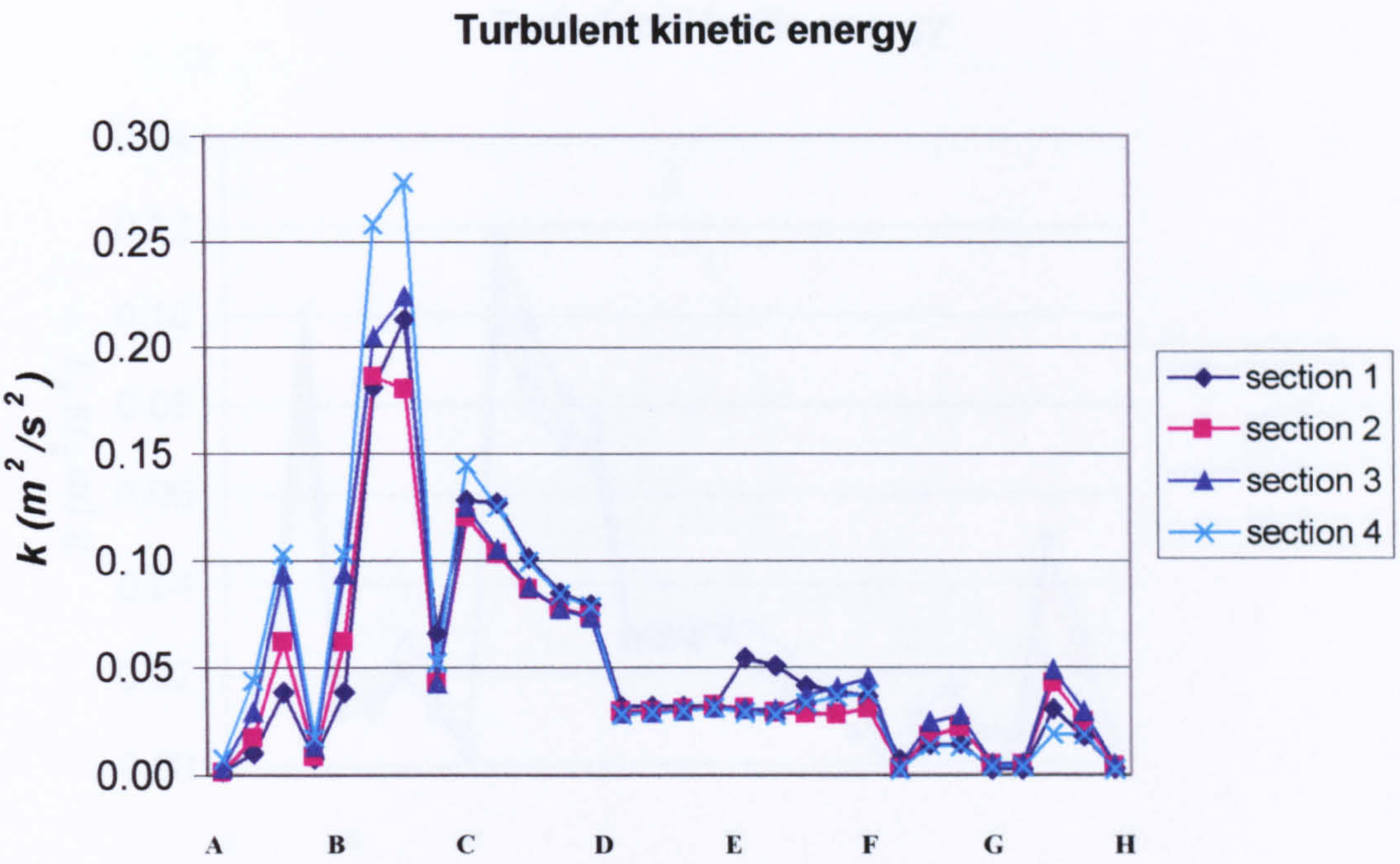

Figure 6.2.15 Turbulent kinetic energy on the first building

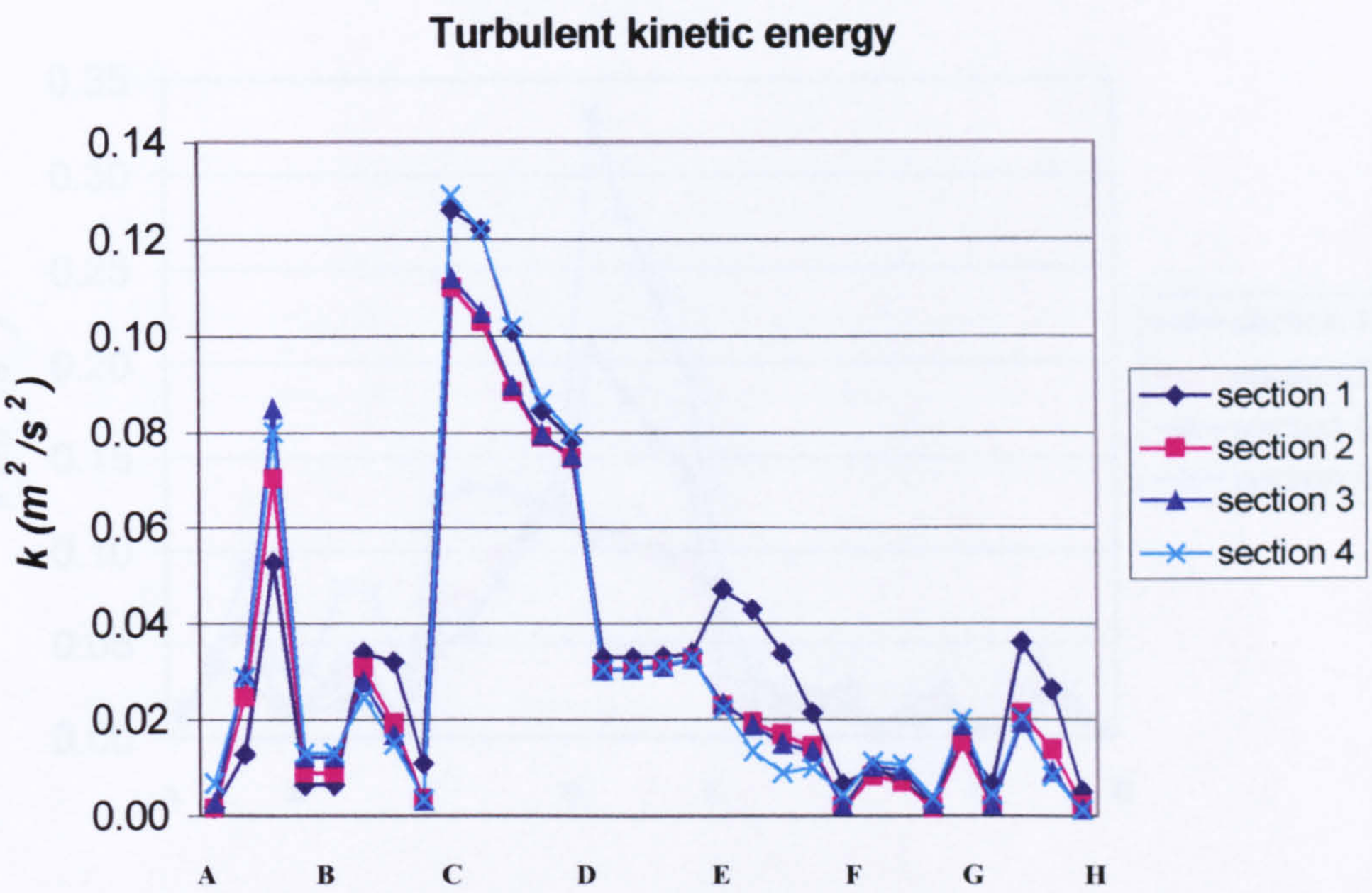

Figure 6.2.16 Turbulent kinetic energy on the second building

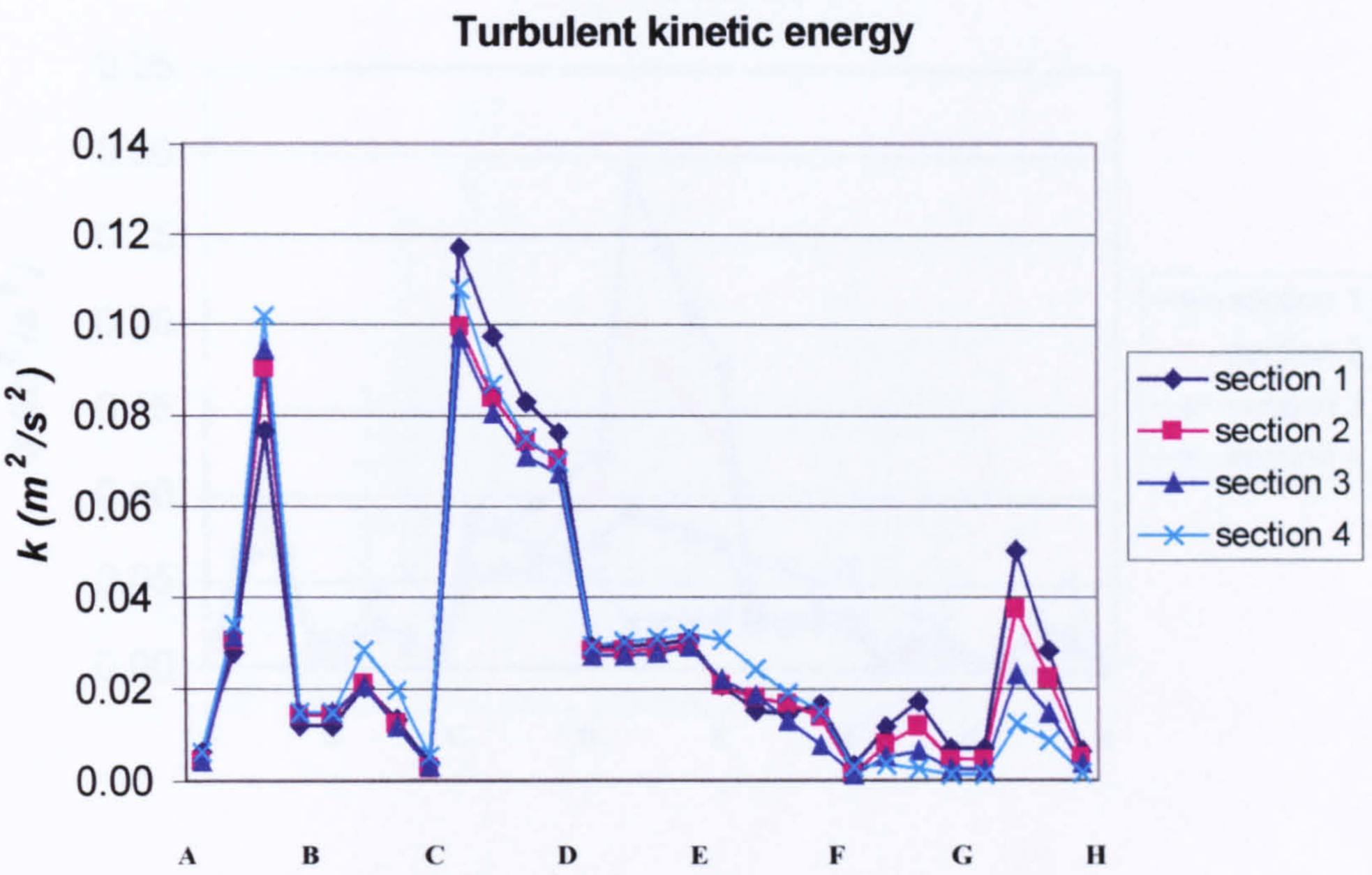

Figure 6.2.17 Turbulent kinetic energy on the third building

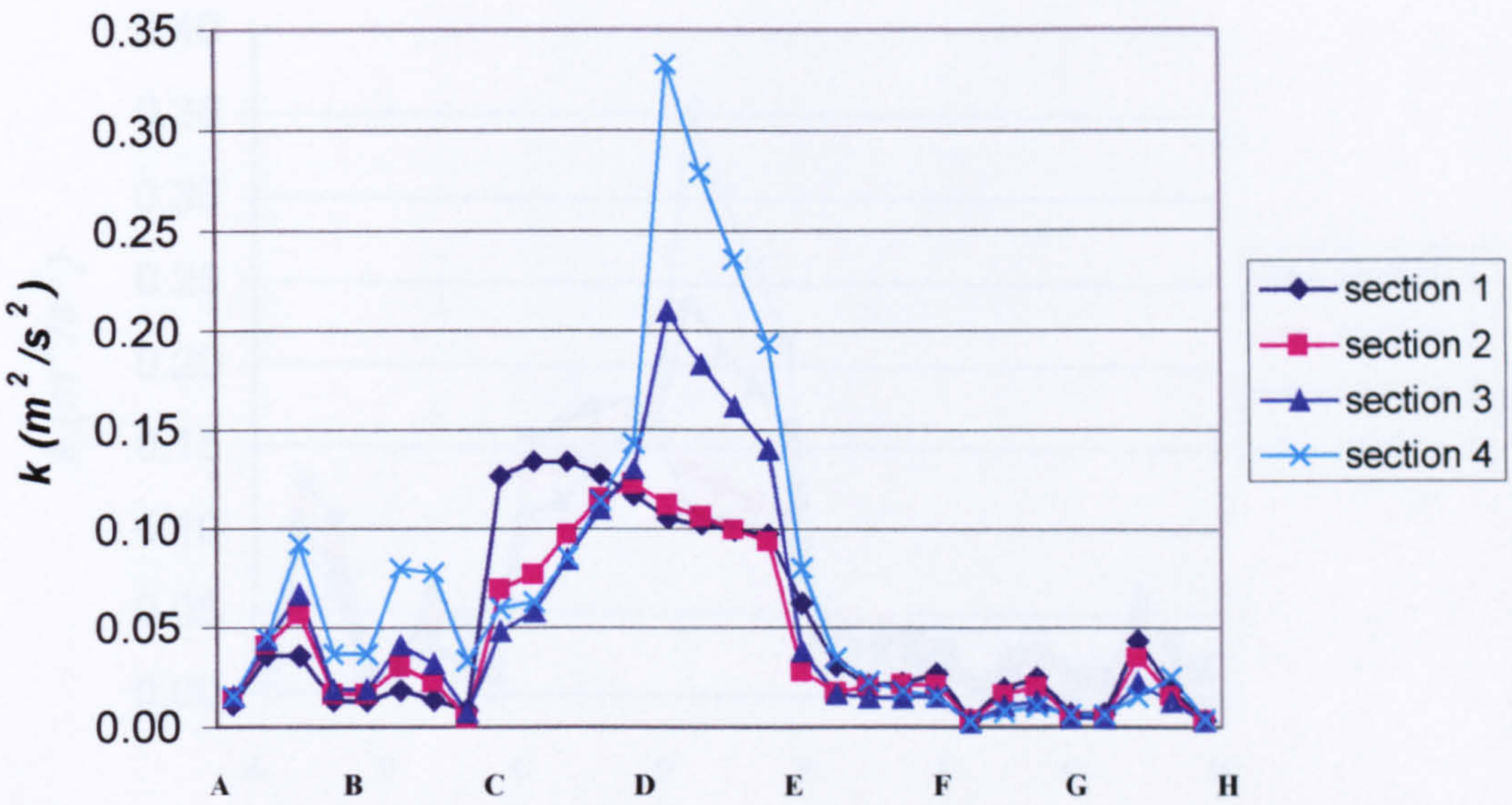

Figure 6.2.18 Turbulent kinetic energy on the fourth building

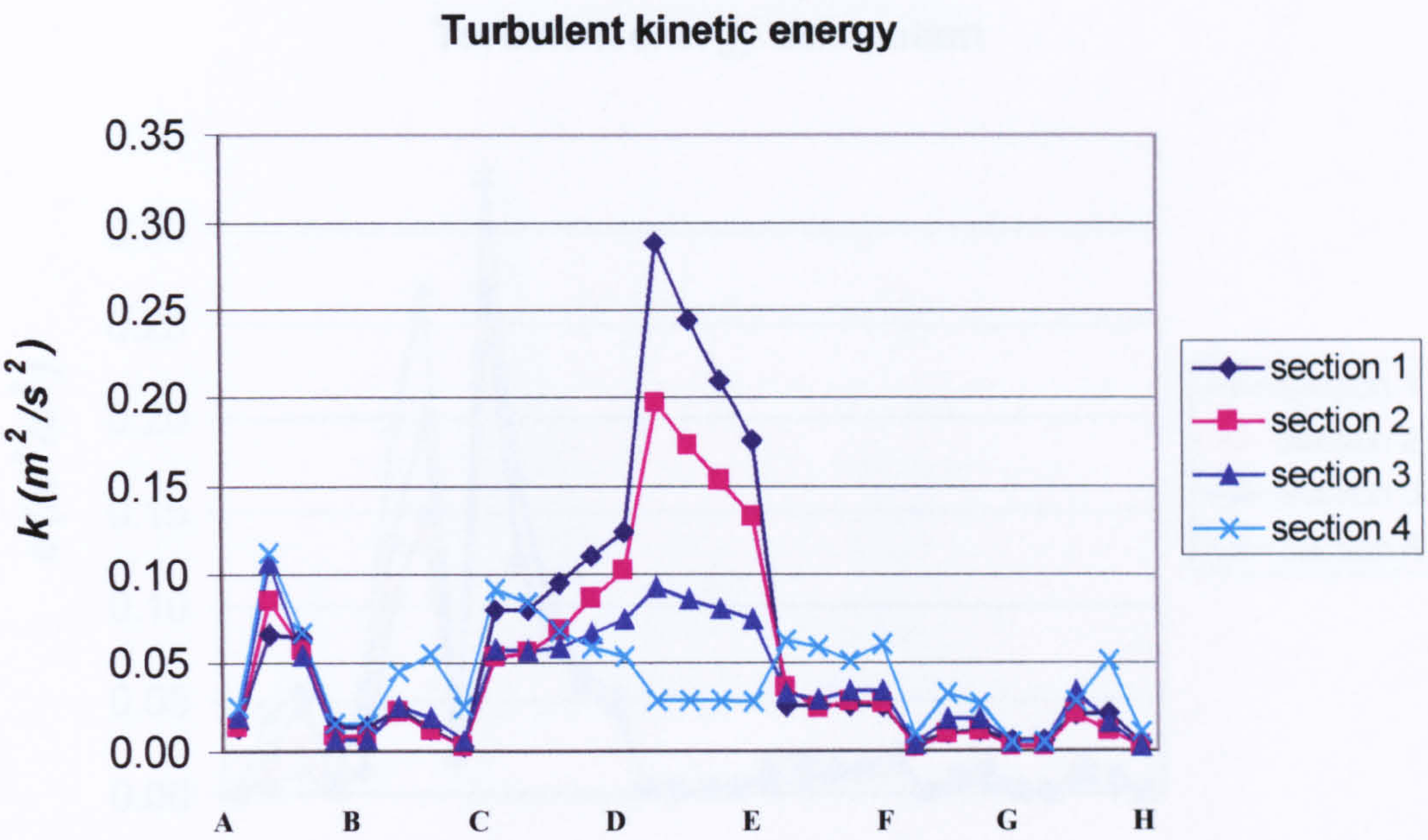

Figure 6.2.19 Turbulent kinetic energy on the fifth building

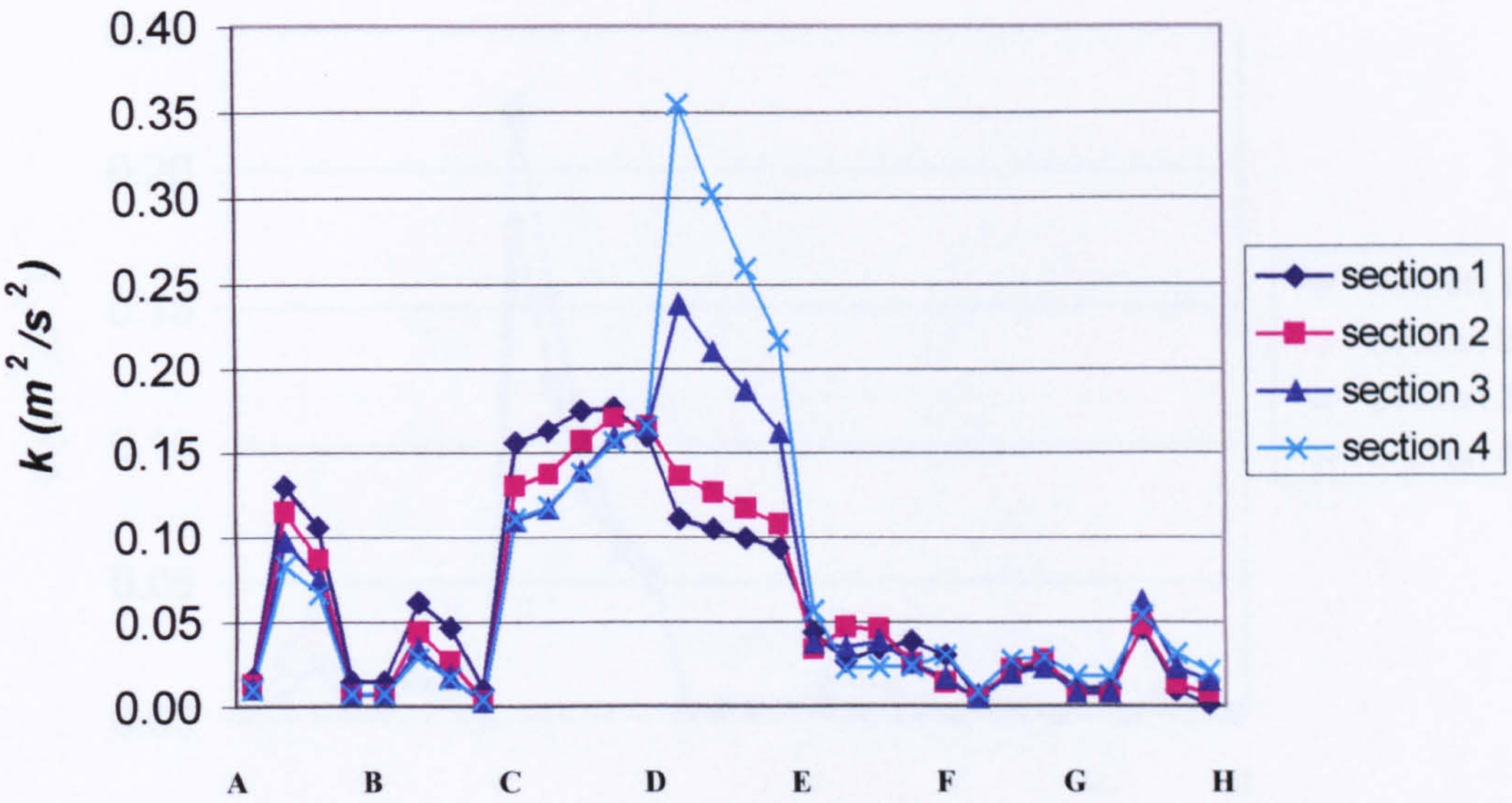

Figure 6.2.20 Turbulent kinetic energy on the sixth building

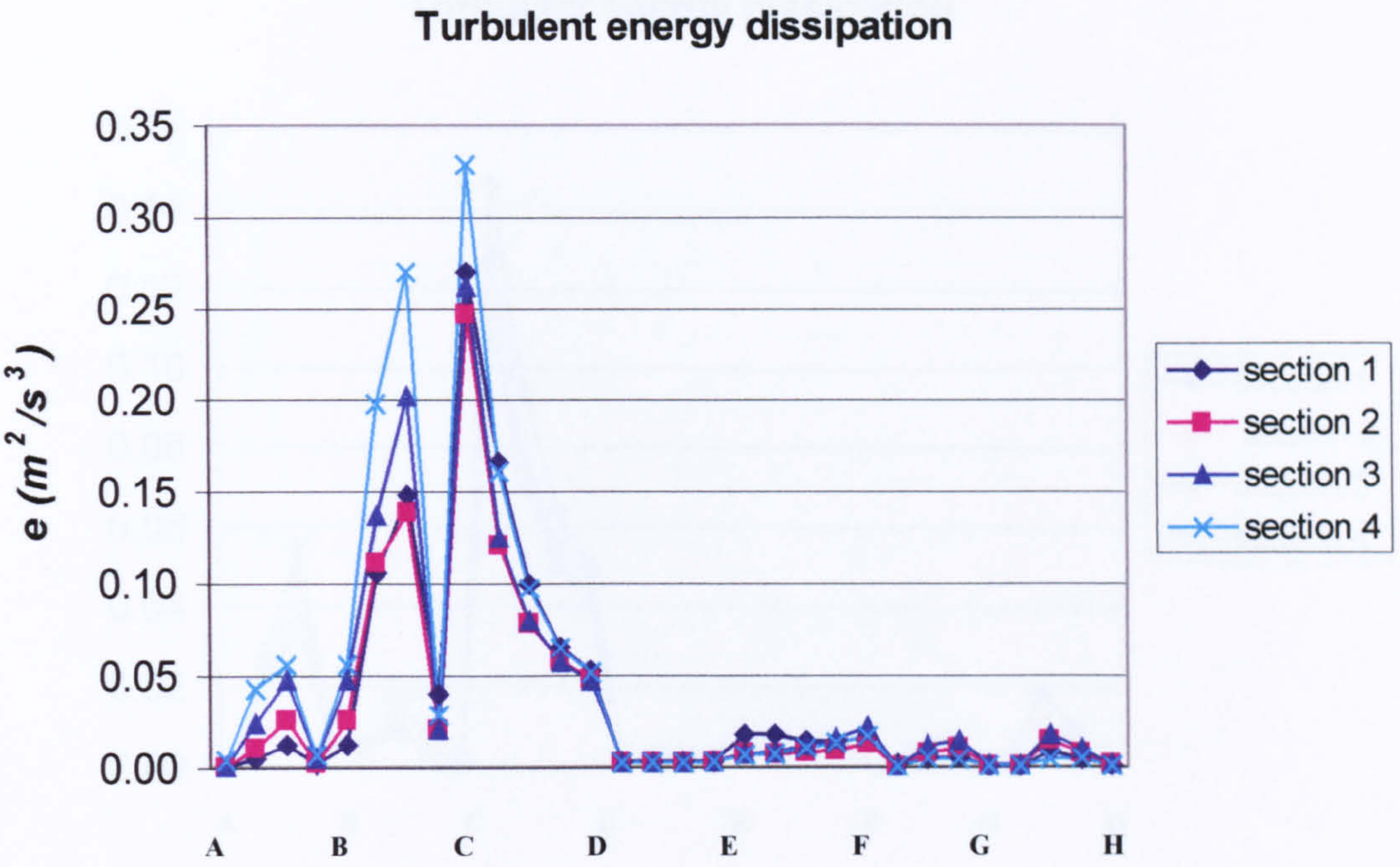

Figure 6.2.21 Turbulent energy dissipation on the first building

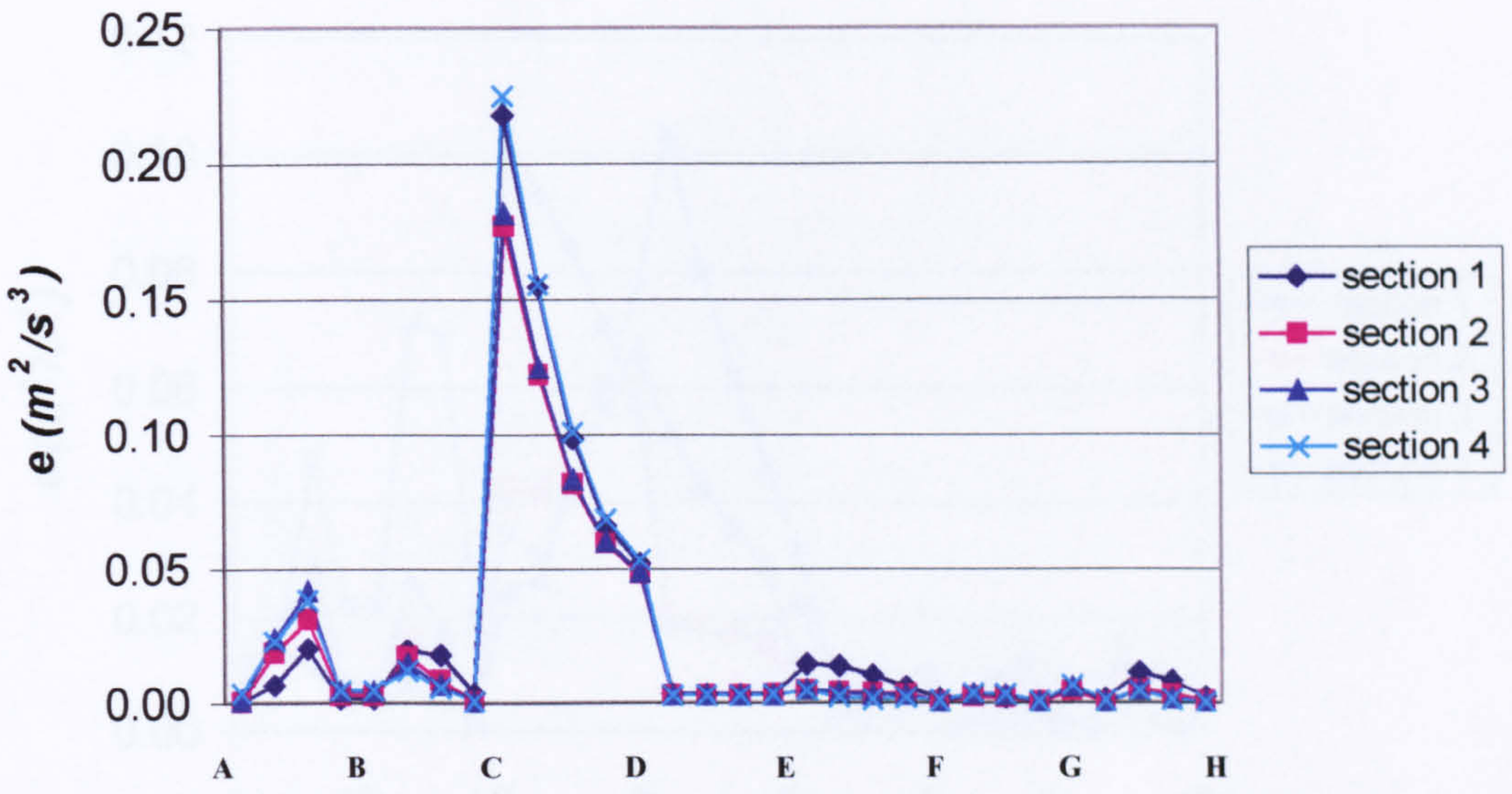

Figure 6.2.22 Turbulent energy dissipation on the second building

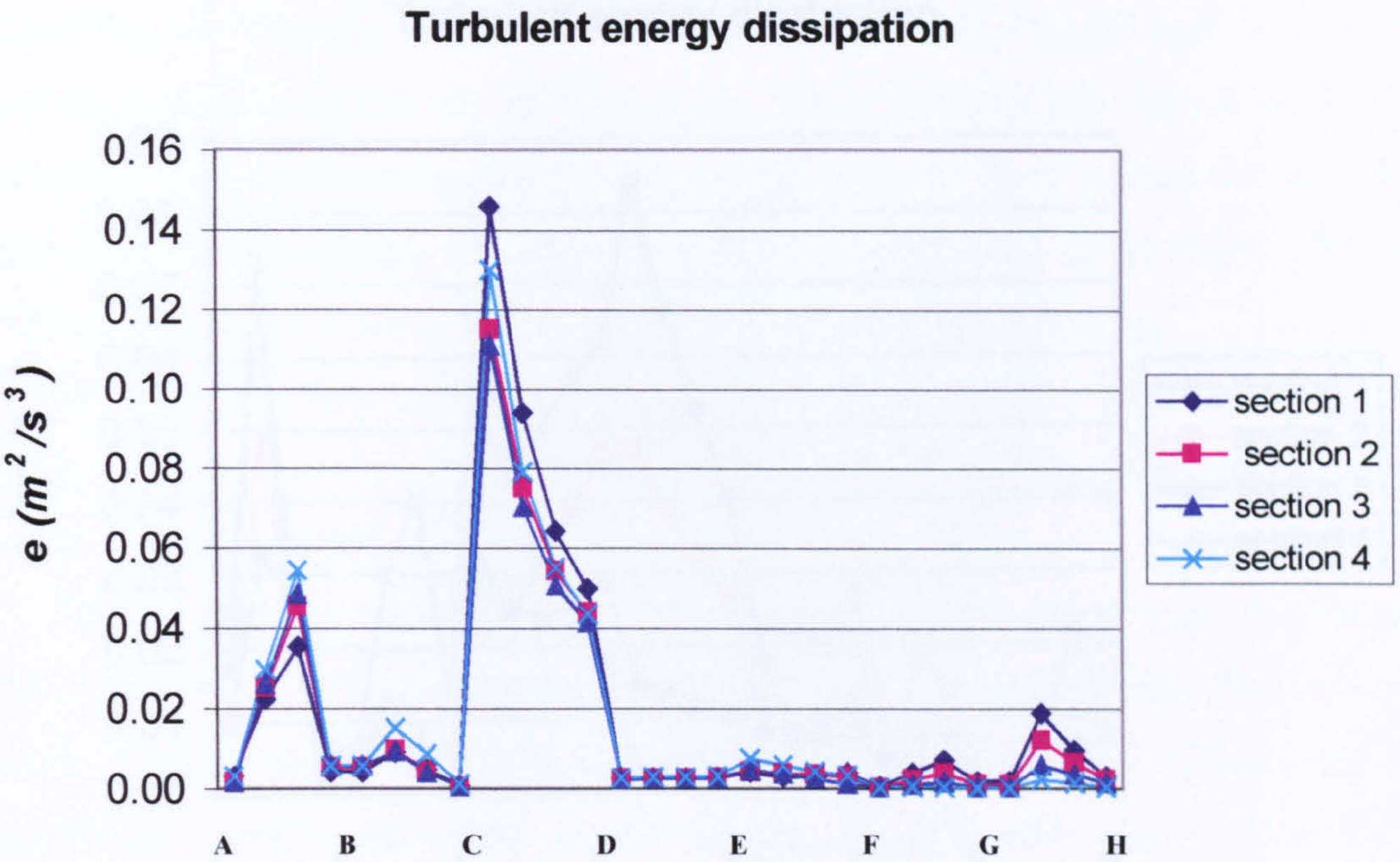

Figure 6.2.23 Turbulent energy dissipation on the third building

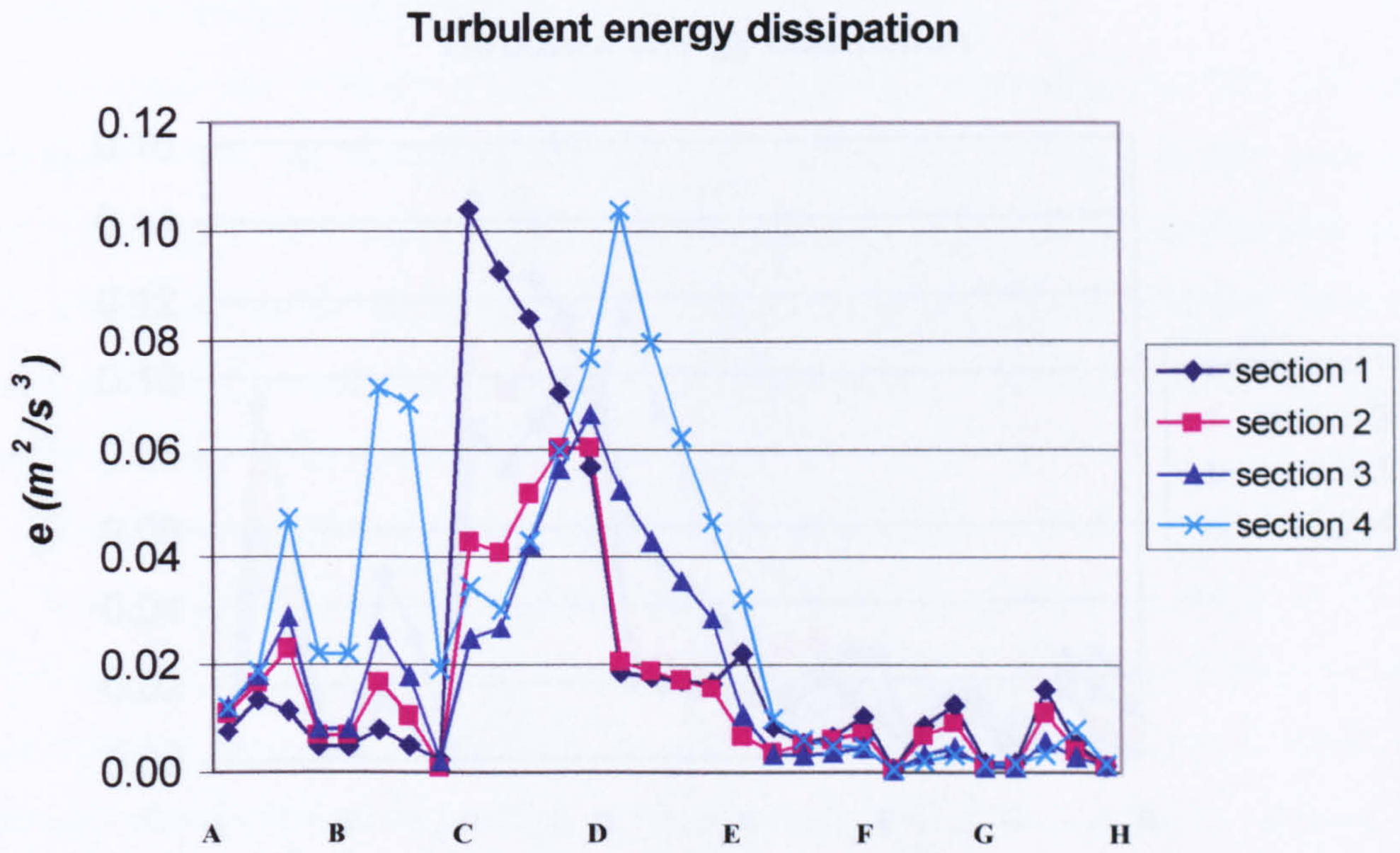

Figure 6.2.24 Turbulent energy dissipation on the fourth building

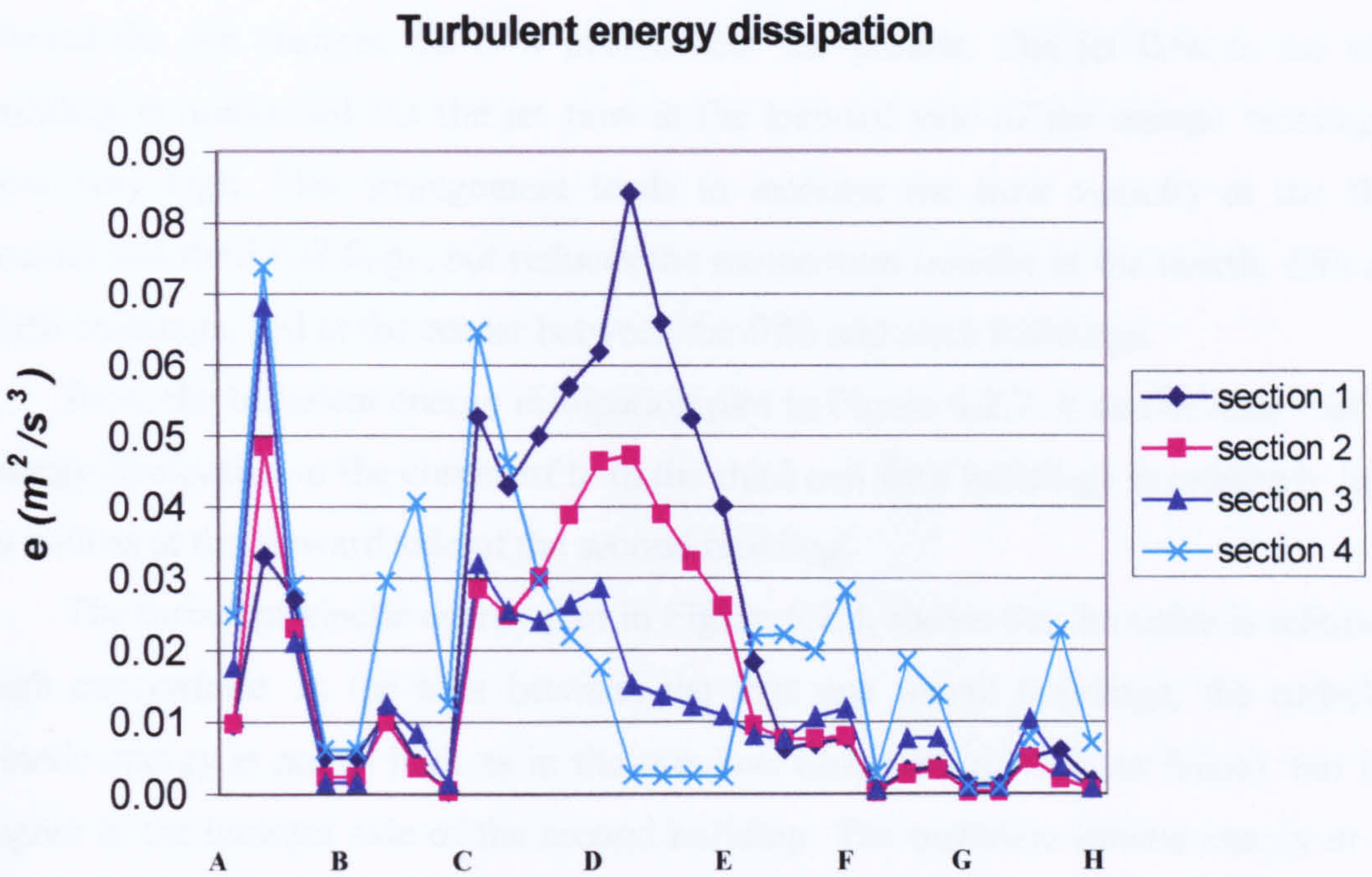

Figure 6.2.25 Turbulent energy dissipation on the fifth building

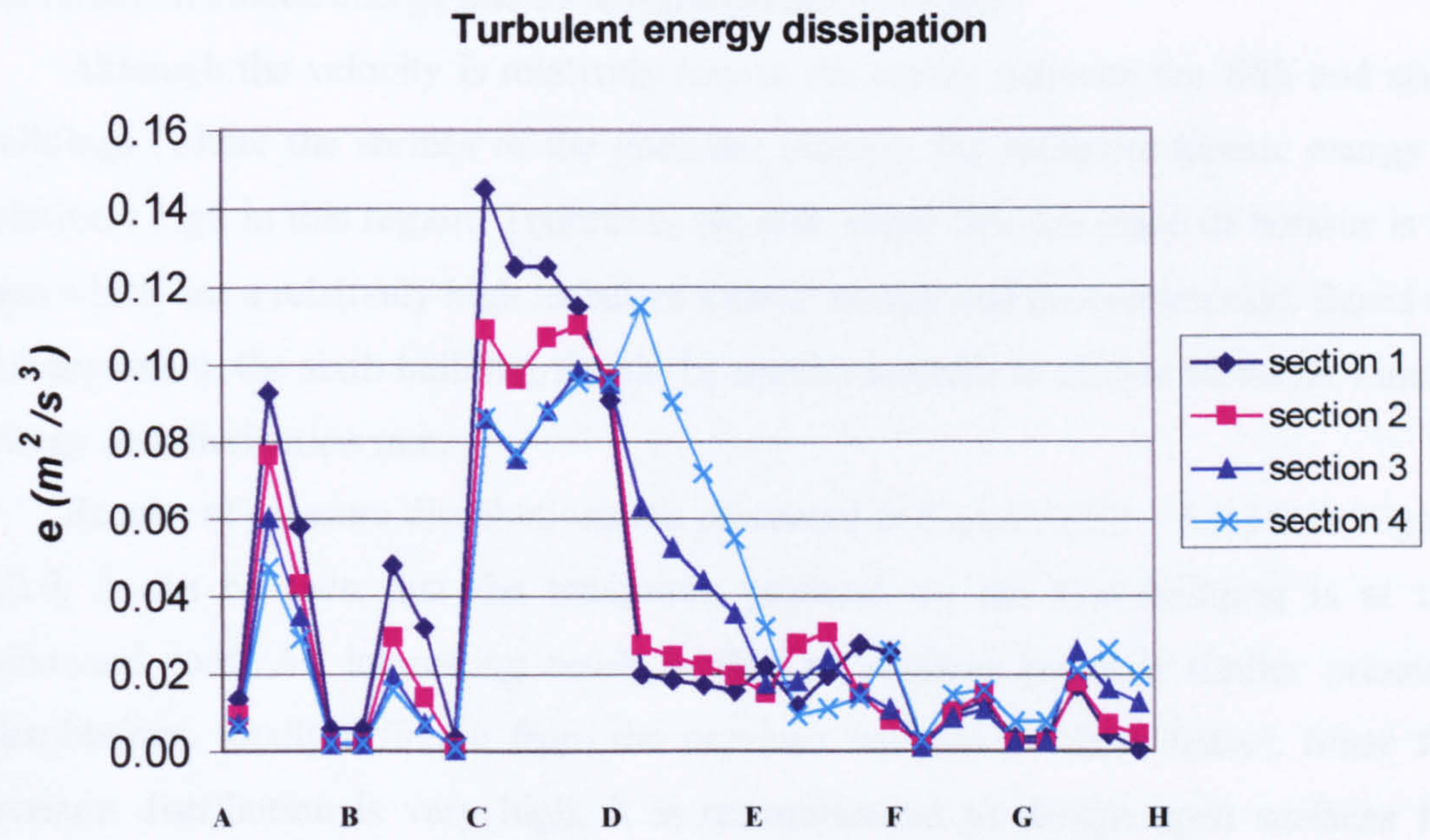

Figure 6.2.26 Turbulent energy dissipation on the sixth building

From streamline plots, it can be seen in Figures 6.2.5 and 6.2.6 that adding fences around the site changes the flow profile near the ground. The jet flow to the sixth building is minimised but the jet flow at the leeward side of the second building is now very high. This arrangement tends to increase the flow velocity at the first, second and third buildings, but reduces the momentum transfer at the fourth, fifth and sixth buildings, and at the corner between the fifth and sixth buildings.

From the turbulent energy dissipation plot in Figure 6.2.7, it can be seen that the energy dissipation at the corner of both the third and fifth buildings is relatively high, as well as at the leeward side of the second building.

The turbulent kinetic energy plot in Figure 6.2.8, shows that its value is relatively high everywhere. In the area between the first and fourth buildings, the turbulent kinetic energy is not as high as in the previous observation (without fence), but it is higher at the leeward side of the second building. The turbulent kinetic energy at the leeward side of the second building decreases in the area between the fourth and fifth buildings. Defining this area as the centre (*natar*), *natar* is then the area where both turbulent kinetic energy and velocity profile decrease. With or without the fence, it can be seen that *natar* is the area where the flow merges and the velocity gradient becomes very low. From this statement, it can also be seen that *natar* is the area where the turbulent kinetic energy and its dissipation rate decrease.

Although the velocity is relatively low at the corner between the fifth and sixth buildings (where the shrines of the gods are placed), the turbulent kinetic energy is relatively high in this region. Therefore, we also argue that the place of honour is an area which has a relatively high turbulent kinetic energy and dissipation rate. Based on this argument, the sixth building should be moved in order to reduce turbulent kinetic energy and dissipation rate.

Results of pressure distributions are presented in Figure 6.2.9 – 6.2.14. In Figure 6.2.9, it can be seen that the maximum pressure on the first building is at the windward roof. An interesting result is that all sections produce similar pressure distributions, totally different from the previous analysis (without fence). Since the pressure distribution is very high, it is recommended to design open surfaces for natural ventilation at the windward roof. Open surfaces on walls can be placed on both windward and leeward sides, but it is recommended to design an open surface at the leeward side, where the pressure decreases.

The pressure variation at the second building is similar to that in the first, as presented in Figure 6.2.10. Therefore, an open surface at the windward roof is recommended for better natural ventilation and an open surface at the leeward side is also suggested.

On the third building, an open surface at the windward roof is also suggested, according to Figure 6.2.11. Therefore, natural ventilation systems at the first, second and third buildings should be designed with open surfaces at the windward roof and at the leeward side of the buildings.

An interesting result occurs at the windward side of the fourth building, as presented in Figure 6.2.12, where the pressure distribution on section 4 is relatively high near the ground. An open surface can be placed on this side in order to produce good natural ventilation. For a better solution, it is suggested to design a natural ventilation system with an opening at the windward roof as an intake, and at the leeward roof as the exhaust. Therefore, the fourth building does not need an open surface at the leeward side, but the ceiling should be fully open.

On the fifth building, it can be seen in Figure 6.2.13 that the pressure distribution on section 4 is the highest one. This result is similar to that in previous analyses (without fence). For natural ventilation design, open surface at the windward roof as an intake and open surface at the leeward roof as an exhaust are preferred. Therefore, both the fourth and fifth buildings are design with open surfaces at roof and the ceiling is fully open.

On the sixth building, an open surface at the windward roof as the intake is recommended on section 2, while an open surface at the leeward roof as the exhaust is preferred on section 1. At the leeward side, an open surface on section 4 will produce a higher pressure variation between the room and its surrounding, as can be seen in Figure 6.2.14.

The highest pressure distribution is received at the windward roof of the first and second buildings, but the maximum value is lower than that in the previous analysis (without fence). From this result, we suggest that the fence has reduced the pressure distribution on the building surfaces. This agrees with our explanation in Chapter Four. The effects of the gate position on the pressure distribution do not seem very clear, since flow patterns at the centre are dominated by the incoming flow from the fence. The maximum pressure decreases at the first and second buildings, but increases at the third, fourth, fifth and sixth buildings. Therefore, effects of the fence

only reduce pressure at the first and second buildings. This agrees with explanations in Chapter Four that a higher fence produces a lower pressure distribution at the first building. The question is, why does the maximum pressure increase at the other buildings? We suggest that this phenomenon is influenced by the gate position.

Similar to the previous observation, the highest value of turbulent kinetic energy occurs on the sixth and fourth buildings, even though a fence has been added, as can be seen in Figures 6.2.15 – 6.2.20. The maximum turbulent kinetic energy for all buildings is lower than in the previous analysis. Therefore, the effect of the fence is to reduce the turbulent kinetic energy everywhere. This result is interesting because the fourth building is used for conventions or meetings, and the sixth building is the parent's sleeping quarters. In Chapter Four, it was clear that there is a relation between turbulent kinetic energy and number of pillars. The highest turbulent kinetic energy occurs at the sixth building. This is interesting since in the previous analysis the maximum turbulent kinetic energy occurred at the fourth building. We suggest that this phenomenon is also influenced by the gate position.

In previous studies (without fence), the turbulent kinetic energy was relatively high near the ground. By adding a gate on the west side, the turbulent kinetic energy on the windward walls becomes greater. The air from the gate directly moves to the first building and create re-circulation at the windward side (in the area between the fence and the building). The flow moves toward the area between the fence and buildings (first, second and third buildings). Therefore, the turbulent kinetic energy on those three buildings should be very high at the windward side, near the ground.

The fence influences the air motion and creates a higher momentum at the roof. The turbulent kinetic energy at the roof of the first building is relatively lower than that on walls. Therefore, the momentum of air from the gate to the first building is greater than that from the fence. In order to minimise this momentum, a fully open surface should be taken into account. By removing the wall, both drag force and turbulent kinetic energy can be minimised.

The turbulent kinetic energy at the roof of the second building is now greater than that near the ground, its maximum near the ground being about 0.1 m^2/s^2 and at the roof about 0.15 m^2/s^2. Therefore, the air momentum which is affected by the fence is a bit greater than those from the gate. Since the turbulent kinetic energy near the ground is relatively high, the second building should have a strong foundation.

And, in order to minimise the effects of drag and turbulent kinetic energy at the roof, the second building should have a strong construction, *e.g.*, by adding several posts.

The turbulent kinetic energy near the ground tends to increase at the third building. This is explainable since air motion from the gate creates a high momentum in the corner where the third building lies. The third building should also have a strong foundation.

At the fourth building, the greatest value of turbulent kinetic energy occurs at the top of the roof, on section 4. The effects of the fence on the air motion have been described in Chapter Four. Since the distance from the fourth building to the fence is relatively short, the air motion around the fence creates a higher momentum on section 4. If the fourth building is moved from section 4 to section 3, the turbulent kinetic energy on the roof can be minimised, similarly to the previous study. Since the turbulent kinetic energy near the ground is not high, the fourth building does not need a strong foundation as in the first, second and third buildings.

The turbulent kinetic energy on the fifth building is relatively high on section 4. In this arrangement, the greatest turbulent kinetic energy occurs on section 1 at the leeward roof. An interesting result occurs on section 4 where the turbulent kinetic energy is the lowest. This indicates that the effects of air motion from the gate are greater than that from the fence. In order to reduce the turbulent kinetic energy on the roof, a strong construction should be considered on the fourth and fifth buildings, or the roof surface moved from section 1 to section 2. Therefore, both the fourth and fifth buildings should be in the same direction to the centre (*natar*).

At the sixth building, the greatest value of turbulent kinetic energy occurs at the top of the roof, on section 4. The air motion in the area between the fence and the fourth buildings creates a high momentum at the corner (between the fourth and sixth buildings) and produces re-circulation at the roof of the sixth building. Since the pressure distribution on section 4 is relatively lower than the others, an open surface at this side is not recommended. The best solution from the building design point of view is to move the sixth building away from the back fence.

Turbulent energy dissipation results are presented in Figures 6.2.21 – 6.2.26. The maximum turbulent energy dissipation occurs at the fourth building. Therefore, the fourth building receives the highest turbulent kinetic energy and its dissipation rate.

In previous studies (without fence), the turbulent energy dissipation at the first building was relatively high near the ground, but by adding a gate on south-west side,

the turbulent energy dissipation increases at the windward wall and roof. To reduce wind forces, turbulent kinetic energy and dissipation rate, the best solution is to remove all building surfaces or create fully open surfaces.

At the second building, it can be seen that the turbulent energy dissipation at the windward side near the ground is also relatively high. Therefore, to minimise the effects of this parameter, the roof should have an open surface as intake and the ceiling be fully open.

The above comments also apply to the third building. Since the turbulent energy dissipation near the ground is also relatively high, it is recommended to create an open surface (or floating foundation) at the windward side.

There is an interesting result at the fourth building where similar values occur on sections 1 and 4 of the roof. The turbulent energy dissipation near the ground is relatively high on section 4, where the turbulent kinetic energy was also relatively high.

At the fifth building, the turbulent energy dissipation is relatively high near the ground. Although the highest turbulent energy dissipation occurs on section 1 of the leeward roof, the turbulent energy dissipation on section 4 is also high. To minimise the effects of turbulent energy dissipation near the ground, it is recommended to design the foundation by using open surfaces.

At the sixth building, the turbulent energy dissipation is also high near the ground. Since the maximum value occurs at the windward side of roof, it is recommended to design open surfaces on section 1. A strong foundation is a possible solution to minimise the effects of turbulent energy dissipation near the ground.

A gate on the west-side increases the pressure on the third, fourth, fifth and sixth buildings and tends to reduce both the turbulent kinetic and energy dissipation on all buildings.

A summary of results for pressure distribution, turbulent kinetic energy and its dissipation rate are presented in Table 6.2.1.

Table 6.2.1 A summary of results for gate at the south-west side

Building number	I	II	III	IV	V	VI
Maximum pressure (Pa) position	9.5 windward roof	9 windward roof	9.5 windward roof	6.2 windward roof	8.4 windward roof	7.5 windward roof
Maximum turbulent kinetic energy (m^2/s^2) position	0.28 windward wall	0.13 windward wall	0.118 windward wall	0.335 top roof	0.28 top roof	0.35 leeward roof
Maximum turbulent energy dissipation (m^2/s^3) position	0.33 windward roof	0.225 windward roof	0.15 windward roof	0.105 windward roof	0.085 top roof	0.15 windward roof

6.2.2 Gate at the North-West Side

The gate of a well-to-do family house usually lies on the west side of the buildings arrangement (as presented in Figure 6.2.2). In order to understand the effects of the gate position on natural ventilation, the gate is now moved at the north-west side of the building site, as presented in Figure 6.2.27.

6.2.2.1 Results and Discussion

From the velocity profile, it can be seen that the air motion is relatively high at the leeward side of the second building near the ground, as well as at the corner where the place of honour lies. Similarly to the previous results, the velocity at 8 m above roof has a uniform profile, indicating that the flow over this level is not affected by the buildings arrangement.

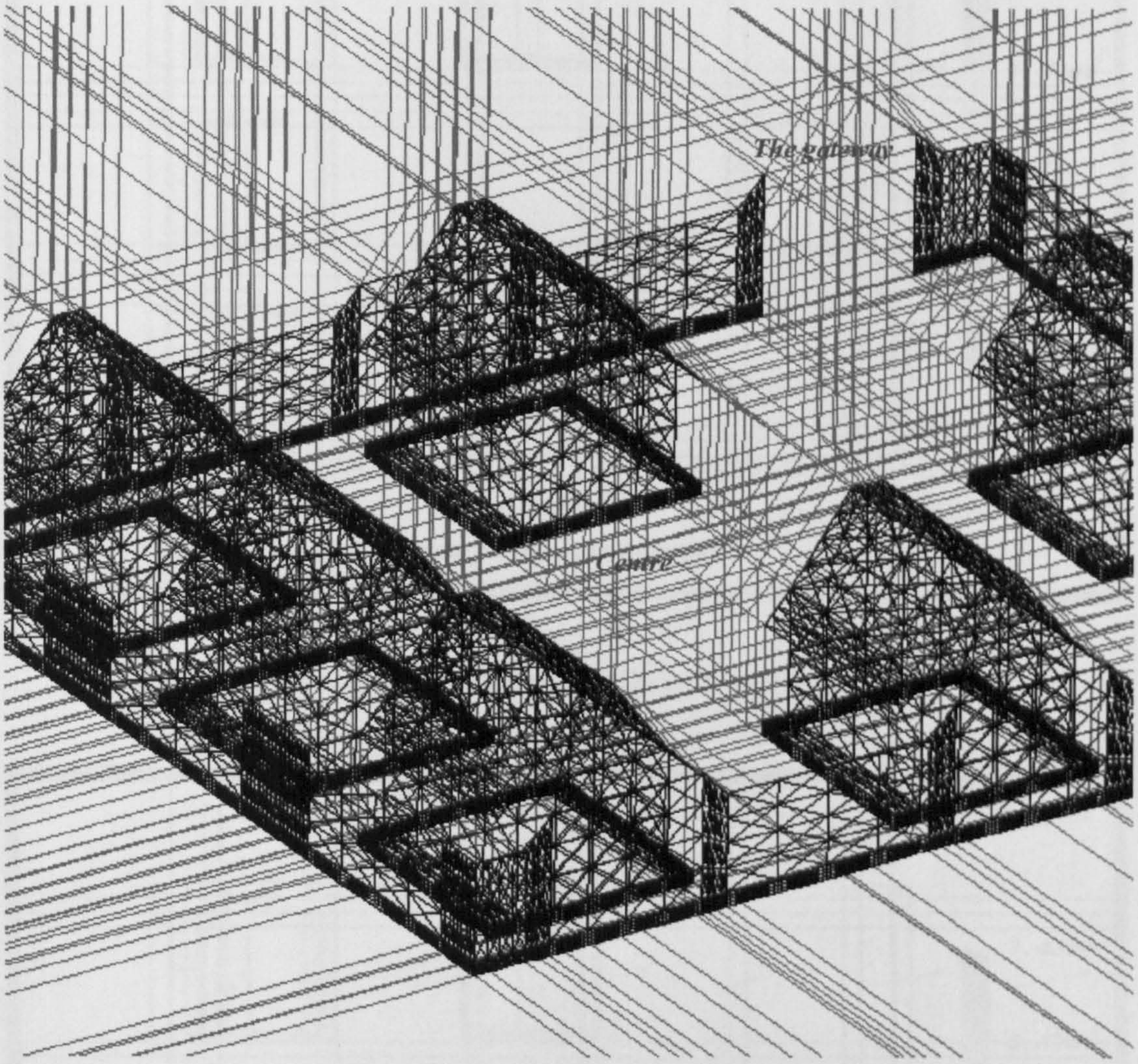

Figure 6.2.27 Side view of buildings arrangement with gate on north-west side

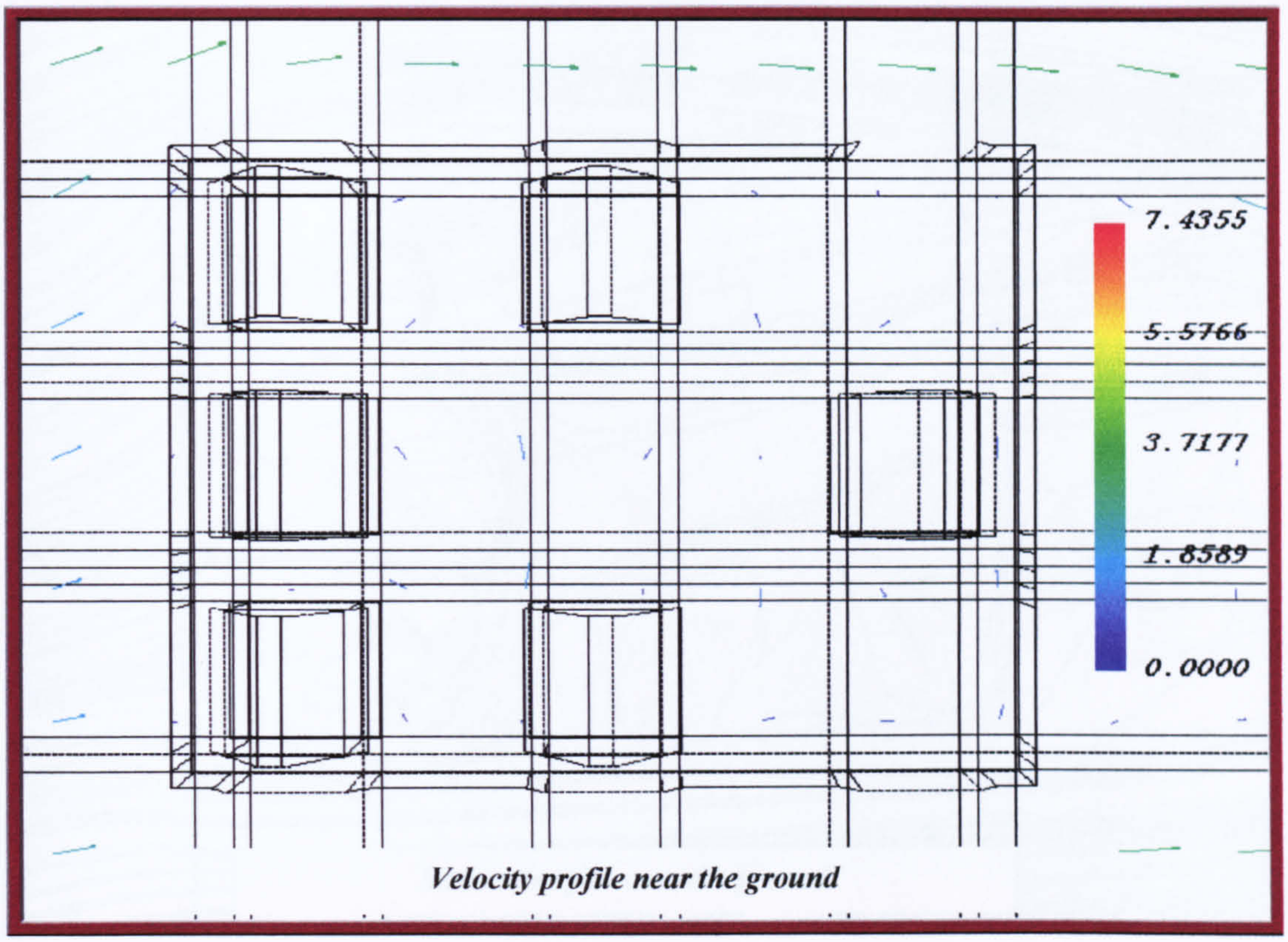

Velocity profile near the ground

Figure 6.2.28 Velocity profile near the ground

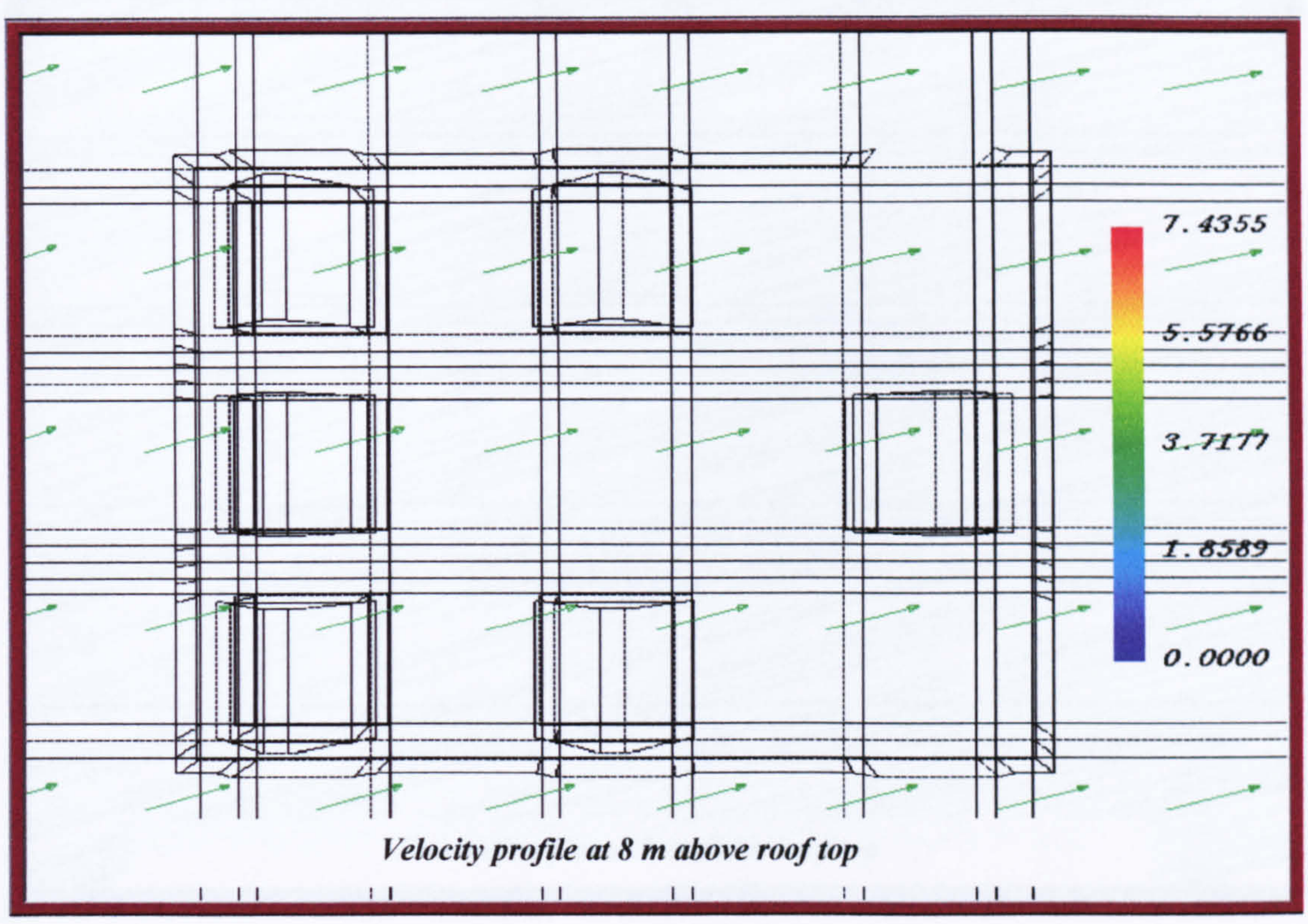

Velocity profile at 8 m above roof top

Figure 6.2.29 Velocity profile at 8 m above roof top

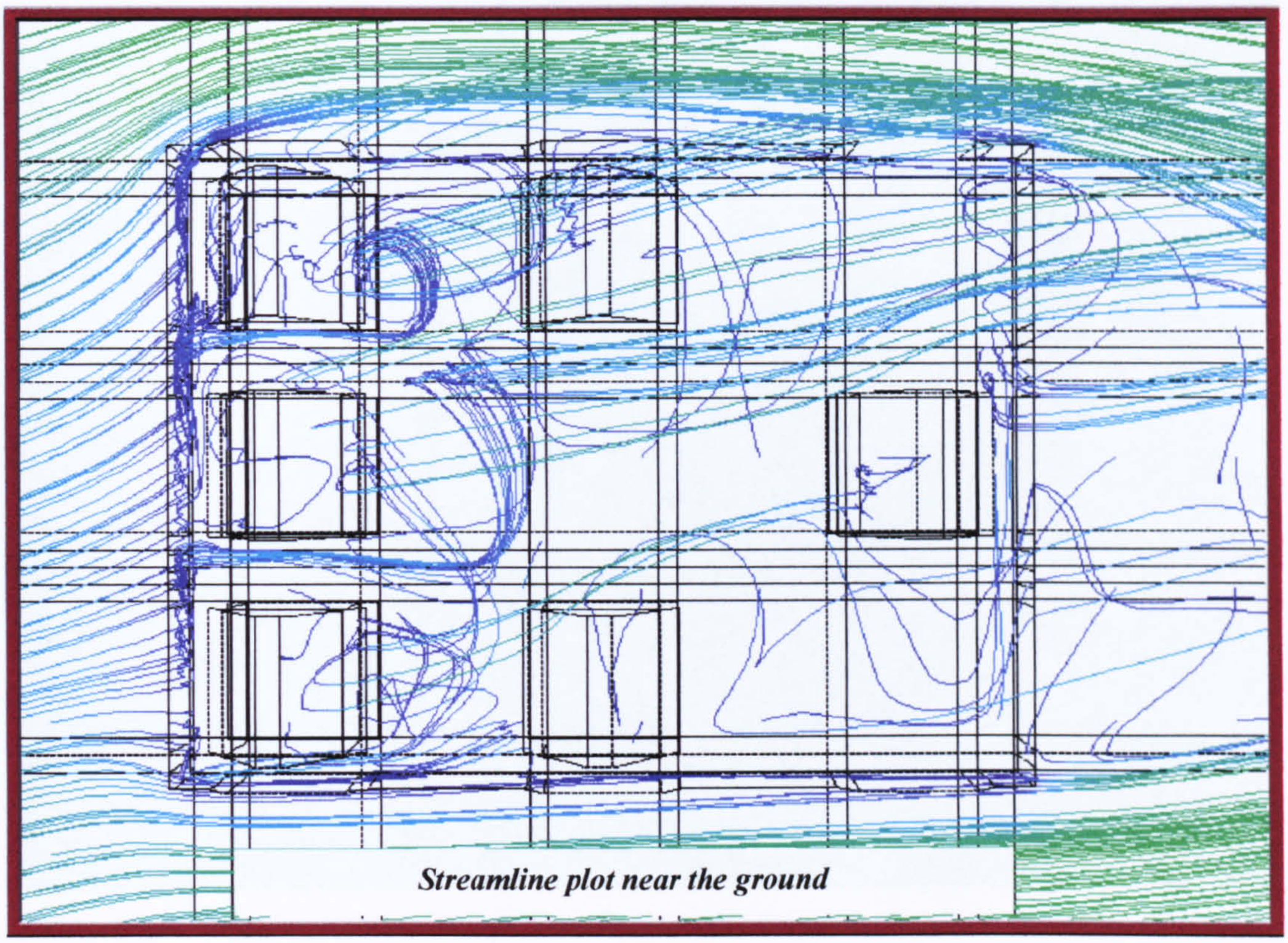

Streamline plot near the ground

Figure 6.2.30 Streamline plot near the ground

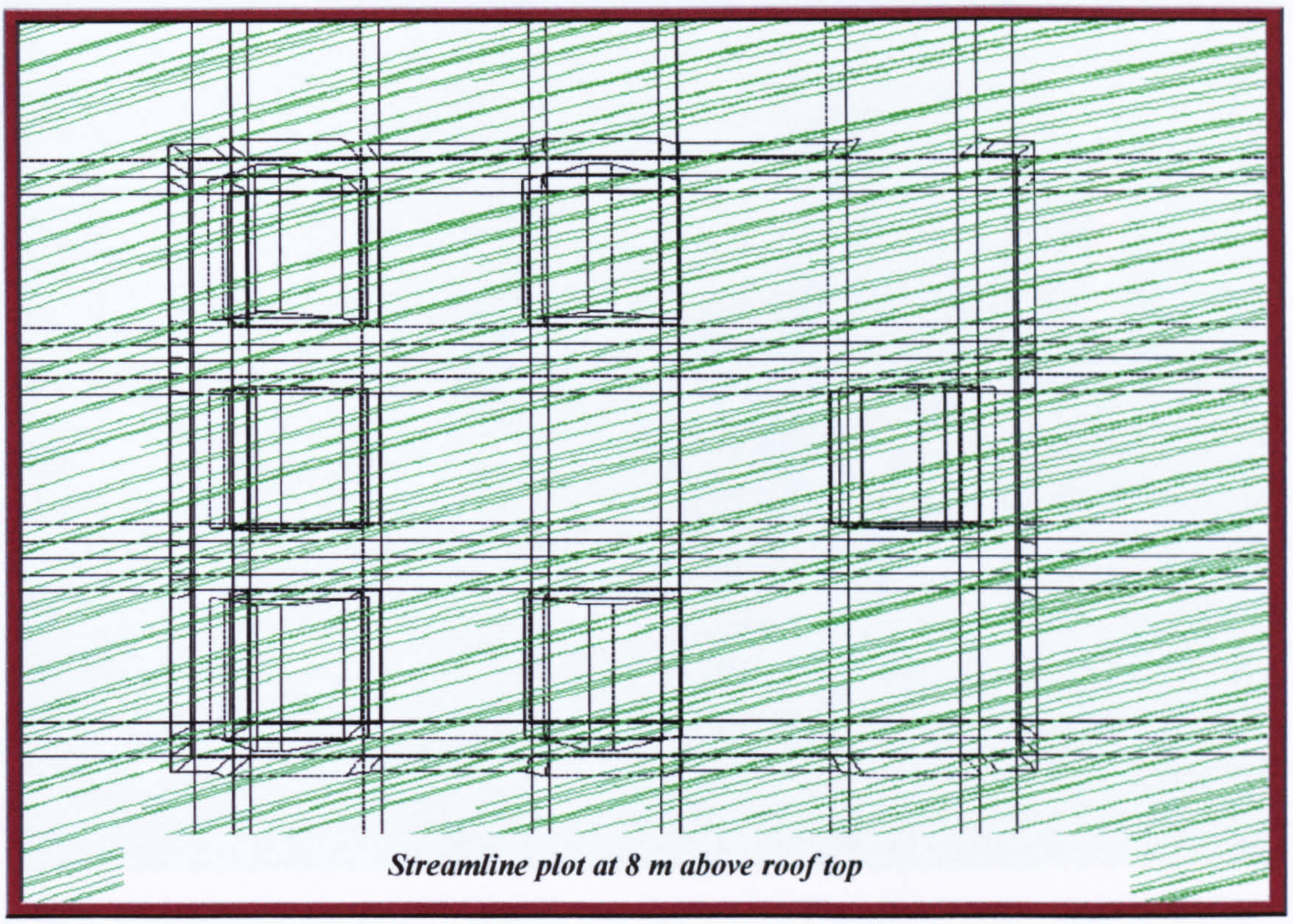

Streamline plot at 8 m above roof top

Figure 6.2.31 Streamline plot at 8 m above roof top

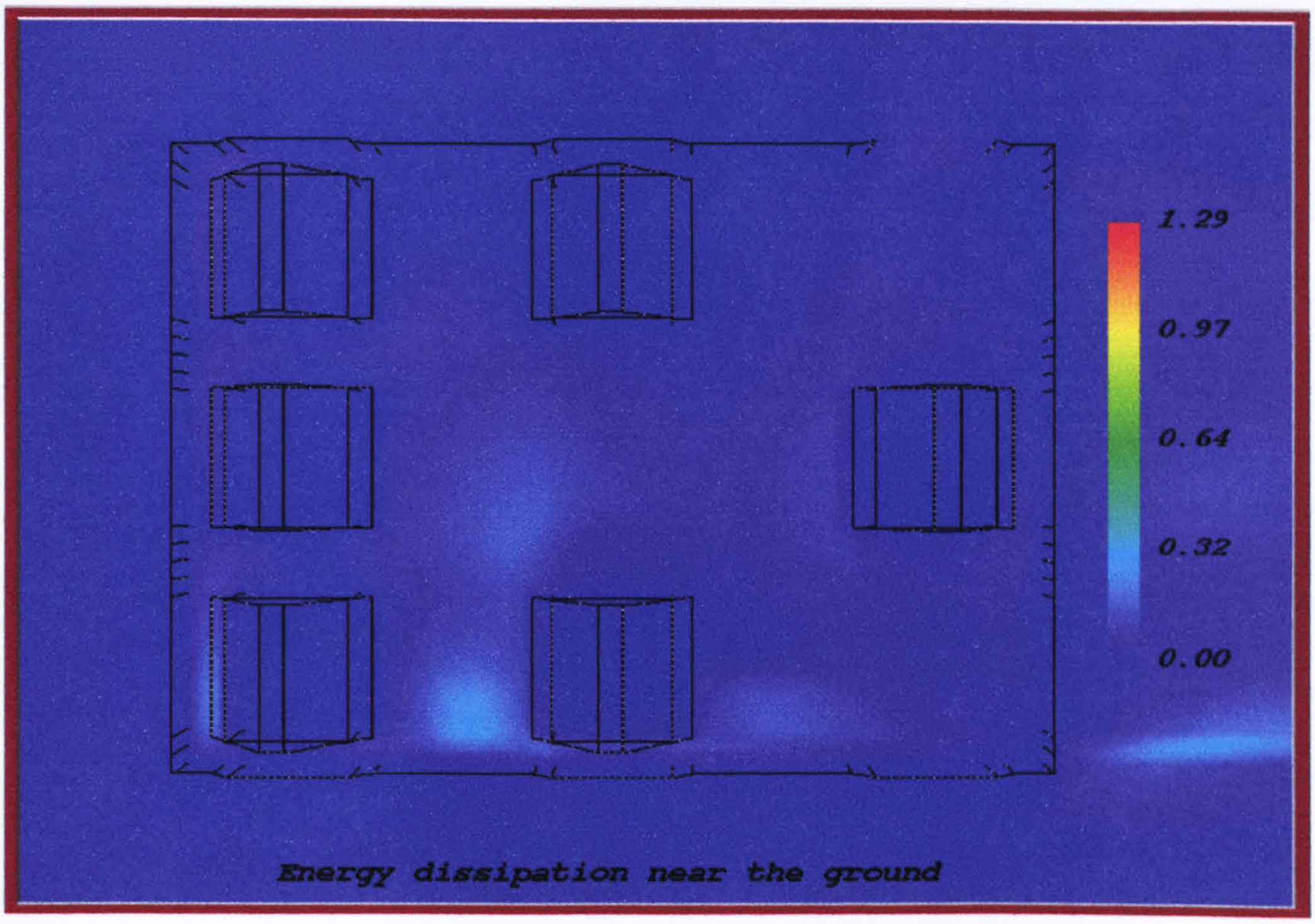

Figure 6.2.32 Turbulent energy dissipation plot near the ground

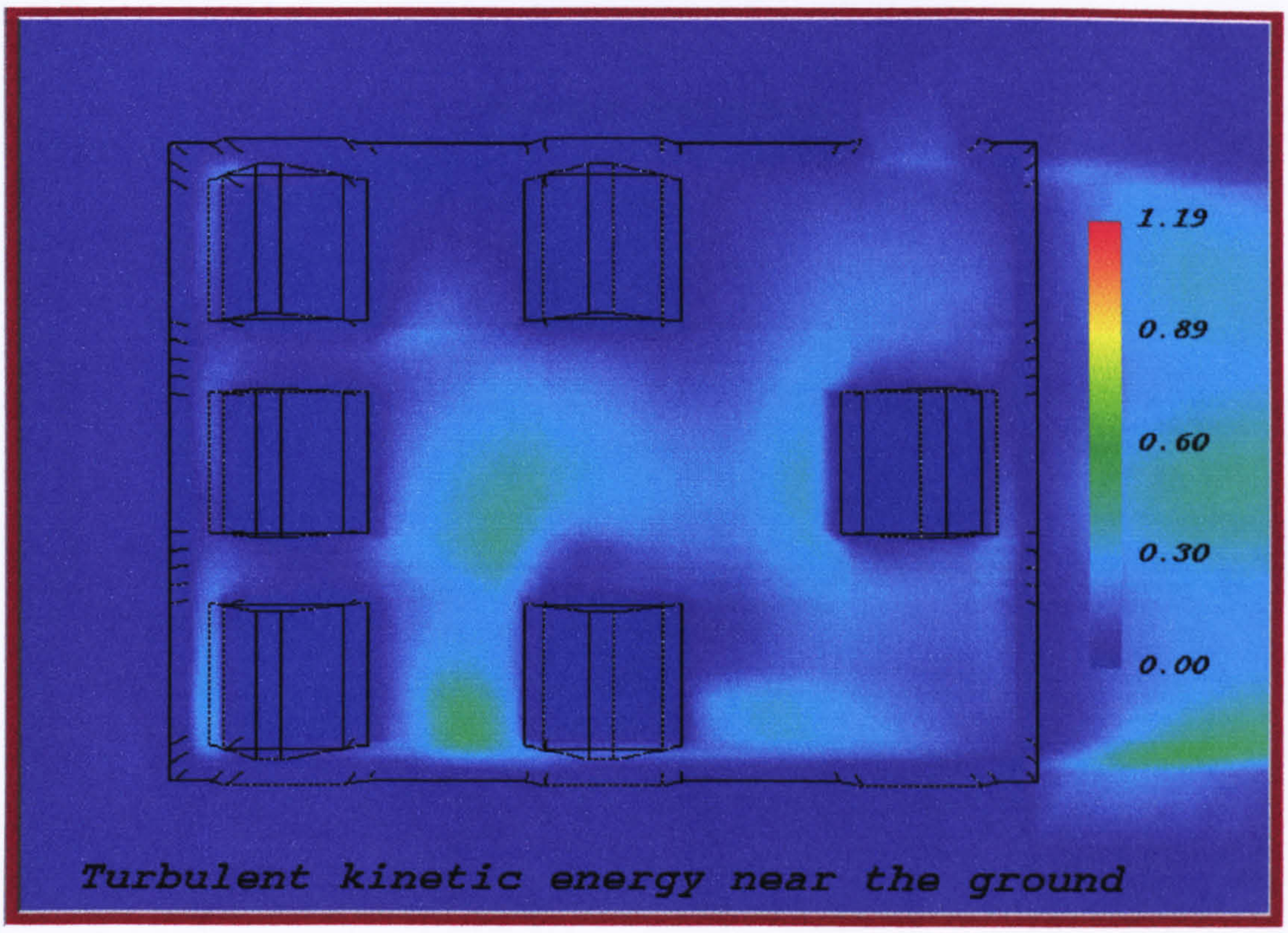

Figure 6.2.33 Turbulent kinetic energy plot near the ground

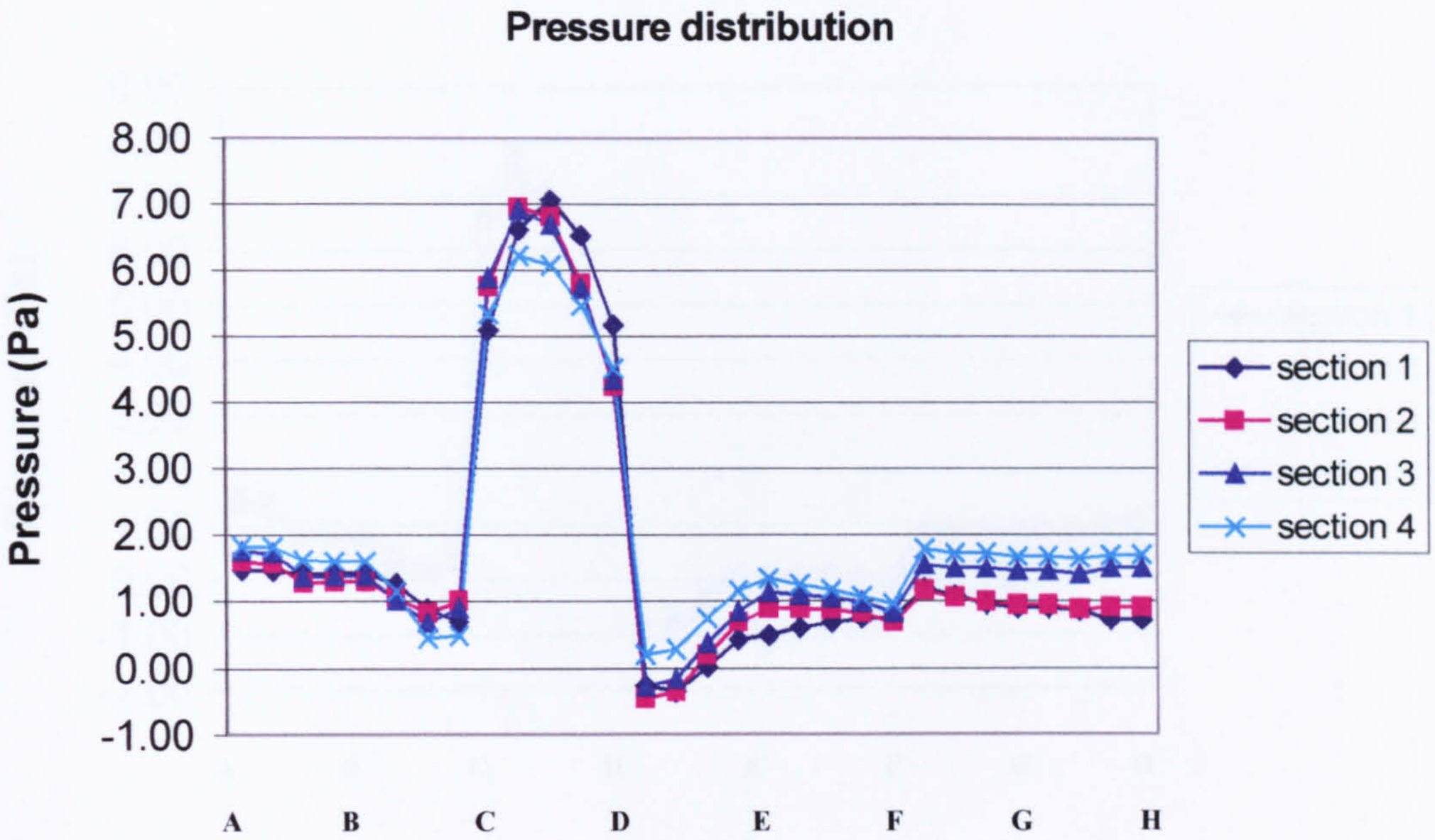

Figure 6.2.34 Pressure distribution on the first building

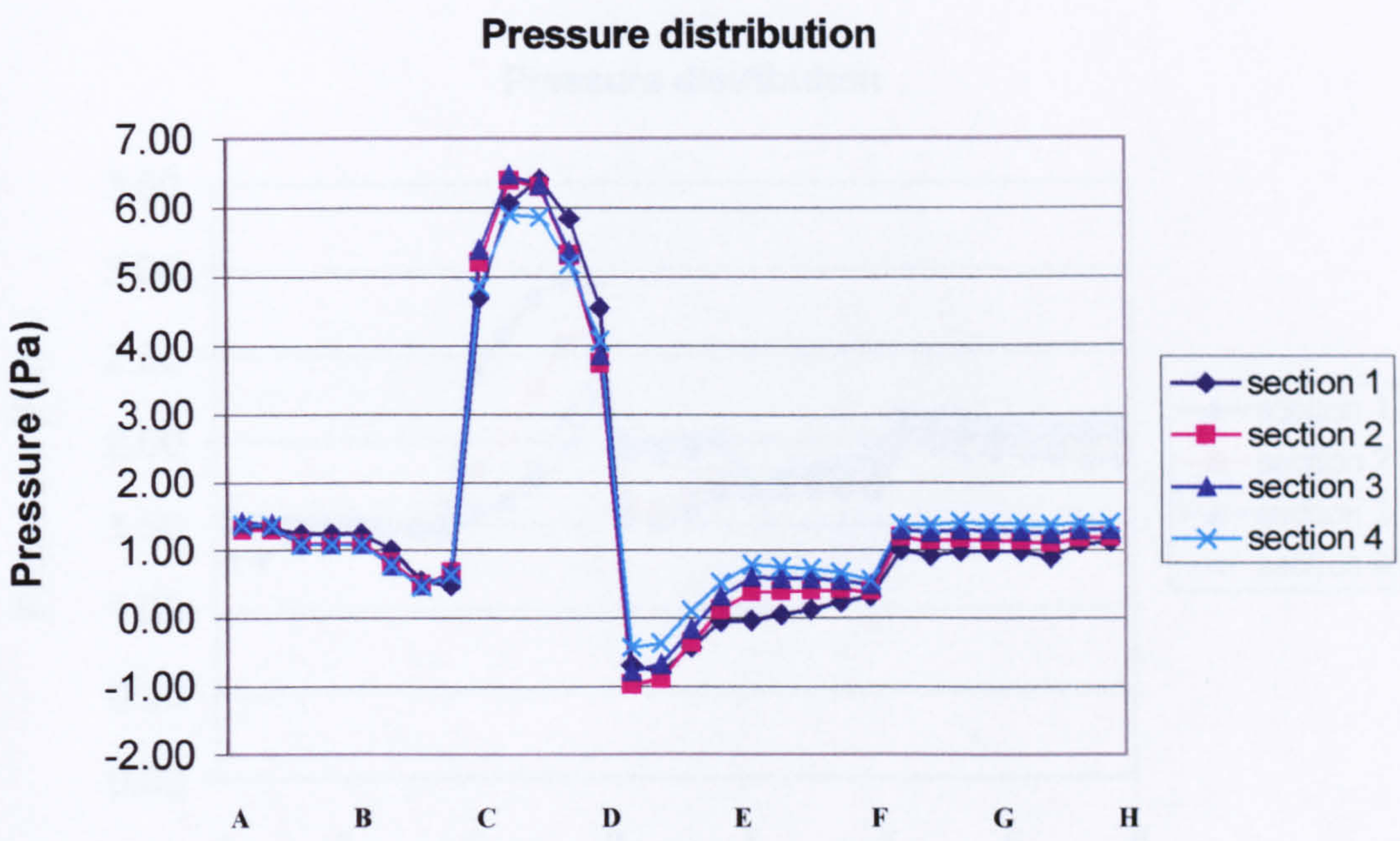

Figure 6.2.35 Pressure distribution on the second building

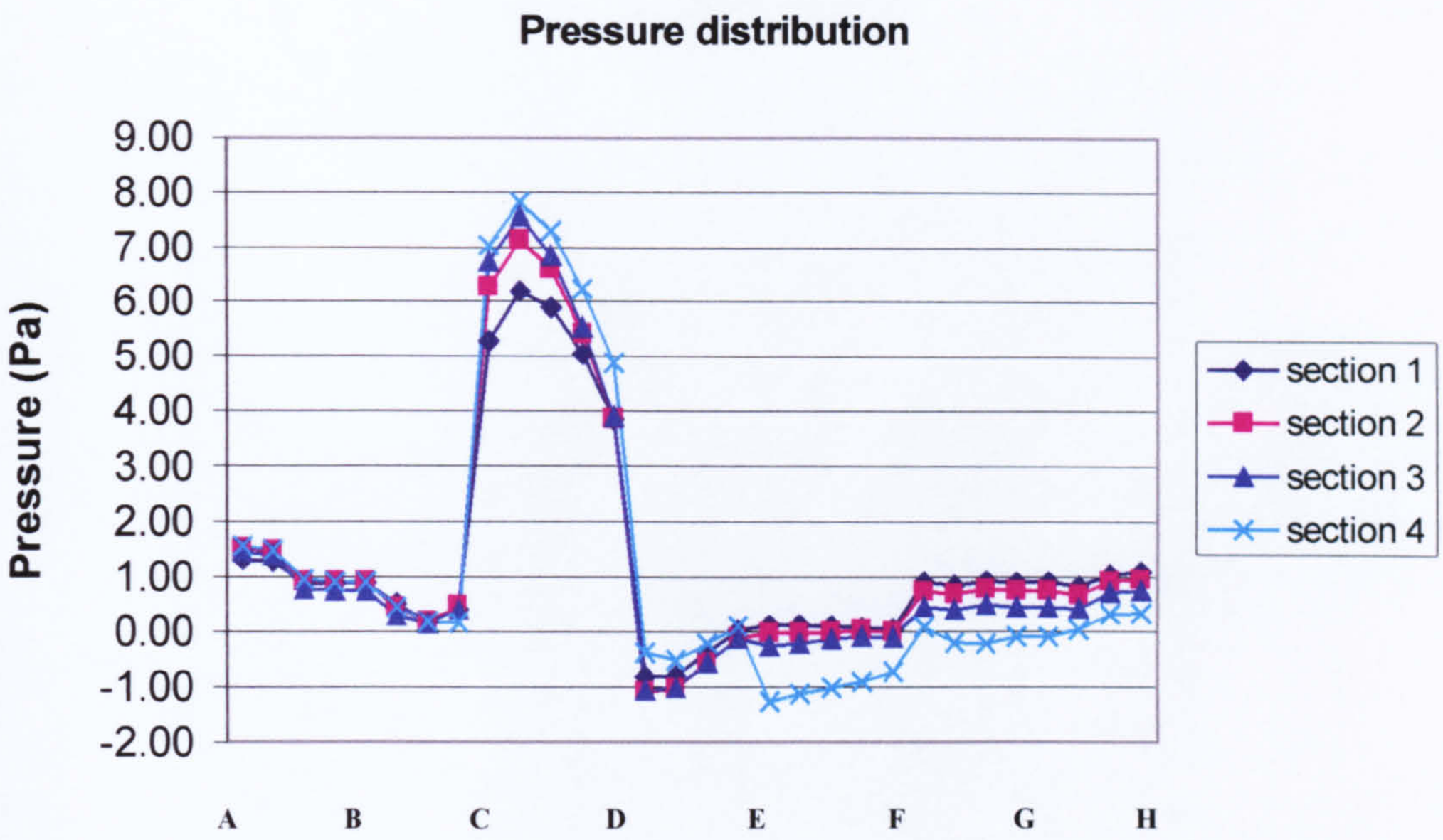

Figure 6.2.36 Pressure distribution on the third building

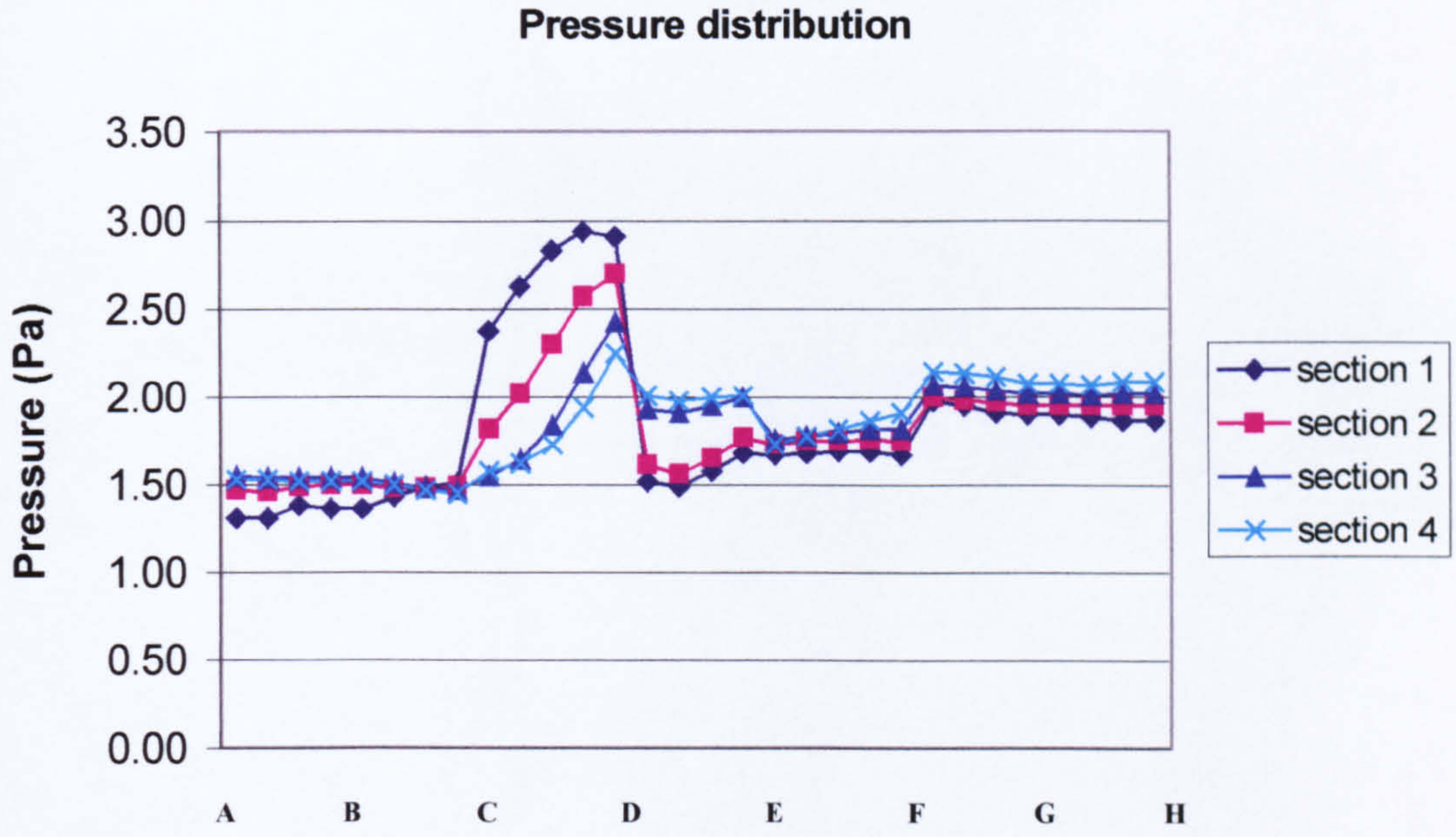

Figure 6.2.37 Pressure distribution on the fourth building

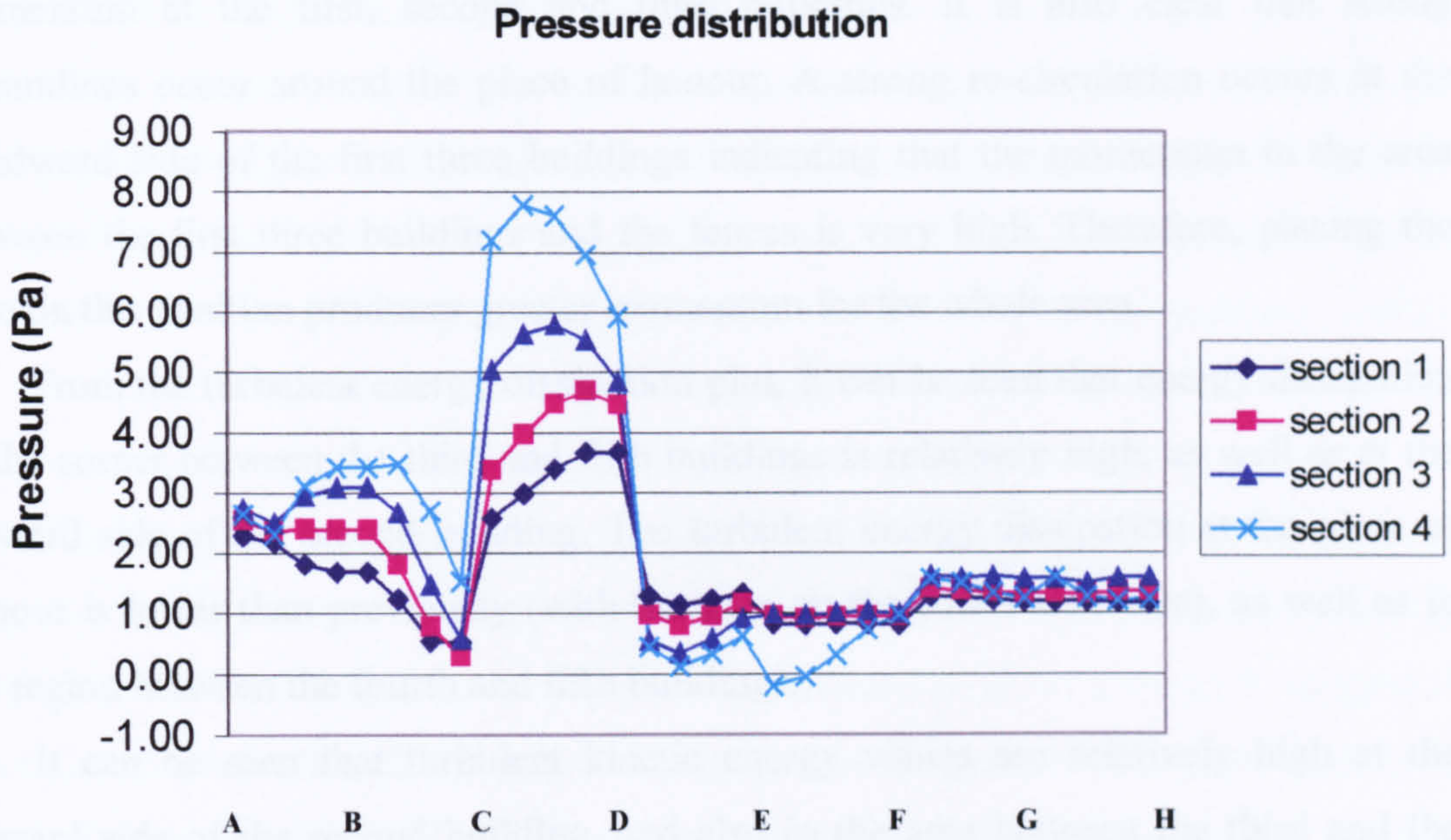

Figure 6.2.38 Pressure distribution on the fifth building

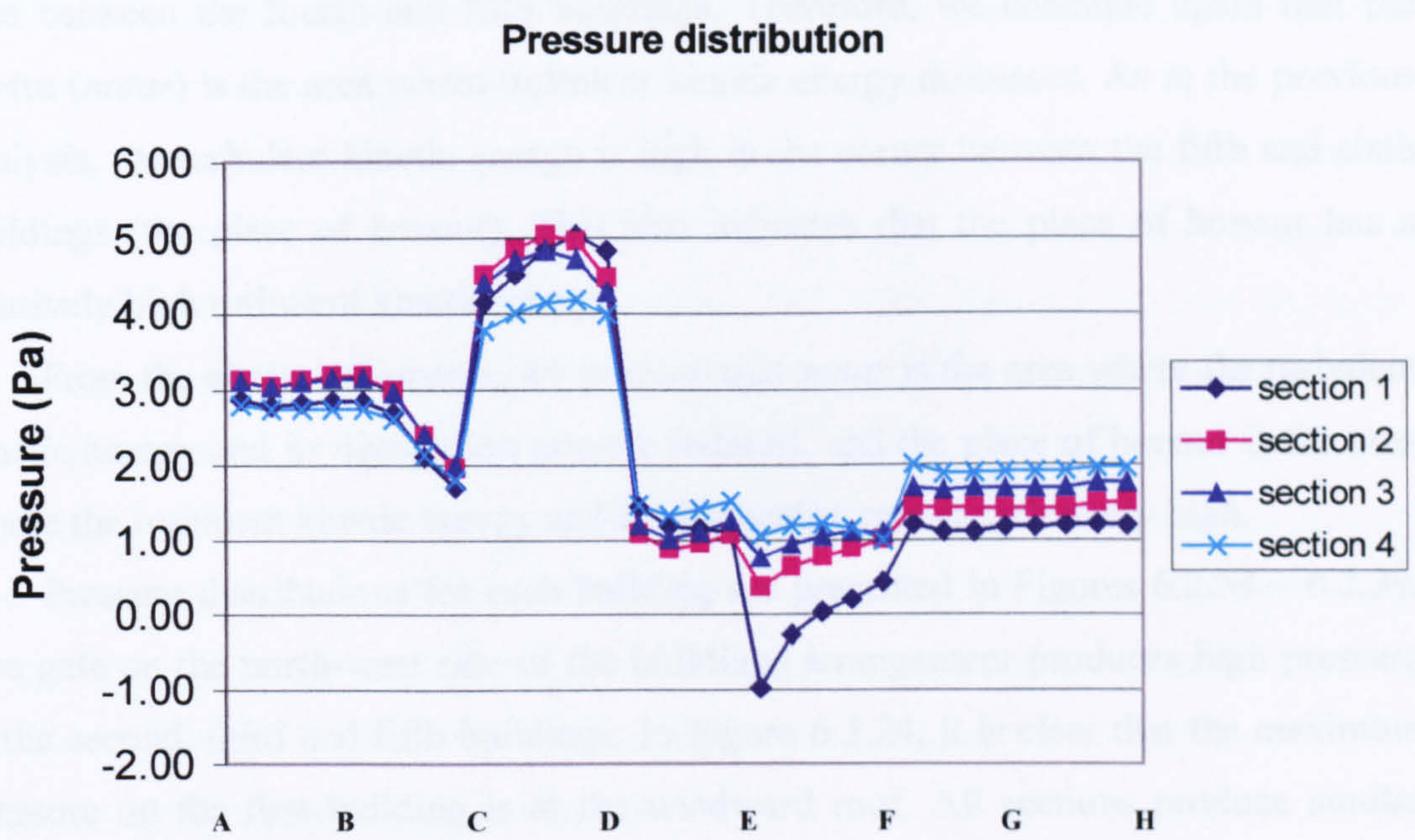

Figure 6.2.39 Pressure distribution on the sixth building

From streamline plots, it can be seen that this model creates very high momentum at the first, second and third buildings. It is also clear that strong streamlines occur around the place of honour. A strong re-circulation occurs at the windward side of the first three buildings indicating that the momentum in the area between the first three buildings and the fences is very high. Therefore, placing the gate on this position produces greater momentum for the whole area.

From the turbulent energy dissipation plot, it can be seen that energy dissipation at the corner between the third and fifth buildings is relatively high, as well as at the leeward side of the second building. The turbulent energy dissipation at the place of honour is lower than previously (with the gate on the south-west side), as well as in the region between the fourth and fifth buildings.

It can be seen that turbulent kinetic energy values are relatively high at the leeward side of the second building, and also in the area between the third and the fifth buildings. Air is moving from the gate to the centre (*natar*), producing high turbulent kinetic energy after hitting the second and third buildings. The turbulent kinetic energy on the sixth building is also very high since the air from the gate is moving to the second building. The turbulent kinetic energy is relatively lower in the area between the fourth and fifth buildings. Therefore, we conclude again that the centre (*natar*) is the area where turbulent kinetic energy decreases. As in the previous analysis, the turbulent kinetic energy is high in the corner between the fifth and sixth buildings (the place of honour). This also indicates that the place of honour has a relatively high turbulent kinetic energy.

From the above statements, we propose that *natar* is the area where the turbulent kinetic energy and its dissipation rate are reduced, and the place of honour is the area where the turbulent kinetic energy and its dissipation rate are relatively high.

Pressure distributions for each building are presented in Figures 6.2.34 – 6.2.39. The gate on the north-west side of the buildings arrangement produces high pressure at the second, third and fifth buildings. In Figure 6.2.24, it is clear that the maximum pressure on the first building is at the windward roof. All sections produce similar pressure distributions to that in the previous analysis (gate on the south-west side), therefore, similar design considerations are recommended.

There is no variation of pressure for the second and third buildings. Similar to the first building (and also to the previous observation in section 6.2.1), an open surface at

the windward roof is recommended and an open surface at the leeward side is also suggested for natural ventilation.

In the previous analysis (gate on the south-west side), the pressure on section 4 of the fourth building was relatively high. In the present simulation, it can be seen that the pressure on section 1 is now the highest one. Therefore, it can be stated that air motion in the area between the fence and the fourth building becomes weaker. Another interesting result is that the pressure variation is relatively small. Therefore, a fully open surface on section 1 is needed for natural ventilation.

The pressure distribution on the fifth building is similar to that in previous simulation with section 4 having the greatest value. An open surface at the windward roof for air intake and an open surface at the leeward roof for exhaust is suggested. Therefore, both the fourth and fifth buildings should be designed with open surfaces at the roof, and the ceiling fully open. From three simulations, we suggest that the fifth building is the building where pressure is high on section 4. Therefore, section 4 should be open, or facing the fence, for better natural ventilation.

At the sixth building, an open surface at the windward roof as intake is recommended on section 2 or 3, and an open surface at the leeward roof as exhaust is preferred on section 1. At the leeward side, an open surface on section 2 will produce higher pressure variation between the room and its surrounding.

The highest pressure values are received at the windward roof of the third and fifth buildings, but the maximum value is lower than in previous simulations. The maximum pressure decreases at all buildings, indicating that the gate on the north-west side reduces pressure. The maximum turbulent kinetic energy decreases at the first, fifth and sixth buildings, increases at the second and third buildings but is constant at the fourth building. A reduction of pressure indicates a reduction of wind forces and their damaging effects on buildings. A reduction of turbulent kinetic energy at the first, fifth and sixth buildings also indicates a reduction of energy on the buildings. The gate on the north-west side as shown in Figure 6.2.27 appears to reduce wind loads and energy transfer on buildings.

The maximum pressure on the fifth building is almost similar to the previous simulations. This indicates that the fifth building is not fully affected by the gate position. As described in Chapter Four, the second building is ideal for ceremonial or meeting rooms. We suggest that this is the reason why, traditionally, the fifth building

has been used as a ceremonial hall since air motion around the fifth produces a similar pressure variations, a good criterion for natural ventilation and thermal comfort.

A summary results for pressure distribution, turbulent kinetic energy and dissipation rate is presented in Table 6.2.2.

Table 6.2.2 A summary of results for gate at the north-west side

Building number	I	II	III	IV	V	VI
Maximum pressure (Pa) position (m)	7.0 windward roof	6.5 windward roof	8.0 windward roof	2.9 windward roof	7.8 windward roof	5.0 windward roof
Maximum turbulent kinetic energy (m^2/s^2) position	0.145 windward roof	0.142 windward roof	0.142 windward roof	0.34 top roof	0.18 windward ground	0.33 top roof
Maximum turbulent energy dissipation (m^2/s^3) and position	0.275 windward roof	0.27 windward roof	0.275 windward roof	0.085 top roof	0.15 windward ground	0.135 windward roof

6.2.3 Gate at the North Side

The gate is now placed at the north side as presented in Figure 6.2.40. This location is very close to the gate in the north-west side but it has a different meaning in traditional reasoning.

6.2.3.1 Results and Discussion

The velocity profile near the ground is relatively high at the leeward side of the second building, as well as at the corner where the shrines of gods are placed.

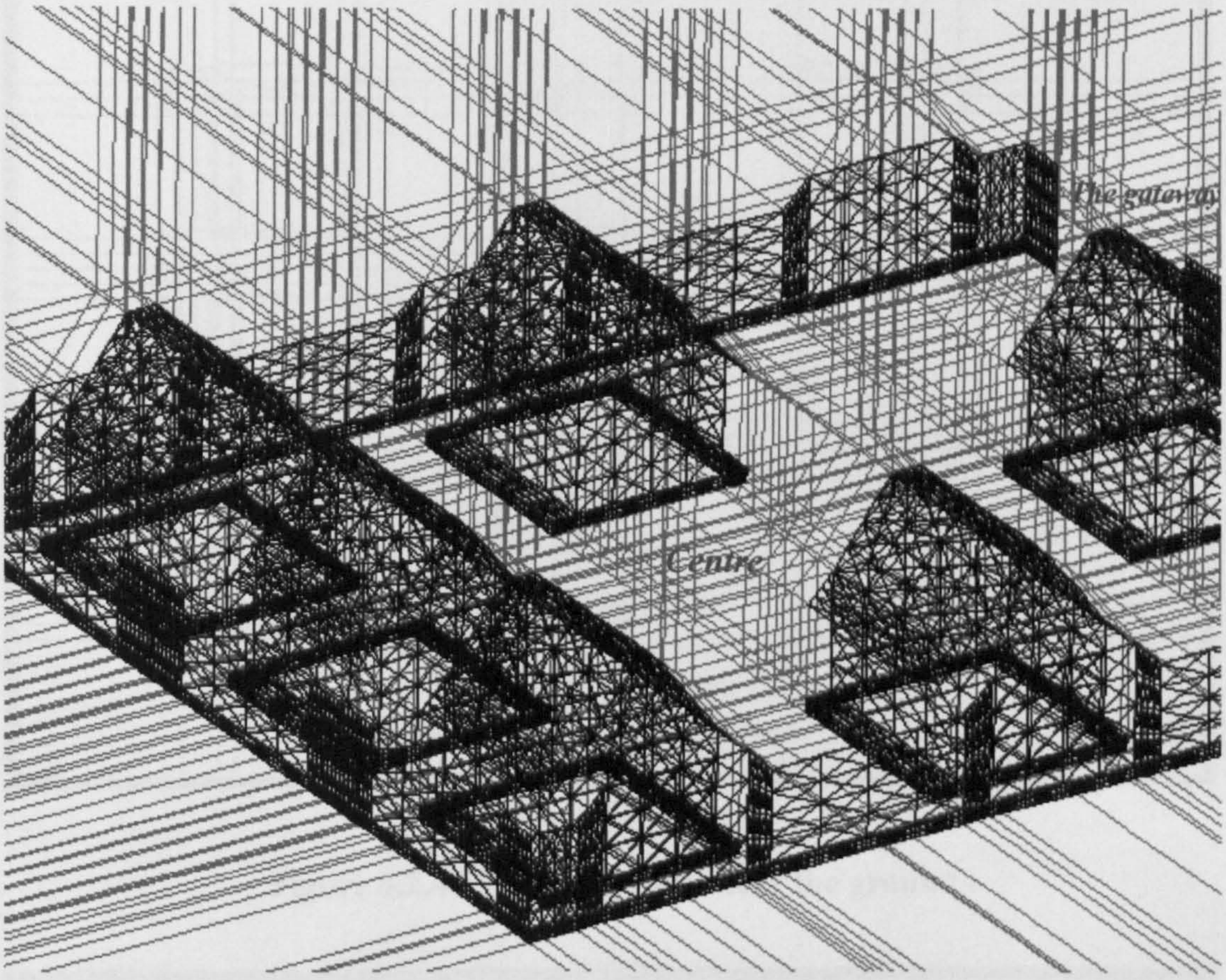

Figure 6.2.40 Side view of buildings arrangement with gate on north side

From streamline plots, it can be seen that this model also produces high momentum at the first, second and third buildings, similarly to the previous observations, except that the momentum is now higher at the first building. This model produces weaker streamline plots than the previous ones, around the place of honour. A strong re-circulation occurs at the windward side of the first, second and third buildings, indicating that air momentum in the area between these three buildings and the fence is very high. It can be noted that placing the gate in this position produces greater momentum at the first, second and third buildings.

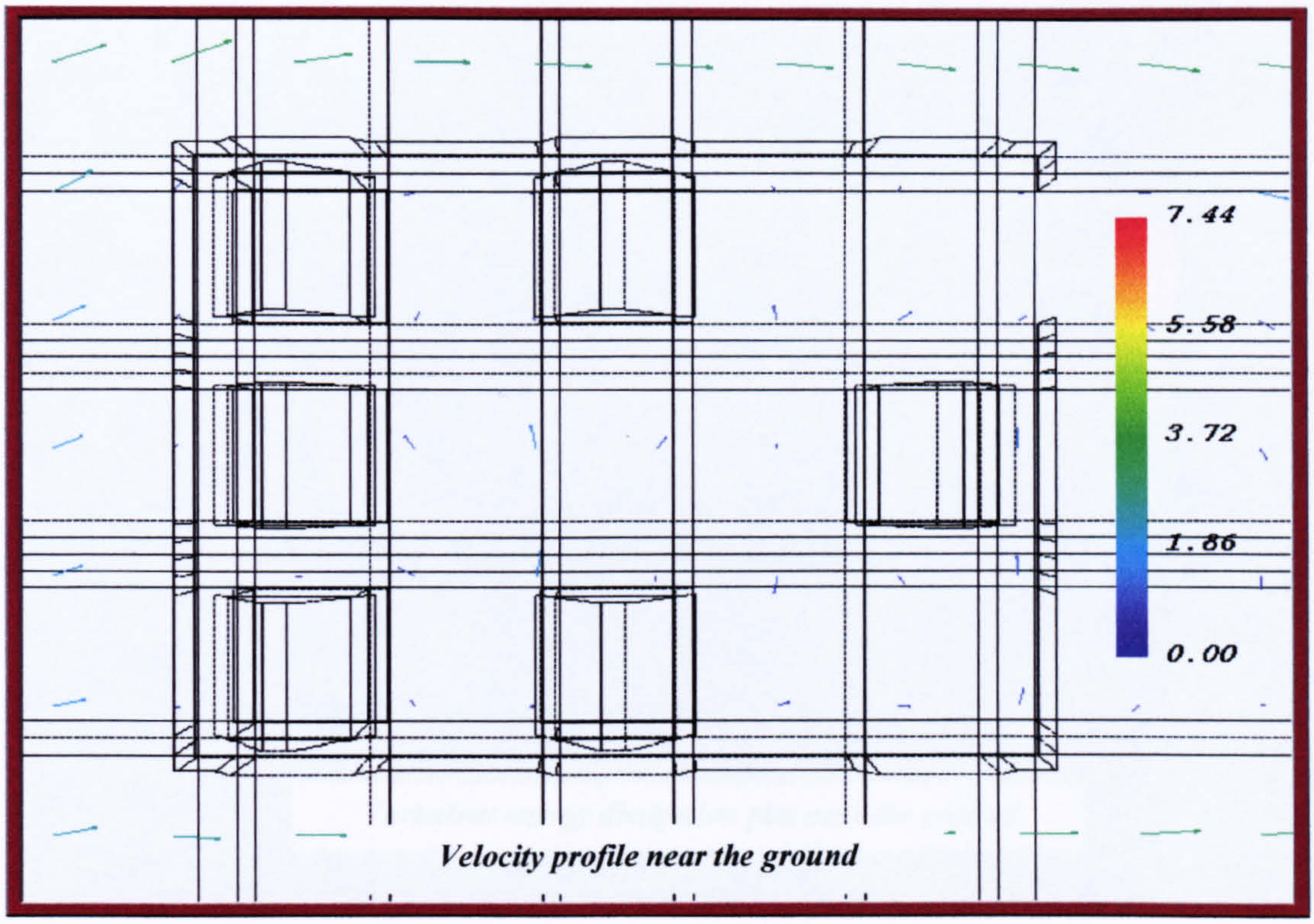

Figure 6.2.41 Velocity profile near the ground

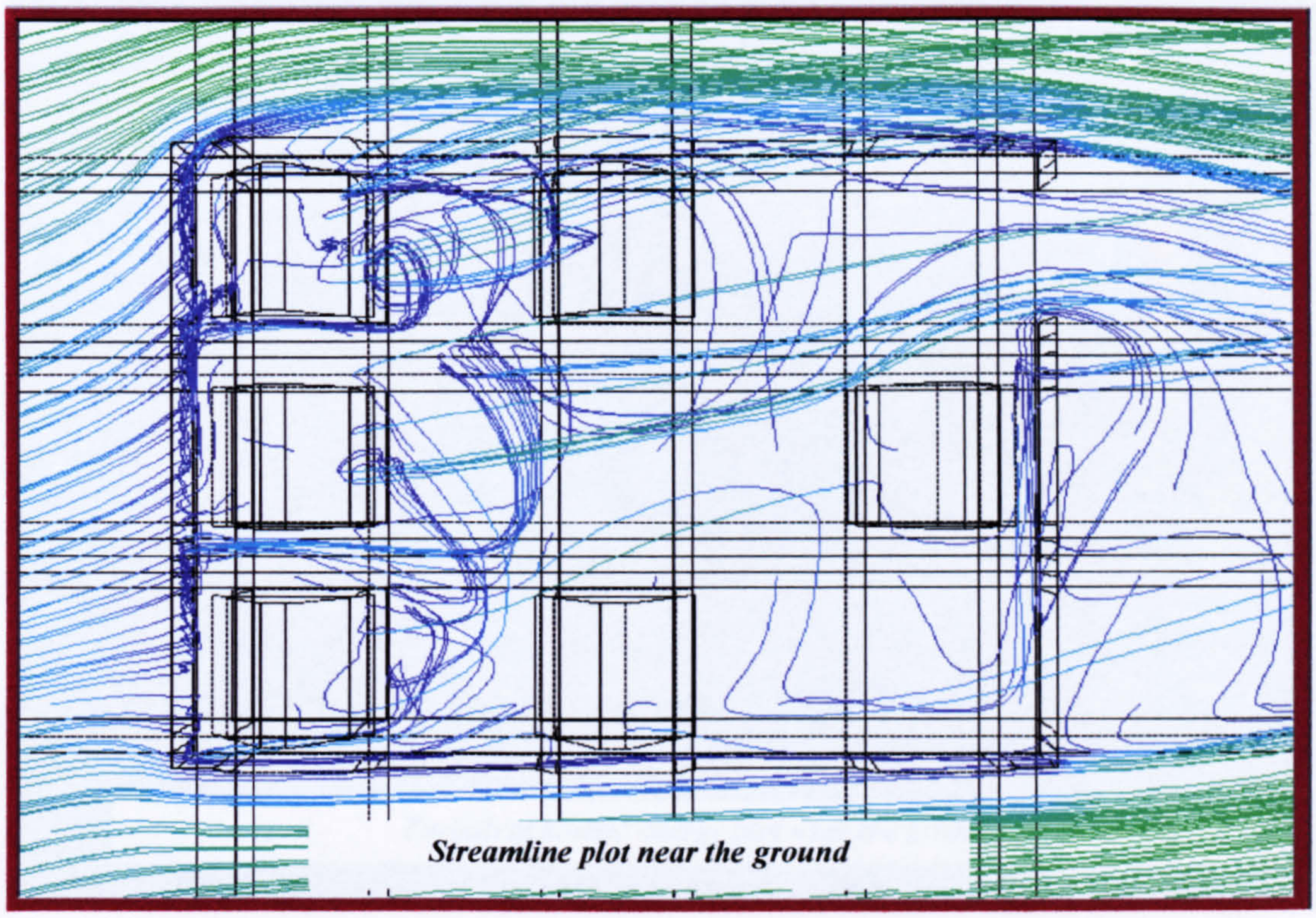

Figure 6.2.42 Streamline plot near the ground

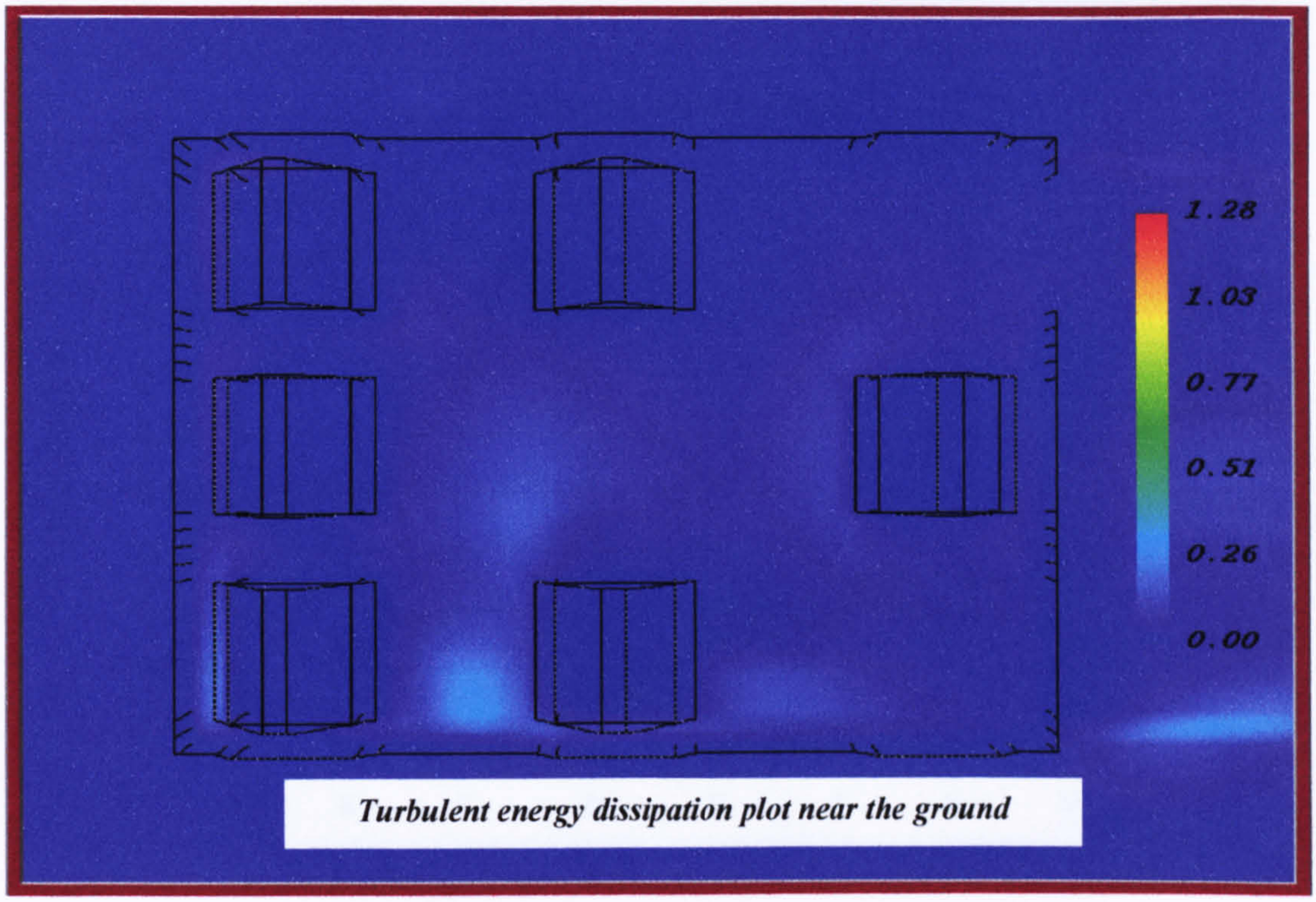

Turbulent energy dissipation plot near the ground

Figure 6.2.43 Turbulent energy dissipation plot near the ground

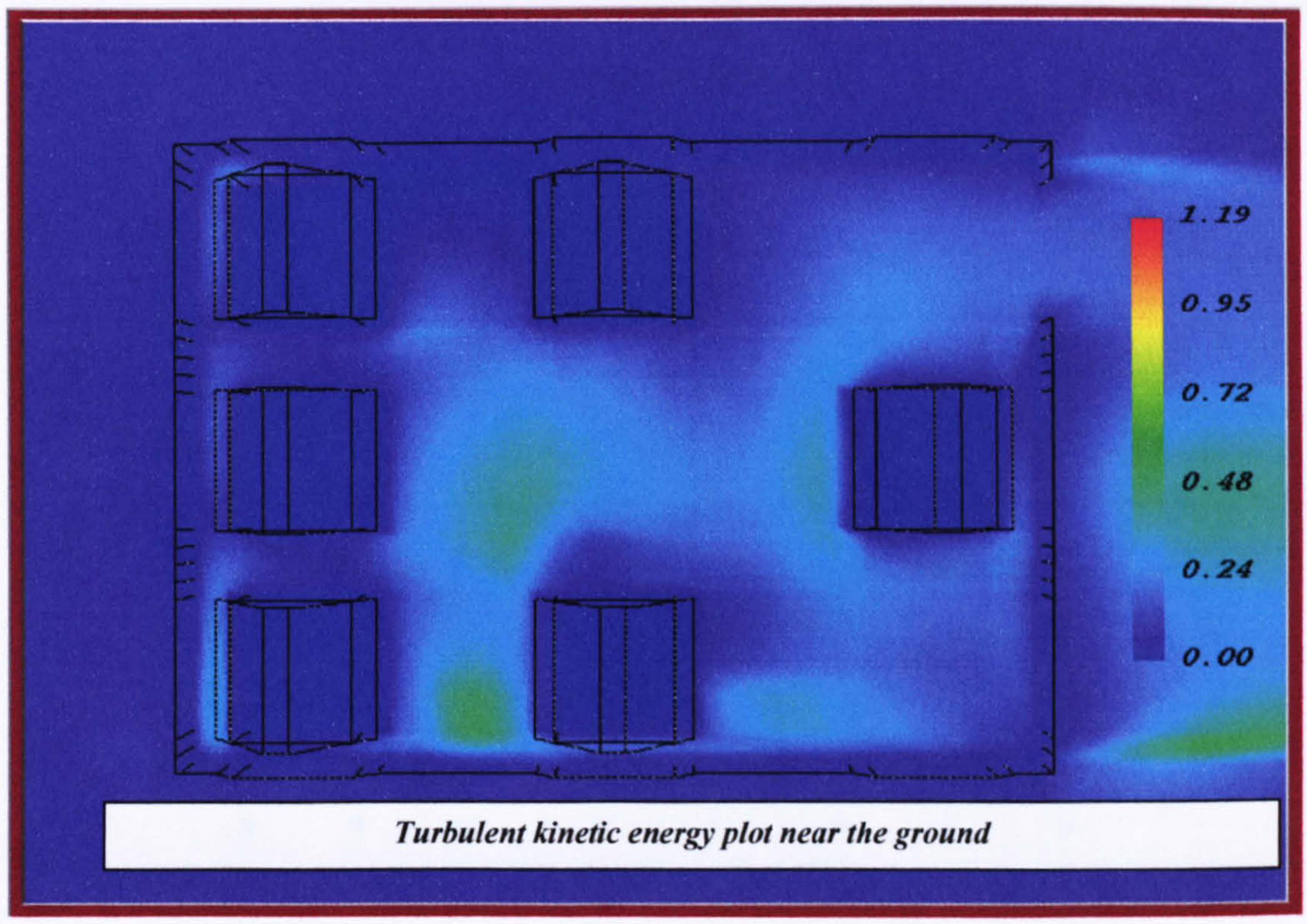

Turbulent kinetic energy plot near the ground

Figure 6.2.44 Turbulent kinetic energy plot near the ground

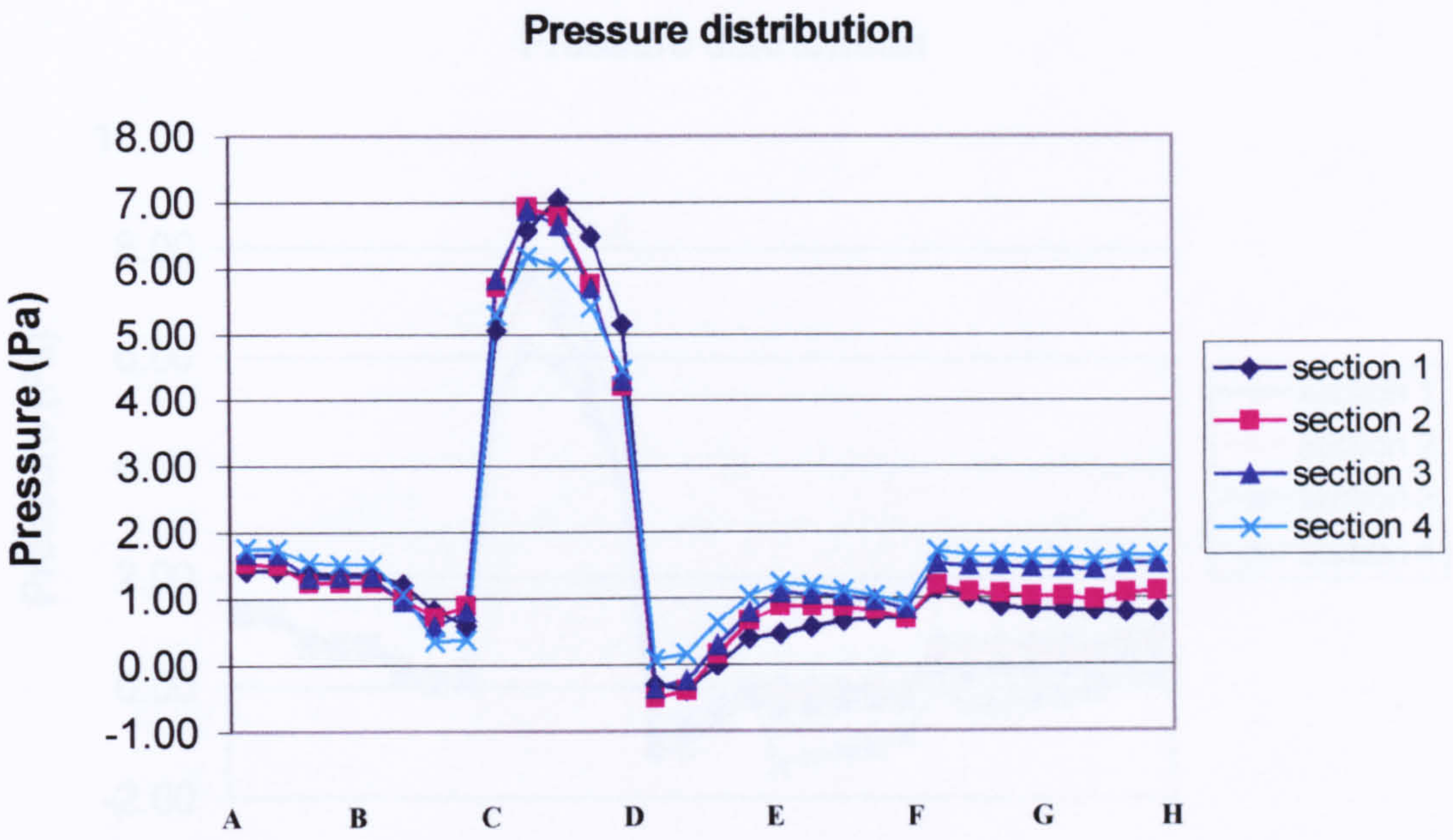

Figure 6.2.45 Pressure distribution on the first building

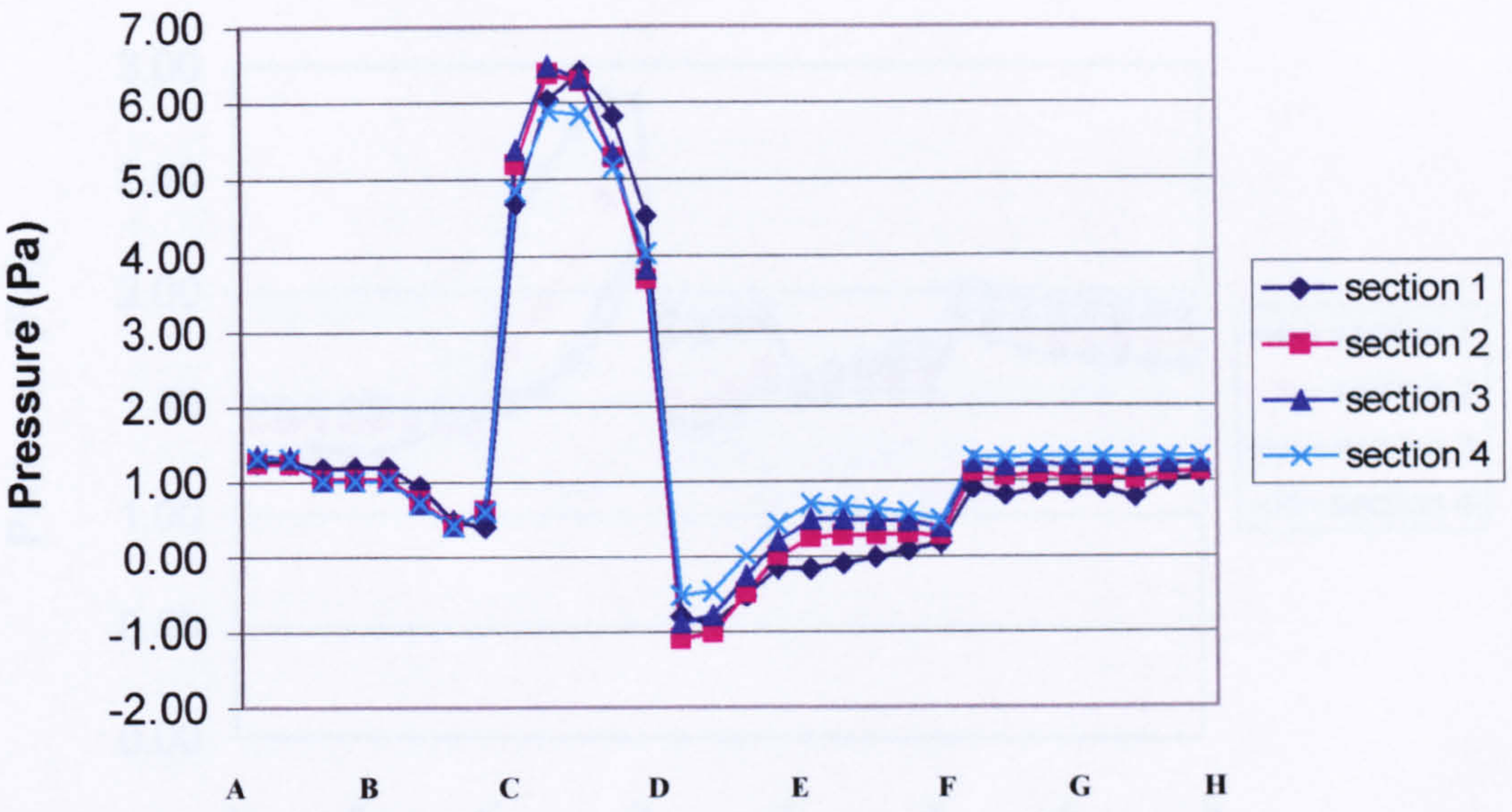

Figure 6.2.46 Pressure distribution on the second building

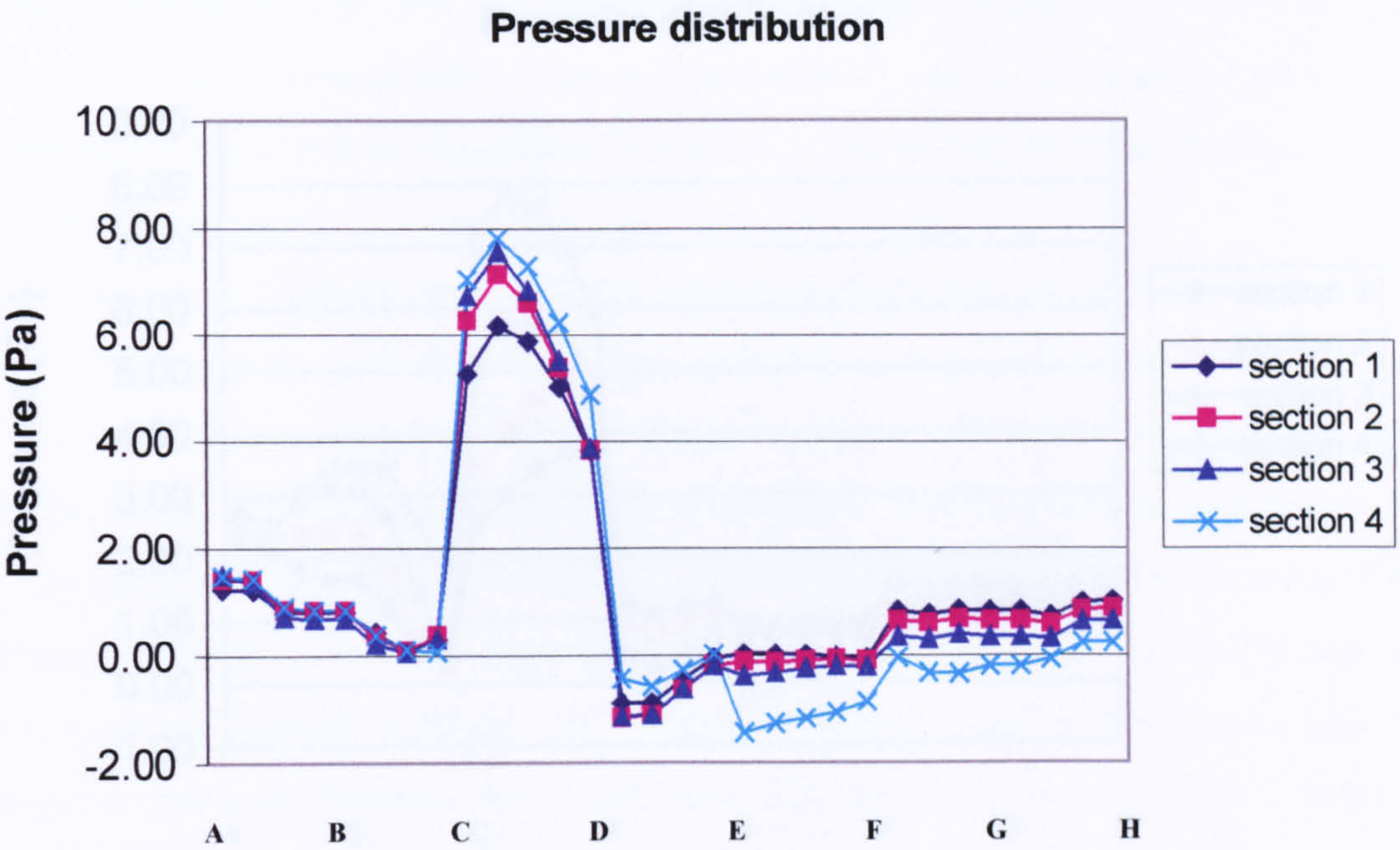

Figure 6.2.47 Pressure distribution on the third building

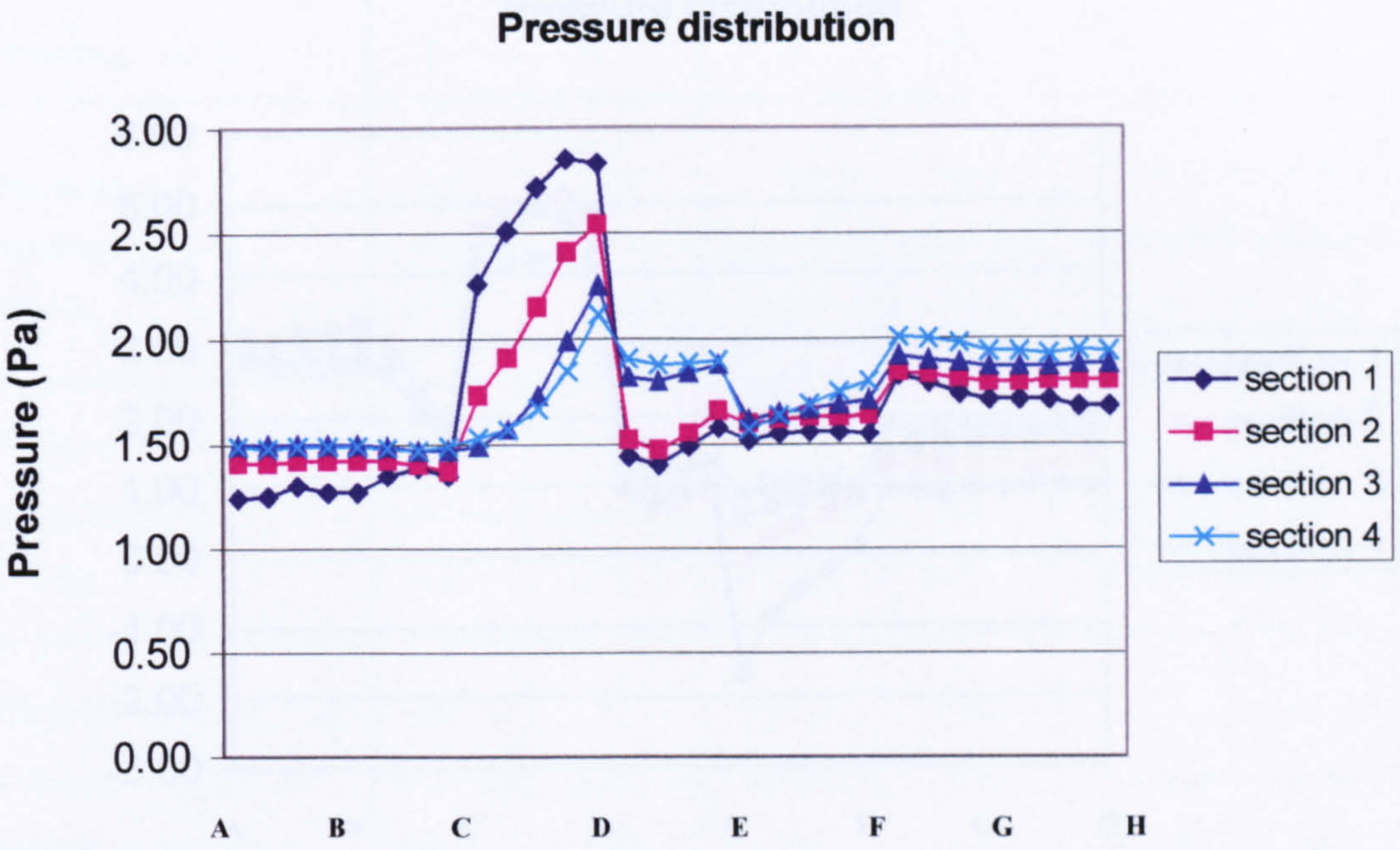

Figure 6.2.48 Pressure distribution on the fourth building

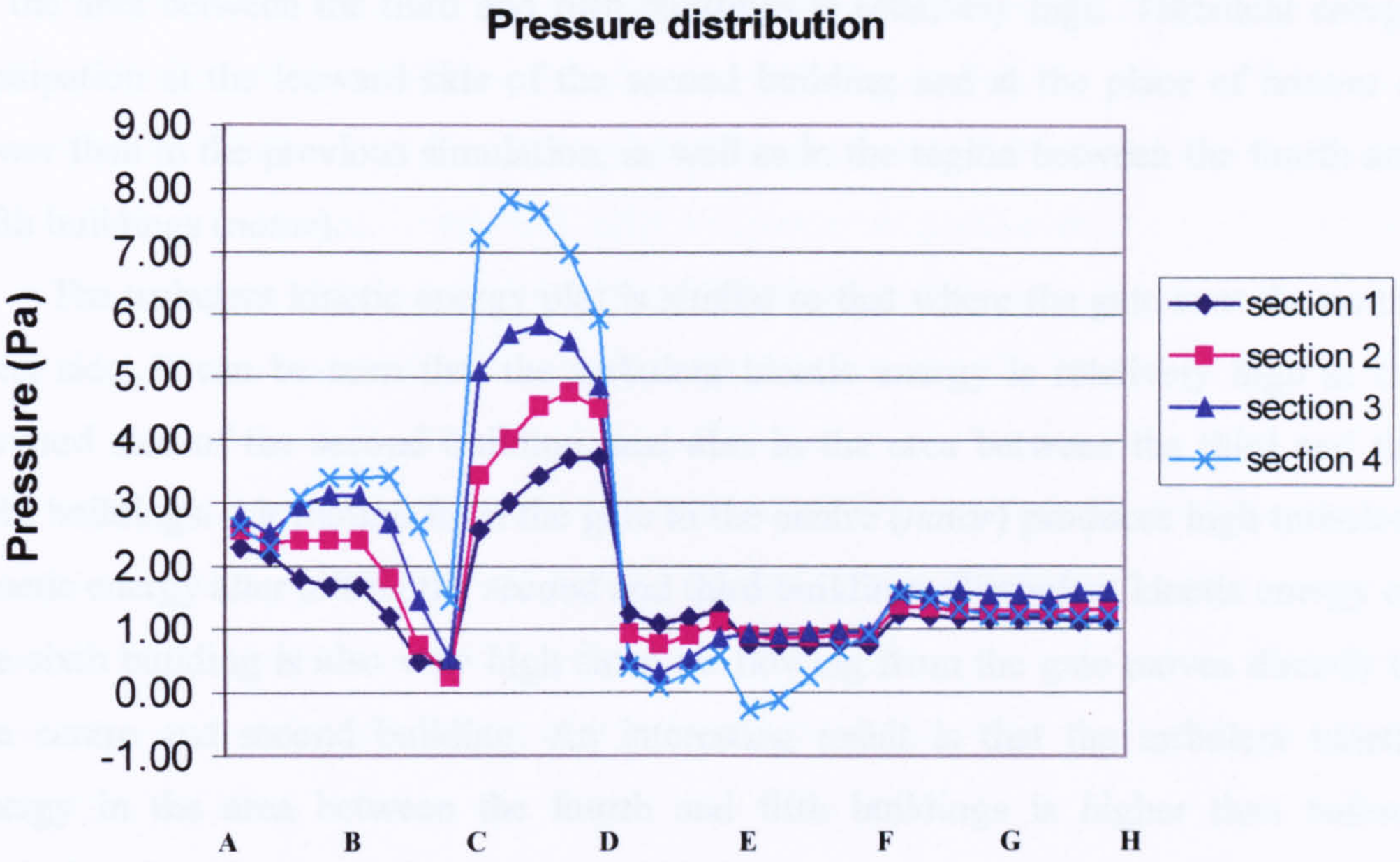

Figure 6.2.49 Pressure distribution on the fifth building

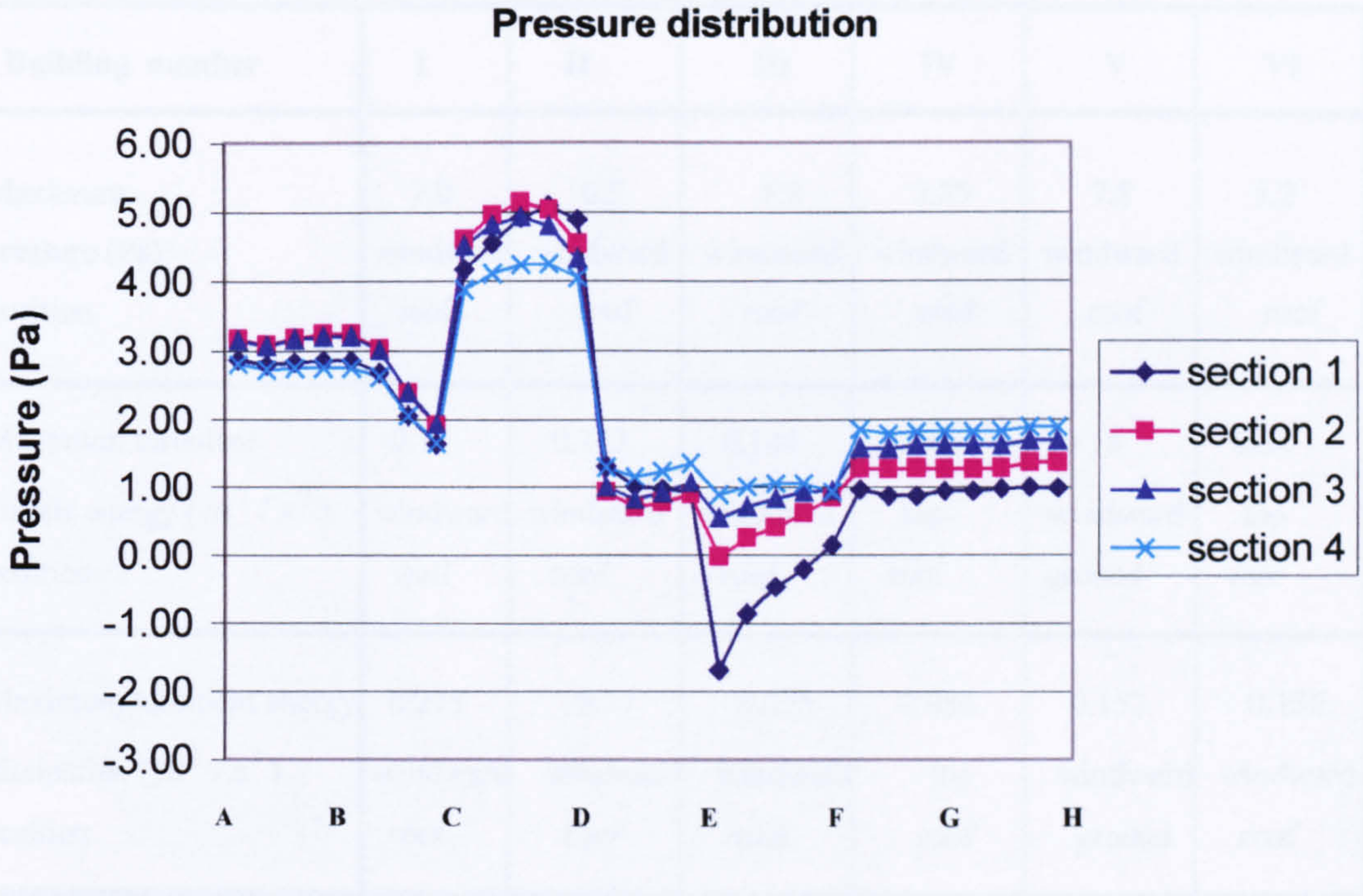

Figure 6.2.50 Pressure distribution on the sixth building

From the turbulent energy dissipation plot, it can be seen that energy dissipation in the area between the third and fifth buildings is relatively high. Turbulent energy dissipation at the leeward side of the second building and at the place of honour is lower than in the previous simulation, as well as in the region between the fourth and fifth buildings (*natar*).

The turbulent kinetic energy plot is similar to that where the gate is at the north-west side. It can be seen that the turbulent kinetic energy is relatively high at the leeward side of the second building, and also in the area between the third and the fifth buildings. Air motion from the gate to the centre (*natar*) produces high turbulent kinetic energy after hitting the second and third buildings. Turbulent kinetic energy on the sixth building is also very high since air flowing from the gate moves directly to the centre and second building. An interesting result is that the turbulent kinetic energy in the area between the fourth and fifth buildings is higher than before. Turbulent kinetic energy is relatively high at the corner between the fifth and sixth buildings where the place of honour lies.

Table 6.2.3 A summary of results for gate at the north side

Building number	**I**	**II**	**III**	**IV**	**V**	**VI**
Maximum pressure (Pa) position	7.0 windward roof	6.5 windward roof	7.9 windward roof	2.85 windward roof	7.8 windward roof	5.2 windward roof
Maximum turbulent kinetic energy (m^2/s^2) position	0.15 windward wall	0.142 windward roof	0.144 windward roof	0.35 top roof	0.18 windward ground	0.32 top roof
Maximum turbulent energy dissipation (m^2/s^3) position	0.275 windward roof	0.27 windward roof	0.275 windward roof	0.086 top roof	0.152 windward ground	0.136 windward roof

From the above statements, we now suggest that *natar* is the area where the turbulent kinetic energy and its dissipation rate are minimum, and the place of honour is the area where they are relatively high.

Pressure distributions for each building are presented in Figures 6.2.45 – 6.3.50. Pressure at the second, third and fifth buildings is greater than in other areas. Therefore, a gate on the north side of the buildings arrangement produces a similar pressure profile to that where the gate is at the north-west side. Similar results for the pressure variation are obtained for all six buildings.

A summary of results for pressure distribution, turbulent kinetic energy and dissipation rate is presented in Table 6.2.3. It can be seen that results for pressure and both turbulent kinetic and energy dissipation are similar to Table 6.2.2. Therefore, traditional meaning of this gate position should be similar to that where the gate is at the north-west side.

6.2.4 Gate at the East Side

The gate is now placed on the east side, as shown in Figure 3.2.51. Traditional meaning for this gate position is presented in Figure 6.2.1, a good value for the occupants.

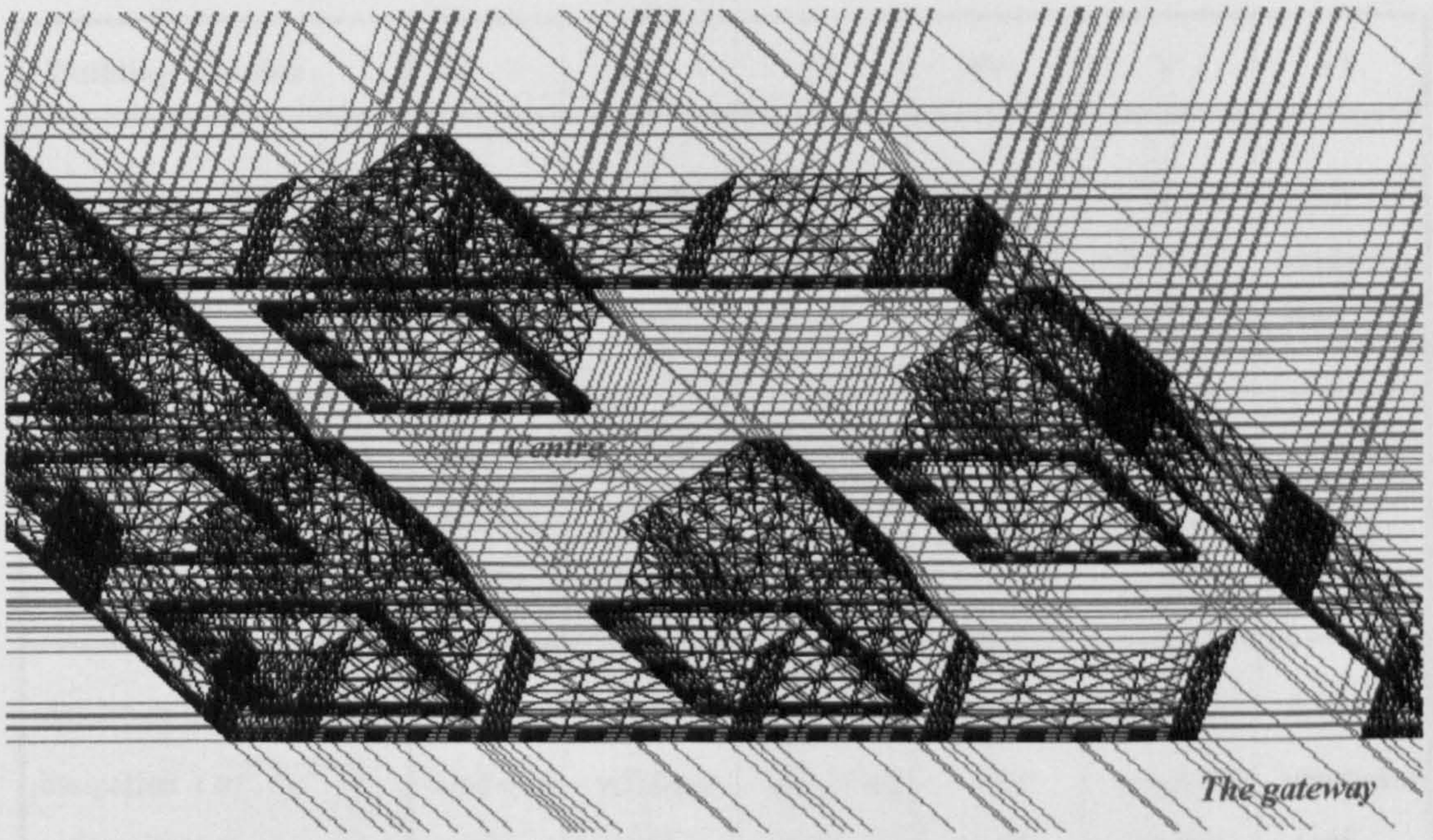

Figure 6.2.51 Side view of buildings arrangement with gate on east side

6.2.4.1 Results and Discussion

The velocity near the ground is relatively high at the leeward side of the second building, as well as at the corner where the shrines of gods is placed. This is similar to the case where the gate was placed on the north side. The velocity at 8 m above roof once more shows a uniform profile.

A summary of results for pressure distribution, turbulent kinetic energy and dissipation rate is presented in Table 6.2.4. It can be seen that the maximum pressure, turbulent kinetic energy and dissipation are similar to that in previous analyses. Therefore, traditional meaning for this gate position should be similar to that for gate positions in Figures 6.2.40 and 6.2.51. Since the traditional meaning of both gates is "good" for occupants, as indicated in Figures 6.2.27 and 6.2.51, we suggest that traditional meaning may have a relation to wind engineering or architectural aerodynamics. It was shown that these gate positions reduce pressure and energy on buildings. Since the results in Table 6.2.3 are similar to that in Tables 6.2.2 and 6.2.4, we now conclude that the traditional meaning for the gate position in Figure 6.2.40 is also a "good" value.

Table 6.2.4 A summary of results for gate at the east side

Building number	**I**	**II**	**III**	**IV**	**V**	**VI**
Maximum pressure (Pa) and position	7.0 windward roof	6.5 windward roof	7.9 windward roof	3.0 windward roof	7.8 windward roof	5.0 windward roof
Maximum turbulent kinetic energy (m^2/s^2) and position	0.144 windward roof	0.144 windward roof	0.144 windward roof	0.348 top roof	0.18 windward ground	0.325 top roof
Maximum turbulent energy dissipation (m^2/s^3) and position	0.275 windward roof	0.27 windward roof	0.275 windward roof	0.085 top roof	0.15 windward ground	0.132 windward roof

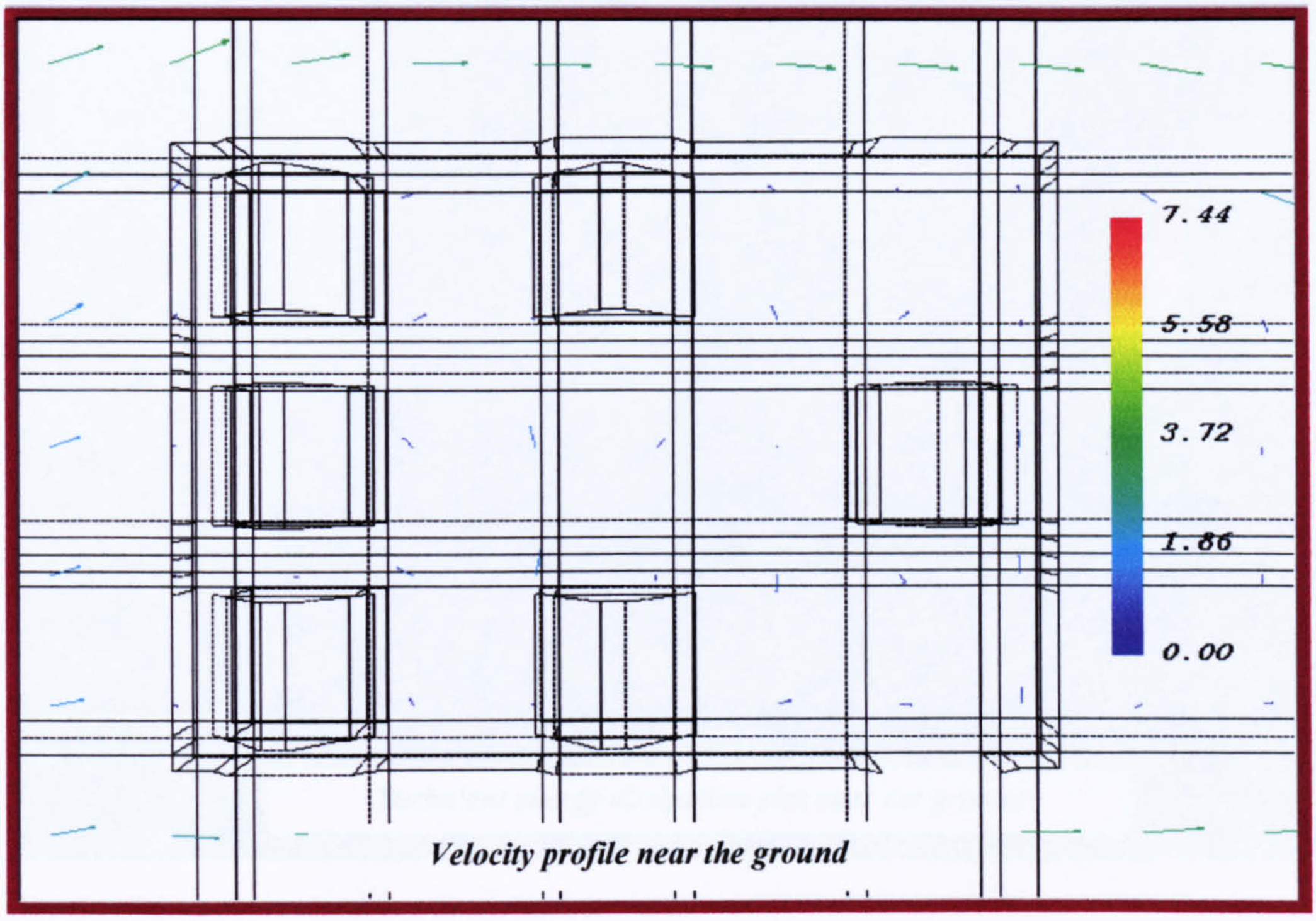

Figure 6.2.52 Velocity profile near the ground

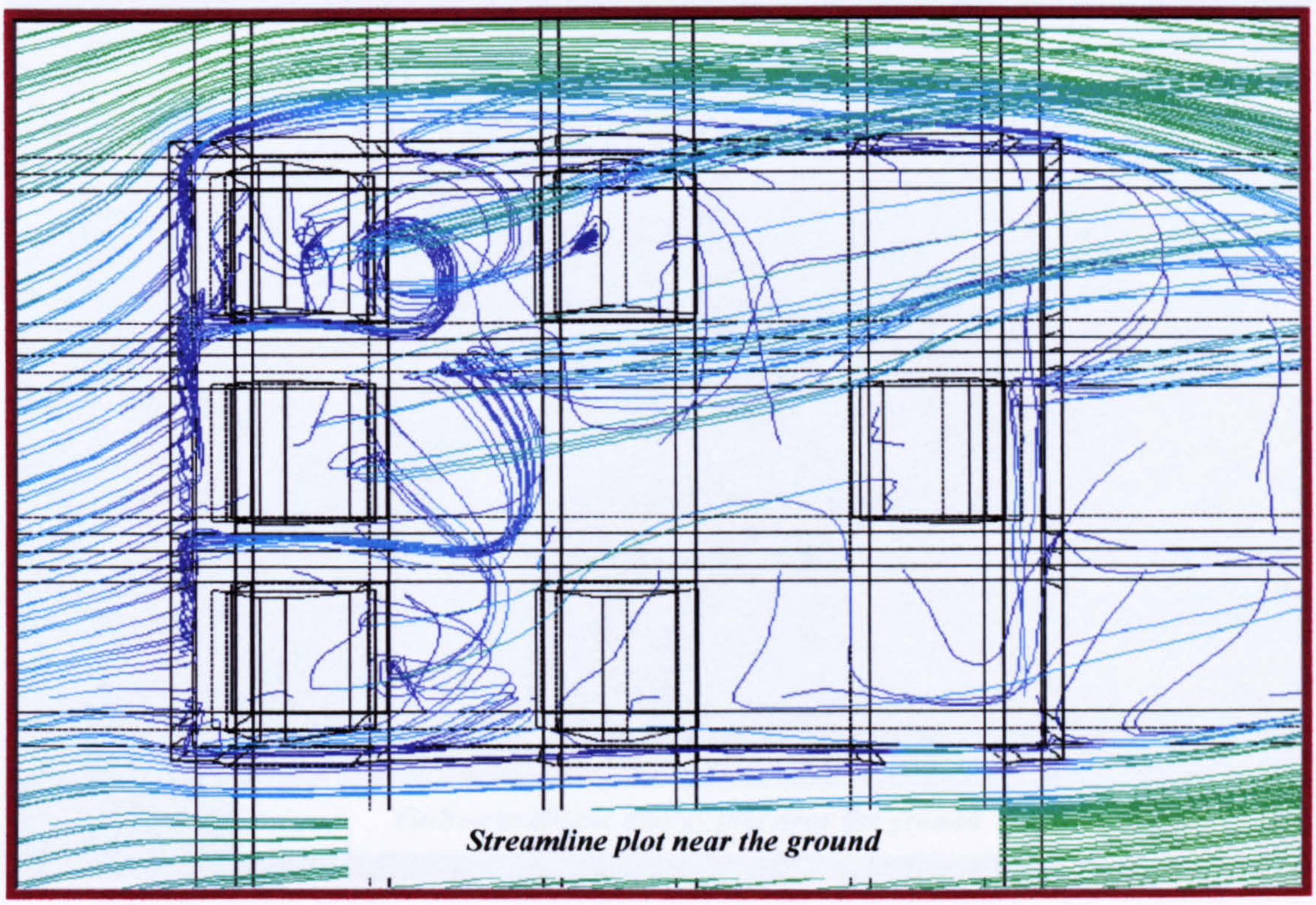

Figure 6.2.53 Streamline plot near the ground

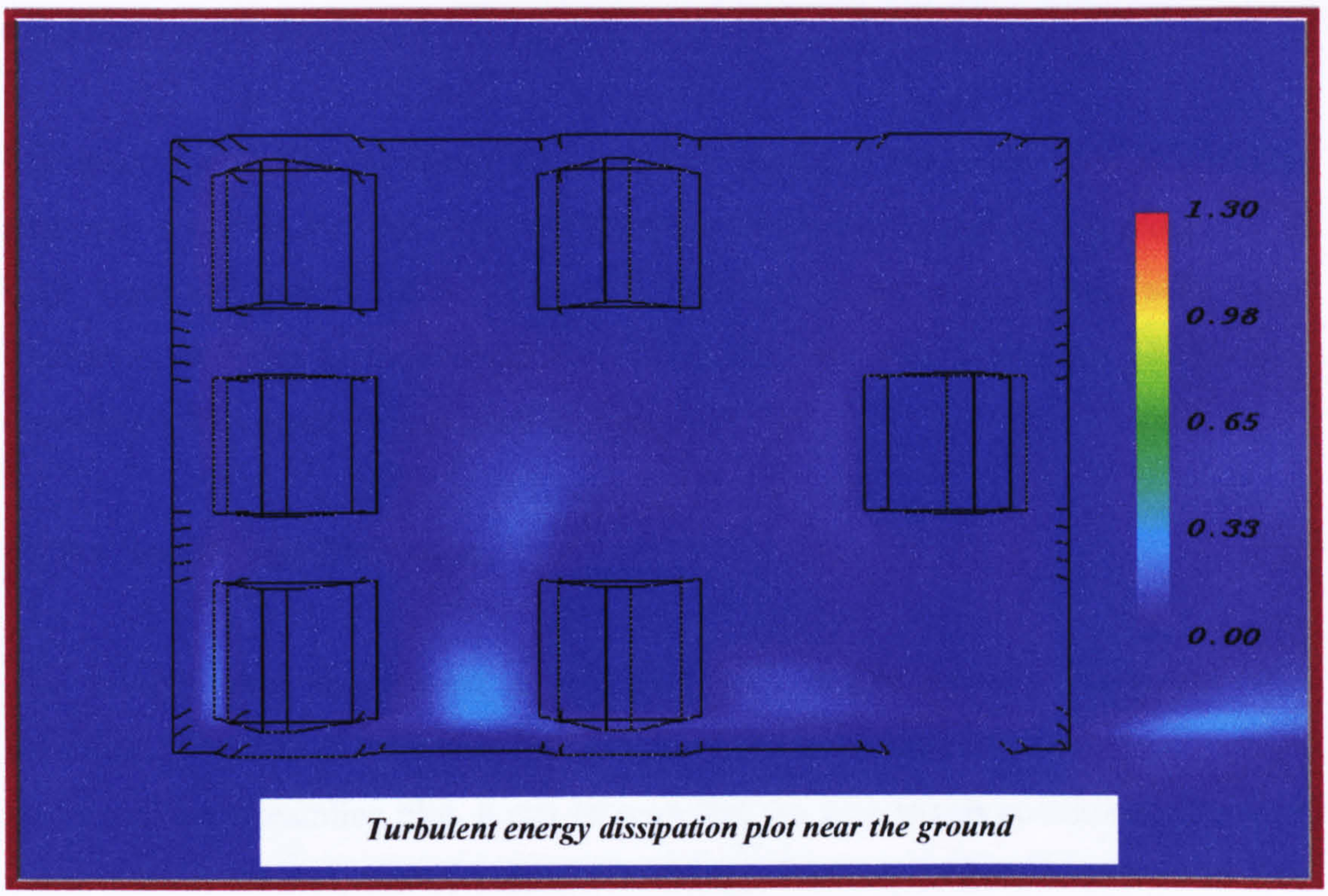

Turbulent energy dissipation plot near the ground

Figure 6.2.54 Turbulent energy dissipation plot near the ground

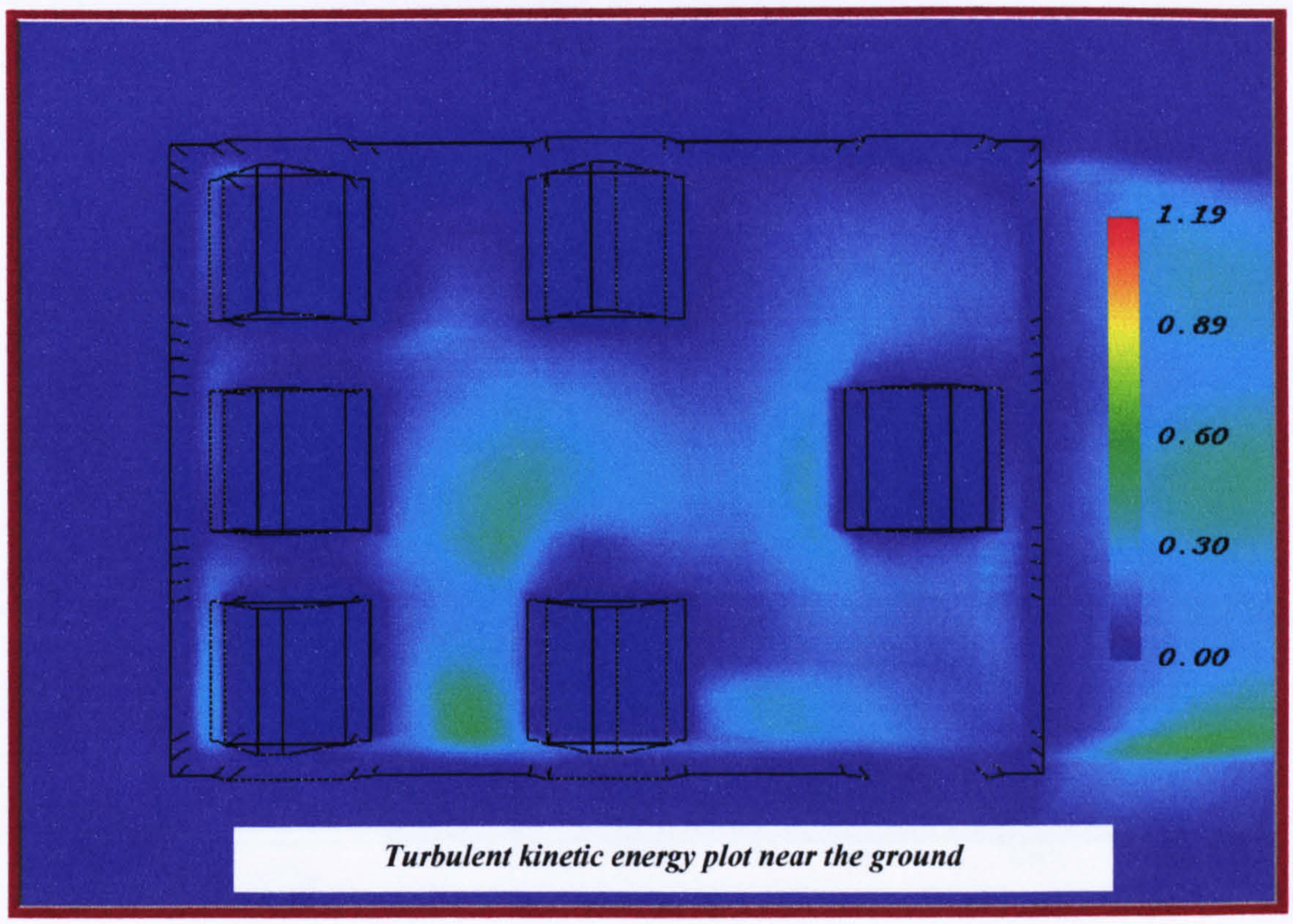

Turbulent kinetic energy plot near the ground

Figure 6.2.55 Turbulent kinetic energy plot near the ground

6.2.5 Gate at the South Side

The gate of a well-to-do-family house is now placed at the south side. In previous analyses, a correlation was observed between traditional meaning and reduction of wind loads and energy on buildings. All gates previously studied were very wide. Therefore, in order to understand the effects the gate size, a smaller gate is now considered. The model is presented in Figure 6.2.56.

6.2.5.1 Results and Discussion

The velocity near the ground is relatively high at the second, fourth and fifth buildings, as well as at the corner between the fourth and sixth buildings.

From the streamline plot, it can be seen that the gate in this position creates high momentum at the first, second and third buildings, similarly to the previous cases. The streamline plot around the place of honour is weaker than previously. A strong re-circulation occurs at the windward side of the first three buildings, indicating that the

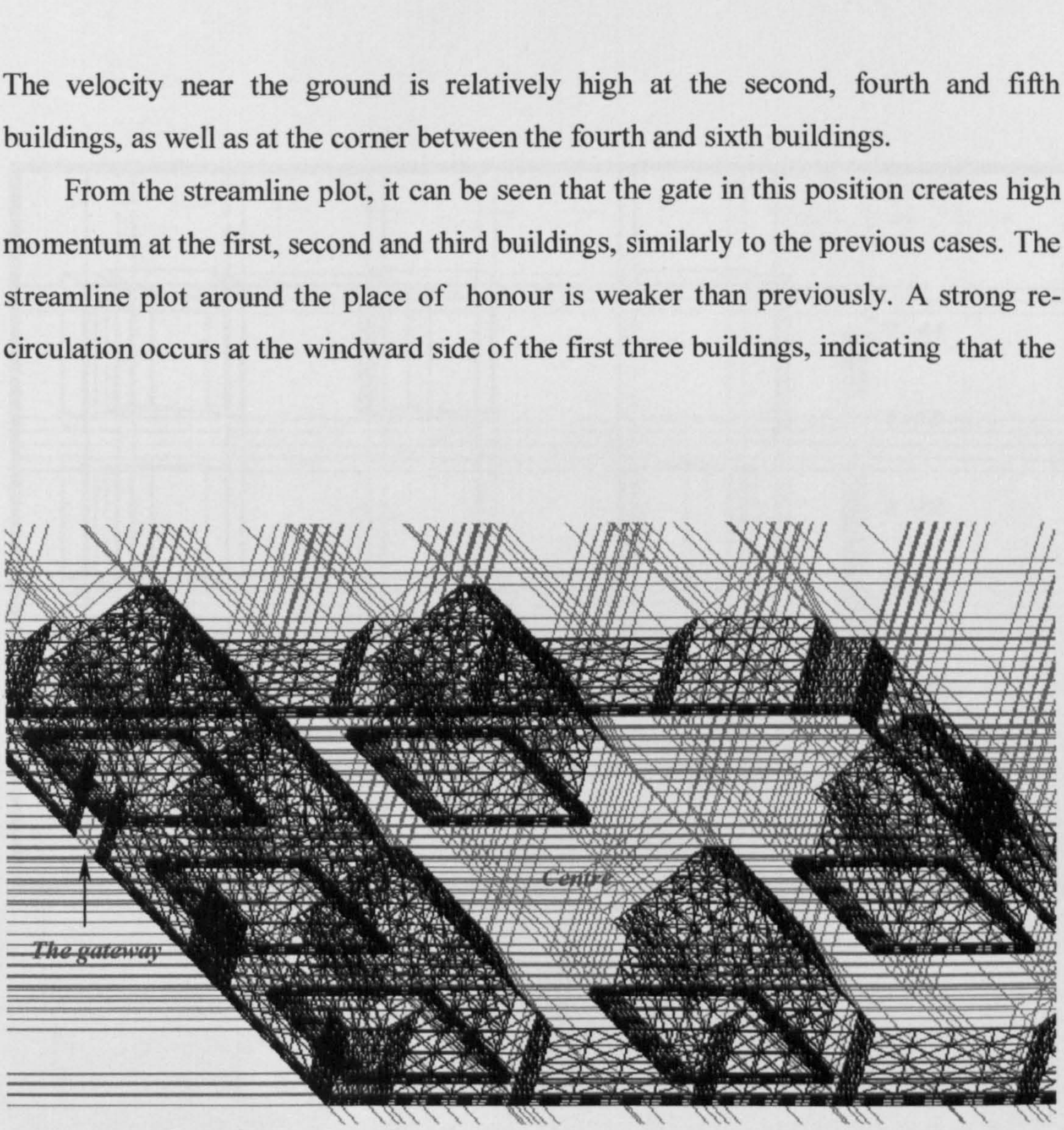

Figure 6.2.56 Side view of buildings arrangement with gate on south side and with a smaller entrance

momentum in the area between the first, second and third buildings and the fences is very high. It can be seen that the streamlines move from the gate to the centre, indicating that the velocity around the buildings also depends on the gate position.

From the turbulent energy dissipation plot, it can be seen that energy dissipation in the area between the third and fifth buildings is relatively high, as it is in the area between the first and second buildings, in the leeward side of the second building, in the windward side of the sixth building and in the place of honour. The turbulent energy dissipation in the place of honour is also similar to the previous cases, as well as in the region between the fourth and fifth buildings (*natar*).

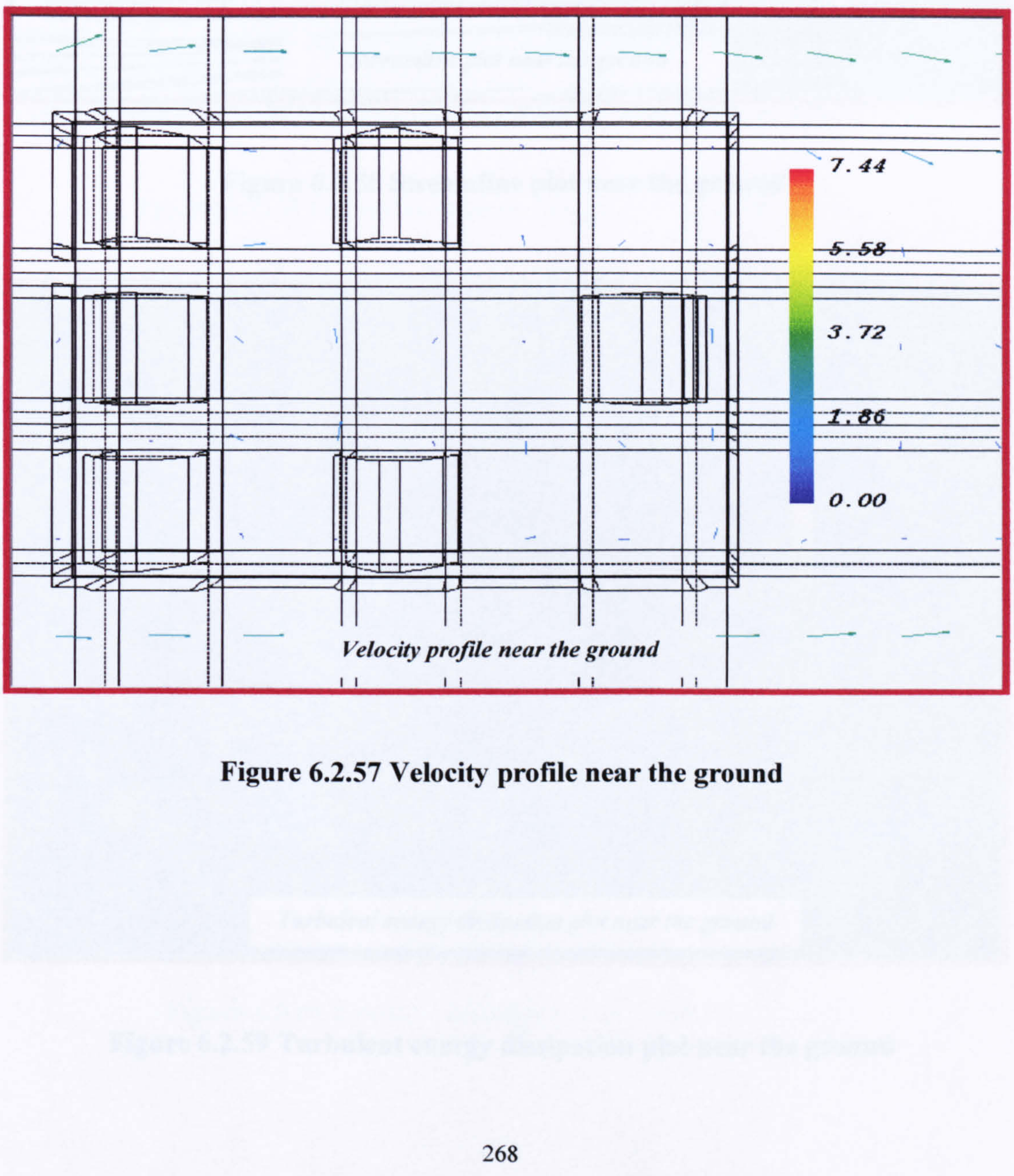

Figure 6.2.57 Velocity profile near the ground

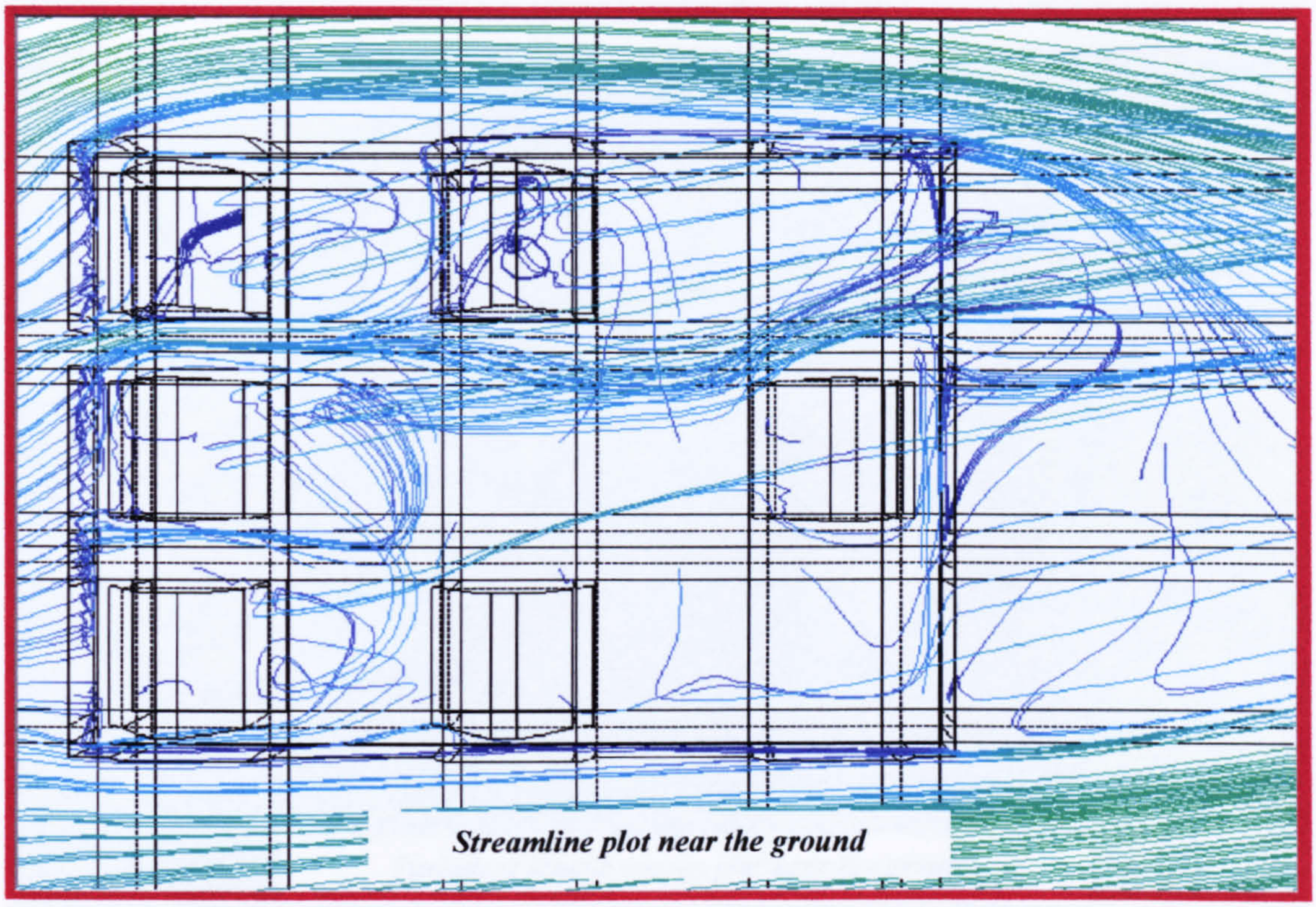

Figure 6.2.58 Streamline plot near the ground

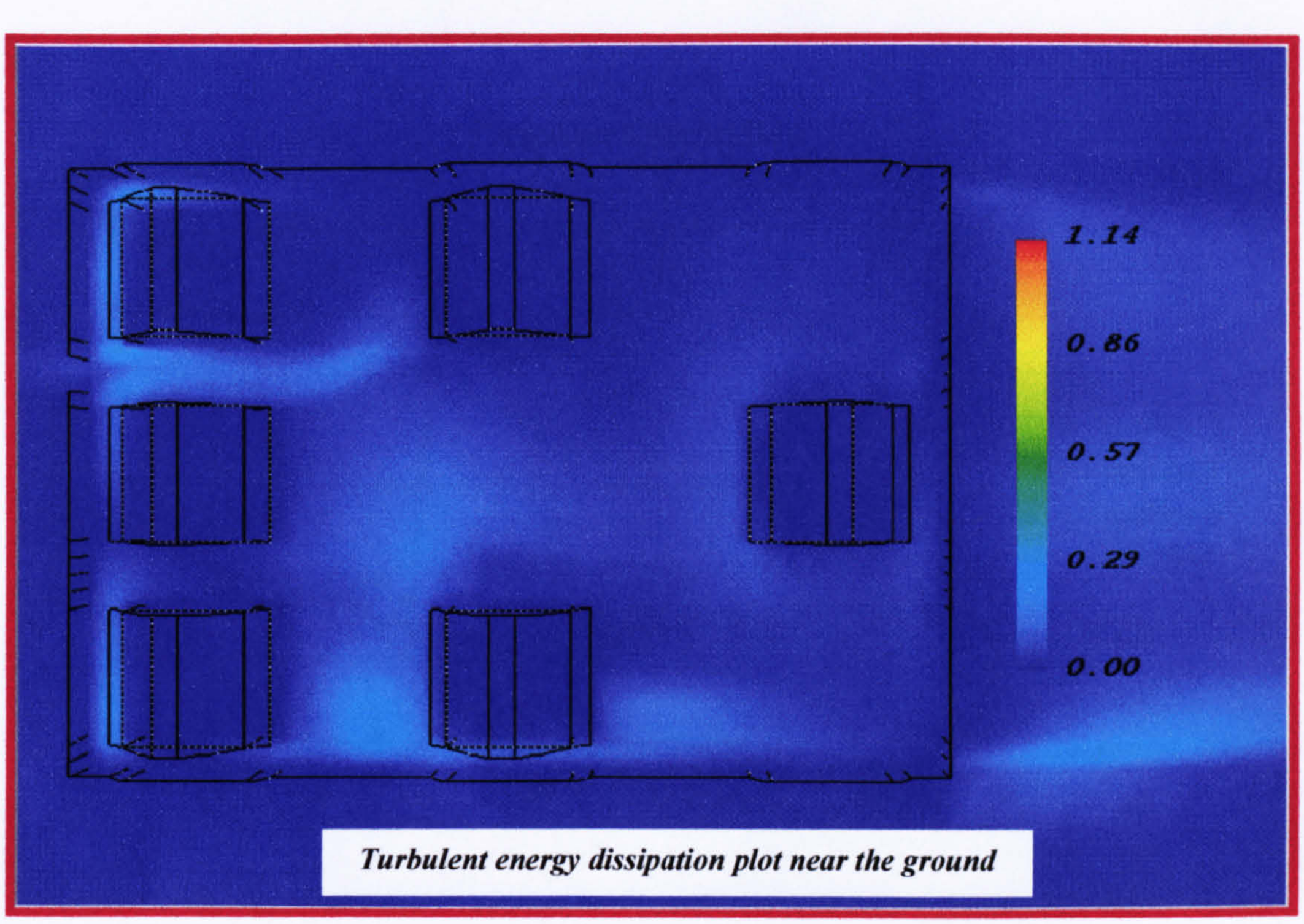

Figure 6.2.59 Turbulent energy dissipation plot near the ground

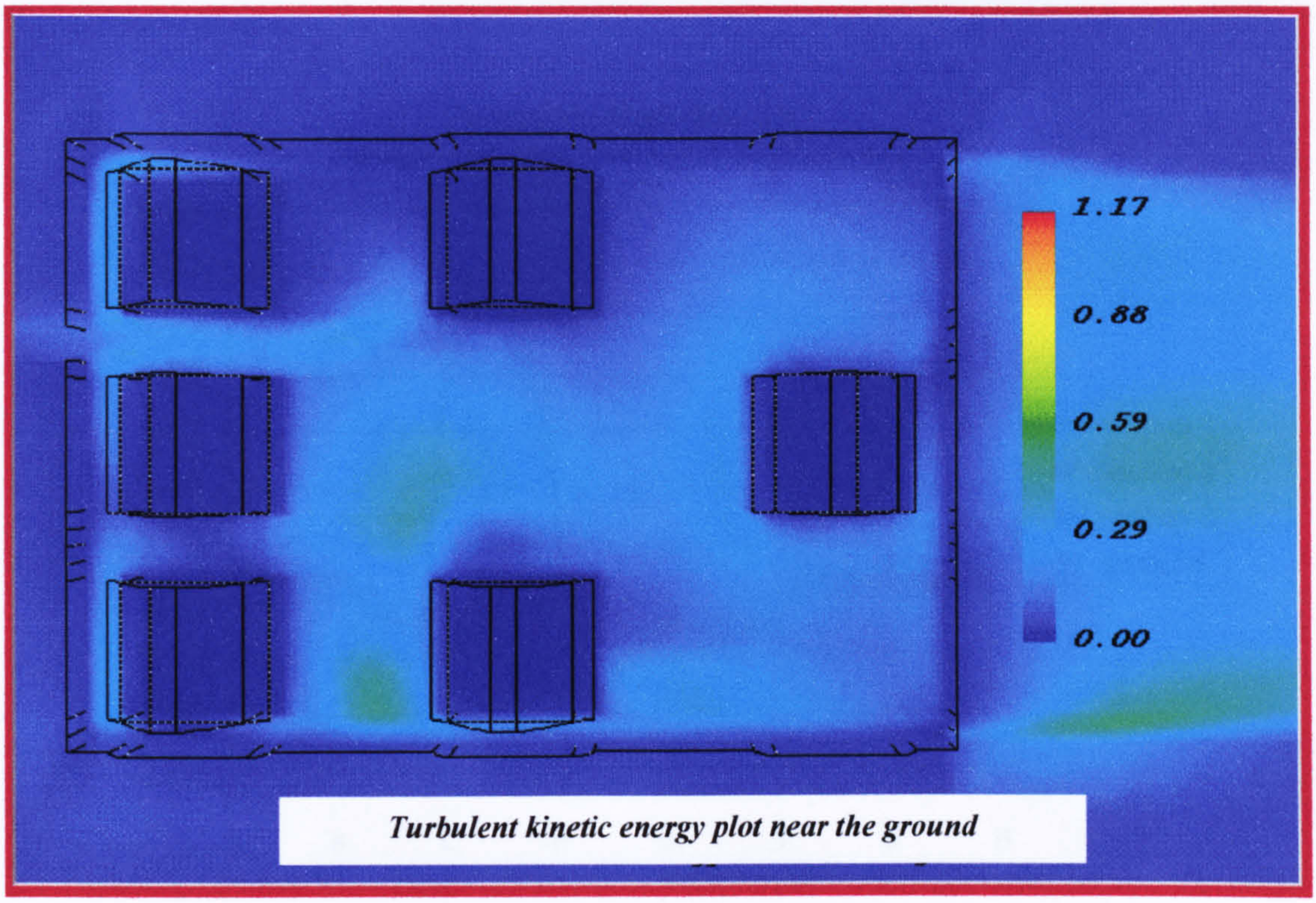

Figure 6.2.60 Turbulent kinetic energy plot near the ground

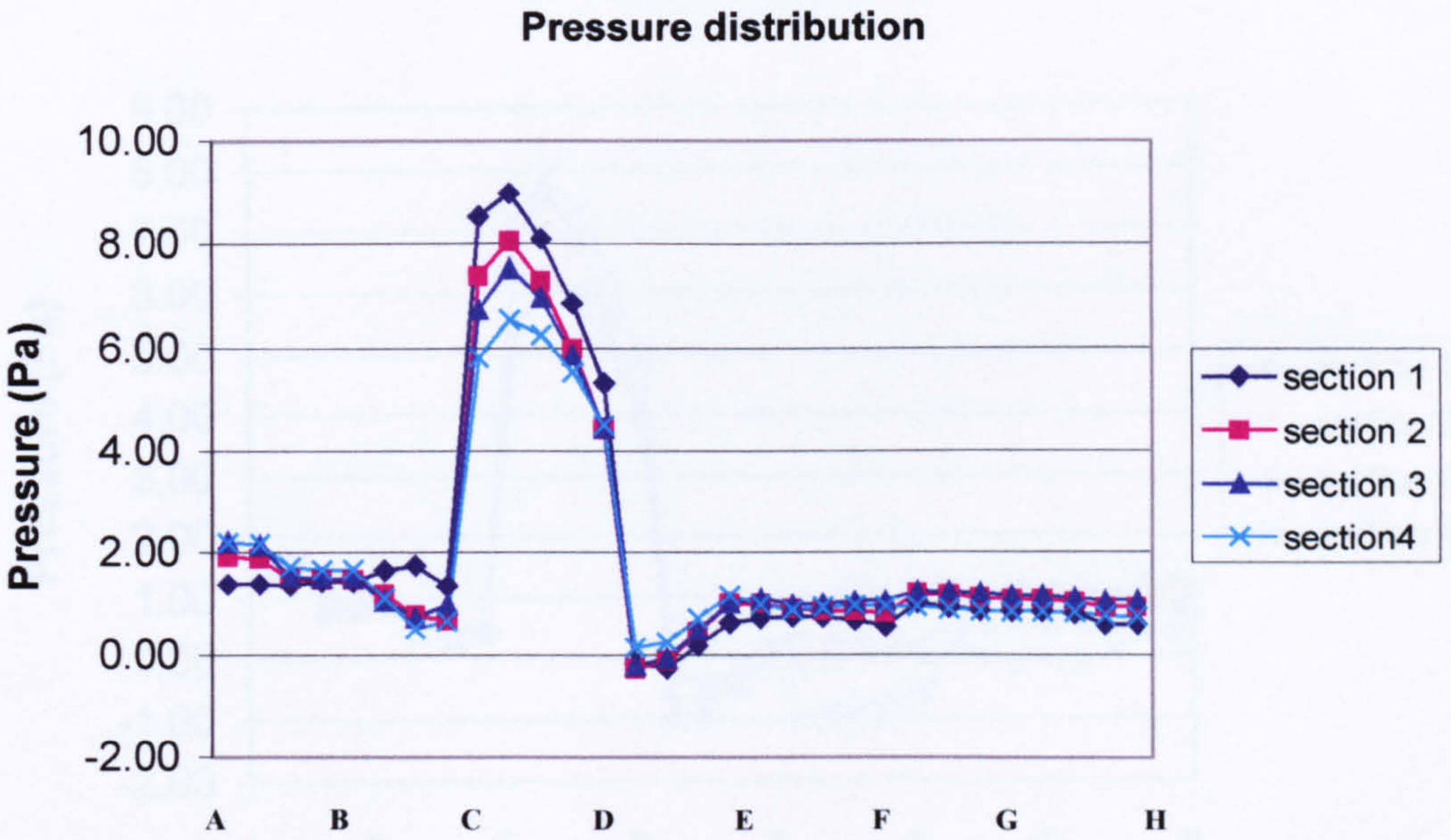

Figure 6.2.61 Pressure distribution on the first building

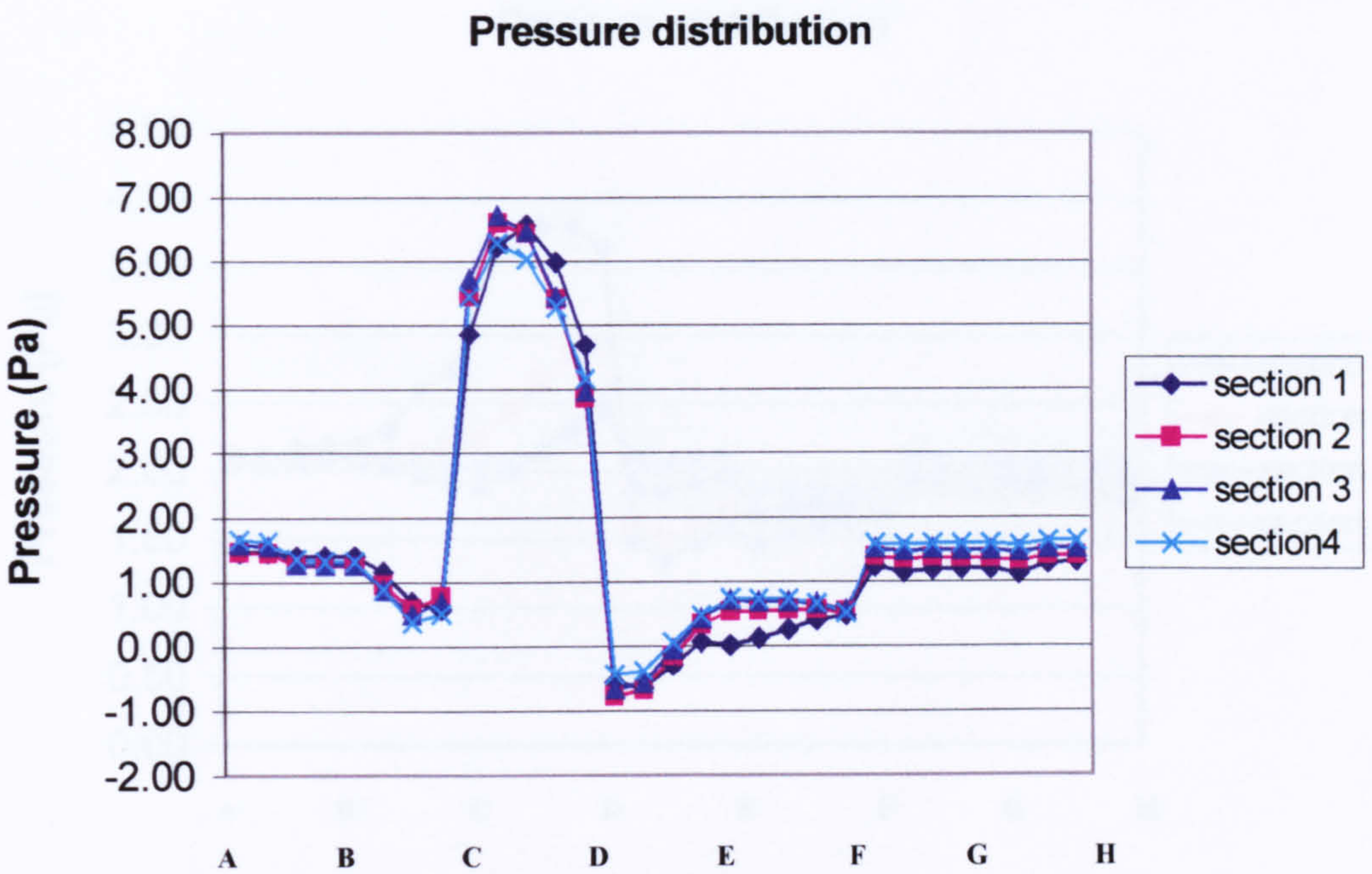

Figure 6.2.62 Pressure distribution on the second building

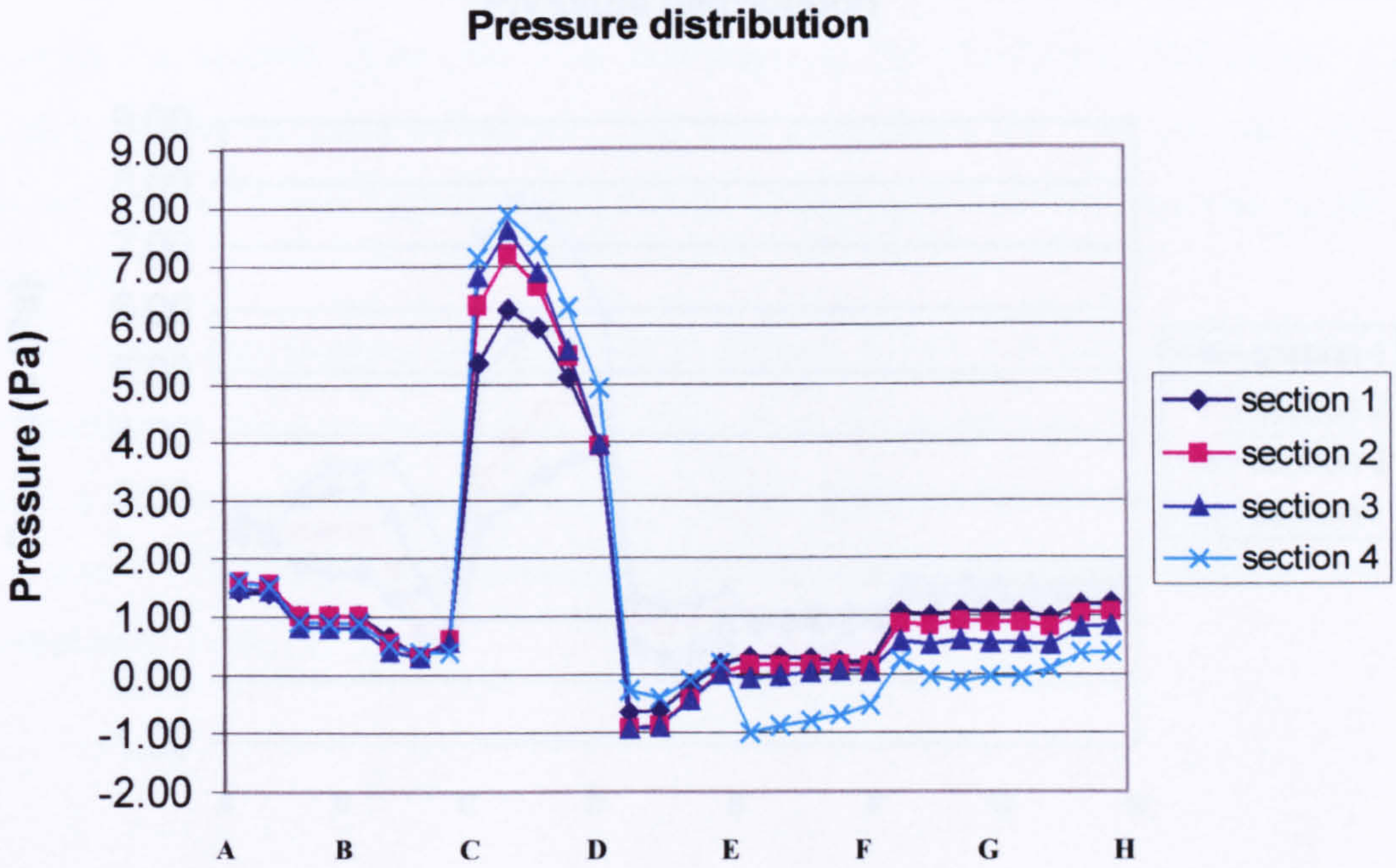

Figure 6.2.63 Pressure distribution on the third building

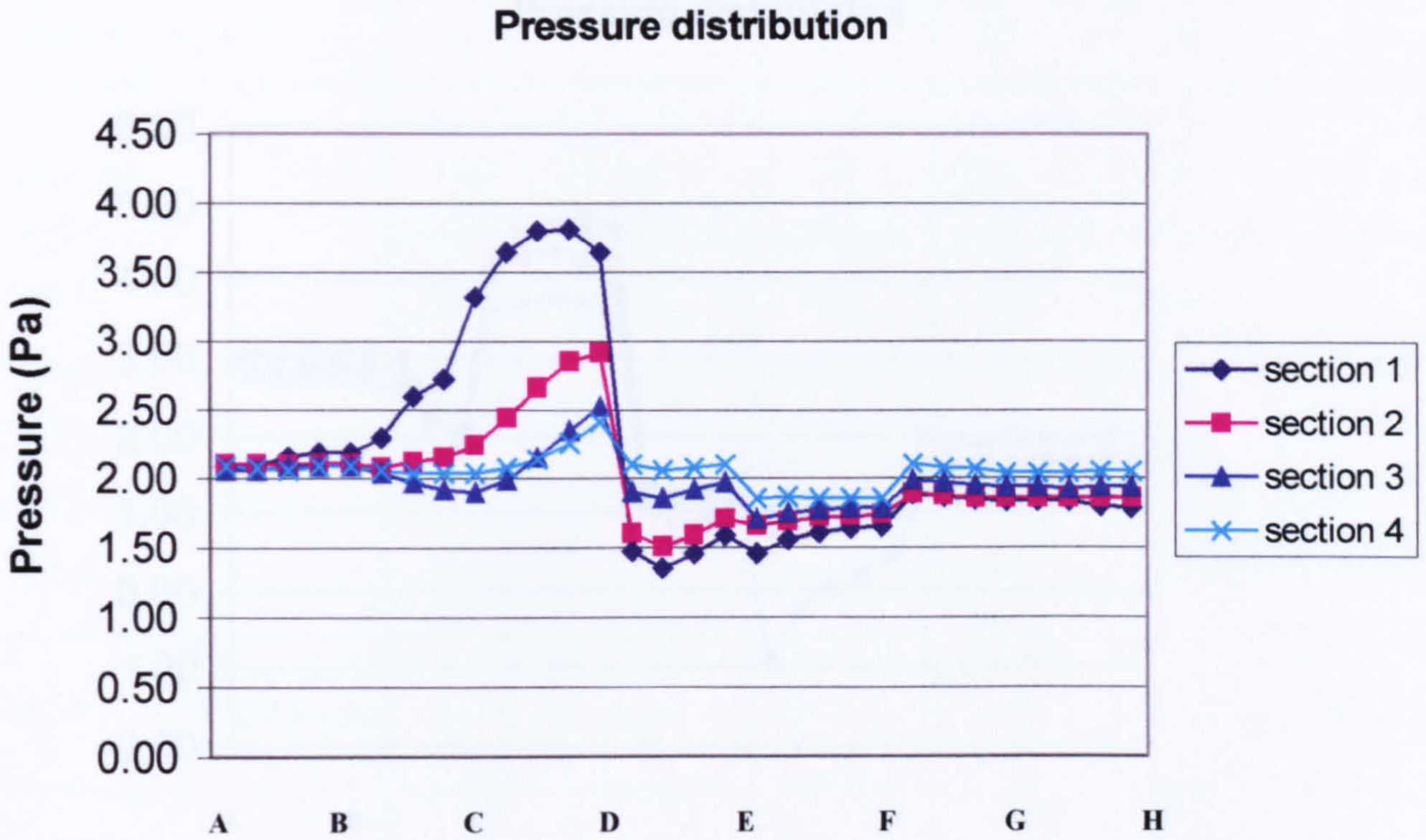

Figure 6.2.64 Pressure distribution on the fourth building

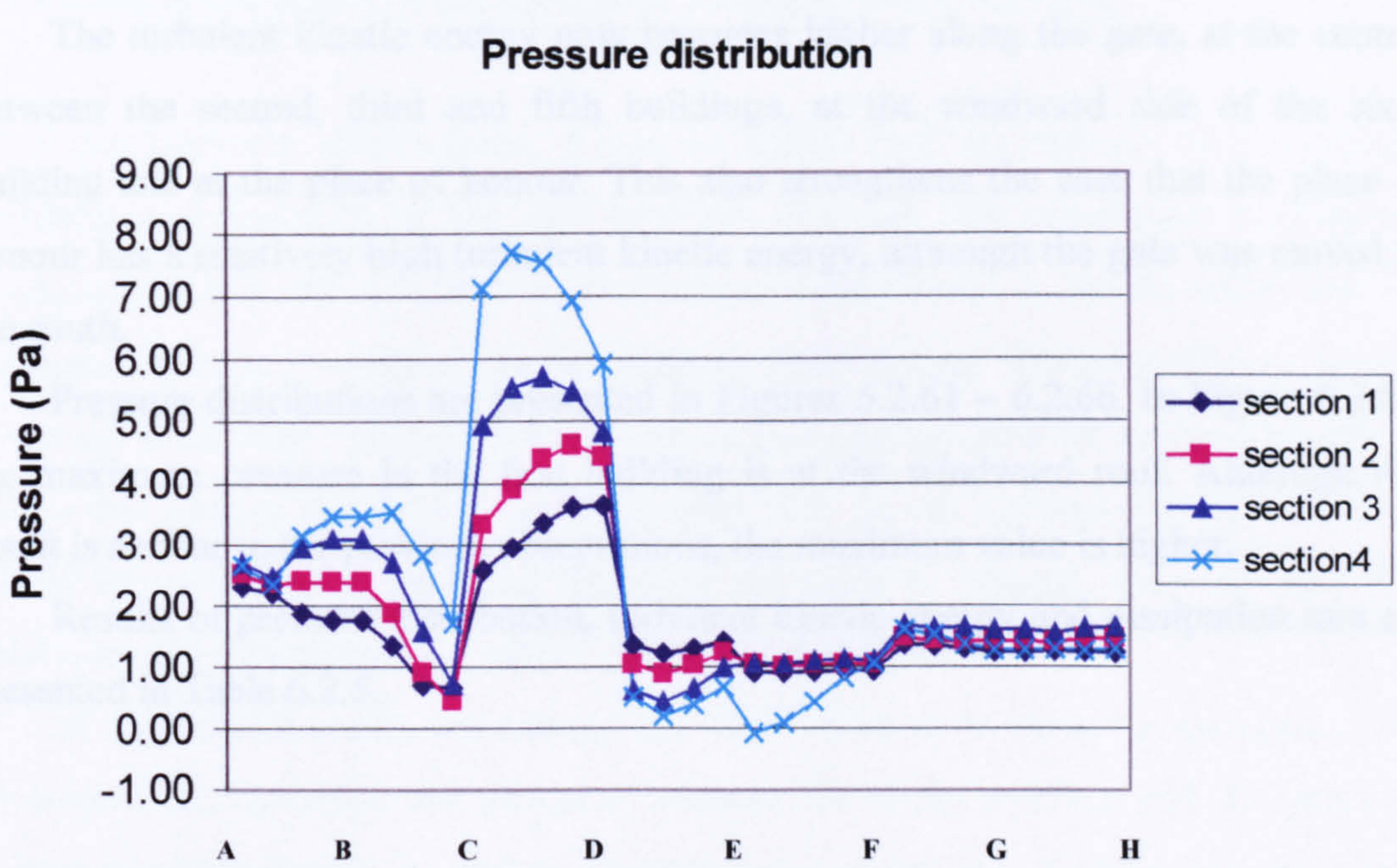

Figure 6.2.65 Pressure distribution on the fifth building

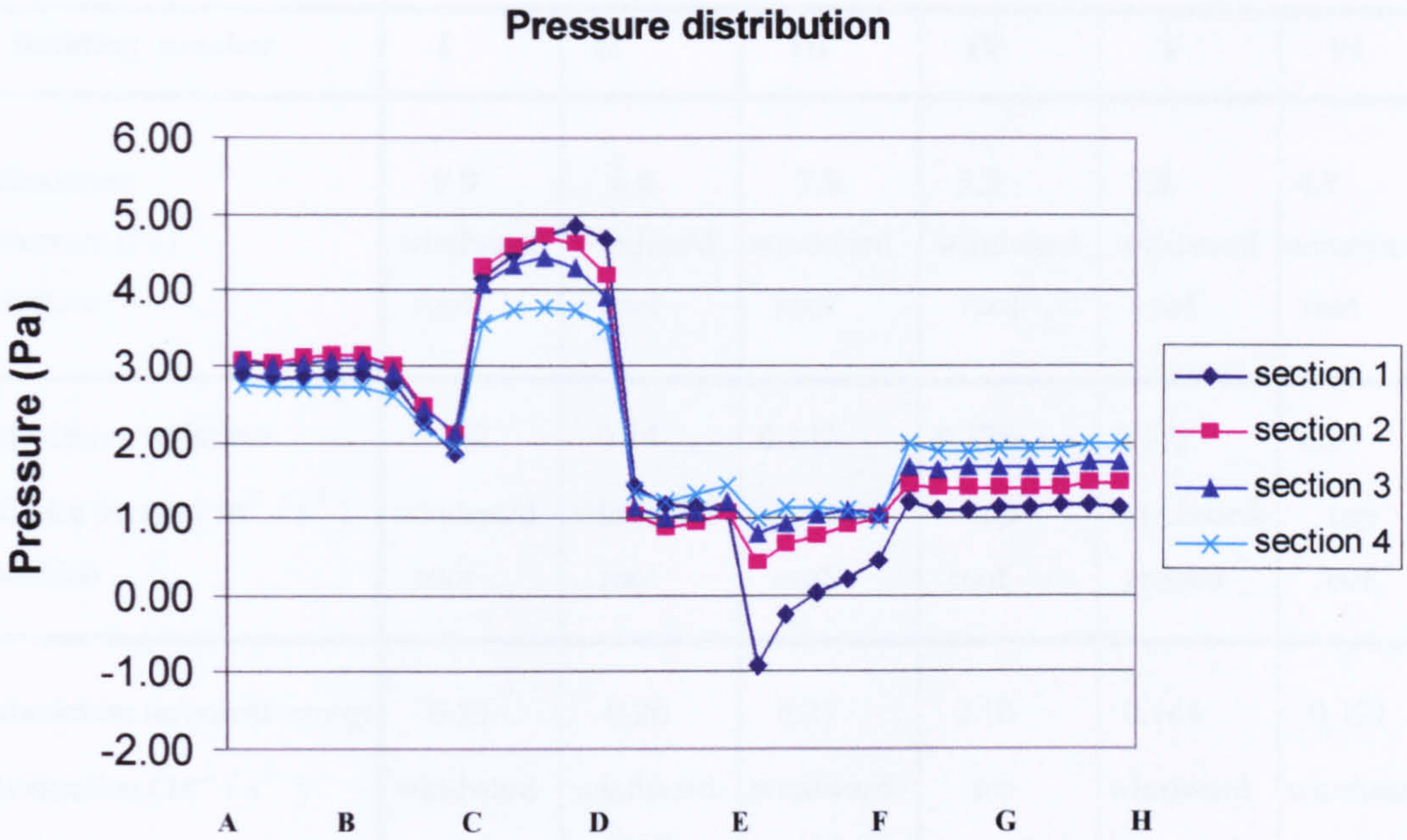

Figure 6.2.66 Pressure distribution on the sixth building

The turbulent kinetic energy now becomes higher along the gate, at the centre, between the second, third and fifth buildings, at the windward side of the sixth building and at the place of honour. This also strengthens the case that the place of honour has a relatively high turbulent kinetic energy, although the gate was moved to the south.

Pressure distributions are presented in Figures 6.2.61 – 6.2.66. In Figure 6.2.61, the maximum pressure in the first building is at the windward roof. Although this result is similar to the previous observations, the maximum value is higher.

Results of pressure distribution, turbulent kinetic energy and dissipation rate are presented in Table 6.2.5.

Table 6.2.5 A summary of results for gate at the south side

Building number	I	II	III	IV	V	VI
Maximum Pressure (Pa) position	9.0 windward roof	6.8 windward roof	7.9 windward roof	3.8 windward roof	7.8 windward roof	4.8 windward roof
Maximum turbulent kinetic energy (m^2/s^2) position	0.162 windward roof	0.14 windward roof	0.142 windward roof	0.375 top roof	0.175 windward ground	0.33 top roof
Maximum turbulent energy dissipation (m^2/s^3) position	0.33 windward roof	0.26 windward roof	0.27 windward roof	0.10 top roof	0.141 windward ground	0.121 windward roof

6.2.6 Gate at the South-West Side, with Enlarged Sixth Building

From the previous observations, it can be stated that the velocity profile around buildings is influenced by the gate position, although this correlation is relatively weak for the east side position. From pressure distributions, it can be stated that the maximum pressure variation on building surfaces occurs where no fences around buildings are added. Pressure distributions on building surfaces are reduced by adding fences and placing the gate at the south-west side. In our opinion, the sixth building should be moved away from the corner or the place of honour, since the turbulent kinetic energy and dissipation rate at this position are relatively high.

In the present study, we enlarge the sixth building in order to understand this phenomenon. Therefore, the distance between the sixth building and the place of honour becomes shorter, as well as distance between the sixth building and the north-west side corner. The gate is now placed at the south-west side, as shown in Figure 6.2.67.

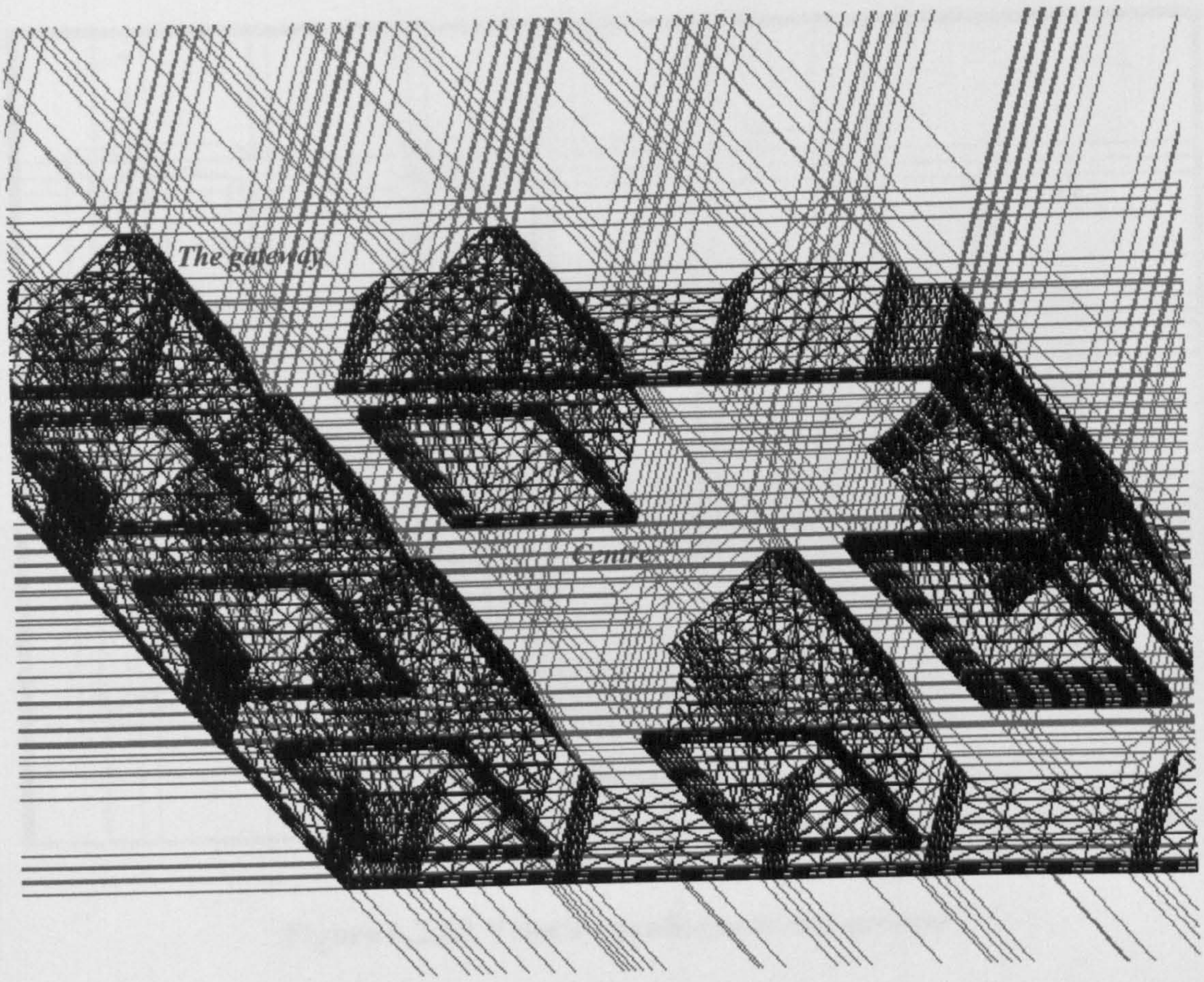

Figure 6.2.67 Side view of buildings arrangement with single gate at the south-west side and enlarged sixth building

6.2.6.1 Results and Discussion

Velocity profile near the ground is relatively high between the second, fourth and fifth buildings, as well as at the corner between the fifth and sixth buildings and between the fourth and sixth buildings.

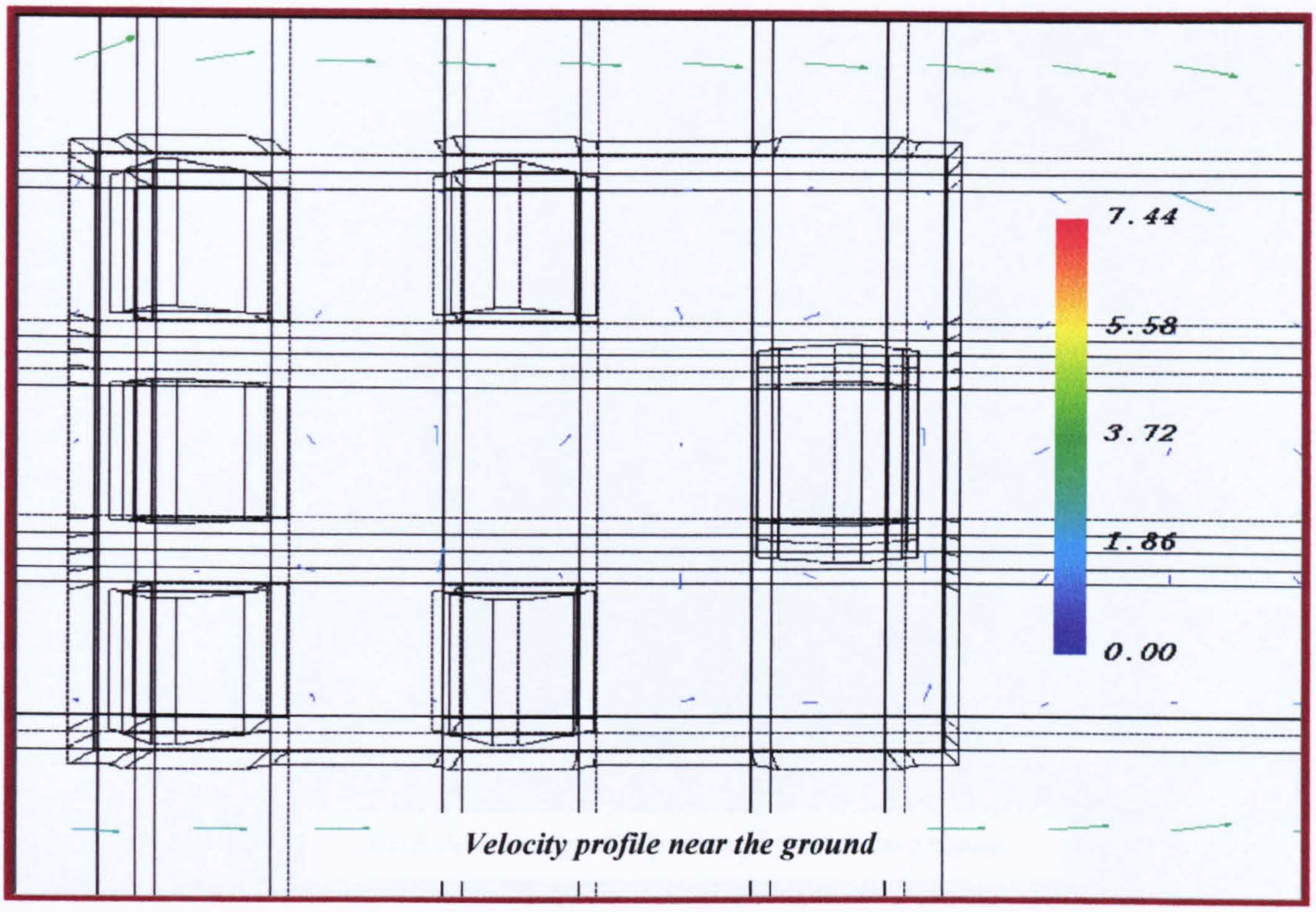

Figure 6.2.68 Velocity profile near the ground

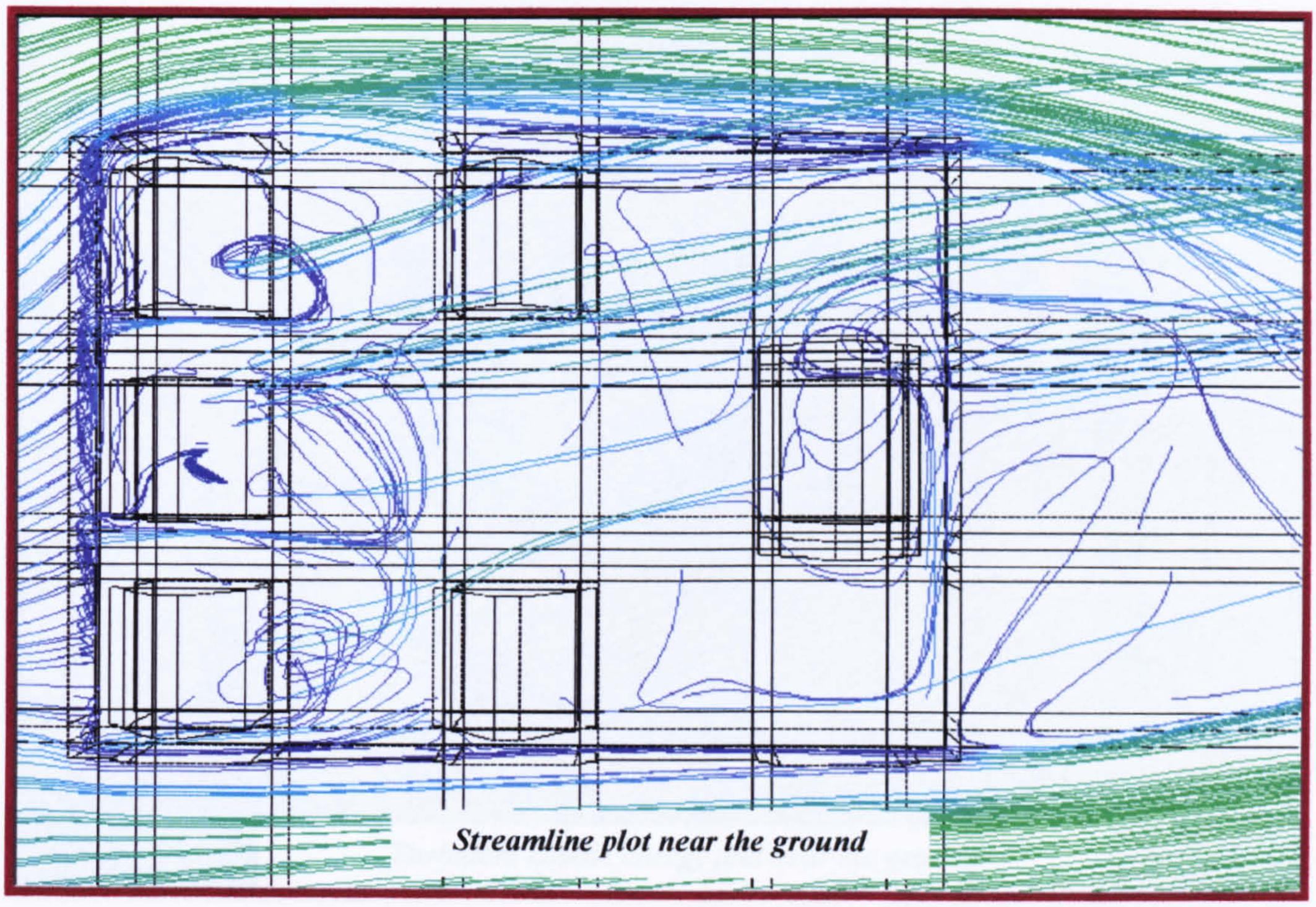

Figure 6.2.69 Streamline plot near the ground

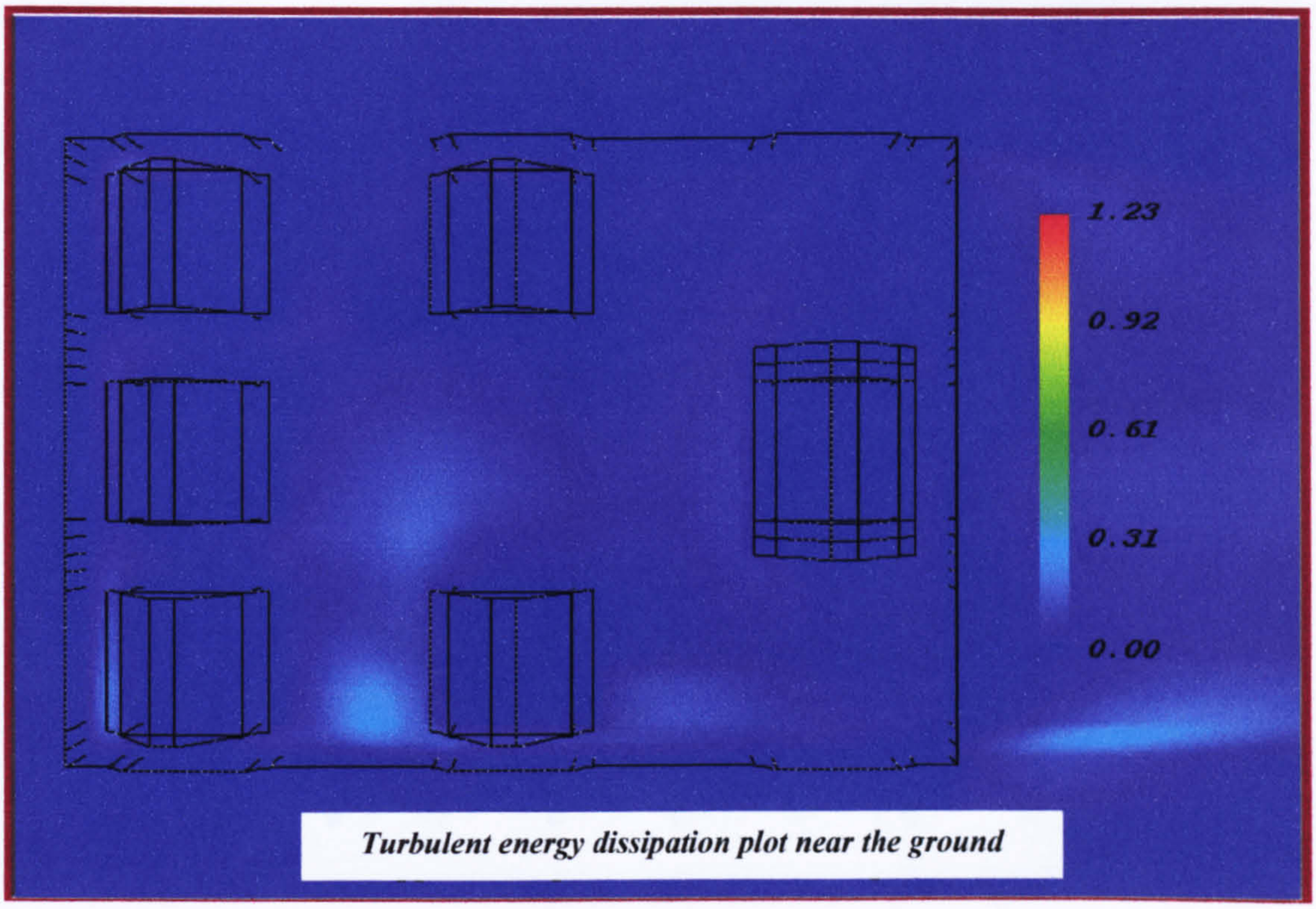

Turbulent energy dissipation plot near the ground

Figure 6.2.70 Turbulent energy dissipation plot near the ground

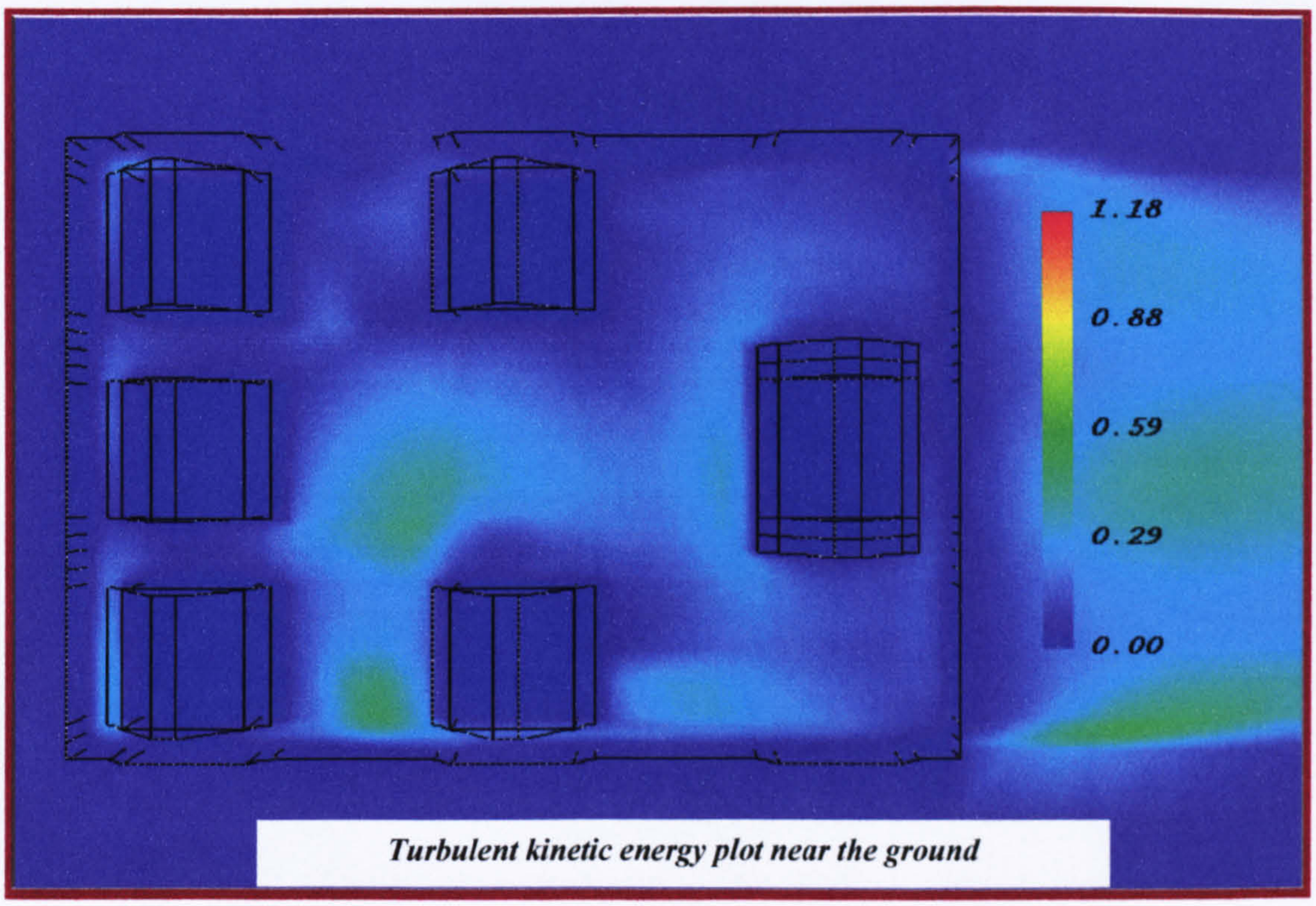

Turbulent kinetic energy plot near the ground

Figure 6.2.71 Turbulent kinetic energy plot near the ground

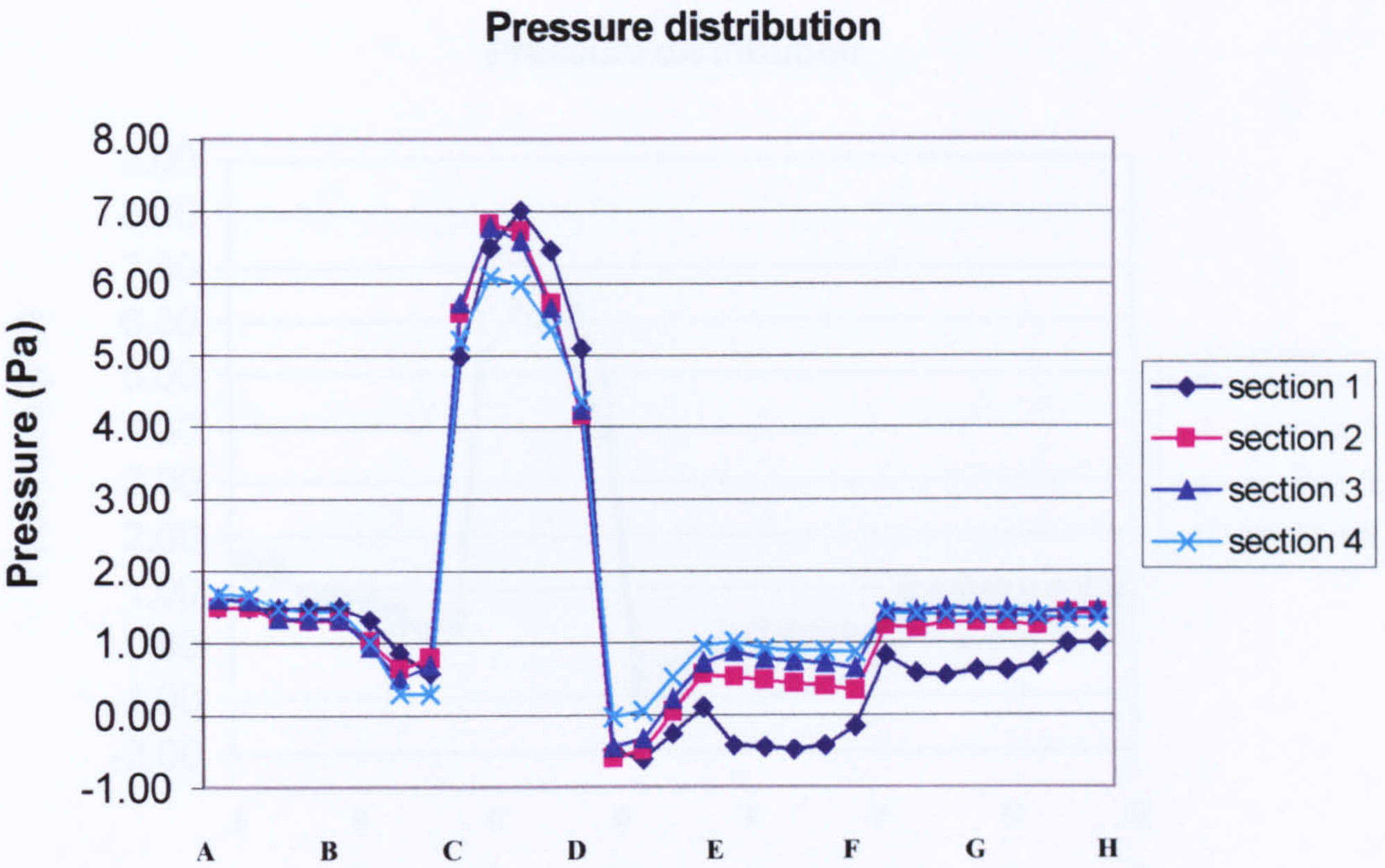

Figure 6.2.72 Pressure distribution on the first building

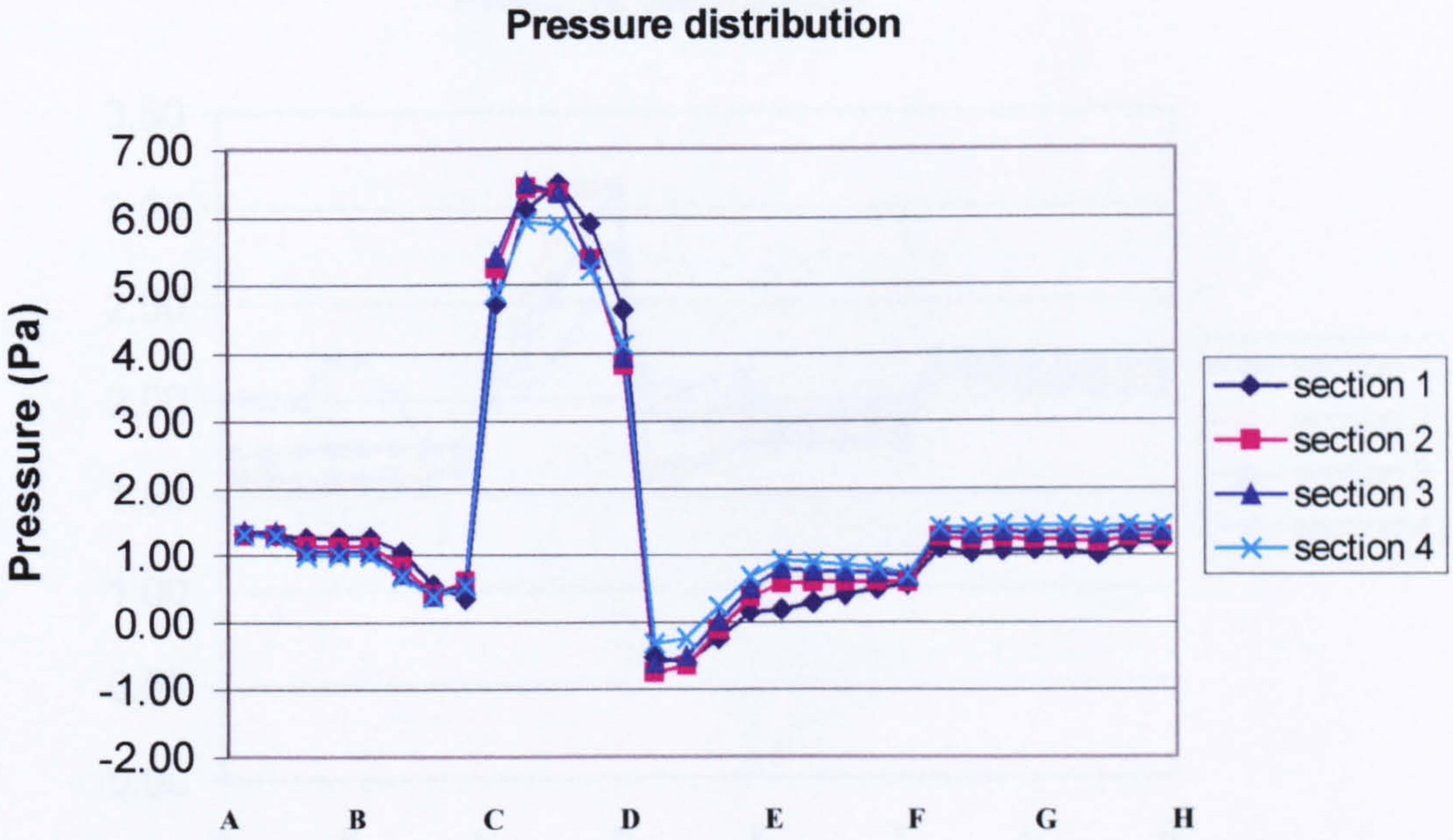

Figure 6.2.73 Pressure distribution on the second building

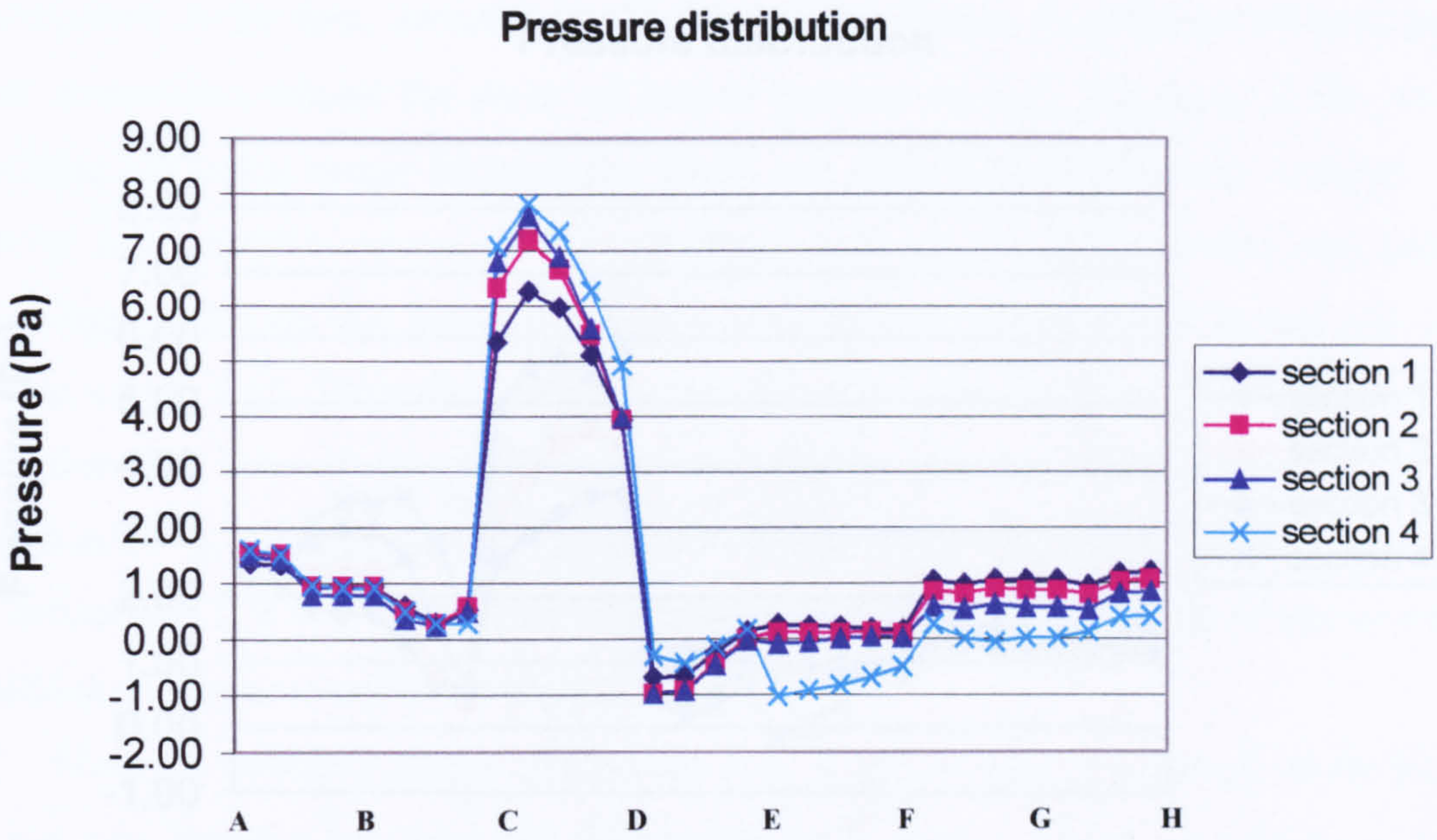

Figure 6.2.74 Pressure distribution on the third building

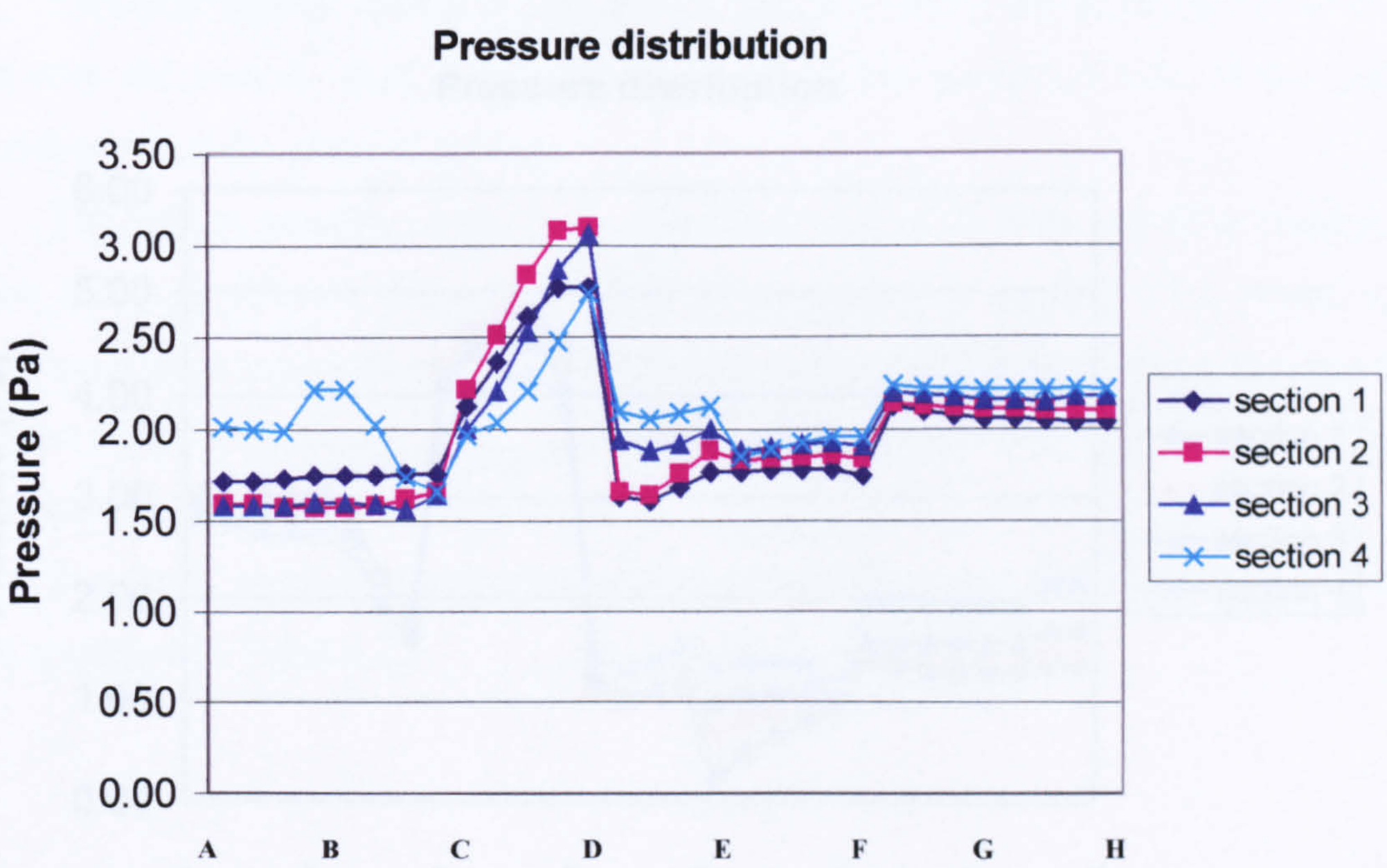

Figure 6.2.75 Pressure distribution on the fourth building

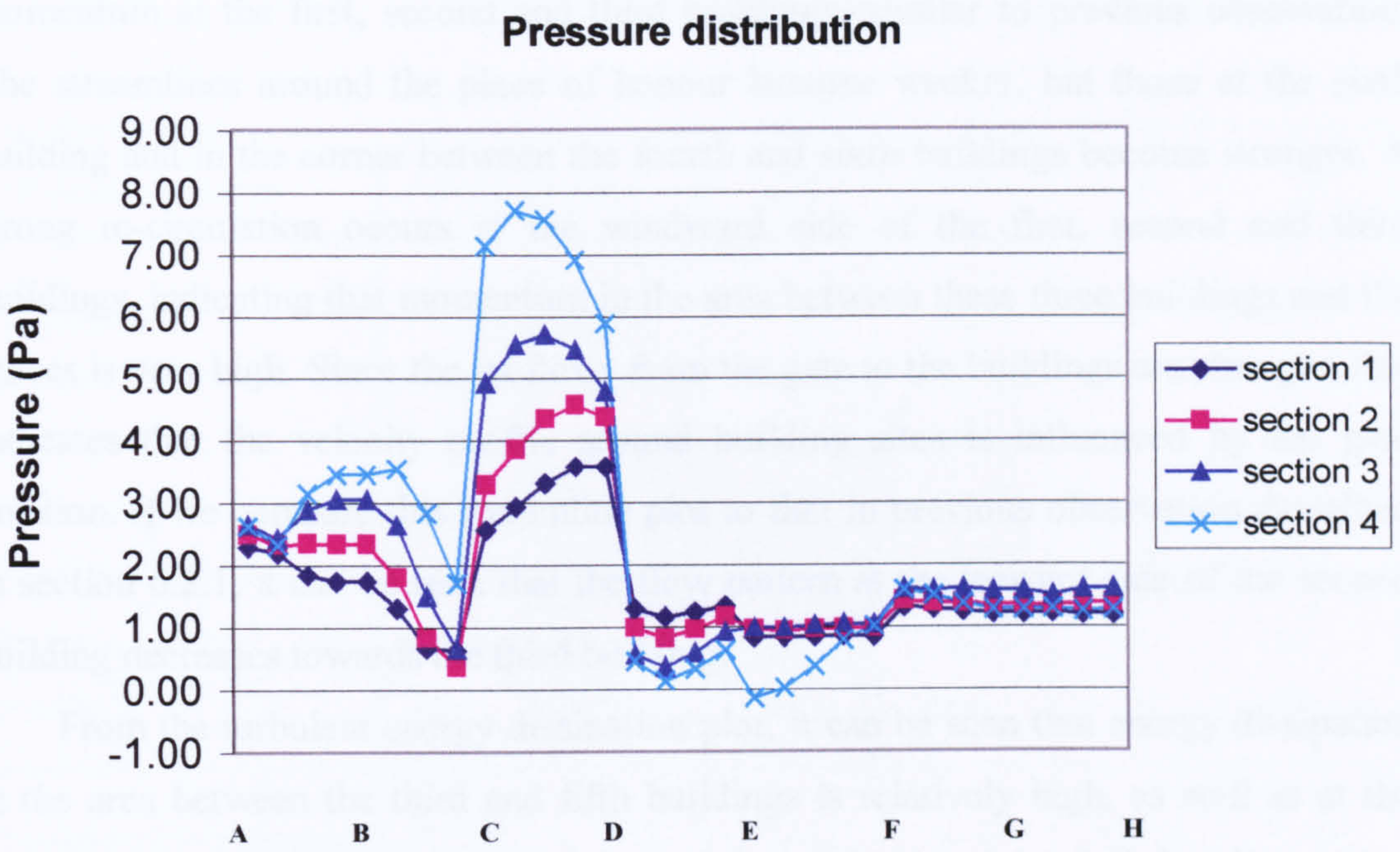

Figure 6.2.76 Pressure distribution on the fifth building

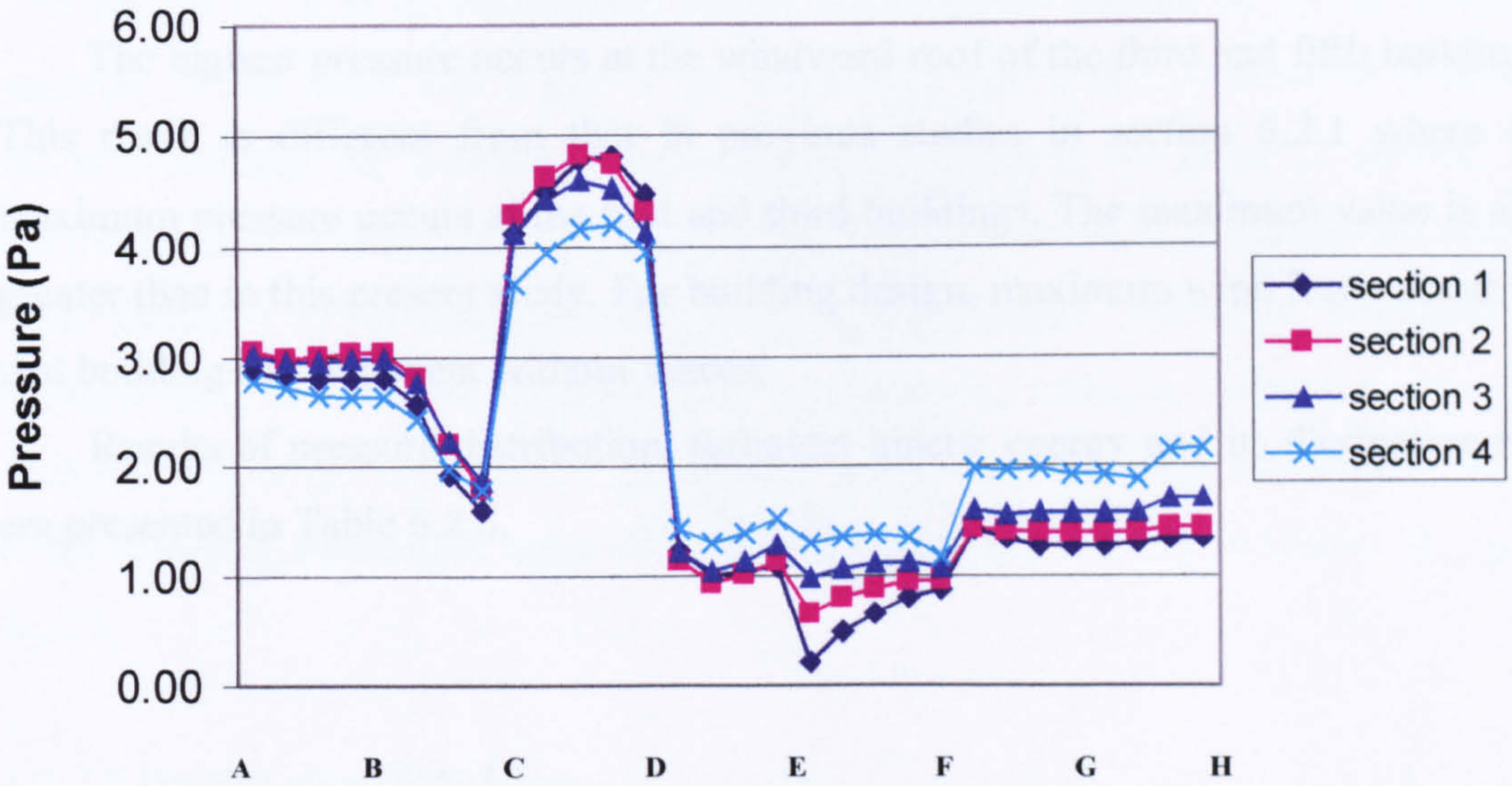

Figure 6.2.77 Pressure distribution on the sixth building

From the streamline plot, it can be seen that the gate at this position creates high momentum at the first, second and third buildings, similar to previous observation. The streamlines around the place of honour become weaker, but those at the sixth building and in the corner between the fourth and sixth buildings become stronger. A strong re-circulation occurs at the windward side of the first, second and third buildings, indicating that momentum in the area between these three buildings and the fences is very high. Since the jet flows from the gate to the buildings are stronger, this indicates that the velocity profile around building sites is influenced by the gate position. If we compare this streamline plot to that in previous observation described in section 6.2.1, it can be seen that the flow pattern at the leeward side of the second building decreases towards the third building.

From the turbulent energy dissipation plot, it can be seen that energy dissipation in the area between the third and fifth buildings is relatively high, as well as at the leeward side of the second building, at the windward side of the sixth building and at the place of honour. Turbulent energy dissipation is also similar to that in previous observations, at the place of honour and in the region between the fourth and fifth buildings (*natar*).

Turbulent kinetic energy is also greater than previously, especially at the centre, between the second, third and fifth buildings, on the windward side of the sixth building and at the place of honour.

The highest pressure occurs at the windward roof of the third and fifth buildings. This result is different from that in previous studies in section 6.2.1 where the maximum pressure occurs at the first and third buildings. The maximum value is also greater than in this present study. For building design, maximum wind loads occur for that buildings arrangement without fences.

Results of pressure distribution, turbulent kinetic energy and its dissipation rate are presented in Table 6.2.6.

Table 6.2.6 A summary of results for gate at the south-west side, with enlarged sixth building

Building number	I	II	III	IV	V	VI
Maximum pressure (Pa) position	7.0 windward roof	6.5 windward roof	7.9 windward roof	3.2 windward roof	7.8 windward roof	4.8 windward roof
Maximum turbulent kinetic energy (m^2/s^2) position	0.144 windward roof	0.142 windward roof	0.142 windward roof	0.28 top roof	0.18 top roof	0.33 top roof
Maximum turbulent energy dissipation (m^2/s^3) position	0.275 windward roof	0.26 windward roof	0.265 windward roof	0.065 top roof	0.142 windward ground	0.104 windward roof

6.2.7 Two Gates at the South-West and North-West Sides

The number of gates of a well-to-do family house is now considered. In our previous analyses, it was noted that a gate at the south-west side produces different results at the first building. By enlarging the sixth building close to the place of honour, the maximum value of pressure, turbulence kinetic energy and dissipation rate are moved from section 4 to section 1 but the value itself decreases. Therefore, this building configuration is preferred since pressure distribution, turbulent kinetic energy and dissipation rate are reduced. In the present study, two gates are considered, in the south-west and north-west sides of the building arrangement, as presented in Figure 6.2.78.

6.2.7.1 Results and Discussion

The velocity profile near the ground seems to be similar to that in the previous observations. The streamline plot shows a very high momentum near the north-west

side gate, and at the sixth building. The streamline at the corner, the place of honour, has a greater value than in previous observations, indicating that using two gates will increase the air motion around the buildings.

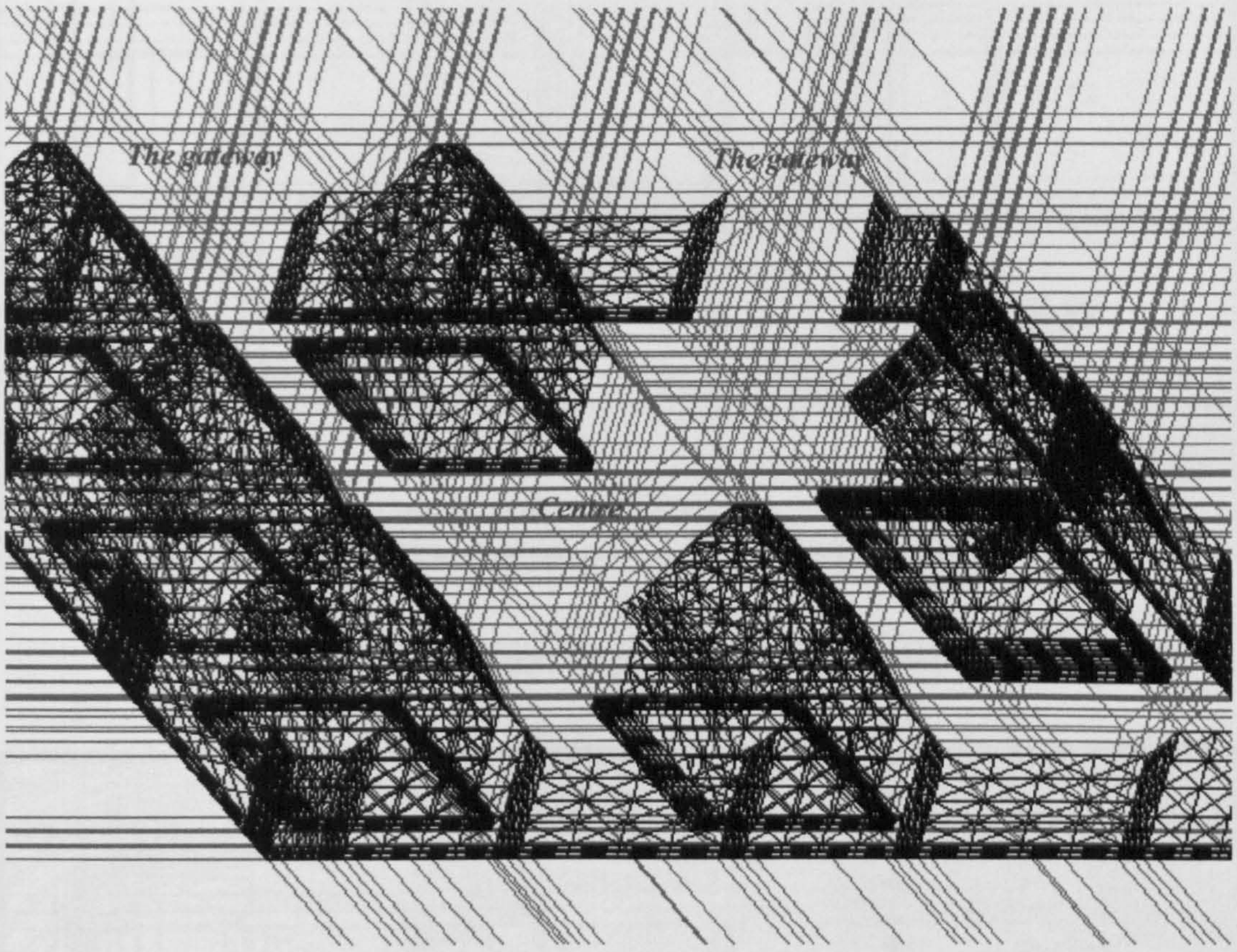

Figure 6.2.78 Side view of buildings arrangement with two gates on south-west and north-west sides of buildings site

The turbulent energy dissipation plot shows that energy dissipation in the area between the third and fifth buildings is relatively high, as well as at the leeward side of the second building, at the windward side of the sixth building and at the place of honour.

The turbulent kinetic energy is also higher, especially at the centre, between the second, third and fifth buildings, at the windward side of the sixth building and at the place of honour.

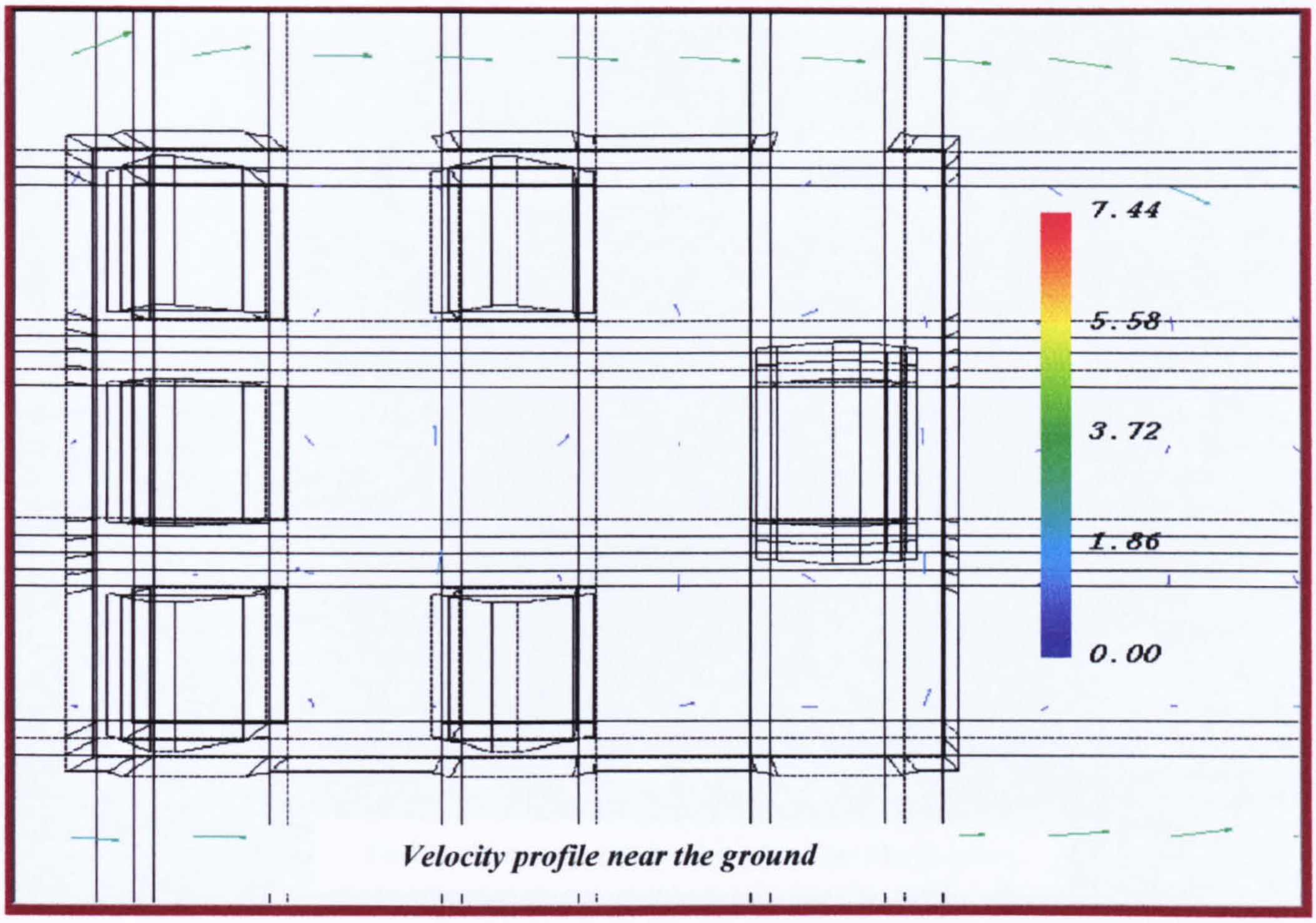

Figure 6.2.79 Velocity profile near the ground

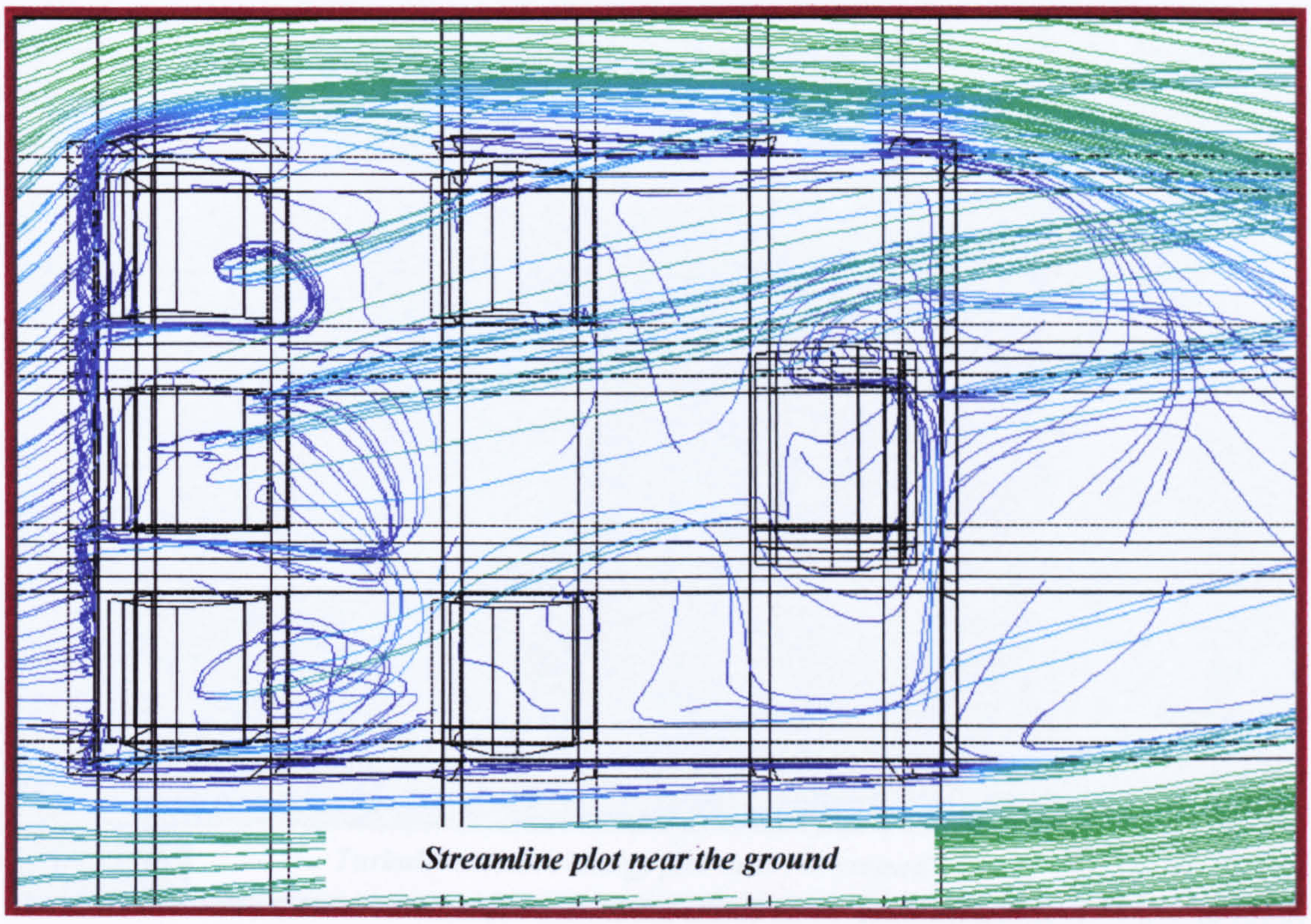

Figure 6.2.80 Streamline plot near the ground

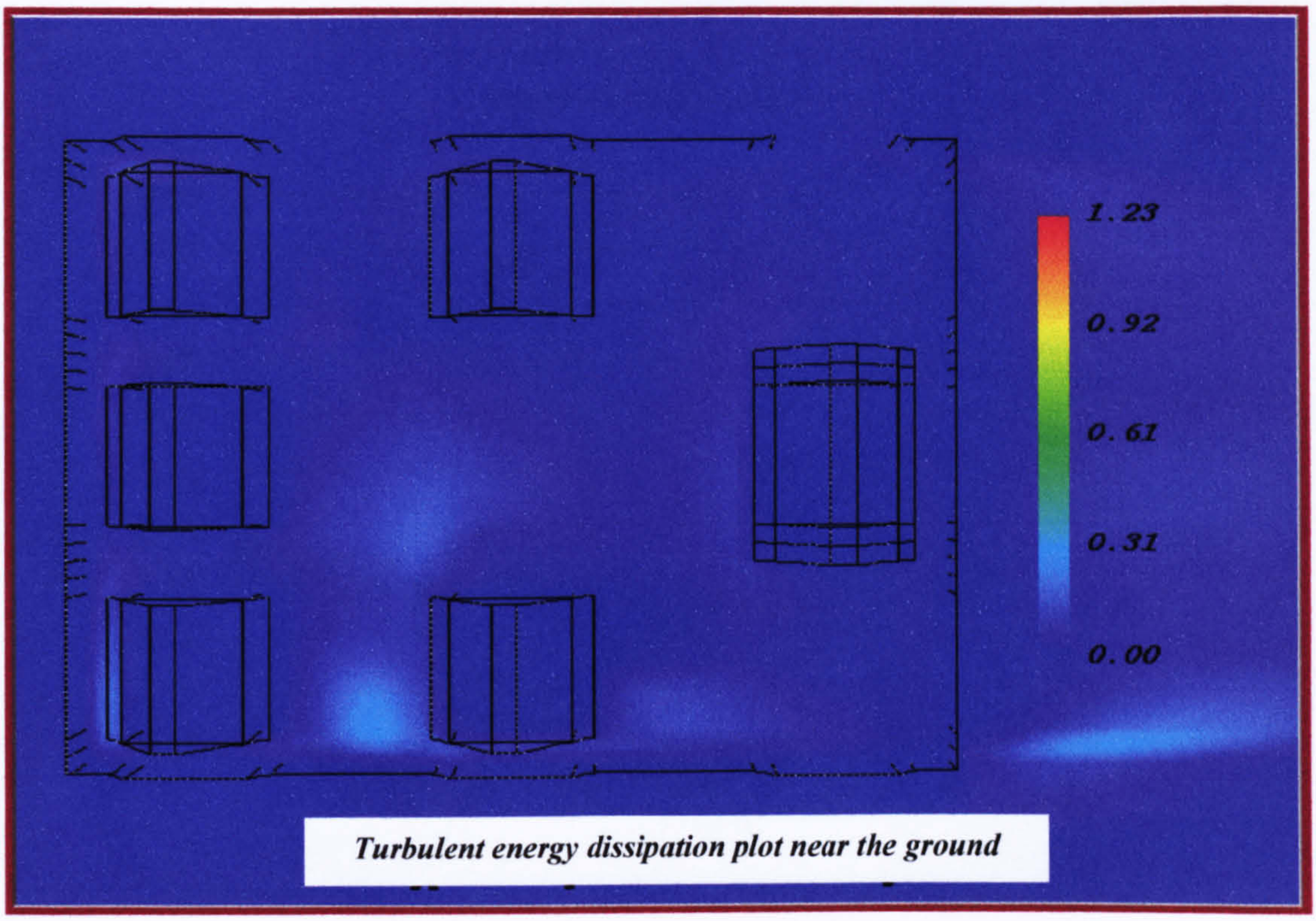

Turbulent energy dissipation plot near the ground

Figure 6.2.81 Turbulent energy dissipation plot near the ground

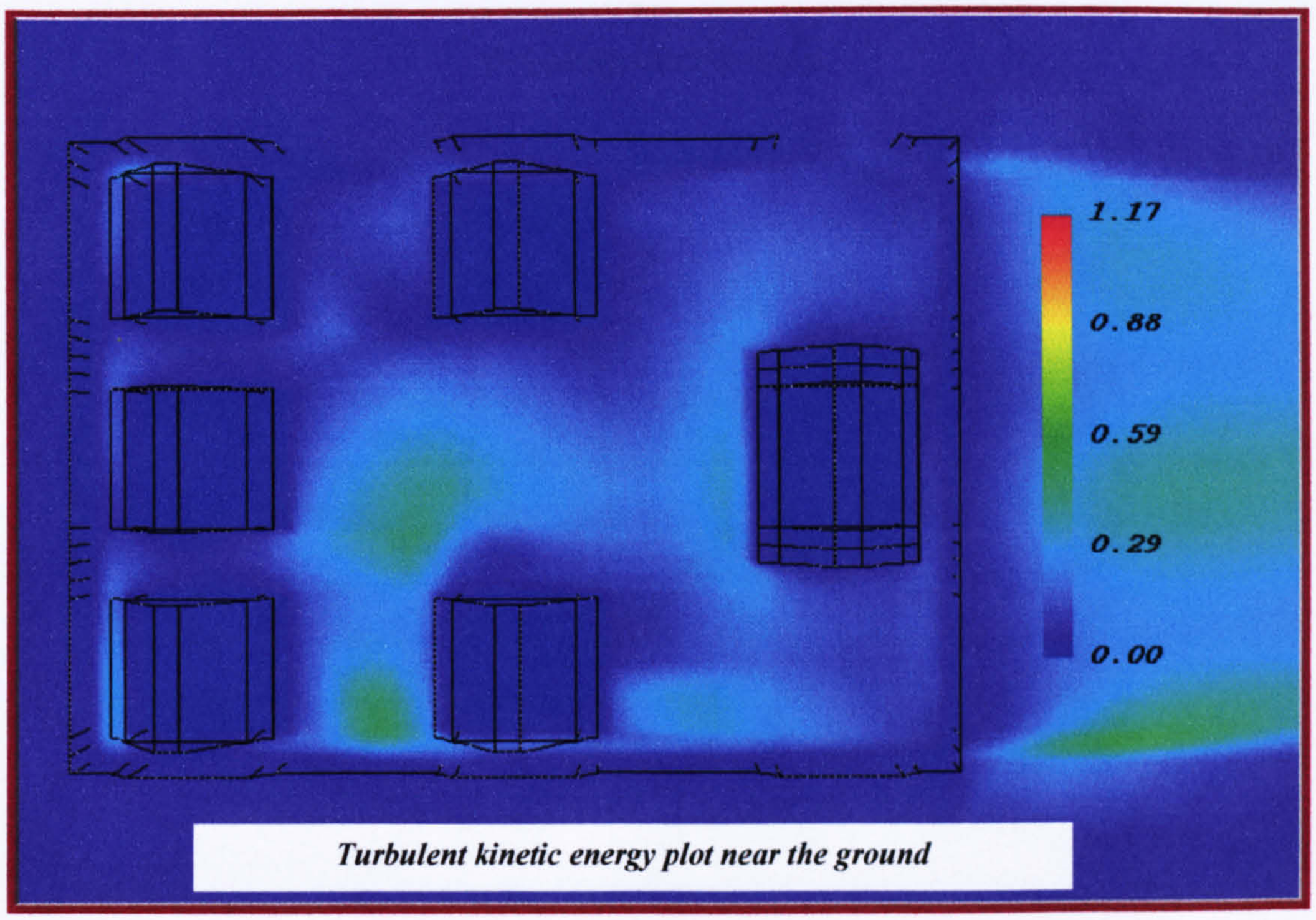

Turbulent kinetic energy plot near the ground

Figure 6.2.82 Turbulent kinetic energy plot near the ground

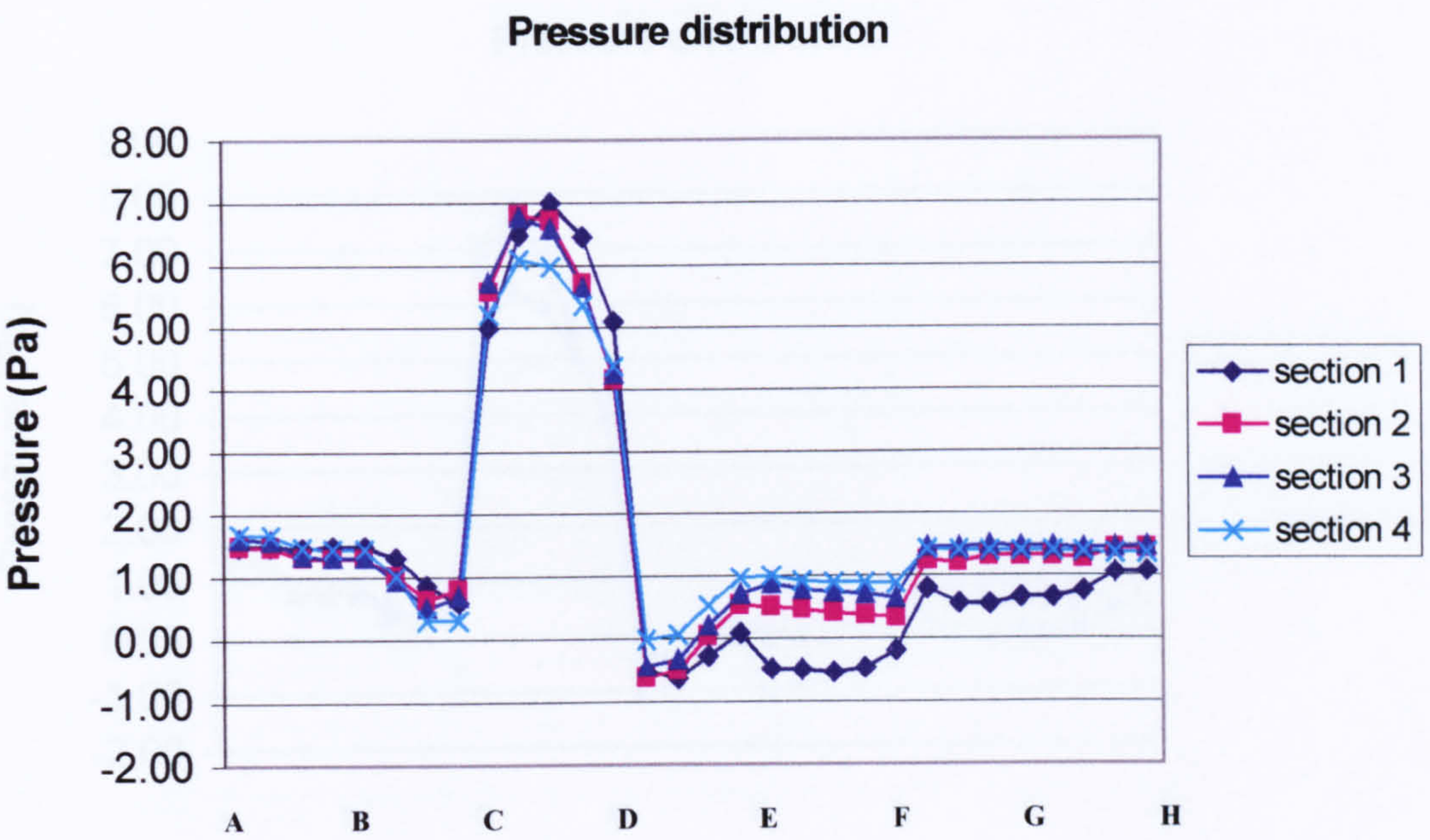

Figure 6.2.83 Pressure distribution on the first building

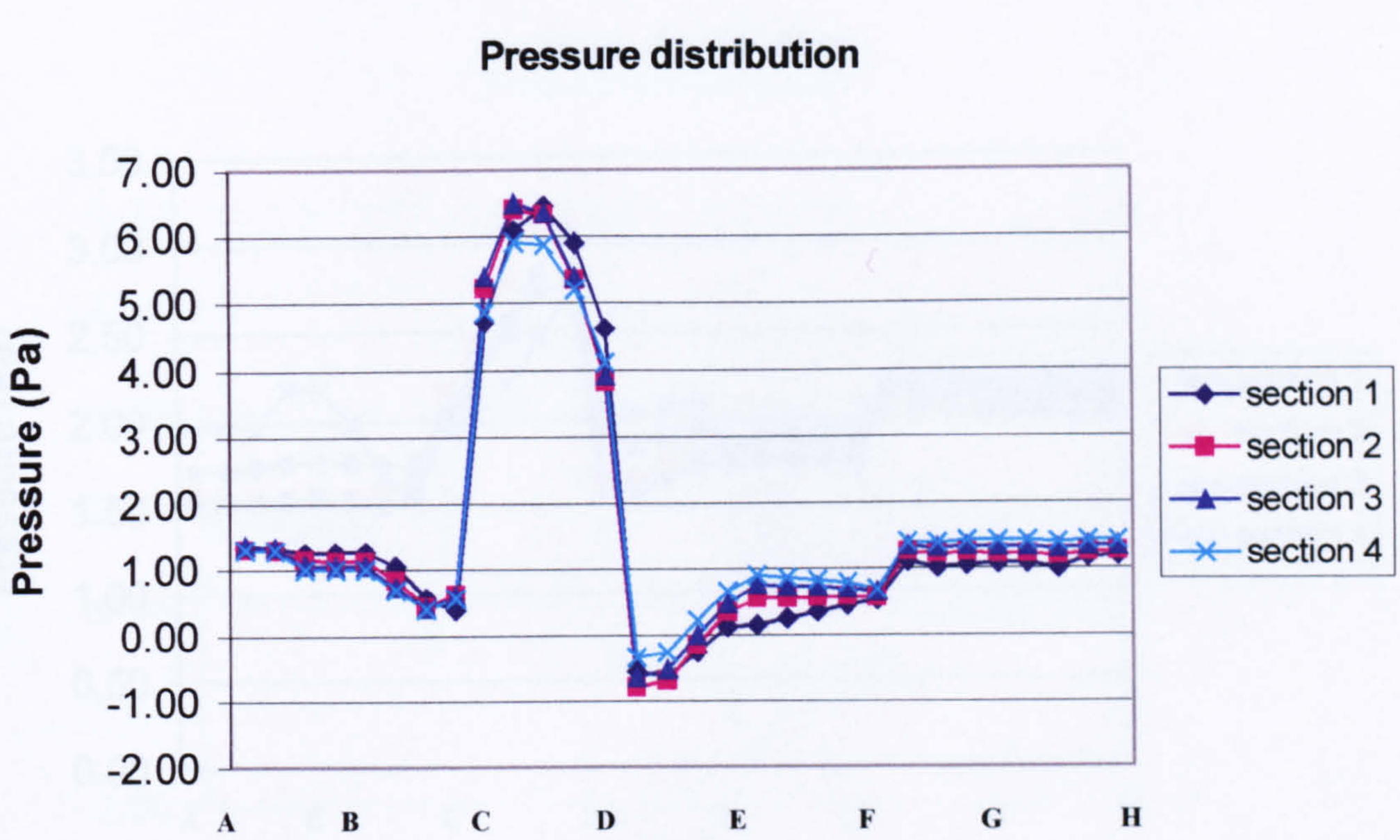

Figure 6.2.84 Pressure distribution on the second building

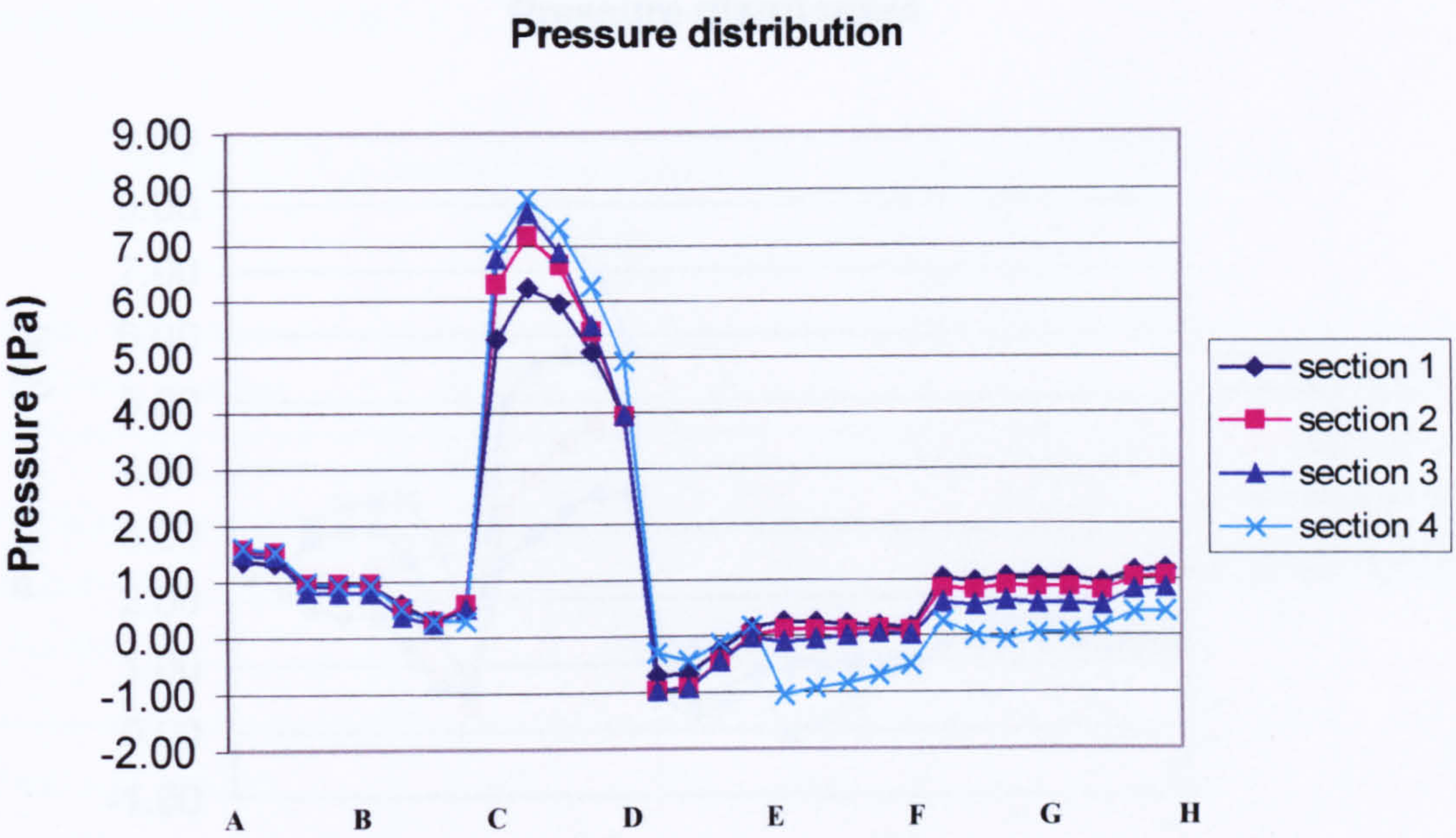

Figure 6.2.85 Pressure distribution on the third building

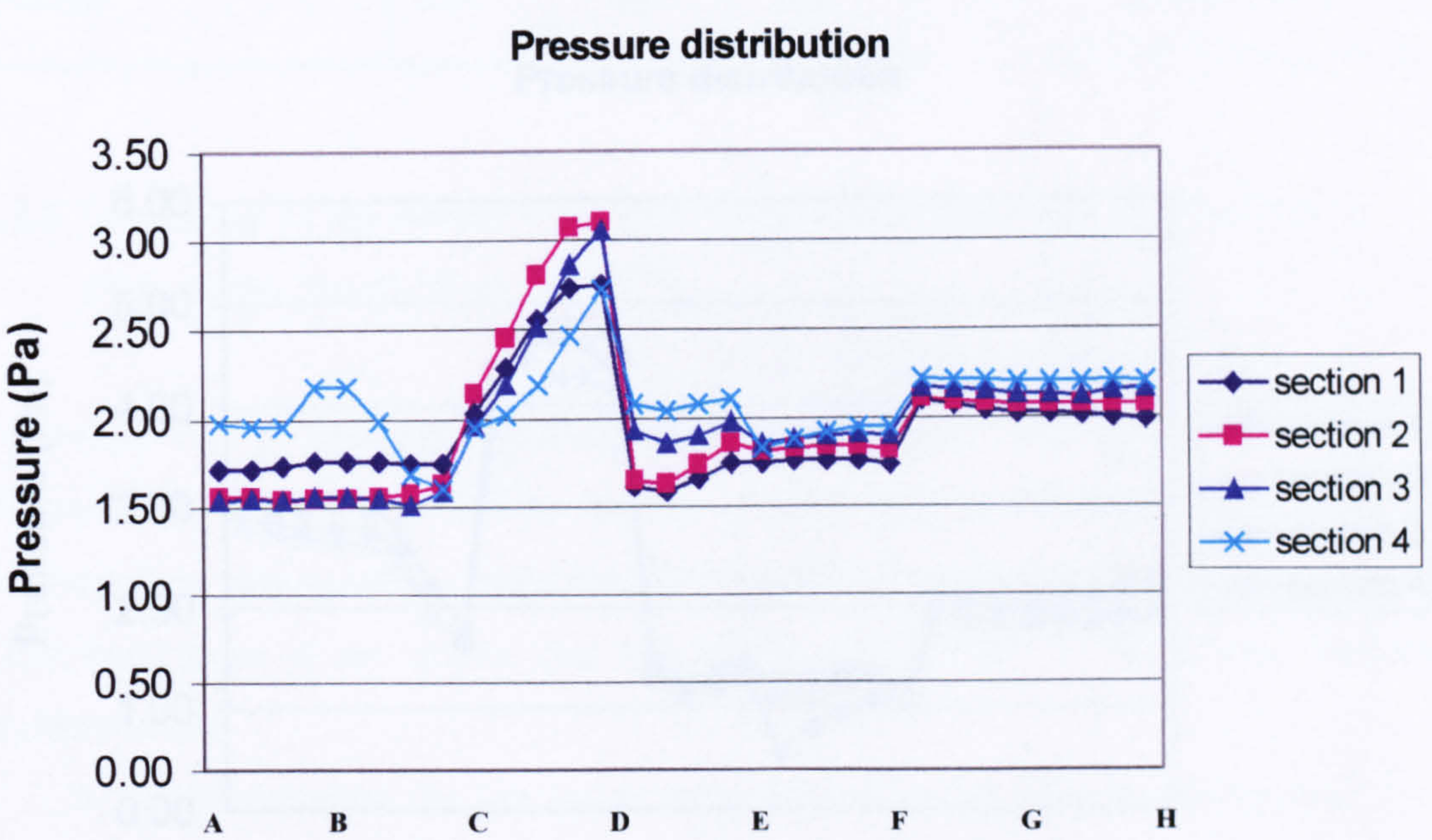

Figure 6.2.86 Pressure distribution on the fourth building

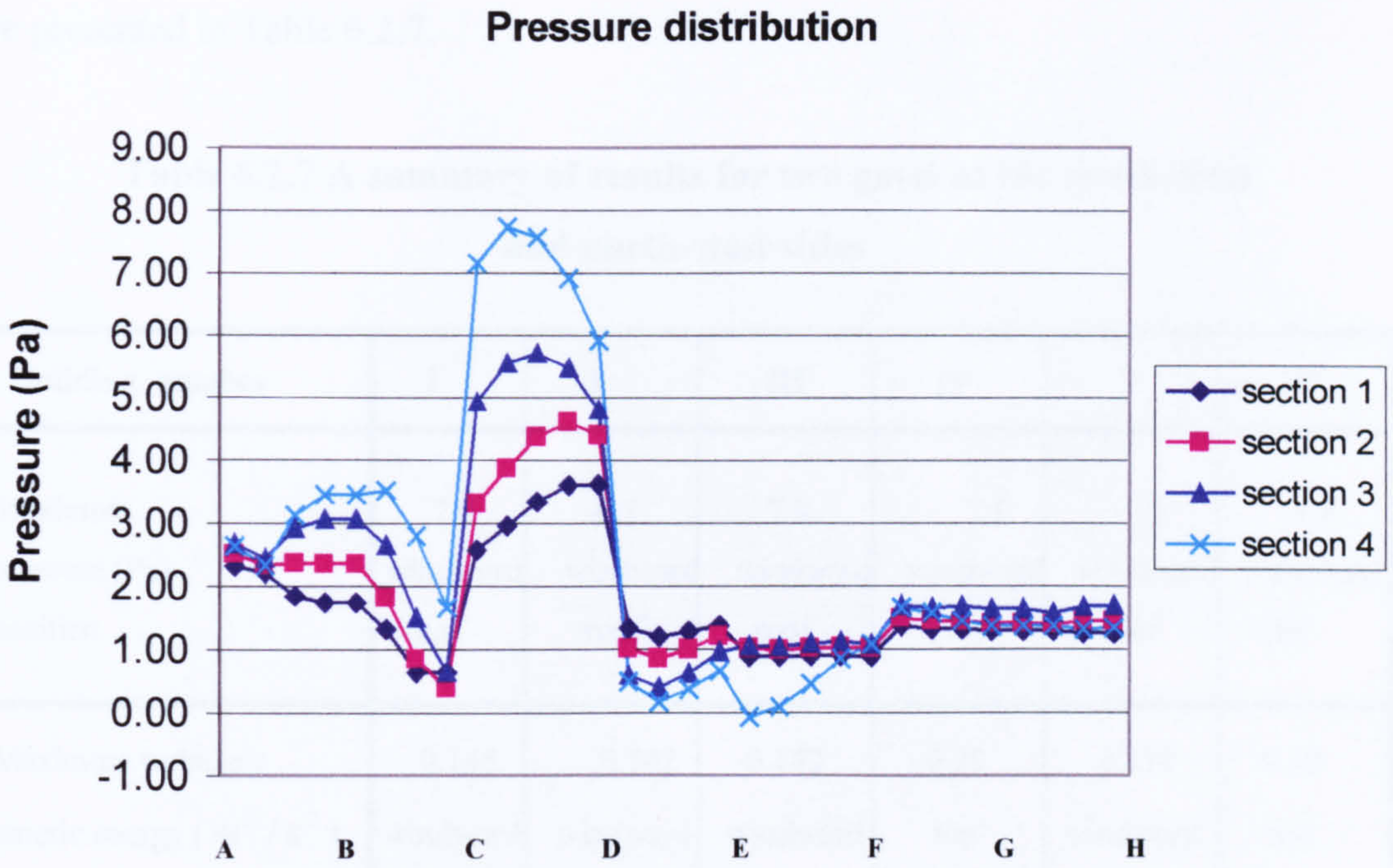

Figure 6.2.87 Pressure distribution on the fifth building

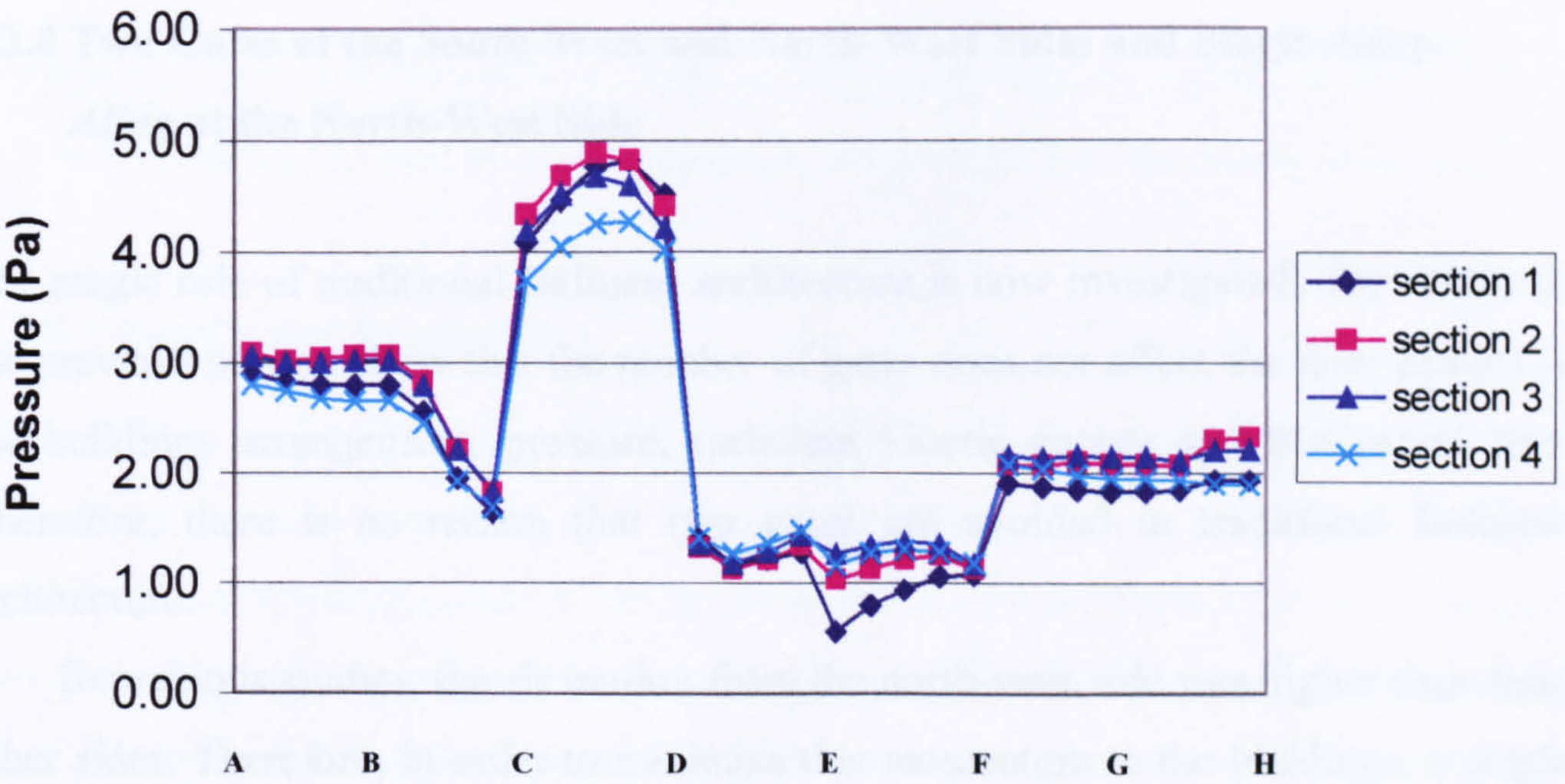

Figure 6.2.88 Pressure distribution on the sixth building

Results of pressure distribution, turbulent kinetic energy and its dissipation rate are presented in Table 6.2.7.

Table 6.2.7 A summary of results for two gates at the south-west and north-west sides

Building number	**I**	**II**	**III**	**IV**	**V**	**VI**
Maximum pressure (Pa) position	7.0 windward roof	6.5 windward roof	7.8 windward roof	3.1 windward roof	7.8 windward roof	4.8 windward roof
Maximum turbulent kinetic energy (m^2/s^2) position	0.145 windward roof	0.142 windward roof	0.142 windward roof	0.28 top roof	0.178 windward ground	0.33 top roof
Maximum turbulent energy dissipation (m^2/s^3) position	0.27 windward roof	0.26 windward roof	0.265 windward roof	0.064 top roof	0.142 windward ground	0.105 windward roof

6.2.8 Two Gates at the South-West and North-West Sides and Single *Aling* – *Aling* at the North-West Side

The magic rule of traditional Balinese architecture is now investigated. The results in the previous section show that the number of gates does not affect the flow pattern in the buildings arrangement, pressure, turbulent kinetic energy and dissipation rate. Therefore, there is no reason that two gates are avoided in traditional Balinese architecture.

In previous studies, the air motion from the north-west side was higher than from other sides. Therefore, in order to minimise this momentum to the buildings, a single screen (***aling – aling***) is now considered at the north-west side. All building configurations are similar to the previous test, as presented in Figure 6.2.89.

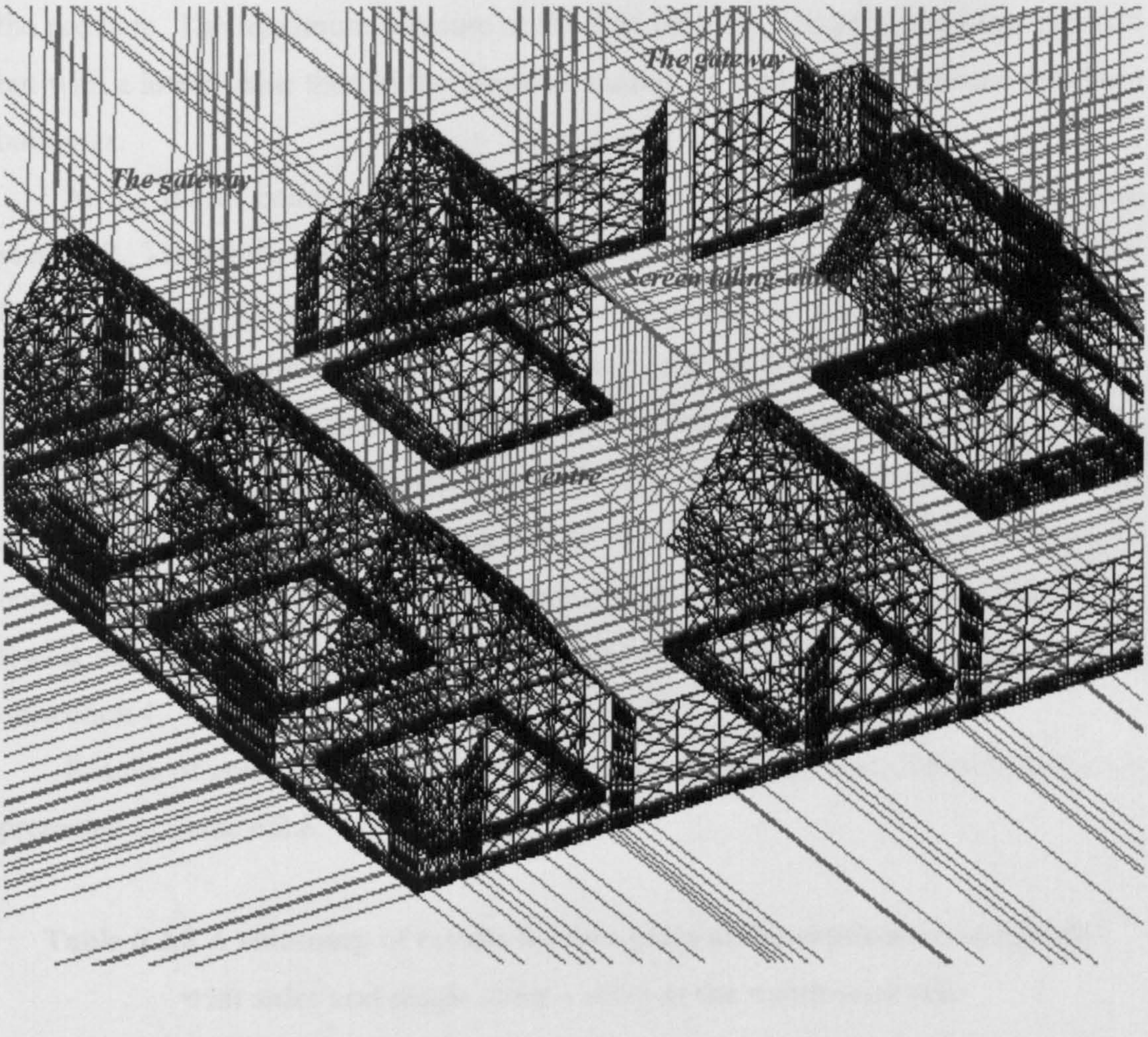

Figure 6.2.89 Side view of buildings arrangement with two gates at the south-west and north-west sides and a single *aling – aling* at the north-west side

6.2.8.1 Results and Discussion

The velocity profile is similar to previously, except at the corner -where the screen lies- where its value decreases.

From the streamline plot, it can be seen that this configuration produces more or less the same pattern as previously, except that the third building now has a weaker flow. It can be seen that the flow patterns from the north-west side gate are stopped in the screen. Therefore, the flow at the sixth building is reduced, compared to the previous study without the screen. It is also clear that the flow at the place of honour is weaker, compared to the previous studies. This indicates that by adding a screen at the north-west side gate, the air motion decreases.

The results shown in Figures 6.3.94 – 6.3.99 indicate that adding screens reduces the pressure. The maximum pressure at the first building occurs at the same position but with a lower value than in the previous studies, as well as at the second and third buildings.

At the fourth building, the maximum pressure occurs at the windward roof on section 2. Therefore, adding a screen moves the air motion from the sixth into the fourth building. This also indicates that the screen influences the flow patterns and its distribution. To minimise the effects of pressure and reduce the cooling loads on the fourth building, an open surface at the windward roof is recommended on section 4.

The position of the maximum pressure at the sixth building shows that the screen not only reduces the flow but also moves the maximum value away from the place of honour or into the middle of the building. Since the pressure on section 4 has the lowest value at the leeward side, this building must be designed with an open surface on section 4.

Results of pressure distribution, turbulent kinetic energy and dissipation rate are presented in Table 6.2.8.

Table 6.2.8 A summary of results for two gates at the south-west and north-west sides and single *aling – aling* at the north-west side

Building number	**I**	**II**	**III**	**IV**	**V**	**VI**
Maximum pressure (Pa) position	7.0 windward roof	6.5 windward roof	7.8 windward roof	3.1 windward roof	7.8 windward roof	4.8 windward roof
Maximum turbulent kinetic energy (m^2/s^2) position	0.145 windward roof	0.142 windward roof	0.142 windward roof	0.28 top roof	0.178 windward ground	0.33 top roof
Maximum turbulent energy dissipation (m^2/s^3) position	0.27 windward roof	0.26 windward roof	0.265 windward roof	0.064 top roof	0.142 windward ground	0.105 windward roof

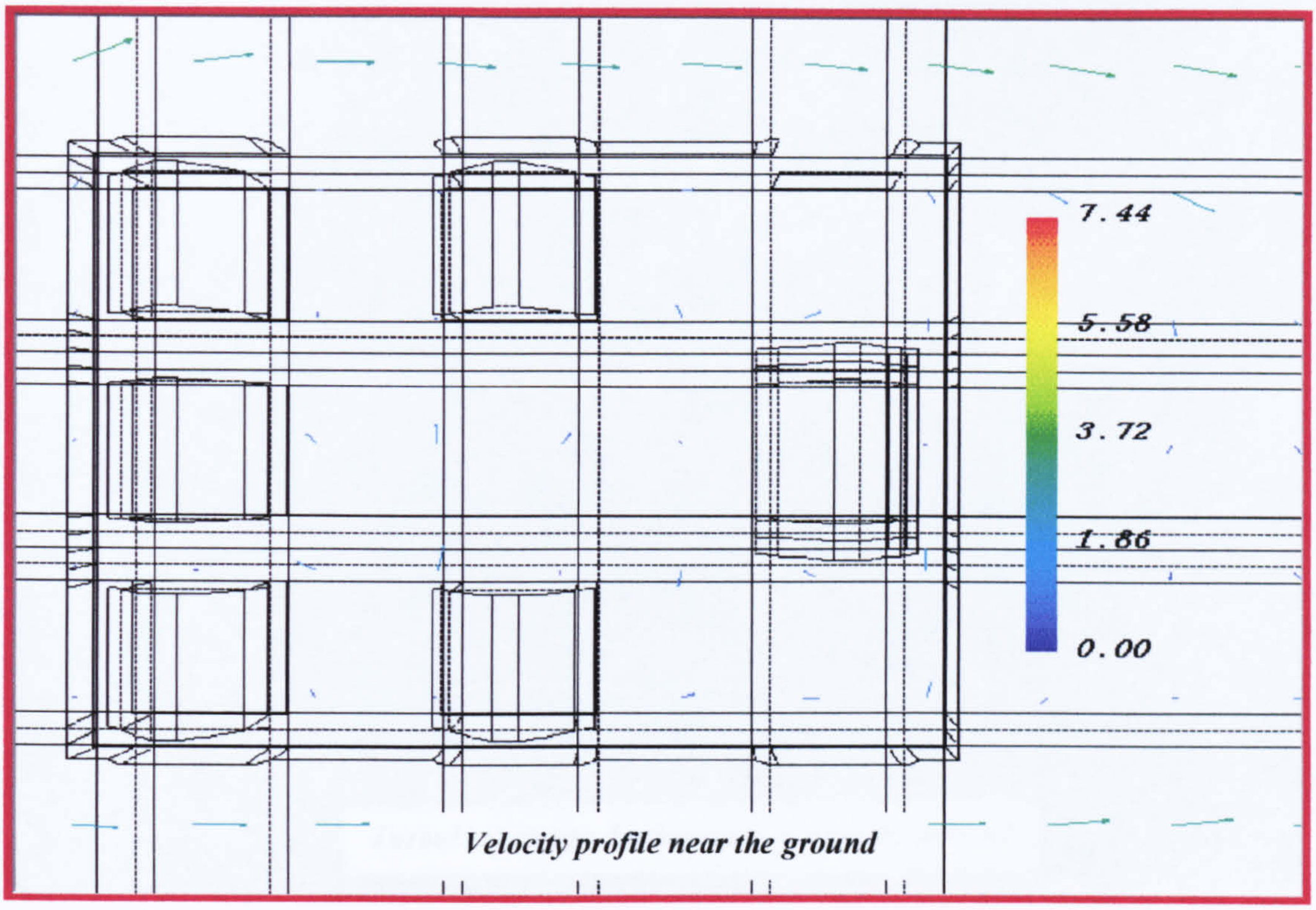

Figure 6.2.90 Velocity profile near the ground

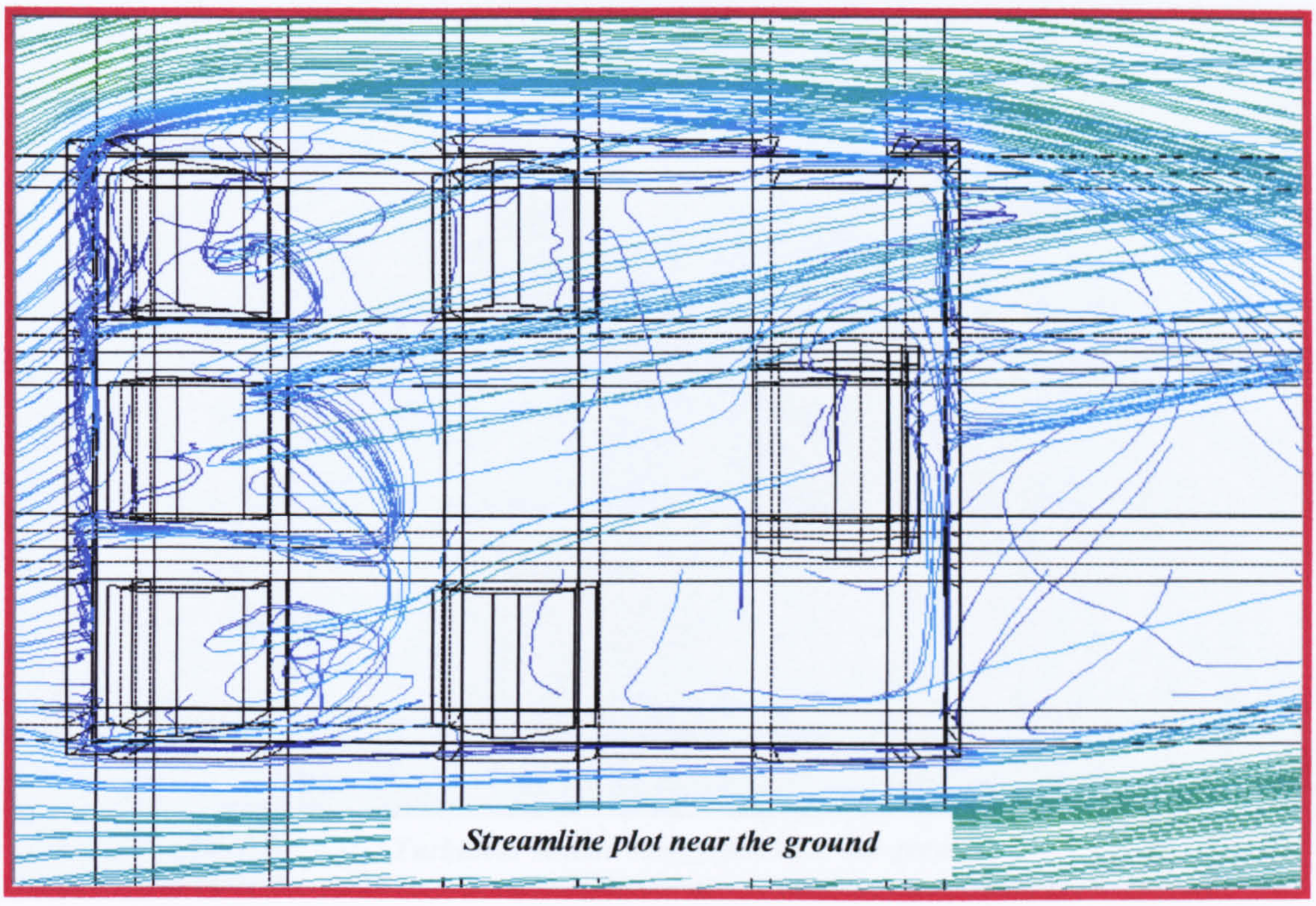

Figure 6.2.91 Streamline plot near the ground

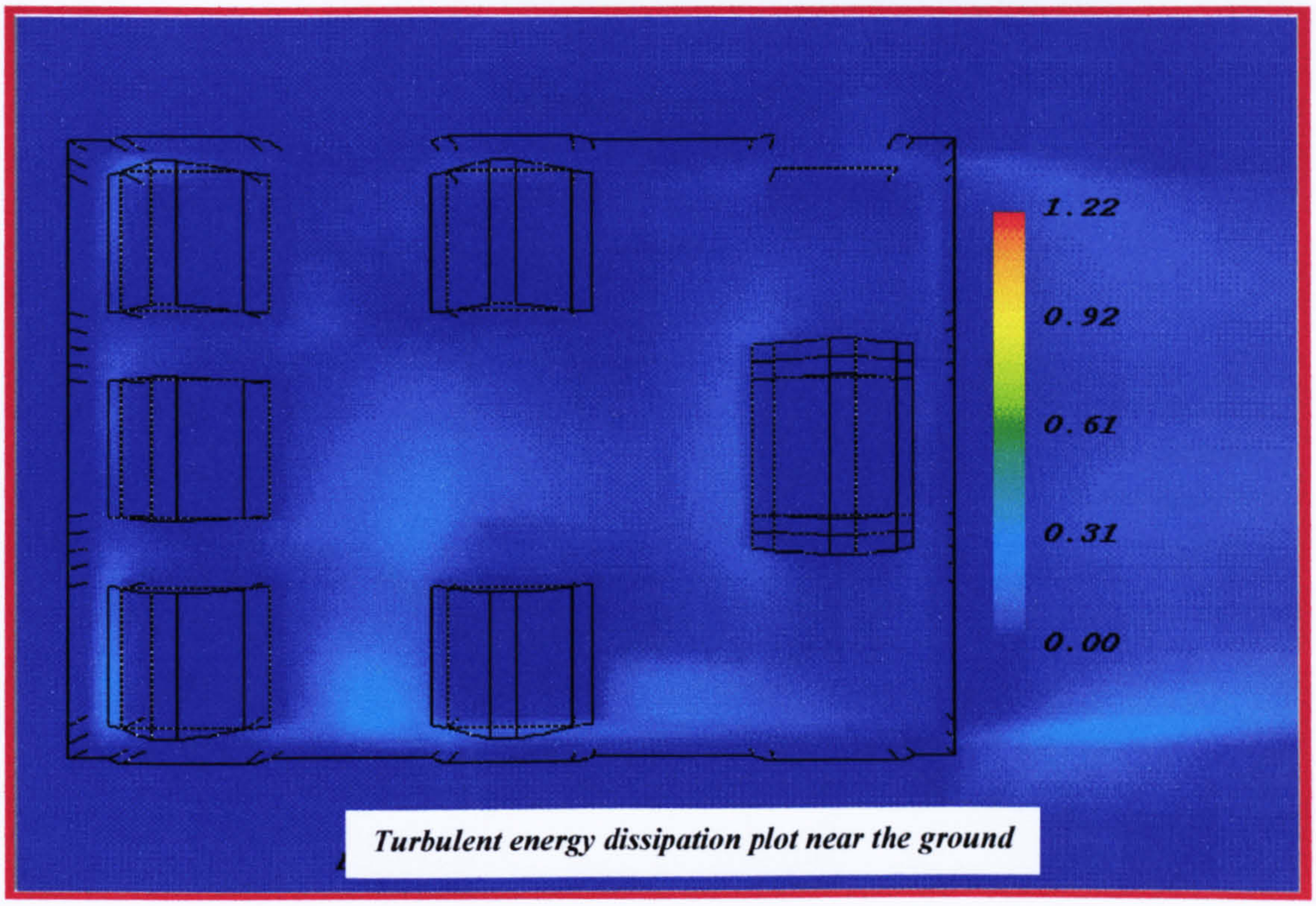

Figure 6.2.92 Turbulent energy dissipation plot near the ground

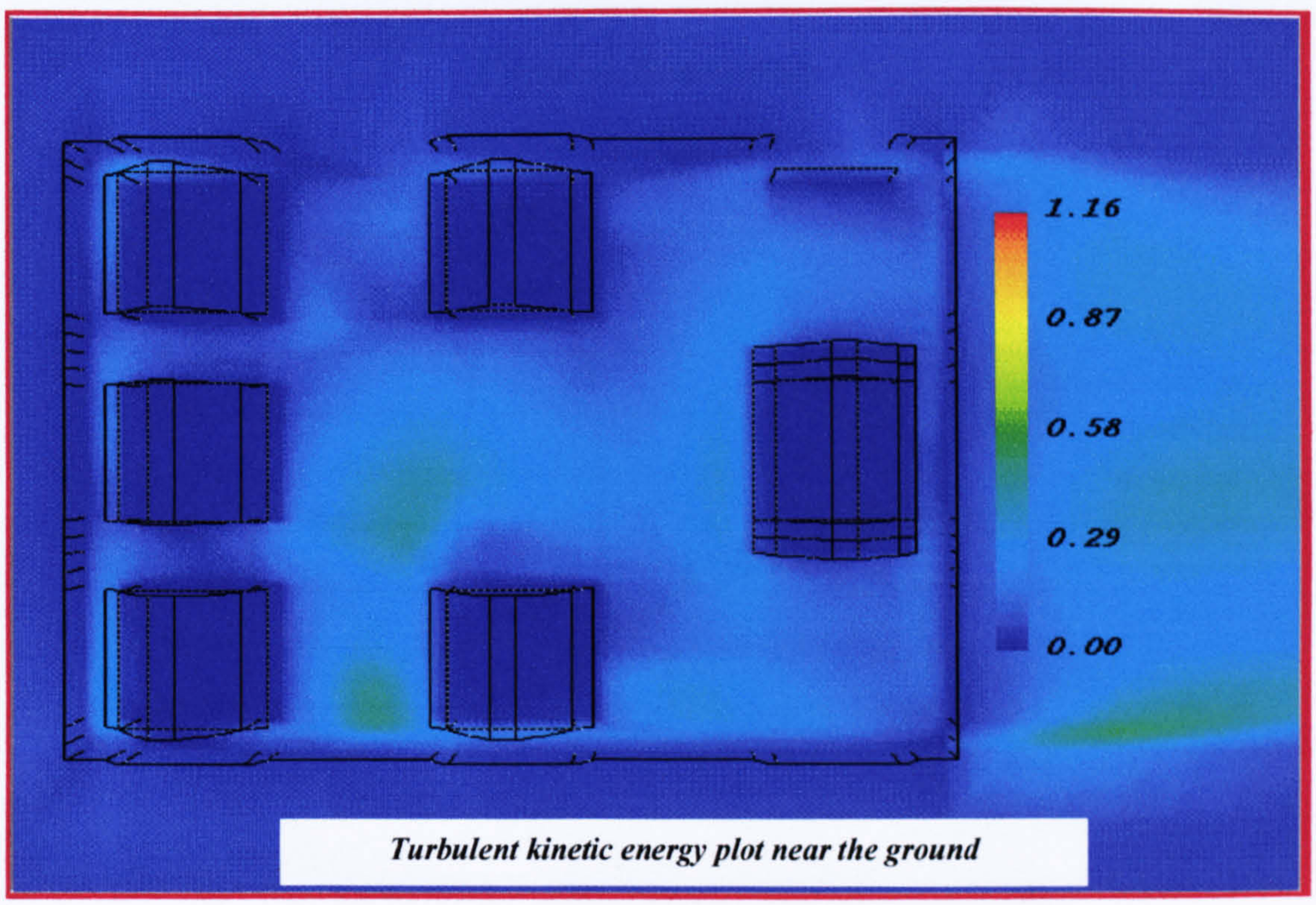

Figure 6.2.93 Turbulent kinetic energy plot near the ground

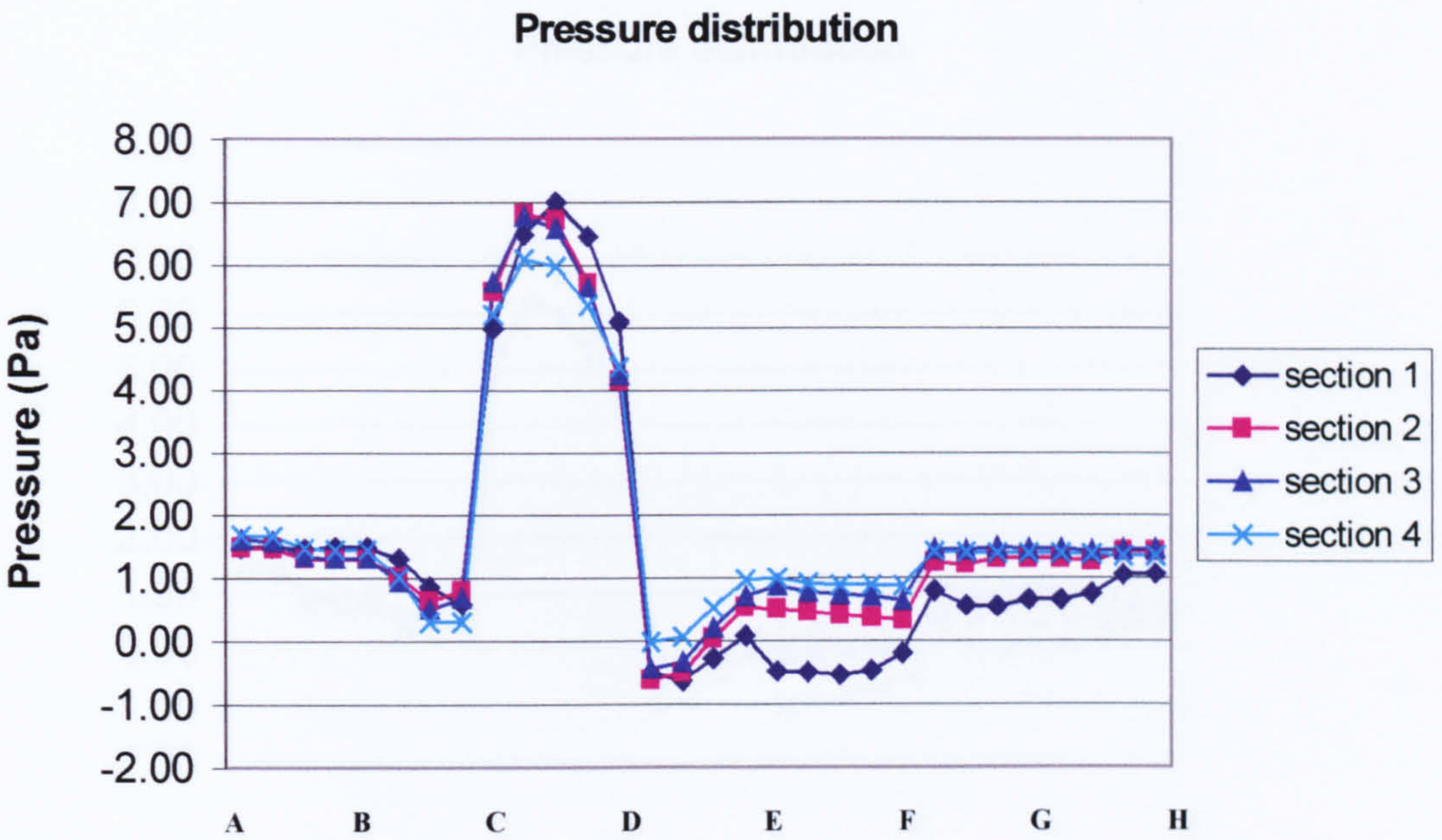

Figure 6.2.94 Pressure distribution on the first building

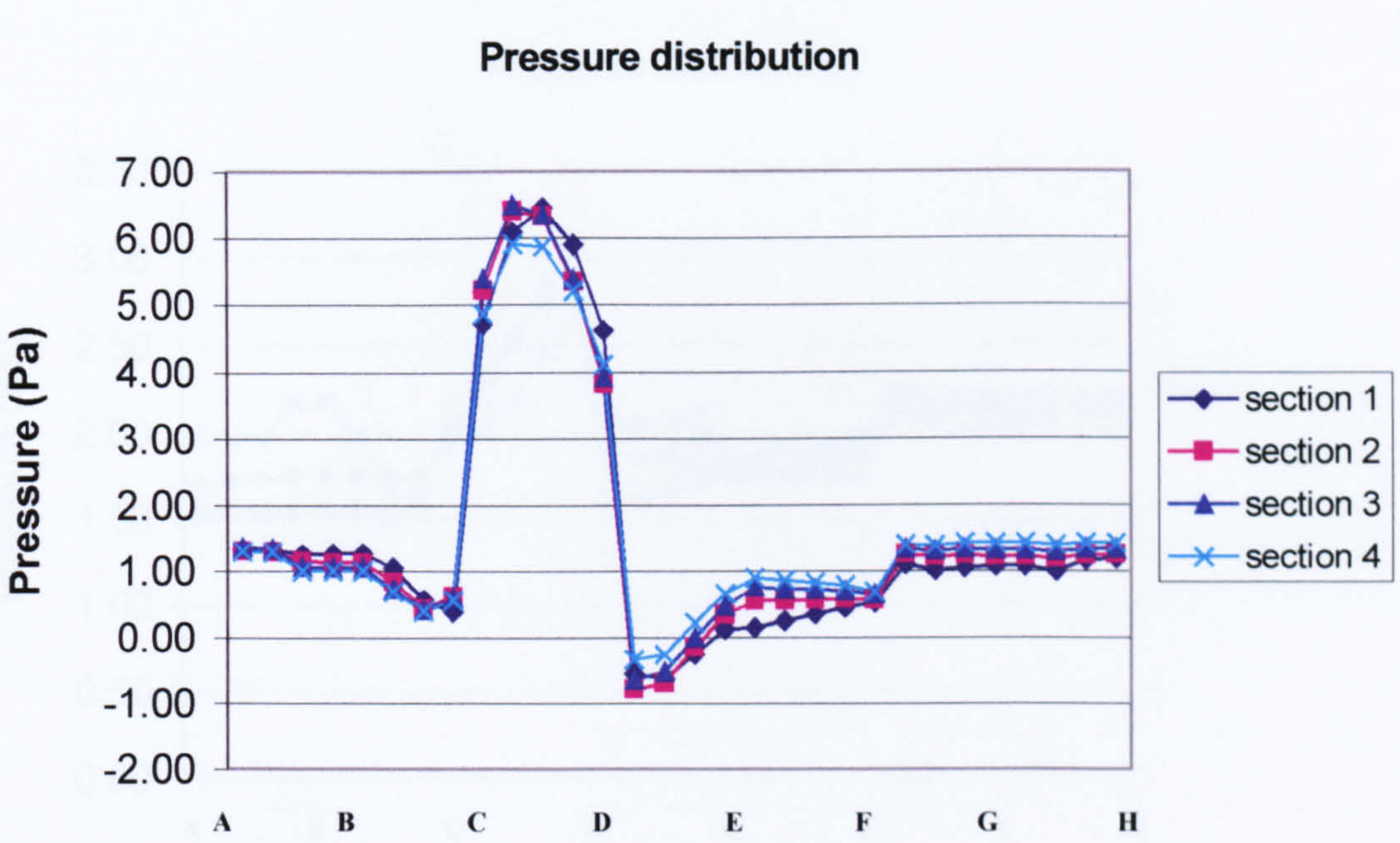

Figure 6.2.95 Pressure distribution on the second building

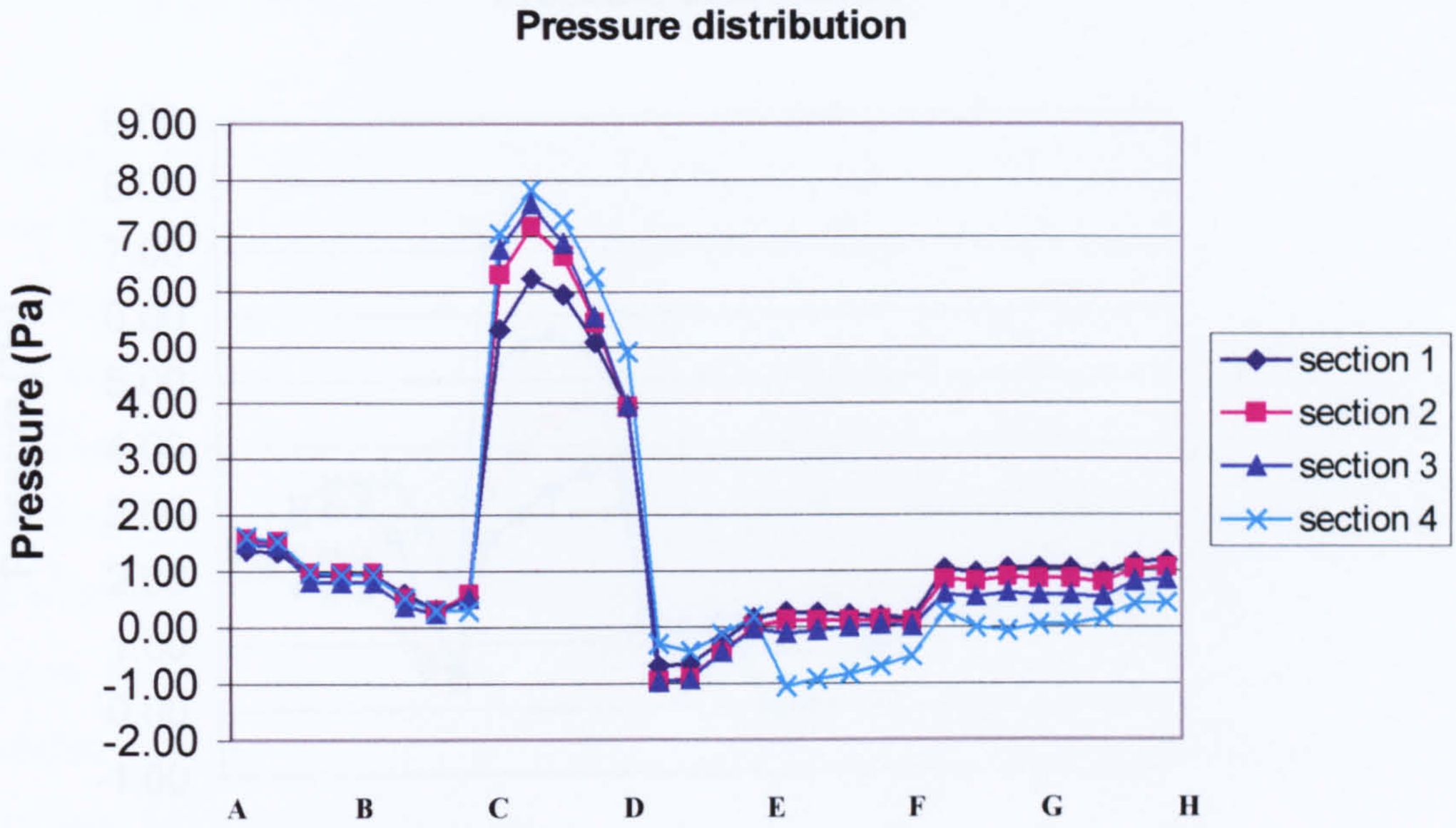

Figure 6.2.96 Pressure distribution on the third building

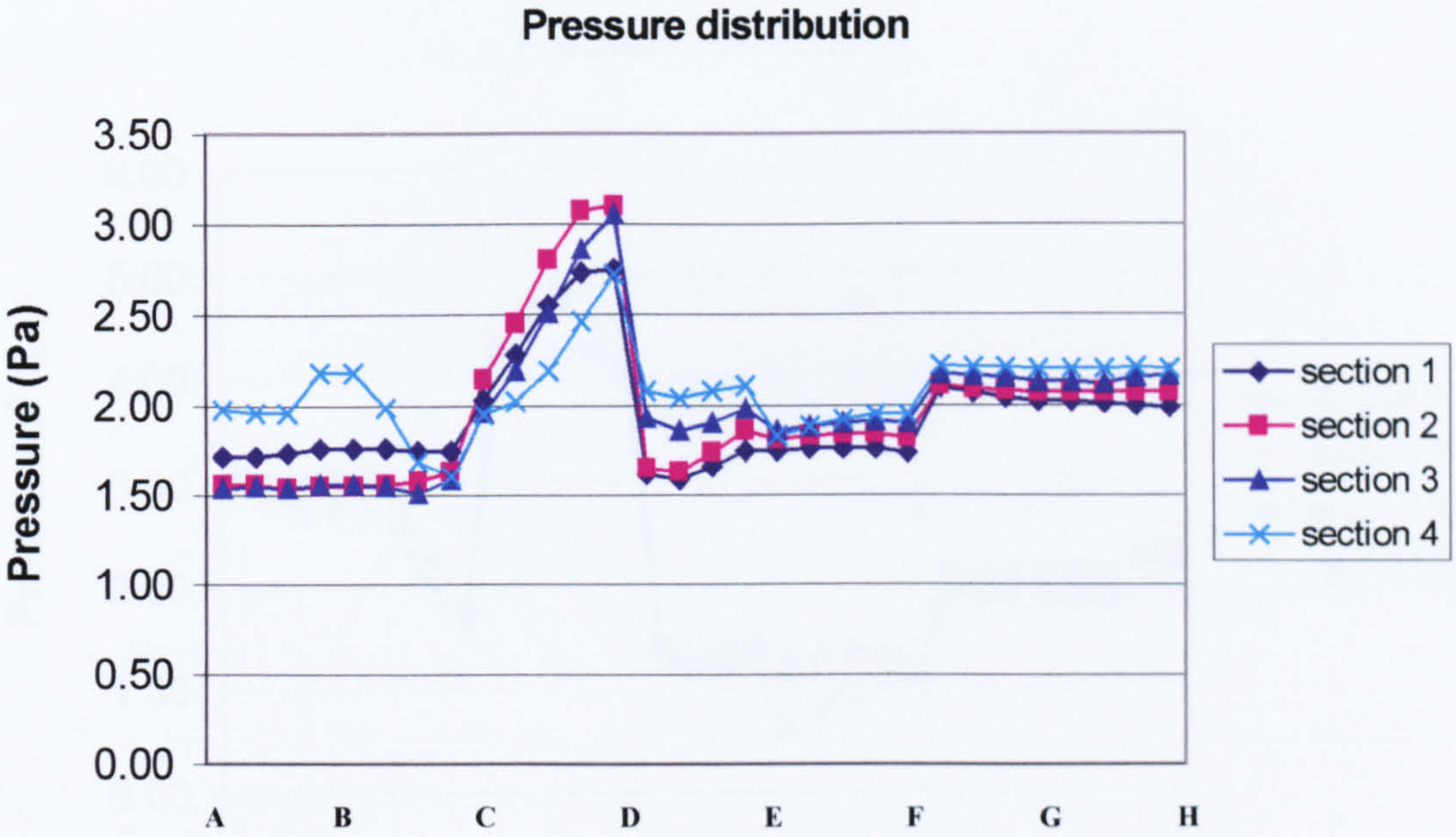

Figure 6.2.97 Pressure distribution on the fourth building

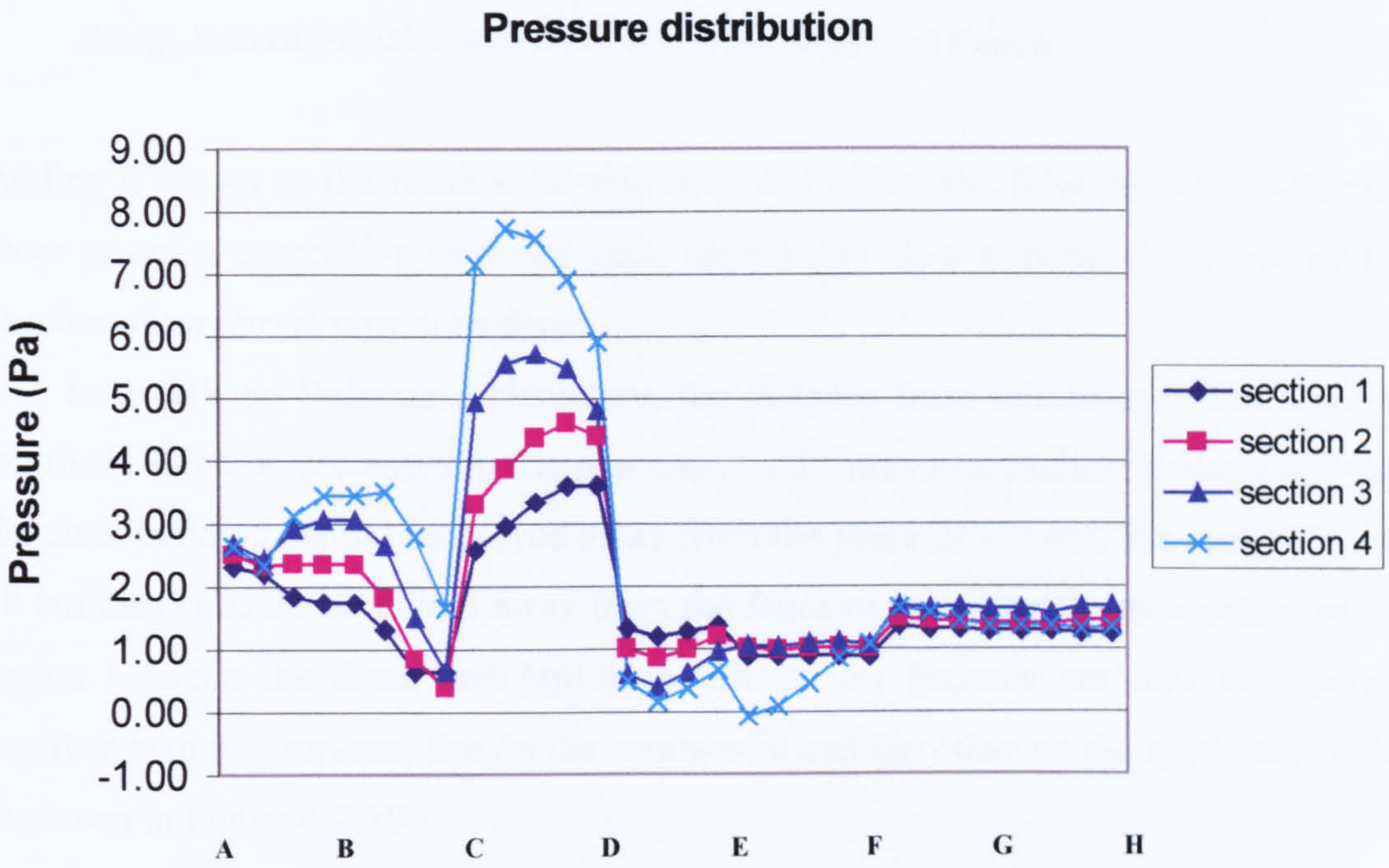

Figure 6.2.98 Pressure distribution on the fifth building

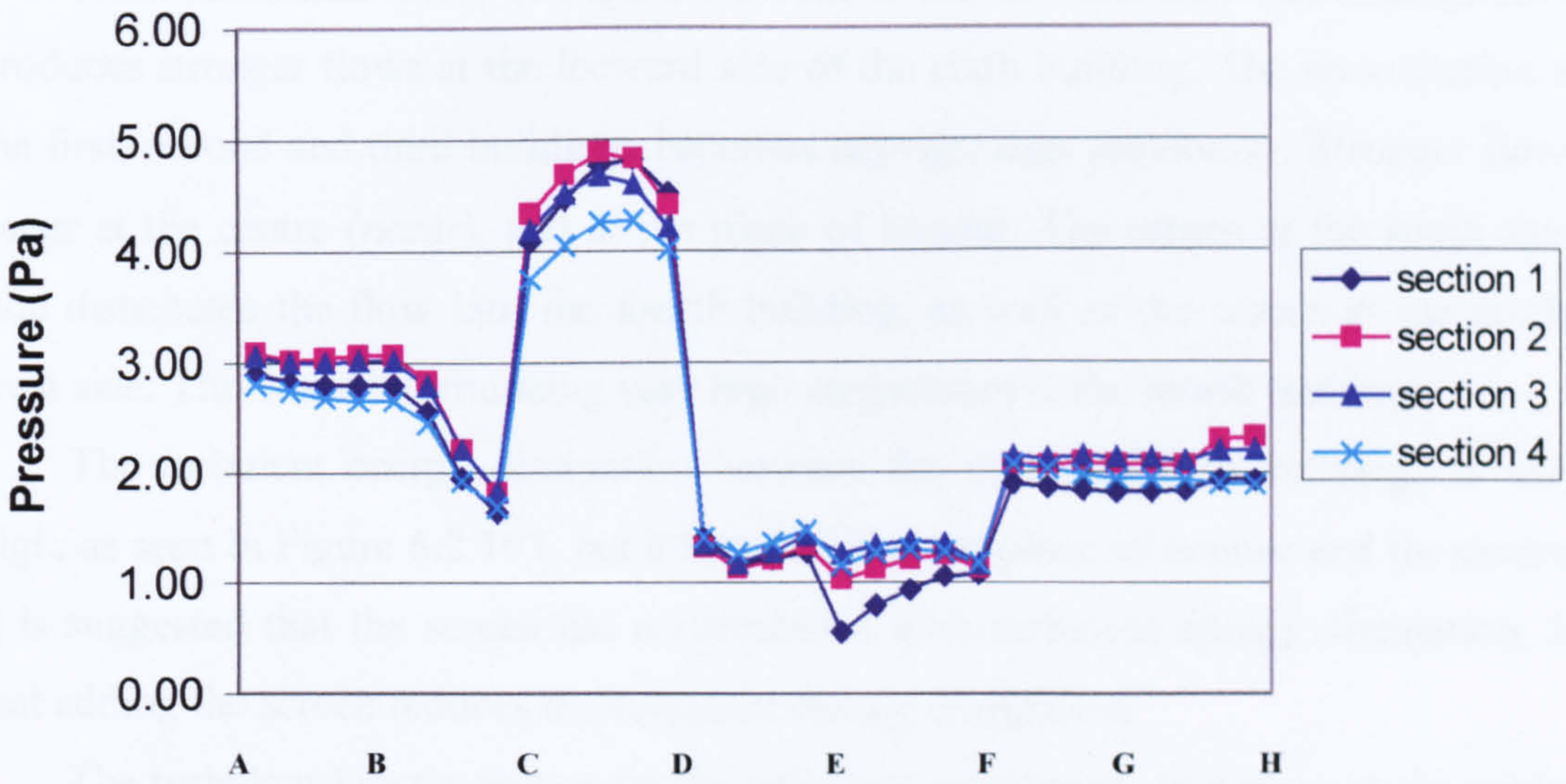

Figure 6.2.99 Pressure distribution on the sixth building

6.2.9 Two Gates at the South-West and North-West Sides with Two *Aling – Aling*, Increased Distance Between Buildings and Fence

Adding a screen at the north-west side does not affect the flow patterns. Although there is not a correlation between gate, screen and flow pattern, the effect of the number of screens is now considered.

In traditional Balinese architecture, the distance from buildings to the fence is relatively short, as presented in Chapter One. In the previous studies, it was noted that the sixth building should be moved away from the place of honour. We also note that all buildings should be moved away from the fence to minimise the momentum in the region between the fence and buildings. These two features are now considered, together with two screens, one on the south-west and the other on the north-west side, as shown in Figure 6.2.100.

6.2.9.1 Results and Discussion

From the velocity profile in Figure 6.2.101, it can be seen that the flow between the building surfaces and the fence decreases. It seems that the flow profile becomes stronger near the place of honour, but weaker near the two screens.

From streamline plots in Figure 6.2.102, it can be seen that this configuration produces stronger flows at the leeward side of the sixth building. The recirculation at the first, second and third buildings becomes stronger than previously. Stronger flows occur at the centre (*natar*), and at the place of honour. The screen at the south-west side distributes the flow into the fourth building, as well as the screen at the north-west side. This leads to producing very high momentum at the fourth building.

The turbulent energy dissipation between the third and fifth buildings is very high, as seen in Figure 6.2.103, but it is reduced at the place of honour and the centre. It is suggested that the screen has a correlation with turbulent energy dissipation, in that adding the screen reduces the turbulent energy dissipation.

The turbulent kinetic energy on the buildings is reduced, as well as at the centre and place of honour.

Pressure distribution plots are presented in Figures 6.2.105 – 6.2.110. By adding two screens and moving the buildings away from the fences, it can be seen that the pressure distribution decreases at the windward side but increases at the leeward side.

The maximum pressure occurs at the windward roof, similarly to the previous studies, but with a lower value. The relationship between the screen and pressure distribution is more clear, in that adding two screen reduces the pressure on the building surfaces.

There is also an interesting result, where the pressure distribution curves are not parabolic, indicating that the flow profile at the windward side of the buildings is not fully developed. This is explainable since the distance between the fences and the first building is longer, therefore the momentum decreases between the fences and the windward building (see also Chapter Three for details of the effects of the fence on pressure distribution). Although the position of the maximum pressure is similar to previously, its value decreases.

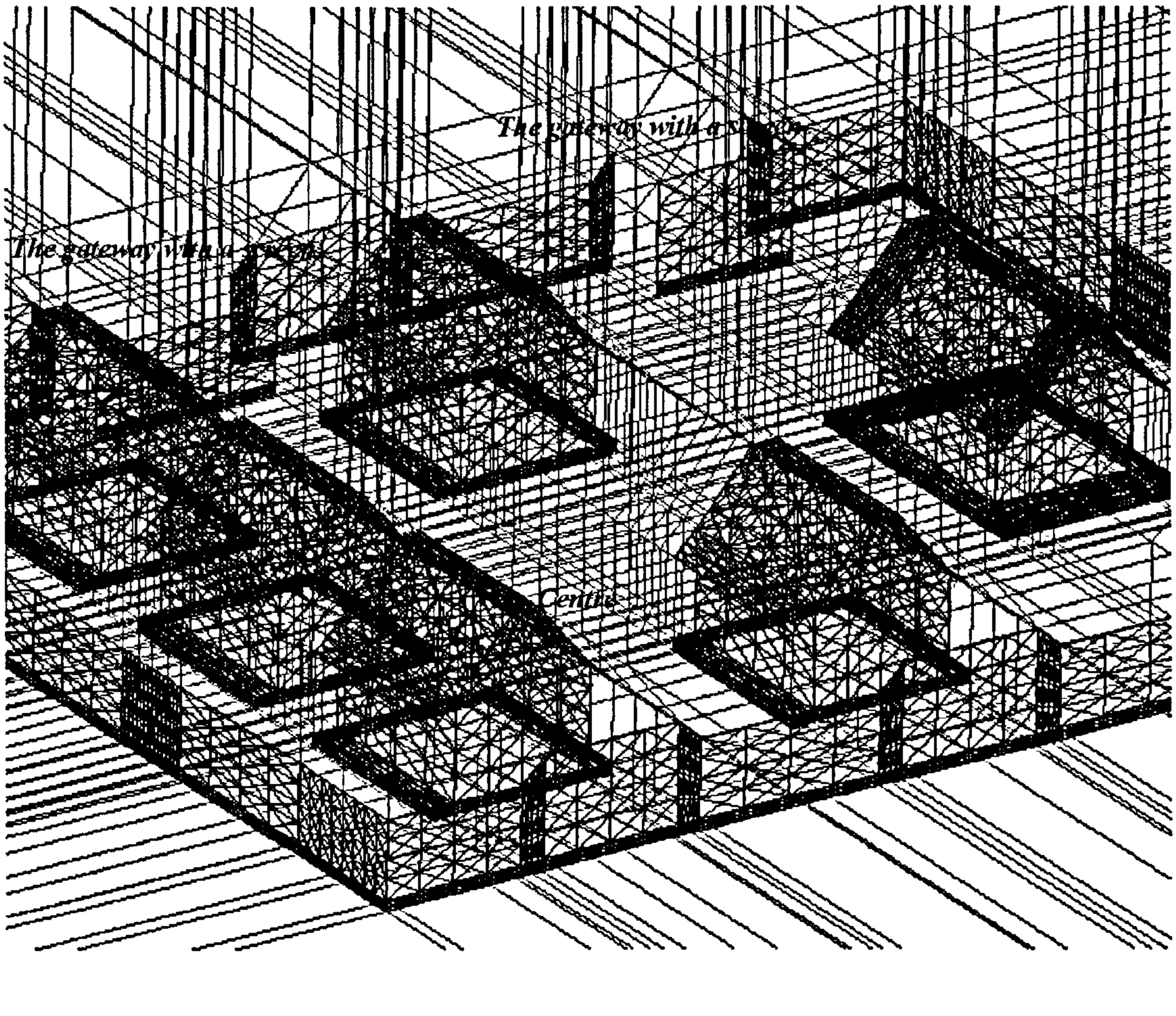

Figure 6.2.100 Side view of buildings arrangement with two gates and two *aling* – *aling* at the south-west and north-west sides of buildings site (increased distance between the fences and buildings)

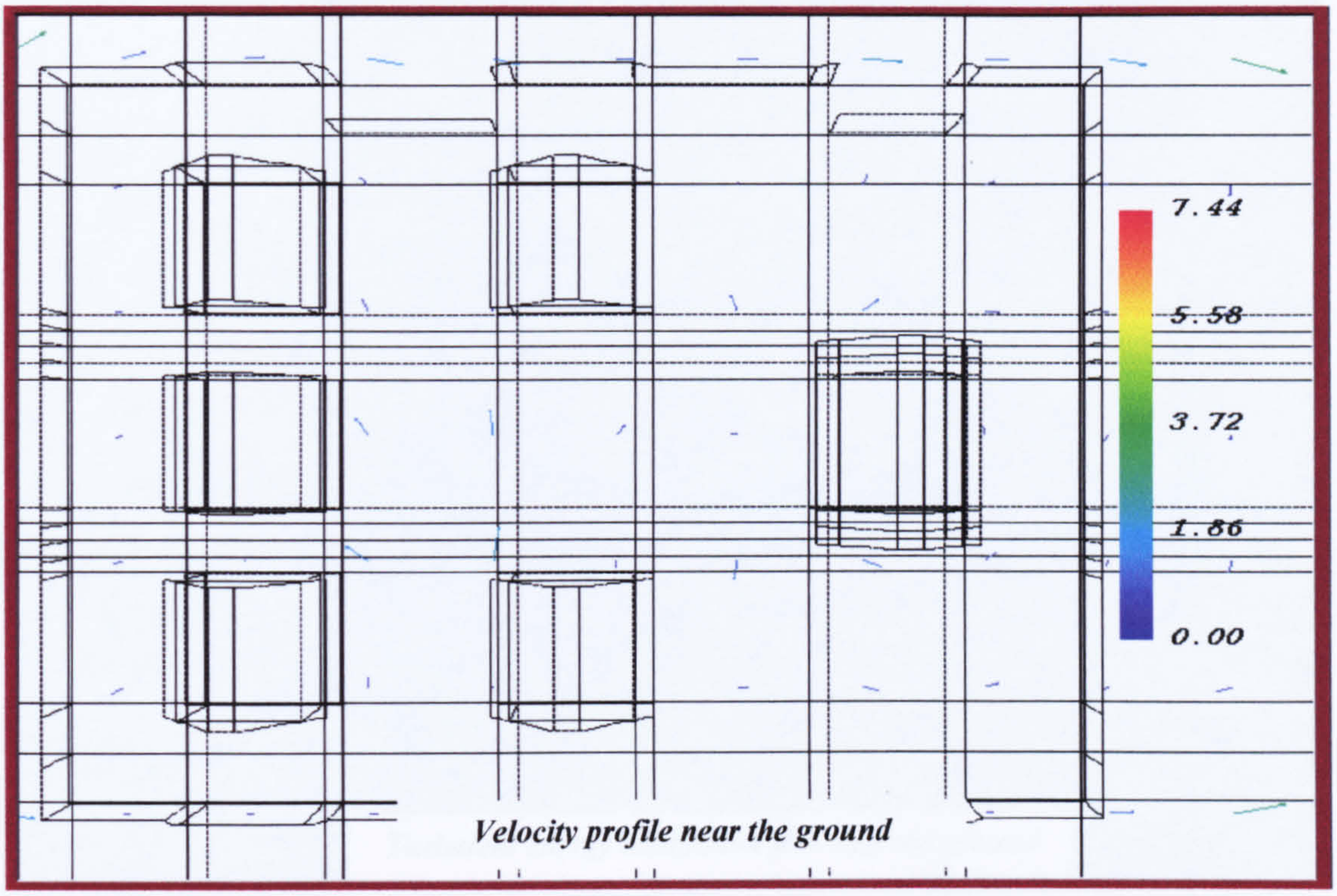

Figure 6.2.101 Velocity profile near the ground

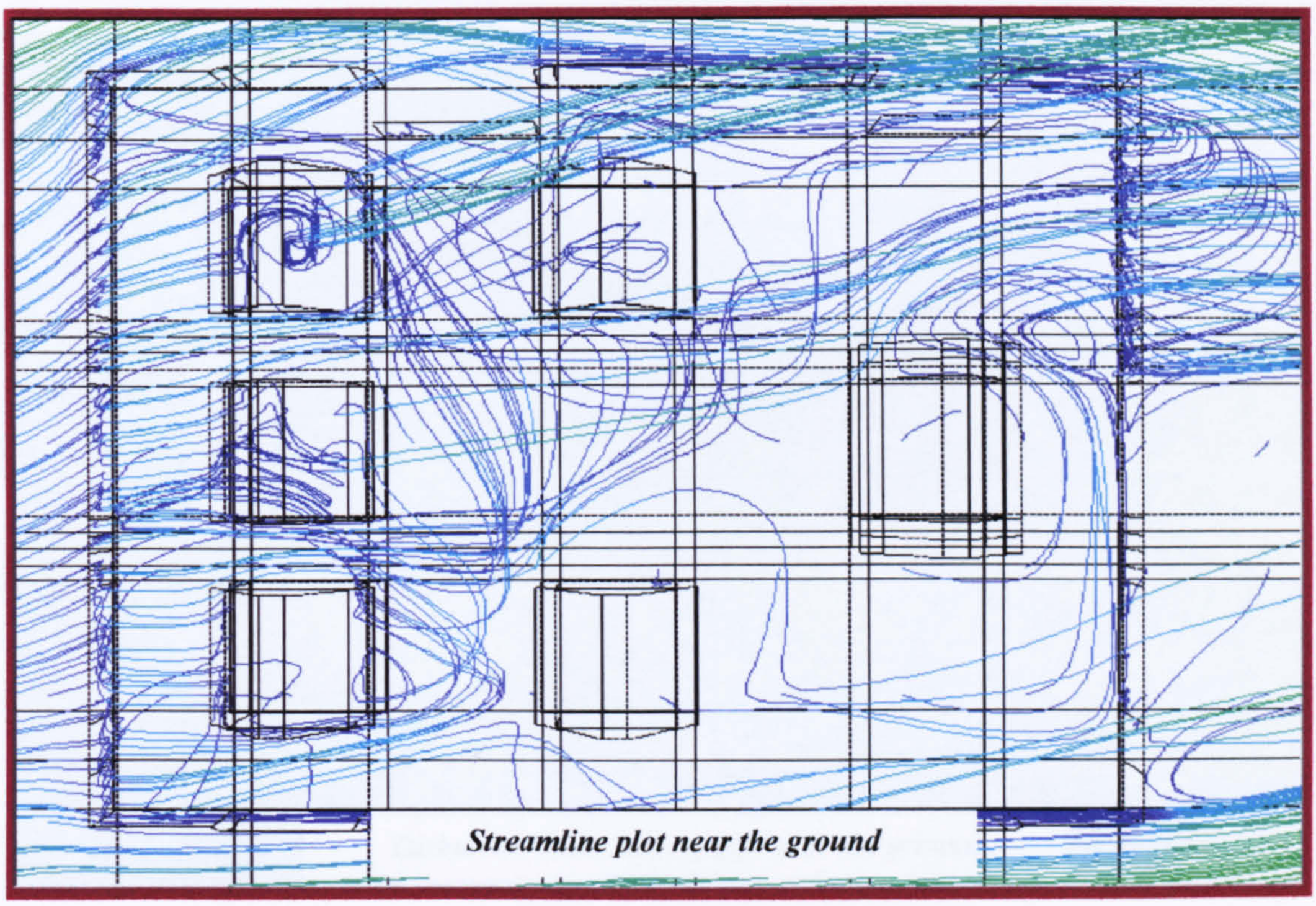

Figure 6.2.102 Streamline plot near the ground

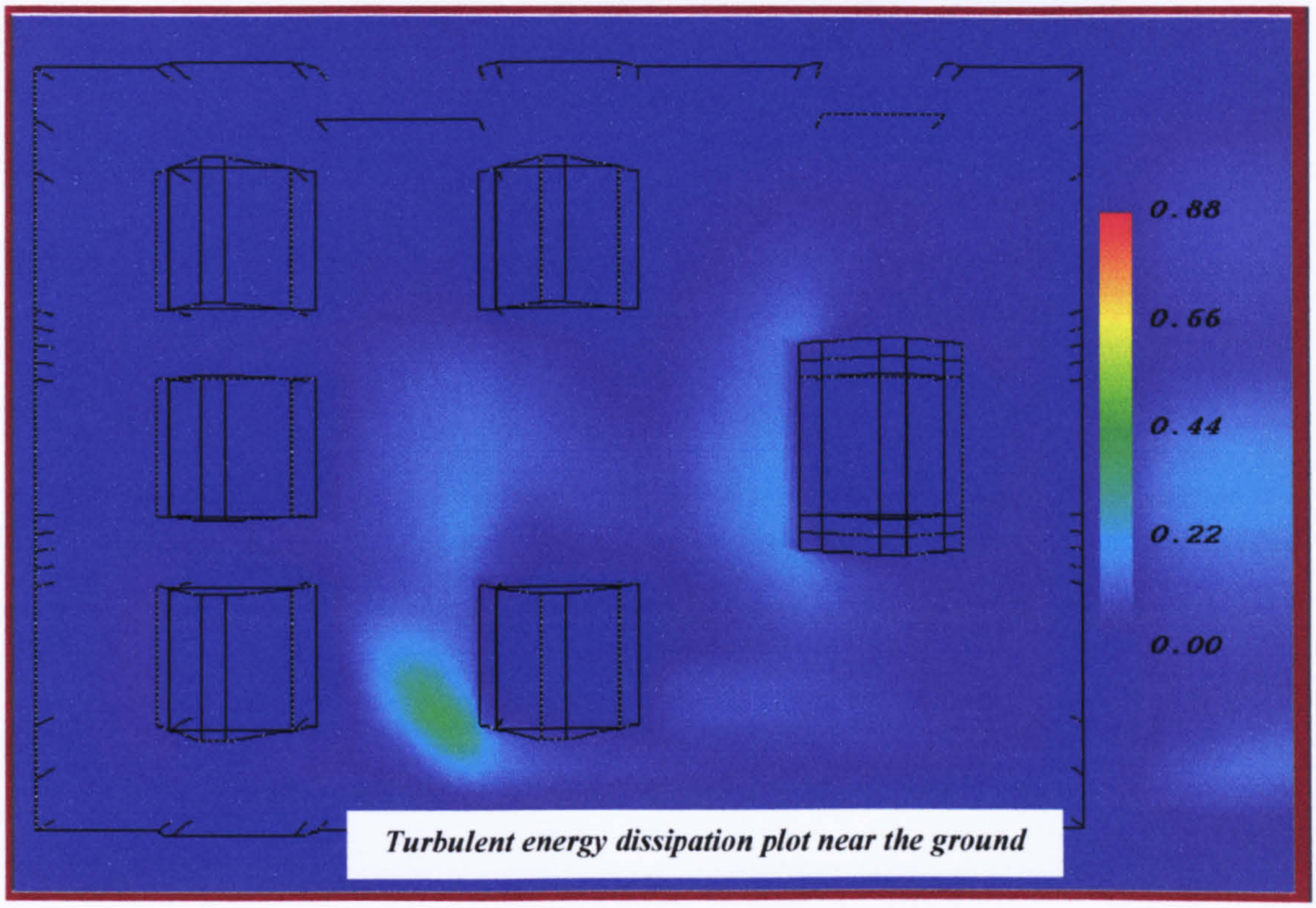

Figure 6.2.103 Turbulent energy dissipation plot near the ground

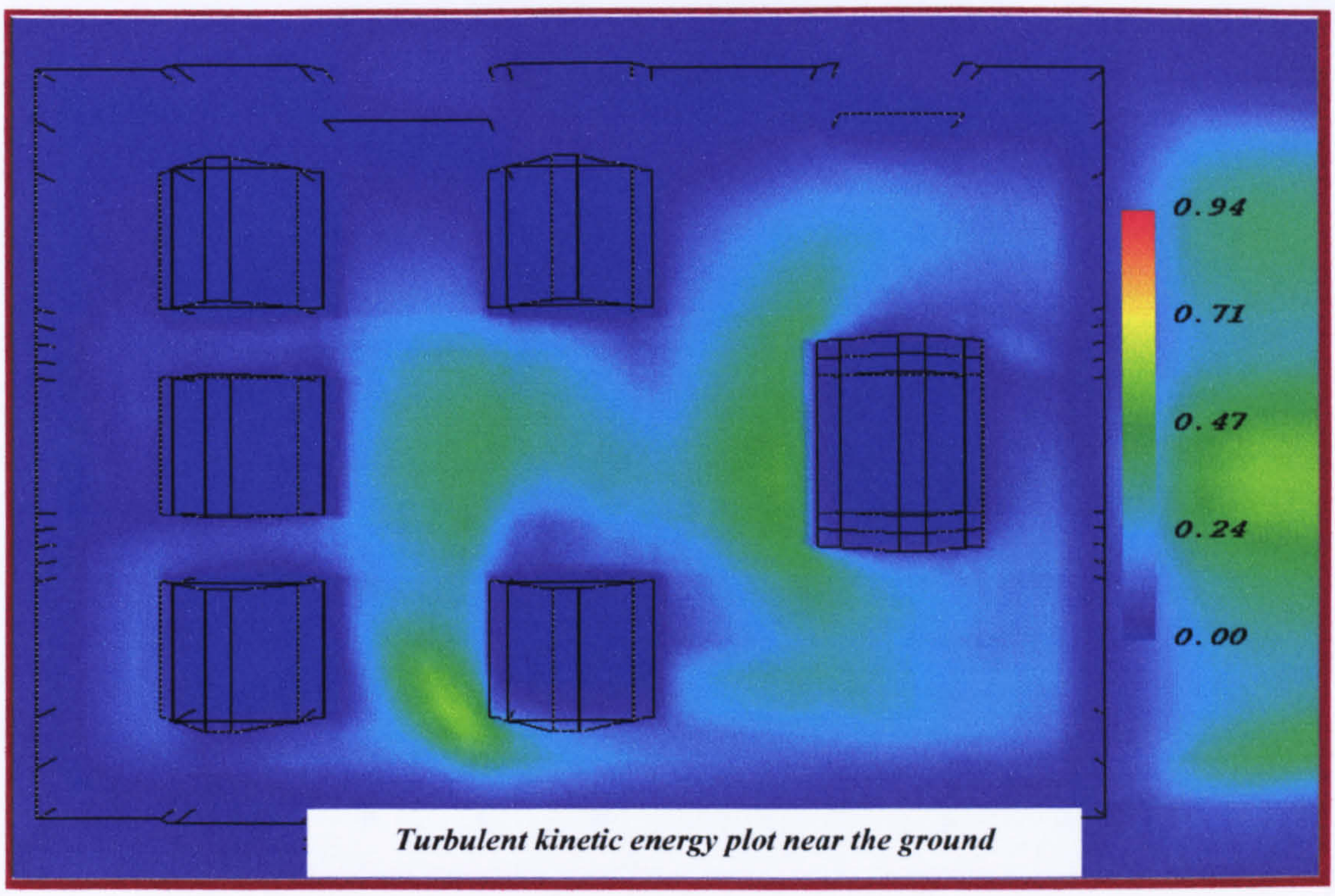

Figure 6.2.104 Turbulent kinetic energy plot near the ground

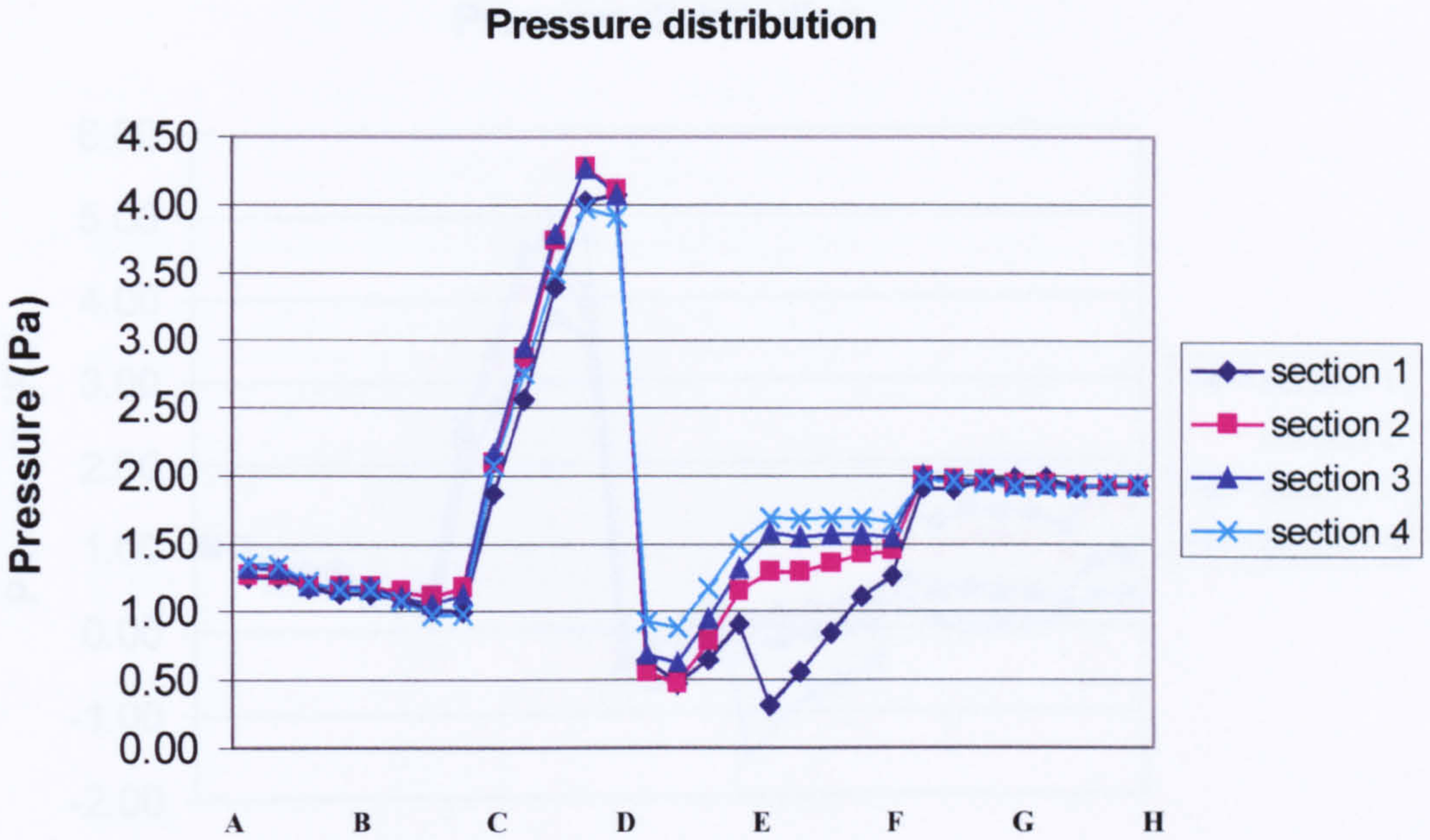

Figure 6.2.105 Pressure distribution on the first building

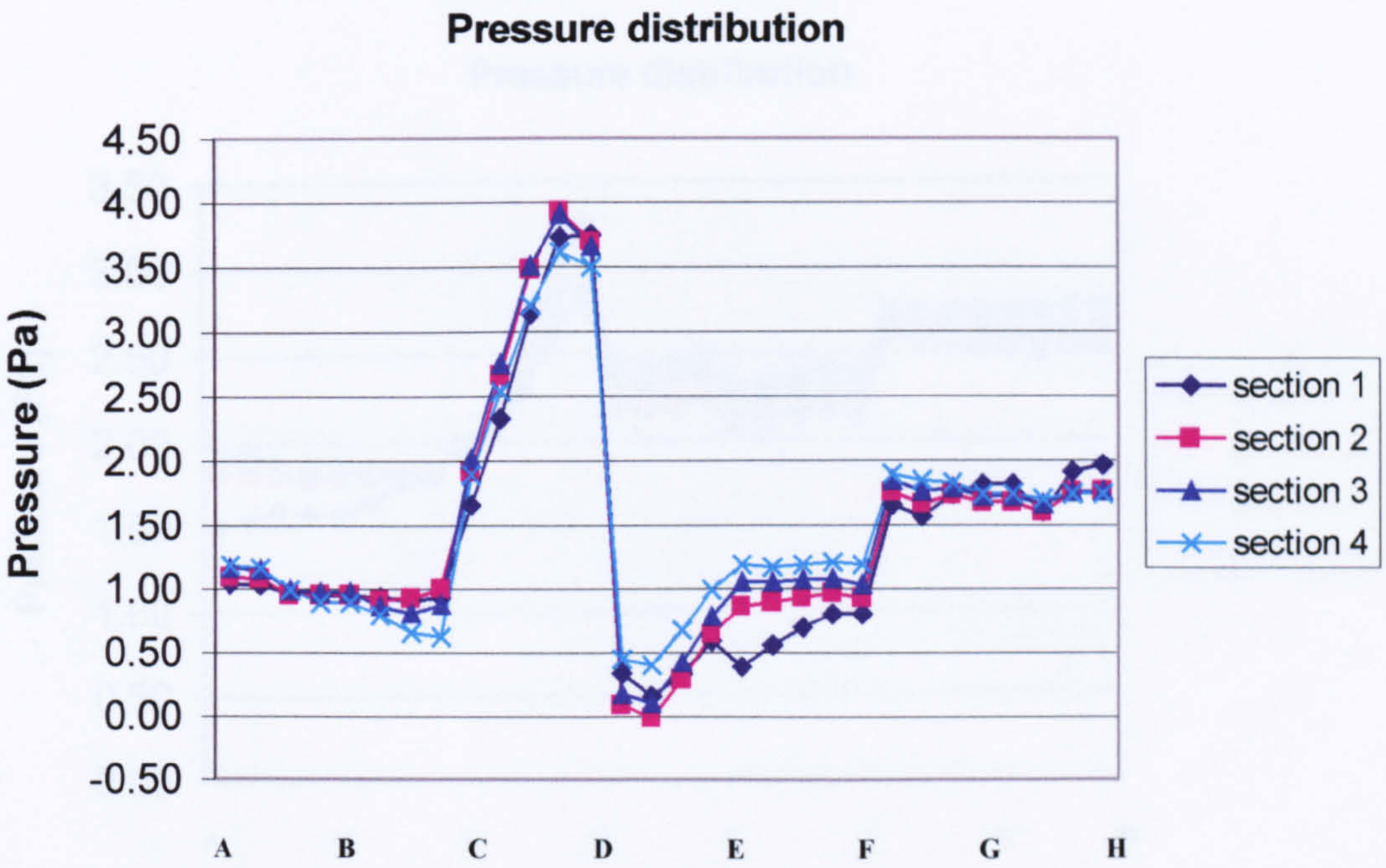

Figure 6.2.106 Pressure distribution on the second building

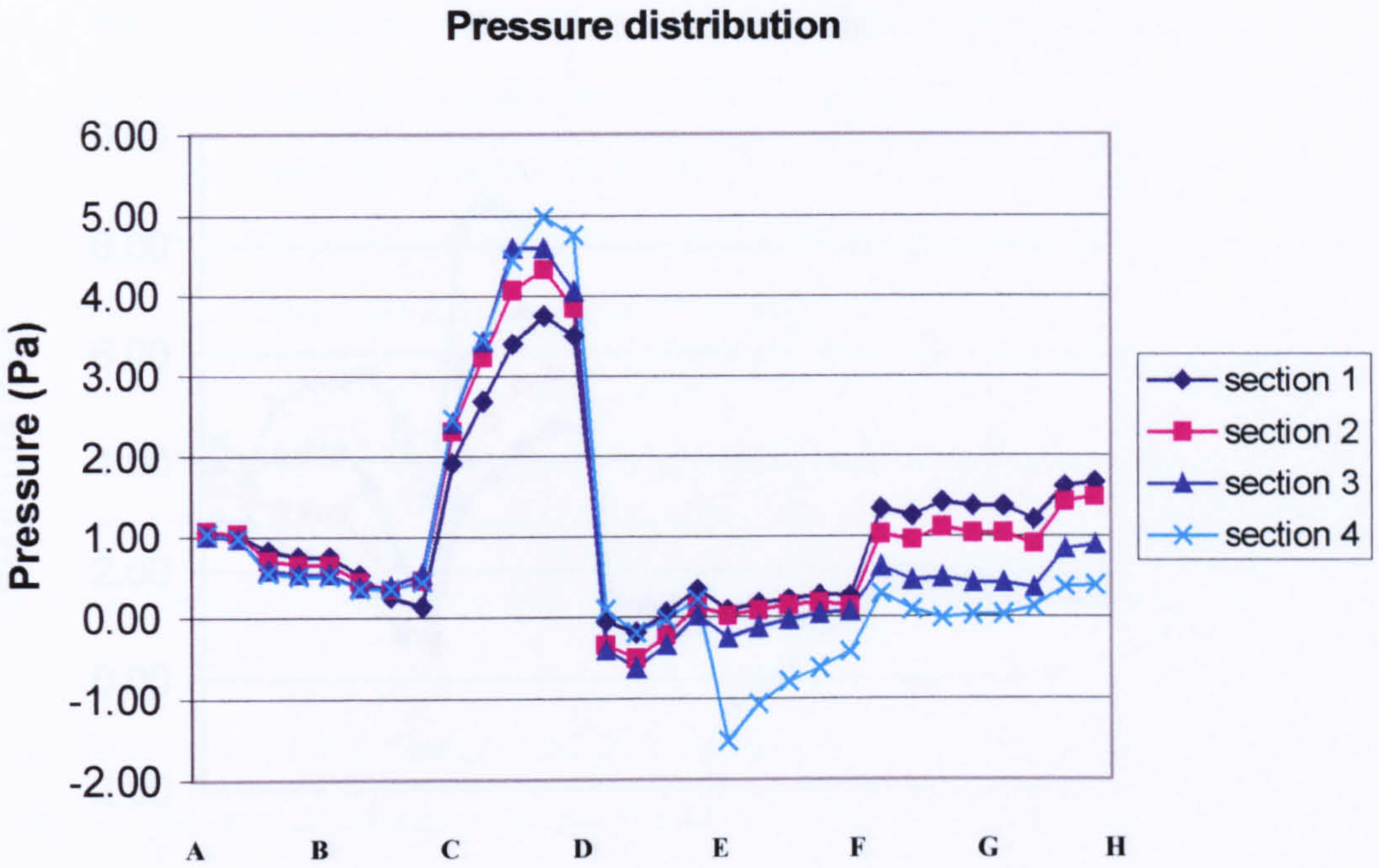

Figure 6.2.107 Pressure distribution on the third building

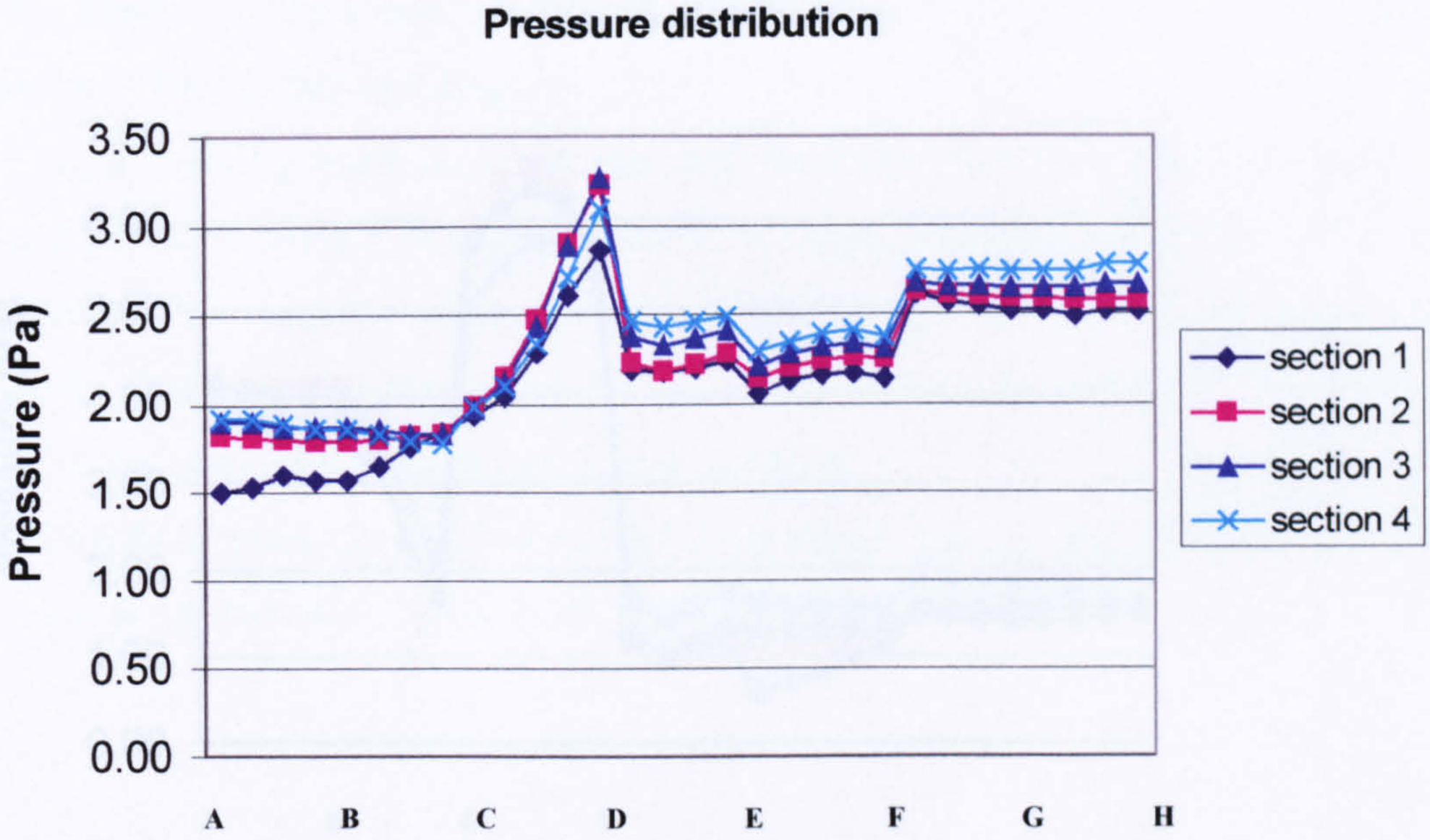

Figure 6.2.108 Pressure distribution on the fourth building

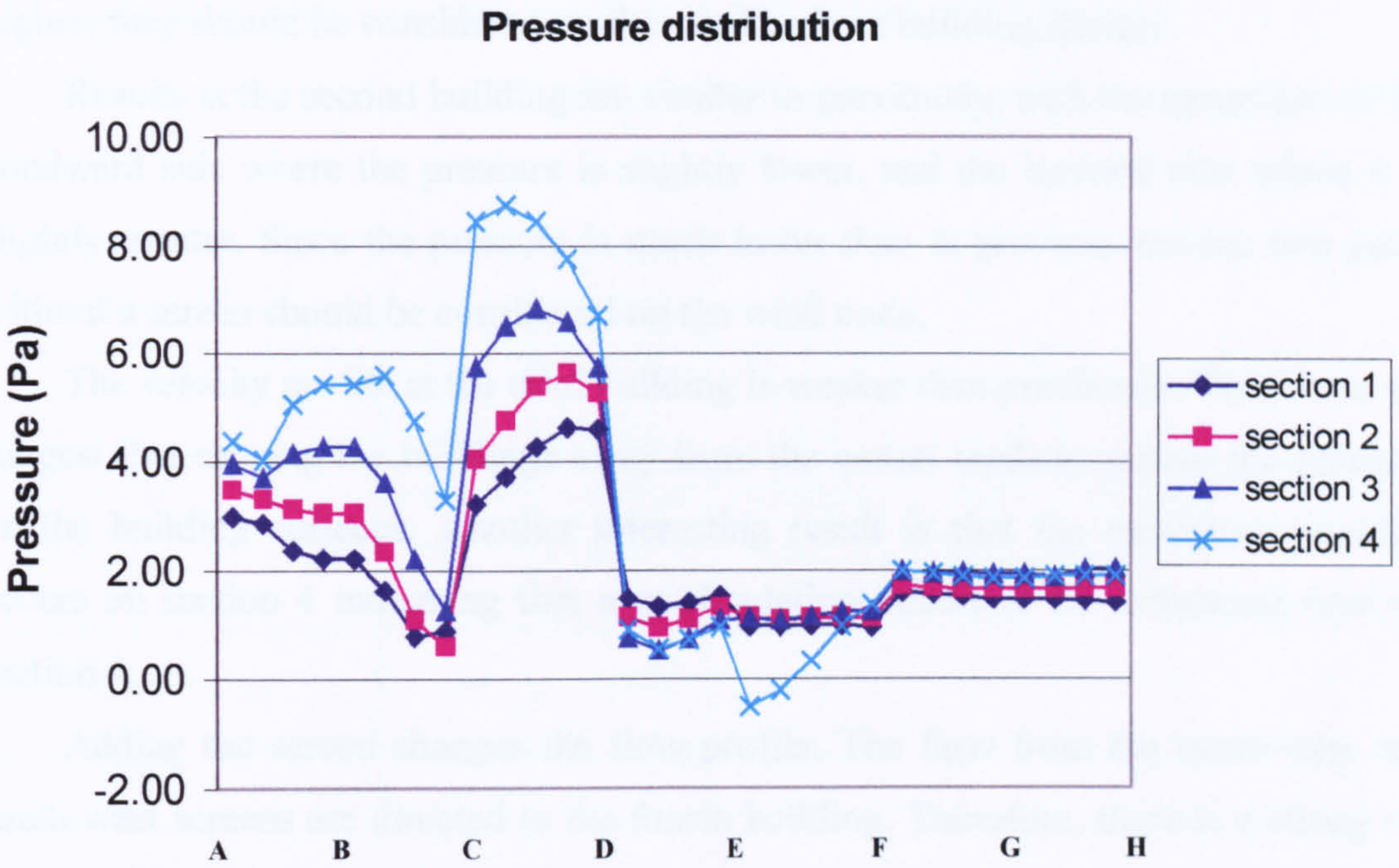

Figure 6.2.109 Pressure distribution on the fifth building

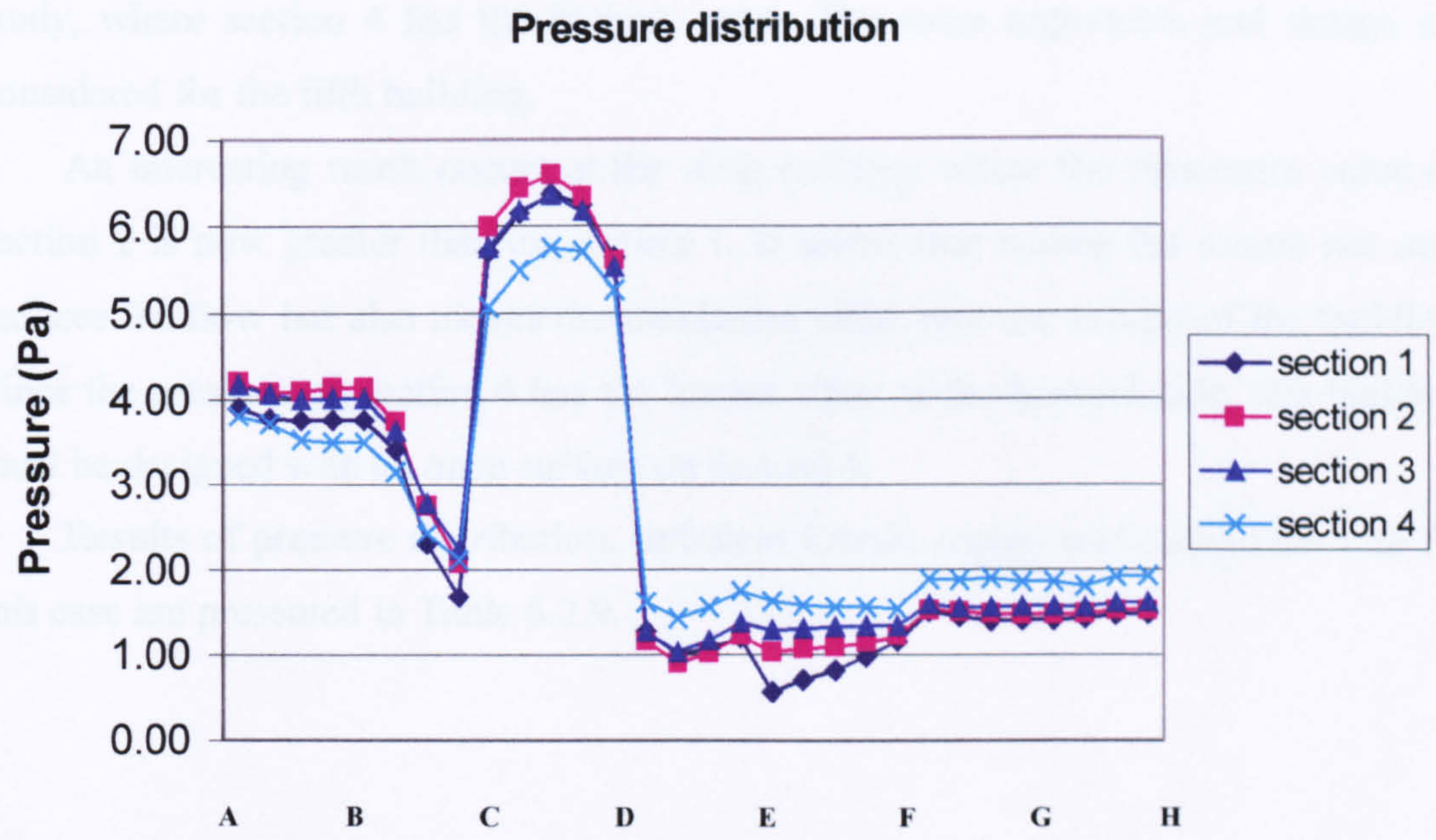

Figure 6.2.110 Pressure distribution on the sixth building

However, since previous pressure distributions -two gates without a screen- were higher, they should be considered on the wind code of building design.

Results at the second building are similar to previously, with the exception of the windward side where the pressure is slightly lower, and the leeward side where it is slightly greater. Since the pressure is much lower than in previous results, two gates without a screen should be considered on the wind code.

The velocity profile at the third building is weaker than previously. Therefore, we suggest that moving the buildings away from the corner tends to reduce the pressure on the building surfaces. Another interesting result is that the maximum pressure occurs on section 4 indicating that a re-circulation occurs at the windward roof on section 4.

Adding the screen changes the flow profile. The flow from the north-west and south-west screens are directed to the fourth building. Therefore, there is a strong re-circulation at the fourth building, shown very clearly where the maximum pressure occurs on sections 2 and 3. From the pressure distribution, it can be seen that the flow profile is not fully developed. Therefore, the distance between buildings and the fences should be decreased.

The pressure distribution at the fifth building is similar to that in the previous study, where section 4 has the highest value. The same arguments and design are considered for the fifth building.

An interesting result occurs at the sixth building where the maximum value on section 2 is now greater than on section 1. It seems that adding the screen not only reduces the flow but also moves the maximum value into the middle of the building. Since the pressure on section 4 has the lowest value at the leeward side, this building must be designed with an open surface on section 4.

Results of pressure distribution, turbulent kinetic energy and dissipation rate for this case are presented in Table 6.2.9.

Table 6.2.9 A summary of results for two gates at the south-west and north- west sides with two *aling – aling*, increased distance between buildings and fence

Building number	I	II	III	IV	V	VI
Maximum pressure (Pa) position	4.25 windward roof	3.8 windward roof	5.0 windward roof	3.3 windward roof	8.5 windward roof	6.6 windward roof
Maximum turbulent kinetic energy (m^2/s^2) position	0.158 windward roof	0.156 windward roof	0.16 windward roof	0.33 top roof	0.21 windward ground	0.245 top roof
Maximum turbulent energy dissipation (m^2/s^3) position	0.095 windward roof	0.092 windward roof	0.10 windward roof	0.08 top roof	0.18 windward ground	0.181 windward ground

6.3 Summary

A summary of results for pressure, turbulent kinetic energy and dissipation rate is presented in Table 6.2.10.

Table 6.2.10 A summary of results

Building number	**I**	**II**	**III**	**IV**	**V**	**VI**
Maximum pressure (Pa) position condition	11 windward wall without gates	10 windward wall without gates	9.5 windward wall without gates	6.2 windward roof gates on south-west	8.4 windward roof gates on south-west	7.5 windward roof gates on south-west
Maximum turbulent kinetic energy (m^2/s^2) position condition	0.28 windward wall gate on south-west	0.19 near ground without gates	0.14 near ground without gates	0.46 windward roof without gates	0.28 top roof without gates	0.42 top roof without gates
Maximum energy dissipation (m^2/s^3) position condition	0.275 windward roof gate on north	0.27 windward roof gate on north	0.275 windward roof gate on north	0.28 windward wall without gates	0.152 windward ground gate on north	0.15 leeward roof without gate

The table shows the maximum values for pressure, turbulent kinetic energy and dissipation rate of a cluster of buildings with a short distance between them. In order to reduce the wind loads on building surfaces, open surfaces should be placed where the highest values occurred.

The highest turbulent kinetic energy at the first building occurred where the gate is on the south-west side. In traditional Balinese architecture, the gate usually lies on this side. Therefore, the first building (granary) always receives high turbulent kinetic energy. To reduce the turbulent kinetic energy at the windward wall of the first building, an open surface should be provided. This leads to reducing the wind forces but produces a higher heat transfer rate. Since the granary shown in Figure 4.4.1 is fully open, we suggest that this phenomenon was taken into account.

The highest turbulent energy dissipation occurred for a building arrangement without fence. This indicates that the distance from the fourth building to the centre is relatively short. Therefore, the fourth building should be moved away from the centre, or a fence added at the front side. From the results, we note that the gate position affects the flow patterns around a cluster of buildings.

From the above results, it was clear that the maximum pressure, turbulent kinetic energy and dissipation rate for the gate position in Figure 6.2.40 are similar to that in Figures 6.2.27 and 6.2.51. Since the traditional meaning of Figures 6.2.27 and 6.2.51 is a "good" value, then the traditional meaning of Figure 6.2.40 should also be a "good" value.

The gate position should be related to wind engineering, architectural aerodynamics, heat transfer and thermal comfort of occupants. A "good" meaning can be related to the percentage of reduction in wind velocity. Reduction of wind velocity at buildings means reduction of heat loss from buildings to the surroundings, or reducing the cooling loads, which can be related to thermal comfort of occupants. Therefore, a "good" meaning of the gate position has a strong relation to the thermal comfort of occupants. We propose that the greater the reduction in wind velocity, heat losses on building surfaces and cooling loads of buildings, the better the value of the gate position. This indicates that the traditional meaning of the gate position should be related to thermal comfort of occupants. The better the thermal comfort of occupants, the better the value of the gate position.

The magic rule described in Chapter One can also be related to wind engineering and heat transfer. A screen behind the gate (*aling –aling*) reduces the pressure, turbulent kinetic energy and dissipation rate. This small wall that screens off the interior and stops evil spirits, can be related to the protection against wind loads and reduction of energy transfer on building surfaces. The connotation of evil spirit and magic rule of traditional Balinese architecture now has a strong relation with

momentum and energy transfer on building surfaces. Therefore, a reduction of momentum and energy transfer (evil spirit) increases the thermal comfort of occupants.

Centre (*natar*) is the area where the flows reattach to the ground. The pressure, turbulent kinetic energy and dissipation rate decrease here. At the reattachment point, the shear stress becomes zero and the heat transfer to the surroundings is reduced. After the reattachment point, the pressure, turbulent kinetic energy, energy dissipation and heat transfer tend to increase. The increase of these parameters is fully affected by the Reynolds number. Therefore, the distance between the sixth building and the centre plays an important role in order to reduce the wind effects at the sixth building. The reattachment length also depends on the distance between the front fence and the first row of buildings, with a shorter distance producing a shorter reattachment length. From the analyses, the reattachment length is around 1.7 times the first row building's height (**H**). A shorter distance between the sixth building and the centre produces a higher turbulent kinetic energy and dissipation rate. This is explainable since the air motions are not fully developed turbulent. The one solution to produce a fully developed turbulent flow is to increase the distance between the sixth building and the centre. Results of Chapter Five have shown that fully developed turbulent flows occur at a point 1.5 times the reattachment length, indicated by the constant value of the static pressure coefficient at the ground. Therefore, the distance between the sixth building and the centre should be around 2.5-2.6 **H**, or a distance of 4.2-4.3 **H** between the first and sixth buildings, as presented in Figure 6.3.1.

At the separation region, the formation of eddy vortices affects the flow patterns. The separation width becomes important to adjacent structures since it becomes small at the reattachment point but enlarges thereafter. In order to reduce the wind effects, the second row of buildings (in this case the fourth and fifth buildings) should lie at the reattachment point, or 1.7 **H** times the first buildings height. To reduce wind effects and cooling loads, the second row of buildings should be moved away from the reattachment point, at least 1.5 times the separation width (w) which depends on the first building width (W), as shown in Figure 6.3.2 (a). A shorter distance between the second row and the first row of buildings results in a longer distance between the second row of buildings and the reattachment point, as presented in Figure 6.3.2 (b). Since the separation width increases after the reattachment point, the distance between the second row of buildings and the centre will also be increased, as presented in

Figure 6.3.2 (c). We recommend that the second row (the fourth and fifth) of buildings should be placed at the reattachment point. Based on the above definition of centre (*natar*), the fourth and fifth buildings should be placed at the centre. This indicates that the reattachment length and separation width have been taken into consideration in traditional Balinese architecture, by reducing their width (**W**) and increase their length (**L**).

For better natural ventilation and beneficial air motion, inlet openings should be located to intercept prevailing winds and direct them towards the living room. Therefore, all buildings should be oriented to the centre (*natar*) in order to optimise the airflow into buildings. This again indicates that building orientation to the centre (*natar*) in traditional Balinese architecture has a strong relation to natural ventilation and thermal comfort of occupants.

The place of honour, the higher north-east corner of the house towards the mountain, was occupied by the family temple (*sanggah kemulan*) for worshipping their ancestors. In our analyses, the place of honour is an area where the turbulent kinetic energy and dissipation rate are relatively high. According to the definition that an evil spirit has a strong relation to momentum and energy transfer, the energy transfer in this area should be eliminated. The evil spirit can be contrasted with the gods. Therefore, the shrines of gods should be built in this area in order to reduce the evil spirits. We propose that the reason for building the family temple at the north-east corner of the house towards the mountains is to dispose of the evil spirit around the buildings. This leads to an increased thermal comfort of occupants.

Based on this analysis, the distance between the sixth building and the place of honour depends on the separation width at the fifth building, as presented in Figure 6.3.3.

A gate without a screen was presented in Figure 1.1.11. In order to avoid the evil spirit entering the site, a protector should be built around the gate. In Balinese words this protector is named *Penunggu Karang*. Therefore, it is clear that traditional Balinese reason is meaningful and can be related to several aspects, even in the modern age.

The name *Ngurah* or *Penunggu Karang* refers to a deity whose function is to "protect the ground", or act as a "guardian" or "protector" or "shelter". They protect the land from natural disasters, crops plagues, earthquakes , volcanic eruptions, floods and hurricanes [3]. Fluid is believed to circulate from the holy mountains to the sea,

from where it returns to the mountain (as wind and rain). So, Balinese life is a constant movement between *kaja* and *kelod*, the main direction of orientation in Bali [4]. Temples and shrines follow a similar logic, where temples are physically located at the upstream edge of whatever system they purport to control [5]. From the above description, we propose that the temples and shrines should be physically located in such a way to protect the buildings and occupants from natural disaster.

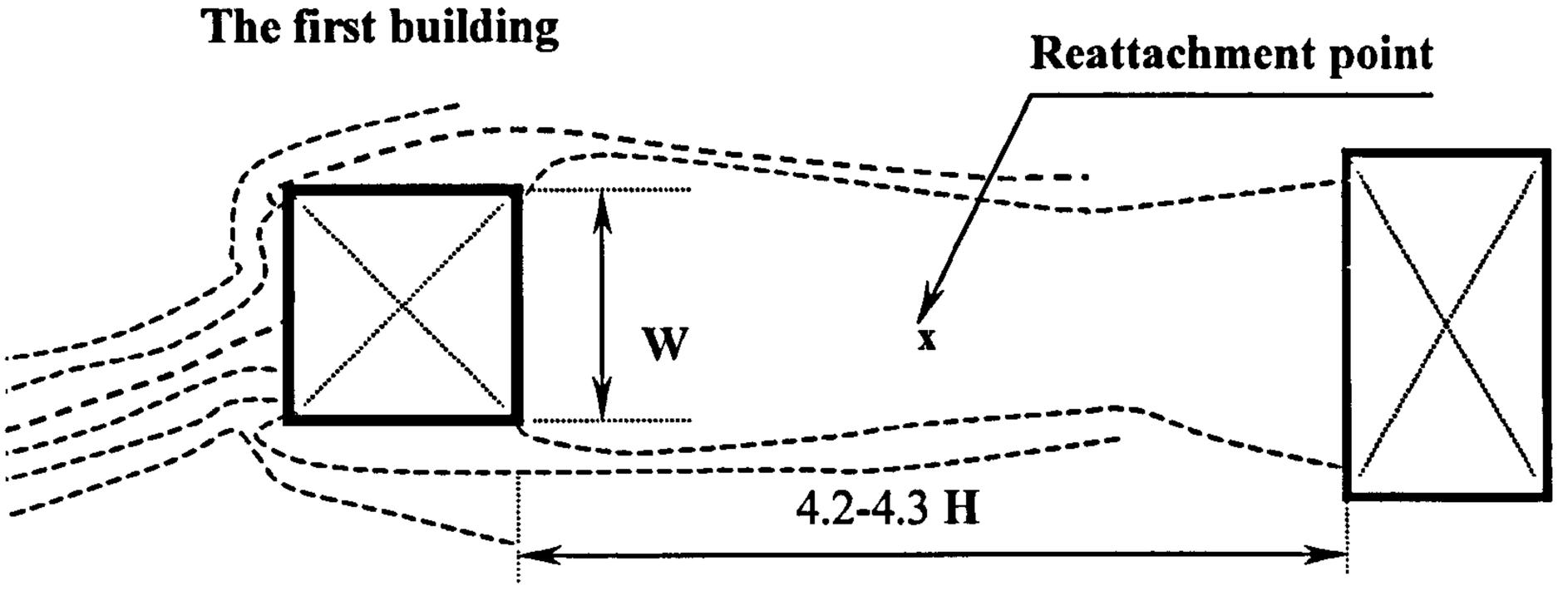

Figure 6.3.1 Design for the sixth building

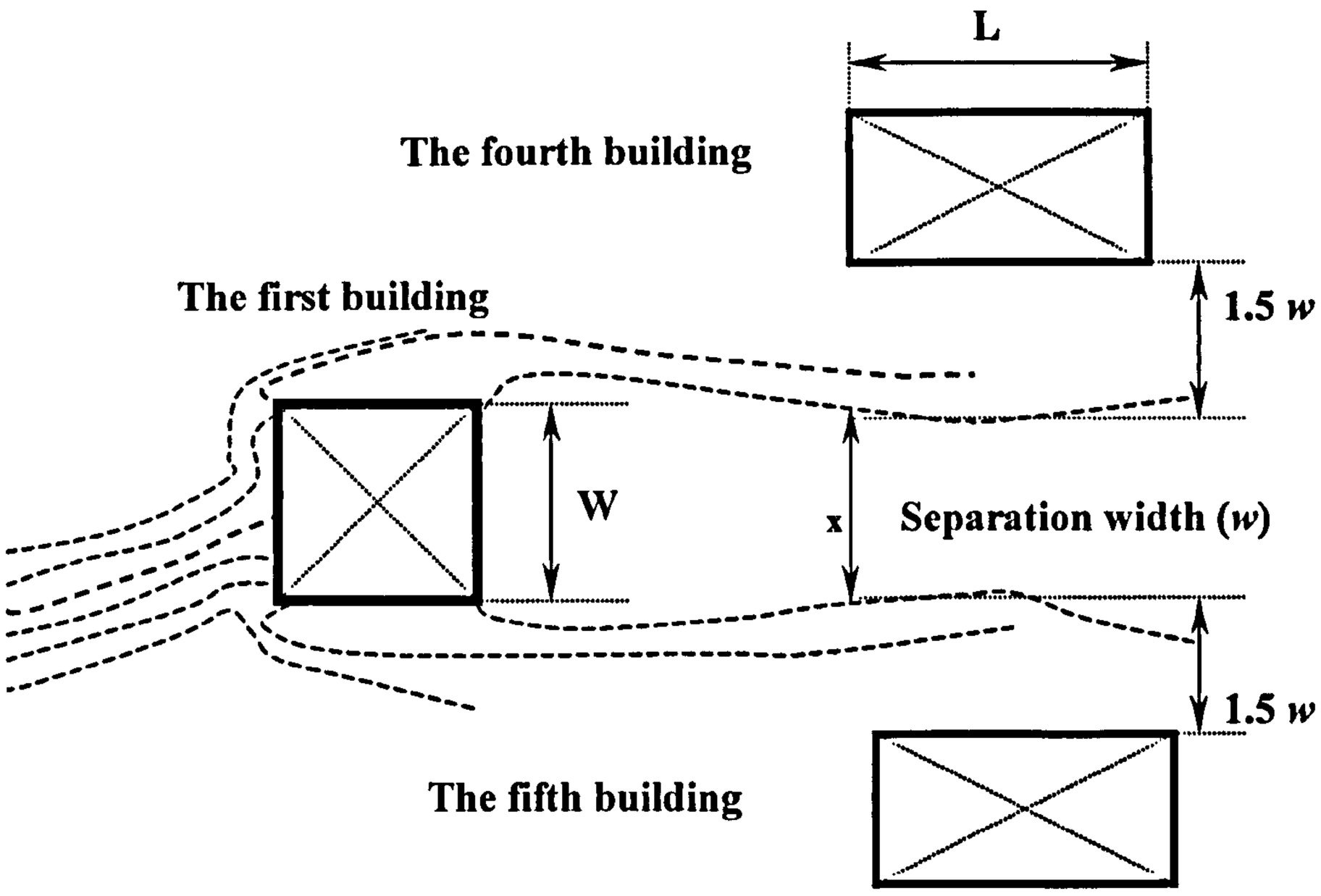

Figure 6.3.2 (a) Design for the fourth and fifth buildings, at the reattachment point

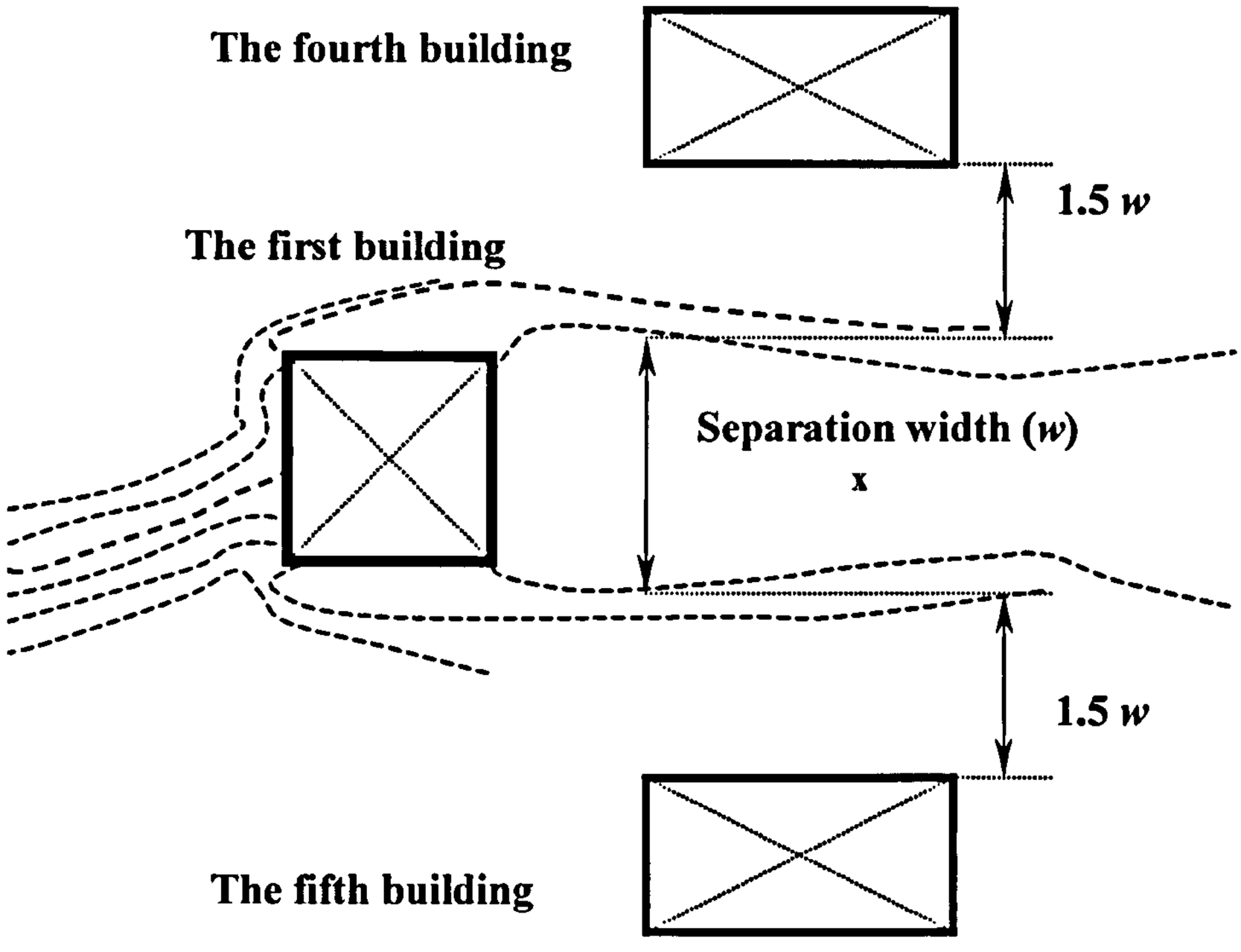

Figure 6.3.2 (b) Design for the fourth and fifth buildings, near the first building

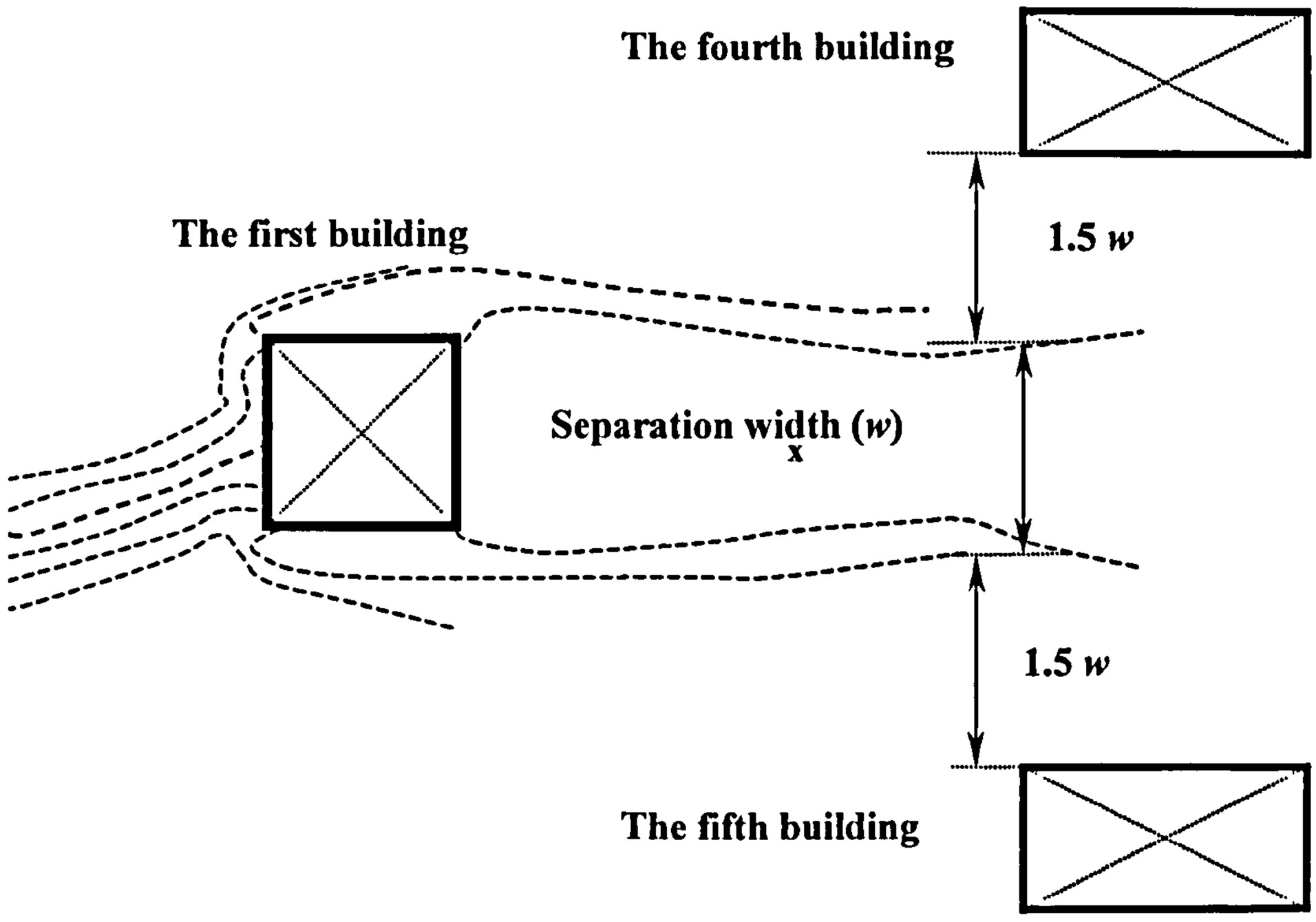

Figure 6.3.2 (c) Design for the fourth and fifth buildings, far from the first building

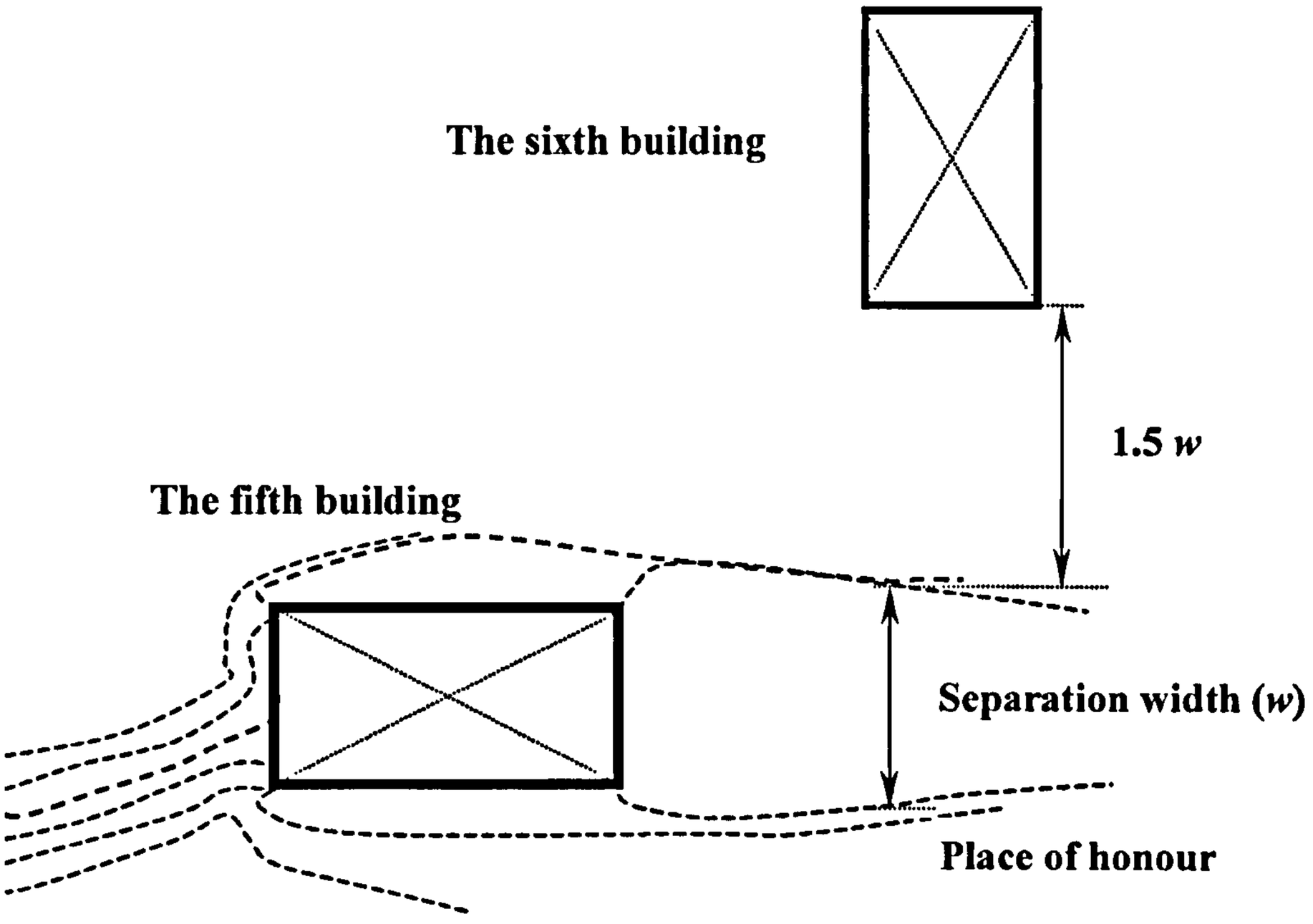

Figure 6.3.3 Design for the sixth building, distance to the place of honour

We conclude that traditional Balinese architecture is not only a traditional way of life, but also has a strong and significant correlation with several engineering fields such as wind engineering, architectural aerodynamics, heat transfer, fluid dynamics and thermal comfort.

Traditional Balinese architecture does not only mean harmonisation between humans and their environment, but also giving protection to humans from environmental disasters. Therefore, new Balinese codes of building design should refer to the *Tri Hita Karana* concept in order to improve thermal comfort of occupants and reduce cooling loads with corresponding energy savings.

REFERENCES

1. D. Delaunay, D. Lakehal and D. Pierrat, Numerical approach for wind loads prediction on buildings and structures, J. Wind Engineering and Industrial Aerodynamics 57 (1995) 307-321.
2. I.G.M. Putra, Nilai-nilai Tata Letak Bangunan dalam Rumah Tradisional Bali, University of Udayana, 1985.
3. C. Geertz, Negara: The Theatre State in Nineteenth-Century Bali, Princeton University Press, New Jersey, 1980.
4. H.S. Nordholt, Bali: Colonial Conceptions and Political Change 1700-1940, from Shifting Hierarchies to "Fixed Order", CASP 15, Rotterdam, 1986.
5. J.S. Lansing, Priests and Programmers: Technologies of Power in the Engineered Landscape of Bali, Princeton University Press, New Jersey, 1991.

CHAPTER SEVEN

CONCLUSIONS AND SUGGESTIONS FOR FUTURE WORK

7.1 Conclusions

Traditional Balinese architecture has always been followed by the people of Bali and contains exalted values which are considered eternal. *Kaja* (towards the mountain, upstream), leading to the sacred, is the area where momentum and energy transfer are relatively high. In Balinese world, these momentum and energy transfer are named evil spirit. Therefore, in order to reduce the negative effects of these parameters to the occupants, the sacred place should lie on this area. *Kelod* (towards the sea, downstream), leading to demons, is the area where momentum and energy are generated. This is understood as the wind which is generated on the sea and moves to the land due to energy differences. Reducing the wind velocity reduces the pressure, turbulent kinetic energy and dissipation rate, or dispose of the evil spirit. Therefore, Balinese life is a constant movement between *kaja* and *kelod*, the main direction of orientation in Bali.

The *Sanga Mandala* concept is thus a concept relative to energy transfer. The wind moves from the sea to the mountain, and energy transfer (heat flux) increases proportionally to the sun-direction. Heat flux is very high at the sea and at 3 pm, but low at the mountain and in the morning. Therefore, the conditions when the heat flux is high and causes discomfort to the populations are downstream. In opposition, the conditions when the heat (*e.g.* sun shine in the morning) causes are upstream.

Since the wind flows at an angle (from the south-east to the north-west), the highest surface friction and drag force due to pressure occur at the south-western area, but the lowest is in the north-eastern area. The south-western thus denotes the poverty-poverty area and the north-eastern denotes the prime-primary area. Since the mountain lies in the middle of Bali island, the local wind in the north becomes opposite (due to eddy vortices) to that in the south of Bali island. By the same explanation relating to wind forces, the poverty and the primary areas in the north are opposite to that in the

south of Bali. This indicates that the *Sanga Mandala* concept has a strong relation to wind forces, where the lower the wind forces the better the area.

Zoning of traditional Balinese architecture can be associated to wind engineering and heat transfer in order to produce better comfort for occupants. The primary zone is the area where the wind forces are relatively high but with the highest heat transfer rate. This area is suitable for convalescent homes and homes for the aged. In traditional Balinese architecture, this primary zone is for the parents' sleeping quarters. The middle zone is the area where the greatest wind forces occur with a relatively high heat transfer rate. This area is then convenient for conference rooms, meeting rooms or auditoriums. In traditional Balinese architecture, the middle area is for assembly halls and ritual places. The poverty zone is the area where the wind forces are relatively high but with the lowest heat transfer rate. This is adequate for kitchens, stores or garages. In traditional Balinese architecture, the granary lies on the poverty area. From the above explanations, it is clear that traditional Balinese arrangement has a strong relation to thermal comfort.

The distance between buildings and distance from buildings to the fence are parameters that should be taken into consideration in building design. The distance between buildings depends on the reattachment length and separation width. The higher and wider the building, the longer the distance should be. A shorter distance between buildings and fence reduces the heat transfer and the wind forces at the first building. The fence height should not be taller than half a building height since it will reduce the heat transfer.

In traditional Balinese architecture, building orientation and air circulation is from the downstream to the upstream through the centre. Therefore, it is clear that the *Sanga Mandala* concept has a strong relation with air motion around buildings.

The use of pillars in buildings will minimise the momentum effects and protect from damage caused by turbulent kinetic energy. Therefore, there is a strong relation between buildings names, *e.g.*, *Sakapat*, *Sakanem*, *Balé Tiang Sanga* and *Balé Sakutus*, the four posts building, the six posts building, the nine posts building and the eight posts building, respectively, and the need to protect against damage caused by turbulent kinetic energy. Therefore, building arrangement should be as follows; the four posts building at the front followed by the six posts building, the nine posts building at the middle, and the eight posts building at the rear. The use of pillars can also reduce wind forces by pressure (drag) on building surfaces.

Increasing the relative surface roughness by using traditional materials reduces the turbulent kinetic energy at the second and third buildings. A rougher surface produces a lower velocity. Therefore, to increase the heat transfer rate on building surfaces, a relatively high surface roughness should be used. A very rough material should be used on the plains and at the shores, but a relatively smooth material can be used at mountains and hills. This material design will improve the wind protection, heat transfer rate and thermal comfort of occupants.

The gate position affects the flow patterns around a cluster of buildings. The gate position should be related to wind engineering, architectural aerodynamics, heat transfer and thermal comfort. The greater the reduction in wind velocity, heat losses on building surfaces and cooling loads of buildings, the better the meaning of the gate.

The magic rule can also be related to wind engineering and heat transfer. A screen behind the gate (*aling –aling*) reduces the pressure, turbulent kinetic energy and dissipation rate. This small wall that screens off the interior and stops evil spirits can be related to the protection against wind loads and the reduction of energy transfer on building surfaces. The connotation of evil spirit and magic rule of traditional Balinese architecture now has a strong relation with momentum and energy transfer on building surfaces.

Centre (*natar*) is the area where the flows reattach to the ground. The pressure, turbulent kinetic energy and dissipation rate decrease here. For better natural ventilation and beneficial air motion, inlet openings should be located to intercept prevailing winds and direct them towards the living room. Therefore, all buildings should be oriented to the centre (*natar*) in order to optimise the airflow into buildings. This again indicates that building orientation to the centre (*natar*) in traditional Balinese architecture has a strong relation to natural ventilation and thermal comfort.

The place of honour, the higher north-east corner of the house towards the mountain, was occupied by the family temple (*sanggah kemulan*) for worshipping their ancestors. The place of honour is an area where the turbulent kinetic energy and dissipation rate are relatively high, then, the shrines of gods should be built in this area in order to reduce the evil spirit or momentum and energy transfer. As previously discussed, the name *Ngurah* or *Penunggu Karang* refers to a deity whose function is to "protect the ground", or act as a "guardian" or "protector" or "shelter".

As an organic unit, the structure, significance, and function of the house have the same fundamental principles of belief that rule larger communities. By understanding

the structure and function of traditional Balinese house, the same principles can be used to improve larger communities or villages. We believe that traditional Balinese architecture and communities can be modified by considering the above aspects and also taking into account the *Tri Hita Karana* concept. Therefore, new Balinese codes of building design should refer to the *Tri Hita Karana* concept in order to improve thermal comfort of occupants and reduce cooling loads with corresponding energy savings.

In a housing complex, the distance between buildings at the front side can be very short but at the leeward side should be at least 1.7 times the first building height **(H)**, as shown in Figure 7.1. This arrangement increases the heat transfer rate and thermal comfort of occupants.

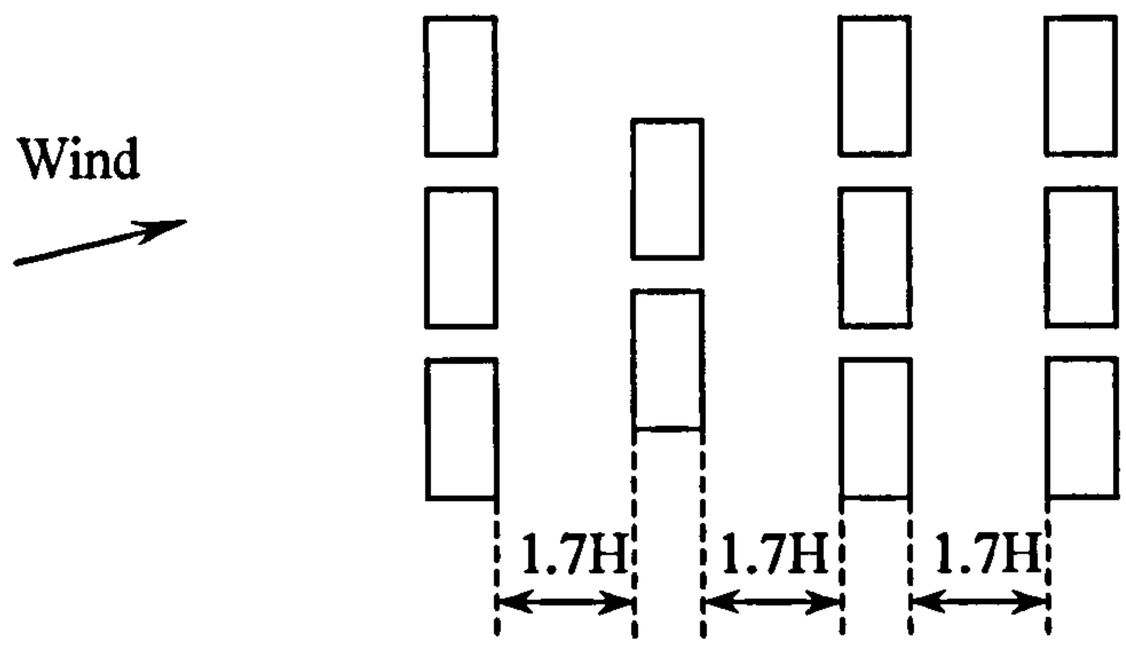

Figure 7.1 Building arrangement in a housing complex

7.2 Suggestions for Future Work

Suggestions for future CFD work are as follows:

1. The first extension of this work would consist of improving the accuracy of the results of the standard k-ε turbulence model, especially in the separation bubble region (top of building), and developing a two-layer method by applying a one-equation model in the inner region. The values of strain (S) of the standard k-ε turbulence model are large in the stagnation region (windward edge) and lead to an excessive value of the production term (P_k) since the fluid deformation near that point is nearly irrotational. Thus, the replacement of the production term is of great importance in future works to improve the accuracy of the results. The modification steps are as follows:
   The dimensionless strain, $S = f(k, \varepsilon, \nabla u)$ and vorticity $\Omega = f(k, \varepsilon, \nabla u)$ can be modified by introducing very low velocity fluctuations at the inlet or at the inner region (for two-layers). The production term of turbulent kinetic energy thus becomes: $P_k = f(C_\mu, \varepsilon, S, \Omega)$. The model of Kato and Launder [1] -as used by Selvam [2]- still gave a high production term around the building and a high pressure distribution at the windward edge, but this was reduced in the present study by using low velocity fluctuations at the inlet. Therefore, the key to improving the accuracy of the results at the top of building lies in values of the strain (S) and C_μ.
2. The meteorological conditions in urban areas (towns and capital of Bali) should be considered in future simulations. These would include:

- Solar irradiation, since it holds an important key to the thermal environment and building design.
- Relative humidity in the wet season (more than 90%), in order to improve thermal comfort of occupants.
- Air pollutants, in order to understand their distribution and concentration in the thermal structure of urban areas. The interactions between air temperature, wind velocity and pollutants concentration should be further studied in connection to reducing solar radiation and gas pollutants.

3. Heat transfer reduction in urban areas by considering plants and vegetation. The ideal distance between vegetation and urban areas (the so-called green belt), permeability of vegetation, and absorption of gas pollutants from the surrounding urban areas are of great importance in future works.
4. Permeability and surface roughness of building materials in order to reduce cooling loads by conduction, convection and radiation and to prevent re-radiation of heat during evenings, by allowing air movement through these materials.
5. Simulation of internal flows in order to reduce heat by cross-ventilation and improving thermal comfort of occupants.

It would also be advantageous if the use of numerical simulation could be extended to cover the details of the *Tri Hita Karana* concept in urban planning, such as shrines of gods and temples, especially when land occupation becomes a major problem in the future.

Given the above conditions, it would be interesting to explore the possibilities of combining the results derived herein with several fields of sciences, as a method of improving and developing the traditional Balinese communities and revising the Balinese code of building design.

REFERENCES

1. M. Kato and B.E. Launder, The modelling of turbulent flow around stationary and vibrating square cylinders, Ninth Symposium on Turbulent Shear Flows, Kyoto, Japan, 10-4 (1993)1-6.
2. R.P. Selvam, Computation of flow around Texas Tech building using k-ε and Kato-Launder k-ε turbulence model, Engineering Structures 18 (1996) 856-860.

GLOSSARY

Alit	small, little
Aling – aling	a small wall that screens off the interior and stops evil spirits
Adat	customary law
Asta Kosala	a manuscript of ground regulation
Asta Kosali	a manuscript of building regulation
Asta Patali	a manuscript of sacred building regulation
Balé	a pavilion, a house, a couch or bed
Balé gedé	a building with twelve beautiful carved posts which is used for social life
Balé Piasan	the place for ritual ceremonies
Balé Sakanem	the six posts building used for ceremonies
Balé Sakapat	the four posts building, used for small building, kitchen
Balé Tiang Sanga	the nine posts building, used for meetings
Bayung Gede	the mountain village originally studied by Gregory Bateson and Margaret Mead in 1936-1939
Besakih	mother temple of all Balinese temples
Bhuwana	world
Bhuwana Agung	the great world; that is, outer reality, the material world, the macrocosm
Bhuwana Alit	the little world; that is, the inner human, the immaterial world, the microcosm
Candi	a sepulchral monument
Candi Bentar	split gate
Desa	a complete and independent community, a village
Gede	great, big
Gedong	building
Gedong Pesimpenan	a building to place all ritual attributes

Gong	name for traditional orchestras and music
Gunung Agung	the highest and sacred mountain in Bali island where the mother temple of *Besakih* lies
Gunung Batur	the sacred mountain in the middle island of Bali, a symbol of prosperity
Hulu	upwards, towards the sacred
Jineng	granary, rice shed
Kaja	direction towards the sacred mountain or the sunrise
Kangin	the direction 'east'
Kauh	the direction 'west'
Kelod	direction towards the sea or the sunset, associated with the evil spirit activity
Kemulan	the ancestors of a nuclear family
Kulkul	a hollowed tree-trunk beaten to give signals, call meetings and sound alarms
Lontar	a manuscript, a book written on dried leaves of the *lontar* Palm (a Palmaceous)
Madya	mean, middle
Manjangan Saluang	a place to worship the holy priest who arrange the traditional Balinese communities
Maospait (Majapahit)	ancient kingdom in Indonesia (11^{th}-14^{th} centuries) where most Balinese people came from
Merajan	comes from *praja*, descendants, family but also followers, to pay respect to the gods
Meru	building with multi-stage roofs, indicating sacred mountain
Natar	a Balinese house yard, consists either of a nuclear family or of a group of connected nuclear families
Ng(r)urah	a deity whose function is to "protect" the ground Applied to a lord, it then indicates his roles as such a "guardian" or "protector"

Nista	poverty
Padmasana	Lotus seat, refers to the throne of God
Paduraksa	ceremonial gate
Paruman	the place of gods and goddesses during ritual day
Pa(w)on	kitchen
Pengijeng	a deity who acts as a "guardian" of a place of honour
Penunggu Karang	a deity whose function is to "protect" the occupants and its surroundings
Pura	the temple
Pura Desa	a village temple
Pura Dalem	the temple of dead
Pura Puseh	Naval Temple, village temple dedicated to commemorating local settlement origins and founding ancestors
Puri	the palace of a prince, castle
Sanga Mandala	nine regions of house yard, each region has a different meaning and functions
Sanggah Kemulan	the family temple for worshipping their ancestors
Saren	the place for ritual ceremonies
Swakarman	a manuscript of building construction regulation
Sumur	waterhole
Tri Hita Karana	concept of harmony and balance of the Balinese Hindu religion involving three factors: microcosm, macrocosm and the Supreme God
Taksu	the power, manifested in the consorts of the gods
Teben	downwards, towards the evil spirit
Uma meten	the building for sleeping-quarters of the occupants
Undagi	traditional architects
Utama	primary
Wantilan	assembly hall of the villagers
Waringin	a banyan tree